

Alma Mater Studiorum – Università di Bologna

DOTTORATO DI RICERCA IN

CHIMICA

Ciclo 29°

Settore Concorsuale: 03/C1

Settore Scientifico Disciplinare: CHIM/06

**ISOLATION AND MODIFICATION OF PLANT GLUCOSINOLATES
AND THEIR ROLE IN THE PREVENTION OF PATHOLOGIES
OF THE CENTRAL NERVOUS SYSTEM**

Presentata da: Gina Rosalinda De Nicola

Coordinatore Dottorato

Prof. Aldo Roda

Supervisore

Prof. Luca Valgimigli

Co-supervisore

Dr. Renato Iori

Esame finale anno 2018

*ISOLATION AND MODIFICATION OF PLANT GLUCOSINOLATES
AND THEIR ROLE IN THE PREVENTION OF PATHOLOGIES OF
THE CENTRAL NERVOUS SYSTEM*

TABLE OF CONTENTS

PREFACE	The research project	7
PART ONE	THE GLUCOSINOLATE-MYROSINASE SYSTEM	
Chapter one	The chemistry of the glucosinolate-myrosinase system and its relevant biological effects – An overview	11
PART TWO	PLANT SCREENING	
Chapter two	Long-chain glucosinolates from <i>Arabis turrita</i> : enzymatic and non-enzymatic degradations	57
Chapter three	Glucosinolate profile of Croatian stenoendemic plant <i>Fibigia triquetra</i> (DC.) Boiss. ex Prantl.	75
Chapter four	Glucosinolate diversity in <i>Bretschneidera sinensis</i> of Chinese origin	97
Chapter five	Probing for the presence of glucosinolates in three <i>Drypetes</i> spp. and two <i>Rinorea</i> spp. from Gabon	117
Chapter six	<i>Isatis canescens</i> is a rich source of glucobrassicin and other health-promoting compounds	131
Chapter seven	<i>Moringa oleifera</i> : study of phenolics and glucosinolates by mass spectrometry	151
PART THREE	GLUCORAPHANIN PURIFICATION AND R-SULFORAPHANE PRODUCTION	

Chapter eight	Tuscan black kale as a multifunctional plant source of glucoraphanin and enantiopure <i>R</i> -sulforaphane	177
PART FOUR	GLUCOSINOLATE MYROSINASE ASSISTED HYDROLYSIS	
Chapter nine	Isothiocyanates and dithiocarbamates production in a biphasic system	204
PART FIVE	GLUCOMORINGIN PURIFICATION AND DERIVATIVES PRODUCTION	
Chapter ten	<i>Moringa oleifera</i> seed cake as a source of medicinal glucomoringin, moringin and other derivatives	253
PART SIX	<i>IN VIVO</i> PHARMACOLOGICAL STUDIES – ROLE OF <i>R</i>-SULFORAPHANE AND MORINGIN IN THE PREVENTION OF PATHOLOGIES OF THE CENTRAL NERVOUS SYSTEM	
Chapter eleven	Glucoraphanin purified from Tuscan black kale and bioactivated with myrosinase enzyme protects against cerebral ischemia/reperfusion injury in rats	277
Chapter twelve	Tuscan black kale sprout extract bioactivated with myrosinase: a novel natural product for neuroprotection by inflammatory and oxidative response during cerebral ischemia/reperfusion injury in rat	302
Chapter thirteen	Moringin attenuates secondary damage in an experimental model of spinal cord injury	331
Chapter fourteen	Moringin delays disease phenotype in SOD1 ^{G93A} rats: a transgenic model of amyotrophic lateral sclerosis	353

Chapter fifteen	Moringin activates Wnt canonical pathway by inhibiting GSK3 β in a mouse model of experimental autoimmune encephalomyelitis	373
Chapter sixteen	Moringin shows potent anti-inflammatory activity in the treatment of murine subacute Parkinson's disease	398
SCIENTIFIC PRODUCTION		427

PREFACE

The research project

The present PhD research activity has been carried out at the research center Agricoltura e Ambiente (CREA-AA, ex-CIN) in Bologna (Italy). The center is part of the CREA network (Consiglio per la ricerca in agricoltura e l'analisi dell'economia agraria) and it is a center of excellence for top-level research of the biochemical plant defensive system known as 'glucosinolate-myrosinase system' with an in-depth experience of more than four decades. Noteworthy, the center has developed a collection of glucosinolate producing plant seed, besides having published a wide number of scientific articles on the subject since 1982. The center CREA-AA has also pioneered the purification of glucosinolates to a high purity level along with the enzyme myrosinase. This system is present in many plants, mainly of the order Brassicales, including several nonfood industrial oleaginous crops such as *Brassica carinata*, and common vegetables like broccoli, cabbage, kale, radish and rocket consumed worldwide. The subject is of big interest and the knowledge about this fascinating biochemical system is still evolving and attracting the combined efforts of scientists of several disciplines.

This PhD research activity was granted by the project 'Role of the glucosinolate-myrosinase system in the prevention of pathologies of central nervous system' in collaboration with IRCCS Centro Neurolesi Bonino-Pulejo (Messina, Italy) and supervised by Prof. Luca Valgimigli (University of Bologna) and Dr. Renato Iori (CREA-AA). The research focused on the multigram-scale isolation of selected glucosinolates, the setting-up of their enzymatic transformation, and the *in-vivo* investigation of their activity in the protection of the central nervous system from neurodegenerative disorders. Furthermore, several plants were analyzed for glucosinolate profiling and quantification over the PhD years, since the analytical plant screening is the first step underlying the research activity when dealing with phytochemicals investigations. One of the main task of the PhD was the screening of different Brassicaceae to identify the most convenient source to isolate glucoraphanin, which pointed towards Tuscan black kale seeds that resulted to be a multifunctional source to achieve several purposes. The procedure for extraction and purification of glucoraphanin from the defatted seed cake was set-up by combining preparative anion exchange chromatography

and gel filtration chromatography. Further, a set of other four glucosinolates, namely thiofunctionalized glucoerucin, glucoraphasatin, glucoraphenin and the atypical glycosylated glucomoringin were isolated and purified using similar experimental approach starting from suitable plant sources. The protocol was able to furnish all glucosinolates on the gram scale with a 95-99% purity level. To prepare the isothiocyanates from the purified glucosinolate precursors, the enzyme myrosinase was extracted and purified from white mustard (*Sinapis alba* L.) seeds by an established method based on two chromatographic steps: affinity chromatography on Con-A-Sepharose followed by gel filtration.

An efficient protocol for the enzymatic transformation of the selected glucosinolates and isolation of the corresponding isothiocyanates was set up and optimized using a biphasic system. The glucosinolates were also hydrolyzed using the same set-up system with the addition of benzyl mercaptan used as a model thiol to trap *in situ* the corresponding isothiocyanates intermediate and directly transform them into dithiocarbamates. This study highlighted a peculiar reactivity of glucoraphenin and an interesting water instability of its enantiopure isothiocyanate known as *R*-sulforaphane. Further investigation on glucoraphenin myrosinase catalyzed assisted hydrolysis led to the discovery of a new small cyclic molecule bearing 3 sulfur atoms that was isolated and characterized.

The pharmacological studies focused on glucoraphenin and glucomoringin that are the precursors of dietary isothiocyanates *R*-sulforaphane and moringin, respectively, recognized for their chemopreventive and medicinal properties. In contrast to the well-known *R*-sulforaphane, little is known about the molecular pathways targeted by moringin. The neuroprotective effects of *R*-sulforaphane and moringin freshly prepared by the action of myrosinase on highly pure glucoraphenin and glucomoringin, was tested in *in vivo* pharmacological investigations, in collaboration with IRCCS – Messina. The results showed neuroprotection by *R*-sulforaphane in a rat model of spinal cord injury. Moringin was tested in four different animal models of Parkinson's disease, autoimmune encephalomyelitis, spinal cord injury and amyotrophic lateral sclerosis proving promising neuroprotection effects.

The results achieved in the three years of research have been documented by twenty-seven scientific articles published in international peer reviewed journals and listed at the end of this PhD thesis. Also, the PhD candidate was the presenter of an oral communication at the main international congress on glucosinolates in 2014, and a coauthor of a poster presentation at a national conference in Zagreb in 2015.

PART ONE

THE GLUCOSINOLATE-MYROSINASE SYSTEM

CHAPTER ONE

The chemistry of the glucosinolate-myrosinase system and its relevant biological effects – An overview

Contents

Summary

- 1.1** Glucosinolate structure and classification
 - 1.1.1** Glucosinolate nomenclature
 - 1.1.2** Types of glucosinolates
- 1.2** Glucosinolate biosynthesis
- 1.3** The glucosinolate-myrosinase system
 - 1.3.1** Myrosinases
 - 1.3.2** The mechanism of myrosinase-catalyzed hydrolysis of glucosinolates to produce isothiocyanates
 - 1.3.3** Other glucosinolate breakdown products
 - 1.3.3.1 Oxazolidinethiones*
 - 1.3.3.2 Specifier proteins*
 - 1.3.3.3 Nitriles and epithionitriles*
 - 1.3.3.4 Thiocyanates*
- 1.4** Biological activity
 - 1.4.1** Plant defense
 - 1.4.2** Human health
 - 1.4.2.1 Indirect antioxidant activity of isothiocyanates*
 - 1.4.2.2 Pro-oxidant activity of isothiocyanates*

References

Keywords

Glucosinolates, Isothiocyanates, Myrosinases, Brassicales

Summary

The objective of this chapter is to present a general overview of the glucosinolates, thiosaccharidic secondary metabolites, found in the plant kingdom and to present their structural diversity depending on the metabolism of the amino acid precursor of the plant species. The occurrence of glucosinolates in plants coincides with the occurrence of specific thioglucosidases, the myrosinases enzymes, which catalyzes the hydrolysis of these compounds. The fascinating glucosinolate breakdown machinery can give rise to the formation of structurally diverse products depending mainly on the chemical structure of the aglycon chain and the experimental conditions. The different hydrolysis pathways leading to the formation of isothiocyanates as well as several others degradation products are presented. Finally, a general overview of the relevant biological effects of glucosinolate breakdown products is described.

1.1 Glucosinolate structure and classification

Glucosinolates (GLs) are an important class of thiosaccharidic secondary metabolites occurring in the botanical order Brassicales which encompass seventeen plant families of dicotyledonous angiosperms including many edible species (Table 1.1) (APG III, 2009). Brassicaceae, also called Cruciferae, is the dominant family within the order Brassicales, with over 330 genera and 3700 species distributed primarily in the temperate and alpine areas of all continents except Antarctica (Blažević et al., 2017). The Brassicaceae family includes many economically important GLs producing plants such as leaf and root vegetables, oilseed and condiment crops that are cultivated worldwide and marketed for animal and human consumption (Ishida et al., 2014). GLs are water soluble organic anions which display a remarkable structural homogeneity based on three moieties: (1) a hydrophilic β -D-glucopyrano unit and (2) a *O*-sulfated anomeric (*Z*)-thiohydroxymate function connected to (3) a variable aglycone side chain derived from an α -amino acid (Figure 1.1). The aglycone can originate from one of eight natural α -amino acids according to which GLs can be classified into three classes as aliphatic (derived from Ala, Leu, Ile, Val, and Met), arylaliphatic (derived from Phe or Tyr) and indolyl GLs (derived from Trp) (Agerbirk and Olsen, 2012). The first comprehensive compilation and cataloging of the chemical structure of all known GLs and the plant families from which they have been isolated was provided by Fahey et al. (2001). This review still represents the milestone reference for the scientific community in the field since it provides a single source of the chemical and common names of 121 GLs along with their chemical structure and their distribution among plant species. A systematic critical review of natural occurring GLs has been more recently provided by Agerbirk and Olsen (2012). These authors updated the number of GL structures fully documented by 2011. They reduced the previously reported number of 121 GLs by 15 structures as these molecules were found insufficiently documented and the supportive evidences not conclusive. On the other hand, they increased the number by 1 as two well documented epimers namely (*S*)-2-hydroxy-2-phenylethyl GL (glucobarbarin) and (*R*)-2-hydroxy-2-phenylethyl GL (*epi*glucobarbarin) were not distinguished in Fahey table (Fahey et al., 2001). In the same review Agerbirk and Olsen (2012) added 26 GLs newly discovered between 2000 and 2011 reaching a total number of 133 identified structures which is still almost invariably the quoted number nowadays. A new GL, 4-hydroxy-3-methoxybenzyl GL, has been isolated from *Bretschneidera sinensis* and fully

characterized during the realization of the present PhD thesis described here at Chapter four and published in 2015 (Montaut et al., 2015). Thus, the quoted number of GLs by 2017 should be increased to 134. For the sake of completeness, the valuable review of Clarke (2010) must be mentioned here. This review focused on the quantitative analysis of GLs in plant materials and provided an electronic database of structures, formulae and accurate masses of 200 structures for use in mass spectrometry. Hence, it appears likely that several new natural structures have already been detected in plants and are awaiting documentation by complete identification after their isolation.

Table 1.1 Seventeen plant families of the botanical order Brassicales. Numbers in parenthesis are the approximate number of genus and species in each family (Blažević et al., 2017). Edible species are reported in italics.

Akaniaceae (2/2)	Limnanthaceae (2/9)
Bataceae (1/2)	Moringaceae (1/12) (<i>moringa</i>)
Brassicaceae (330/3700) (<i>cabbages</i>)	Pentadiplandraceae (1/1)
Capparaceae (16/480) (<i>capers</i>)	Resedaceae (6/85) (<i>reseda</i>)
Caricaceae (4-6/34) (<i>papaya</i>)	Salvadoraceae (3/11)
Cleomaceae (2-6/300)	Setchellanthaceae (1/1)
Emblingiaceae (1/1)	Tovariaceae (1/2)
Gyrostemonaceae (6/20)	Tropaeolaceae (1/105) (<i>Indian cress</i>)
Koeberliniaceae (1/2)	

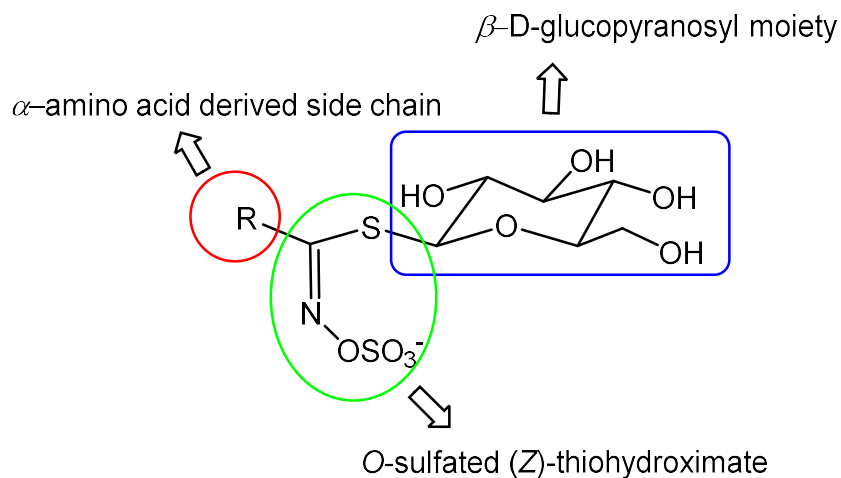


Figure 1.1 General structure of glucosinolates. The three common constitutive moieties are indicated: a hydrophilic β -D-glucopyrano unit, a O-sulfated anomeric (Z)-thiohydroximate function and a variable aglycone side chain derived from an α -amino acid precursor.

1.1.1 Glucosinolate nomenclature

The systematic nomenclature of each individual GL is greatly simplified by the convention of naming the entire anionic core invariable structure as GL. Because of this convention, most natural GLs can be named simply by adding the systematic name of the side chain to the term GL. Many GLs also carry common names most often given according to the plant from which they have been isolated or indirectly identified for the first time. Also, GL acronyms have been developed as a three letters code which is an abbreviated form of the common name (Wathelet, 2004). For example, 3-methylsulfinylpropyl GL was isolated from *Iberis amara*, its common name is glucoiberin and its code GIB (Schultz and Gmelin, 1954). The use of these codes is not recommendable because it relies on the existence of trivial names instead of referring to the chemistry of the side chain group. These codes are by no way officially assigned to the compounds and they should be avoided, though they still are of common use in the community of GL specialists with many differences depending on the laboratory tradition of the research groups.

1.1.2 Types of glucosinolates

GLs are conveniently grouped into several chemical classes based on structural similarities of the α -amino acid derived side chain. The generally accepted chemical classification is the one reported by Fahey et. al (2001) and modified by Clarke (2010) as follow:

- A. Sulfur-containing side chain,
- B. Aliphatic, straight-chain,
- C. Aliphatic, branched-chain,
- D. Olefins straight and branched chain and alcohols,
- E. Aliphatic straight and branched chain alcohols,
- F. Aliphatic straight chain ketones and esters,
- G. Aromatic,
- H. Benzoates,
- I. Indole,
- J. Glycosylated,
- K. Benzyl glucosides,
- L. Cinnamic glucosides.

All the 134 documented naturally occurring GLs are reported as follows in Table 1.2 and Chart 1.1 based on the classification described before. Table 1.2 shows chemical name, common name and acronym, if known, for each GL numbered progressively within each chemical class listed alphabetically. The numeration used by Agerbirk and Olsen (2012) is also reported in the last column of the table to keep consistency with this PhD thesis and their recent review. Compound numbers 1-120 in Agerbirk and Olsen (2012) refer to the alphabetical numbering system proposed by Fahey et al. (2001), whereas numbers 121-142 refer to the 26 structures (of which 4 couples of epimers that carry the same number) newly discovered and identified between 2000 and 2011. Reported acronyms are those used at CREA-AA (Bologna, Italy) where the research activity of this PhD thesis has been carried out, as well as at other European research centers, and that can be found in many published articles (Wathelet et al. 2004).

Table 1.2 Chemical names, common names and known acronyms of glucosinolates identified in higher plants. Class assignment refers to the chemical classification based on structural similarity of the side chain as explained in the text. The last column shows the numeration used by Agerbirk and Olsen (2012).

Glucosinolate					
No.	Class	Chemical name	Common name	Acronym	No.
A					
Sulfur-containing side chains					
Methyl-sulfanyl-alkyl					
1	A	3-Methylsulfanylpropyl	Gluciberberin	GIV	95
2	A	4-Methylsulfanylbutyl	Glucoerucin	GER	84
3	A	5-Methylsulfanylpentyl	Glucoberteroin	GBE	94
4	A	6-Methylsulfanylhexyl	Glucosquerellin		88
5	A	7-Methylsulfanylheptyl			87
6	A	8-Methylsulfanyloctyl			92
7	A	9-Methylsulfanylnonyl			89
8	A	10-Methylsulfanyldecyl			85
Methyl-sulfinyl-alkyl					
9	A	2-Methylsulfinylethyl			137
10	A	3-Methylsulfinylpropyl	Gluciberin	GIB	73
11	A	4-Methylsulfinylbutyl	Glucoraphanin	GRA	64
12	A	5-Methylsulfinylpentyl	Glucosalyssin	GAL	72
13	A	6-Methylsulfinylhexyl	Glucosesperin		67
14	A	7-Methylsulfinylheptyl	Glucobarin		66
15	A	8-Methylsulfinyloctyl	Glucosirsutin		69
16	A	9-Methylsulfinylnonyl	Glucosarabin		68
17	A	10-Methylsulfinyldecyl	Glucoscamelinin		65
18	A	11-Methylsulfinylundecyl			74
Methyl-sulfonyl-alkyl					
19	A	3-Methylsulfonylpropyl	Glucoscheirolin	GCH	82
20	A	4-Methylsulfonylbutyl	Glucoscherysolin		76
21	A	5-Methylsulfonylpentyl			81
22	A	6-Methylsulfonylhexyl			78
23	A	8-Methylsulfonyloctyl			80
24	A	9-Methylsulfonylnonyl			79
25	A	10-Methylsulfonyldecyl			77
Methyl-sulfanyl-alkene					
26	A	4-Methylsulfanyl-3-butenyl	Glucosraphasatin	GRH	83
Methyl-sulfinyl-alkene					
27	A	4-Methylsulfinyl-3-butenyl	Glucosraphenin	GRE	63
Methyl-sulfonyl-alkene					
28	A	4-Methylsulfonyl-3-butenyl			75
Methyl-sulfanyl-hydroxy-alkyl					
29	A	3-Hydroxy-5-methylsulfanylpentyl			37

Glucosinolate

No.	Class	Chemical name	Common name	Acronym	No.
30	A	3-Hydroxy-6-methylsulfanylhexyl			36
Methyl-sulfinyl-hydroxy-alkyl					
31	A	3-Hydroxy-5-methylsulfinylpentyl			33
32	A	3-Hydroxy-6-methylsulfinylhexyl			32
Methyl-sulfonyl-hydroxy-alkyl					
33	A	3-Hydroxy-5-methylsulfonylpentyl			35
34	A	3-Hydroxy-6-methylsulfonylhexyl			34
Methyl-sulfanyl-oxo-alkyl					
35	A	6-Methylsulfanyl-3-oxohexyl			91
36	A	7-Methylsulfanyl-3-oxoheptyl			90
37	A	8-Methylsulfanyl-3-oxooctyl			93
Methyl-sulfinyl-oxo-alkyl					
38	A	7-Methylsulfinyl-3-oxoheptyl			70
39	A	8-Methylsulfinyl-3-oxooctyl			71
Mercapto-alkyl					
40	A	4-Mercaptobutyl			133
Disulfanyl					
41	A	Dimeric 4-mercaptobutyl			134
42	A	4-(β -(Glucopyranosyl)disulfanyl)butyl			135
Cysteine-sulfanyl-alkyl					
43	A	4-(Cystein-S-yl)butyl			136
	B	Aliphatic, straight chain			
44	B	Methyl	Glucocapparin	GCA	51
45	B	Ethyl			16
46	B	n-Propyl			108
47	B	n-Butyl			13
48	B	n-Pentyl			102
49	B	n-Hexyl			20
	C	Aliphatic, branched chain			
50	C	1-Methylethyl	Glucoputranjivin, isopropyl	GPU	56
51	C	1-Methylpropyl	Glucocochlearin, sec-butyl, 2-butyl	GCC	61
52	C	2-Methylpropyl	Isobutyl		62
53	C	1-Methylbutyl			53
54	C	2-Methylbutyl			54
55	C	3-Methylbutyl			55
56	C	3-Methylpentyl			58
57	C	4-Methylpentyl			59

Glucosinolate					
No.	Class	Chemical name	Common name	Acronym	No.
D Olefins					
Straight and branched chain					
58	D	2-Propenyl	Sinigrin, Allyl	SIN	107
59	D	2-Methyl-2-propenyl			60
60	D	3-Butenyl	Gluconapin	GNA	12
61	D	3-Methyl-3-butenyl			52
62	D	1-Pentenyl			100
63	D	4-Pentenyl	Glucobrassicinapin	GBN	101
Alcohols					
64R	D	2(<i>R</i>)-hydroxy-3-butenyl	Progoitrin	PRO	24a
64S	D	2(<i>S</i>)-hydroxy-3-butenyl	<i>Epi</i> progoitrin	ePRO	24b
65	D	2-Hydroxy-4-pentenyl	Gluconapoleiferin	GNL	38
E Aliphatic alcohols					
Straight chain					
66	E	2-Hydroxyethyl			27
67	E	3-Hydroxypropyl			42
68	E	3-Hydroxybutyl			25
69	E	4-Hydroxybutyl			26
Branched chain					
70	E	1-Methyl-2-hydroxyethyl	Glucosismbrin	GSY	57
71	E	1-(Hydroxymethyl)propyl			30
72	E	2-Hydroxy-2-methylpropyl	Glucoconringiin	GCN	31
73	E	2-Hydroxy-2-methylbutyl	Glucocleomin	GCL	29
74	E	3-(Hydroxymethyl)pentyl			141
75	E	4,5,6,7-Tetrahydroxydecyl			113
F Aliphatic straight chain ketons					
76	F	4-Oxoheptyl	Glucocapangulin, glucopangulin		96
77	F	5-Oxoheptyl	Glucocappasalin		97
78	F	5-Oxoocetyl	Gluconorcappasalin		98
Esters					
79	F	3-Methoxycarbonylpropyl	Glucoeypestrin		1
G Aromatic					
Benzyl					
80	G	Benzyl	Glucotropaeolin	GTL	11
81	G	2-Hydroxybenzyl			21
82	G	3-Hydroxybenzyl	Glucolepigramin		22
83	G	4-Hydroxybenzyl	Glucosinalbin	SNB	23
84	G	2-Methoxybenzyl			44
85	G	3-Methoxybenzyl	Glucolimnanthin	GLI	45
86	G	4-Methoxybenzyl	Glucoaubrietin	GAU	46

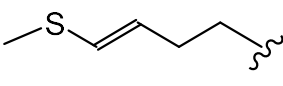
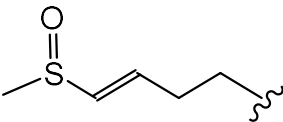
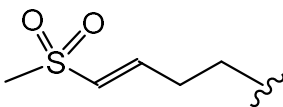
Glucosinolate					
No.	Class	Chemical name	Common name	Acronym	No.
87	G	3,4-Dihydroxybenzyl	Glucomatronalin		14
88	G	3,4-Dimethoxybenzyl			15
89	G	4-Hydroxy-3-methoxybenzyl	Glucobretschneiderin	GBR	
90	G	3,4,5-Trimethoxybenzyl			114
Phenylethyl					
91	G	2-Phenylethyl	Gluconasturtiin, phenethyl	GST	105
92R	G	2(<i>R</i>)-Hydroxy-2-Phenylethyl	Glucobarbarin	GBB	40S
92S	G	2(<i>S</i>)-Hydroxy-2-Phenylethyl	<i>Epigluco</i> barbarin	eGBB	40R
93	G	2-Hydroxy-2-(4-methoxyphenyl)ethyl			50
94	G	2,2-Dimethyl-2-(4-methoxyphenyl)ethyl			49
95R		2(<i>R</i>)-Hydroxy-2-(4-hydroxyphenyl)ethyl	4-Hydroxy-glucobarbarin	4-OHGBB	139R
95S	G	2(<i>S</i>)-Hydroxy-2-(4-hydroxyphenyl)ethyl			139S
96	G	4-Hydroxyphenylethyl	Homosinalbin		140
97	G	2(<i>R</i>)-Hydroxy-2-(3-hydroxyphenyl)ethyl			142R
H Benzoates					
98	H	Benzoyloxymethyl			8
99	H	2-(Benzoyloxy)ethyl			6
100	H	3-(Benzoyloxy)propyl	Glucomalcomiin		10
101	H	4-(Benzoyloxy)butyl			5
102	H	5-(Benzoyloxy)pentyl			117
103	H	6-(Benzoyloxy)hexyl			118
104	H	2-Benzoyloxy-1-methylethyl	Glucobenzosisymbirin		9
105	H	2-Benzoyloxy-1-ethylethyl	Glucobenzosisaustricin		7
106	H	2-Benzoiloxo-3-butenyl	2-Benzoylprogoitrin		123
I Indol					
107	I	Indol-3-ylmethyl	Glucobrassicin	GBS	43
108	I	4-Hydroxyindol-3-ylmethyl	4-Hydroxyglucobrassicin	4-OHGBS	28
109	I	1-Methoxyindol-3-ylmethyl	Neoglucobrassicin	NeoGBS	47
110	I	4-Methoxyindol-3-ylmethyl	4-Methoxyglucobrassicin	4-OMeGBS	48
111	I	1-Sulfo-indol-3-ylmethyl	Glucobrassicin-1-sulfate		112
112	I	1,4-Dimethoxyindol-3-ylmethyl	1,4-Dimethoxyglucobrassicin		138
113R	I	Glucoisatin		GIT	121R
113S	I	<i>Epigluco</i> isatin		eGIT	121S
114R	I	3'-Hydroxyglucoisatin			122R
114S	I	3'-Hydroxyepiglucoisatin			122S
J Multiple glycosilated					
115	J	2-(α -L-Rhamnopyranosyloxy)benzyl			109
116	J	4-(α -L-Rhamnopyranosyloxy)benzyl	Glucomoringin	GMG	110

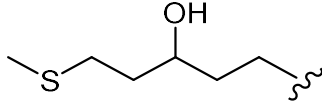
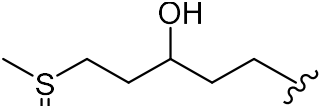
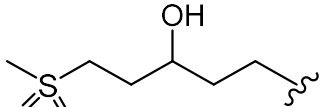
Glucosinolate

No.	Class	Chemical name	Common name	Acronym	No.
117	J	4-(4'-O-Acetyl- α -L-Rhamnopyranosyloxy)benzyl			3
118	J	2-(α -L-Arabinopyranosyloxy)-2-phenylethyl			4
119	J	6-Sinapoyl- β -D-1-thioglucoside of 4-methylsulfinyl-3-butenyl			111
	K	Benzoyl glucosides			
120	K	6'-benzoyl-4-(benzoyloxy)butyl			125
121	K	6'-benzoylglucoraphanin			126
122	K	6'-benzoylglucoerucin			127
	L	Cinnamic glucosides			
123	L	6'-(p-coumaroyl)glucoraphanin			128
124	L	6'-isoferuloylgluconasturtiin			129
125	L	6'-isoferuloylglucobrassicin			130
126R	L	6'-isoferuloylglucobarbarin			131R
126S	L	6'-isoferuloylglucobarbarin			131S
127R	L	6'-isoferuloylgluarabihirin			132R
128	L	Sinapoylated 3-hydroxypropyl			124

A. SULFUR-CONTAINING SIDE-CHAINS

	Methyl-sulfanyl-alkyl	Methyl-sulfinyl-alkyl	Methyl-sulfonyl-alkyl
n			
2	-	9	-
3	1	10	19
4	2	11	20
5	3	12	21
6	4	13	22
7	5	14	-
8	6	15	23
9	7	16	24
10	8	17	25
11	-	18	-
12			

	Sulfanyl-alkene	Sulfinyl-alkene	Sulfonyl-alkene
			
	26	27	28

	Methyl-sulfanyl-hydroxy-alkyl	Methyl-sulfinyl-hydroxy-alkyl	Methyl-sulfonyl-hydroxy-alkyl
			
	29	31	33

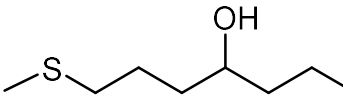
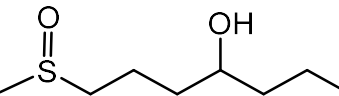
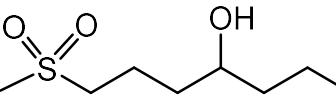
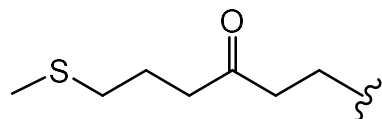
	Methyl-sulfanyl-hydroxy-alkyl	Methyl-sulfinyl-hydroxy-alkyl	Methyl-sulfonyl-hydroxy-alkyl
			
	30	32	34

Chart 1.1 Reported glucosinolate structures by chemical class. The number of each structure is the progressive numeration used in Table 1.1.

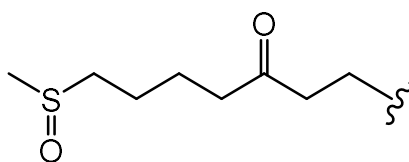
A. SULFUR-CONTAINING SIDE-CHAINS

Methyl-sulfanyl-oxo-alkyl

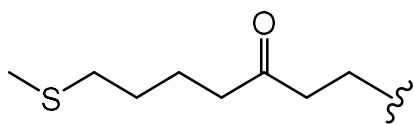


35

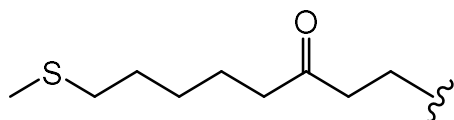
Methyl-sulfinyl-oxo-alkyl



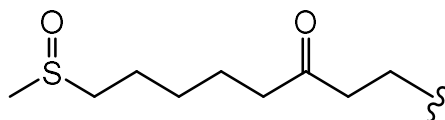
38



36

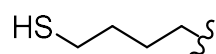


37



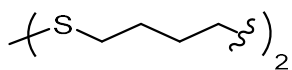
39

Mercapto-alkyl

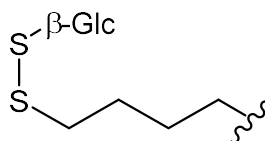


40

Disulfanyl

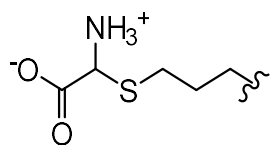


41



42

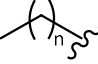
Cysteine-sulfanyl-alkyl



43

Chart 1.1 (*continued*) Reported glucosinolate structures by chemical class. The number of each structure is the progressive numeration used in Table 1.1.

B. ALIPHATIC, STRAIGHT CHAIN

	
n	
0	44
1	45
2	46
3	47
4	48
5	49

C. ALIPHATIC, BRANCHED CHAIN

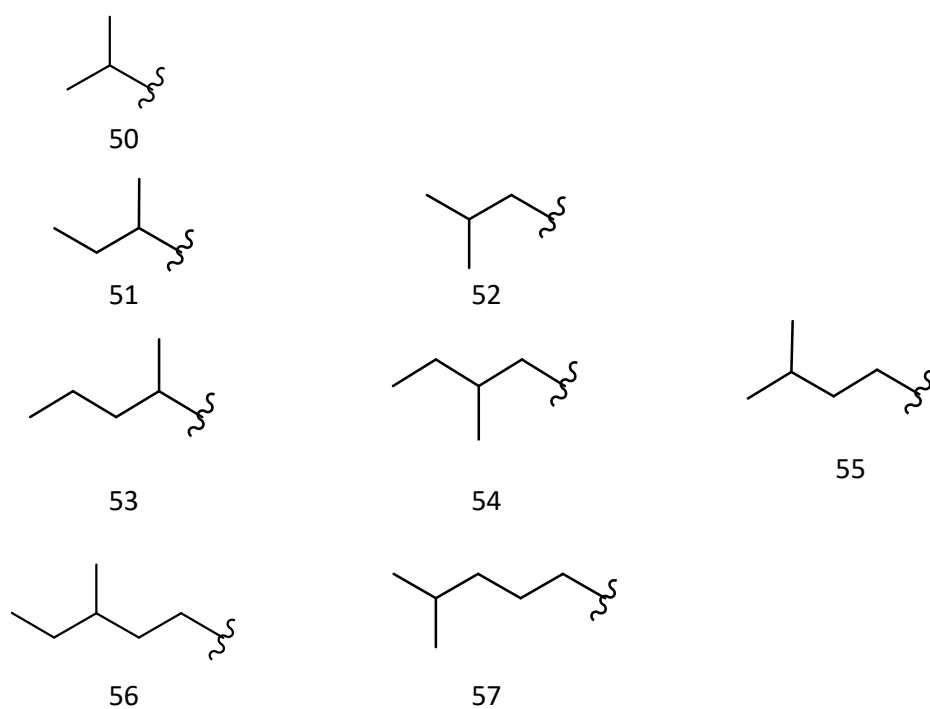
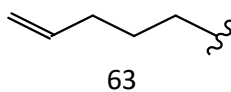
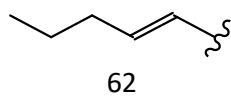
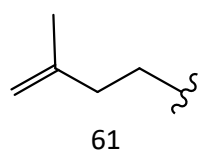
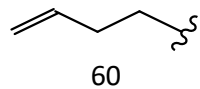
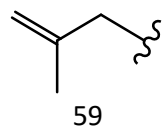
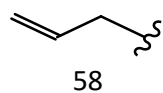


Chart 1.1 (continued) Reported glucosinolate structures by chemical class. The number of each structure is the progressive numeration used in Table 1.1.

D. OLEFINS

Straight and branched
chain



Alcohols

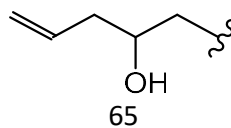
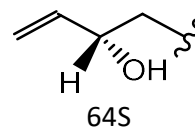
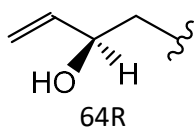
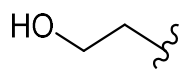
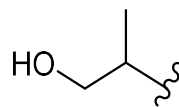


Chart 1.1 (*continued*) Reported glucosinolate structures by chemical class. The number of each structure is the progressive numeration used in Table 1.1.

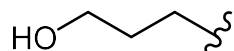
E. ALIPHATIC STRAIGHT AND BRANCHED CHAIN ACOHOLS



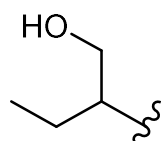
66



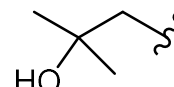
70



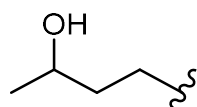
67



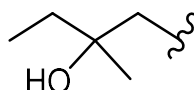
71



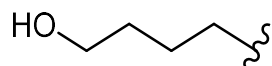
72



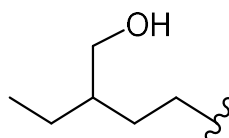
68



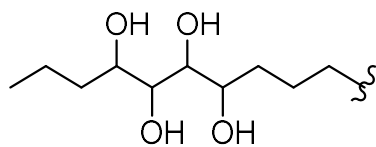
73



69



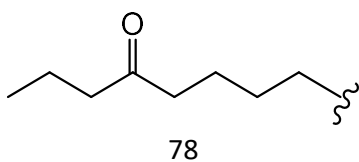
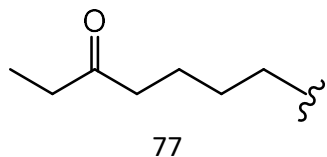
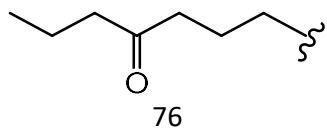
74



75

Chart 1.1 (*continued*) Reported glucosinolate structures by chemical class. The number of each structure is the progressive numeration used in Table 1.1.

F. ALIPHATIC STRAIGHT CHAIN KETONS



ESTERS

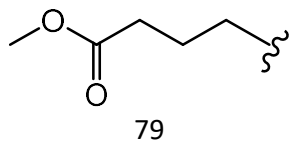
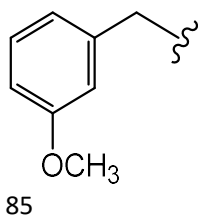
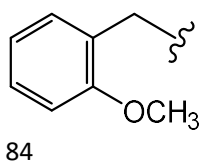
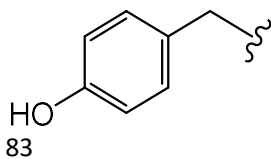
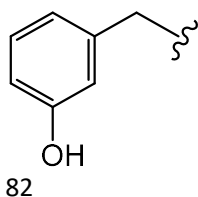
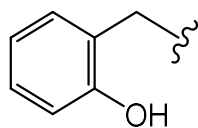
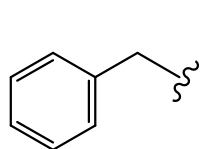


Chart 1.1 (*continued*) Reported glucosinolate structures by chemical class. The number of each structure is the progressive numeration used in Table 1.1.

G. AROMATIC

BENZYL



PHENYLETHYL

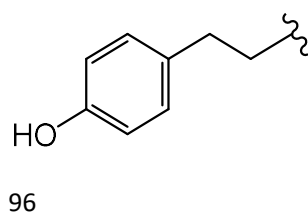
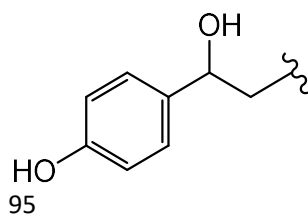
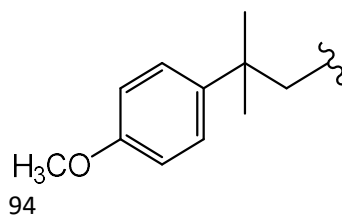
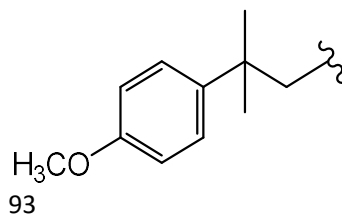
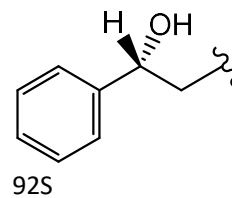
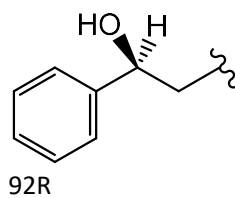
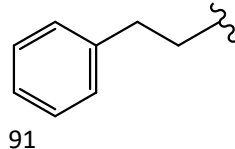
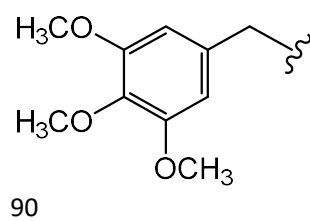
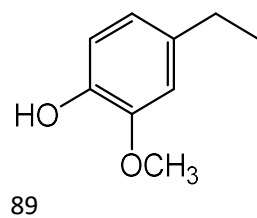
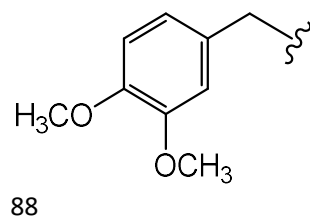
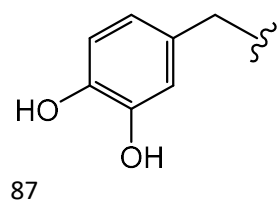
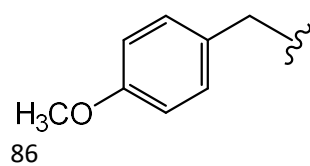


Chart 1.1 (continued) Reported glucosinolate structures by chemical class. The number of each structure is the progressive numeration used in Table 1.1.

G. AROMATIC

BENZYL



PHENYLETHYL

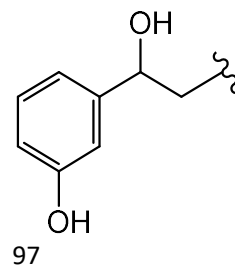
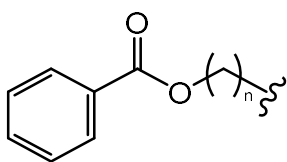


Chart 1.1 (*continued*) Reported glucosinolate structures by chemical class. The number of each structure is the progressive numeration used in Table 1.1.

H. BENZOATES

	
n	
1	98
2	99
3	100
4	101
5	102
6	103

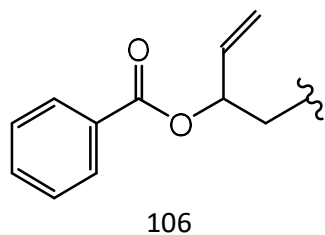
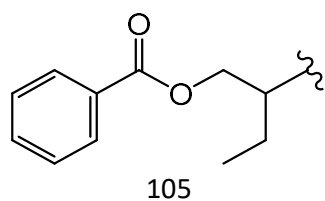
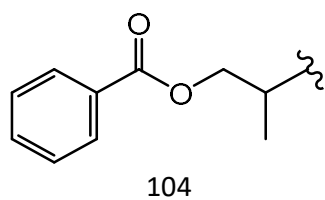
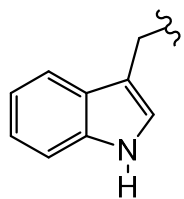


Chart 1.1 (*continued*) Reported glucosinolate structures by chemical class. The number of each structure is the progressive numeration used in Table 1.1.

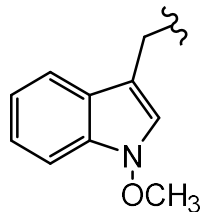
I. INDOLE



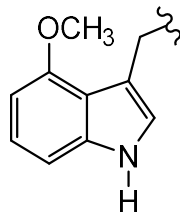
107



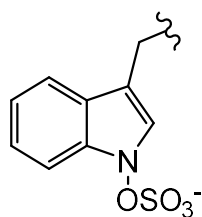
108



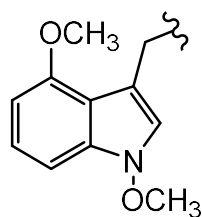
109



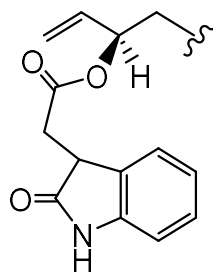
110



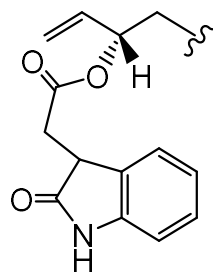
111



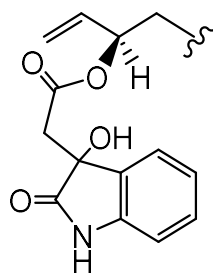
112



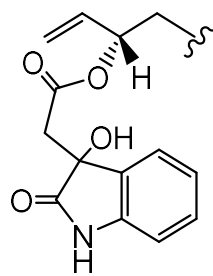
113R



113S



114R



114S

Chart 1.1 (continued) Reported glucosinolate structures by chemical class. The number of each structure is the progressive numeration used in Table 1.1.

J. MULTIPLE GLYCOSILATED

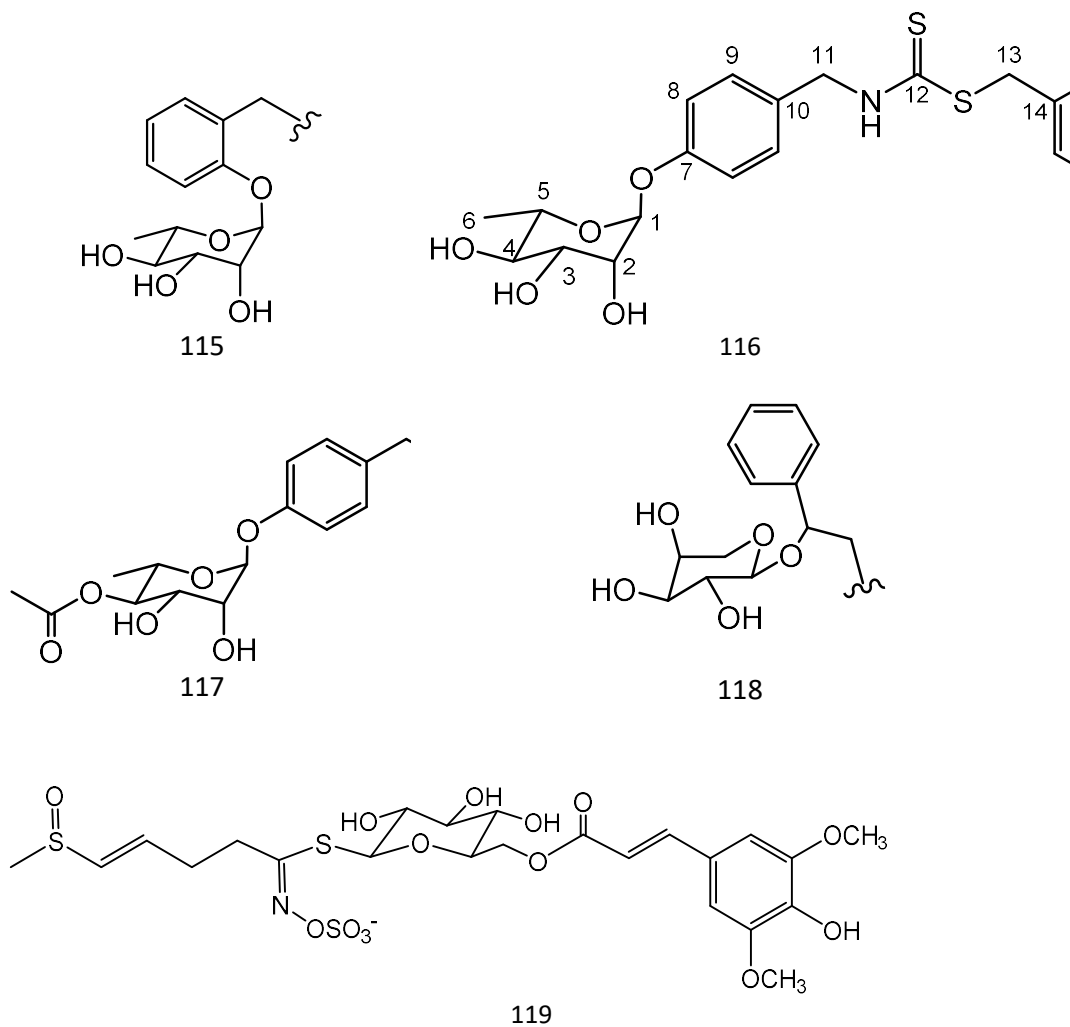


Chart 1.1 (*continued*) Reported glucosinolate structures by chemical class. The number of each structure is the progressive numeration used in Table 1.1.

K. BENZOYL GLUCOSIDES

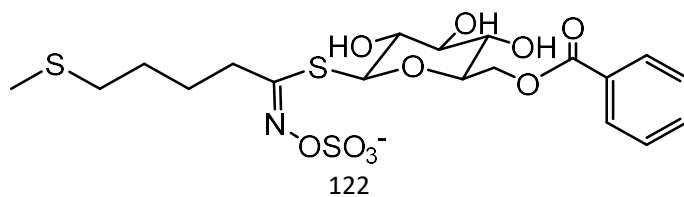
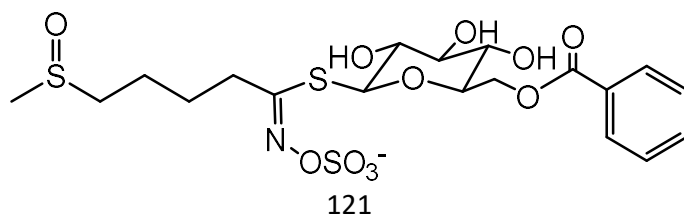
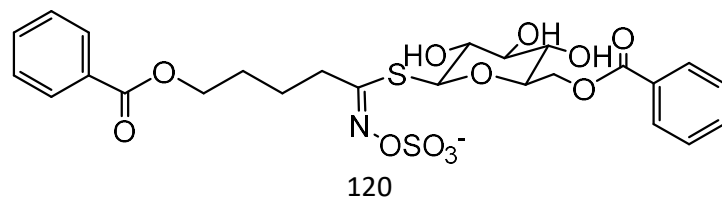


Chart 1.1 (*continued*) Reported glucosinolate structures by chemical class. The number of each structure is the progressive numeration used in Table 1.1.

L. CINNAMIC GLUCOSIDES

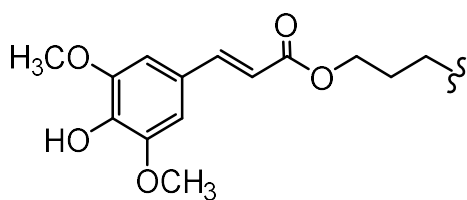
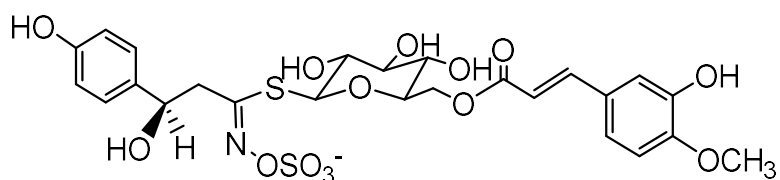
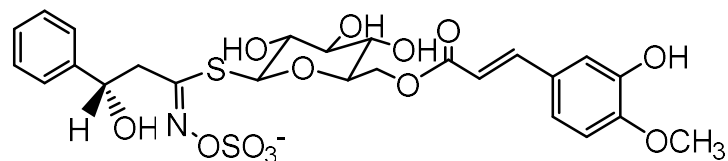
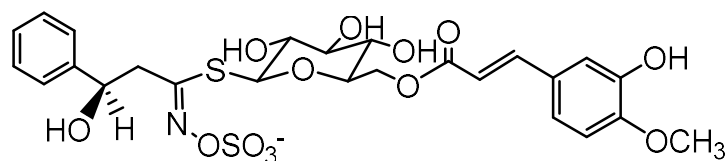
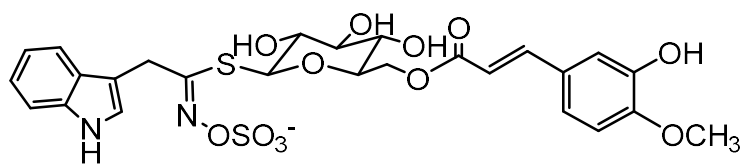
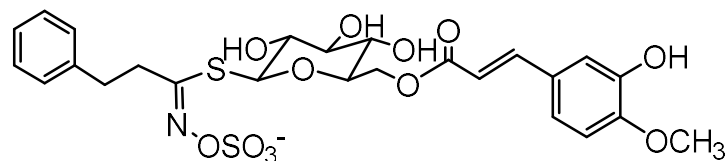
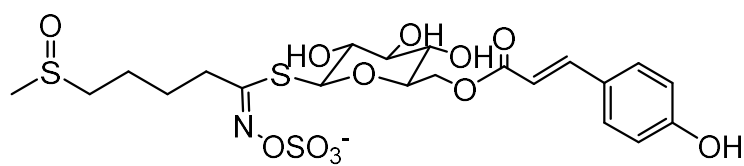


Chart 1.1 (continued) Reported glucosinolate structures by chemical class. The number of each structure is the progressive numeration used in Table 1.1.

1.2 Glucosinolates biosynthesis

The biosynthesis of GLs includes a number of common steps responsible for the formation of the core structure, as well as several steps responsible for the side chain diversification and has recently been reviewed (Grubb and Abel, 2006; Halkier and Gershenzon, 2006; Sønderby et al., 2010). The biosynthetic pathway of GLs has been almost entirely elucidated using *Arabidopsis thaliana* (Brassicaceae) that was selected as the first GL-producing model plant to have its genome sequenced because of its small genome and short life cycle and genetics (Meyerowitz, 2001). It is important to point out that, although GL biosynthesis is considered a secondary pathway, it is firmly embedded in plant metabolism as it requires cofactors and intermediates derived from primary metabolism. Indeed, GLs are primarily seen as α -amino acid derived secondary compounds, but they are clearly also an important component of sulfur metabolism in the plant. Each GL contains two sulfur atoms, one in the thioglucosidic bond and a second one in the sulfate group. In addition, around one third of aliphatic GLs possess a third sulfur atom in their side chain (Table 1.2). Most of the genes encoding the biosynthetic enzymes have been identified, as well as transporters necessary for moving the metabolic intermediates in the cell and the final products between the cells and organs (Sønderby et al., 2010). The biosynthesis is rather complex with more than 40 genes participating, creating the variety of GLs, depending on α -amino acid used for the synthesis and its modifications. The biosynthesis can be divided roughly into three modules: (1) amino acid chain elongation, (2) formation of a core GL structure and (3) side chain secondary modifications. However, there is no side chain elongation that occurs for indole GL biosynthesis (Figure 1.2 and Figure 1.3). Although the core pathway is well understood, several transporters necessary for optimal distribution of GLs and their precursors are still unknown and the knowledge about the metabolic context of GL synthesis pathway is far from being ultimate (Kopriva and Gigolashvili, 2016).

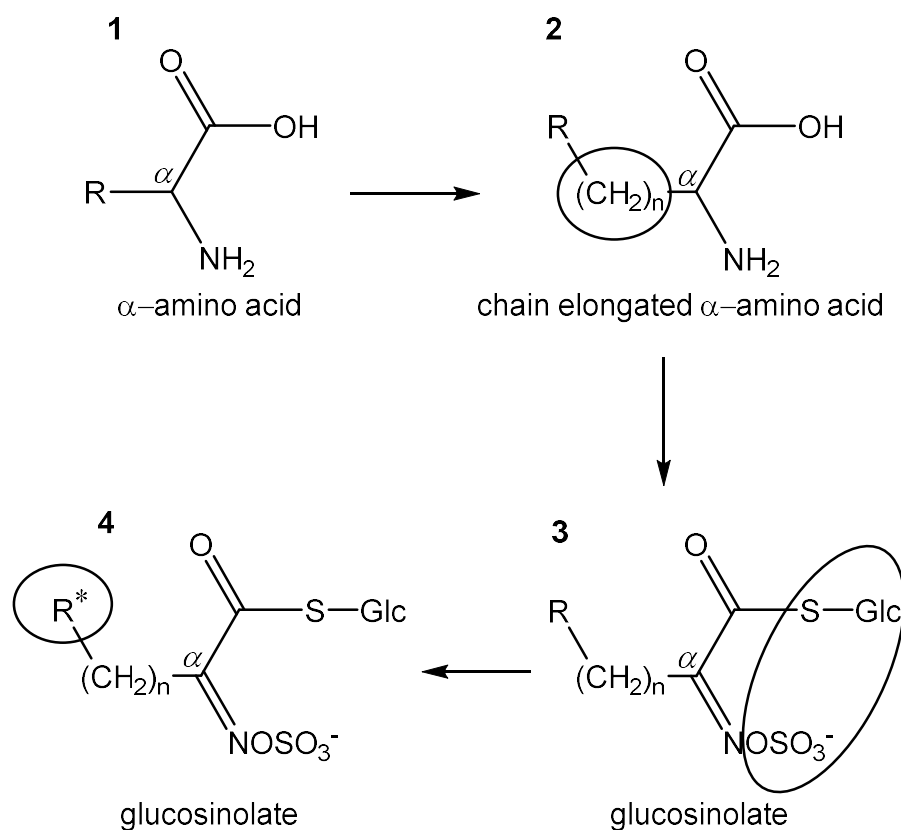


Figure 1.2 General scheme of the chemical reactions involved in the glucosinolate biosynthesis pathway. **1** Precursor α -amino acid, **2** chain elongated α -amino acid, **3** glucosinolate core formation, **4** glucosinolate R group undergoing secondary modification reactions.

Step 1: Amino acid chain elongation

Aliphatic GLs have various side chains with different lengths determined by the chain elongation step (Figure 1.3). The first process of chain elongation is the deamination of amino acids such as Met to the corresponding 2-oxoacids by a branched-chain amino acid aminotransferase (BCAT). The 2-oxoacids are precursors of the elongation reaction by a methylene group. The elongation proceeds by methylthioalkylmalate synthase (MAM), isopropylmalate isomerase (IPMI), and isopropylmalate dehydrogenase (IPMDH). Finally, the elongated 2-oxoacids are transformed to the corresponding amino acids by BCAT. This chain elongation also takes place in the biosynthesis of aromatic GLs but does not occur in the formation of indole GLs.

Step 2: Formation of a core glucosinolate structure

Amino acids, including elongated ones, undergo the formation of the core GL structure (Figure 1.3). Cytochromes P450 (CYP79s) convert the amino acids to aldoximes, which are then oxidized to the activated forms by CYP83s. The activated forms are transformed to thiohydroximates via glutathione conjugation and the C-S lyase (SUR1) reaction. The thiohydroximates are first converted to the desulfoGL structure by the S-glucosyltransferases of the UGT74 family and then finally to the GL structure by the sulfotransferases SOTs.

Step 3: Side chain modification

After the GL structure formation has taken place, the side chain can be modified by a variety of reactions such as oxygenation, hydroxylation, alkenylation, benzoylation, and methoxylation. The S-oxygenation of aliphatic GLs is a common modification conducted by flavin monooxygenases FMO_{GS-OXs}. The side chain of GLs derived from Met and its chain-elongated homologues is especially subjected to further modifications, such as the stepwise oxidation of the sulfur atom in the methylsulfanylalkyl side chain leading successively to methylsulfinylalkyl and methylsulfonylalkyl moieties. Methylsulfinylalkyl side chains can be further modified by oxidative cleavage to afford alkenyl chains produced by 2-oxoglutarate-dependent dioxygenases AOPs (Figure 1.3). The indole GL secondary modifications involve a series of hydroxylations and methoxylations catalyzed by several CYP family enzymes. Glucobrassicin, which is a common indole GL, is hydroxylated by CYP81F2 in *A. thaliana*. Methoxylations might occur by unidentified O methyltransferases.

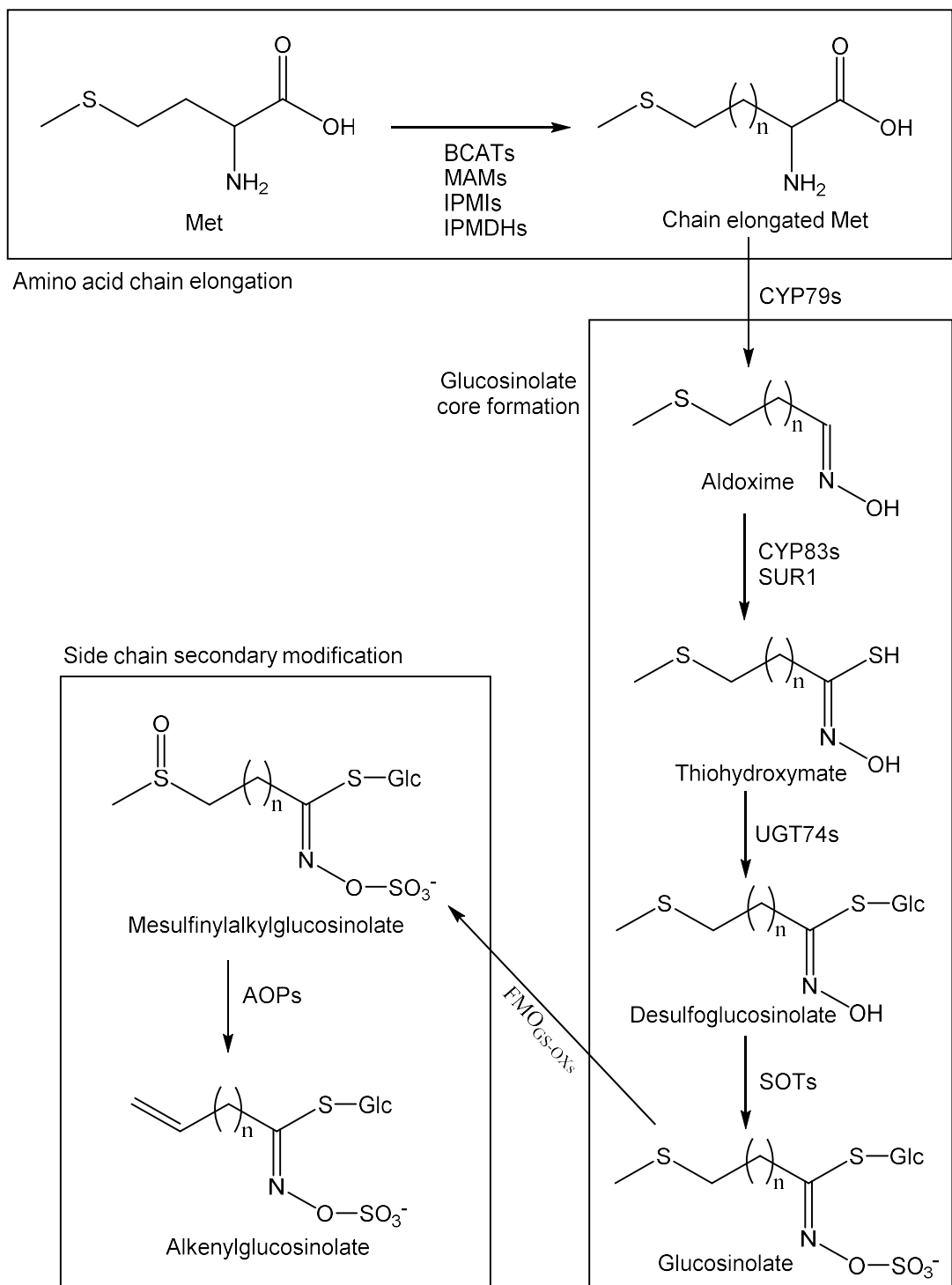


Figure 1.3 Schematic pathway of aliphatic glucosinolate biosynthesis. The pathway consists of three main steps: (1) amino acid chain elongation, (2) core glucosinolate formation and (3) side chain secondary modification.

1.3 The glucosinolate-myrosinase system

The occurrence of GLs throughout the order Brassicales coincides with the presence of specific thioglucosidases, the myrosinases (MYRs), which can hydrolyze these compounds. GLs in intact form are known to be generally inactive in nature and they act as precursors of a variety of bioactive hydrolysis products. In plants, MYRs are located in specialized cells known as myrosin cells/idioblast cells of the phloem parenchyma, whereas the GLs are held separately in the vacuoles or S-cells of most plant tissues. This compartmentalization prevents hydrolysis in natural conditions and self-intoxication (Augustine and Bisht, 2016). This system has been long referred to as the 'mustard oil bomb' and constitutes an endogenous defense setup against pests and diseases (Matile 1980). In *A. thaliana*, GLs have been reported to be stored at high levels (>130 mM) in the specific sulfur-rich S-cells. This concentration is about 20 times higher in comparison to surrounding tissue. Upon damage, the S-cell works as a high-pressure mustard bomb as the large GL (mustard oil glucoside) content is released producing the deterring hydrolysis products (Koroleva et al., 2010). The products of MYR-catalyzed GL hydrolysis are β -D-glucose, a sulfate anion and a labile aglycon that can be converted to a broad variety of final degradation compounds depending on the substrate, the pH value and the presence of MYR cofactors. PH values close to neutrality generally favor the formation of rather lipophilic, irritant and toxic isothiocyanate (ITC) (mustard oil) through a Lossen-type rearrangement of the detached aglycon (Figure 1.4).

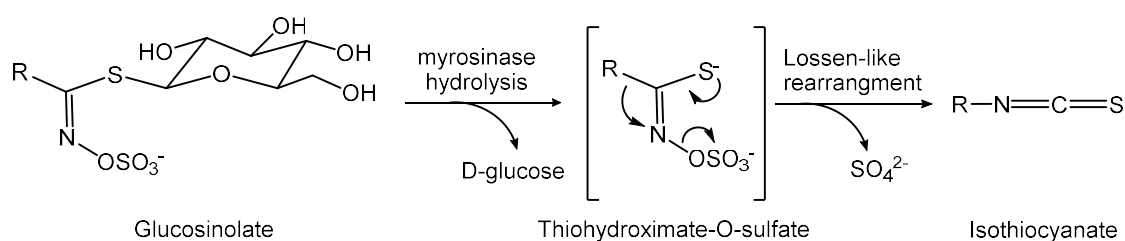


Figure 1.4 Myrosinase-catalyzed hydrolysis of a glucosinolate at neutral pH. The labile aglycon thiohydroximate-O-sulfate undergoes a spontaneous 'Lossen-like' rearrangement to isothiocyanate.

1.3.1 Myrosinases

Myrosinases (MYRs) are thioglucosidases (thioglucoside glucohydrolases, EC 3.2.1.147) that catalyze the hydrolysis of the thioglucosidic bond of GLs. They are members of glycoside hydrolase family I along with other β -glycosidases that are involved in plant defense. MYRs are unique because they are the only enzymes able to break an anomeric carbon-sulfur bond. MYRs are usually composed of two identical 55-65 kDa polypeptides which are heavily glycosylated resulting in a native molecular weight of 120-150 kDa of the dimeric proteins as reported for the main MYR isoenzyme isolated from ripe seeds of white mustard (*Sinapis alba* L.) (Burmeister et al., 1997; 2000). The dimeric structure is maintained through tetrahedral coordination of a Zn^{2+} by two conserved residues of each monomer (His 56 and Asp 70 in the *S. alba* MYR) (Burmeister et al., 1997). Common properties of MYRs are their heat stability (with temperature optima of up to 70 °C) and their activation by ascorbic acid at low millimolar concentrations (typically 1-2 mM). MYRs accept GLs of different structural types as substrates but differ in their affinity to individual GLs and the efficiency of their hydrolysis (Bernardi et al., 2003).

1.3.2 The mechanism of myrosinase-catalyzed hydrolysis of glucosinolates to produce isothiocyanates

The determination of the structures of the native MYR enzyme from *S. alba* seed and the covalent glycosyl-enzyme intermediate obtained after reaction with a modified GL (2-deoxy-2-fluoroglucotropaeolin) made it possible to elucidate the mechanism of MYR-assisted hydrolysis of GLs (Burmeister et al., 2000). Each MYR monomer has a substrate-binding pocket with three different subsites for recognition of the glucosyl moiety, the sulfate group and the hydrophobic side chain of the GL. In the first step of the catalysis MYR bioactivates the GL by nucleophilic attack of Glu 409 positioned in its catalytic center at the anomeric carbon, which initiates the detachment of the aglycone and results in the formation of a glucosyl intermediate. The removal of the glucosyl group is sufficient to initiate a Lossen-like rearrangement of the labile aglycone thiohydroximate-*O*-sulfate with the release of a sulfate ion without the need for additional sulfatase activity and formation of ITC. While the ITC and the sulfate diffuse away, Gln 187 located in the MYR pocket and dedicated to the recognition

of sulfate positions a water molecule close to the anomeric carbon to enable hydrolysis of the glucosyl-enzyme. Finally, after this hydrolysis, ITC, sulfate and β -D-glucose are released from the MYR active site (Figure 1.5) (Burmeister et al., 2000).

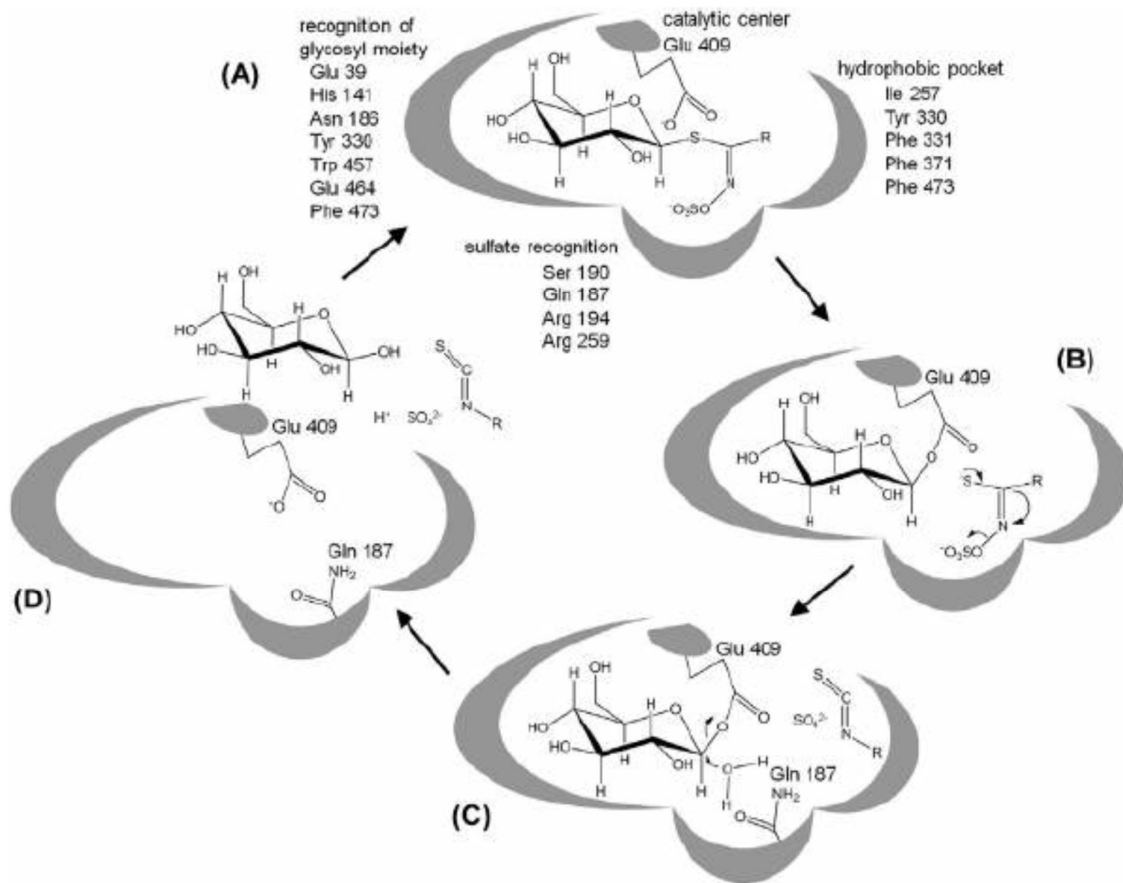


Figure 1.5 The mechanism of myrosinase-catalyzed hydrolysis of glucosinolates. Step (A): recognition of the glucosinolate in the myrosinase catalytic center. Step (B): nucleophilic attack at the anomeric carbon of glucosinolate. Step (C): hydrolysis of the glucosyl-enzyme intermediate. Step (D): release of ITC, sulfate ion and β -D-glucose. Source: Wittstock et al. (2016).

1.3.3 Other glucosinolate breakdown products

The catabolism of GLs is likely to follow several pathways leading to the delivery of products different from ITCs. The variety of GLs combined with the diversity of reactions that may occur upon their hydrolysis gives rise to a fascinating breakdown machinery to produce structurally diverse breakdown products.

1.3.3.1 Oxaxolidinethione

In the case of GLs bearing in the aglycone a hydroxyl group in β position, the ITC produced cannot be isolated because it undergoes a fast cyclization process to afford a 1,3-oxazolidine-2-thione (Figure 1.6). The first identified ITC-derived compound of this kind was goitrin (5-ethenyl-1,3-oxazolidine-2-thione), which is a cyclization product of the ITC generated upon hydrolysis of (*S*)-2-hydroxy-3-butenyl GL (progoitrin) (Figure 1.7). Its name refers to the observation that intake of high amounts of this compound through Brassica (a genus within the Brassicaceae family) vegetables consumption may cause an enlargement of the thyroid gland (goiter) as explained next in section 1.4.

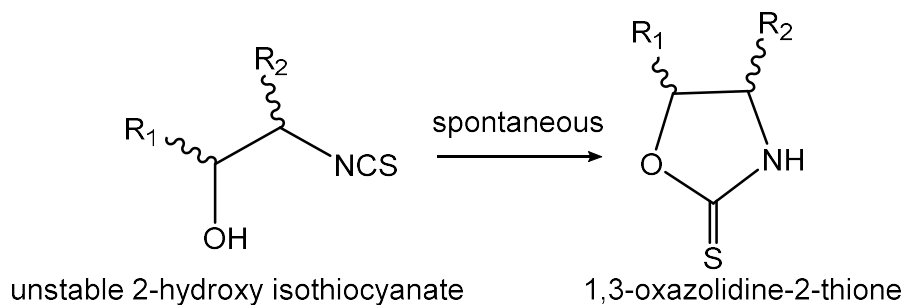


Figure 1.6 Formation of 1,3-oxazolidine-2-thione from the spontaneous cyclisation of a 2-hydroxy isothiocyanate.

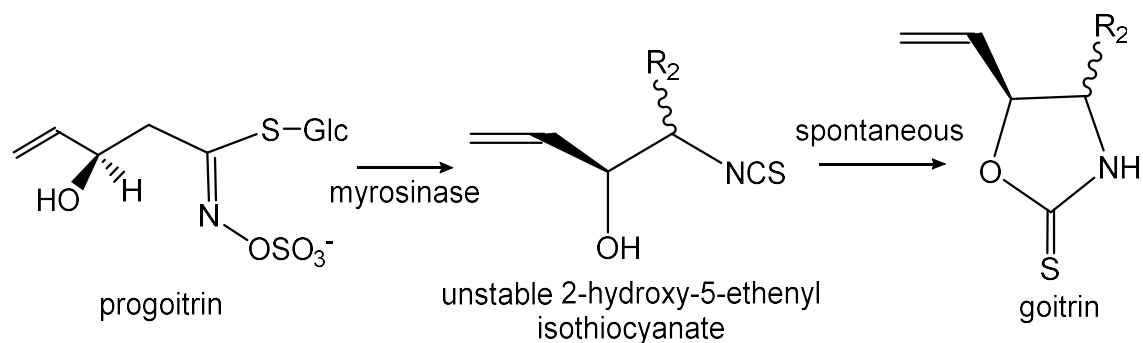


Figure 1.7 Formation of 5-ethenyl-1,3-oxazolidine-2-thione (goitrin) from (S)-2-hydroxy-3-butenylglucosinolate (progoitrin) myrosinase catalyzed hydrolysis through the spontaneous cyclisation of unstable 2-hydroxy-5-ethenyl isothiocyanate.

1.3.3.2 Specifier proteins

The presence of so-called ‘specifier proteins’ may promote the formation of alternative products such as nitriles, epithionitriles and thiocyanates. According to their product profiles, specifier proteins are grouped into three different types: nitrile-specifier proteins (NPSs), epithio-specifier proteins (ESPs) and thiocyanate-forming proteins (TFPs). Specifier proteins themselves do not convert GLs but affect the outcome of MYR GL hydrolysis. With increasing amounts of specifier protein, the amount of non-ITC products increases whereas the amount of ITC decreases. While simple nitriles may also be formed in the absence of NSP under certain conditions (Figure 1.8), formation of epithionitriles and organic thiocyanates is strictly dependent on the presence of specifier proteins (Figure 1.9 and 1.10) (Wittstock et al., 2016).

Nitriles and epithionitriles

NSPs as well as acidic conditions and/or the presence of a reducing agent (ferrous ion, cysteine) favor the formation of nitriles, with concomitant extrusion of elemental sulfur (Figure 1.8).

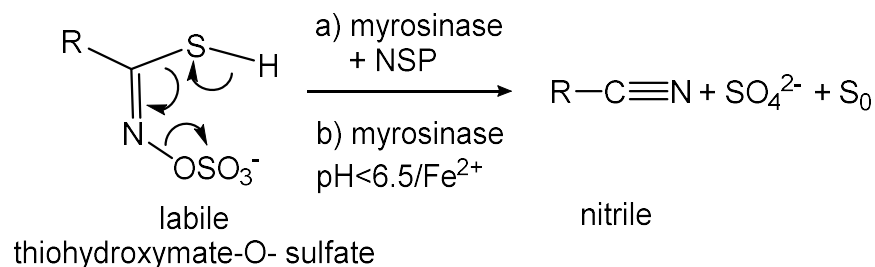


Figure 1.8 Formation of nitriles from the thiohydroximate-*O*-sulfate intermediate in glucosinolate hydrolysis catalyzed by enzyme myrosinase in the presence of a) nitrile specifier protein (NSP) or b) acidic environment and/or ferrous ions.

Simple nitriles are also formed in the presence of ESP unless the GL side chain bears a terminal double bond to enable epithionitriles formation. Epithionitriles are nitriles with a terminal thiirane moiety (Figure 1.7). Labelling studies demonstrated that the sulfur of the thiirane ring originates from the thioglucosidic bond of the GL.

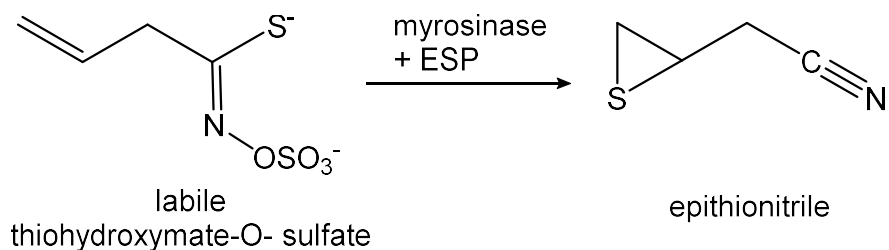


Figure 1.9 Formation of epithionitriles from the thiohydroximate-*O*-sulfate intermediate in glucosinolate hydrolysis catalyzed by enzyme myrosinase in the presence of epithio-specifier protein (ESP).

1.3.3.3 Thiocyanates

TFPs can promote the formation of organic thiocyanates (Figure 1.10) that has only been observed for three GLs, namely allyl (sinigrin), benzyl (glucotropaeolin) and 4-methylsulfanylbutylGL (glucoerucin). It has been proposed that the ability to form stable carbocations is a common feature of the aglucones of these three GLs and a prerequisite for organic thiocyanate formation.

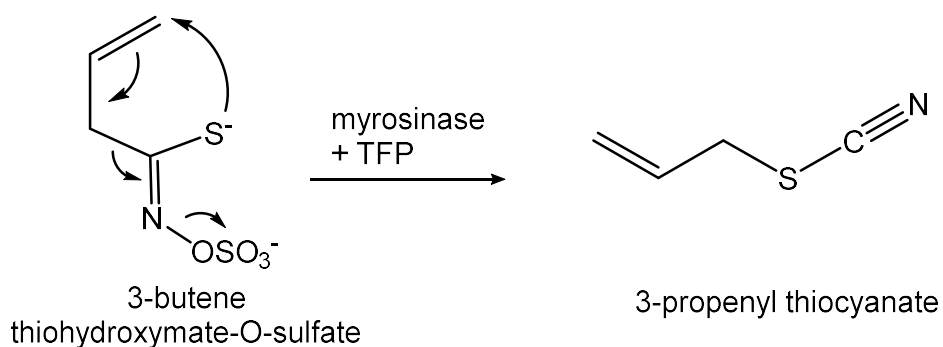


Figure 1.10 Formation of allyl thiocyanate from but-3-ene thiohydroximate-*O*-sulfate intermediate in sinigrin hydrolysis catalyzed by the enzyme myrosinase in the presence of thiocyanate forming protein (TFP).

1.4 Biological activity of glucosinolate breakdown products

1.4.1 Plant defense

GL breakdown products play an important role in the interactions between plant and insects/herbivores. They can act both as poisons and deterrents to generalist insect/herbivores, or, on the contrary, as signaling molecules to attract specialist insects/herbivores laying their eggs or feeding on that specific plant. Several studies have shown that GLs determine a growth inhibition or represent a feeding deterrent to a wide range of herbivorous animals such as birds, slugs and generalist insects. Moreover, it has been observed that volatile hydrolysis products can attract natural enemies of herbivores such as parasitoids and therefore determine an indirect protection of the plant (Possenti et al., 2017). GLs and their breakdown products are also detrimental to many microorganisms like fungi

and bacteria (Brown and Morra, 2005). Their biocidal activity can be successfully exploited in agriculture in an integrated plant defense strategy for their protection against weeds and various pathogens, using a technique known as biofumigation. This technique essentially consists in soil incorporation of selected Brassica plants, both as biofumigant or catch crop green manures, or derived materials as biofumigant pellets based on Brassica defatted seed meal (De Nicola et al., 2013). Several studies have also proven biofumigation by means of GL-containing processed Brassica plants as a promising treatment to reduce postharvest damage due to fungi and bacteria (Ugolini et al., 2014; Ugolini et al., 2017).

1.4.2 Human health

Initially, GLs have been studied for their toxic activity and goitrogenic effects, especially when used for animal feeding. Earlier studies initiated in the mid 1970s with plant breeders starting to select oilseed rape (*Brassica juncea*) varieties with a reduced content of GLs because of their antinutritional properties, such as goiter, growth retardation, poor egg production and liver damage in animals fed with defatted rapeseed meal. In addition, their bitterness and off-taste limited the intake by animals (Schnug and Haneklaus, 2016). Rapeseed contains progoitrin and it has become clear now that its metabolic product 5-ethenyl-1,3-oxazolidine-2-thione (goitrin) (Figure 1.7) can decrease iodine uptake resulting in a reduced thyroxine secretion by the gland that stimulates the growing of the organ (goiter). A similar goitrogenic activity has been reported also for thiocyanate ions that are possible GL breakdown products (Possenti et al., 2017). In the last three decades, GLs along with their breakdown products, especially ITCs, have gained enormous interest because these compounds have shown a wide array of health promoting properties in relation to prevent the risk of carcinogenesis and certain chronic diseases such as cardiovascular, articular and neurological diseases, asthma, diabetes and cholesterol (Avato and Argentieri, 2015). Above all, ITCs are known and investigated for their chemopreventive properties showing a strong potential against the risk of various cancers at different target organs like lung, prostate, ovary, breast and colon. The biological interactions of ITCs are strongly related to the cellular redox state and many studies have documented their indirect antioxidant properties, particularly related to the induction of phase-2 detoxification enzymes, as well as their pro-oxidant properties related to the induction of phase-1 enzymes, as reviewed by Valgimigli and Iori (2009) and summarized in

Figure 1.11. Especially, evidences suggest that beneficial effects of ITCs could be mainly ascribed to their peculiar capacity to activate the nuclear factor erythroid-derived 2-related factor 2 (Nrf2)/ARE (antioxidant responsive element) pathway, consequently exerting antioxidant functions.

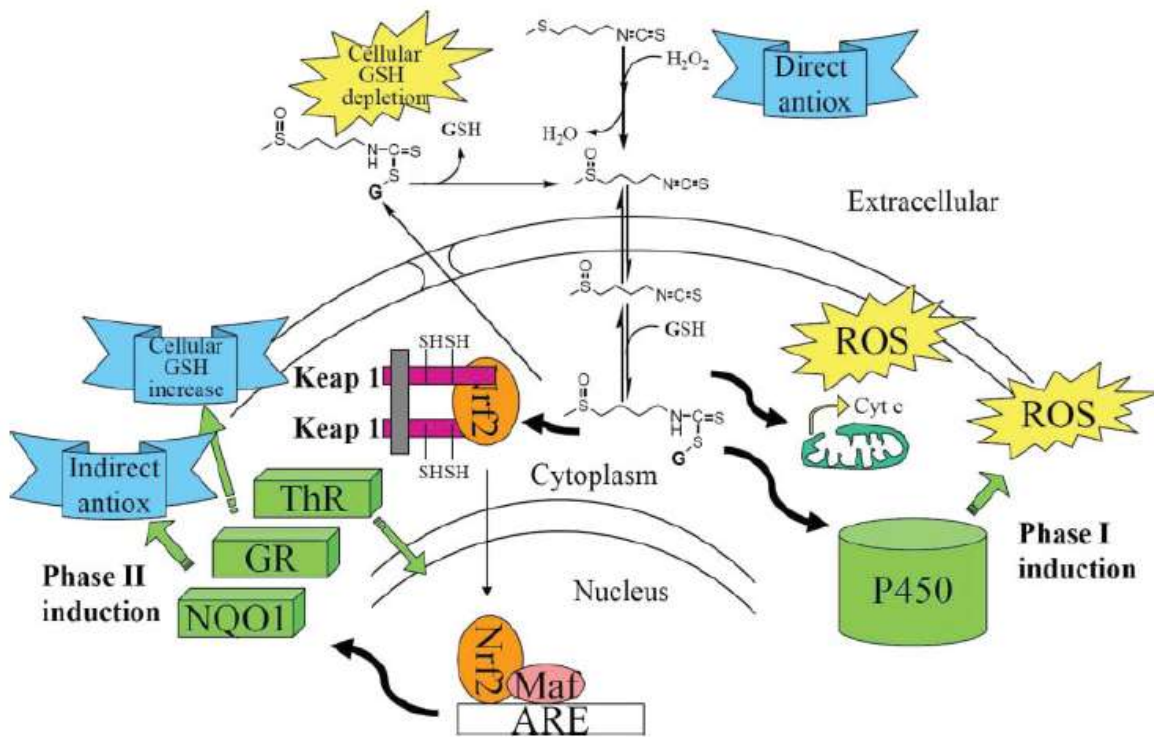


Figure 1.11 Complex interplay of cellular anti- and pro-oxidant activities of isothiocyanates exemplified for 4-methylsulfonyl isothiocyanate (erucin). Removal of hydrogen peroxide (or organic hydroperoxides) leads to the formation of 4-methylsulfonyl isothiocyanate (sulforaphane), which enters the cell by simple diffusion and concentrates in the cytoplasm bound to glutathione (GSH). The adduct is pumped out of the cell, where it can reversibly dissociate. In the cytoplasm, sulforaphane (free or conjugated with GSH) interacts with Keap1 proteins leading to the release of NR2 factor that translocates in the nucleus and, binding with antioxidant responsive elements (ARE), activates transcriptional overexpression of antioxidant phase-2 enzymes, increasing the productions of reactive oxygen species (ROS). Furthermore, damage to mitochondria and release of cytochrome c is another potential cause of induced oxidative stress. Figure and caption taken from Valgimigli and Iori, 2009.

1.4.2.1 Indirect antioxidant activity of isothiocyanates

ITCs cross the cell membrane freely, possibly by simple diffusion, and accumulate in the cytoplasm where they bind to glutathione and other cellular thiols, reacting with the -SH groups (thiocarbamoylation). This reaction is due to the electrophilicity of the -N=C=S moiety and is further catalyzed by glutathione S-transferase (GST). Although this reaction is reversible, it is believed to be the main driving force for accumulation of ITCs, and intracellular levels of 100–200 fold over the extracellular concentrations have been reported (Zhang, 2000). Intracellular accumulation of ITCs is an essential step in their antioxidant activity. On exposure to ITCs, Nrf2 dissociates from Keap1, translocates into the nucleus where it associates with other nuclear factors, like small Maf, and binds to ARE to activate the transcription of the downstream gene. Direct reactions of ITCs with the sulfhydryl groups of specific cysteine residues in Keap1 has been reported, resulting in conformational changes that would force the release of Nrf2 (Dinkova-Kostova et al., 2017). It is currently unknown which of the two-equilibrating species within the cell, the free ITC and the GSH-conjugated form, is responsible for enzyme induction and other interactions. Since it has been estimated that about 5% or less than 1% of ITCs is in the free form inside the cell, it's likely that the GSH-conjugated species at least contribute to the activity (Valgimigli and Iori, 2009). Phase-2 enzymes are generally regarded as antioxidants as many of them have been proven to increase the cellular levels of antioxidant molecules like GSH or protect the cell from reactive oxygen species (ROS) and oxidizing species (Figure 1.11).

1.4.2.2 Pro-oxidant activity of isothiocyanates

The early view of ITCs as selective monofunctional inducers of phase-2 antioxidant/detoxifying enzymes has lately given way to a more realistic consideration of their very complex oxidative stress modulation. As discussed above, ITCs rapidly accumulate in the cell, the driving force for accumulation being the reaction with SH groups of cellular thiols, particularly GSH. The thiocarbamoylation reaction of the -N=C=S group with thiols is spontaneous, although it is further enhanced by GST (Zhang, 2001) which promotes GSH conjugation with ITCs (Valgimigli and Iori, 2009). ITCs are very interesting polyhedral modulators of oxidative stress. The double-edged-sword behavior they express in biological

environments, namely antioxidant versus pro-oxidant, is the result of the multiple induction of phase-1 and phase-2 enzymes, superimposed on their direct antioxidant activity (Figure 1.11). It is of interest to point out that, although accumulation of ITCs in the cell is the first fundamental step for their beneficial activity, it is also one potential cause of their pro-oxidant behavior. Unfortunately, there appears to be no fully distinctive dose range for the two actions and, although pro-oxidant activity prevails at the highest doses, there is a large overlap between the two dose ranges. Most studies where a clear pro-oxidant behavior was observed were based on cell exposures $\gg 1\text{-}2\ \mu\text{M}$ or on administration *in vivo* of doses $\gg 2\text{-}4\ \mu\text{mol/kg}$ of ITCs (or GLs), which are the normal dietary exposures; they do however indicate the potential threats associated with high-dose intake. There appears also to be consensus on the idea that the pro-oxidant activity is functional to the cancer-protective role of ITCs because the variation of the redox status within the cell triggers apoptosis and other defensive mechanisms (Valgimigli and Iori, 2009). ITCs can also modulate other pathways, such as inflammation and apoptosis, which could be involved in neurodegenerative disease development as will be discussed in Chapters twelve to twenty.

References

- Agerbirk N, Olsen CE (2012) Glucosinolate structures in evolution. *Phytochemistry* 77:16-45.
- APG III (2009) An update of the angiosperm phylogeny group classification for the orders and families of flowering plants: APG III. *Bot J Linn Soc* 161:105-121.
- Augustine R, Bisht NC. Regulation of glucosinolates metabolism: from model plant *Arabidopsis thaliana* to brassica crops. In Méryllon J-M, Ramawat KG (eds), *Glucosinolates, Reference Series in Phytochemistry*. Springer International Publishing Switzerland 2017: pp. 163-200.
- Avato P, Argentieri MP (2015) Brassicaceae: a rich source of health improving phytochemicals. *Phytochem Rev* 14:1019-1033.
- Bernardi R, Finiguerra MG, Rossi AA, Palmieri S (2003) Isolation and biochemical characterization of a basic myrosinase from ripe *Crambe abyssinica* seeds, highly specific for epi-progoitrin. *J Agric Food Chem* 51(9):2737-44.
- Blažević I, Montaut S, Burčul F, Rollin, P. Glucosinolates: novel sources and biological potential. In Méryllon J-M, Ramawat KG (eds), *Glucosinolates, Reference Series in Phytochemistry*. Springer International Publishing Switzerland 2017: pp. 3-60.
- Brown J, Morra MJ (2005) Glucosinolate-containing seed meal as a soil amendment to control plant pests: 2000-2002. NREL/SR-510-35254. doi:10.2172/15016728 Available online at <http://www.osti.gov/bridge> (Accessed on March 13th, 2018).
- Burmeister WP, Cottaz S, Driguez H, Iori R, Palmieri S, Henrissat B (1997) The crystal structures of *Sinapis alba* myrosinase and a covalent glycosyl-enzyme intermediate provide insights into the substrate recognition and active-site machinery of an S-glycosidase. *Structure* 5:663-75.

Burmeister WP, Cottaz S, Rollin P, Vasella A, Henrissat B (2000) High resolution X-ray crystallography shows that ascorbate is a cofactor for myrosinase and substitutes for the function of the catalytic base. *J Biol Chem* 275:39385-39393.

Clarke DB (2010) Glucosinolates, structures and analysis in food. *Anal Methods* 2(4):310-325.

De Nicola GR, D'Avino L, Curto G, Malaguti L, Ugolini L, Cinti S, Patalano G, Lazzeri L (2013) A new biobased liquid formulation with biofumigant and fertilizing properties for drip irrigation. *Industrial Crops and Products* 42:113-118.

Dinkova-Kostova AT, Fahey JW, Kostov RV, Kensler TW (2017) KEAP1 and NRF2: Targeting the NRF2 pathway with sulforaphane. *Trends in Food Sci & Technol* 69:257-269.

Fahey JW, Zalcmann AT, Talalay P (2001) The chemical diversity and distribution of glucosinolates and isothiocyanates among plants. *Phytochemistry* 56(1):5-51.

Grubb CD, Abel S (2006) Glucosinolate metabolism and its control. *Trends Plant Sci* 11:89-100.

Halkier BA, Gershenzon J (2006) Biology and biochemistry of glucosinolates. *Ann Rev Plant Biol* 57:303-333.

Ishida M, Hara M, Fukino N, Kakizaki T, Morimitsu Y (2014) Glucosinolates metabolism, functionality and breeding for the improvement of Brassicaceae vegetables. *Breeding Science* 64:48-59.

Kopriva S, Gigolashvili T. Glucosinolate synthesis in the context of plant metabolism. In Kopriva S (ed), *Glucosinolates, Advances in Botanical Research Volume 80*. Elsevier Ltd. 2016: pp. 99-124.

Koroleva OA, Gibson TM, Cramer R, Stain C (2010) Glucosinolates-accumulating S-cells in *Arabidopsis* leaves and flowers stalks undergo programmed cell death at early stages of differentiation. *Plant Journal* 64:456-469.

Matile P (1980) The mustard oil bomb. Compartmentalization of the myrosinase system. *Biochemie und Physiologie der Pflanzen* 175:722-731.

Meyerowitz EM (2001) Prehistory and history of Arabidopsis research. *Plant Physiology* 125(1):15-19.

Montaut S, Zhang W-D, Nuzillard J-M, De Nicola GR, Rollin P (2015) Glucosinolate diversity in *Bretschneidera sinensis* of Chinese origin. *J Nat Prod* 78:2001-2006.

Possenti M, Baima S, Raffo A, Durazzo A, Giusti AM, Natella F. Glucosinolates in food. In Méridon J-M, Ramawat KG (eds), *Glucosinolates, Reference Series in Phytochemistry*. Springer International Publishing Switzerland 2017: pp. 87-132.

Schnug E, Haneklaus S Glucosinolates - The agricultural story. In Kopriva S (ed), *Glucosinolates, Advances in Botanical Research Volume 80*. Elsevier Ltd. 2016: pp.281-302.

Schultz OE, Gmelin R (1954) Das Senfölglykosid "Glucoiberin" und der bitterstoff "Ibamarin" von *iberis amara* L. (Schleifenblume). *Arch Pharm* 287 (7):404-412.

Sønderby IE, Geu-Flores F, Halkier, BA (2010) Biosynthesis of glucosinolates-gene discovery and beyond. *Trends Plant Sci* 15:283-290.

Ugolini L, Martini C, Lazzeri L, D'Avino L, Mari M (2014) Control of postharvest grey mould (*Botrytis cinerea* Per.: FR.) on strawberries by glucosinolate-derived allyl-isothiocyanate treatments. *Postharvest Biology and Technology* 90:34-39.

Ugolini L, Righetti L, Carbone K, Paris R, Malaguti L, Di Francesco A, Micheli L, Paliotta M, Mari M, Lazzeri L (2017) Postharvest application of brassica meal-derived allyl isothiocyanate to kiwifruit: effect on fruit quality, nutraceutical parameters and physiological response. *J Food Sci Technol* 54:751-760.

Valgimigli L, Iori R (2009) Antioxidant and pro-oxidant capacities of ITCs. *Environmental and Molecular Mutagenesis* 50:222-237.

Wathelet J-P, Iori R, Leoni O, Rollin P, Quinsac A, Palmieri S (2004) Guidelines for glucosinolate analysis in green tissues used for biofumigation. *Agroindustria* 3(3):257-266.

Wittostock U, Kurzbach E, Herfurth AM, Stauber EJ. Glucosinolate breakdown. In Kopriva S (ed), *Glucosinolates, Advances in Botanical Research Volume 80*. Elsevier Ltd. 2016: p. 131.

Zhang Y (2000) Role of glutathione in the accumulation of anticarcinogenic isothiocyanates and their glutathione conjugates by murine hepatoma cells. *Carcinogenesis* 21:1175-1182.

Zhang Y (2001) Molecular mechanism of rapid cellular accumulation of anticarcinogenic isothiocyanates. *Carcinogenesis* 22:425-431.

PART TWO
PLANT SCREENING

Glucosinolates investigation is an ongoing research activity and the subject of various disciplines. Glucosinolates are found in many plants widely used as food and as medicinal plants and they show versatile biological potential together with their breakdown products. Therefore, glucosinolate screening in plants is the key step at the basis of a wider spectrum of investigation and possible application. The type and concentration of glucosinolates have been found to vary between the seventeen plant families belonging to the order Brassicales, between genera in the same family, between species of the same genus as well as between cultivars of the same species. Moreover, different tissues of the same plant also present qualitative and quantitative differences in their glucosinolate content, due to factors such as genetics, plant age and environmental growth conditions. Characteristic glucosinolate profiles can be found in the roots, seeds, leaf and stem of the plant. Plant screening brings knowledge for a multiple array of purposes including profiling of scarcely or not investigated plants, documenting new and/or rare glucosinolates, and searching for glucosinolate rich sources suitable for isolation. Given the aforementioned consideration, investigation of different plants screened for glucosinolate and their breakdown products are reported in this part of the thesis, as follows:

1. *Arabis turrata* L.

Arabis turrata L. is one of the 17 species of the genus *Arabis* and it belongs to the Brassicaceae family within the order Brassicales. Together with *Nasturtium* and *Lepidium*, *Arabis* is one of the few species within the Brassicaceae containing rare long-chain-length aliphatic thiofunctionalized glucosinolates (C7-C10).

2. *Fibigia triquetra* (DC.) Boiss. ex Prantl.

Fibigia triquetra (DC.) Boiss. ex Prantl. is a rare Croatian paleostenoendemic plant species included in the Croatia Red Book in the category of near threatened plants. It belongs to the Brassicaceae family and has never been investigated before for glucosinolates.

3. *Bretschneidera sinensis* Hemsl.

Bretschneidera sinensis Hemsl. is a Chinese rare and threatened plant belonging to Akaniaceae, a different family from Brassicaceae within the same order Brassicales. Glucosinolate content was determined for the first time in different organs of plant samples

from three different Chinese locations. In the context of this study, a new aromatic glucosinolate, 4-hydroxy-3-methoxybenzyl (glucobretschneiderin, GBR listed as n. 89 in Table 1.2 at Chapter one) was isolated and characterized by NMR and HRMS.

4. *Drypetes* spp and *Rinorea* spp.

Drypetes and *Rinorea* genera belong to two different families within the order Malpighiales outside the order Brassicales. *Drypetes* is a genus belonging to the Putranjivaceae family, whereas *Rinorea* belongs to the Violaceae family. Plants of these families are used in traditional African medicine. Plant parts of three different *Drypetes* species (*Drypetes euryodes* (Hiern) Hutch., *Drypetes gossweileri* S. Moore, *Drypetes laciniata* Hutch.), and two different *Rinorea* species (*Rinorea subintegrifolia* O. Ktze and *Rinorea woermanniana* (Büttner) Engl.) were investigated proving the presence of glucosinolate outside the order Brassicales.

5. *Isatis canescens*

I. canescens flower buds collected in different localities of Sicily were screened for the content of 3-indolylmethyl glucosinolate (glucobrassicin; GBS), the natural precursor of recognized anti-cancer and chemopreventive agents, such as indole-3-carbinol and 3,3'-diindolylmethane. The available plant material proved to be a remarkable source for GBS, whose purification was performed at gram scale following the chromatographic procedure described.

6. *Moringa oleifera*

Moringa oleifera is an edible medicinal plant belonging to the Moringaceae family within the order Brassicales. It is a promising plant as a food commodity as well as the source of natural phytochemicals for the prevention and the treatment of several diseases. 12-day old seedlings of *M. oleifera* were screened for the first time for the profile of glucosinolates and phenolics, as well as to assess the glucosinolate content in pulp seed, seed coat, leaves and roots of the seedlings. 11 GLs were simultaneously analyzed in the different tissues by using mass spectrometric approaches.

CHAPTER TWO

Long-chain glucosinolates from *Arabis turrita*: enzymatic and non enzymatic degradations

Contents

Summary

2.1 Introduction

2.2 Experimental

2.2.1 General

2.2.2 Plant material

2.2.3 Thermal degradation

2.2.4 Enzymatic hydrolysis

2.2.5 Chemical degradation

2.2.6 GC-MS analysis

2.2.7 HPLC-ESI-MS analysis of intact glucosinolates

2.2.8 Identification and quantification

2.3 Results and discussion

References

Keywords

Arabis turrita, Glucosinolates, Thermal, Enzymatic, Chemical degradation, HPLC-MS, GC-MS

Summary

C8-C10 methylsulfinylalkyl glucosinolates, and C8-C10 methylsulfonylalkyl glucosinolates were identified in the seed of *Arabis turrita* L. by HPLC-MS/ESI analysis of intact glucosinolates. Enzymatic (with myrosinase) and non-enzymatic (thermal at 100 °C, and chemical at different pH) hydrolyses were performed and the volatile isolates were analyzed by GC-MS. Only the enzymatic and chemical (pH 10) degradations produced volatiles which were originating from glucosinolate degradation. GC-MS analysis showed the presence of long-chain olefinic isothiocyanates along with other long-chain thiofunctionalized glucosinolates breakdown products.

2.1 Introduction

Arabis or rockcress, is a genus of flowering plants within the family Brassicaceae which includes at least 17 known species that are wild growing in Croatia (Nikolić, 2012). The species are annual or perennial plants, 20–80 cm tall, usually densely hairy, with simple entire to lobed leaves, and small white four-petaled flowers. The fruit is a long, slender capsule containing 10-20 or more seeds (Figure 2.1).



Figure 2.1 *Arabis turrata* L.

Glucosinolates (GLs) are multifunctional secondary plant metabolites of great chemotaxonomical importance for classification within the order Brassicales and the Brassicaceae family. Many *Arabis* species contain significant concentrations of long-chain C8-C10 GLs, either alone or in combination with modified arylaliphatic GLs (Bennet et al., 2004; Fahey et al., 2001). Long-chain aliphatic GLs (C7-C10) are generally less common and restricted to a few species within the Brassicaceae (Bennet et al., 2004). *Nasturtium*, *Camelina*, *Neslia* and certain wild *Lepidium* species contain aliphatic GLs with more than seven carbons in the side chain (Bennet et al., 2004; Fahey et al., 2001; Agerbirk and Olsen, 2012; Songsak and Lockwood, 2002; Daxenbichler et al., 1991). *Biscutella laevigata* is also a particularly good source of 8-methylsulfinyloctyl GL (Bennet et al., 2004). *Capsella bursa-*

pastoris seed contains several methylsulfinylalkyl GLs, including 9-methylsulfinylnonyl GL (glucoarabin) and 10-methylsulfinyldecyl GL (gluocamelinin) (Vaughn and Berhow, 2005; Daxenbichler et al., 1991). To our knowledge, although some of these plants are known as food and medicinal plants - mostly due to the biological properties of GL breakdown products - information on the volatiles produced by long-chain GL degradation due to different influences is not available. Thus, the aim of this study was to identify GLs contained in *Arabis turrita* L. seed by HPLC-ESI-MS analysis of the intact GLs (Figure 2.2, Table 2.1) and to investigate degradation products obtained by enzymatic and non-enzymatic (thermal and chemical) hydrolysis. The obtained volatile extracts were subjected to GC-MS analysis and the results are given in Table 2.1 and Table 2.2.

2.2 Experimental

2.2.1 General

All the solvents employed were purchased from Fluka Chemie, Buchs, Switzerland. Anhydrous sodium sulfate was obtained from Kemika, Zagreb, Croatia. Myrosinase (β -thioglucoside glucohydrolase; E.C. 3.2.1.147; 361 U g⁻¹; MYR) from *Sinapis alba* L. seed was purchased from Sigma-Aldrich Chemie GmbH, Steinheim, Germany. Intact GLs were analyzed by high-performance liquid chromatography using an Agilent model 1100 (New Castle, Delaware, USA) equipped with a quaternary pump, automatic injector, diode-array detector (wavelength range 190-600 nm), degasser, and a Hypersil ODS column (5 μ m, 4.6 x200 mm). The HPLC was interfaced to an Agilent model 6120 mass spectrometer (Toronto, ON) with a Chemstation data system LC-MSD B.03.01. GC analyses were performed on a gas chromatograph (model 3900; Varian Inc., Lake Forest, CA, USA) equipped with mass spectrometer (model 2100T; Varian Inc.) and VF-5MS capillary column (30 m \times 0.25 mm i.d., coating thickness 0.25 μ m (Varian Inc.)).

2.2.2 Plant material

Arabis turrita L. seeds were collected near Split, Croatia, in June 2012 from a wild-growing population. The botanical identity of the plant material was confirmed by a local botanist, Dr.

Mirko Ruščić from the Faculty of Natural Sciences, University of Split and the voucher specimens (no. ZOKAT2013) are deposited at the Department of Organic Chemistry, Faculty of Chemistry and Technology, Split, Croatia.

2.2.3 Thermal degradation

The essential oil was isolated by hydrodistillation in a Clevenger-type apparatus for 3 h using 3 mL of *n*-pentane–diethylether (1:1, v/v) for trapping. The whole air-dried plant material (75 g) was mixed with previously heated H₂O (500 mL). As a consequence of thermal degradation (at 100 °C), GL breakdown volatiles are found in the hydrodistillate. The latter was dried over anhydrous sodium sulfate and concentrated by careful fractional distillation to a small volume (*ca.* 1 mL), which was used for GC–MS analysis (Blazević et al., 2014).

2.2.4 Enzymatic hydrolysis

Crushed and dried undefatted seeds (1 g) were homogenized separately with H₂O (100 mL), and MYR (1-2 U) and left for 17 h at room temperature (*ca.* 30 °C). During this period, volatiles are produced from GLs by MYR catalyzed hydrolysis, and from several different precursors by the action of other endogenous enzymes. Then, sufficient redistilled CH₂Cl₂ (3 x 20 mL) was added, the mixtures were shaken for 30 min and separated by centrifugation for 5 min at 4000 rpm. The separated organic layer was dried over anhydrous sodium sulfate. The CH₂Cl₂ layer was concentrated to 100 µL and kept (in a tightly closed vial) in a freezer at -20 °C until GC-MS analysis (Blazević et al., 2014).

2.2.5 Chemical degradation

The seed meal was defatted with *n*-hexane in a Soxhlet extractor for 24 h. The hexane extract was analyzed by GC-MS and showed no GL breakdown products (data not shown). For chemical degradation of GLs in defatted seeds (10 g), different conditions were applied: basic (0.05 M Tris buffer), acidic (0.1 M HCl), and very acidic (2 M HCl). CH₂Cl₂ (50 mL) was then added to each flask, and the flasks were placed into an incubator shaker set at 25 °C and 200 rpm for 8 h. Following hydrolysis, sodium chloride and anhydrous sodium sulfate were added

to the solution, which was mixed thoroughly. The CH₂Cl₂ was filtered and the residual seed meal was extracted 3 more times with an excess of CH₂Cl₂. The combined crude CH₂Cl₂ extract was evaporated under reduced pressure and analyzed by GC-MS (Blazević et al., 2014).

2.2.6 GC-MS analysis

Chromatographic conditions were as follows: helium carrier gas at 1 mL min⁻¹, injector temperature 250 °C. VF-5MS, column temperature was programmed at 60 °C isothermal for 3 min, and then increased to 246 °C at a rate of 3 °C min⁻¹ and held isothermal for 25 min. The injected volume was 1 µL and the split ratio was 1:20. MS conditions were: ionization voltage 70 eV; ion source temperature 200 °C; mass scan range: 40–350 mass units. The analyses were carried out in duplicate (Blazević et al., 2014).

2.2.7 HPLC-ESI-MS analysis of intact glucosinolates

Seeds (516 mg) were frozen in liquid N₂ then ground with a mortar and pestle. The powder was extracted for 5 min at 80 °C in 2 x 5 mL EtOH-H₂O (70:30 v/v). The solutions were combined and evaporated under reduced pressure. The extract (84.2 mg) was dissolved in 5 mL of EtOH-H₂O (70:30 v/v) and filtered through a plug of cotton prior to HPLC analysis, which was performed by injecting a 10 µL aliquot of the solution of crude extract into the HPLC-ESI-MS. The mobile phase solvents, MeOH and H₂O, were prepared with 0.15% Et₃N and 0.18% HCO₂H, added as ion-pairing reagents. Both solutions were filtered using 0.45 µm nylon membranes. The initial mobile phase was 100% HPLC-grade H₂O. At 10 min, the mobile phase was switched to a linear gradient of 100% H₂O to 100% MeOH over 60 min. After each run, the initial mobile phase conditions were set, and the system was allowed to equilibrate. The flow rate was kept constant at 1 mL min⁻¹. The column was maintained at room temperature. The electrospray interface was a standard ES source operating with a capillary voltage of 4 kV and temperature of 350 °C. The system was operated in the negative and positive ion electrospray modes. N₂ was used as nebulizing and drying gas at a flow rate of 10 L min⁻¹ (35 psig). The mass spectrometer was programmed to perform full scans between m/z 100 and 1000 (Zrybko et al., 1997).

2.2.8 Identification and quantification

Individual peaks of volatiles were identified by comparing their retention indices and mass spectra with those of authentic samples, as well as by computer matching against the Wiley 275-library spectra database and comparison of the mass spectra with literature data (Fahey et al., 2001; Adams, 1995). The percentages in Table 2.1 and Table 2.2 were calculated as the mean value of component percentages on the VF-5MS column for analyses run in duplicate. The intact 9-methylsulfinylnonyl GL was identified by comparison of the retention time and the UV and mass spectra of an isolated authenticated standard (Berhow et al., 2013). Other GLs were identified from their degradation products and/or comparison of the specific product ion and its abundance in ESI-MS with those of the literature (Bennet et al., 2004).

2.3 Results and discussion

The HPLC-ESI-MS analysis of the intact GLs revealed 6 GLs *i.e.* C8-C10 methylsulfinylalkyl GLs, and C8-C10 methylsulfonylalkyl GLs (Figure 2.2, Table 2.1).

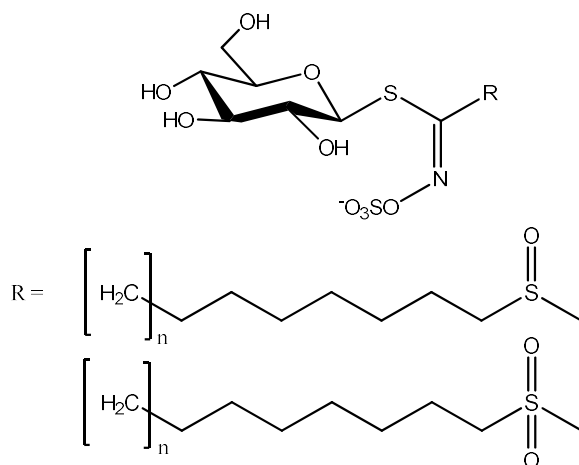


Figure 2.2 GLs ($n = 0-2$) of *Arabis turrata* L. identified by HPLC-MS/ESI.

Previous HPLC-MS analysis showed only 3 long-chain GLs, *i.e.* 8-methylsulfinyl- octyl- (glucohirsutin), 8-methylsulfonyloctyl- and 10-methylsulfonyldecyl GLs (Bennet et al., 2004). Daxenbichler et al. (1991) and Cole (1976) reported C3 and C8 methylsulfonylalkyl-, C8-C10 methylsulfinylalkyl-, and C8-C9 methylsulfonyl GLs by using GC-MS analysis of GL breakdown products (mostly isothiocyanates (ITCs)). After enzymatic hydrolysis of the seeds and CH₂Cl₂

extraction, 21 compounds (95.5 %) were identified, 13 of which (68.3%) originated from GL degradation. The volatile degradation products corresponded to 4 thiofunctionalized GLs also identified by HPLC- ESI-MS analysis: 9-methylsulfonylnonyl- (47.6%), 8-methylsulfonyloctyl- (3.4%) ITCs and 9-methylsulfonylnonanenitrile (0.6%), 10-methylsulfonyldecyl- (0.9%) and 8-methylsulfinyloctyl- (0.3%) ITCs originating from 9-methylsulfonylnonyl-, 8-methylsulfonyloctyl-, 10-methylsulfonyl- decyl-, and 8-methylsulfinyloctyl (glucohirsutin) GLs, respectively. In addition, GC-MS analysis revealed another previously reported thiofunctionalized volatile (Daxenbichler et al., 1991; Cole, 1976) 8-methylsulfonyloctyl ITC (0.7%), which can derive from the corresponding 8-methylsulfonyloctyl GL. Volatiles originating from the degradation 9-methylsulfonylnonyl- (glucoarabin) and 10-methylsulfonyldecyl (glucocamelinin) GLs, identified by HPLC-ESI-MS analysis, were not detected.

Table 2.1 Glucosinolate profile of *Arabis turrita* L. seeds obtained by GC-MS analysis of volatiles originating from glucosinolates and HPLC-ESI-MS of intact glucosinolates.

Parent glucosinolate (GL) Identified compound	LC-MS [M] ^{-a)}	RI ^{b)}	Myr ^{c)}	Tris ^{d)}	Hyd ^{e)}
Hept-6-enyl GL					
Hept-6-enyl ITC	- ^{f)}	1296	Tr ^{g)}	Tr	-
Oct-7-enyl GL					
Non-2-enenitrile ^{h)}	-	1174	Tr	-	-
Non-2-enenitrile ^{h)}	-	1283	Tr	-	-
Oct-7-enyl ITC	-	1404	2.1	8.3	-
Non-8-enyl GL					
Non-8-enyl ITC	-	1518	10.0	8.5	-
Dec-9-enyl GL					
Dec-9-enyl ITC	-	1615	0.3	1.6	-
Undec-10-enyl GL					
Undec-10-enyl ITC	-	1683	2.4	Tr	-
8-Methylsulfanyloctyl GL					
8-Methylsulfanyloctyl ITC	-	1895	0.7	2.0	-
8-Methylsulfonyloctyl GL 508.0					
9-Methylsulfonylnonanenitrile	-	1946	0.6	Tr	-
8-Methylsulfonyloctyl ITC	-	2391	3.4	Tr	-
8-Methylsulfinyloctyl GL 492.0					
(glucohirsutin)					
8-Methylsulfinyloctyl ITC	-	2303	0.3	Tr	-
9-Methylsulfonylnonyl GL 522.0					
9-Methylsulfonylnonyl ITC	-	2500	47.6	35.7	-
9-Methylsulfinylnonyl GL 506.0					
(glucoarabin)					
10-Methylsulfonyldecyl GL 536.0					
10-Methylsulfonyldecyl ITC	-	2625	0.9	0.4	-
10-Methylsulfinyldecyl GL 520.0					
(glucocamelinin)					
Total (%)					
			68.3	56.5	-

^{a)} [M]⁻; specific product ion for GL identification in ESI⁻-MS and its abundance (100%); ^{b)} RI, retention indices determined on a VF-5MS capillary column; ^{c)} Myr, volatiles obtained after enzymatic hydrolysis by myrosinase; ^{d)} Tris, volatiles obtained after chemical degradation in Tris buffer (pH 10); ^{e)} Hyd, volatiles obtained after thermal degradation (100 °C); ^{f)} -, not detected; ^{g)} Tr, traces; ^{h)} E or Z isomers, hypothesized to originate from the rearrangement of non-8-enenitrile.

Among volatiles, along with the thiofunctionalized GLs, long-chain olefinic ITCs and nitriles, also identified, originated from the corresponding intact GLs that were undetected by HPLC-ESI-MS analysis. Although the existence of the long-chain olefinic GLs in nature was reported by GC-MS identification of the GL breakdown products (Songsak and Lockwood, 2002), the report by Chiang et al. (1998) of 4-methylsulfinylbutyl ITC (sulforaphane) degradation to but-3-enyl ITC during GC/MS analyses put this report in question. The most abundant non-8-enyl ITC (10.0%) can derive either from the corresponding non-8-enyl GL (not confirmed by HPLC-ESI-MS) or from degradation of 9-methylsulfonylnonyl ITC, issued in turn from the 9-methylsulfonylnonyl GL (confirmed by HPLC-ESI-MS). The presence of undec-10-enyl- (2.4%), oct-7-enyl- (2.1%), dec-9-enyl- (0.3%), and hept-6-enyl (Tr) ITCs also suggests the presence of the corresponding GLs, *i.e.* undec-10-enyl-, oct-7-enyl-, dec-9-enyl-, and hept-6-enyl GLs, respectively, or breakdown of the corresponding methylsulfonylalkyl ITCs. In addition, stereoisomers of non-2-enenitrile (*E/Z* correct isomer not assigned) were identified by comparison of MS spectra with those in the Wiley library of different retention indices. The presence of these unusual nitriles can be suggested to originate from rearrangement of the non-8-enenitrile terminal double bond. Non-8-enenitrile, not detected in the volatile isolates, can be formed through the known scheme of GL degradation (Fahey et al., 2001; Vaughn and Berhow, 2005) from oct-7-enyl GL (not confirmed by HPLC-ESI-MS), or by degradation of the only other nitrile detected in the sample, 9-methylsulfonylnonanenitrile, which originates from the 9-methylsulfonylnonyl GL (confirmed by HPLC-ESI-MS).

Table 2.2 GC-MS analysis of miscellaneous volatiles not originating from glucosinolates obtained after hydrolysis from *Arabis turrita* L.

Identified compound	RI ^{b)}	Myr ^{c)}	Tris ^{d)}	Hyd ^{e)}
Dimethyl disulfide	<900	Tr ^{g)}	-	- ^{f)}
Dimethyl trisulfide	966	-	Tr	-
S-Methyl methanethiosulfonate	1066	1.1	Tr	-
(E)-Non-2-en-1-ol	1103	-	-	Tr
Dimethyl tetrasulfide	1221	Tr	0.1	Tr
3-Ethyl-4-methyl-1H-pyrrole-2,5-dione	1268	-	-	Tr
2-Methoxy-4-vinylphenol	1334	Tr	-	Tr
4-Hydroxy-3-methoxy-benzaldehyde (vanillin)	1426	0.2	-	-
Diethyl phtalate	1560	Tr	-	-
Dodecanoic acid	1624	-	-	Tr
Tetradecanoic acid	1827	-	-	Tr
6,10,14-Trimethyl-2-pentadecanone	1861	-	-	9.8
Dibutylphtalate	1892	-	-	16.2
Hexadecanoic acid	2026	6.4	5.1	16.9
Ethyl linoleate	2223	19.5	20.2	49.8
Total (%)		27.2	25.4	92.7

From ^{b)} to ^{g)}: same as in Table 2.1.

In addition to enzymatic hydrolysis, GL degradation into various volatiles can be induced thermally and chemically. In order to investigate thermal influence (100 °C) on the present GLs, the dried plant material was subjected to hydrodistillation. Ten molecules representing 92.7% of the total volatile compounds were identified (Table 2.2, *Hyd*). No GL degradation products were identified in the analyzed volatile isolate (Table 2.1, *Hyd*). Previous analysis of volatile extracts obtained by hydrodistillation included mostly C3-C5 alkenyl, methylsulfanylalkyl, methylsulfinylalkyl, and arylaliphatic GL degradation products (Blazević and Mastelić, 2008; Blazević and Mastelić, 2009; Blazević et al., 2010; Blazević et al., 2011; Blazević et al., 2013a; Blazević et al., 2013b; Mastelić et al., 2006; Mastelić et al., 2010; Radonić et al., 2011). Although thermally induced degradation of individual GLs was not

mostly considered, it is widely accepted that indole GLs are more labile than aliphatic ones (Chevolleau et al, 1997; Hanschen et al., 2014). Hanschen et al. (2012a, 2012b, 2014) reported differences in the thermal stability within the group of sulfur-containing aliphatic GLs *i.e.* the investigated methylsulfanylalkyl GLs (C3 and C4, namely glucoiberberin and glucoerucin) being more susceptible to thermal degradation. In a previous report on the volatile extract of *Cardaria draba*, 4-methylsulfanylbutyl GL, 4-methylsulfinylbutyl GL and 4-methylsulfonylbutyl GL degradation products were identified in the extract obtained by enzymatic hydrolysis, while in the hydrodistillate only degradation products of 4-methylsulfanylbutyl GL were identified (Radonić et al., 2011). According to these reports it can be suggested that the long-chain C8-C10 aliphatic GLs with sulfoxide- or sulfone- containing side chain were stable in water at 100 °C (Table 2.1, *Hyd*).

GLs can also degrade under several other conditions such as strong acids or bases or different type of salts (Hanschen et al., 2014). Previous reports suggested that acid-catalyzed hydrolysis (Ettlinger and Lundeen, 1956) of GLs leads to the corresponding carboxylic acid together with hydroxylammonium ion and sugar, and this fact has been used by Olsen and Sørensen (1979, 1980) in the identification of new GLs of *Reseda* species. On the other hand, the base-catalyzed hydrolysis of GLs can result in several products (Bones and Rossiter, 2006). Basic hydrolysis can lead to the formation of alkyl amino acids and 1- β -D-thioglucose through a Neber-type rearrangement (Bones and Rossiter, 2006; Friis et al., 1977). In order to investigate the chemical degradation of the present GLs, different conditions were applied: basic (pH 10), acidic (~pH 2) and very acidic (~pH 0). The GC-MS analysis of the CH₂Cl₂ extracts showed that only the basic extract contained GL degradation products, *i.e.* 11 compounds (56.5%) among which ITCs predominate (Table 2.1, *Tris*). According to the GL degradation products obtained by this analysis, the same GL profile can be suggested as in the case of the volatile isolate obtained after enzymatic hydrolysis. 9-Methylsulfonylnonyl- (35.7%), 10-methylsulfonyldecyl- (0.4%), 8-methylsulfonyloctyl (Tr) ITCs, 9-methylsulfonylnonanenitrile (Tr) and 8-methyl- sulfinyloctyl ITC (Tr) originate from 9-methylsulfonylnonyl-, 10-methylsulfonyldecyl-, 8-methylsulfonyloctyl-, and 8-methylsulfinyloctyl GLs, respectively (confirmed by HPLC-ESI-MS). In addition to the thiofunctionalized ITCs, long-chain alkenyl ITCs were also identified: non-8-enyl- (8.5%), oct-7-enyl- (8.3%), dec-9-enyl- (1.6%), undec-10-enyl- (Tr) and hept-6-enyl ITCs (Tr) originating from the corresponding long-chain olefinic GLs, *i.e.* non- 8-enyl-, oct-7-enyl-, dec-9-enyl-, undec-10-enyl-, and hept-6-enyl GLs, respectively.

The acidic and strongly acidic conditions did not degrade GLs into ITCs and/or nitriles. Also, in contrast to the previous reports (Ettliger and Lundeen, 1956; Olsen and Sørensen, 1979; Olsen and Sørensen, 1980; Bones and Rossiter, 2006; Friis et al., 1977), no carboxylic acids that could correspond to the identified GLs were detected by GC-MS analysis (data not shown). Such observations showing that GLs easily degrade under basic conditions into their corresponding ITCs were previously reported in the study of *Lunaria annua* (Blazević et al., 2014) and *Capsella bursa pastoris* (Vaughn and Berhow, 2005) seed. Thus, in contrast to previous reports of the acidic and basic GL hydrolyses (Bones and Rossiter, 2006), the basic conditions using Tris buffer (pH 10) can easily degrade GLs, mostly into their corresponding ITCs, whereas acidic conditions (pH 0 and 2) are not appropriate for generating characteristic volatiles usually obtained by enzymatic degradation. It is worth noticing that next to the major degradation products of C5 and C6 methylsulfanylalkyl GLs (glucoberteroin and glucolesquerellin) and methylsulfinylalkyl GLs (glucoalyssin and glucohesperin) of *L. annua*, the C5-C7 alkenyl volatiles were also present (Blazević et al., 2014). A large number of degradation products identified in the volatile isolate belong to the long-chain olefinic GL degradation products that were not identified in the previous reports of *A. turrita*, nor of other *Arabis* species (Bennet et al., 2004; Fahey et al., 2001). According to previous reports, only prop-2-enyl GL (sinigrin) was identified as an olefinic GL in 3 species of *Arabis* (Fahey et al., 2001; Daxenbichler et al., 1991). Those long-chain GLs can be important as chemotaxonomic tags of this species. However, such GLs were suggested previously only from their degradation products in other plants, e.g. hept-6-enyl GL, reported in *Wasabi japonica* (Fahey et al., 2001), and three long-chain unsaturated C8-C10 ITCs in autolysates of *Nasturtium montanum*, along with structurally related methylsulfonylalkyl long-chain ITCs (Songsak and Lockwood, 2002). The corresponding GLs were concluded to exist in the intact plant. The suggested occurrence of alkenyl GLs in a plant also accumulating similar Met derived GLs seems likely. Contrary to GC-MS analysis, our HPLC-ESI-MS confirmed only thiofunctionalized GLs, and their conversion into olefinic ITCs during GC-MS analyses can be presumed. Hence, the isolation and purification of these long-chain olefinic GLs and recording of their NMR data should be performed in order to confirm their occurrence in nature (Agerbirk and Olsen, 2012). Except for the above-mentioned molecules, all volatile fractions from the investigated species contained compounds devoid of nitrogen and sulfur (Table 2.2) – mostly hexadecanoic acid (5.1-16.9%) and ethyl linoleate (19.5-49.8%) in all volatile isolates.

Next to these volatiles, the hydrodistillate contained a high concentration of dibutylphthalate (16.2%) and 6,10,14-trimethyl-2-pentadecanone (9.8%).

References

Adams RP. (1995) Identification of essential oil components by gas chromatography/mass spectroscopy, Allured Publishing Corp., Carol Stream, IL, 469 pp.

Agerbirk N, Olsen CE. (2012) Glucosinolate structures in evolution. *Phytochemistry* 77:16–45.

Bennett RN, Mellon FA, Kroon PA. (2004) Screening crucifer seeds as sources of specific intact glucosinolates using ion-pair high-performance liquid chromatography negative ion electrospray mass spectrometry. *J Agric Food Chem* 52:428-438.

Berhow MA, Polat U, Glinski JA, Glensk M, Vaughn SF, Isbell T, Ayala-Diaz I, Marek L, Gardner C. (2013) Optimized analysis and quantification of glucosinolates from *Camelina sativa* seeds by reverse-phase liquid chromatography. *Ind Crops Prod* 43:119-125.

Blažević I, Mastelić J. (2008) Free and bound volatiles of garlic mustard (*Alliaria petiolata*). *Croat Chem Acta* 8:607-613.

Blažević I, Mastelić J. (2009) Glucosinolate degradation products and other bound and free volatiles in the leaves and roots of radish (*Raphanus sativus* L.). *Food Chem* 113:96-102.

Blažević I, Radonić A, Mastelić J, Zekić M, Skocibušić M, Maravić A. (2010) Hedge mustard (*Sisymbrium officinale*): Chemical diversity of volatiles and their antimicrobial activity. *Chem Biodiversity* 7:2023-2034.

Blažević I, Radonić A, Skocibušić M, De Nicola GR, Montaut S, Iori R, Rollin P, Mastelić J, Zekić M, Maravić A (2011) Glucosinolate profiling and antimicrobial screening of *Aurinia leucadea* (Brassicaceae). *Chem Biodiversity* 8:2310-2321.

Blažević I, Burcul F, Rušić M, Mastelić J (2013a) Glucosinolates, volatile constituents, and acetylcholinesterase inhibitory activity of *Alyssoides utriculata*. *Chem Nat Compd* 49:374-378.

Blažević I, De Nicola GR, Montaut S, Rollin P (2013b) Glucosinolates in two endemic plants of the *Aurinia* genus and their chemotaxonomic significance. *Nat Prod Commun* 8:1463-1466.

Blažević I, Maleš T, Ruščić M (2014) Glucosinolates of *Lunaria annua*: thermal, enzymatic, and chemical degradation. *Chem Nat Compd* 49:1154-1157.

Bones AM, Rossiter JT. (2006) The enzymic and chemically induced decomposition of glucosinolates, *Phytochemistry* 67:1053-1067.

Chevolleau S, Gasc N, Rollin P, Tulliez J. (1997) Enzymatic, chemical and thermal breakdown of 3H-labeled glucobrassicin, the parent indole glucosinolate. *J Agric Food Chem* 45:4290-4296.

Chiang WCK, Pusateri DJ, Leitz REA. (1998) Gas chromatography/mass spectrometry method for the determination of sulforaphane and sulforaphane nitrile in broccoli. *J Agric Food Chem* 46:1018-1021

Cole RA. (1976) Isothiocyanates, nitriles and thiocyanates as products of autolysis of glucosinolates in Cruciferae. *Phytochemistry* 15:759-762.

Daxenbichler ME, Spencer GF, Carlson DG, Rose GB, Brinker AM, Powell RG (1991). Glucosinolate composition of seeds from 297 species of wild plants. *Phytochemistry* 30:2623-2638

Ettlinger MG, Lundeen AJ. (1956) The structures of sinigrin and sinalbin: an enzymic rearrangement. *J Am Chem Soc* 78:4172-4173.

Fahey JW, Zalcmann AT, Talalay P. (2001) The chemical diversity and distribution of glucosinolates and isothiocyanates among plants. *Phytochemistry* 56:5- 51.

Friis P, Larsen PO, Olsen CE. (1977) Base-catalyzed Neber-type rearrangement of glucosinolates 1-(β -D-glucosylthio)-N-(sulphonate-oxy)alkylideneamines. J Chem Soc, Perkin Trans 1:661-665.

Hanschén FS, Rohn S, Mewis I, Schreiner M, Kroh LW. (2012a) Influence of the chemical structure on the thermal degradation of the glucosinolates in broccoli sprouts. Food Chem 130:1–8.

Hanschén FS, Platz S, Mewis I, Schreiner M, Rohn S, Kroh LW. (2012b) Thermally induced degradation of sulfur-containing aliphatic glucosinolates in broccoli sprouts (*Brassica oleracea* var. *italica*) and model systems. J Agric Food Chem 60:2231-2241.

Hanschén FS, Lamy E., Schreiner M, Rohn S (2014) Reactivity and stability of glucosinolates and their breakdown products. Angew Chem, Int Ed 53:11430-11450.

Mastelić J, Blažević I, Jerković I (2006) Free and bound sulphur containing and other volatile compounds from evergreen candytuft (*Iberis sempervirens* L.). Croat Chem Acta 79:591- 597.

Mastelić J, Blažević I, Kosalec I (2010) Chemical composition and antimicrobial activity of volatiles from *Degenia velebica*, a European stenoendemic plant of the Brassicaceae family. Chem Biodiversity 7:2755-2765.

Nikolić T. Flora Croatica Database, On-Line (<http://hirc.botanic.hr/fcd>), Department of Botany, Faculty of Science, University of Zagreb, Zagreb, 2012.

Olsen O, Sørensen H (1979). Isolation of glucosinolates and the identification of O-(α -L-rhamnopyranosyloxy)benzylglucosinolate from *Reseda odorata*. Phytochemistry 18:1547–1552.

Olsen O, Sørensen H (1980) Glucosinolates and amines in *Reseda media*. Phytochemistry 19:1783–1787.

Radonić A, Blažević I, Mastelić J, Zekić M, Skocibušić M, Maravić A (2011) Phytochemical analysis and antimicrobial activity of *Cardaria draba* (L.) Desv. volatiles. Chem Biodiversity 8:1170-1181.

Songsak T, Lockwood GB (2002) Glucosinolates of seven medicinal plants from Thailand. Fitoterapia 73:209-216.

Vaughn SF, Berhow MA (2005) Glucosinolate hydrolysis products from various plant sources: pH effects, isolation, and purification. Ind Crops Prod 21:193–202.

Zrybko CL, Fukuda EK, Rosen RT (1997) Determination of glucosinolates in domestic and wild mustard by high-performance liquid chromatography with confirmation by electrospray mass spectrometry and photodiode-array detection. J Chromatogr A 767:43-52.

CHAPTER THREE

Glucosinolate profile of Croatian stenoendemic plant *Fibigia triquetra* (DC.) Boiss. ex Prantl.

Contents

Summary

3.1 Introduction

3.2 Experimental

3.2.1 General

3.2.2 Plant material

3.2.3 HPLC of desulfoglucosinolates and glucosinolates

3.2.3.1 Extraction of glucosinolates and desulfation

3.2.3.2 HPLC-DAD analysis of desulfoglucosinolates

3.2.3.3 HPLC-ESI-MS analysis of intact glucosinolates

3.2.4 GC-MS analysis of glucosinolate breakdown products

3.2.4.1 Enzymatic hydrolysis of glucosinolates and extraction

3.2.4.2 GC-MS analysis

3.2.5 Identification and quantification

3.3 Results

3.4 Discussion

3.5 Conclusions

References

Keywords

Fibigia triquetra, Brassicaceae, glucosinolates, desulfo-glucosinolates, isothiocyanates.

Abbreviations

GL: glucosinolate;

DS-GL: desulfo-glucosinolate;

NT: near threatened; ITC: isothiocyanate;

GC-MS: gas chromatography-mass spectrometry;

HPLC-DAD: high-performance liquid chromatography - diode array detector;

HPLC-ESI-MS: high-performance liquid chromatography - electrospray mass spectrometry;

RPF: relative proportionality factor;

GRA: glucoraphanin;

GPU: glucopturanjivin;

GNA: gluconapin;

GCC: glucocochlearin;

GBN: glucobrassicinapin;

GER: glucoerucin;

GBE: glucoberteroin;

GAL: glucoalyssin;

Met: methionine;

Leu: leucine;

Tyr: tyrosine;

Val: valine;

DNA: deoxyribonucleic acid;

ITS: internal transcribed spacer;

a.s.l.: above sea level.

Summary

Different plant parts (flower, leaf, stem, and seed) of *Fibigia triquetra* were characterized and quantified for glucosinolates (GLs) according to the ISO 9167-1 EU official method based on the HPLC analysis of desulfo-GLs for the first time. A taxonomic screening showed that *F. triquetra* contained relatively high levels of C-4 GLs, namely but-3-enyl GL (gluconapin, 1a), 4-methylsulfanylbutyl GL (glucoerucin, 3a), and 4-methylsulfinylbutyl GL (glucoraphanin, 5a). GC-MS analysis of the volatile fractions obtained after enzyme hydrolysis and/or HPLC-ESI-MS of intact GLs confirmed the GL profile. Four minor GLs, namely isopropyl GL (glucoputranjivin, 6a), *sec*-butyl GL (glucocochlearin, 7a), pent-4-enyl GL (glucobrassicinapin, 2a), and 5-methylsulfanylpentyl GL (glucoberteroin, 4a) were also identified and quantified while 4-methylpentyl GL, 5-methylhexyl GL, and *n*-heptyl GL, were tentatively identified by GC-MS of their degradation products. Based on the major, as well as the minor GLs, this study showed differences in chemotaxonomy between *F. triquetra* and the related *Degenia velebitica* (Degen) Hayek as well as other investigated species of the genus *Fibigia*.

3.1 Introduction

Croatia is hosting significant populations of many plant species that are threatened at the European level. One of the reasons for the large number of endemics in Croatia, and especially tertiary relics, is the fact that this area was not greatly affected by glaciation. Among the 13 known species in the genus *Fibigia* (Brassicaceae) (Cetin et al., 2012) two wild-growing are known in the Flora of Croatia, namely *Fibigia clypeata* (L.) Medik. and *Fibigia triquetra* (DC.) Boiss. ex Prantl. The latter species is a rare Croatian paleostenoendemic plant species included in the Croatia Red Book in the category of near threatened (NT) plants (Fukarek and Šolić, 1982; Kostović-Vranješ et al., 1998). *F. triquetra* is a perennial plant, characterized by subshrubby growth (up to 5–20 cm in height), large yellow flowers, and compact rosettes of hairy, and grey leaves. The fruit forms an elliptical or elongated ellipsoidal silique (Figure 3.1).



Figure 3.1 *Fibigia triquetra* (DC.) Boiss. ex Prantl.

The natural area of distribution is restricted to the rocky grounds of Dalmatia (Kostović-Vranješ et al., 1994; Prevalek-Kozlina et al., 1997) on altitudes ranging from 10 to 1000 m above sea level (a.s.l.). There is a striking similarity in morphology, anatomy, and taxonomy between *F. triquetra* and *Degenia velebitica* (Degen) Hayek, which was reported as a Croatian stenoendemic chasmophytic herbaceous plant (Mayer, 1981; Prevalek-Kozlina et al., 1999; De Nicola et al., 2011; Mastelić et al., 2010). According to a phylogenetic relationship study, *F. triquetra* seems to be closer to *D. velebitica* than any other *Fibigia* species (Rešetnik et al., 2013). The restriction fragment length PCR amplified ribosomal DNA (ITS regions), as well as the size of the genome types of *F. triquetra* and *D. velebitica* were determined and compared.

These analyses indicated that *F. triquetra* varied from *D. velebica*. Studies based on non-morphological characters, such as chemical features together with other biological or genetic informations can help in discriminating species and understanding real relationships among the taxa. The plants of the Brassicaceae family are strikingly chemocharacterized by the presence of glucosinolates (GLs). GLs are genetically variable within plant species. The chemistry of *F. triquetra* has never been investigated, and thus its GL composition is not established. As a matter of fact, information on GLs present in other plants of the genus *Fibigia* are very scarce and only include early approaches regarding the characterization of the GLs present, *i.e.* comparison with the authentic sample on TLC, paper chromatography, and GC-MS analysis of their degradation products - which are mostly isothiocyanates (ITCs). *F. eriocarpa* (DC.) Boiss. seeds were reported to contain 3-methylsulfinyl propyl GL (glucoiberin, GIB), *p*-hydroxybenzyl GL (sinalbin, SNB), and benzyl GL (glucotropaeolin, GTL) (Boudjidanian et al., 1974). Pent-4-enyl GL (glucobrassicinapin, GBN, 2a) (Figure 3.2) and 2-hydroxy-3-butenyl GL (progoitrin, PRO or epiprogoitrin, EPRO) were reported in the seeds of *F. clypeata* (L.) Medik. (Al-Shehbaz et al., 1987). and *F. macrocarpa* (Boiss.) Boiss. (Al-Shehbaz et al., 1987; Daxenbichler et al., 1991). Next to those GLs, *F. macrocarpa* was reported also to contain but-3-enyl GL (gluconapin, GNA, 1a) 4-methylsulfonylbutyl GL (glucoerucin, GER, 3a) and 4-methylsulfinylbutyl GL (glucoraphanin, GRA, 5a) (Al-Shehbaz et al., 1987). Bennett et al. (2004) used ion-pairing LC-MS methodology for the identification of the GLs in *F. clypeata* seeds, which confirmed the previous report of GLs, *i.e.* EPRO (100–125 $\mu\text{mol g}^{-1}$ of dry weight) and PRO (0.1–10 $\mu\text{mol g}^{-1}$ of dry weight). Conversely to GC-MS and other techniques previously mentioned, this latter method ensured accurate measurement of all classes of GLs (Bennett et al., 2004). All previous reports dealt with GLs in *Fibigia* seeds. However, the nature of GLs and their relative amounts can vary greatly with plant species and variety, tissue type (seed, root, stem, leaf, flower) and developmental stage of the tissue (De Nicola et al., 2011; Blazević et al., 2011; Blazević et al., 2013a). Thus, the aim of the present study was to investigate the qualitative and quantitative GL profile in the various aerial parts (flower, leaf, stem, seed) of *F. triquetra*. The identification and quantification were performed by HPLC-DAD of the desulfo-glucosinolates (DS-GLs) and comparison with standards. The analyses were confirmed by direct HPLC-ESI-MS analysis of intact GLs and/or indirectly by GC-MS of their breakdown products.

3.2 Experimental

3.2.1 General

DS-GLs were analyzed on HPLC Agilent model 1100 (New Castle, Delaware, USA) equipped with a diode array detector (DAD) and an Inertsil ODS-3 column (250 × 3 mm, particle size 5 μm), thermostated at 30 °C. Intact GLs were analyzed on a HPLC Agilent model 1100 equipped with a quaternary pump, automatic injector, diode-array detector (wavelength range 190–600 nm) degasser, and a Hypersil ODS column (200 × 4.6 mm, particle size 5 μm). The HPLC was interfaced to an Agilent model 6120 mass spectrometer (Toronto, ON) with a Chemstation data system LC-MSD B.03.01.

GC analyses were performed with a Varian model 3900 system (Varian Inc., Lake Forest, CA, USA) equipped with a Varian mass spectrometer model 2100T, non-polar capillary column VF-5MS (30 m × 0.25 mm i.d., coating thickness 0.25 μm ; Varian Inc.). Homogenization was done by U-Turrax (IKA T25) homogenizer.

All the solvents employed were purchased from Fluka Chemie, Buchs, Switzerland. Anhydrous sodium sulfate was obtained from Kemika, HR-Zagreb, DEAE- Sephadex A-25 anion-exchange resin from GE Healthcare). Enzymes thioglucosidase (myrosinase EC 3.2.1.147; 361 U g^{-1} ; MYR) from *Sinapis alba* seeds and sulfatase Type H-1 from *Helix pomatia* were purchased from Sigma-Aldrich Chemie GmbH, D-Steinheim. GLs and DS-GLs were available as pure standards isolated in the laboratory (Montaut et al., 2009; Wathelet et al., 2004).

3.2.2 Plant Material

The aerial parts (leaf-flower, stem, and seed) of *Fibigia triquetra* (DC.) Boiss. ex Prantl were collected on the island of Brač (Mt. Vidova Gora, 770 m a.s.l.; Gauss-Kruger coordinates $X = 5631845$; $Y = 4794051$) - near Split, during flowering in March (flower, leaf, stem) and June (seed) in 2011 from wild-growing populations. The botanical identity of the plant material was confirmed by the local botanist Dr. Mirko Ruščić, and voucher specimens (no. DBFT001) have been deposited at the Department of Biology, Faculty of Sciences, Split, Croatia.

3.2.3 HPLC of desulfoglucosinolates and glucosinolates

3.2.3.1 Extraction of glucosinolates and desulfation

GLs were extracted from the different plant parts of *F. triquetra* (leaf-flower, stem, and seed) according to the EU standard procedure (EEC, 1990) albeit with some modifications (Blazević et al., 2011). Plant samples were reduced to a fine powder. Samples of ca 500 mg were extracted for 5 min at 80 °C in 2x5 mL EtOH–H₂O (70:30 v/v), homogenized and then centrifuged. Supernatants were combined, and the final volume was measured. Each extract (1 mL) was loaded onto a mini-column filled with 0.6 mL of DEAE-Sephadex A-25 anion-exchange resin conditioned with 25 mM acetate buffer (pH 5.6). After washing with 3 mL buffer, 200 µL (0.35 U mL⁻¹) of purified sulfatase (Leoni et al., 1998) was loaded onto the mini-column which was left on the bench overnight. The DS-GLs were then eluted with 3 mL of ultra-pure H₂O and were analyzed by HPLC-DAD. In addition, seeds (540 mg) were frozen in liquid N₂ and ground with a mortar and pestle. The powder was extracted for 5 min at 80 °C in 2 x 5 mL EtOH–H₂O (70:30 v/v). The solutions were combined and evaporated under reduced pressure and intact GLs were analyzed by HPLC-ESI-MS.

3.2.3.2 HPLC-DAD analysis of desulfoglucosinolates

The chromatography of DS-GLs (20 µL injected solution) was performed with an Inertsil ODS-3 column at a flow rate of 1 mL min⁻¹ eluting with a gradient of H₂O (A) and acetonitrile (B) following the program: 1 min 1 % B; 22 min linear gradient up to 22 % B; 3 min linear gradient down to 1 % B. DS-GLs were detected monitoring the absorbance at 229 nm (Blazević et al., 2011).

3.2.3.3 HPLC-ESI-MS analysis of intact glucosinolates

The extract (121.3 mg) was dissolved in 4 mL EtOH–H₂O (70:30 v/v) and filtered through a plug of cotton prior to HPLC analysis, which was performed by injecting a 5 µL aliquot of the

solution of crude extract into HPLC-ESI-MS. The two mobile phase solvents, MeOH and H₂O, were prepared with 0.15 % Et₃N and 0.18 % HCO₂H, added as ion-pairing reagents. Both solutions were filtered using 0.45 mm nylon membranes. The initial mobile phase was 100 % HPLC-grade H₂O. At 10 min, the mobile phase was switched to a linear gradient of 100 % H₂O to 100 % MeOH over 60 min. After each run, the initial mobile phase conditions were set, and the system was allowed to equilibrate. The flow rate was kept constant at 1 mL min⁻¹. The column was maintained at room temperature. The electrospray interface was a standard ES source operating with a capillary voltage of 4 kV and temperature of 350 °C. The system was operated in the negative and positive ion electrospray modes. N₂ was used as nebulizing and drying gas at a flow rate of 10 L min⁻¹ (35 psig). The mass spectrometer was programmed to perform full scans between *m/z* 100 and 1.000 (Zrybko et al., 1997).

3.2.4 GC-MS analysis of glucosinolate breakdown products

3.2.4.1 Enzymatic hydrolysis of glucosinolates and extraction

Crushed and dried flower with leaf (10 g), stem (10 g), and seed (1 g), were homogenized separately with deionized H₂O (100 mL, pH~6) and MYR (1-2 U), then allowed to hydrolyze during 17 h at room temperature (*ca* 30 °C). Sufficient redistilled CH₂Cl₂ (3x20 mL) was then added, the mixtures were taken for 30 min and separated by centrifugation for 5 min at 4,000 rpm. The separated organic layer was dried over anhydrous sodium sulfate and concentrated to 100 µL. All the obtained hydrolysates were kept (in a tightly closed vial) in a freezer at -20 °C until GC-MS analysis (Blazević et al., 2010).

3.2.4.2 GC-MS analysis

Chromatographic conditions were as follows: helium was the carrier gas at 1 mL min⁻¹, injector temperature was 250 °C. VF-5MS column temperature was programmed at 60 °C isothermal for 3 min, and then increased to 246 °C at a rate of 3 °C min⁻¹ and held isothermal for 25 min. The injected volume was 1 µL and the split ratio was 1:20. MS conditions were:

ionization voltage 70 eV; ion source temperature 200 °C; mass scan range: 40–350 mass units. The analyses were carried out in duplicate (Bezić et al., 2011).

3.2.5 Identification and quantification

The identification of DS-GLs was performed based on the retention time and UV spectra of each DS-GL compared with pure standards (Leoni et al., 1998). The GL amount was quantified by using a calibration curve of pure DS-sinigrin solution (range from 0.14 to 1.4 mM, $y = 36.3 + 5854.3 \cdot x$, $R^2 = 0.9998$, LOD (limit of detection) 0.013 mM, LOQ (limit of quantitation) 0.041 mM. LOD and LOQ were both determined based on the DS-sinigrin calibration curve according to the European Medicines Agency (EMA, 2009) guidelines relating to the validation of analytical methods) and RPFs for each individual DS-GL. The published RPFs for DS-GLs (Wathelet et al., 2004; Clarke, 2010) were used, with the exception of 5b, for which an arbitrary RPF value equal to 1 was set.

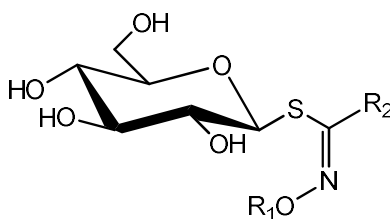
Peaks of the intact GLs, 1a, 3a, and 5a, were identified by comparison of UV spectra, retention times and mass spectra of commercial standards in the LC-MS library. Glucoberberoin (5-methylsulfanylpenylGL, GBE, 4a) was identified by comparison of the UV spectrum, retention time and mass spectrum with those of a previously isolated GBE stored in the LC-MS library (Montaut et al., 2009).

Individual peaks of volatiles were identified by comparing their retention indices and mass spectra to those of authentic samples, as well as by computer matching against the Wiley 275-library spectra database and comparison of the mass spectra with literature data (Adams, 2001). The percentages in Table 3.2 and 3.3 were calculated as the mean value of component percentages on column VF-5MS column for analyses run in duplicate.

3.3 Results

The aerial parts of *Fibigia triquetra* leaf-flower, stem and seed were analyzed for GL identification and quantification. The extractions were made according to the EU official

method. Each extraction was performed in duplicate. The structures of the major GLs and their DS-counterparts are given in Figure 3.2.



	R ₁	R ₂		R ₁	R ₂
1a	SO ₃ ⁻	CH ₂ =CH-(CH ₂) ₂	1b	H	CH ₂ =CH-(CH ₂) ₂
2a	SO ₃ ⁻	CH ₂ =CH-(CH ₂) ₃	2b	H	CH ₂ =CH-(CH ₂) ₃
3a	SO ₃ ⁻	CH ₃ -S-(CH ₂) ₄	3b	H	CH ₃ -S-(CH ₂) ₄
4a	SO ₃ ⁻	CH ₃ -S-(CH ₂) ₅	4b	H	CH ₃ -S-(CH ₂) ₅
5a	SO ₃ ⁻	CH ₃ -SO-(CH ₂) ₄	5b	H	CH ₃ -SO-(CH ₂) ₄
6a	SO ₃ ⁻	CH ₃ -CH(CH ₃)	6b	H	CH ₃ -CH(CH ₃)
7a	SO ₃ ⁻	CH ₃ -CH ₂ -CH(CH ₃)	7b	H	CH ₃ -CH ₂ -CH(CH ₃)

Figure 3.2 Chemical structures of glucosinolates in *F. triquetra*: gluconapin (1a), glucobrassicinapin (2a), glucoerucin (3a), glucoberteroin (4a), glucoraphanin (5a), glucoputranjivin (6a), glucocochlearin (7a), and their desulfo-counterparts (1b–7b).

The obtained HPLC chromatograms are given in Figure 3.3 and the GL contents are summarized in Table 3.1. The identity of each DS-GL was determined by the comparison of the t_R and UV spectra of each product with those of DS-GL standards. The leaf - flower extract and the stem extract of *F. triquetra* showed almost the same DS-GL chromatographic qualitative profile. DS-GNA (1b) - the major DS-GL in both samples - DS-GER (3b) and DS-GRA (5b) were identified at t_R 9.4, 5.2, and 14.3 min, respectively. In contrast to other plant parts analyzed, the major DS-GL identified in seed extracts was 3b, followed by 1b and 5b. The other minor DS-GLs present in all the samples were DS-GPU (desulfo isopropyl GL, 6b) and DS-GCC (desulfo *sec*-butyl GL, 7b). In addition, DS-GBN (desulfo pent-4-enyl GL, 2b) was detected in the stem, and DS-GBE (desulfo 5-methylsulfanylpentyl GL, 4b) in the seed only. The structures of those minor GLs and their DS-counterparts are also given in Figure 3.2. The HPLC chromatograms showed also unidentified peaks at 20.1 and 20.9 min (seed extract) as well as at 21.6 min (flower - leaf extract) which did not match with any available standards.

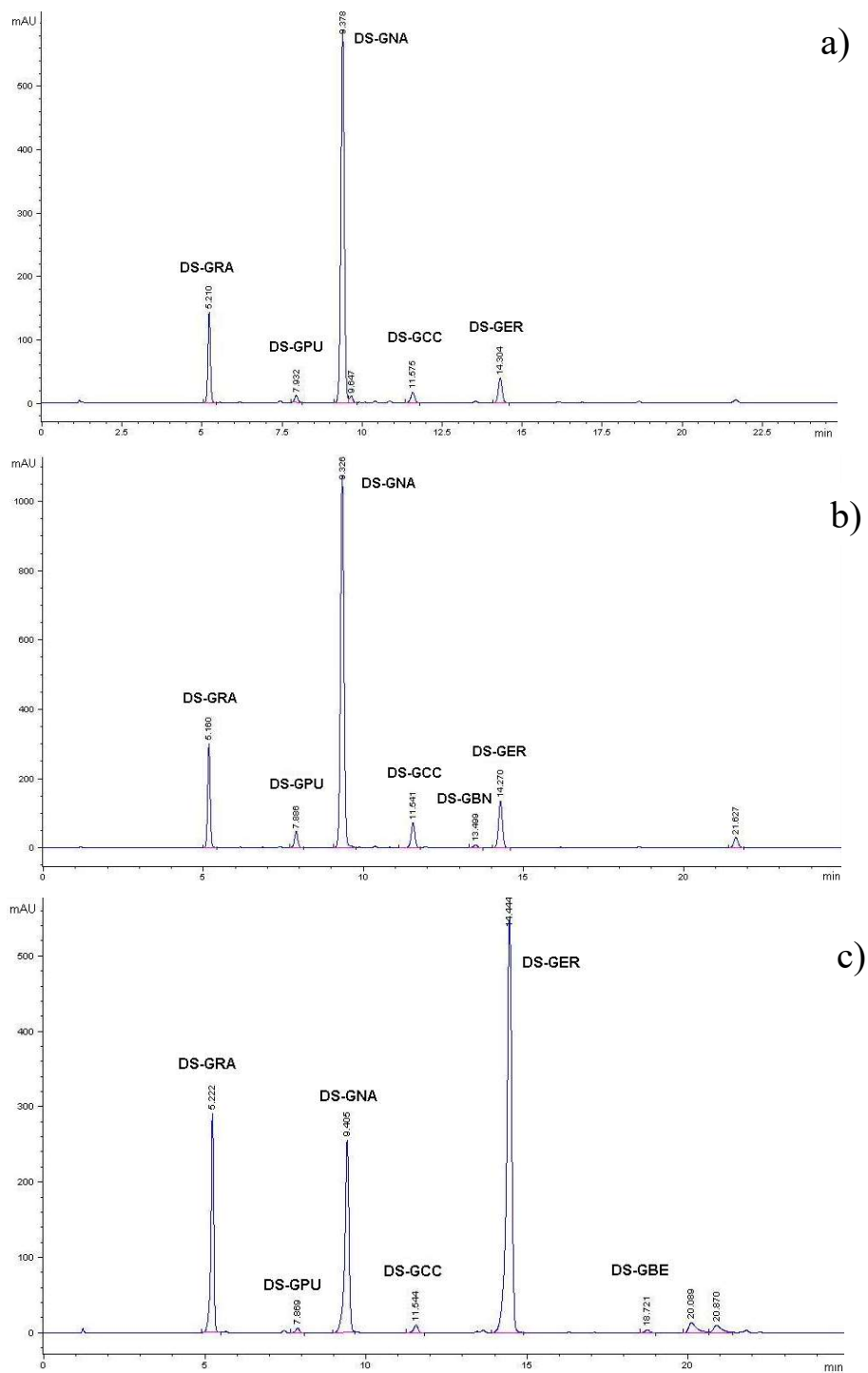


Figure 3.3 HPLC-DAD chromatograms of desulfoglucosinolates isolated from a) leaf and flower; b) stem; c) seed of *F. triquetra* (DC.) Boiss. ex Prantl. Peaks correspond to glucosinolates, as follows: DS-GRA, desulfo-glucoraphanin; DS-GPU, desulfo-glucopturanjivin; DS-GNA, desulfo-gluconapin; DS-GCC, desulfo-glucochlearin; DS-GBN, desulfo-glucoberberoin; DS-GER, desulfo-glucoerucin; DS-GBE, desulfo-glucoberteroin.

For GL quantification, we used the relative proportionality factors (RPFs) reported in the literature (Wathelet et al. 2004; EMEA, 2009). Since the RPFs for DS-GCC and DS-GBE are not reported, an arbitrary RPF value of 1 was set for DS-GCC, whereas for DS-GBE the RPF of DS-GER was used. The results for quantification are given in Table 3.1. In comparison to the stem extract, the leaf - flower extract showed a similar content of the major GLs, *i.e.* 77.9 and 68.2 % of 1a, 12.8 and 15.4 % of 5a, and 5.6 and 8.7 % of 3a, respectively. The seed contained 56.6 % of 3a, 24.1 % of 1a, and 17.3 % of 5a. The total GL content is strikingly high in all aerial parts, with the highest content in the seed. It is worth mentioning that the upper plant parts (leaf - flower and stem) have a 2–3 fold higher content of 5a than 3a, while this content in the seed is *vice versa*. This phenomenon was previously reported for *D. velebica* (De Nicola et al., 2011) and *Raphanus sativus* L. (Barillari et al., 2005) and one could speculate a biological oxidation of 3a to 5a during the sprouting of the seeds.

Table 3.1 Glucosinolate content of leaf-flower, stem, and seed in *F. triquetra* (DC.) Boiss. ex Prantl.

Glucosinolates ^(a)	Leaf-flower	Stem	Seed	LC-MS [M] ^{-(b)}
Glucoraphanin (5a)	8.0 ± 1.7 ^(c)	15.1 ± 3.0	23.4 ± 1.6	436.0
Glucoputranjivin (6a)	0.9 ± 0.1	2.5 ± 0.1	0.7 ± 0.1	–
Gluconapin (1a)	48.7 ± 1.7	66.7 ± 3.4	32.6 ± 1.1	372.0
Glucocochlearin (7a)	1.4 ± 0.1	4.3 ± 0.1	1.3 ± 0.1	373.8
Glucobrassicinapin (2a)	–	0.7 ± 0.0	–	–
Glucoerucin (3a)	3.5 ± 0.2	8.5 ± 0.5	76.7 ± 2.4	420.0
Glucoberteroin (4a)	–	–	0.7 ± 0.1	434.0
Total content (µmol / g dry weight)	62.5 ± 3.8	97.8 ± 7.1	135.4 ± 5.4	
Yield, (w / w) / %	2.7	4.2	6.1	

^(a) GLs are listed according to elution of their corresponding DS-GL on *Inertsil ODS-3* column. An arbitrary RPF value of DS-GL equal to 1 was used only for quantification of 5a.

^(b) [M]⁻ (%): specific product ion for GL identification in ESI⁻-MS having 100 % abundance.

^(c) Value is the mean ± standard error (*n* = 2).

The identification of GLs was confirmed by the GC-MS analysis of the corresponding volatile degradation products resulting from enzymatic hydrolysis. The most common breakdown products are ITCs, which are characterized by odd mass of the molecular ion, and a fragment ion of *m/z* = 72. Some GLs form unstable ITCs, such as 2-hydroxyalkenyl ITCs which cyclize to

oxazolidine-2-thiones, while 4-hydroxybenzyl ITC and the very reactive indole ITCs are degraded into their corresponding alcohols, releasing the thiocyanate ion (Hanshen et al., 2014). Beside identified ITCs, other breakdown products, mostly nitriles, can be helpful in confirming the parent GL identification. Individual GLs identified by GC-MS analysis of their hydrolysis products in different *F. triquetra* plants parts are shown in Table 3.2.

Table 3.2 Individual glucosinolates identified by GC-MS analysis of their hydrolysis products in different *F. triquetra* (DC.) Boiss. ex Prantl. plant parts.

Parent GL Identified compound	RI ^{a)}	Leaf-flower	Stem	Seed
Glucoputranjivin (6a) Isopropyl isothiocyanate	836	0.4	1.6	0.9
Glucocochlearin (7a) sec-Butyl isothiocyanate	939	- ^{b)}	-	0.7
Gluconapin (1a) But-3-enyl isothiocyanate	998	22.9	48.7	32.0
Glucobrassicinapin (2a) Pent-4-enyl isothiocyanate	1090	0.2	0.2	0.2
4-Methylpentyl GL 4-Methylpentyl isothiocyanate	1169	0.2	0.1	0.1
n-HeptylGL n-Heptyl isothiocyanate	1269	tr	0.4	0.3
5-Methylhexyl GL 5-Methylhexyl isothiocyanate	1276	-	0.2	0.1
Glucoerucin (3a) 5-Methylsulfanylpentanenitrile	1213	-	tr ^{c)}	tr
4-Methylsulfanylbutyl isothiocyanate (erucin)	1457	0.3	4.7	6.0
Glucoberteroin (4a) 5-Methylsulfanylpentyl isothiocyanate (berteroin)	1542	-	-	0.3
Glucoraphanin (5a) 4-Methylsulfanylbutyl isothiocyanate (sulforaphane)	1791	4.3	5.5	3.3
Group sum (%)		28.3	61.4	43.9

^{a)} RI, Retention indices determined on a VF-5MS capillary column. ^{b)} -, not detected. ^{c)} tr, traces.

GC-MS analysis confirmed the presence of the GLs identified by HPLC analysis of the corresponding DS-GLs, through detection of the following ITCs: i) isopropyl- and sec-butyl ITCs, originating from the branched GLs, 6a, and 7a, respectively; ii) but-3-enyl- and pent-4-enyl ITCs, from olefinic GLs 1a and 2a; and iii) 4-methylsulfanylbutyl- (erucin), 5-methylsulfanylpentyl- (berteroin) and 4-methylsulfanylbutyl (sulforaphane) ITCs confirming 3a, 4a, and 5a, respectively. In addition to the present ITCs, 5-(methylsulfanyl)pentanenitrile

confirmed the presence of 3a. GC-MS analysis was particularly useful for the correct identification of two minor peaks, namely 6a and 7a. Three additional minor ITCs, 4-methylpentyl-, 5-methylhexyl-, and *n*-heptyl ITCs were detected via GC-MS analysis. Those GL breakdown products belonging to the saturated C-6 C-7 aliphatic group were tentatively identified by their t_R and MS spectra. DS-GLs often bring difficulties in interpreting results of the individual GLs, due to concerns over the impact of pH value, time, and enzyme sulfatase (EC 3.1.6.1) concentration on desulfation products (Wathelet et al., 2014; Hennig et al., 2012). In addition, some GL breakdown products lack volatility or prove unstable in the conditions used during the analysis, and this represents a major drawback of this indirect method (Chiang et al., 1998). Therefore, a direct analysis of intact GLs present in the seed was performed by LC-MS for more specific and accurate qualitative determination and for better interpretation of analytical results. Specific product ion for GL identification in ESI-MS, having abundance 100%, is given in Table 3.1. The major intact GLs, 1a, 3a, and 5a, as well as 4a were clearly identified in chromatograms of crude seed extracts. GCC (7a) peak, notwithstanding the low amount (1.0 %), was also observed with specific product ion 373.8 (100 %). On the contrary, LC-MS analysis of intact GLs in the seed did not allow to confirm the presence of either 2a or 6a, previously identified by their corresponding DS-GLs and ITCs (Table 3.1 and 3.2). Moreover, it was not possible to confirm the tentatively identified 4-methylpentyl-, 5-methylhexyl- and *n*-heptyl GLs hypothesized by GC-MS analysis of ITCs (Table 3.2). Hence, the three HPLC peaks of DS-GLs at 20.1, 20.9 and 21.6 min could not be assigned (Figure 3.2). Except for the above-mentioned molecules, all volatile fractions from the investigated species contained compounds devoid of nitrogen or sulfur (Table 3.3) - mostly fatty acids, esters, alkanes, phenols, phenylpropanoids and related derivatives. The major products belonging to this class were hexadecanoic acid (12.6–19.9 %) and ethyl linoleate (15.0–25.7 %).

Table 3.3 GC-MS analysis of miscellaneous volatile compounds from different *F. triquetra* (DC.) Boiss. ex Prantl. plant parts.

Identified compound	RI ^{a)}	Flower and leaf	Stem	Seed
Alkanes				
1-Phenyl-1-propanone	1178	tr ^{b)}	tr	- ^{c)}
Tricosane	2300	0.9	-	0.5
Pentacosane	2500	1.9	-	-
Heptacosane	2700	12.9	2.6	2.6
Octacosane	2800	3.4	0.7	0.5
Phenols, phenylpropane derivatives and related compounds				
2-Phenylethyl alcohol	1133	tr	0.7	-
Eugenol	1366	0.3	0.3	-
4-Hydroxy-3-methoxy benzaldehyde	1422	tr	-	-
Dihydroactinidiolide	1547	-	0.1	0.1
6,10,14-Trimethyl-2-pentadecanone	1838	0.3	-	0.5
Fatty acid and esters				
Octanoic acid	1216	tr	-	-
Nonanoic acid	1310	tr	-	tr
Decanoic acid	1405	tr	tr	tr
Dibutyl phtalate	1861	0.3	0.4	tr
Pentadecanoic acid	1890	tr	tr	0.2
Hexadecanoic acid	2017	19.9	12.6	19.0
Ethyl linoleate	2195	25.7	15.0	23.7
Other compounds				
Dimethyl trisulfide	981	tr	0.1	0.1
Dimethyl tetrasulfide	1228	tr	0.9	1.0
Phytol	2110	0.2	1.9	-
Group sum (%)		65.8	35.3	48.2
Total sum (%)		94.2	96.9	92.3

(a) Same as in Table 3.2.

(b) tr: traces.

(c) -: not detected.

3.4 Discussion

GL profile analyses in the diverse plant tissues of *Fibigia triquetra* revealed aliphatic GLs to be the major ones. The C-4 and C-5 GLs 1a–5a originate from L-methionine (Met) *via* chain elongation by one carbon atom at a time, while C-3 and C-4 GLs 6a and 7a are derived from L-valine (Val) and L-leucine (Leu), respectively. The suggested natural occurrence of C-6 and

C-7 GLs, 4-methylpentyl-, 5-methylhexyl-, and *n*-heptyl GLs in a plant also accumulating similar Met-, Val-, and Leu-derived GLs seems likely. Reports of alkyl GLs bearing C-6 and longer chains are scarce and analyses revealing their occurrence are mostly based on GC-MS of the derived ITCs (Blazević et al., 2015). The presence of Leu-derived 4-methylpentyl GL (Sawada et al., 2009) was previously reported in *Alyssoides utriculata* (L.) Medik., *Raphanus sativus* L., *Eruca sativa* Mill by using GC-MS analysis of the ITC (Blazević et al., 2009; Blazević et al., 2015; Fahey et al., 2001) and LC-MS analysis of intact GLs (Lelario et al., 2012; Cataldi et al., 2007). Natural occurrence of both 5-methylhexyl- and *n*-heptyl GLs was also inferred from GC-MS analysis of their breakdown products. Val-derived 5-methylhexyl GL (Sawada et al., 2009) was previously inferred from 5-methylhexyl ITC analysis, while identification of *n*-heptyl GL was based on degradation to octanenitrile and *n*-heptyl ITC (Blazević et al., 2009; Blazević et al., 2013a; Blazević et al., 2013b). It is worth mentioning that until recent years, *n*-heptyl GL has been considered “unnatural” as claimed for example by Davidson et al. (2001). The present study has shown that C-4 GLs *i.e.* 1a, 3a, 5a are the major ones in *F. triquetra* whereas a C-5 GL, 4a, is dominant in *D. velebatica*. In addition, minor GLs can be suggested to be important tags which differentiate *F. triquetra* from *D. velebatica*. Previous studies of *D. velebatica* has shown the presence of glucoaubrietin (4-methoxybenzyl GL), as one minor GL present in the seed. Thus, it seems that, next to the major Met derived GLs, *F. triquetra* accumulates also Val and Leu derived GLs, whereas *D. velebatica* accumulates Tyr-derived GLs, next to the major Met derived GLs. Earlier reports on other *Fibigia* species showed prevalence of C-4 GLs such as 1a and 5a, but also of (*R*)- and (*S*)-2-hydroxy-3-butenyl GLs (PRO and EPRO), which were not identified in *F. triquetra* (Boudjikianian et al., 1974; Daxenbichler et al., 1991; Bennett et al., 2004). Previous studies focused on the GL profile of endemic plants of the tribe *Alyseae*, which comprises seven genera: *Alyssoides*, *Alyssum*, *Aurinia*, *Berteroa*, *Clypeola*, *Degenia* and *Fibigia*. Those investigations (De Nicola et al., 2011; Blazević et al., 2011; Blazević et al., 2013a; Blazević et al., 2013b; Blazević et al., 2015) of, namely, *D. velebatica*, *Aurinia sinuata* (L.) Griseb. and *A. leucadea* (Guss.) C. Koch., suggested that species in this tribe represent appropriate sources for Met derived GLs bearing a C-4 and/or C-5 olefinic aglycon chain (1a, 2a) and/or a thiofunctionalized chain (3a–5a, GAL). With high GL contents ranging from 9.9 to 135.4 $\mu\text{mol g}^{-1}$ of dried material in different plant

parts - especially in the seed (over 4.0 % w/w with the highest, 6.1 % w/w in *F. triquetra*) - those *Alysseae* are found to represent a good GL source

3.5 Conclusions

The GLs of an ice-age survived plant *F. triquetra* were analyzed by using a multiple method approach, involving HPLC-DAD analysis of DS-GLs and their comparison to standards, HPLC-ESI-MS analysis of intact GLs and GC-MS of the breakdown products obtained by enzymatic degradation of GLs. This approach established the qualitative and quantitative GL profile of *F. triquetra* and the present study revealed differences in the GL chemistry with the most similar paleostenoendemic plant *Degenia velebitica*, the only species in this genus.

References

Adams RP. Identification of essential oils components by gas chromatography/quadrupole mass spectrometry. Allured Publishing Cooperation, Illinois 2001.

Al-Shehbaz IA, Al-Shammary KI (1987) Distribution and chemotaxonomic significance of glucosinolates in certain Middle-Eastern cruciferae. *Biochem Syst Ecol* 15(5):559-569.

Barillari J, Canistro D, Paolini M, Ferroni F, Pedulli GF, Iori R, Valgimigli L (2005) Direct antioxidant activity of purified glucoerucin, the dietary secondary metabolite contained in rocket (*Eruca sativa* Mill.) seeds and sprouts. *J Agric Food Chem* 53(7):2475-2482.

Bennett RN, Mellon FA, Kroon PA (2004) Screening crucifer seeds as sources of specific intact glucosinolates using ion-pair high-performance liquid chromatography negative ion electrospray mass spectrometry. *J Agric Food Chem* 52(3):428-438.

Bezić N, Vuko E, Dunkić V, Ruščić M, Blažević I, Burčul F (2011) Antiphytoviral activity of sesquiterpene-rich essential oils from four croatian *teucrium* species. *Molecules* 16(9):8119-8129.

Blažević I, Mastelić J (2009) Glucosinolate degradation products and other bound and free volatiles in the leaves and roots of radish (*Raphanus sativus* L.). *Food Chem* 113(1):96-102.

Blažević I, Radonić A, Mastelić J, Zekić M, Skočibušić M, Maravić A (2010) Glucosinolates, glycosidically bound volatiles and antimicrobial activity of *Aurinia sinuata* (Brassicaceae). *Food Chem* 121(4):1020-1028.

Blažević I, Radonić A, Skočibušić M, De Nicola GR, Montaut S, Iori R, Rollin P, Mastelić J, Zekić M, Maravić A (2011) Glucosinolate profiling and antimicrobial screening of *aurinia leucadea* (Brassicaceae). *Chem Biodiversity* 8(12):2310-2321.

Blažević I, De Nicola GR, Montaut S, Rollin P (2013a) Glucosinolates in two endemic plants

of the *Aurinia* genus and their chemotaxonomic significance. *Nat Prod Commun* 8(10):1463-1466.

Blazević I, Burcul F, Ruscic M, Mastelic J (2013b) Glucosinolates, volatile constituents, and acetylcholinesterase inhibitory activity of *Alyssoides utriculata*. *Chem Nat Compd* 49(2):374-378.

Blažević I, Montaut S, De Nicola GR, Rollin P (2015) Long-chain glucosinolates from *Arabis turrita*: enzymatic and non-enzymatic degradations. *Nat Prod Commun* 10(6):1043-1046.

Boudjikianian HA, Abdel Gawad MM, Raynaud J (1974) Sulfur glycosides of *Fibigia eriocarpa* [LES GLUCOSIDES SOUFRES DE FIBIGIA ERIOCARPA]. *Planta Med* 26(2):144-149.

Cataldi TRI, Rubino A, Lelario F, Bufo SA (2007) Naturally occurring glucosinolates in plant extracts of rocket salad (*Eruca sativa* L.) identified by liquid chromatography coupled with negative ion electrospray ionization and quadrupole ion-trap mass spectrometry. *Rapid Commun Mass Spectrom* 21(14):2374-2388.

Çetin Ö, Duran A, Martin E, Tustas S (2012) A taxonomic study of the genus *Fibigia* Medik. (Brassicaceae). *Afr J Biotechnol* 11:109-119.

Chiang WCK, Pusateri DJ, Leitz REA (1998) Gas chromatography/mass spectrometry method for the determination of sulforaphane and sulforaphane nitrile in Broccoli. *J Agric Food Chem* 46(3):1018-1021.

Clarke DB (2010) Glucosinolates, structures and analysis in food. *Anal Methods* 2(4):310-325.

Davidson NE, Rutherford TJ, Botting NP (2001) Synthesis, analysis and rearrangement of novel unnatural glucosinolates. *Carbohydr Res* 330(3):295-307.

Daxenbichler ME, Spencer GF, Carlson DG, Rose GB, Brinker AM, Powell RG (1991)

Glucosinolate composition of seeds from 297 species of wild plants. *Phytochemistry* 30(8):2623-2638.

De Nicola GR, Blažević I, Montaut S, Rollin P, Mastelić J, Iori R, Tatibouët A (2011) Glucosinolate distribution in aerial parts of *degenia velebitica*. *Chem Biodiversity* 8(11):2090-2096.

European Economic Community, Commission Regulation, EEC No. 1864/90. Oilseeds – determination of glucosinolates high performance liquid chromatography. *Off J Eur Comm* 1990 L170 27-34.

European Medicines Agency (EMA). Quality guidelines. Validation of analytical procedures. Text and methodology (ICHQ2) 2009 Available online at http://www.ema.europa.eu/docs/en_GB/document_library/Scientific_guideline/2009/09/WC500002662.pdf (Accessed on March 13th, 2018).

Fahey JW, Zalcmann AT, Talalay P (2001) The chemical diversity and distribution of glucosinolates and isothiocyanates among plants. *Phytochemistry* 56(1):5-51.

Fukarek P, Šolić EM (1982) *Acta Biokovica* 2:243.

Hanschen FS, Lamy E, Schreiner M, Rohn S (2014) Reactivity and stability of glucosinolates and their breakdown products in foods. *Angew Chem Int Ed* 53(43):11430-11450.

Hennig K, Verkerk R, Bonnema G, Dekker M (2012) Pitfalls in the desulphation of glucosinolates in a high-throughput assay. *Food Chem* 134(4):2355-2361.

Kostović-Vranješ V, Vladović D, Papeš D (1994) Cytogenetics and new localities of endemic species *Fibigia triquetra* (DC.) Boiss. *Period Biol* 96(4):372-374.

Kostović-Vranješ V, Bohanec B, Javornik B, Papeš D. Variability of ITS region of nrDNA among stenoendemic species of Croatian *Fibigia triquetra* and two *Fibigia* species from Macedonia

(Brassicaceae) (Ed. B. Vitale), *Periodicum Biologorum*, Hvar, Hrvatska, 1998, p. 30.

Lelario F, Bianco G, Bufo SA, Cataldi TRI (2012) Establishing the occurrence of major and minor glucosinolates in Brassicaceae by LC-ESI-hybrid linear ion-trap and Fourier-transform ion cyclotron resonance mass spectrometry. *Phytochemistry*, 73:74-83.

Leoni O, Iori R, Haddoum T, Marlier M, Wathelet JP, Rollin P, Palmieri S (1998) Approach to the use of immobilized sulfatase for analytical purposes and for the production of desulfo-glucosinolates. *Ind Crop Prod* 7(2-3):335-343.

Mastelić J, Jerković I, Blažević I, Radonić A, Krstulović L (2008) Hydrodistillation-adsorption method for the isolation of water-soluble, non-soluble and high volatile compounds from plant materials. *Talanta* 76(4):885-891.

Mastelić J, Blažević I, Kosalec I (2010) Chemical composition and antimicrobial activity of volatiles from *Degenia velebitica*, a European stenoendemic plant of the Brassicaceae family. *Chem Biodiversity* 7(11):2755-2765.

Mayer E (1981) *Degenia velebitica* Deg. Hay. in *Fibigia triquetra* (DC.) Boiss.-morfološko taksonomska paralela. *Acta Biokovica* 1:283-290.

Montaut S, Grandbois J, Righetti L, Barillari J, Iori R, Rollin P (2009) Updated glucosinolate profile of *Dithyrea wislizenii*. *J Nat Prod* 2009, 72 (5):889-893.

Prevalek-Kozlina B, Kostović-Vranješ V, Slade D (1997) In vitro propagation of *Fibigia triquetra* (DC.) Boiss., a rare stenoendemic species. *Plant Cell Tiss Org Cult* 51(2):141-143.

Prevalek-Kozlina B, Pavlica M, Vujević M (1999) Micropropagation of *Degenia velebitica* (Deg.) Hay., a Croatian endemic plant species. *Phyton Ann Rei Bot A* 39(3):293-296.

Rešetnik I, Satovic Z, Schneeweiss GM, Liber Z (2013) Phylogenetic relationships in

Brassicaceae tribe Alysseae inferred from nuclear ribosomal and chloroplast DNA sequence data. *Mol Phylogenet Evol* 69(3):772-786.

Sawada Y, Kuwahara A, Nagano M, Narisawa T, Sakata A, Saito K, Yokota Hirai M (2009) Omics-based approaches to methionine side chain elongation in arabidopsis: Characterization of the genes encoding methylthioalkylmalate isomerase and methylthioalkylmalate dehydrogenase. *Plant Cell Physiol* 50(7):1181-1190.

Wathelet J-P, Iori R, Leoni O, Rollin P, Quinsac A, Palmieri S (2004) Guidelines for glucosinolate analysis in green tissues used for biofumigation. *Agroindustria* 3(3):257-266.

Zrybko CL, Fukuda EK, Rosen RT (1997) Determination of glucosinolates in domestic and wild mustard by high-performance liquid chromatography with confirmation by electrospray mass spectrometry and photodiode-array detection. *J Chromatogr A* 767(1-2):43-52.

CHAPTER FOUR

Glucosinolate diversity in *Bretschneidera sinensis* of Chinese origin

Contents

Summary

4.1 Introduction

4.2 Experimental

4.2.1 General

4.2.2 Plant material

4.2.3 HPLC analysis and quantification of desulfoglucosinolates

4.2.4 Isothiocyanate and nitrile production from *B. sinensis* fruits

4.2.5 GC-MS analysis of isothiocyanates and nitriles

4.2.6 LC-MS analysis of glucosinolates

4.2.7 Extraction and isolation of glucobretschneiderin

4.2.7.1 Glucobretschneiderin characterization

4.3 Results and discussion

References

Summary

The glucosinolate (GL) profile in several plant parts (leaf, branch, bark, root, and fruit) of *Bretschneidera sinensis* from three geographical regions of the People's Republic of China was established for the first time by HPLC. During this investigation, benzyl GL (1), 4-hydroxybenzyl GL (2), 2-hydroxy-2-methylpropyl GL (3), and 4-methoxybenzyl GL (4) were identified. In addition, one new GL, 3-hydroxy-4-methoxybenzyl GL (5), was isolated in a minor amount from the fruit and characterized by spectroscopic data interpretation. Furthermore, traces of 4-hydroxy-3-methoxyphenylacetonitrile were detected by GC-MS analysis in the fruits, thus confirming the presence of the regioisomeric 4-hydroxy-3-methoxybenzyl GL (6). GLs 1–5 were also quantified for the first time by HPLC in the various plant organs.

4.1 Introduction

Bretschneidera sinensis Hemsl. (syn. *B. yunshanensis* Chun & F.C. How.) (Akaniaceae), Chinese common name “bo le shu”, is a tree growing in Southeast mainland China (provinces of Fujian, Guangdong, Guangxi, Guizhou, Hubei, Hunan, Jiangxi, Sichuan, Yunnan, and Zhejiang), northern Taiwan, and northern Vietnam (Hemsley, 1901; Zheng et al., 2005). It was described for the first time by Hemsley in 1901 and placed originally in the Sapindaceae family (Hemsley, 1901). However, its taxonomic position has always been a point of discussion, and this plant has been the subject of many botanical studies (Tobe et al., 1990; Lü et al., 1994a; Lü et al., 1994b; Doweld, 1996; Carlquist, 1996; Ronse De Craene et al., 2002; Qiao et al., 2010a; Qiao et al., 2010b; Qiao et al., 2012; Tu et al., 2012; Chaw, 1987). The chromosome cytology [chromosome number, $2n=18$, and karyotypic formula, $8m+6sm+4sm$ (SAT)] was not sufficient to suggest a systematic relationship (Yang et al., 1995). An initial pollen morphology observation of *B. sinensis* suggested for the family Bretschneideraceae a closer classification and systematic position relationship with Connaraceae rather than with Papaveraceae (Liu, 1996). Another pollen morphology investigation suggested that *Bretschneidera* is related to Sapindaceae, Hippocastanaceae, Moringaceae, and Caesalpinioideae (Chaw, 1987). In addition, some genetic and cladistic studies have been carried out on *B. sinensis* (Guan et al., 2012; Rodman, 1991a; Rodman, 1991b; Gadek et al., 1992; Rodman et al., 1993; Rodman et al., 1998; Bayer et al., 2003; Peng et al., 2011). In a phenetic study based on a sparser data set, *Akania* and *Bretschneidera* clustered together but were not close to Sapindaceae (Rodman, 1991a). Cladistic pairings by Rodman were congruent with phenetic linkages (Rodman, 1991b). Based on comparative sequence data for the ribulose-1,5-bisphosphate carboxylase chloroplast encoded gene (*rbcl*), a close affinity between *Bretschneidera* and the Capparales was demonstrated and especially with the genus *Tropaeolum* (Rodman, 1993). Other cladistic analyses based on the comparison of the sequence data for *rbcl* showed that the genus *Akania* clustered robustly with *Bretschneidera* and then *Tropaeolum*, within the clade of Capparalean families (Gadek, 1992). An investigation on DNA sequencing of the nuclear 18S rRNA gene and the combination of the two gene data sets (DNA sequencing of the chloroplast *rbcl* gene and DNA sequencing of the nuclear 18S rRNA gene) yielded the same result (Rodman, 1998). Later, Bayer and Appel included *B. sinensis* in the family Akaniaceae (order Brassicales) (Bayer et al., 2003). This plant still belongs to the family Akaniaceae

according to the Angiosperm Phylogeny Group classification III system (APG, 2009) *B. sinensis* is the only known species of the genus *Bretschneidera*. This plant is rare and threatened in mainland China (Qiao et al., 2010a; Qiao et al., 2010b; Qiao et al., 2012; Peng et al., 2011; Qiao et al., 2010c; He et al., 2005; Wang et al., 2007). An analysis of the nutrients in leaves of *B. sinensis* has shown that the plant is a magnesium accumulator (Wan et al., 2009). In the leaf, the concentrations of N, P, K, Ca, Mg, and Fe were found to be 15.17, 1.18, 4.17, 20.75, 8.16, and 226.5 mg g⁻¹, respectively, and those of Mn, Zn, Cu, Ni, Na, and Al were found to be 493.8, 30.16, 4.41, 9.38, 123.3, and 70.3 mg kg⁻¹, respectively (Wan et al., 2009). Moreover, *B. sinensis* has been described as an excellent wild vegetable because the concentration levels of nitrite, nitrate, and vitamin C in the juvenile stems and leaves were 0.04–0.08, 5.91–6.17, and 15.10–217.0 mg kg⁻¹, respectively (Guo et al., 2009). A review of the scientific literature shows that 5,5-dimethyl-2-oxazolidinethione can be isolated from *B. sinensis* leaves after myrosinase (MYR) hydrolysis of the plant extract, indicating the presence of 2-hydroxy-2-methylpropyl glucosinolate (glucoconringiin, GCN). In addition, 3,4-dihydroxybenzyl glucosinolate and other glucosinolates (GLs) in trace amounts were detected by GC-MS (Boufford et al., 1989). In 2010, glucotropaeolin (GTL), hydroxymethylpropyl- and hydroxybenzyl GLs were detected by LC-MS in leaves of a single herbarium specimen of *B. sinensis* collected from mainland China in 1919 (Mithen et al., 2010). In addition, in the trunk of *B. sinensis*, 3-*epi*-betulinic acid, 3,5,7-trihydroxyflavonol, daucosterol, and β -sitosterol were isolated (Ma et al., 1992). Recently, two heterocyclic compounds, bretschnneiderazines A and B, and six aromatic diglycosides, bretschnneiderosides A–C, benzyl 6'-O- β -D-apiofuranosyl- β -D-glucopyranoside, 3,4,5-trimethoxyphenyl- β -D-apiofuranosyl-(1→6)- β -D-glucopyranoside, and canthoside C, were isolated from the stem of the plant (Liu et al., 2010). Furthermore, bretschnneiderazine A showed moderate activity against the NCI-H446 human lung carcinoma cell line (Liu et al., 2010). Shortly after this, the total synthesis of bretschnneiderazines A and B was described (Liu et al., 2011). A review of the literature indicates that *B. sinensis* contains glucosinolates, sulfur-containing secondary metabolites that are present in all plants of the order Brassicales. Their degradation products mainly isothiocyanates (ITCs), nitriles, thiocyanates, and oxazolidinethiones are known to be responsible for various biological activities (Fahey et al., 2001). However, all the minor compounds present have not been identified, and, so far, only the leaves of *B. sinensis* have been investigated. Thus, the aim of the present work was to investigate the GL profile in the

various plant parts (leaf, branch, trunk, root, and fruit) of *B. sinensis*. GLs were extracted and quantified as desulfoglucosinolates (DS-GLs) by HPLC. In addition, an extract of the fruits was analyzed for ITCs and nitriles by GC-MS analysis. Finally, one new GL (5) was isolated in minor amount from *B. sinensis* fruits and characterized by NMR and HRMS.

4.2 Experimental

4.2.1 General

All solvents were ACS grade and used as such, except for CHCl_3 , which was redistilled. D_2O was purchased from Eurisotop (Saint-Aubin, France). Formic acid was purchased from BDH (Toronto, ON, Canada). HPLC-grade MeOH, Et_3N (Reagent grade), and thymol were purchased from Fisher Scientific (Whitby, ON, Canada). 4-Hydroxy-3-methoxyphenylacetonitrile was purchased from Sigma-Aldrich Chemie (Steinheim, Germany). Potassium phosphate, FeSO_4 , and sodium acetate were purchased from Merck (Darmstadt, Germany). Potassium sulfate was purchased from Sigma-Aldrich (Seelze, Germany). HPLC-grade H_2O was generated in the laboratory through a Nanopure Diamond Ultrapure water system provided by Barnstead (Dubuque, IA, USA). Kieselgel 60 F_{254} analytical TLC aluminum sheets were purchased from EM Science (Gibbstown, NJ, USA); compounds were visualized under UV light and by dipping the plates into a 95% ethanol solution containing 1% (w/v) thymol and 10% (v/v) H_2SO_4 followed by heating. Preparative TLC was performed on precoated 20 cm \times 20 cm silica gel 60 (0.5 mm thickness, Merck) plates. Flash column chromatography was carried out using SPE bulk sorbent large-pore C-18 from Alltech (State College, PA, USA). C-18 silica gel cartridges (Mega Bond Elut Flash, 10 g sorbent mass, 60 mL volume) were obtained from Varian, Inc. (Mississauga, ON, Canada). The UV spectrum was determined on a Cary 60 UV/visible spectrophotometer from Agilent Technologies (Santa Clara, CA, USA). The infrared spectrum was recorded with a Bruker Optics FTIR microscope using a mercury cadmium telluride detector cooled with liquid N_2 . The sample was dissolved in MeOH and deposited on a gold-coated glass, and 1000 coadded scans were collected in grazing angle reflectance mode with a 40 \times objective. The baseline was corrected using OPUS software. The atmospheric compensation algorithm from the OPUS software was used to correct for carbon dioxide and

water vapor. NMR spectra were recorded in D₂O at 600 MHz (¹H) and 150 MHz (¹³C) on a Bruker Avance III 600 spectrometer equipped with a TXI cryoprobe at the Institut de Chimie Moleculaire de Reims (Reims, France); δ values (ppm) are referenced to 3-(trimethylsilyl)-2,3,2',3'-tetradeuteropropanoic acid (Sigma-Aldrich, Saint Quentin Fallavier France), and coupling constants *J* are given in Hz. HRESIMS measurements were recorded using an API Qstar XL mass spectrometer at the Saskatchewan Structural Science Centre (Saskatoon, Canada).

4.2.2 Plant Material

B. sinensis was collected on October 2011 in the People's Republic of China: (1) at the Xishuangbanna Tropical Botanical Garden, Yunnan Province (branch and leaf); (2) in Xiushui County, Jiangxi Province (leaf, branch, bark, and root), and (3) in Wuning County, Jiangxi Province (leaf, branch, and fruit). The plant parts were dried in the shade for several days. The plant was identified by Prof. Han-Ming Zhang at the Department of Pharmacognosy, Second Military Medical University, Shanghai, China. A voucher specimen (20080823) is kept at the Herbarium of the School of Pharmacy, Second Military Medical University, Shanghai, People's Republic of China.

4.2.3 HPLC analysis and quantification of desulfoglucosinolates

GLs were extracted as previously reported with some modifications (De Nicola et al., 2012). Dried samples (~500 mg) were frozen in liquid N₂, ground in a mortar, and immediately extracted for 5 min at 80 °C twice with EtOH/H₂O (5 mL, 7:3 v/v). The solution was filtered, concentrated to dryness, and dissolved in 10 mL of EtOH. Each extract (2 mL) was loaded onto a minicolumn filled with 0.6 mL of DEAE-Sephadex A-25 anion-exchange resin (GE Healthcare) conditioned with 25 mM acetate buffer (pH 5.6). After washing with 3 mL of buffer, 150 μ L (0.36 U/mL) of purified sulfatase (Leoni et al., 1998) was loaded onto the minicolumn that was left overnight. The DS-GLs were then eluted with 1 mL of ultrapure H₂O for GL profiling and with a second addition of 1 mL of H₂O for quantification purposes. Desulfations were performed in duplicate. HPLC analysis of DS-GLs was performed on an

Agilent model 1100 equipped with an Inertsil ODS-3 column (250 × 3.0 mm, 5 μm particle size), thermostated at 30 °C, and having a diode array as detector. The chromatography was performed at a flow rate of 1 mL min⁻¹ eluting with a gradient of H₂O (A) and acetonitrile (B) following the following program: 1 min 1% B; 22 min linear gradient up to 22% B; 3 min linear gradient down to 1% B. DS-GLs were detected by monitoring the absorbance at 229 nm. Identification of the peaks was performed on the basis of retention times and UV spectra of pure standards available in our laboratory. The amount of GL was quantified by using a calibration curve of pure desulfosinigrin solution (range from 0.07 to 1.29 mM) and the relative proportionality factors (RPFs) for each individual DS-GL. The published RPFs for DS-GLs were used, with the exception of compound 5, for which an arbitrary RPF value equal to 1 was set for quantification (De Nicola et al., 2012; Clarke, 2010).

4.2.4 Isothiocyanate and nitrile production from *B. sinensis* fruits

Dried fruits (2.3 g) were first dehulled (net weight 1.7 g), then reduced to a fine powder, which was extracted by boiling absolute EtOH. The mixture was homogenized for 10 min at 80 °C using an Ultra Turrax T-25 and then centrifuged to afford 7.4 mL of clear supernatant. For ITC production, the EtOH extract (1 mL) was concentrated to dryness and the residue dissolved in 0.1 M potassium phosphate buffer pH 7 (1 mL). ITCs were produced by enzymatic hydrolysis of the GL crude extract by the addition of MYR (100 μL, 34 U mL⁻¹) to the buffer solution. After 15 min at 37 °C, the resulting ITCs were extracted with CH₂Cl₂ (1 mL) and analyzed by GC-MS after drying with K₂SO₄ (De Nicola et al., 2012). For nitrile production, the EtOH extract (1 mL) was concentrated to dryness and the residue dissolved in 25 mM acetate buffer pH 5.6 (1 mL) containing 10 mM FeSO₄. Nitriles were produced by enzymatic hydrolysis of the GL crude extract by the addition of MYR (100 μL, 34 U mL⁻¹) to the buffer solution. After 15 min at 37 °C, the resulting nitriles were extracted with CH₂Cl₂ (1 mL) and analyzed by GC-MS after drying with K₂SO₄ (Velasco et al., 2011).

4.2.5 GC-MS analysis of isothiocyanates and nitriles

GC-MS analyses of ITCs and nitriles were carried out using a Bruker Scion SQ Premium instrument (Bruker Daltonics), equipped with a 30 m × 0.25 mm capillary column (HP-5MS). The flow rate of the carrier gas He was 1 mL min⁻¹. Temperature programming was from 60 °C (hold 1 min) to 260 °C at 8 °C min⁻¹ (hold 1 min). The temperatures of the injector and the detector were 250 and 280 °C, respectively. All MS runs were conducted in the electron impact (EI⁺) mode at 70 eV. The mass range was from *m/z* 40 to 650, and chromatograms were acquired as total ion currents. The identification of ITCs and nitriles was assigned based on retention times (*t_R*) and mass spectra of hydrolysis products obtained by MYR catalyzed degradation of pure GLs available in our laboratory and by matching the recorded mass spectra with the mass spectrum library of the GC-MS data system.

4.2.6 LC-MS analysis of glucosinolates

LC-MS analysis was performed by injecting a 20 µL aliquot of the solution of crude extract or fraction into an Agilent Technologies HP 1100 (New Castle, DE, USA) high-performance liquid chromatograph equipped with a quaternary pump, automatic injector, diode-array detector (wavelength range 190–600 nm), degasser, and a Hypersil ODS column (5 µm, 4.6 × 200 mm). The two mobile phase solvents, MeOH and H₂O, were prepared with 0.15% Et₃N and 0.18% HCO₂H, added as ion-pairing reagents. Both solutions were filtered using 0.45 µm nylon membranes. The initial mobile phase was 100% HPLC-grade H₂O. At 10 min, the mobile phase was switched to a linear gradient of 100% H₂O to 100% MeOH over 60 min. After each run, the initial mobile phase conditions were set, and the system was allowed to equilibrate. The flow rate was kept constant at 1 mL min⁻¹. The column temperature was held at room temperature (Montaut et al., 2009). The HPLC was interfaced to an Agilent model 6120 mass spectrometer (Toronto, ON, Canada) with a Chemstation LC-MSD B.03.01 data system. The electrospray interface was a standard ES source operating with a capillary voltage of 4 kV and temperature of 350 °C. The system was operated in the negative and positive ion electrospray modes. Nitrogen was used as nebulizing and drying gas at a flow rate of 10 L min⁻¹ (35 psig).

The mass spectrometer was programmed to perform full scans between m/z 100 and 1000 amu.

4.2.7 Extraction and isolation of glucobretschneiderin

Dried fruits (17 g) were frozen in liquid N_2 , ground in a mortar, and immediately extracted for 5 min at 80 °C twice with EtOH/ H_2O (90 mL, 7:3 v/v). The solution was filtered and concentrated to dryness (3.9 g). This extract was dissolved in H_2O (10 mL) and submitted to liquid-liquid extractions with EtOAc. The organic layer (EtOAc fraction 512 mg) and the aqueous layer (2.7 g) were concentrated to dryness. The aqueous fraction was separated by flash column chromatography (C-18 phase, 40 × 80 mm, gradient $H_2O/MeOH$, 100:0 and 0:100 v/v, 25 mL fractions). Fractions 8 to 15 were combined (335 mg) and submitted to solid-phase separation (C-18 cartridge, $H_2O/MeOH$, 100:0 and 0:100 v/v, 3 mL fractions). The combined fractions 6 to 25, obtained from the solid-phase separation, were submitted to preparative TLC ($CHCl_3/MeOH/H_2O$, 65:45:10), yielding glucobretschneiderin (5) (3.4 mg) and glucotropaeolin (1) (74.9 mg) (Prester et al., 1996, Dini et al., 2002; Piacente et al., 2002) after filtration.

4.2.7.1 Glucobretschneiderin characterization

White, amorphous powder.

UV (MeOH) λ_{max} (log ϵ) 204 (4.2), 229 (3.7), 283 (3.2) nm.

IR ν_{max} 3373, 2915, 2847, 1658, 1621, 1596, 1511, 1438, 1247, 1130, 1059, 801, 668 cm^{-1}

1H NMR (D_2O , 600 MHz) δ 7.06 (1H, d, $^3J_{H-7-H-8} = 8.8$ Hz, H-7), 6.92 (2H, m, H-4 and H-8), 4.73 (1H, m, H-1'), 4.06 (1H, d, $^3J_{H-2A-H-2B} = 16.1$ Hz, H-2A), 4.02 (1H, d, $^3J_{H-2B-H-2A} = 16.1$ Hz, H-2B), 3.87 (3H, s, $-OCH_3$), 3.64 (2H, m, H-6'), 3.42 (1H, m, H-4'), 3.33 (2H, m, H-2' and H-3'), 3.21 (1H, m, H-5').

^{13}C NMR (D_2O , 150 MHz) δ 165.6 (C-1), 149.6 (C-6), 148.1 (C-5), 130.9 (C-3), 123.1 (C-8), 118.0 (C-4), 115.9 (C-7), 84.2 (C-1'), 82.7 (C-5'), 79.8 (C-3'), 74.6 (C-2'), 71.5 (C-4'), 63.0 (C-6'), 58.8 ($-OCH_3$), 40.4 (C-2).

HRESIMS m/z 454.0479 $[M]^-$ (calculated for $C_{15}H_{20}NO_{11}S_2$, 454.0483).

HPLC, t_R = 22.2 min

4.3 Results and discussion

The different parts of *B. sinensis* were harvested from three geographical regions in the People's Republic of China (branch and leaf at the Xishuangbanna Tropical Botanical Garden, Yunnan Province; leaf, branch, bark, and root in Xiushui County, Jiangxi Province; and leaf, branch, and fruit in Wuning County, Jiangxi Province). The extractions were performed according to the EEC standard procedure. Next, each plant extract was analyzed by HPLC to detect the DS-GLs resulting from enzyme-catalyzed hydrolytic desulfation. The t_R data and UV spectra of the products were compared with the values for standards from our DS-GLs library.

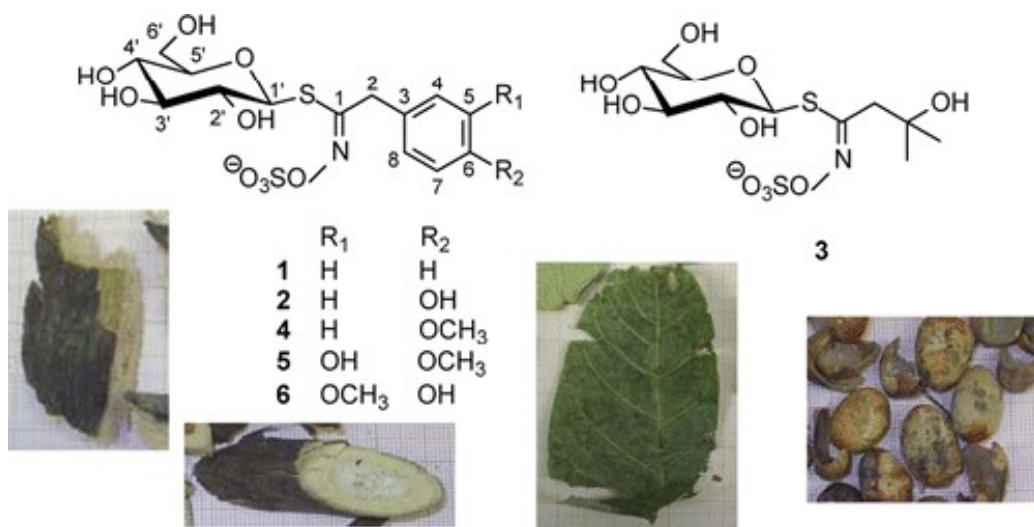


Chart 4.1 Structures of glucosinolates 1–6 from *Bretschneidera sinensis*.

Two GLs, benzyl GL (1, GTL, 79% in leaf, 97.5% in branch) and 4-hydroxybenzyl GL (2, glucosinalbin, SNB, 21% in leaf, 2.5% in branch) were identified in the leaf and branch harvested at the Xishuangbanna Tropical Botanical Garden (Table 4.1). No GL was detected in the leaf and root of *B. sinensis* from Xiushui County. However, GLs 1 (51% in branch, 76.5% in bark) and 2 (5% in branch, 1.1% in bark) as well as 2-hydroxy-2-methylpropyl GL (3, glucoconringiin, 44% in branch, 22.4% in bark) have been identified in the branch and in the

bark of *B. sinensis* originating from the same county. In addition, no GL was detected in the leaf extract of *B. sinensis* from Wuning County. However, the bark contained the three GLs 1 (88.3%), 2 (6.3%), and 3 (5.4%), whereas the fruit contained the four GLs 1 (77.7%), 3 (9.3%), 4-methoxybenzyl GL [4, glucoaubrietin (GAU), 6.8%], and a minor unidentified GL (5, 6.2%). The fruit extract was submitted to MYR hydrolysis process, producing ITCs, and to another procedure leading to nitriles. GC-MS analysis revealed the presence of benzyl ITC, 5,5-dimethyl-1,3-oxazolidine-2-thione, and 4-methoxybenzyl ITC, thus confirming the presence of 1, 3, and 4 as already identified by HPLC analysis of the DS-GLs. An additional unidentified peak displayed a spectrum with fragments compatible with 4-hydroxy-3-methoxybenzyl ITC with major ions at m/z 195 $[M^+]^+$ and m/z 137 $[M^+-NCS]^+$, as reported for *Brassica elongata* Ehrh. (Brassicaceae) by Schroeder et al. (1983). However, no standard spectrum of this ITC was available for comparison. The GC-MS analysis of the nitrile-containing extract confirmed the presence of 1, 3, and 4 in the fruit extract. Two additional minor peaks, traces of the first one at 15.4 min and the second one at 15.9 min, displayed the same mass spectrum with fragmentations matching those of 4-hydroxy-3-methoxyphenylacetonitrile present in the mass spectrum library of our GC-MS data system. The nitrile-containing fraction was co-injected with a commercial standard of 4-hydroxy-3-methoxyphenylacetonitrile in the GC-MS system. The chromatogram showed that the standard had the same t_R value as the trace peak at 15.4 min, indicating that minor amounts of 4-hydroxy-3-methoxybenzyl GL (6) were present in the fruit extract. The peak at 15.9 min remained unidentified, but at this stage of the investigation it was reasonable to speculate that it could be a regioisomer of 4-hydroxy-3-methoxyphenylacetonitrile.

Table 4.1 Glucosinolate content in different organs of *B. sinensis* from Xishuangbanna tropical botanical garden, Wuning County, and Xiushui County.

	glucosinolates ($\mu\text{mol/g}$ dry weight)					total DS-GLs
	1a (DS-GTL, t_R 14.0 min)	2a (DS-SNB, t_R 8.3 min)	3a (DS-GCN, t_R 4.9 min)	4a (DS-GAU, t_R 15.6 min)	5a (DS-GBR, t_R 11.1 min)	
Xishuangbanna Tropical Botanical Garden						
leaf	0.44 \pm 0.07	0.12 \pm 0.01 ^{a,b}				0.56 \pm 0.08
branch	0.78 \pm 0.02	0.02 \pm 0.00				0.80 \pm 0.02
Wuning County						
leaf						
bark	0.98 \pm 0.13	0.07 \pm 0.01	0.06 \pm 0.00			1.11 \pm 0.14
fruit	7.11 \pm 0.17		0.85 \pm 0.10	0.62 \pm 0.00	0.57 \pm 0.02	9.15 \pm 0.29
Xiushui County						
leaf						
root						
branch	0.22 \pm 0.00	0.02 \pm 0.00	0.19 \pm 0.04			0.43 \pm 0.04
bark	0.65 \pm 0.04	0.01 \pm 0.02	0.19 \pm 0.00			0.85 \pm 0.06

^aDuplicate. ^bStandard error.

Identification of compound 5 required its isolation, which was performed from 17 g of fruit, producing *ca.* 3.4 mg of 5. Its structure was elucidated using UV, IR, NMR (^1H , ^{13}C , HMBC, and HMQC), and mass spectrometric data. The UV spectrum indicated that 5 belongs to the arylalkyl GL class (Wathelet et al., 2004). The mass spectrum of 5 gave a mass of 454 amu, and the molecular formula $\text{C}_{15}\text{H}_{20}\text{NO}_{11}\text{S}_2$ was established by HRMS. FTIR data showed absorption bands at 3373 (OH), 2915 (CH), 1658 (CN), 1059 (C–O), 801 (sulfate), and 668 (C–S) cm^{-1} . The ^1H and multiplicity edited HSQC NMR spectra revealed the presence of three aromatic protons, a pair of nonequivalent protons from an isolated methylene group (δH 4.06, 4.02 and δC 40.4), a singlet due to a methoxy group (δH 3.87 and δC 58.8), and signals attributable to a thioglucose unit (see Experimental Section). These observations supported the hypothesis of 5 being a benzylic GL, for which the aromatic substitution pattern needed to be determined. The signal of the anomeric proton (δH 4.73) may be expected to appear as a doublet, caused by the coupling of H-1' with H-2'. However, as observed in the ^1H NMR spectra of other benzylic GLs (Figure 4.1), such as glucolimnanthin (3-methoxybenzyl GL), glucotropaeolin (1), and glucosinalbin (2), the nearly identical chemical shifts of H-2' and H-3' make the first-order analysis of the H-1' signal difficult. The similarity of the complex coupling patterns in Figure 4.1 is consistent with a β -anomeric configuration (Cox et al., 1984).

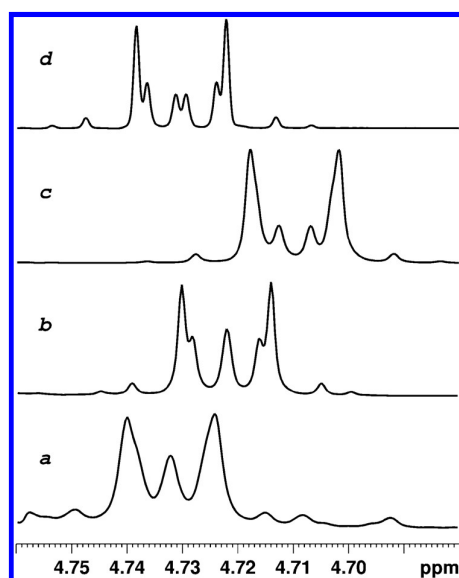


Figure 4.1 NMR spectrum expansions of the anomeric ^1H signal region of (a) compound 5, (b) glucolimnanthin, (c) glucotropaeolin (1), and (d) glucosinalbin (2).

The signals of the CH₂ group at position C-6' were identified easily in the multiplicity-edited HSQC spectrum. The chemical shifts of H-5', H-4', and H-3' were successively deduced from the COSY spectrum. The remaining sugar moiety peak in the HSQC spectrum (δ H 3.33, δ C 74.6) led to the assignment of the position C-2'. The chemical shifts of the sugar moiety carbons followed the usual decreasing order for C-1', C-5', C-3', C-2', C-4', and C-6' (Montaut et al., 2009; De Nicola et al., 2012). Strong coupling effects were also visible in the aromatic ring. The HSQC spectrum revealed two methine groups for which the ¹H NMR chemical shifts were almost identical (δ H 6.92, H-4 and H-8), a broad one (δ C 123.1, C-8) and a narrow one (δ C 118.0, C-4), broadening being related to the large (³J = 8.8 Hz) ¹H-¹H coupling constant observed. The third methine group exhibited a ¹H-NMR signal that appeared as a broad doublet (δ H 7.06, H-7), with its coupling partner being therefore H-8. The coupling pattern of the aromatic ¹H-NMR signals fully supported the occurrence of a trisubstituted aromatic ring with H-7/H-8 *ortho* coupling and H-4/H-8 *meta* coupling. The HMBC spectrum (Figure 4.2) showed the coupling of C-3, C-4, and C-8 with H-2.

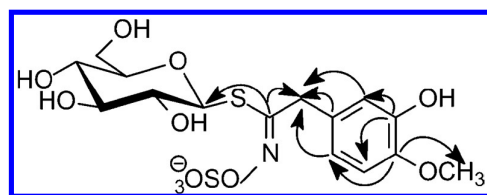


Figure 4.2 Selected HMBC correlations for glucobretschneiderin (5).

The quaternary C-3 was therefore identified as the attachment point of the aromatic ring to C-2, immediately surrounded by C-4 and C-8. The C-6/H-8 HMBC correlation was explained by the occurrence of a C-6/C-7 bond. The remaining aromatic carbon C-5 must be bound to C-4 and C-6. The methoxy group was placed at C-6 by means of the HMBC spectrum. Carbon C-5 was bound to a hydroxy group, as pointed out by its high chemical shift (δ C 148.1), thus resulting in the structure and NMR spectroscopic assignments proposed for compound 5. Therefore, the NMR data reported here suggested that compound 5 is 3-hydroxy-4-methoxybenzyl GL (glucobretschneiderin; GBR).

The major GLs were quantified in the different plant organs of *B. sinensis* by HPLC (Table 4.1). Quantitatively, the fruit was found to be about nine times richer in GLs than the bark and about 15–16 times richer than the branch and leaf. In comparison with other GL-containing plants recently studied, *B. sinensis* is not particularly rich in total GLs (De Nicola et al., 2012).

The number of plant samples investigated was too small to assume whether their geographic locations would have an impact on the GL content. Qualitatively, the phenylalanine-derived GTL 1 was found in all *B. sinensis* GL-containing extracts, no matter the organ type and the geographical origin. In summary, the first experiments to examine the comprehensive GL profile in *B. sinensis* have been performed using the HPLC method for analysis of DS-GLs and GC-MS methods for the analysis of ITCs and nitriles. As a result, benzyl (1), 4-hydroxybenzyl (2), 2-hydroxy-2-methylpropyl (3), and 4-methoxybenzyl (4) GLs were identified. Moreover, spectroscopic data are reported for 3-hydroxy-4-methoxybenzyl GL (5), a new GL, isolated from *B. sinensis* fruit. GLs 1–5 were also quantified for the first time by HPLC in various plant parts. In addition, traces of 4-hydroxy-3-methoxyphenylacetonitrile were detected in the fruit, indicating the presence of traces of 4-hydroxy-3-methoxybenzyl GL (6). The present findings agree with the identification of 3 by Boufford et al. (1989). The latter group also mentioned the detection of 3,4-dihydroxybenzyl DS-GL in *B. sinensis* leaf; however, this GL was not detected in *B. sinensis* (Boufford et al. (1989). This may be due to genetic and environmental factors. The GL profile of *B. sinensis* is close to that established for *Akania bidwillii* (R. Hogg) Mabb. (Akaniaceae), featuring benzyl, hydroxybenzyl, dihydroxybenzyl, and methoxybenzyl GLs (Mithen et al., 2010). In addition, as some cladistic studies have suggested, the profile of arylalkyl GLs in *B. sinensis* is consistent with a close affinity of the plant with *Tropaeolum* species (Gadek et al., 1992; Rodman et al., 1993). However, arylalkyl GLs are also predominant in plants of the families Limnanthaceae, Caricaceae, Moringaceae, and Pentadiplandraceae and in some members of the family Brassicaceae. Furthermore, 2-hydroxy-2-methylpropyl GL (3) is also found in plants of the families Brassicaceae, Limnanthaceae, Moringaceae, Resedaceae, and Tropaeolaceae (Fahey et al., 2001). In a recent study, GTL (1) was shown to possess a very low peroxy radical scavenging capacity and a very weak antioxidant capacity toward ABTS^{•+} (Natella et al., 2014). Furthermore, this GL failed to inhibit Cu-catalyzed LDL oxidation or to reduce Cu(II)/H₂O₂-induced bleaching of crocin (Natella et al., 2014) according to Aires et al. (2009) GTL (1) has no antimicrobial activity but is likely to have potential inhibition against HIV-1 integrase (Ma et al., 2011). However, several studies have shown that benzyl ITC possesses potential cancer chemopreventive properties (Hwang and Lee, 2008; Ho et al., 2011; Kim et al., 2011), antifungal activity toward plant pathogenic fungi (Manici et al., 1997), and antimicrobial activity (Aires et al., 2009; Ma et al., 2011; Hwang et al., 2008; Ho et al., 2011; Kim et al., 2011; Manici et al., 1997; Radulović et al., 2012). Therefore, it would also

be of great interest to test the potential of 5 and its MYR degradation product 3-hydroxy-4-methoxybenzyl ITC for their possible health benefits.

References

Aires A, Mota VR, Saavedra MJ, Rosa EAS, Bennett RN (2009) The antimicrobial effects of glucosinolates and their respective enzymatic hydrolysis products on bacteria isolated from the human intestinal tract. *J Appl Microbiol* 106(6):2086–2095.

Bayer C, Appel O. In *Flowering Plants, Dicotyledons: Malvales, Capparales and Non-betalain Caryophyllales*. Kubitzki K and Clemens C (Eds) Springer-Verlag: Heidelberg, 2003. Vol. 5:pp 21-24.

Boufford DE, Kjær A, Madsen JØ, Skrydstrup T (1989) Glucosinolates in *Bretschneideraceae* (1989) *Biochem Syst Ecol* 17:375–379.

APG III (2009) An update of the angiosperm phylogeny group classification for the orders and families of flowering plants: APG III. *Bot J Linn Soc* 161:105-121.

Carlquist, S (1996) Wood anatomy of *Akaniaceae* and *Bretschneideraceae*: a case of near-identity and its systematic implications. *Syst Bot* 21(4):607–616.

Clarke DB (2010) Glucosinolates, structures and analysis in food. *Anal Methods* 2(4):310-325.

Chaw SW, Peng CI (1987) Palynological notes on *Bretschneidera sinensis* Hemsl. *Bot Bull Acad Sin* 28:55-60.

Cox IJ, Hanley AB, Belton PS, Fenwick GR (1984) N.m.r. spectra (^1H , ^{13}C) of glucosinolates. *Carbohydr Res* 132(2):323–329.

De Nicola GR, Nyegue M, Montaut S, Iori R, Menut C, Tatibouët A, Rollin P, Ndoyé C, Amvam Zollo P-H (2012) Profile and quantification of glucosinolates in *Pentadiplandra brazzeana* Baillon. *Phytochemistry* 73:51-56.

Dini I, Tenore GC, Dini A (2002) Glucosinolates from Maca (*Lepidium meyenii*). *Biochem Syst Ecol* 30(11):1087-1090.

Doweld AB (1996) The carpology and taxonomic relationships of *Bretschneidera* (*Bretschneideraceae*). *Acta Bot Malacit* 21:79-90.

European Economic Community, Commission Regulation, EEC No. 1864/90. Oilseeds – determination of glucosinolates high performance liquid chromatography. *Off J Eur Comm* 1990 L170 27-34.

Fahey JW, Zalcmann AT, Talalay P (2001) The chemical diversity and distribution of glucosinolates and isothiocyanates among plants. *Phytochemistry* 56(1):5-51.

Guan BC, Song G-R, Ge G (2012) Sixteen microsatellite markers developed from *Bretschneidera sinensis* (*Bretschneideraceae*). *Conserv Genet Resour* 4(3):673–675.

Gadek PA, Quinn CJ, Rodman JE, Karol KG, Conti E, Price RA, Fernando ES (1992) Affinities of the australian endemic akaniaceae: New evidence from *rbcl* sequences. *Aust Syst Bot* 5(6): 717–724.

Guo Z and Yang Z (2009) *Shipin Yu Fajiao Gongye* 35:141-143.

He K-J and Li Y-D (2005) [Plant resources of national protection grade I in Guangdong Province.] *J Trop Subtrop Bot* 13:519-525.

Leoni O, Iori R, Haddoum T, Marlier M, Wathelet J-P, Rollin P, Palmieri S (1998) Approach to the use of immobilized sulfatase for analytical purposes and for the production of desulfo-glucosinolates. *Ind Crops Prod* 7(2-3):335-343.

Lü J and Hu Y-X (1994) Structural study of secondary xylem in *Bretschneidera sinensis* Hemsl. *Acta Bot Sin* 36:459-465.

Lü J, Hu Y-X, Hu Y-S (1994) Anatomy of the young stem and secondary phloem in *Bretschneidera sinensis* Hemsl. *Chin J Bot* 6:112-117.

Liu C (1986) Studies of pollen morphology in the *Bretschneideraceae* and the relative families. *Acta Bot Yunnan* 8:441-450.

Liu C-M, Li B, Shen YH, Zhang WD (2010) Heterocyclic compounds and aromatic diglycosides from *Bretschneidera sinensis*. *J Nat Prod* 73(9):1582-1585.

Liu QC, Guo TT, Fan Z, Li D, Li, WH (2011) First total synthesis of two new heterocyclic compounds: Bretschneiderazines A and B. *Chin Chem Lett* 22(7):801-803.

Hwang E-S and Lee H-J (2008) Benzyl isothiocyanate inhibits metalloproteinase-2/-9 expression by suppressing the mitogen-activated protein kinase in SK-Hep1 human hepatoma cells. *Food Chem Toxicol* 46(7):2358-2364.

Ho C-C, Lai KC, Hsu S-C, Kuo C-L, Ma C-Y, Lin M-L, Yang J-S, Chung J-G (2011) Benzyl isothiocyanate (BITC) inhibits migration and invasion of human gastric cancer AGS cells via suppressing ERK signal pathways. *Hum Exp Toxicol* 30(4):296-306.

Kim EJ, Hong JE, Eom SJ, Lee J-Y, Park JHY (2011) Oral administration of benzyl-isothiocyanate inhibits solid tumor growth and lung metastasis of 4T1 murine mammary carcinoma cells in BALB/c mice. *Breast Cancer Res Treat* 130(1):61-71.

Manici LM, Lazzeri L, Palmieri S (1997) In vitro fungitoxic activity of some glucosinolates and their enzyme-derived products toward plant pathogenic fungi. *J Agric Food Chem* 45(7):2768-2773.

Ma S-K, Wu K-Z, Li A-X (2011) Virtual screening for natural product inhibitors of HIV-1 integrase *Interdiscip Sci: Comput Life Sci* 3(1):17-21.

Ma Z-W and He G-F (1992) *Acta Bot Sin* 34:483-484.

Mithen R, Bennett R, Marquez J (2010) Glucosinolate biochemical diversity and innovation in the Brassicales. *Phytochemistry* 71(17-18):2074-2086.

Montaut S, Grandbois J, Righetti L, Barillari J, Iori R, Rollin P (2009) Updated glucosinolate profile of *Dithyrea wislizenii*. *J Nat Prod* 72(5):889-893.

Natella F, Maldini M, Leoni G, Scaccini C (2014) Glucosinolates redox activities: can they act as antioxidants? *Food Chem* 149:226-232.

Peng S-S, Huang HH, Tong Z-K, Zhou H-J, Shi J, Yu G-M, Luo W-J (2011) *J Plant Genet Resour* 12:362-367.

Piacente S, Carbone V, Plaza A, Zampelli A, Pizza C (2002) Investigation of the tuber constituents of maca (*Lepidium meyenii* Walp.). *J Agric Food Chem* 50(20):5621-5625.

Prester T, Fahey JW, Holtzclaw WD, Abeygunawardana C, Kachinski JL, Talalay P (1996) Comprehensive chromatographic and spectroscopic methods for the separation and identification of intact glucosinolates. *Anal Biochem* 239(2):168-179.

Qiao Q, Xing F-W, Chen H-Q, Fu LJ (2010a) *J Wuhan Bot Res* 28:229-233.

Qiao Q, Wen X-Y, Chen H-F, Xing F-W (2010b) *J Wuhan Bot Res* 28:544-549.

Qiao Q, Xing F-W, Chen H-F, Zhong W-C (2010c) *Acta Bot Boreal-Occident Sin* 30:377-384.

Qiao Q, Chen H, Xing F, Wang F, Zhong W, Wen X, Hou X (2012) Pollination ecology of *Bretschneidera sinensis* (hemsley), a rare and endangered tree in China. *Pak J Bot* 44(6):1897-1903.

Radulović NS, Dekić MS, Stojanović-Radić ZZ (2012) Antimicrobial volatile glucosinolate autolysis products from *Hornungia petraea* (L.) Rchb. (Brassicaceae). *Phytochem Lett* 5(2):351-357.

Rodman JE (1991) A taxonomic analysis of glucosinolate-producing plants. Part 1 Phenetics. *Syst Bot* 16:598-618.

Rodman JE (1991) A taxonomic analysis of glucosinolate-producing plants. Part 2 Cladistics. *Syst Bot* 16:619-629.

Rodman J, Price RA, Karol K, Conti E, Systma KJ, Palmer JD (1993) Nucleoside sequences of the *rbcl* gene indicate monophyly of mustard oil plants. *Ann Mo Bot Gard* 80:686-699.

Rodman JE, Soltis PS, Soltis DE, Sytsma KJ, Karol KG (1998) Parallel evolution of glucosinolate biosynthesis inferred from congruent nuclear and plastid gene phylogenies. *Am J Bot* 85(7):997-1006.

Ronse De Craene LP, Yang TYA, Schols P, Smets EF (2002) Floral anatomy and systematics of *Bretschneidera* (Bretschneideraceae). *Bot J Linn Soc* 139(1):29-45.

Schroeder WP, Daxenbichler ME, Spencer GF, Weisleder D (1983) 4-hydroxy-3-methoxybenzylglucosinolate, a new glucosinolate in seeds of *brassica elongata*. *J Nat Prod* 46(5):667-670.

Tu Q, Wu T, Zhao L-C, Liu Y-C, Liu R-L, Zhang Z-X (2012) *Zhiwu Fenlei Yu Ziyuan Xuebao* 34:248-256.

Tobe H and Peng CI (1990) The embryology and taxonomic relationships of *Bretschneidera* (Bretschneideraceae) *Bot J Linn Soc* 103(2):139-152.

Velasco P, Slabaugh MB, Reed R, Kling J, Kishore VK, Stevens JF, Knapp S (2011) Glucosinolates in the new oilseed crop meadowfoam: natural variation in section *inflexae* of *Limnanthes*, a new glucosinolate in *L. floccosa*, and QTL analysis in *L. alba*. *J Plant Breed* 130(3):352-359.

Yang D-Q and Hu C-M (1985) The chromosomes of *Bretschneidera* Hemsl. *Notes R Bot Gard Edinburgh* 42:347-349.

Wan K-Y, Chen F, Tao Y, Chen S-S (2009) Nutrient elements in leaves of rare and endangered species in wuhan botanical garden, China. *J Plant Nutr* 32(11):1914-1940.

Wang F-G, Zhang R-J, Xing F-W, Ng SC, Ye Y-S, Chen H-Q (2007) *J Wuhan Bot Res* 25:303-309.

Wathelet J-P, Iori R, Leoni O, Rollin P, Quinsac A, Palmieri S (2004) Guidelines for glucosinolate analysis in green tissues used for biofumigation. *Agroindustria* 3(3):257-266.

Zheng W and Raven PH. *Flora of China*; Harvard University Herbaria: Cambridge, MA, 2005.

CHAPTER FIVE

Probing for the presence of glucosinolates in three *Drypetes* spp. and two *Rinorea* spp. from Gabon

Contents

Summary

5.1 Introduction

5.2 Experimental

5.2.1 General

5.2.2 Plant material

5.2.3 HPLC analysis and quantification desulfoglucosinolates

5.3 Results and discussion

5.3.1 Glucosinolates in *Drypetes gossweileri*

5.3.2 Glucosinolates in *Rinorea subintegrifolia*

5.4 Conclusions

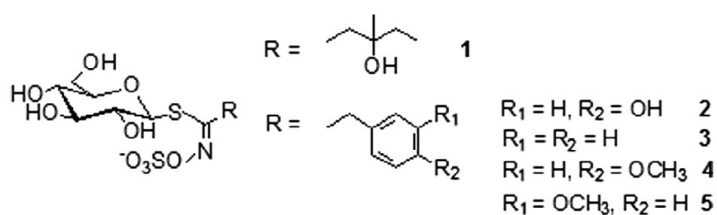
References

Keywords

Drypetes spp; *Rinorea* spp; glucosinolates; Malpighiales

Summary

Drypetes euryodes (Hiern) Hutch., *Drypetes gossweileri* S. Moore, *Drypetes laciniata* Hutch. (Putranjivaceae), *Rinorea subintegrifolia* O. Ktze, and *Rinorea woermanniana* (Büttner) Engl. (Violaceae) from Gabon were probed for the presence of glucosinolates (GLs). When present, the GLs were identified and quantified by HPLC analysis. 2-Hydroxy-2-methyl GL (1) was the major GL in the cork of *D. euryodes*. Moreover, 4-hydroxybenzyl GL (2) was the major GL in the seed of *D. gossweileri* whereas the bark contained 2 as the minor GL and benzyl GL (3) was the major one. In addition, 4-methoxybenzyl GL (4), 3-methoxybenzyl GL (5), and 3 were found in the root of *R. subintegrifolia*. However, no GL was detected in *D. laciniata* (leaf and stem), *D. euryodes* (leaf and stem), and *R. woermanniana* (leaf and stem-branch). Our results support the hypothesis of the existence of GLs in plants of the Putranjivaceae and Violaceae families (order Malpighiales).



5.1 Introduction

Drypetes gossweileri S. Moore (Putranjivaceae) is a tree used in Africa for diverse therapeutic applications such as the treatment of headache, intercostal pain, kidney pain, and bronchopneumonia. It has also been used as vermifuge, aphrodisiac, and against gonorrhoea (Bouquet, 1969). The stem bark extract was found to have antifungal properties (Ngouana et al., 2011) and to display some toxicity towards mice (Tessier and Paris, 1978). However, no toxic effect was noticed in albinos Wistar rats (Ngouana et al., 2011). Furthermore, a methanolic extract of *D. gossweileri* stem bark was found to have cytotoxic and DNA-damaging activities (Ngouela et al., 2003). The ethanolic and crude aqueous extracts of *D. gossweileri* bark were also active against bacteria responsible for urinary tract infections (Ijah and Oyebanji, 2003). Dichloromethane and ethyl acetate extracts of *D. gossweileri* have shown effective insecticide activities against *Sitophilus zeamais* (Motsch.) and *Rhyzoperthadominica* (F.) (Aba Toumou et al., 2013). The crude stem bark extract of *D. gossweileri* has shown anti-microbial and phytotoxic properties against *Lemna minor* L. (Schmelzer and Gurib-Fakim, 2008). Phytochemical screenings of stem bark extract and fractions indicated the presence of alkaloids, phenols, flavonoids, saponins, anthocyanins, anthraquinones, sterols, lipids, cardiac glycosides, tannins, phlobatannins, and essential oils (Ijah and Oyebanji, 2003; Ngouana et al., 2011; Aba Toumou et al., 2013). The essential oil of *D. gossweileri* bark (origin Gabon) did not show good antioxidant or antiradical activities but has shown bacteriostatic and bactericidal activities (Agnaniet et al., 2003; Voundi et al., 2015). This essential oil contained benzyl isothiocyanate (ITC) (56.5, 93.9 and 86.7% in plants from Gabon, Central African Republic and Cameroon, respectively) and benzyl cyanide (42.3, 5.7 and 12.6%, respectively) (Eyele Mvé-Mba et al., 1997; Voundi et al., 2015). Those constituents are indicative of the existence of benzyl glucosinolate (GL) (3) in the plant (Figure 5.1).

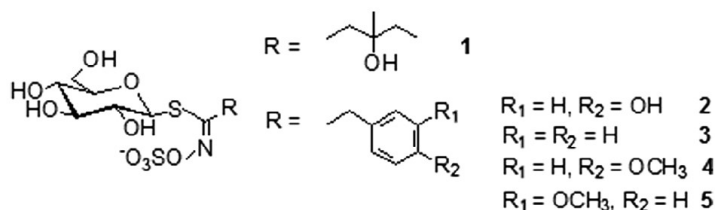


Figure 5.1 Glucosinolates identified in *D. euryodes*, *D. gossweileri*, and *R. subintegrifolia*.

Another study confirmed the presence of the above major constituents in *D. gossweileri* bark essential oil, together with benzyl alcohol, several benzyl esters, and terpenes (Agnaniet et al., 2003). In addition, non-volatiles have been isolated from the stem bark of *D. gossweileri* (Dupont et al., 1997). In other respects, several other secondary metabolites were isolated from the stem bark of *D. gossweileri* (Ngouela et al., 2003; Ata et al., 2011). The whole stems of *Drypetes laciniata* Hutch. (Putranjivaceae) were shown to contain several friedelane-type ketones, olean-12-en-28-oic acid derivatives, a mixture of sterols, and chikusetsusaponin IVa methyl ester (Fannang et al., 2011). In African traditional medicine, *Rinorea subintegrifolia* O. Ktze (Violaceae) is used as a fragrant agent during ancestral cults, as expectorant, against eye diseases and to treat heart disease, fever, headache, rheumatism, stomach ache, constipation, oedema, and malaria (Agnaniet et al., 2003; Tokuoka, 2008; Lekana-Douki et al., 2011). However, the methanolic extract of *R. subintegrifolia* was not active *in vitro* against *Plasmodium falciparum* Welch (Lekana-Douki et al., 2011). The essential oil obtained from roots of Gabonese *R. subintegrifolia* contained benzyl- and *p*-methoxybenzyl cyanides, benzyl- and *p*-methoxybenzyl ITCs, benzyl- and *p*-methoxybenzyl alcohols (Agnaniet et al., 2003). This investigation led to think that the plant would contain 3 and *p*-methoxybenzyl GL (4) (Figure 5.1). Furthermore, the essential oil of *R. subintegrifolia* did not have good antioxidant or antiradical activities (Agnaniet et al., 2003). No previous phytochemical study was reported in the literature for *Drypetes euryodes* (Hiern) Hutch. (Putranjivaceae) or *Rinorea woermanniana* (Büttner) Engl. (Violaceae). GLs are present in all species of the order Brassicales and in some families of the order Malpighiales (Eyele Mvé- Mba et al., 1997; Agnaniet et al., 2003; Voundi et al., 2015). GL degradation products – mainly ITCs, nitriles, thiocyanates and oxazolidinethiones – are known to be responsible for various biological activities (Mithen et al., 2000; Brader et al., 2006). The aim of this work was to probe for the presence of GLs in *D. euryodes*, *D. gossweileri*, *D. laciniata*, *R. subintegrifolia* and *R. woermanniana* growing wild in Gabon. GLs were extracted, analyzed as desulfoglucosinolates (DS-GLs) and quantified by HPLC.

5.2 Experimental

5.2.1 General

HPLC-grade acetonitrile was purchased from Sigma Aldrich Chemie GmbH, (Steinheim, D). Potassium phosphate and sodium acetate were purchased from Merck (Darmstadt, Germany). Ultrapure water (pH 5.0 ± 0.2) was obtained from a Milli-Q Gradient instrument (Millipore SAS, Molsheim, F) equipped with a Millipack filter 0.22 µm (Millipore, SAS, Molsheim, F).

5.2.2 Plant Material

The plants were collected in February 2010 in Gabon. The samples were harvested in a forest near Andem village (Kougouleu) at least 30 km north of Libreville for *D. laciniata*, in a forest near Libreville (Estuaire) for *D. gossweileri*, *D. euryodes*, *R. woermanniana* and for *R. subintegrifolia* near Ngounié. They were identified by Mr. Raoul Niangadouma from the National Herbarium of Gabon by comparison with authenticated plants in the herbarium. The information regarding the voucher numbers are reported in Table 5.1.

Table 5.1 Studied plants from Gabon

Plant	Voucher numbers in Gabon
<i>Drypetes euryodes</i>	JJFE de Wilde 233
<i>Drypetes gossweileri</i>	AM Louis 3407
<i>Drypetes laciniata</i>	AM Louis 1849
<i>Rinorea subintegrifolia</i>	Breteler 14738
<i>Rinorea woermanniana</i>	Wieringa 4352

5.2.3 HPLC analysis and quantification of desulfoglucosinolates

Glucosinolates (GLs) were extracted as previously reported with some modifications (Barillari et al., 2005). Plant samples were reduced to a fine powder. Samples of about 500 mg were extracted for 5 min at 80 °C in 2 x 5 mL EtOH-H₂O (70:30 v/v), using a U-Turrax (IKA T25) homogenizer and then centrifuged. Supernatants were combined 4 and each extract (1 mL) was loaded onto a mini-column filled with 0.6 mL of DEAE Sephadex A-25 anion-exchange

resin (Amersham Biosciences) conditioned with 25 mM acetate buffer (pH 5.6). After washing with 3 mL of buffer, 200 μL (0.35 U mL^{-1}) of purified sulfatase (Leoni et al. 1998) was loaded onto the mini-column which was left overnight at 30 °C. The desulfoglucosinolates (DS-GLs) were then eluted with 3 mL of ultrapure H_2O and finally injected into an HPLC. The DS-GLs were analyzed on an Agilent 1100 HPLC system equipped with an Inertsil ODS-3 column (250 x 3.0 mm, 5 μm particle size), thermostated at 30 °C, and using a diode array detector. The chromatography was performed at a flow rate of 1 mL min^{-1} eluting with a gradient of H_2O (A) and acetonitrile (B) following the program: 1 min 1% B; 22 min linear gradient up to 22% B; 3 min linear gradient down to 1% B. DS-GLs were detected monitoring the absorbance at 229 nm. The amount of GL was quantified by using a calibration curve of pure DS-sinigrin solution (range from 0.14 to 1.4 mM) and the RPFs of each individual DS-GLs (Clarke, 2010; De Nicola et al., 2012). Identification of the peaks was performed based on retention time and UV spectra of spiked DS-GL pure standards available in our laboratory (Leoni et al., 1998).

5.3 Results and discussion

The extraction of various plant parts of *D. euryodes*, *D. gossweileri*, *D. laciniata*, *R. subintegriifolia* and *R. woermanniana*, the HPLC analysis and quantification of DS-GLs (Barillari et al., 2005; Clarke, 2010; De Nicola et al., 2012) were performed as described in the experimental section (Figures 5.2–5.5 and Tables 5.1–5.2).

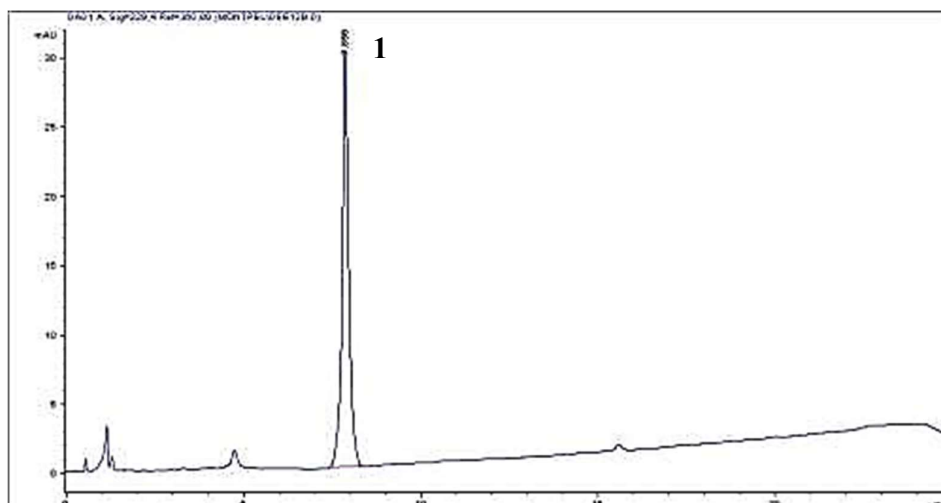


Figure 5.2 HPLC chromatogram of desulfoglucosinolates in *Drypetes euryodes* cork ethanolic extract. 1: Desulfo 2-hydroxy-2-methylbutyl glucosinolate (DS glucocleomin) (t_R 7.9 min).

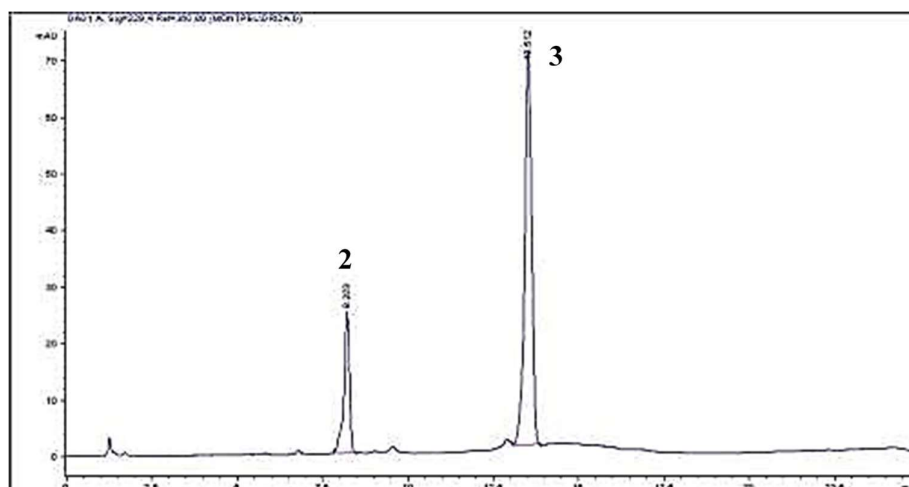


Figure 5.3 HPLC chromatogram of desulfoglucosinolates in *Drypetes gossweileri* bark ethanolic extract. 2: desulfo 4-hydroxybenzyl glucosinolate (DS glucosinalbin) (t_R 8.2 min), 3: desulfo benzyl glucosinolate (DS glucotropaeolin) (t_R 13.5 min).

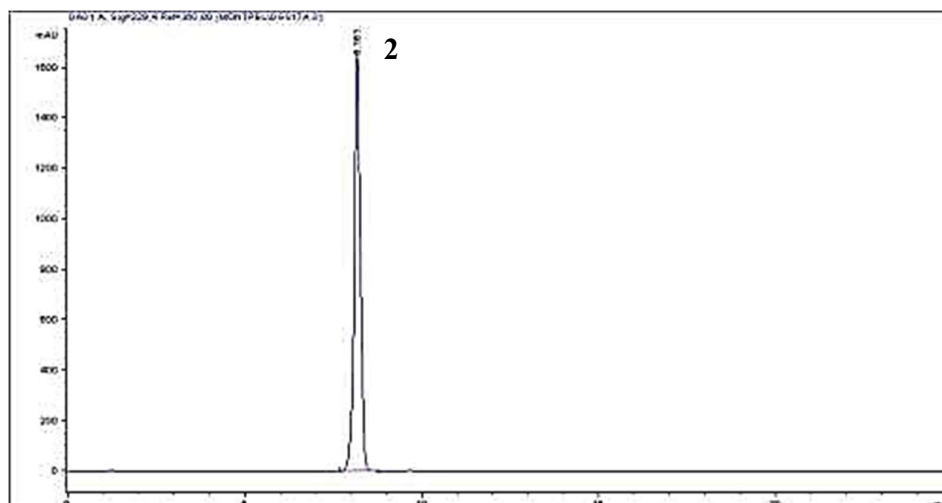


Figure 5.4 HPLC chromatogram of desulfoglucosinolates in *Drypetes gossweileri* seed ethanolic extract. 2: desulfo 4-hydroxybenzyl glucosinolate (DS glucosinalbin) (t_R 8.2 min).

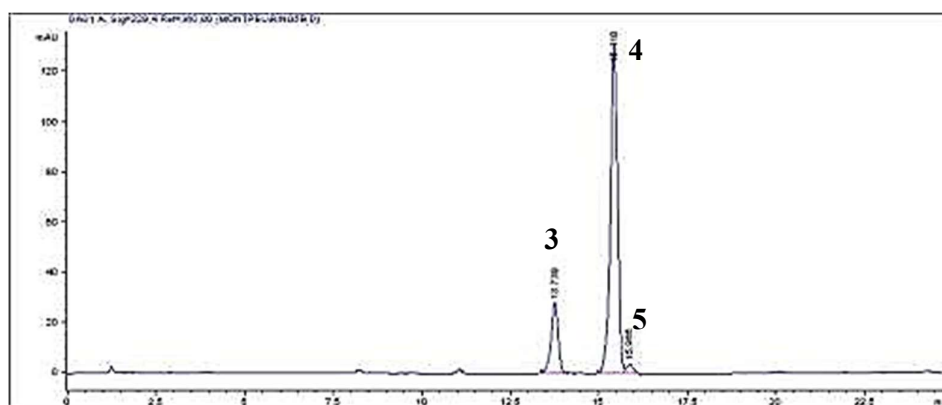


Figure 5.5 HPLC chromatogram of desulfoglucosinolates in *Rinorea subintegrifolia* root ethanolic extract. 3: desulfo benzyl glucosinolate (DS glucotropaeolin) (t_R 13.7 min), 4: desulfo 4-methoxybenzyl glucosinolate (DS glucoaubrietin) (t_R 15.4 min), 5: desulfo 3-methoxybenzyl glucosinolate (DS glucolimnanthin) (t_R 15.9 min).

Table 5.2 Distribution of glucosinolates in *Drypetes euryodes*, *Drypetes gossweileri*, *Drypetes laciniata*, *Rinorea subintegrifolia*, and *Rinorea woermanniana*.

Plant	Glucosinolates ^{a)} (μmol/g dry weight)					Total
	1	2	3	4	5	
<i>D. euryodes</i>						
Leaf	ND ^{b)}	ND	ND	ND	ND	ND
Stem	ND	ND	ND	ND	ND	ND
Cork	3.19 ± 0.49 ^{c)}	ND	ND	ND	ND	3.19 ± 0.49
<i>D. gossweileri</i>						
Bark	ND	2.30 ± 0.12	16.11 ± 0.56	ND	ND	18.41 ± 0.68
Seed	ND	171.41 ± 8.93	ND	ND	ND	171.41 ± 8.93
<i>D. laciniata</i>						
Leaf	ND	ND	ND	ND	ND	ND
Stem	ND	ND	ND	ND	ND	ND
<i>R. subintegrifolia</i>						
Root	ND	ND	2.56 ± 0.52	5.99 ± 1.06	0.20 ± 0.03	8.75 ± 1.61
<i>R. woermanniana</i>						
Leaf	ND	ND	ND	ND	ND	ND
Stem and branch	ND	ND	ND	ND	ND	ND

Legend: 1: 2-Hydroxy-2-methylbutyl glucosinolate (glucocleomin), 2: 4-hydroxybenzyl glucosinolate (glucosinalbin), 3: benzyl glucosinolate (DS glucotropaeolin), 4: 4-methoxybenzyl glucosinolate (DS glucoaubrietin), 5: 3-methoxybenzyl glucosinolate (DS glucolimnanthin).

No GL was detected in the leaf and stem of *D. laciniata* or in the leaf and stem-branch of *R. woermanniana*. This could be paralleled to the fact that these species are odorless (Raponda-Walker and Sillans, 1995). Additionally, no GL was detected in the leaf and stem of *D. euryodes* whereas 2-hydroxy-2-methylbutyl GL (glucocleomin, 1) was identified for the first time as the only GL in the cork of this species (Figure 5.2).

5.3.1 Glucosinolates in *Drypetes gossweileri*

The results of the investigations showed that 4-hydroxybenzyl- (glucosinalbin, 12.5%, 2) and benzyl GL (glucotropaeolin, 87.5%, 3) are present in the bark of *D. gossweileri*. Furthermore, 2 was the only GL found in the seeds of *D. gossweileri*. The unusual high quantity of 2 (171.14 $\mu\text{mol/g}$ dry weight) (Table 5.2) in this plant is indicative that *D. gossweileri* represents a sound novel source of this GL. Our investigations confirmed the presence of 3 in the cork of *D. gossweileri*, as surmised by the detection of benzyl ITC in the essential oil obtained from the plant bark (Eyele Mvé-Mba et al., 1997; Voundi et al., 2015). However, we were able to identify 2 as a minor GL in the bark, whereas no previous study mentioned the presence of 4-hydroxybenzyl ITC in *D. gossweileri* essential oil. This can be explained by the fact that this ITC, resulting from the degradation of 2, is unstable in aqueous media, producing 4-hydroxybenzyl alcohol under release of a thiocyanate ion (Borek and Morra 2005). Interestingly, the smell of the bark of *D. gossweileri* was reported to be very similar to the smell of *Pentadiplandra brazzeana* Baill. root (family Pentadiplandraceae, order Brassicales) and described as a particular mixture of horseradish and methyl salicylate (Bouquet, 1969). This similarity could be attributed partly to the presence of 3, which is prone to undergo degradation into benzyl ITC in both plants.

5.3.2 Glucosinolates in *Rinorea subintegrifolia*

The HPLC profile of *R. subintegrifolia* root revealed the presence of three GLs, the major being 4-methoxybenzyl GL (glucoaubrietin, 68.5%, 4) followed by 3 (29.2%), and 3-methoxybenzyl GL (glucolimnanthin, 2.3%, 5). Our investigations confirmed the presence of 3 and 4 in the root of *R. subintegrifolia* hypothesized from the detection of benzyl- and 4-methoxybenzyl ITCs in the essential oil of the root by one of us (Agnaniet et al., 2003). We also have been able to identify 5 as a minor GL in the root whereas no previous study ever mentioned the presence of 3-methoxybenzyl ITC in *R. subintegrifolia* root essential oil. Our GL profile based on DS-GL analysis does not fit previous results regarding the composition of the essential oil from the root. In fact, the essential oil was constituted of benzyl ITC (1.4–29%), benzyl cyanide (64–87.7%), 4-methoxybenzyl ITC (0.6–0.8%), and 4-methoxybenzyl alcohol (0.4–0.5%)

(Agnaniet et al., 2003). This apparent discrepancy can be explained by the high instability of arylaliphatic ITCs under hydrodistillation conditions (De Nicola et al., 2013). Genetic and environmental factors may also account for the observed differences. Interestingly, a similar GL profile was observed for the root of *R. subintegrifolia* and for the root of *P. brazzeana* (De Nicola et al., 2012). Arylaliphatic GLs, biosynthesized from Tyr and Phe, were found in *D. gossweileri* and *R. subintegrifolia* whereas the aliphatic GL 1 was identified in *D. euryodes*. The close GL profiles of *D. gossweileri* and *R. integrifolia* would indicate a close relationship between these two genera. This is supported by a phylogenetic analysis of the order Malpighiales which showed that Putranjivaceae and Violaceae are grouped in the same clade (Tokuoka and Tobe, 2006).

5.4 Conclusions

The probing of the presence of GLs in plants of the order Malpighiales (*D. euryodes*, *D. gossweileri*, *D. laciniata*, *R. subintegrifolia* and *R. woermanniana*) growing wild in Gabon enabled the identification and quantification of 5 known GLs. More species in the Violaceae and Putranjivaceae families and other families of the order Malpighiales should be screened in the future for the presence of GLs, to delineate a better overview of the distribution and diversity of GLs in these plant families.

References

Aba Toumnou L, Seck D, Lakouetene DPB, Bolevane Ouantinam SF, Gueye Momar T, Traoré A, Namkosséréna S, Noba K, Sembène M, Syssa-Magalé J-L (2013) Chemical characterization and insecticidal activity of ethyl acetate and dichloromethane extracts of *Drypetes gossweileri* against *Sitophilus zeamais*, *Tribolium castaneum* and *Rhyzopertha dominica*. J Life Sci 7:1030–1040.

Agnaniet H, Mounzeo H, Menut C, Bessiere J-M, Criton M (2003) The essential oils of *Rinorea subintegrifolia* O. Ktze and *Drypetes gossweileri* S. Moore occurring in Gabon. Flavour Fragrance J 18:207–210.

Ata A, Tan DS, Matochko WL, Adesanwo JK (2011) Chemical constituents of *Drypetes gossweileri* and their enzyme inhibitory and anti-fungal activities. Phytochem Lett 4:34–37.

Barillari J, Iori R, Rollin P, Hennion F (2005) Glucosinolates in the subantarctic crucifer Kerguelen cabbage (*Pringlea antiscorbutica*). J Nat Prod 68:234–236.

Borek V and Morra MJ (2005) Ionic thiocyanate (SCN^-) production from 4-hydroxybenzyl glucosinolate contained in *Sinapis alba* seed meal. J Agric Food Chem 53:8650–8654.

Bouquet A. Féticheurs et médecines traditionnelles du Congo (Brazzaville). Mémoires ORSTOM Paris 1969: p. 36.

Brader G, Mikkelsen MD, Halkier BA, Tapio Palva E. 2006. Altering glucosinolate profiles modulates disease resistance in plants. Plant J 46:758–767.

Clarke DB (2010) Glucosinolates, structures and analysis in food. Anal Methods 2:310–325.

De Nicola GR, Montaut S, Rollin P, Nyegue M, Menut C, Iori R, Tatibouët A (2013) Stability of benzylic-type isothiocyanates in hydrodistillation-mimicking conditions. J Agric Food Chem 61:137–142.

De Nicola GR, Nyegue M, Montaut S, Iori R, Menut C, Tatibouët A, Rollin P, Ndoyé C, Amvam Zollo P-H (2012) Profile and quantification of glucosinolates in *Pentadiplandra brazzeana* Baill. *Phytochemistry* 73:51–56.

Dupont MP, Llabrés G, Delaude C, Tchissambou L, Gastmans JP (1997) Sterolic and triterpenoidic constituents of stem bark of *Drypetes gossweileri*. *Planta Med* 63:282–284.

Eyele Mvé-Mba C, Menut C, Bessière JM, Lamaty G, Nzé Ekekang L, Denamganai J (1997) Aromatic plants of tropical Central Africa. XXIX. Benzyl isothiocyanate as major constituent of bark essential oil of *Drypetes gossweileri* S. Moore. *J Essent Oil Res* 9:367–370.

Fannang SV, Kuete V, Djama CM, Dongfack MDJ, Wansi JD, Tillequin F, Seguin E, Chosson E, Wandji J (2011) A new friedelane triterpenoid and saponin with moderate antimicrobial activity from the stems of *Drypetes laciniata*. *Chin Chem Lett* 22:171–174.

Ijah UJJ, Oyebanji FO (2003) Effects of tannins and polyphenols of some medicinal plants on bacterial agents of urinary tract infections. *Global J Pure Appl Sci* 9:193–198.

Lekana-Douki JB, Bongui JB, Oyegue Liabagui SL, Zang Edou SE, Zatra R, Bisvigou u, Druilhe P, Lebibi J, Toure Ndouo FS, Kombila M (2011) *In vitro* antiplasmodial activity and cytotoxicity of nine plants traditionally used in Gabon. *J Ethnopharmacol* 133:1103–1108.

Leoni O, Iori R, Haddoum T, Marlier M, Wathelet J-P, Rollin P, Palmieri S (1998) Approach to the use of immobilized sulfatase for analytical purposes and for the production of desulfo-glucosinolates. *Ind Crops Prod* 7:335–343.

Mithen RF, Dekker M, Verkerk R, Rabot S, Johnson It. 2000. The nutritional significance, biosynthesis and bioavailability of glucosinolates in human foods. *J Sci Food Agric* 80:967–984.

Ngouela S, Ngoupayo J, NOUNGOUÉ DT, Tsamo E, Connolly JD (2003) Gossweilone: a new podocarpane derivative from the stem bark of *Drypetes gossweileri* (Euphorbiaceae). Bull Chem Soc Ethiop 17:181–184.

Ngouana V, Tsouh Fokou PV, Saha Foudjo Bu, Ngouela SA, Fekam Boyom F, Amvam Zollo PH (2011) Antifungal activity and acute toxicity of stem bark extracts of *Drypetes gossweileri* S. Moore – Euphorbiaceae from Cameroon. Afr J Tradit Complementary Altern Med 8:328–333.

Raponda-Walker A and Sillans R. Les plantes utiles du Gabon. Sepia ed. Libreville: Fondation Raponda-Walker, Centre Culturel Français de Libreville 1995.

Schmelzer GC, Gurib-Fakim A. Medicinal plants. Wageningen: Kluwer Publishers 2008: pp 233–236.

Tessier AM and Paris RR (1978) Sur des Euphorbiacées toxiques africaines à Cucurbitacines [Study of some African toxic Euphorbiaceae containing cucurbitacins]. Toxicol Eur Res 1:329–336.

Tokuoka T (2008) Molecular phylogenetic analysis of Violaceae (Malpighiales) based on plastid and nuclear DNA sequences. J Plant Res 121:253–260.

Tokuoka T and Tobe H (2006) Phylogenetic analyses of Malpighiales using plastid and nuclear DNA sequences, with particular reference to the embryology of Euphorbiaceae sens. str. J Plant Res 119:599–616.

Voundi SO, Nyegue M, Lazar I, Raducanu D, Ndoye FF, Stamate M, Etoa F-X (2015) Effect of essential oils on germination and growth of some pathogenic and spoilage spore-forming bacteria. Foodborne Pathog Dis 12:551–559.

CHAPTER SIX

Isatis canescens is a rich source of glucobrassicin and other health-promoting compounds

Contents

Summary

- 6.1** Introduction
- 6.2** Experimental
 - 6.2.1** Plant materials and sample preparation
 - 6.2.2** Determination of glucosinolate content
 - 6.2.3** Extraction and purification of glucobrassicin
 - 6.2.4** Determination of total phenol and flavonoid content
 - 6.2.5** Oxygen radical absorbance capacity assay
 - 6.2.6** Statistical analysis
- 6.3** Results and discussion
 - 6.3.1** Glucosinolate content
 - 6.3.2** Purification of glucobrassicin
 - 6.3.3** Total phenol, flavonoid content and antioxidant activity
- 6.4** Conclusion

References

Keywords

Isatis; glucosinolate; glucobrassicin; ORAC; phenol; flavonoid; chemoprevention

Summary

Glucobrassicin (GBS), a glucosinolate contained in many brassica vegetables, is the precursor of chemopreventive compounds such as indole-3-carbinol. Large amounts of GBS would be needed to perform studies aimed at elucidating its role in the diet. This study was mainly undertaken to evaluate the flower buds of *Isatis canescens* as a source for GBS purification. To investigate the health-promoting potential of this species, glucosinolate, phenol and flavonoid content as well as the whole antioxidant capacity were also determined. Flower bud samples were collected in four localities around Mount Etna in Sicily, Italy, where *I. canescens* is widespread, as they are locally traditionally eaten. *I. canescens* flower buds displayed high GBS concentrations, up to 60 $\mu\text{mol g}^{-1}$ dry weight. The purification method consisted of two chromatographic steps, which made it possible to obtain GBS with a purity of 92–95%, with a yield of 21 g Kg^{-1} . The total glucosinolates, phenols, flavonoids and antioxidant activity were considerable, with the southern locality showing the highest concentrations for all the phytochemicals. *I. canescens* flower buds represent a naturally rich source of GBS, at a level suitable for its purification. Furthermore, flower bud consumption could provide an intake of health-promoting compounds, with possible antioxidant and chemopreventive properties.

6.1 Introduction

Glucobrassicin (GBS), or 3-indolylmethyl glucosinolate (GL), a secondary metabolite contained in many Brassicaceae plants (Fahey et al., 2001) is the natural precursor of recognized anti-cancer and chemopreventive agents, such as indole-3-carbinol and 3,3'-diindolylmethane. These compounds have been widely investigated and have been shown to suppress the proliferation of various cancer cell lines, such as those of breast, colon, prostate and endometrium (Weng et al., 2008). Indole-3-carbinol and 3,3'-diindolylmethane are generated after hydrolysis of GBS, catalyzed by the plant endogenous myrosinase (β -thioglucoside glucohydrolase, EC 3.2.1.147; MYR), following tissue disruption (chewing, cutting or processing the vegetable) or by enzymatic activity of the intestinal microflora (Jeffery and Jarrel, 2001). GBS hydrolysis gives firstly an unstable isothiocyanate (ITC) which is spontaneously transformed into indole-3-carbinol (Figure 6.1) and, in an acidic environment, the latter generates a series of biologically active oligomeric products including 3,3'-diindolylmethane (Agerbirk et al., 2009).

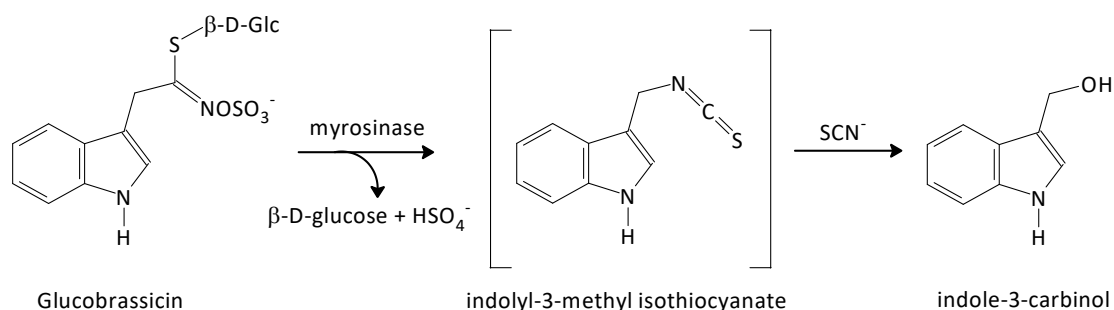


Figure 6.1 Myrosinase-catalyzed hydrolysis reaction of glucobrassicin.

GBS is also the most abundant GL ingested by the consumption of *Brassica* vegetables, such as Brussels sprouts, broccoli and cauliflower (Steinbrecher and Linseisen, 2009), whose high intake has been associated with a reduced risk for developing cancer as shown by several epidemiological studies (Verhoeven et al., 1996; Higdon et al., 2007; Herr and Buchler, 2010). This effect is mainly attributed to the ability of ITC to induce detoxification enzymes (Keum et al., 2005; Valgimigli and Iori, 2005). Recently, a possible synergizing role for indole GLs, as GBS, has been suggested (Zhu et al., 2010). For these reasons, the role of GBS in the diet, as

well as its potential as a chemopreventive compound, merits in-depth investigation, but research is slowed down by the unavailability of the pure compound in suitable amounts, since the organic synthesis of GBS is difficult and expensive (Cassel et al., 1998). A previous study indicated a northern Italy accession of woad (*Isatis tinctoria* L.) from Casolavalsenio (Ravenna, Italy) as a valuable source for the purification of GBS (Galletti et al., 2006) far better than broccoli, which instead contains GBS in small amounts and combined with other indole GLs (Ageribirk et al., 1998). However, the purification of GBS from the young leaves of *I. tinctoria* needs a preliminary step to increase its concentration up to a suitable level of at least 1% on a dry weight basis, which can be obtained by repeated mechanical wounding or by treatment with jasmonic acid (Galletti et al., 2006). Both these treatments are effective, but they are time consuming and/or expensive, and the search for naturally rich sources of GBS is therefore still of great interest to allow the purification of the compound on the gram-scale and at low cost. In this perspective, attention has been focused on *I. canescens* DC., which tends to replace *I. tinctoria* in the south of Italy and in Sicily (Pignatti, 1982; Guarino et al. 2000). *I. canescens* is an herbaceous biennial or, according to some (Strobl, 1885), a perennial hemicryptophyte, very similar to *I. tinctoria* but characterized by densely tomentose siliqua (Pignatti, 1982). Some botanists actually consider *I. canescens* as a subspecies of *I. tinctoria* (Greuter and Raus, 1986). An interesting characteristic of *I. canescens* is the traditional local use as food, unlike *I. tinctoria*, which is not considered as an edible green worldwide. In the region of Mount Etna, the largest active volcano in Europe on the north-eastern coast of Sicily, Italy, rural people are accustomed, in late winter, to collecting the not yet flowered tops of the wild plants of the *I. canescens* sub-species, which are abundant in the countryside, and to eat them after cooking, for their slightly bitter taste (Branca, 1991). Since the inflorescences generally represent the organ with maximum GL accumulation, after seeds (Brown et al., 2003), the main objective of the present study was to determine the GL content in different samples of *I. canescens* flower buds, collected over 2 years in the Mount Etna area, to evaluate their potential as a source for GBS purification. Because of this traditional consumption of *I. canescens* flower buds, the total phenol and flavonoid content, as well as the antioxidant capacity, tested by the oxygen radical absorbance capacity (ORAC) assay, were also determined, to complete their profile as health-promoting compounds (Manchali et al., 2012).

6.2 Experimental

6.2.1 Plant materials and sample preparation

In March-April 2007 and 2008 large samples [about 1 Kg fresh weight (FW)] of flower buds of wild populations of *I. canescens* were collected in four localities around Mount Etna in Sicily, Italy, at different altitudes and slopes: Linguaglossa at 550 m a.s.l. on the northern slope, Pedara at 700 m a.s.l. on the southern slope, S. Alfio at 870 m a.s.l. on the eastern slope and Maletto at 960 m a.s.l. on the western slope (Figure 6.2). Samples were stored at -20 °C, then freeze-dried and ground to a fine powder prior to analysis. The botanical identity of the plant material was confirmed by a local botanist, Prof. Gian Pietro Giusso del Galdo from the Department of Biological, Geological and Environmental Science, University of Catania, Italy, and the voucher specimen is deposited at the Botanical garden belonging to the same department under the following denomination: *I. tinctoria* L. ssp. *canescens* (DC.) Arcang., Mascali (CT), 3.IV.2008, Argento, Bagatta, Branca & Galletti, s.n. (CAT). For comparison purposes, samples of flower buds from plants of the Casolavalsenio accession of *I. tinctoria*, cultivated at the CRA-CIN experimental site of Budrio (Bologna, Italy), were collected in April 2008 at the same development stage and stored for analysis as above.

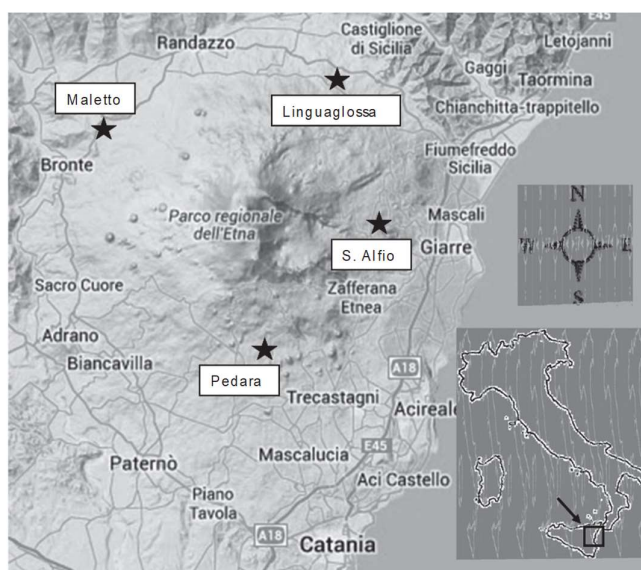


Figure 6.2 Map of *Isatis canescens* sampling localities on the four different slopes of Mount Etna, Sicily, Italy: Linguaglossa (northern), Pedara (southern), Maletto (eastern), S. Alfio (western).

6.2.2 Determination of glucosinolate content

Freeze-dried powder samples of *I. canescens* and *I. tinctoria* flower buds were analyzed for GL content according to the EU official ISO 9167-1 method (EEC, 1990), which is based on the high-performance liquid chromatography (HPLC) analysis of desulfo-GL, with some modifications (Wathelet et al., 2004). Each sample (250 mg) was extracted by adding boiling 70% EtOH (5 mL) with the addition of a standard solution of sinigrin (2-propenyl GL) as internal standard (200 μ L, 0.038 μ mol L⁻¹). The mixture was homogenized for 5 min at 80 °C using a U-Turrax T25 (IKA-Werke, Staufen, Germany). The residue after centrifugation was extracted again with the same amount of boiling 70% EtOH, and the centrifugation repeated. Supernatants were combined, and each extract was treated as already reported (Galletti et al., 2006). Desulfo-GLs were analyzed using an Agilent 1100 HPLC system (Agilent Technologies, Waldbronn, Germany) equipped with an Inertsil ODS3 column (250 \times 3 mm, 5 μ m), thermostated at 30 °C, and having a diode array as detector. Chromatography was performed at a flow rate of 1 mL min⁻¹, eluting with a gradient of H₂O (A) and CH₃CN (B) following the program: 1 min 1% B; 22 min linear gradient up to 22% B; 3 min linear gradient down to 1% B. Desulfo-GLs were detected by monitoring the absorbance at 229 nm. Identification of the peaks was performed based on retention times and UV spectra of the desulfo-GL standards available in our laboratory, then GL content was quantified considering the amount of the internal standard and the relative proportionality factor values (Clarke, 2010).

6.2.3 Extraction and purification of glucobrassicin

GBS was isolated from *I. canescens* flower buds harvested in the locality of S. Alfio (Catania, Italy) in 2007, following the procedure developed at CRA-CIN and reported in a previous article (Iori et al., 2003), with some modifications. A sample of freeze-dried powder (10 g) was added to 300 mL of boiling methanol 70% (v/v) and homogenized by U-Turrax at medium speed for 15 min at 75 °C. The mixture was centrifuged at 25 900 $\times g$ for 30 min at 4 °C. The solid residue was extracted again, homogenized and centrifuged, as before. The two extracts were pooled and loaded onto an open preparatory column (20 cm \times 2.5 cm i.d.) containing DEAE-Sephadex A-25 (GE Healthcare, Freiburg, Germany) conditioned with 25 mmol L⁻¹

acetate buffer pH 4.2. After loading, the column was washed sequentially with water, a formic acid/2-propanol/water (3/2/5) solution and water again. The column was then eluted stepwise with starting 1 × 150 mL of a 0.2 mol L⁻¹ water solution of potassium sulfate, and sequentially with 1 × 100 mL and 3 × 150 mL of a 0.8 mol L⁻¹ water solution of the same salt. The fractions of collected eluate were then checked by HPLC for GL content, as described before, after salt precipitation with ethanol. The fractions containing GBS were dried using a rotary evaporator at 40 °C under vacuum. Boiling methanol was then added to the solid, up to approximately the initial volume, and the mixture was left at room temperature to allow potassium sulfate salt to settle. After filtration, the methanolic extract was analyzed and concentrated to a few milliliters. The purity of GBS was further improved by gel filtration performed on an XK 16/70 column containing Sephadex LH-20 chromatography media (GE Healthcare), connected to an AKTA fast protein liquid chromatograph system (GE Healthcare). A 500 µL methanolic sample of GBS was loaded onto the column and elution was performed using a mobile phase of ethanol 70% (v/v) at a flow rate of 1.0 mL min⁻¹. After the void volume (approximately 50 mL) was discarded, 4-mL fractions were collected. Individual fractions were analyzed by HPLC and those containing pure GBS were pooled and freeze-dried, after removing the organic solvent by rotary evaporation at 40 °C. Purified GBS was characterized by ¹H and ¹³C NMR spectroscopy in agreement with previous reports (Iori et al., 2003). The purity of GBS was determined by HPLC analysis of the desulfo-derivative, according to ISO 9176-1 method, as reported above.

6.2.4 Determination of total phenol and flavonoid content

Freeze-dried powder samples (250 mg) of *I. canescens* flower buds were extracted in 70% acetone (5 mL). Total phenolic content was determined according to the Folin-Ciocalteu method (Singleton, 1999). The values are expressed as µmol of gallic acid equivalents (GAE) g⁻¹ dry weight (DW). The Folin-Ciocalteu reagent was purchased from Sigma-Aldrich (St. Louis, MO, USA). Flavonoids were determined by the method of Liu et al. (2002) and the amount of total flavonoids is expressed as mg of (+)-catechin equivalents (CE) g⁻¹ DW.

6.2.5 Oxygen radical absorbance capacity assay

The antioxidant activity of *I. canescens* extracts was determined by the hydrophilic ORAC assay (oxygen radical absorbance capacity) (Ninfali et al., 2009). The assay was carried out using a Fluostar Optima plate reader fluorimeter (BMG Labtech, Offenburgh, Germany) equipped with a temperature-controlled incubation chamber and an automatic injection pump. Incubator temperature was set at 37 °C. The reaction mixture was the following: 200 µL of 0.096 µmol L⁻¹ fluorescein sodium salt (Sigma-Aldrich) in 0.075 mol L⁻¹ sodium phosphate buffer (pH 7.0), and 20 µL of sample or 6-hydroxy-2,5,7,8-tetramethyl-2-carboxylic acid (Trolox; Sigma-Aldrich) as standard. A calibration curve was made each time with the standard Trolox (100, 50, 25 µmol L⁻¹). The blank was 0.075 sodium phosphate buffer (pH 7.0). The reaction was initiated with 80 µL of 0.33 mol L⁻¹ 2,2'-azobis(2-amidinopropane) dihydrochloride (Polysciences, Warrington, PA, USA). Fluorescence was read at 485 nm excitation and 520 nm emission until complete extinction. ORAC values are expressed as µmol Trolox equivalents (TE) g⁻¹ DW. The TEAC assay (Trolox equivalent antioxidant capacity), which utilizes the 2,2'-azino-bis(3-ethylbenzothiazoline-6-sulfonic acid) (ABTS) radical scavenging method, was also used for a comparison with the ORAC assay, following the procedure described by Re et al. (1999), using Trolox as a standard.

6.2.6 Statistical analysis

Results were expressed as the mean ± standard deviation (SD) of three independent assays. Data were submitted to analysis of variance by Statgraphics plus 5.1 statistical program (StatPoint Inc., Herndon, Virginia) and means were separated by least significance difference (LSD) test at $P \leq 0.05$ significance level.

6.3 Results and discussion

6.3.1 Glucosinolate content

Figure 6.3 shows a typical HPLC profile obtained during the analysis of GL in *I. canescens* flower buds. In the profile, besides the internal standard (peak 1), two main peaks are present:

peak 2, desulfo-GNA, corresponding to gluconapin (3-butenyl GL, GNA) and desulfo-GBS (peak 3), corresponding to GBS in the crude extract of flower buds.

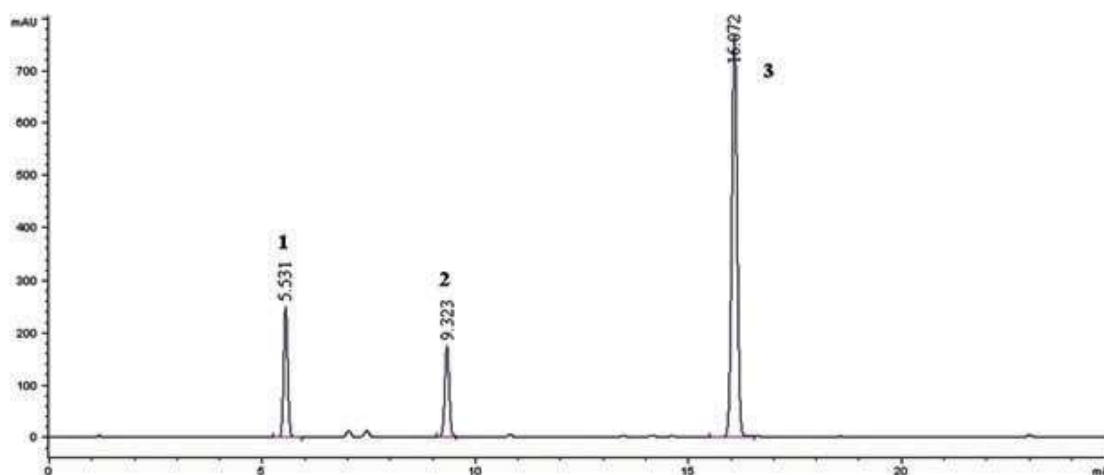


Figure 6.3 HPLC chromatogram showing the desulfo-glucosinolate profile of a sample of *Isatis canescens* flower buds. Peak numbers are identified as follows: (1) desulfo-sinigrin (internal standard); (2) desulfo-gluconapin; (3) desulfo-glucobrassicin.

Values ranged from about 30 up to 69 $\mu\text{mol g}^{-1}$ DW for both GNA and GBS, depending on the collecting site and year (Table 6.1). In comparison, *I. tinctoria* flower buds, cultivated at the experimental site of CRA-CIN, contained lower levels of GBS ($12.4 \pm 0.7 \mu\text{mol g}^{-1}$ DW) and $38.2 \pm \mu\text{mol g}^{-1}$ DW of GNA. Unlike *I. canescens*, *I. tinctoria* samples also contained *epi*-progoitrin ((2*S*)-2-hydroxy-3-butenyl GL) ($13.6 \pm 0.4 \mu\text{mol g}^{-1}$ DW).

Table 6.1 Gluconapin, glucobrassicin and total glucosinolate content ($\mu\text{mol g}^{-1}$ DW) of floral buds of *Isatis canescens* sampled in four Mount Etna localities (Sicily, Italy) in 2007 and 2008

Locality	Gluconapin		Glucobrassicin		Total glucosinolates	
	2007	2008	2007	2008	2007	2008
Linguaglossa	45.4 ± 2.9 ^a	47.2 ± 4.0 ^c	34.1 ± 3.0 ^c	35.3 ± 1.7 ^b	79.5 ± 5.9 ^c	82.5 ± 5.7 ^d
Pedara	34.6 ± 1.9 ^c	40.8 ± 2.7 ^d	68.7 ± 6.0 ^a	60.9 ± 0.5 ^a	103.3 ± 7.9 ^a	101.6 ± 2.4 ^a
S. Alfio	33.5 ± 2.1 ^c	55.4 ± 1.3 ^b	68.8 ± 3.3 ^a	35.7 ± 0.3 ^b	102.3 ± 5.2 ^{ab}	91.2 ± 1.4 ^c
Maletto	43.4 ± 3.3 ^b	65.1 ± 4.6 ^a	56.1 ± 6.4 ^b	33.1 ± 2.6 ^b	99.5 ± 9.6 ^b	98.2 ± 2.0 ^b
Mean	39.2 ± 6.1	52.1 ± 10.5	56.9 ± 16.3	41.3 ± 13.1	96.1 ± 11.2	93.4 ± 8.4

Means in columns with a common letter are not significantly different for $P \leq 0.05$ after ANOVA (LSD test). Results are expressed as means ± SD for triplicates.

To identify the richest source of GBS, samples of *I. canescens* from the four sites in the Mount Etna area were compared over 2 years. In both the investigated years, the Pedara samples (700 m a.s.l., southern slope) showed the highest GBS content (over 60 $\mu\text{mol g}^{-1}$ DW), while the Linguaglossa samples (550 m a.s.l., northern slope) showed the lowest values (around 35 $\mu\text{mol g}^{-1}$ DW) (Table 6.1). S. Alfio and Maletto samples showed higher values in 2007 than in 2008, suggesting an effect of the environmental factors, as confirmed by the analysis of variance, which highlighted a significant year \times locality interaction. Similarly, a significant year \times locality interaction was found both for GNA and total GLs. In general, a high content of GBS corresponded to a lower amount of GNA and vice versa (Table 6.1). A possible explanation of this occurrence could be that the biosynthesis of one type of GL down-regulates the synthesis of the other type of GL. GBS derives from tryptophan, while GNA derives from methionine. A reciprocal negative control of methionine and tryptophan derived GL pathways was already demonstrated in *Arabidopsis thaliana* (Gigolashvili et al., 2009). The total GL values showed the same behavior as GBS: in both years the Pedara samples showed the highest GL content (over 100 $\mu\text{mol g}^{-1}$ DW), while the Linguaglossa samples showed the lowest but still remarkable amount (around 80 $\mu\text{mol g}^{-1}$ DW) (Table 6.1). GL synthesis is regulated by genetic and environmental factors, but the latter are reported to exert a stronger effect than the former on indole GLs (Brown et al., 2002). High temperature, light intensity, water stress and long days caused a total and indole GL content increase in several cultivars of *Brassica oleracea* (Charron et al., 2005). Therefore, the highest values found on the southern slope (Pedara) of the Mount Etna region could partly depend on the occurrence of favorable environmental conditions. The climate in the Mount Etna area varies greatly with the variation of altitude and slope. Rainfall is intense, with more than 1000 mm per year. The hilly area is dominated by a sub-humid climate (meso-Mediterranean), while in the mountain area a humid climate (supra-Mediterranean) prevails (Brullo et al., 1996). Figure 6.4 reports the thermo-pluviometric monthly data recorded in 2007 at Pedara, showing the occurrence of mild temperatures (8-19 °C) and abundant rainfall during winter, before the collection time. The thermo-pluviometric trends of the other sampling localities were similar, and the longer sun exposure of Pedara could therefore have played a major role in favoring GL biosynthesis.

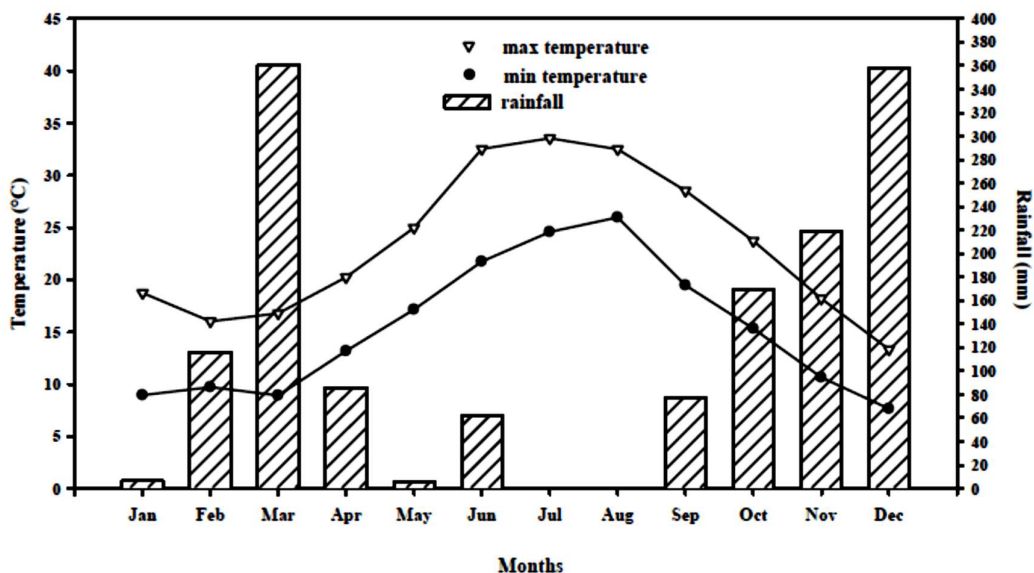


Figure 6.4 Monthly rainfall, minimum and maximum temperatures recorded at the collection site of Pedara, in the Mount Etna area, Italy, in 2007.

From a dietary point of view, since *I. canescens* flower buds are traditionally consumed in Sicily, it is worth comparing their GL content to that of other brassica vegetables. Interestingly, the total GL content in *I. canescens* flower buds is considerably higher than those generally reported for other commonly eaten brassica (Table 6.2). Looking at the GBS maximum value of *I. canescens* flower buds, it was at least 3.5-fold higher than those of the other brassica vegetables (Table 6.2).

Species	Total glucosinolate range	Glucobrassicin maximum content	Reference
<i>Isatis canescens</i>	80 – 103	69	–
Broccoli	19 – 25	8	Charron et al. (2005)
Brussels sprouts	15 – 36	19	Charron et al. (2005)
Turnip greens	8 – 74	1	Padilla et al. (2007)
Cauliflower	24 – 33 ^a	15 ^a	Volden et al. (2009)
Cabbage	9 – 41	3	Kushad et al. (1999)

^a Assuming 10% dry weight (DW).

Notably, the GNA mean value of *I. canescens* samples is also higher than that of the most commonly consumed brassica cultivars (0-7 $\mu\text{mol g}^{-1}$ DW) (Kushad et al., 1999), whereas some accessions of turnip greens showed similar GNA levels (Padilla et al., 2007).

The health promoting potential of *I. canescens* depends on GBS hydrolysis by MYR, with formation of the unstable 3-indolylmethyl ITC and its spontaneous conversion into indole-3-carbinol (Figure 6.1), one of the most studied compounds for its chemopreventive and anti-cancer properties (Weng et al., 2008). The presence of MYR activity in *I. canescens* samples was therefore demonstrated by means of a gas chromatography assay which revealed the presence of 3-butenyl ITC derived from GNA (data not shown).

6.3.2 Purification of glucobrassicin

The remarkable GBS values found in *I. canescens* flower buds demonstrated that they represent a naturally rich source of this GL and prompted us to set up its purification which was achieved by means of two chromatographic steps, the first on Sephadex DEAE-A25 and the second on Sephadex LH-20. The presence of GNA in the *I. canescens* samples did not represent a drawback for the purification of GBS. In fact, GNA and GBS showed a different affinity for the Sephadex DEAE-A25 resin, GBS being more adsorbed because of the indole structure of its aglycon side chain (Agerbirk et al., 1998). Indeed, the method of elution by fractions made it possible to isolate GBS by using a solution of potassium sulfate with two different concentrations. The elution carried out with 0.2 mol L⁻¹ of the salt made it possible to recover GNA, whereas GBS was selectively isolated by using 0.8 mol L⁻¹ of potassium sulfate solution (Table 6.3).

Table 6.3 Distribution of gluconapin (GNA) and glucobrassicin (GBS) among the anion exchange chromatographic fractions				
Fraction	K ₂ SO ₄ eluent (mol L ⁻¹)	Volume (mL)	GNA (μmol)	GBS (μmol)
I	0.2	150	290.7	6.3
II	0.8	100	4	53.6
III	0.8	150	–	280.9
IV	0.8	150	–	227.5
V	0.8	150	–	29.1

Fraction II was discarded because of the presence of GNA, whereas fractions III and IV, containing about 85% of GBS, were pooled and further processed. Fraction V was discarded because of the negligible amount of GBS content. GBS collected after anion exchange was refined with gel filtration by exploiting the dual hydrophilic and lipophilic nature of the Sephadex LH-20 media. Finally, the purity of freeze-dried GBS (potassium salt) (212 mg) estimated by HPLC analysis of the desulfo-derivative was 99% (peak purity HPLC) and 92–95% on weight basis, for a yield of about 21 g Kg⁻¹ on the starting vegetal material. Based on this yield, a gram-scale production of GBS is thus achievable simply starting from a larger quantity of *I. canescens* flower buds.

6.3.3 Total phenol, flavonoid content and antioxidant activity

To better define the health-promoting profile of *I. canescens* flower buds, the total phenol and flavonoid content as well as the antioxidant activity were evaluated.

As for GLs, a significant year × locality interaction was found both for phenol and flavonoid content. Total phenol content mean values ranged from 22 up to 27 mg GAE g⁻¹ DW, while flavonoid content ranged from 5 up to 8 mg CE g⁻¹ DW (Table 6.4). Significant differences were recorded for both classes of compounds among localities, especially in 2007, even if the range of variation was not as marked as observed for GLs. In general, the samples collected at Pedara tended to display the highest values.

Table 6.4 Total phenol and flavonoid content of floral buds of *Isatis canescens* sampled in four Mount Etna localities (Sicily, Italy) in 2007 and 2008.

Locality	Total phenols (mg GAE g ⁻¹ DW)		Flavonoids (mg CE g ⁻¹ DW)	
	2007	2008	2007	2008
Linguaglossa	24.1 ± 2.3 ^C	26.7 ± 1.5 ^a	7.0 ± 0.2 ^a	7.0 ± 0.1 ^b
Pedara	24.7 ± 2.2 ^b	26.4 ± 0.8 ^a	7.0 ± 0.1 ^a	8.3 ± 0.3 ^a
S. Alfio	26.5 ± 2.2 ^a	25.1 ± 1.2 ^a	6.5 ± 0.1 ^b	7.1 ± 0.2 ^b
Maletto	23.3 ± 1.9 ^d	22.3 ± 0.1 ^b	5.3 ± 0.1 ^c	7.2 ± 0.0 ^b
Mean	24.7 ± 1.4	25.1 ± 2.0	6.5 ± 0.8	7.4 ± 0.6

Results are expressed as means ± SD for triplicates.

Means in columns with common letters are not significantly different for $P \leq 0.05$ after ANOVA (LSD test).

CE, catechinequivalents; DW, dry weight; GAE, gallic acid equivalents.

The total phenol values found for flower buds are two- to six-fold higher than those generally reported for other common edible brassica vegetables (Heimler et al., 2006; Volden et al., 2009). Values similar to our data were reported for broccoli, cabbage and cauliflower (Wu et al., 2004; Sultana et al., 2008). The large phenol quantity measured was explained in terms of high solar radiation received by the plants grown in the mountain regions of Pakistan (Sultana et al., 2008) Thus, the considerable phenol content found in *I. canescens* flower buds could be related to the strong solar radiation occurring on the Mount Etna slopes. Similarly to phenol, the flavonoid content, ranging from 5.3 up to 8.3 mg CE g⁻¹ DW (Table 6.4), was also found to be similar to the maximum values reported for broccoli or red cabbage, which were 6.7 and 9.7 mg CE g⁻¹ DW, respectively (Heimler et al., 2006; Chun et al., 2004), or even greater than those recorded for other common brassica vegetables (Ninfali et al., 2005). About the antioxidant activity measured by the ORAC assay, the mean values were stable over the years, thus only the mean values over the years were reported (Table 6.5). Statistically significant differences were only highlighted among the localities, with Pedara samples showing the maximum value (326 µmol TE g⁻¹ DW), as previously observed for total GLs and GBS. The mean value of about 300 µmol TE g⁻¹ DW found in *I. canescens* (Table 6.5) is among the highest reported for other brassica vegetables, whose ORAC values range from 42 up to 318 µmol TE g⁻¹ DW (Volden et al., 2009; Wu et al., 2004; Ninfali et al., 2005; Kurlich et al., 2002). In addition, the ORAC/phenol ratio was calculated since it is considered a valuable parameter to describe the antioxidant quality of the phenolic compounds and the synergy among them (Ninfali et al., 2009). The ORAC/phenol ratio in our samples ranged from 10 up to 13 (Table 6.5), being either higher than those reported for other common brassica vegetables (under 10), and in the highest slot of many fruit and vegetable values (from 5 up to 15) (Wu et al., 2004). To obtain a better insight of the antioxidant quality, the ABTS radical scavenging method was considered for standardization. By this way the relative differences found among the antioxidant capacity values of floral buds in the four Mount Etna localities were maintained when expressed in TEAC units (Table 6.5).

Table 6.5 Antioxidant activity reported as ORAC, ORAC/phenols ratio and TEAC of floral buds of *Isatis canescens* sampled in four Mount Etna localities (Sicily, Italy) in 2007 and 2008

Locality	ORAC ($\mu\text{mol TE g}^{-1}\text{ DW}$)	ORAC/ phenols	TEAC ($\mu\text{mol TE g}^{-1}\text{ DW}$)
Linguaglossa	300 \pm 25 ^{ab}	11.9 \pm 0.6 ^{ab}	562 \pm 44 ^{ab}
Pedara	326 \pm 4 ^a	12.8 \pm 0.8 ^a	610 \pm 47 ^a
S. Alfio	276 \pm 7 ^b	10.8 \pm 0.7 ^b	516 \pm 32 ^b
Maletto	282 \pm 4 ^b	12.4 \pm 0.1 ^a	528 \pm 43 ^b

Results are expressed as means \pm SD (triplicates \times 2 years). Means in columns with common letters are not significantly differ for $P \leq 0.05$ after ANOVA (LSD test). DW, dry weight; ORAC, oxygen radical absorbance capacity; TE, Trolox equivalents; TEAC, Trolox equivalent antioxidant capacity.

6.4 Conclusion

The results of this study highlighted that *I. canescens* flower buds represent a remarkable source for GBS, whose purification can be easily performed at gram scale following the chromatographic procedure described. The availability of this pure compound at low cost could allow studies and clinical trials to be performed on this molecule, which is normally present in brassica vegetables as part of the human diet, and on its derivatives, elucidating their chemopreventive role. As *I. canescens* flower buds could also represent a rich source of dietary GLs and antioxidants, with possible health-promoting effects, mild cooking methods, like steaming, able to preserve the actual bioavailability of these heat-labile compounds, should be evaluated in future studies. Since the availability of the fresh flower buds is restricted to a relatively short period of the year, dried standardized extracts could be produced and proposed as dietary supplements, once the positive role of these phytochemicals, particularly GBS, for human health had been clearly established. Breeding and agronomic research would be needed to explore the variability among *I. canescens* populations, to reproduce genotypes with stable characters and to establish appropriate cultivation protocols. The ruderal habit of *I. canescens* and its invasive behavior suggest the possibility of easily cultivating it even in marginal areas under mild climates.

References

Agerbirk N, De Vos M, Kim JH, Jander G (2009) Indole glucosinolate breakdown and its biological effects. *Phytochem Rev* 8:101-120.

Agerbirk N, Olsen CE, Sørensen H (1998) Initial and final products, nitriles, and ascorbigens produced in myrosinase-catalyzed hydrolysis of indole glucosinolates. *J Agric Food Chem* 46:1563-1571.

Branca F (1991) Studi su specie spontanee di interesse alimentare. PhD thesis, Università degli Studi di Catania, Italy.

Brown PD, Tokuhisa JG, Reichelt M, Gershenzon J (2003) Variation of glucosinolate accumulation among different organs and developmental stages of *Arabidopsis thaliana*. *Phytochemistry* 62:471-481.

Brown AF, Yousef GG, Jeffery EH, Klein BP, Wallig MA, Kushad MM, Juvik JA (2002) Glucosinolate profile in broccoli: Variation in levels and implications in breeding for cancer chemoprotection. *J Am Soc Hort Sci* 127:807-813.

Brullo S, Scelsi F, Siracusa G, Spampinato G (1996) Caratteristiche bioclimatiche della Sicilia. *Giornale Botanico Italiano* 130:177-185.

Cassel S, Casenave B, Déléris G, Latxague L, Rollin P (1998) Exploring an alternative approach to the synthesis of arylalkyl and indolylmethyl glucosinolate. *Tetrahedron* 54:8515-8524.

Charron CS, Saxton AM, Sams CE (2005) Relationship of climate and genotype to seasonal variation in the glucosinolate – myrosinase system. I. Glucosinolate content in ten cultivars of *Brassica oleracea* grown in fall and spring seasons. *J Sci Food Agric* 85:671-681.

Chun OK, Smith N, Sakagawa A, Lee CY (2004) Antioxidant properties of raw and processed cabbages. *Int J Food Sci Nutr* 55:191-199.

- Clarke DB (2010) Glucosinolates, structures and analysis in food. *Anal Methods* 2:310-325.
- EEC Regulation No 1864/90, Enclosure VIII (1990). Oilseeds – determination of glucosinolates – high performance liquid chromatography. *Off J Eur Commun* L170:27-34.
- Fahey JW, Zalcmann AT, Talalay P (2001) The chemical diversity and distribution of glucosinolates and isothiocyanates among plants. *Phytochemistry* 56:5-51.
- Galletti S, Barillari J, Iori R, Venturi G (2006) Glucobrassicin enhancement in woad (*Isatis tinctoria*) leaves by chemical and physical treatments. *J Sci Food Agric* 86:1833-1838.
- Gigolashvili T, Berger B, Flugge UI (2009) Specific and coordinated control of indolic and aliphatic glucosinolate biosynthesis by R2R3-MYB transcription factors in *Arabidopsis thaliana*. *Phytochem Rev* 8:3-13.
- Greuter W and Raus T (1986) Med-Checklist Notulae, 12. *Wildenowia* 15:413-432.
- Guarino C, Casoria P, Menale B (2000) Cultivation and use of *Isatis tinctoria* L. (Brassicaceae) in southern Italy. *Econ Bot* 54:395-400.
- Heimler D, Vignolini P, Dini MG, Vincieri FF, Romani A (2006) Antiradical activity and polyphenol composition of local Brassicaceae edible varieties. *Food Chem* 99:464-469.
- Herr I and Buchler MW (2010) Dietary constituents of broccoli and other cruciferous vegetables: Implications for prevention and therapy of cancer. *Cancer Treat Rev* 36:377-383.
- Higdon JV, Delage B, Williams DE, Dashwood RH (2007) Cruciferous vegetables and human cancer risk: epidemiologic evidence and mechanistic basis. *Pharmacol Res* 55:224-236.
- Iori R, Barillari J, Galletti S, Venturi G, Marotti M, Rollin P (2003) Production of glucobrassicin, a phytochemical of major interest, through jasmonic acid treatment of woad (*Isatis tinctoria* L.) leaves. *Agroindustria* 2:69-72.

Jeffery EH and Jarrel V. Cruciferous vegetables and cancer prevention, in Handbook of Nutraceuticals and Functional Foods, ed. by Wildman REC. CRC Press, Boca Raton, FL, 2001: pp 169-192.

Keum Y-S, Jeong W-S, Kong A-NT (2005) Chemopreventive functions of isothiocyanates. Drug News Perspect 18:445-451.

Kurilich AC, Jeffery EH, Juvik JA, Wallig MA, Klein BP (2002) Antioxidant capacity of different broccoli (*Brassica oleracea*) genotypes using the oxygen radical absorbance capacity (ORAC) assay. J Agric Food Chem 50:5053-5057.

Kushad MM, Brown AF, Kurilich AC (1999) Variation of glucosinolates in vegetable crops of *Brassica oleracea*. J Agric Food Chem 47:1541-1548.

Liu M, Li XQ, Weber C, Lee CY, Brown J, Liu RH (2002) Antioxidant and antiproliferative activities of raspberries. J Agric Food Chem 50:2926-2930.

Manchali S, Chidambara Murthy KN, Patil BS (2012) Crucial facts about health benefits of popular cruciferous vegetables. J Funct Foods 4:94-106.

Ninfali P, Gennari L, Biagiotti E, Cangi F, Mattioli L, Maidecchi A (2009) Improvement in botanical standardization of commercial freeze-dried herbal extracts by using the combination of antioxidant capacity and constituent marker concentrations. J AOAC Int 92:797-805.

Ninfali P, Mea G, Giorgini S, Rocchi M, Bacchiocca M (2005) Antioxidant capacity of vegetables, spices and dressings relevant to nutrition. Br J Nutr 93:257-266.

Padilla G, Cartea ME, Velasco P, de Haro A, Ordás A (2007) Variation of glucosinolates in vegetables crops of *Brassica rapa*. Phytochemistry 68:536-545.

- Pignatti S, Flora d'Italia, Edagricole, Bologna, Italy, 1982 vol 1:p 381.
- Re R, Pellegrini N, Proteggente A, Ananth A, Yang M, Rice-Evans C (1999) Antioxidant activity applying an improved ABTS radical cation decolorization assay. *Free Radical Biol Med* 26:1231-1237.
- Singleton VL, Orthofer R, Lamuela-Raventós RM (1999) Analysis of total phenols and other oxidant substrates and antioxidants by means of Folin–Ciocalteu reagent. *Method Enzymol* 299:152-178.
- Steinbrecher A and Linseisen J (2009) Dietary intake of individual glucosinolates in participants of the EPIC-Heidelberg cohort study. *Ann Nutr Metab* 54:87-96.
- Strobl PG (1885) Flora des Etna. *Österreichische botanische Zeitschrift* 35:97-101.
- Sultana B, Anwar F, Iqbal S (2008) Effect of different cooking methods on the antioxidant activity of some vegetables from Pakistan. *Int J Food Sci Technol* 43:560-567.
- Valgimigli L and Iori R (2009). Antioxidant and pro-oxidant capacities of ITCs. *Environ Mol Mutagen* 50:222-237.
- Verhoeven DT, Goldbohm RA, van Poppel G, Verhagen H, van den Brandt PA (1996) Epidemiological studies on brassica vegetables and cancer risk. *Cancer Epidemiol Biomarkers Prev* 5:733-748.
- Volden J, Borge GIA, Hansen M, Wicklund T, Bengtsson GB (2009) Processing (blanching, boiling, steaming) effects on the content of glucosinolates and antioxidant-related parameters in cauliflower (*Brassica oleracea* L. ssp. *botrytis*). *Food Sci Technol-Leb* 42:63-73.
- Wathelet J-P, Iori R, Leoni O, Rollin P, Quinsac A, Palmieri S (2004) Guidelines for glucosinolate analysis in green tissues used for biofumigation. *Agroindustria* 3:257-266.

Weng J-R, Tsai C-H, Kulp SK, Chen C-S (2008) Indole-3-carbinol as a chemopreventive and anti-cancer agent. *Cancer Lett* 262:153-163.

Wu X, Beecher GR, Holden JM, Haytowitz DB, Gebhardt SE, Prior RL (2004) Lipophilic and hydrophilic antioxidant capacities of common foods in the United States. *J Agric Food Chem* 52:4026-4037.

Zhu N, Soendergaard M, Jeffery EH, Lai RH (2010) The impact of loss of myrosinase on the bioactivity of broccoli products in F344 rats. *J Agric Food Chem* 58:1558-1563.

CHAPTER SEVEN

Moringa oleifera: study of phenolics and glucosinolates by mass spectrometry

Contents

Summary

7.1 Introduction

7.2 Experimental

7.2.1 Materials

7.2.2 Plant material

7.2.3 Extraction and sample preparation

7.2.4 ESI-MS and ESI-MS/MS analysis

7.2.5 HPLC-ESI-MS and HPLC-ESI-MS/MS analyses

7.2.6 Principal component analysis procedure

7.2.7 Calibration and quantification of glucosinolates

7.2.8 Method validation

7.3 Results

7.4 Conclusion

References

Keywords

Moringa oleifera; glucosinolates; PCA; LC-MS; MRM

Summary

Moringa oleifera is a medicinal plant and an excellent dietary source of micronutrients (vitamins and minerals) and health promoting phytochemicals (phenolic compounds, glucosinolates and isothiocyanates). Glucosinolates and isothiocyanates are known to possess anti-carcinogenic and antioxidant effects and have attracted great interest from both toxicological and pharmacological points of view, as they are able to induce phase 2 detoxification enzymes and to inhibit phase 1 activation enzymes. Phenolic compounds possess antioxidant properties and may exert a preventative effect regarding the development of chronic degenerative diseases. The aim of this work was to assess the profile and the level of bioactive compounds in all parts of *M. oleifera* seedlings, by using different MS approaches. First, flow injection electrospray ionization mass spectrometry (FI-ESI-MS) fingerprinting techniques and chemometrics (PCA) were used to achieve the characterization of the different plant organs in terms of profile of phenolic compounds and glucosinolates. Second, LC-MS and LC-MS/MS qualitative and quantitative methods were used for the identification and/or determination of phenolics and glucosinolates in *M. oleifera*.

7.1 Introduction

Moringa oleifera Lam. (synonym: *M. ptreygosperma* Gaertn.) (Moringaceae) is a tree native of India, Pakistan, Bangladesh and Afghanistan, widely distributed in tropical and sub-tropical areas of the world (Manguro et al., 2007; Kashiwada et al., 2012). *Moringa*, the sole genus in the family Moringaceae, consists of 13 species, among which *M. oleifera* is the best known and most widely distributed and naturalized. *M. oleifera*, also called 'Miracle Vegetable', is a multiuse plant used for human nutrition as functional food, animal feeding and for medicinal purposes (Verma et al., 1976). In fact, a wide variety of nutritional and medicinal virtues have been attributed to its roots, bark, leaves, flowers, fruits and seeds. All these parts are used in folk medicine for the treatment of various ailments including the treatment of inflammation and infectious diseases along with cardiovascular, gastrointestinal, hematological and hepatorenal disorders. In addition, extracts of various *Moringa* tissues have been used for anti-bacterial and anti-cancer activity (*M. oleifera* seeds) (Oluduro et al., 2012), anti-inflammatory and hepatoprotective agents (*M. oleifera* fruits and bark) (Cheenpracha et al., 2010), while leaf extracts have been shown to regulate thyroids status and cholesterol levels in rats (Anwar et al., 2004). Recently, this plant has attracted great interest as an important food commodity because of its high nutritional value. Leaves, flowers and green pods are used traditionally as vegetable, whereas the seed can be consumed fresh, fried, roasted or ground to meal. The seed is also the source of a high quality edible oil known as moringa oil, or ben oil, that can be used in several applications such as cooking, cosmetics and as a lubricant. *M. oleifera* is an excellent dietary source of micronutrients, vitamins and minerals, and health-promoting phytochemicals such as glucosinolates (GLs) and phenolic compounds (Mbkay, 2012). The stem bark has also been reported to contain alkaloids (moringinine and moringine) (Sreelatha et al., 2009). In particular, this plant genus contains unusual sugar-substituted hydroxy-aromatic GLs (Bennett et al., 2003; Faizi et al., 1997). *M. oleifera* contains several uncommon members of the GLs family with peculiar characteristics given by the presence in their structure of a second saccharide residue in the aglycon side chain (Smiechowska et al., 2010; Jahangir et al., 2009; Brunelli et al., 2010). The predominant GL in this species is 4-(α -L-rhamnopyranosiloxy)benzyl GL, known as glucomoringin (GMG). Due to its atypical structure, this compound could display biological properties distinctly different from those of other GLs (Brunelli et al., 2010). Since GLs and their derivatives possess different

relevant biological activities, their identification and quantification in plant tissues have become of great importance (Kusznierewicz et al., 2013). Several published indirect methods are based on the determination of their enzymatic volatile breakdown products by GC-MS analysis, but unfortunately some GL breakdown products are unstable in the conditions applied, and they cannot be correctly detected. Therefore, the current tendency is to determine intact GLs or desulfoglucosinolates by more accurate and robust LC-MS methods (Bennett et al., 2004). LC coupled with tandem mass spectrometry (LC-MS/MS) is an important tool that can be used for both qualitative and quantitative analysis, especially in the case of the characterization of GLs composition in less investigated species (Kusznierewicz et al., 2013; Bennett et al., 2004; Maldini et al., 2012).

Phenolics are a large class of secondary metabolites widely distributed in plant kingdom. Previous phytochemical studies on different tissues of *M. oleifera* reported the highest level of phenolic compounds in leaves extracts, mainly flavonoids and caffeic acid derivatives (Bennett et al., 2003). Crypto-chlorogenic acid, caffeoylquinic acids (5- and 3-isomers), isoquercetin and astragalin were detected to be the major compounds isolated and identified in the leaves of *M. oleifera* (Bennett et al., 2003; Vongsak et al., 2013; Manguro and Lemmen, 2007; Kashiwada et al., 2012). Concerning flavonoids, their profiles were found more complex and characterized by flavonol glycosides (kaempferol 3-O-rutinoside, kaempferol 3-O-glucoside, quercetin 3-O-glucoside and rutin). Amaglo et al. (2010) reported leaves as the tissue with the highest and most complex flavonoid contents, while in roots or seeds any phenolic compounds are detected. Phenolics and flavonoids are active antioxidant components in the leaves of *M. oleifera*, responsible also for anti-inflammatory, atherosclerotic and anti-diabetics activities (Sreelatha et al., 2009; Verma et al., 2009; Ndong et al., 2007; Chumark et al., 2008). The aim of the present study was to determine the profile of GLs and phenolics, as well as to assess the GL content in pulp seed, seed coat, leaves and roots of *M. oleifera* 12-day old seedlings. Furthermore, we investigated whether ESI-MS coupled to statistical analysis (principal components analysis (PCA)) could be used as a simple and reliable technique to distinguish extracts from different tissues. Direct infusion ESI-MS offers several advantages since it is a very fast, versatile, reproducible and sensitive technique (Fenn et al. 1989) which requires little or no sample preparation and provides almost instantaneous information. On the other hand, PCA is a chemometric approach that combines mathematical, statistical and computing methods which allows obtaining the maximum

information from chemical data analyses (Hopke, 2003). First, based on ESI-MS and ESI-MS/MS results, the profiles of GLs, along with proanthocyanidins and phenolic compounds, in *M. oleifera* tissues were described. Second, the occurrence and level of GLs were determined in pulp and coat of dried seeds, as well as in roots and leaves of 12-day-old seedlings, by LC-MS/MS analysis and a rapid and sensitive LC-MS/MS (MRM) method.

7.2 Experimental

7.2.1 Materials

Solvents used for extraction, HPLC grade methanol, acetonitrile and formic acid were from Sigma-Aldrich Chemical Company (St Louis, MO). HPLC grade water (18 mΩ) was prepared by using a Millipore (Bedford, MA, USA) Milli-Q purification system. Glucoraphanin (GRA) potassium salt, glucoiberin (GIB) potassium salt, glucotropaeolin (GTL) potassium salt, glucosinalbin (SNB) potassium salt, glucobarbarin (GBB) potassium salt and glucoraphenin (GRE) potassium salt were purchased from PhytoLab GmbH & Co. KG (Vestenbergsgreuth, Germany).

Glucomoringin purification.

GMG was isolated from *M. oleifera* Lam. seed cake powder as described in detail at Chapter ten. GMG was unambiguously characterized by ¹H- and ¹³C-NMR spectrometry, and the purity was assessed by HPLC analysis of the desulfo-derivative according to the ISO9167-1 method (EEC, 1990) yielding GMG with a purity of 99% based on peak area value and 95% on a weight basis.

7.2.2 Plant material

M. oleifera Lam. seeds were kindly provided from Moringa society of Egypt. A part of dried seeds was separated in coat and pulp, whereas another part was kept 2 days in water for imbibition and then germinated in field for 12 days. Afterwards, young leaves and roots of 12-day-old seedlings were rapidly and gently collected, immediately frozen in liquid nitrogen and then stored at 80 °C prior analysis.

7.2.3 Extraction and sample preparation

Each sample of *M. oleifera* (pulp seed, seed coat, leaves and roots) was ground to a fine powder and extracted with methanol:water (70:30 v/v; sample to solvent ratio 1:25 w/v) at 70 °C for 30 min under vortex mixing to facilitate the extraction. The samples were successively centrifuged (4000 rpm, 30 min, 4 °C), the supernatants were collected, and the solvent was completely removed using a rotary evaporator under vacuum at 40 °C. The dried samples were dissolved in ultrapure water with the same volume of extraction and filtered through 0.20- μ m syringe PVDF filters (Whatmann International Ltd., UK).

7.2.4 ESI-MS and ESI-MS/MS analyses

Full scan ESI-MS and collision-induced dissociation (CID) ESI-MS/MS analyses of samples were performed on an ABSciex API2000 (Foster City, CA, USA) spectrometer. The analytical parameters were optimized by infusing a standard solution of GMG (1 μ g mL⁻¹ in methanol 50%) into the source at a flow rate of 10 μ l min⁻¹. The optimized parameters were declustering potential 40 eV, focusing potential 400 eV and entrance potential 10 eV. Data were acquired in the negative ion MS and MS/MS modes. Full scan ESI-MS, MS/MS and MS³ analyses of standards and samples were performed on an ABSciex API32000 Q-Trap (Foster City, CA, USA) spectrometer. The analytical parameters were optimized by infusing a standard solution of GMG (1 μ g mL⁻¹ in methanol 50%) into the source at a flow rate of 10 μ l min⁻¹. The optimized parameters were declustering potential 73.6 eV, entrance potential 4 eV, collision energy 39 eV and collision cell exit potential 5 eV. Data were acquired in the negative ion MS and MS/MS modes.

7.2.5 HPLC-ESI-MS and HPLC-ESI-MS/MS analyses

Qualitative on-line HPLC-ESI-MS/MS analysis of extracts was performed using an HPLC system interfaced to an Applied Biosystems (Foster City, CA, USA) API3200 Q-Trap instrument in ion trap mode. LC analyses were conducted using a system equipped with a 200-binary pump (Perkin-Elmer, USA). Samples were injected (10 μ l) into a Luna C18 column (Phenomenex, USA) (150 \times 2.1 mm i.d., 5 μ m d) and eluted at a flow rate of 0.3 mL min⁻¹. Mobile phase A

was H₂O containing 0.1% formic acid, while mobile phase B was acetonitrile containing 0.1% formic acid. Elution was carried out using a gradient commencing at 100% A (gradient:1) and changing to 20:80 (A:B) in 55 min (gradient: 4), then from 20:80 (A:B) to 100%B in 5 min (gradient: 1). The column was kept at 25 °C, using a Peltier Column Oven Series 200 (Perkin Elmer). The flow from the chromatograph was injected directly into the ESI source. Qualitative analysis of the compounds was performed using IDA (information dependent acquisition). The IDA method created included an IDA criterion (specify the charge state, mass range), enhanced MS scan, enhanced resolution, enhanced product ion scan or MS/MS scan. The source temperature was held at 450 °C, and MS parameters were those optimized for the ESI-MS and ESI-MS/MS analyses with ion spray voltage at 4500. MS data were acquired using the software provided by the manufacturer (Analyst software 1.5.1) and extracted ion chromatograms (XIC) were elaborated to identify GLs from their deprotonated molecular ions and retention time. Quantitative on-line HPLC-ESI-MS/MS analyses were performed using the same LC-ESI-MS/MS equipment, but the mass spectrometer worked with triple quadrupole analyzer in Multiple Reaction Monitoring (MRM) mode. Elution was carried out using a gradient commencing at 98% A (gradient:1) and changing to 88:12 (A:B) in 5 min (gradient: 4), then from 88:12 (A:B) to 75:25 (A:B) in 21 min (gradient: 1). The API 3200 ES source was operated in negative ion mode and was tuned by infusing solutions of standards (1 µg µl⁻¹ in methanol 50%) into the source at a flow rate of 10 µl min⁻¹. The optimized parameters, fragmentation reactions selected for each compound, dwell time and retention times were reported in Table 7.1. The voltage applied was -4500. Data acquisition and processing were performed using Analyst software 1.5.1.

7.2.6 Principal component analysis procedure

A $m \times n$ matrix (where m is the number of samples, and n is the number of variables) was used in PCA. For the flow injection ESI-MS matrix construction, the mass spectra were expressed as the intensities of the individual $[M-H]^{-1}$ ions (variables) of the most intense ions in the fingerprint of each sample. The data were autoscaled and PCA was run. Thus, quantitative data of each chemical marker were used to define a data set with 12 observations and 545 variables. The resulting metabolomics data were processed using SIMCA P+ software 12.0 (Umetrix AB, Umea, Sweden).

7.2.7 Calibration and quantification of glucosinolates

To prepare the calibration plot, a sample (1 mg) of each standard was weighted accurately into a 1-mL volumetric flask, dissolved in methanol 50% (v/v) and the volume made up to the mark with methanol. The resulting stock solution was diluted with methanol in order to obtain reference solutions containing 0.5, 1, 5, 10, 25, 50, 100 and 200 $\mu\text{g mL}^{-1}$ of external standards. A suitable amount of Internal Standard (IS), namely GBB for GMG, SNB and GTL determination, and GRE for GRA and GIB analysis, was added to each reference solution to give a final concentration of 20 $\mu\text{g mL}^{-1}$ and 5 $\mu\text{g mL}^{-1}$ for GBB and GRE, respectively. Calibration curves were constructed by analyzing reference/IS solutions in triplicate at each concentration level. The ratios of the peak areas of the external standard to those of the IS were calculated and plotted against the corresponding standard concentration using weighted linear regression to generate standard curves. All quantitative data were elaborated with the aid of Analyst software (Applied Biosystems).

7.2.8 Method validation

LC-MS/MS method was validated according to the European Medicines Agency (EMA) guidelines relating to the validation of analytical methods. Precision was evaluated at three concentration levels for each compound through triplicate intra-day assays and inter-day assays over 3 days; the intra-day precision (coefficient of variance) was within 8%, while the inter-day was within 9% for all analytes (Table 7.2). Specificity was defined as the non-interference by other analytes detected in the region of interest. About the LC-MS/MS method, which was developed on the basis of the characteristic fragmentation of detected GLs, no other peaks interfered with the analytes in the MS/MS detection mode. Accuracy of the analytical procedure was evaluated using the recovery test. Pulp seed samples were added with three different amounts of the eight standards, and recoveries were calculated from the difference between the number of analytes measured before and after standards addition. The mean recoveries for each standard and each concentration level are reported in Table 7.2. The calibration graphs, obtained by plotting the area ratio between the external and internal standards against the known concentration of external standards, were linear in the range used for the analysis of all GLs. The sensitivity of the method was determined with

respect to limit of quantification (LOD) and limit of detection (LOQ). The LOQ (equivalent to sensitivity of the quantitative method), defined as the lowest concentration of analyte that could be quantified with acceptable accuracy and precision, was estimated by injecting a series of increasingly dilute standard solutions until the signal-to-noise ratio was reduced to 10. The LOD (equivalent to sensitivity of the qualitative method), defined as the lowest concentration of analyte that could be detected, was estimated by injecting a series of increasingly dilute standard solutions until the signal-to-noise ratio was reduced to 2. Linearity (calibration curves equations and regression), together with LOQ and LOD for each of the five compounds analyzed, is reported in Table 7.3.

7.3 Results

Direct infusion electrospray ionization mass spectrometry in the negative ion mode was initially used to obtain the fingerprints of the extracts of the following different tissues: seed pulp and coat, and leaves and root of 12-day-old seedlings of *M. oleifera*. The full spectrum of each sample was recorded in triplicate with the aim to rapidly provide a visual and statistical evaluation of similarities and differences of secondary metabolites among tissues. The ESI-MS fingerprints of samples were very characteristic, thus showing distinctive sets of polar markers for each different tissue. Considering the large amount of data set obtained by negative ion ESI-MS fingerprints of extracts under investigation, a chemometric approach was performed using PCA, to characterize the different plant's tissue and to evaluate differences in terms of metabolites. The PCA, using SIMCA-P+ Software, was applied to the matrix as described in the experimental section, resulting in the intensity of each compared signal which shows the quantitative level of each marker compound in each of the overall 12 samples (4 tissues \times 3 replicates). PCA is an unsupervised method and was used to reduce the dataset to obtain the maximum variation between the samples. Pareto scaling was chosen for scaling data. Figure 7.1 shows the 2D projection plot of the 12 *M. oleifera* samples. The first component (R^1X) explained the 57% of variance whilst, and the second (R^2X) the 16%. Principal component's choice was done based on the fitting (R^2X) and predictive (Q^2X) values for the PCA model. In our case, the second component gave the closest value to 1 for both. Variance was evaluated by significance level for Hotelling's T^2 . The 2D diagram showed confined cluster areas, representing each a link to a different part of the plant extracted; in fact, we can observe separated regions related to

samples of pulp seed, seed coat, root and leaves. To evaluate the influence of each variable on the classification of the samples, the loading plot obtained for the same dataset was then studied, and it is reported in Figure 7.2. For each region of the 2D space, the loading plot shows the m/z values corresponding to the peak observed in the specific samples. The variables that contribute most to the differentiation of the samples and to their location in a specific area of the space can be highlighted. Interesting, values like m/z 288.9 and m/z 577.0 are localized in the area corresponding to the seed coat in the score plot, whereas values like m/z 570, m/z 612, m/z 407.9 and m/z 912, are confined in the area corresponding to pulp seed, and leaves and roots of 12-day-old seedlings in the score plot.

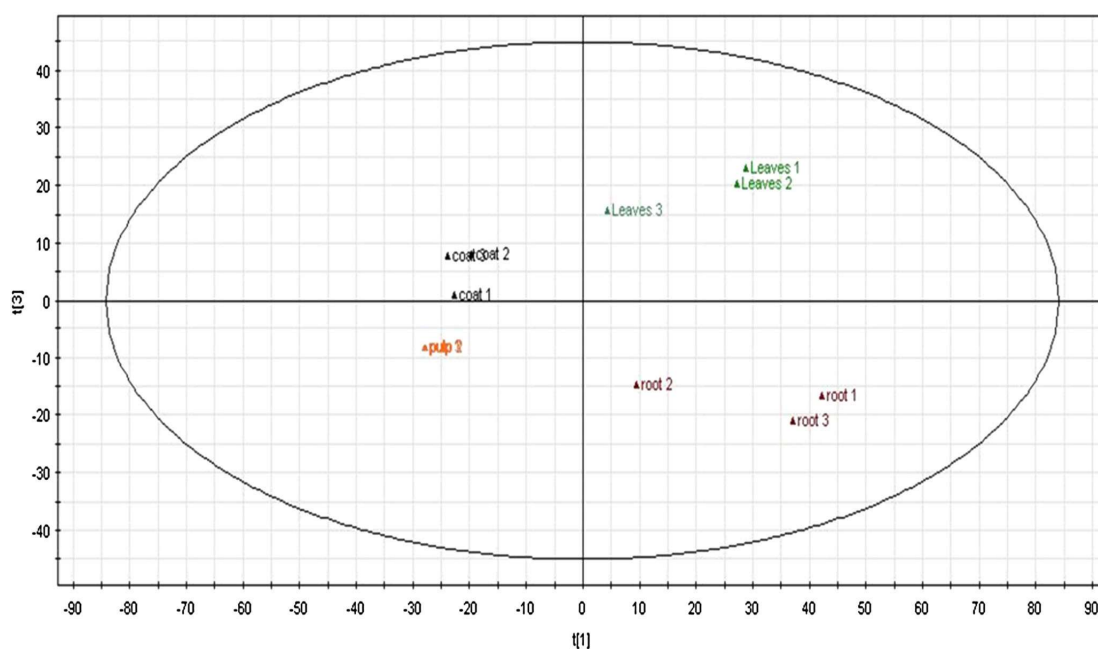


Figure 7.1 Principal component analysis score plot.

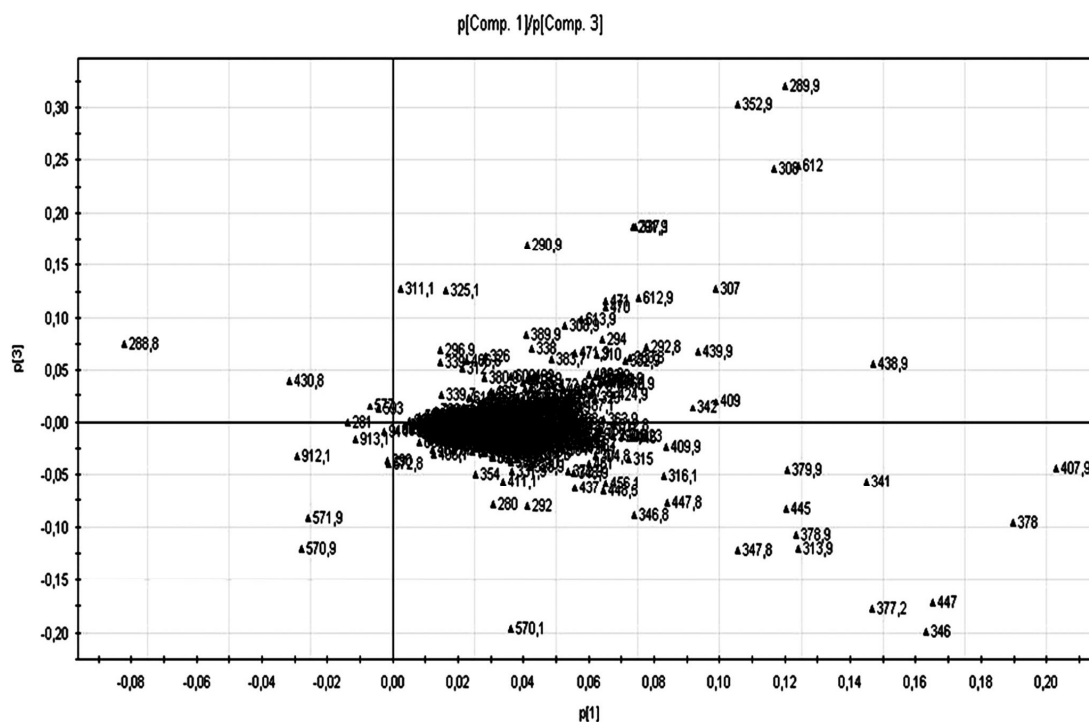


Figure 7.2 Principal component analysis loading plot.

As evidenced by PCA, the ESI-MS fingerprint obtained for seed coat extract showed the $[M-H]^-$ ions at m/z values of 289, 577 and 865 corresponding at catechin/epicatechin and dimeric and trimeric procyanidins, respectively (Figure 7.3A). We confirmed the presence of these compounds by opportune ESI-MS/MS experiments (data not shown). To our knowledge, this is the first study showing the profiling of proanthocyanidins in seed of *M. oleifera*; in fact, previous published works reported just the total proanthocyanidin content (Compaoré et al., 2011). The full negative mass spectrum recorded for seed pulp extract (Figure 7.3B) revealed a major intense ion peak at m/z of 570, relative to GMG together with 3-hydroxy-4-(α -L-rhamnopyranosyloxy)benzyl GL (m/z 586) and three GLs with close structure similarity to GMG, except for the presence of an acetyl group in the compound located at C-2', C-3' and C-4' on the α -L-rhamnopyranosyl unit (m/z 612). The identity of the revealed GLs was verified by the comparison of the MS^2 spectra recorded for each compound with those of the standards and/or with those reported in literature.

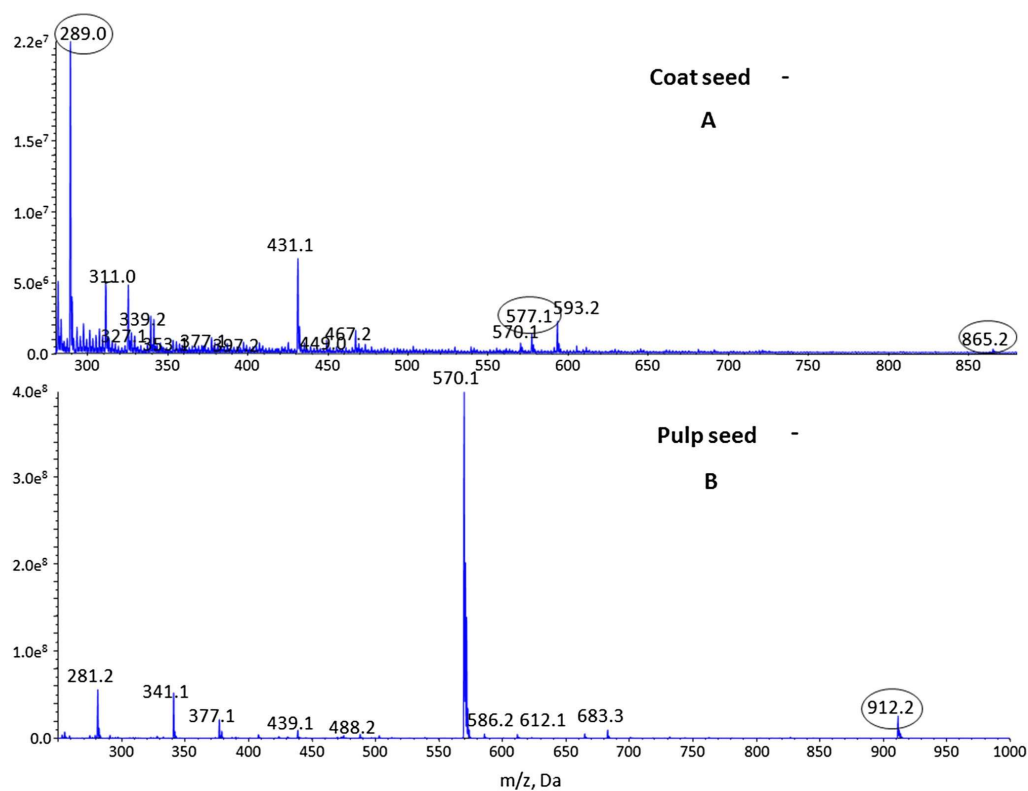


Figure 7.3 ESI-MS (negative ion mode) fingerprints of coat (A) and pulp seed (B).

Another most abundant unknown ion peak was evidenced in this spectrum at m/z value of 912. Fragmentation experiments were performed with the aim to individuate the nature of this compound. MS^2 spectrum (Figure 7.4A) evidenced only one major ion peak at m/z value of 570 corresponding to the deprotonated ion of GMG. Sequential MS^3 spectrum of m/z 570 (Figure 7.4B) displayed most intense fragment ions at values of m/z 424, 328, 275 and 259. The first two were presumably generated by the subsequent loss of a rhamnopyranosyloxy moiety $[M - H - 146]^-$, followed by the loss of sulfate ion $[M - H - 146 - 96]^-$. The last two fragments resulted to be characteristic diagnostic ions typical of fragmentation pattern of GLs. Comparing these results with the fragmentation pattern obtained for GMG standard in using ESI-QqQ-MS and ESI-QqQ-MS/MS (Figure 7.4C), we could hypothesize that the ion at m/z 912 is a GL structurally correlated to GMG. Further studies are needed to clearly identify this compound.

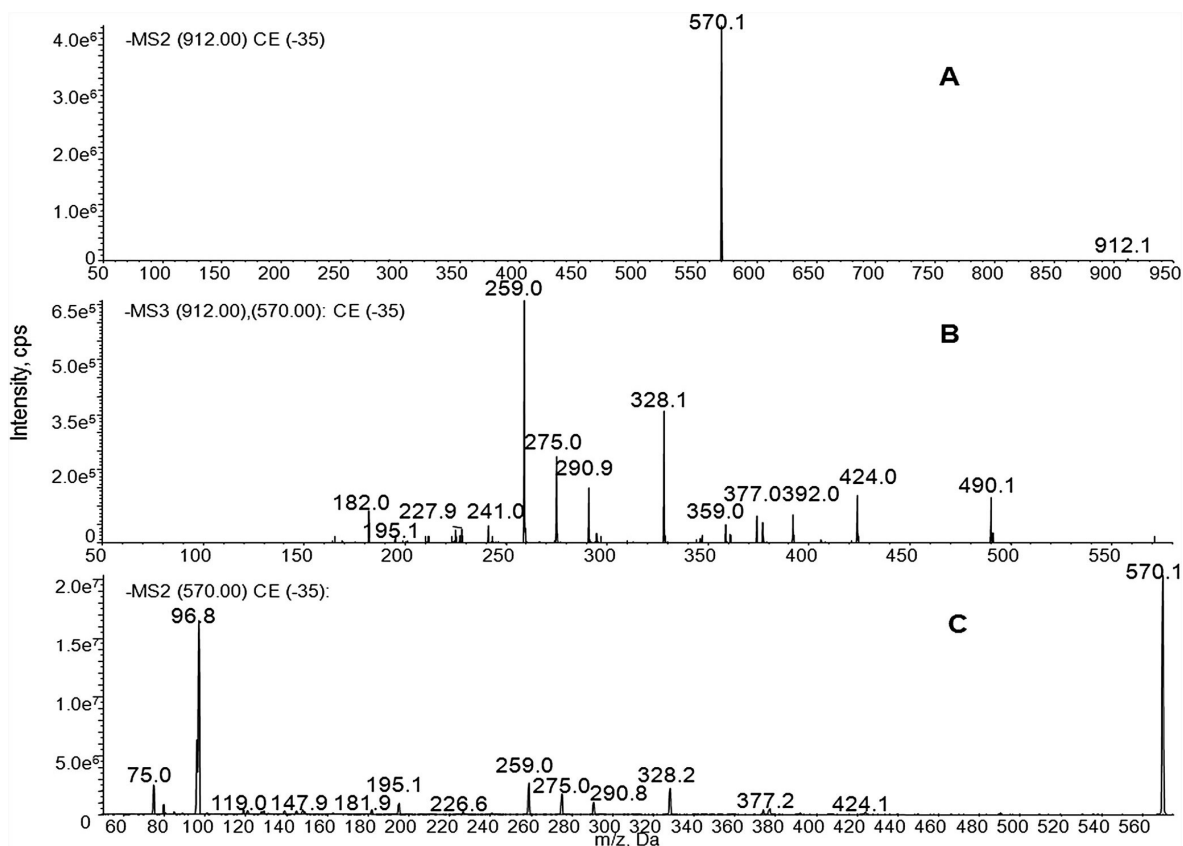


Figure 7.4 ESI-IT-MS/MS (A), ESI-IT-MS³ (B) spectra of compound at m/z 912 and ESI-IT-MS/MS (C) of GMG.

The negative ion ESI-MS spectra of leaves and roots extracts were more complicated, suggesting the high complexity of the mixtures analyzed (data not shown). The deprotonated spectrum of roots extract showed over all a most intense peak at m/z of 408 corresponding to GL GTL, along with minor ion relative to GMG (m/z 570). The comparison of the MS² spectra recorded for each compound with those of the standards confirmed the nature of revealed compounds. The ESI-MS spectrum of leaves extract showed, along with major ion peak of GMG (m/z 570), the acetyl- α -L-rhamnopyranosyloxy-benzyl GL (m/z 612), GTL (m/z 408) and another most abundant ion at m/z value of 353, ascribable to chlorogenic acid. The identity of this compound was confirmed by the comparison of MS/MS spectrum with that of the standard. As evidenced by PCA (Figure 7.2), this variable contributes to the differentiation of leaves sample. Moreover, negative ESI-MS spectrum evidenced other minor ion peaks at m/z value of 447, 463, 593 and 609 corresponding to kaempferol 3-O- β -glucoside, quercetin 3-O- β -glucoside, kaempferol 3-O-rutinoside and rutin, respectively. The identity of the revealed phenolic compounds was verified by the comparison of the MS² spectra with those of the

corresponding standards and/or with those reported in literature (Bennett et al., 2003; Amaglo et al., 2010; Vongsak et al., 2013; Manguro and Lemmen, 2007; Kashiwada et al., 2012). By using IDA software, phenolics found in *M. oleifera* leaves were characterized according to their retention time and their MS and MS/MS spectra and by comparison with standard reference compounds, when available (data not shown). Besides confirming the presence of the revealed compounds, LC-ESI-MS/MS analysis allowed to identify three chlorogenic acid isomers (m/z 353). Focusing on GLs, an opportune IDA method with EMS survey scans, ER and EPI scans was developed to clearly identify these compounds by comparison of both their MS^2 and retention times with those observed for the analytical standards in LC-ESI-MS/MS analyses (data not shown).

Besides GMG, GTL (benzyl GL), 3-hydroxy-4-(α -L-rhamnopyranosyloxy)benzyl GL, 4-(-2'-O-acetyl- α -L-rhamnopyranosyloxy)benzyl GL, 4-(-3'-O-acetyl- α -L-rhamnopyranosyloxy)benzyl GL and 4-(-4'-O-acetyl- α -L-rhamnopyranosyloxy)benzyl GL, LC-ESI-MS/MS analyses allowed to evidence the presence of other GLs at m/z values of 424, 422 and 436. The comparison of MS^2 spectra and the retention times with those of reference standards allowed us to identify these compounds as SNB (4-hydroxybenzyl GL), GIB (3-methylsulfinylpropyl GL) and GRA (4-methylsulfinylbutyl GL), respectively. Except for SNB, these latter GLs have never been previously reported in *M. oleifera*. To obtain accurate data concerning the amounts of revealed GLs in different tissue extracts, a quantitative LC-ESI/MS (MRM) analysis was performed using a method previously described with the opportune modifications (Maldini et al., 2012). MS/MS spectra of GMG and 3-hydroxy-4-(α -L-rhamno-pyranosyloxy)benzyl GL showed the most intense peak at specific product ion at m/z value of 97 corresponding to the $[SO_4H]^-$ ion, while the MS^2 spectra of 4-(O-acetyl- α -L-rhamnopyranosyloxy)benzyl GL and SNB showed a major ion peak at m/z value of 259 due to a sulfated glucose moiety. For the unknown compounds at m/z 912, the only intense product ion generated was the ion at m/z 570. Based on the results, the specific transitions from deprotonated molecular ions to the corresponding fragment ions for each compound were selected to develop an MRM method. IS (internal standards) were characterized by MRM through the transitions from precursor ion m/z 438.0 to product ion m/z 97.0 for GBB and from precursor ion m/z 434.0 to product ion m/z 259.0 for GRE. The structures of detected compounds and selected IS are reported in Figure 7.5. The calibration curves, obtained by plotting the area ratios between the external standards and internal standards against the known concentration of each

compound, were linear in the range of 0.5–200 $\mu\text{g mL}^{-1}$ with r^2 values of >0.993 (Table 7.3). Retention times and selected transitions for analyzed compounds are reported in Table 7.1. The method based on the characteristic fragmentation reactions of GLs was highly specific with no other peaks interfering at the retention times of the marker compounds in the MRM chromatograms (Figure 7.6).

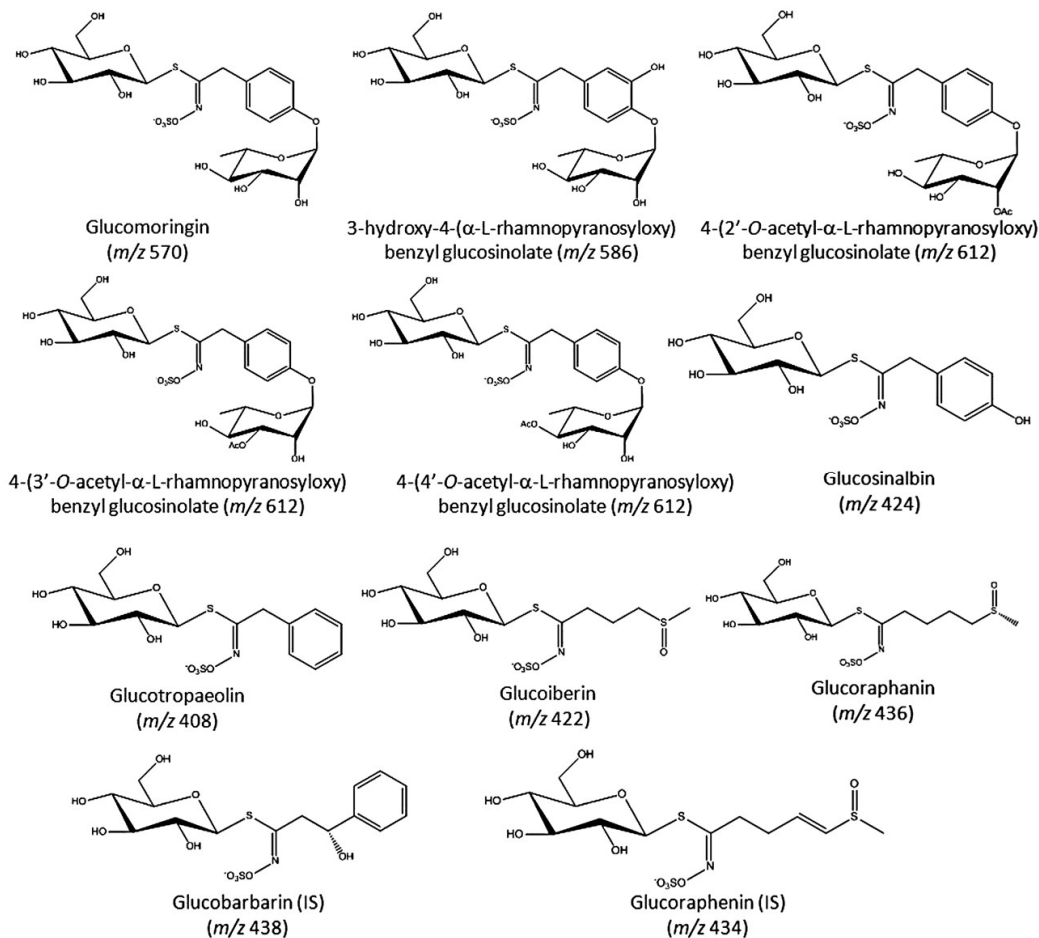


Figure 7.5 Molecular structure of glucosinolates.

Table 7.1 LC-MS/MS conditions for quantitation of glucosinolates by negative ion MRM.

Compound	t_R	Precursor ion [M – H] [–]	Product ion [A – H] [–]	Dwell time (ms)	Declustering potential	Entrance potential	Collision energy	Collision cell exit potential
Glucomoringin	11	570	97	60	–73.6	–6.1	–56.4	–1.13
3-Hydroxy-4-(α -L-rhamnopyranosyloxy)benzyl GL	10.74	586	97	60	–78	–6	–57	–4
4-(2'-O-Acetyl- α -L-rhamnopyranosyloxy)benzyl GL	15.45	612	259	10	–76	–11	–41	–5.6
4-(3'-O-Acetyl- α -L-rhamnopyranosyloxy)benzyl GL	16.01			0				
4-(4'-O-Acetyl- α -L-rhamnopyranosyloxy)benzyl glucosinolate	19.85							
unknown (m/z 912)	10.8	912	570	20	–49	–4.1	–30	–8
	11.3			0				
Glucotropaeolin	17.6	408	328	60	–44	–4	–20	–9
Glucosinalbin	11.6	424	97	60	–61.5	–4.34	–37	–1.8
Glucoraphanin	9.3	436	178	60	–51	–5	–37.8	–4
Glucoiberin	8.8	422	358	60	–48.5	–4	–26	–11.6
Glucobarbarin (I.S.)	16.9	438	97	60	–55	–7.7	–40	–1.7
Glucoraphenin (I.S.)	9.6	434	259	60	–56	–4.8	–35.1	–6.5

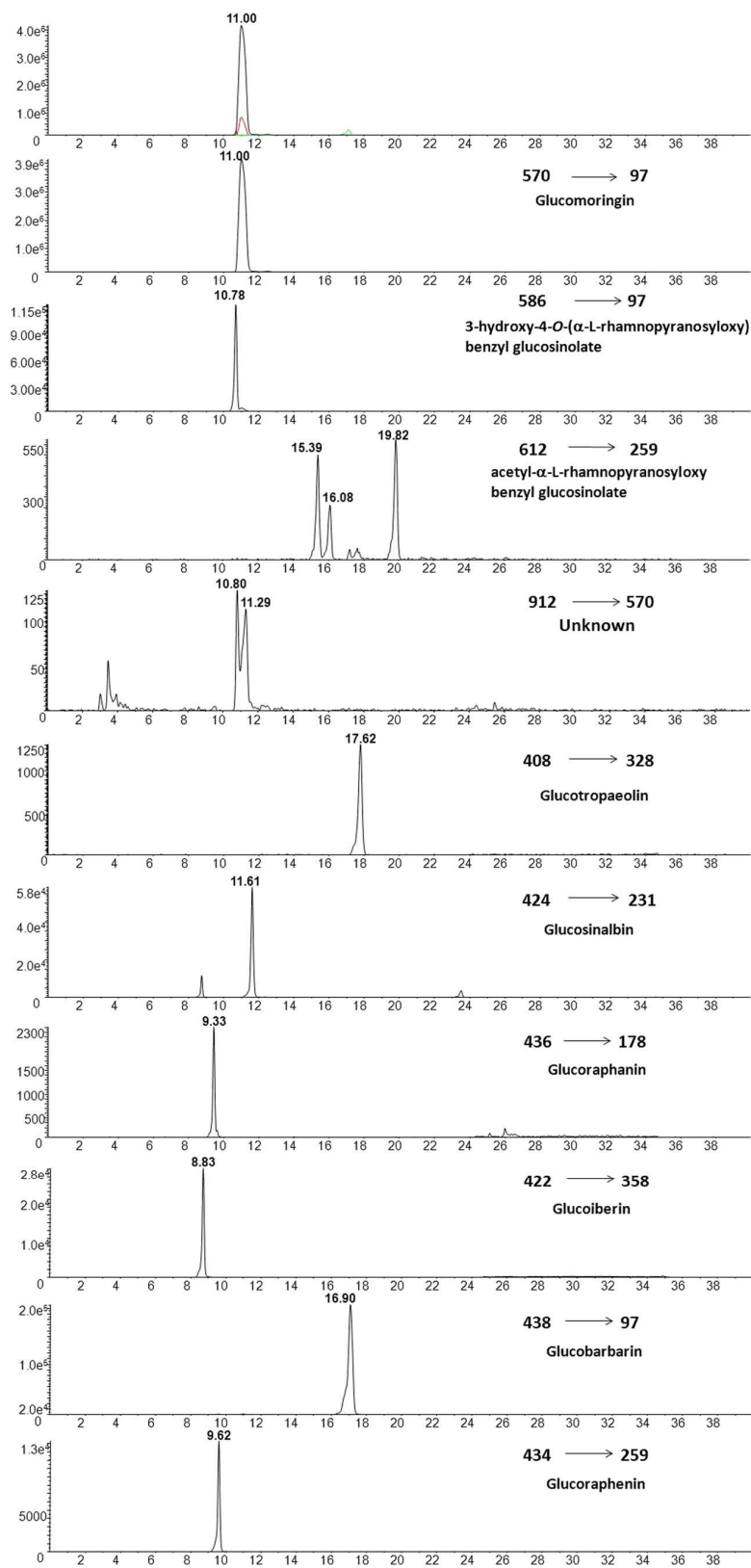


Figure 7.6 LC/ESI(QqQ)/MS/MS XICs (extracted ion chromatograms) of MRM analysis of glucosinolates in *M. oleifera*.

Table 7.2 Accuracy and precision of eight analytes at three concentration levels				
Compound	Concentration ($\mu\text{g/mL}$)	Accuracy (% recovery)	Precision	
			Intra-day (CV%)	Inter-day (CV%)
Glucomoringin	5	112	1.8	3
	50	101	1.2	4.3
	100	99	4.7	3.6
Glucotropaeolin	1	87	8	8
	10	99	2.4	1
	50	98	4.4	2.2
Glucosinalbin	1	112	5.3	6.4
	10	113	2.7	3.2
	50	98	3.1	0.3
Glucoraphanin	1	109	6.3	4.6
	10	110	5.1	2.2
	50	101	3.6	9.8
Glucoiberin	1	106	4.1	8.2
	10	110	3.5	6
	50	100	5.4	1.9

Precision and accuracy were evaluated at three concentration levels for each compound through triplicate intra-day assays and inter-day assays over 3 days

Table 7.3 Linearity, LOQ and LOD of LC-ESI-QqQ-MS/MS MRM method for the analysis of standard compounds.				
Compound	Calibration curve equation	R ²	LOQ ($\mu\text{g mL}^{-1}$)	LOD ($\mu\text{g mL}^{-1}$)
Glucomoringin	$y = 0.0757x + 0.705$	0.993	0.02	0.005
Glucotropaeolin	$y = 0.0241x + 0.0156$	0.999	0.05	0.0015
Glucosinalbin	$y = 0.149x - 0.00236$	0.999	0.011	0.005
Glucoraphanin	$y = 0.883x + 1.72$	0.998	0.06	0.009
Glucoiberin	$y = 0.565x + 1.07$	0.994	0.0019	0.05

The quantitative analysis results are summarized in Table 7.4. It is possible to observe that GMG is the most abundant GL in all parts of *M. oleifera*, particularly in the pulp seed, followed by 3-hydroxy-4-(α -L-rhamnopyranosyloxy)benzyl GL in the pulp seed and seed coat, and by GTL in the leaves. In the pulp, we can also evidence, for the first time in *M. oleifera*, the presence of GRA and SNB and minor quantities of 4-(2'-O-acetyl- α -L-rhamnopyranosyloxy)benzyl GL, 4-(3'-O-acetyl- α -L-rhamnopyranosyloxy)benzyl GL, 4-(4'-O-acetyl- α -L-rhamnopyranosyloxy)benzyl GL, GTL, GIB and in addition two unidentified compounds, most likely GLs.

Table 7.4 Quantitative results for glucosinolates detected in extracts of seed pulp, seed coat, roots and leaves of 12-day-old seedlings of *Moringa oleifera*

Compound	Glucosinolates (mg/100 g)			
	Pulp	Coat	Roots	Leaves
Glucomoringin	8619.44 ± 573.20	28.27 ± 0.6	3.99 ± 0.47	77.7 ± 8.07
3-Hydroxy-4-(α -L-rhamnopyranosyloxy)benzyl glucosinolate	65.75 ± 10.85	3.3 ± 0.02	0.02 ± 0.01	0.45 ± 0.05
4-(2'-O-Acetyl- α -L-rhamnopyranosyloxy)benzyl glucosinolate	(tr15.45) 0.29 ± 0.03	ND	0.01 ± 0.01	0.50 ± 0.01
or 4-(3'-O-acetyl- α -L-rhamnopyranosyloxy)benzyl glucosinolate	(tr16.01) 0.16 ± 0.01	ND	0.01 ± 0.01	0.35 ± 0.05
or 4-(4'-O-acetyl- α -L-rhamnopyranosyloxy)benzyl glucosinolate ^a	(tr19.85) 0.39 ± 0.11	ND	0.02 ± 0.01	2.22 ± 0.26
Unknown (<i>m/z</i> 912) ^a	(tr10.8) 0.14 ± 0.11 (tr11.3) 0.14 ± 0.05	ND	ND	ND
Glucotropaeolin	ND	ND	ND	ND
Glucosinalbin	3.17 ± 0.67	ND	0.27 ± 0.03	15.66 ± 1.04
Glucoraphanin	3.57 ± 0.32	ND	0.05 ± 0.01	0.84 ± 0.19
Glucobrassicin	0.09 ± 0.02	0.86 ± 0.22	0.58 ± 0.03	2.2 ± 0.27
		ND	0.02 ± 0.01	0.05 ± 0.02

Each data is the mean of three replicates (mean ± SD); ND: not detected; ^aQuantified as equivalent of glucomoringin.

To our knowledge, this is the first paper showing a direct quantitative determination of predominant GMG and the other glucosinolates in seeds and different tissues of *M. oleifera* 12-day-old seedlings. Previously, Bennett et al. (2003, 2004) reported the identification (by a LC-MS method) and the indirect quantification (by LC-UV method) of the major GLs present in seeds (Kusznierewicz et al., 2013) and in tissues of 1-year-old plants of *M. oleifera* (Bennett et al., 2003). In another study, performed by Amaglo et al. (2010) a direct quantitative analysis of GMG and congeners in 100-, 320- and 380-day-old plants is reported. Furthermore, the study of Bellostas et al. (2010) measured the total GL level in leaves of 2-3-year-old plants of three different *Moringa* species. Despite showing similar patterns, the levels of GLs obtained in our study are different from those already reported (Amaglo et al., 2010; Bellostas et al., 2010). These differences could be attributed to several reasons. In addition to the different analytical methods used, difference in the varieties examined, the growth conditions, as well as the plant health and nutrition could represent important factors. Our data demonstrated that seed and seedlings of *M. oleifera* can represent a good source of GMG. This compound, as well as its acetyl derivatives and hydrolyzed products, can exert a broad biological activity, from antimicrobial to antiproliferative properties (Cheenpracha et al., 2010; Park et al., 2011; Lee et al., 2009; Juge et al., 2007; Leuck and Kunz, 1998; Fahey, 2005; Galuppo et al., 2013), as well as an effective anticarcinogenic activity (Brunelli et al., 2010; Galuppo et al., 2013; Anwar et al., 2007; Guevara et al., 1999; Dayal et al., 2013).

7.4 Conclusion

This study describes for the first time the MS profiling of proanthocyanidins in seed coat and the simultaneous determination of 11 GLs in different *M. oleifera* tissues by using mass spectrometric approaches. ESI-MS and ESI-MS/MS fingerprints of seed coat have not been previously performed and allowed us to emphasize the presence of dimeric and trimeric proanthocyanidins together with the related monomer (catechin/epicatechin). Furthermore, the use of the full ESI-MS spectra along with the PCA approach proved to be a potentially useful and effective tool to rapidly provide both visual and statistical evaluation of similarities and differences in *M. oleifera* tissues. The LC-ESI-MS/MS IDA method allowed us to individuate two GLs (GIB and GRA) never reported in *M. oleifera* before. Moreover, an LC-MS/MS MRM method allowed us to quantify all the identified GLs in different tissues of *M. oleifera*. *M. oleifera* pulp resulted a very rich source of GMG, an uncommon member of the GL family with promising antimicrobial, anticarcinogenic and neuroprotective properties. Finding of phenolic compounds is interesting because they are active antioxidant components of *M. oleifera* responsible for its anti-inflammatory, atherosclerotic and antidiabetic activities.

References

Amaglo NK, Bennett RN, Lo Curto RB, Rosa EAS, Lo Turco V, Giuffrida A, Lo Curto A, Crea F, Timpo GM (2010) Profiling selected phytochemicals and nutrients in different tissues of the multipurpose tree *Moringa oleifera* L., grown in Ghana. *Food Chem* 122:1047.

Anwar F, Latif S, Ashraf M, Gilani AH (2007) *Moringa oleifera*: a food plant with multiple medicinal uses. *Phytother Res* 21:17.

Bellostas N, Sørensen JC, Nikiema A, Sørensen H, Pasternak D, Kumar S (2010) Glucosinolates in leaves of *Moringa* species grown and disseminated in Niger. *Afr J Agric Res* 5:1338.

Bennett RN, Mellon FA, Foidl N, Pratt JH, Dupont MS, Perkins L, Kroon PA (2003) Profiling glucosinolates and phenolics in vegetative and reproductive tissues of the multi-purpose trees *Moringa oleifera* L. (horseradish tree) and *Moringa stenopetala* L. *J Agric Food Chem* 51:3546.

Bennett RN, Mellon FA, Kroon PA (2004) Screening crucifer seeds as sources of specific intact glucosinolates using ion-pair high-performance liquid chromatography negative ion electrospray mass spectrometry. *J Agric Food Chem* 52:428.

Brunelli D, Tavecchio M, Falcioni C, Frapolli R, Erba E, Iori R, Rollin P, Barillari J, Manzotti C, Morazzoni P, D'Incalci M (2010) The isothiocyanate produced from glucomoringin inhibits NF- κ B and reduces myeloma growth in nude mice in vivo. *Biochem Pharmacol* 79:1141–1148.

Cheenpracha S, Park EJ, Yoshida WY, Barit C, Wall M, Pezzuto GM, Chang LC (2010) Potential anti-inflammatory phenolic glycosides from the medicinal plant *Moringa oleifera* fruits. *Bioorg Med Chem* 18:6598–6602.

Compaoré WR, Nikiéma PA, Bassolé HIN, Savadogo A, Mouecoucou J, Hounhouigan DJ, Traoré SA (2011) Chemical composition and antioxidative properties of seeds of *Moringa oleifera* and pulps of *Parkia biglobosa* and *Adansonia digitata* commonly used in food fortification in Burkina Faso. *Curr Res J Biol Sci* 3: 64.

Chumark P, Khunawat P, Sanvarinda Y, Phornchirasilp S, Morales NP, Phivthong-ngam L, Ratanachamnong P, Srisawat S, Pongrapeeporn KU (2008) The in vitro and ex vivo antioxidant properties, hypolipidaemic and antiatherosclerotic activities of water extract of *Moringa oleifera* Lam. Leaves. J Ethnopharmacol 116:439.

Dayal B, Yannamreddy VR, Amin R, Lea MA, Attygalle AB. Bioactive Compounds in *Moringa oleifera*: isolation, structure elucidation and their antiproliferative properties. In Tropical and Subtropical Fruits: flavors, color and health benefits. Patil B. et al. ACS Symposium Series. American Chemical Society Washington DC 2013.

European Economic Community, Commission Regulation, EEC No. 1864/90. Oilseeds – determination of glucosinolates high performance liquid chromatography. Off J Eur Comm 1990 L170 27-34.

European Medicines Agency (EMA). Quality guidelines. Validation of analytical procedures. Text and methodology (ICH Q2) 2009 Available online at http://www.ema.europa.eu/docs/en_GB/document_library/Scientific_guideline/2009/09/WC500002662.pdf (Accessed on March 13th, 2018).

Fahey JW. *Moringa oleifera*: a review of the medical evidence for its nutritional, therapeutic, and prophylactic properties. Part 1. Trees for Life J. www.TFLJournal.org 2005.

Faizi S, Siddiqui BS, Saleem R, Noor F, Husnain S (1997) Isolation and structure elucidation of a novel glycoside niazidin from the pods of *Moringa oleifera* J Nat Prod 60:1317.

Fenn JB, Mann M, Meng CK, Wong SF, Whitehouse CM (1989) Electrospray ionization for mass-spectrometry of large biomolecules. Science 246:64.

Galuppo M, De Nicola GR, Iori R, Dell'Utri P, Bramanti P, Mazzon E (2013) Antibacterial activity of glucomoringin bioactivated with myrosinase against two important pathogens affecting the health of long-term patients in hospitals. Molecules 18:14340–14348.

Guevara AP, Vargas C, Sakurai H, Fujiwara Y, Hashimoto K, Maoka T, Kozuka M, Ito Y, Tokuda H, Nishino H (1999). An antitumor promoter from *Moringa oleifera*. *Mutat Res* 440:181.

Hopke PK (2003) The evolution of chemometrics. *Anal Chim Acta* 500:65.

Jahangir M, Abdel-Farid IB, Kim HK, Choi YH, Verpoorte R (2009) Healthy and unhealthy plants: the effect of stress on the metabolism of Brassicaceae. *Environ Exp Bot* 67:23.

Juge N, Mithen RF, Traka M (2007) Molecular basis for chemoprevention by sulforaphane: a comprehensive review. *Cell Mol Life Sci* 64:1105.

Kashiwada Y, Ahmed FA, Kurimoto S, Kim SY, Shibata H, Fujioka T, Takaishi Y (2012) New α -glucosides of caffeoyl quinic acid from the leaves of *Moringa oleifera* Lam. *J Nat Med* 66:217.

Kusznierewicz B, Iori R, Piekarska A, Namieśnik J, Bartoszek A (2013) Convenient identification of desulfoglucosinolates on the basis of mass spectra obtained during liquid chromatography-diode array-electrospray ionisation mass spectrometry analysis: method verification for sprouts of different Brassicaceae species extracts. *J Chromatogr A* 1278:108.

Lee YM, Seon MR, Cho HJ, Kim JS, Park JH (2009) Benzylisothiocyanate exhibits anti-inflammatory effects in murine macrophages and in mouse skin. *J Mol Med* 87:1251.

Leuck U and Kunz H (1998) Synthesis of active principles from the leaves of *Moringa oleifera* using S-pent-4-enyl thioglucosides. *Carbohydr Res* 312:33.

Maldini M, Baima S, Morelli G, Scaccini C, Natella F (2012) A liquid chromatography-mass spectrometry approach to study "glucosinoloma" in broccolisprouts. *J Mass Spectrom* 47:1198.

Manguro LOA and Lemmen P (2007) Phenolics of *Moringa oleifera* leaves. *Nat Prod Res* 21:56.

Mbikay M (2012) Therapeutic potential of *Moringa oleifera* leaves in chronic hyperglycemia and dyslipidemia: a review. *Front Pharmacol* 3:24.

Ndong M, Uehara M, Katsumata S, Suzuki K (2007) Effects of oral administration of *Moringa oleifera* Lam. on glucose tolerance in gotokakizaki and wistar rats. J Clin Biochem Nutr 40:229.

Oluduro OA, Idowu TO, Aderiyi BI, Famurewa O, Omoboye OO (2012) Evaluation of antibacterial potential of crude extract of *Moringa oleifera* seed on orthopaedics wound isolates and characterization of phenylmethanamine and benzyl isothiocyanate derivatives. Res J Med Plant 6:383.

Park EJ, Cheenpracha S, Chang LC, Kondratyuk TP, Pezzuto JM (2011) Inhibition of lipopolysaccharide-induced cyclooxygenase-2 and inducible nitric oxide synthase expression by 4-[(2'-O-acetyl- α -L-rhamnosyloxy) benzyl] isothiocyanate from *Moringa oleifera*. Nutr Cancer 63:971.

Smiechowska A, Bartoszek A, Namiesnik J (2010) Determination of glucosinolates and their decomposition products-indoles and isothiocyanates in cruciferous vegetables. Crit Rev Anal Chem 40:202.

Sreelatha S and Padma PR (2009) Antioxidant activity and total phenolic content of *Moringa oleifera* leaves in two stages of maturity. Plant Foods Hum Nutr 64:303.

Verma SC, Banerji R, Misra G, Nigam SK (1976) Nutritional value of *Moringa*. Curr Sci 45:769.

Verma AR, Vijayakumar M, Mathela CS, Rao CV (2009) In vitro and in vivo antioxidant properties of different fractions of *Moringa oleifera* leaves. Food Chem Toxicol 47:2196.

B. Vongsak, P. Sithisarn, W. Gritsanapan. Simultaneous HPLC quantitative analysis of active compounds in leaves of *Moringa oleifera* Lam. J. Chromatogr. Sci. 2013 4,1.

PART THREE

*GLUCORAPHANIN PURIFICATION AND
R-SULFORAPHANE PRODUCTION*

Tuscan black kale as a multifunctional plant source of glucoraphanin and enantiopure *R*-sulforaphane

Contents

Summary

- 8.1** Focus on dietary enantiopure *R*-Sulforaphane
- 8.2** Plant source selection
 - 8.2.1** Screening of broccoli and Tuscan black kale seeds
- 8.3** Purification of glucoraphanin on the gram-scale
 - 8.3.1** Plant source
 - 8.3.2** Glucoraphanin extraction and purification
 - 8.3.3** Glucoraphanin characterization
 - 8.3.3.1 Glucoraphanin molar extinction coefficient determination*
 - 8.3.3.2 NMR analysis of glucoraphanin*
- 8.4** Production of enantiopure *R*-sulforaphane on the gram-scale
- 8.5** Production of a standardized freeze-dried Tuscan black kale seed extract powder
- 8.6** Production of a standardized freeze-dried Tuscan black kale sprout powder
- 8.7** Production of a standardized freeze-dried Tuscan black kale sprout extract powder
- 8.8** Treatment of TBK-SE with myrosinase
 - 8.8.1** GC-MS analysis of isothiocyanates
 - 8.8.2** HPLC analysis of total isothiocyanates
 - 8.8.3** Results
- 8.9** Conclusions

References

Keywords

Glucoraphanin; *R*-sulforaphane; Tuscan black kale; Broccoli; *Brassica oleracea*

Abbreviations

GER: glucoerucin;

GBS: glucobrassicin;

GIB: glucoiberin;

GRA: glucoraphanin;

4-OH-GBS: 4-hydroxy-glucobrassicin;

DS-GL: desulfo-glucosinolate;

MYR: myrosinase;

PPB: potassium phosphate buffer;

R-SF: *R*-sulforaphane.

Summary

In this chapter, the use of Tuscan black kale seed (*Brassica oleracea* (L.) ssp *acephala* (DC) var. *Sabellica* L.) as a multifunctional plant source suitable to achieve several purposes is described. Tuscan black kale proved to be a rich source of natural glucoraphanin (4*R*-methylsulfinylbutyl glucosinolate), the precursor of the most popular dietary enantiopure *R*-sulforaphane. Natural sulforaphane exists as a single *R*-configured enantiomer and this enantiopurity appears critical for its biological activity. However, only few studies up to now have evaluated the influence of the sulfoxide chirality on the beneficial health effects of sulforaphane. Therefore, there is the need to make natural glucoraphanin and *R*-sulforaphane available in large quantities for investigations in animal and clinical studies. The selected seed resulted to be the ideal source to perform the following research activities:

1. isolation and purification of natural glucoraphanin on the gram scale;
2. production of *R*-sulforaphane on the gram scale;
3. preparation of a standardized glucoraphanin enriched freeze-dried seed extract;
4. preparation of a standardized freeze-dried sprout powder;
5. preparation of a standardized glucoraphanin enriched freeze-dried sprout extract.

Tuscan black kale proved to be a better alternative to broccoli. In fact, Tuscan black kale contains a minor number of glucosinolates along with a higher concentration of glucoraphanin and this occurrence enables a more efficient purification of the glucosinolate of interest. Moreover, Tuscan black kale does not contain antinutritional glucosinolates such as the goitrogenic progoitrin present in most screened broccoli varieties. The different research activities described in this chapter proved that seed and sprout of Tuscan black kale can be successfully used for the purification of glucoraphanin and *R*-sulforaphane on the gram scale, as well as for the preparation of standardized glucoraphanin rich plant powder for application in the food/nutraceutical industry.

8.1 Focus on dietary enantiopure *R*-Sulforaphane

Sulforaphane (4-methylsulfinylbutyl isothiocyanate, SF) was first isolated from the leaves of hoary cress (*Lepidium draba* L.), an invasive weed belonging to the Brassicaceae family (Procházka, 1959). About thirty years later in 1992, Professor Paul Talalay of the Johns Hopkins School of Medicine University in Baltimore discovered SF as the main phytochemical in broccoli sprouts responsible for phase 2 enzymes induction (Zhang et al., 1992). This pioneer study opened the way to a new era in cancer research coined as ‘green chemoprevention’ influencing dietary habits and agricultural practices worldwide. Talalay was indeed defined as ‘the catalyst’ (Johnson, 2016) of the steady increase in the number of studies on SF (Figure 8.1). A total number of 2684 publication was found between 1992 and 2018 through a search in Scopus using the keyword ‘sulforaphane’. In particular, the keyword combination ‘sulforaphane’ and ‘cancer’ yielded 1331 scientific articles evidencing the great scientific interest on the anti-cancerogenic activity of this compound (Scopus, February 2018).

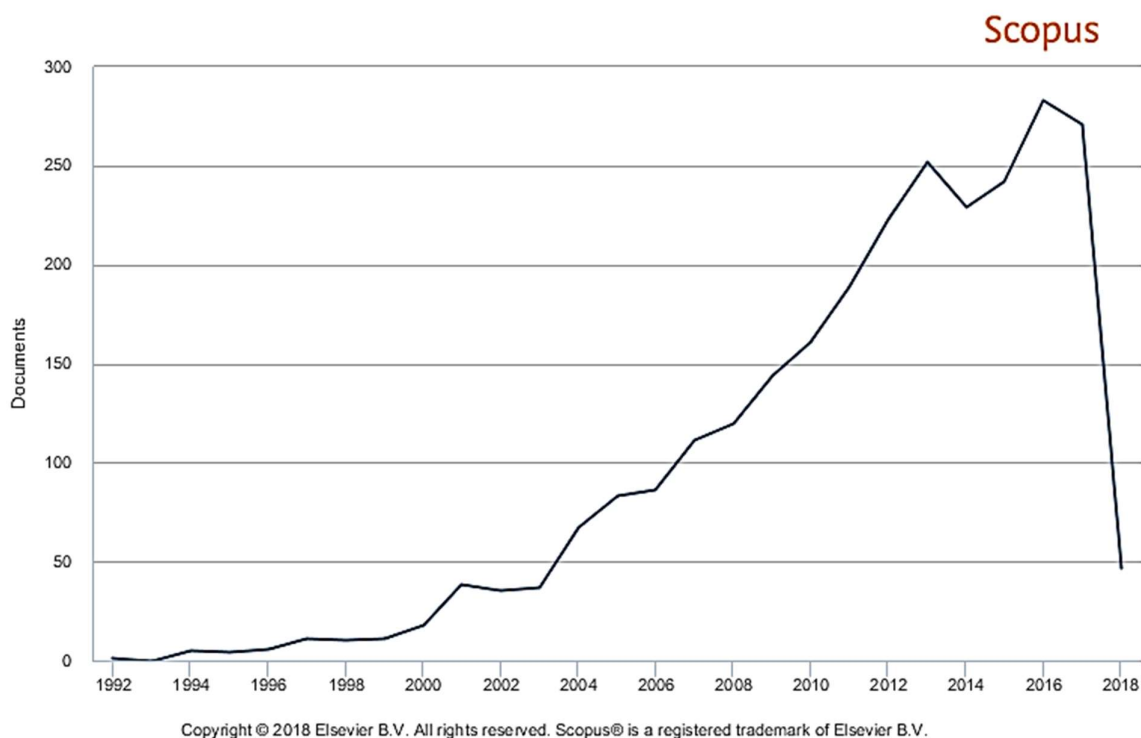
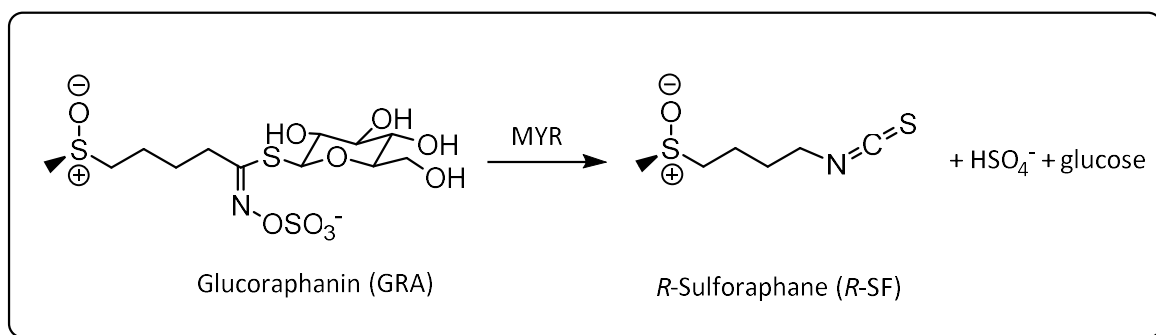


Figure 8.1 Chronology of the number of publications appearing in Scopus between 1992 and 2018 with the keyword ‘sulforaphane’.

Furthermore, SF is currently being used in clinical trials to assess its effects against different tumour processes, cardiovascular diseases, autism disorder, aging, dementia and other pathologies (Clinicaltrials.gov, 2018). SF is not produced as such by the plant, but rather released by the enzymatic action of myrosinase (β -thioglucoside glucohydrolase, E.C. 3.2.1.147; MYR) on the glucosinolate (GL) precursor glucoraphanin (4-methylsulfinylbutyl GL; GRA) following plant cell damage (Schema 8.1). The configuration of the sulfoxide stereogenic center in the GRA side chain was recently ascertained by NMR to be R_S , a configuration retained in the hydrolysis product R -SF (Vergara et al., 2008). It must be also clarified that the stereochemical absolute configuration of natural R -SF has been established unequivocally: the incorrect and confusing designation 'L-sulforaphane' currently found in many articles, clumsily refers to the levorotatory nature of the compound. Up to now, most studies on the biological activities of SF have been conducted using R,S -SF, the racemic form obtained by chemical synthesis, as early studies had shown that the chirality of the sulfoxide group in SF did not affect its potency as an enzyme inducer (Zhang et al., 1992).



Scheme 8.1. Reaction of myrosinase (MYR) catalyzed hydrolysis of 4*R*-methylsulfinylbutyl glucosinolate (glucoraphanin; GRA) to produce 4*R*-methylsulfinylbutyl isothiocyanate (*R*-sulforaphane; *R*-SF).

As humans are exposed exclusively to R -configured SF through the diet, investigations of the effectiveness of this enantiomer to provide beneficial health effects should be carried out in comparison with the S -enantiomer and with the racemic mixture. As a matter of fact, marked differences in the modulation of cytochrome P450 and of the phase II enzymes, by the two enantiomers of SF, have been recently reported. In precision-cut tissue slices of both liver and lung of rats, R -SF enhanced quinone reductase and glutathione S -transferase activities, whereas S -SF either was ineffective or provoked a much weaker response (Abdull

Razis et al., 2011). Future investigations in animal or clinical trials on the pharmacological properties of *R*-SF, as a promising natural compound in chemopreventive therapy, are suggested in recent reviews of existing studies (Abdull Razis and Noor, 2013; Kelsey et al., 2010). There is therefore the need for making available large quantities of enantiopure *R*-SF. Several methods for the purification of natural *R*-SF are based on the separation of the compound from complex mixtures of isothiocyanates (ITCs) present in water extracts of broccoli seed or seed meal after MYR hydrolysis. Those methods are based on low-pressure column chromatography (Liang et al., 2005), solid phase extraction coupled with preparative HPLC (Liang et al., 2007), and macroporous resin (Li et al., 2008), but generally, the yield and/or purity of the obtained *R*-SF were limited. An efficient methodology to produce enantiopure *R*-SF based on the enzymatic hydrolysis of its natural precursor GRA is described in this Chapter and published in De Nicola et al. (2014). In the next sections, the selection of an appropriate vegetable source for GRA purification on the gram scale and its conversion to *R*-SF are reported.

8.2 Plant source selection

In a recent report, the GLs content of 32 cvs of cabbage and 24 cvs of kale was analyzed (Sasaki et al., 2012). The authors mentioned in particular five cvs of kale from Italy, categorized as black kale (*Cavolo nero*), as excellent sources of GRA, hence as potential plant material to produce *R*-SF. Accordingly, broccoli seeds and Tuscan black kale seeds were screened for GLs profile and content.

8.2.1 Screening of broccoli and Tuscan black kale seeds

Selected seeds for sprout production were provided by Suba Seeds Company (Longiano, FC, Italy). Eight different broccoli (*Brassica oleracea* (L.) spp. *italica*) seed cvs. (labelled as A to H), and four Tuscan black kale (*Brassica oleracea* (L.) ssp. *acephala* (DC) var. *Sabellica* L.) seed cvs. (labelled as TBK⁻¹ to TBK-4) were analyzed. GLs were extracted from duplicate samples (about 100 mg) of finely powdered seed meal. Each extract (1 mL) was loaded onto a mini-column filled with DEAE Sephadex A-25 anion exchanger (0.6 mL), conditioned with 25 mM acetate buffer pH 5.6. After washing with the same buffer (3 mL), purified sulfatase (100 µL, 0.26 U

mL⁻¹) was loaded onto the mini-column which was left overnight at room temperature. The desulfo glucosinolates (DS-GLs) were then eluted with ultrapure water (3 mL) and finally injected into an HPLC Agilent 1100 system equipped with a PDA detector and an Inertsil ODS-3 column (250 × 3.0 mm, 5 μm) thermostated at 30 °C. The chromatography and the quantification were achieved as already reported at Chapter three (see Section 3.2.5). All desulfation procedures were carried out in quadruplicate. The typical profile of DS-GLs chromatogram of broccoli and Tuscan black kale is presented in Figure 8.2 and Figure 8.3, respectively. The individual and total content of GL present in each different seed are summarized in Table 8.1. Tuscan black kale resulted to have only five GLs with predominant GRA. The cv labeled as TBK-4, and commercialized as OD74, showed the highest content of GRA with a value of 3.4% (w/w) on whole seed. This cv was therefore chosen as the starting plant material for all the studies, including GRA purification for R-SF production.

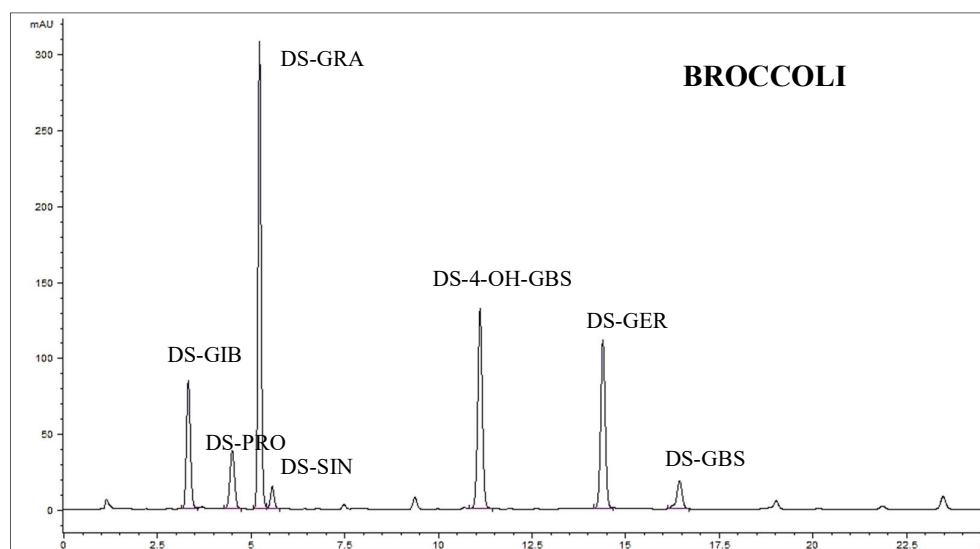


Figure 8.2. HPLC chromatogram of desulfo glucosinolates (DS-GLs) isolated from broccoli (*Brassica oleracea* (L.) *spp italica*) seed extract. Legend: DS-GIB, desulfo glucoiberin; DS-PRO, desulfo progoitrin; DS-GRA, desulfo glucoraphanin; DS-SIN, desulfo sinigrin; DS-4-OH-GBS, desulfo 4-hydroxy glucobrassicin; DS-GER, desulfo glucoerucin; DS-GBS, desulfo glucobrassicin.

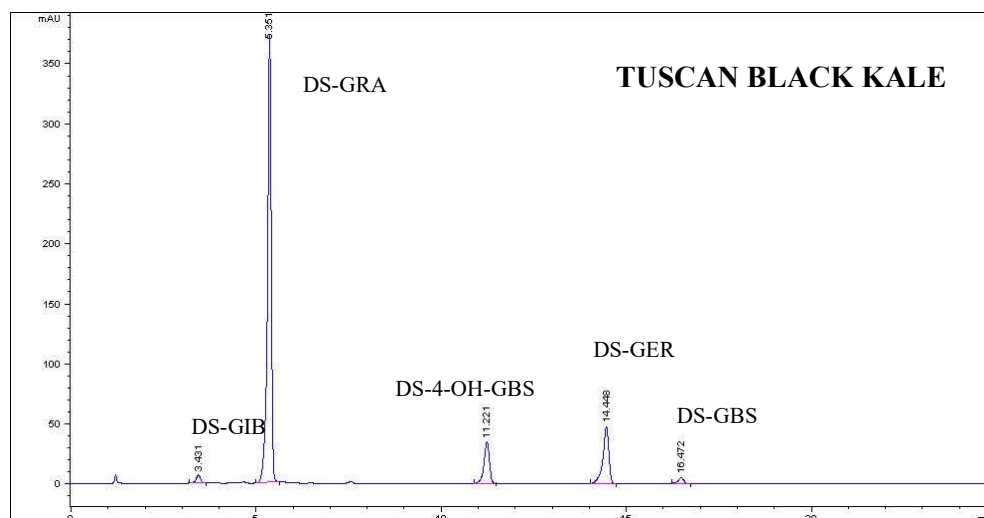


Figure 8.3. HPLC chromatogram of desulfo glucosinolates (DS-GLs) isolated from Tuscan black kale (*Brassica oleracea* (L.) ssp *acephala* (DC) var. *Sabellica* L.) seed extract. Legend: DS-GIB, desulfo glucoiberin; DS-GRA, desulfo glucoraphanin; DS-4-OH-GBS, desulfo 4-hydroxy glucobrassicin; DS-GER, desulfo glucoerucin; DS-GBS, desulfo glucobrassicin.

Table 8.1 Glucosinolate (GL) content in eight different broccoli (*Brassica oleracea* (L.) ssp *italica*) seed cvs. (labeled as A to H) and four different Tuscan black kale (*Brassica oleracea* (L.) ssp *acephala* (DC) var. *Sabellica* L.) seed cvs. (labeled as TBK-1 to TBK-4).

SEED	GLUCOSINOLATE (μmolg^{-1})							TOTAL GLs
	GIB	PRO	GRA	SIN	4-OH-GBS	GER	GBS	
A	10.96 ± 0.44	2.26 ± 0.07	33.44 ± 1.43	0.96 ± 0.00	3.00 ± 0.10	7.96 ± 0.26	0.54 ± 0.02	59.12
B	11.91 ± 0.77	4.31 ± 0.04	31.82 ± 2.75	1.85 ± 0.06	3.63 ± 0.10	9.45 ± 0.02	0.72 ± 0.02	63.69
C	10.36 ± 0.89	1.68	29.10 ± 2.68	-	3.70 ± 0.31	9.24 ± 0.39	0.64 ± 0.04	54.72
D	7.87 ± 0.48	2.14 ± 0.04	20.64 ± 1.32	-	3.56 ± 0.04	6.58 ± 0.12	0.46 ± 0.12	41.25
E	9.09 ± 0.52	2.05 ± 0.00	22.74 ± 1.27	-	3.81 ± 0.01	7.55 ± 0.06	0.62 ± 0.00	45.86
F	7.66 ± 1.08	2.03 ± 0.02	23.09 ± 3.37	-	3.99 ± 0.04	7.36 ± 0.03	0.51 ± 0.00	44.64
G	6.79 ± 1.07	2.56 ± 0.11	22.76 ± 1.04	0.98 ± 0.10	2.56 ± 0.16	9.55 ± 0.19	0.54 ± 0.02	45.74
H	1.09 ± 0.12	-	27.19 ± 0.81	-	1.90 ± 0.31	14.61 ± 0.50	-	44.79
TBK-1	4.10 ± 0.40	-	55.01 ± 4.01	-	3.30 ± 0.61	13.00 ± 0.95	-	76.04
TBK-2	0.65 ± 0.31	-	35.46 ± 2.49	-	3.57 ± 0.50	9.05 ± 1.72	0.61 ± 0.15	49.34
TBK-3	3.47 ± 0.65	-	50.22 ± 4.21	-	4.36 ± 0.38	12.59 ± 0.87	-	70.64
TBK-4	1.32 ± 0.16	-	72.12 ± 3.21	-	2.76 ± 0.28	14.15 ± 0.75	-	90.35

Legend: GIB, glucoiberin; PRO, progoitrin; GRA, glucoraphanin; SIN, sinigrin; 4-OH-GBS, 4-hydroxy glucobrassicin; GER, glucoerucin; GBS, glucobrassicin.

8.3 Purification of glucoraphanin on the gram scale

8.3.1 Plant source

Ripe seeds of Tuscan black kale (*Brassica oleracea* (L.) ssp *acephala* (DC) var. *Sabellica* L. cv. 0D74) were supplied by Suba Seeds Company (Longiano, FC, Italy) and stored in a dry and dark place at room temperature. Seeds were identified by a lot number and guaranteed by the producer for the quality and the homogeneity of the product. Tuscan black kale (Cavolo nero di Toscana) seeds were first ground to a fine powder and defatted overnight in hexane.

8.3.2 Glucoraphanin extraction and purification

A sample of dried defatted seed meal (150 g) was treated with boiling 70% ethanol (700 mL) to quickly deactivate the endogenous MYR. GLs were extracted using an Ultraturrax homogenizer T50 at medium speed for 20 min. The resulting homogenate was centrifuged at 14,000 *g* for 30 min and the extraction repeated on the solid as before. The two extracts were pooled, and 0.5 M acetate buffer pH 4.2 (100 mL) was added and diluted with water (up to a final volume of 3 L). The treated extract was left overnight at 4 °C for protein precipitation. The isolation of GLs from the extract was carried out by one-step ion exchange chromatography. The extract was filtered and loaded on a glass column (Econo-Column 2.5 × 20 cm, Bio-Rad Laboratories, Milan, Italy) packed with DEAE Sephadex A-25 anion exchanger (90 mL) conditioned with 25 mM acetate buffer (pH 4.2). After washing with distilled water (2 L), the GLs were eluted with a 0.2 M aqueous solution of potassium sulfate (500 mL). The collected solution was concentrated to dryness using a rotary evaporator Laborota 4002 (Heidolph Instruments, Schwabach, Germany). The solid residue was then submitted to three subsequent extractions with boiling methanol (3 × 100 mL). The alcoholic extracts were then filtered and concentrated by rotary evaporation to about 10% of the initial volume. Afterwards, the solution was warmed, and slowly added dropwise under stirring to absolute ethanol (≥99.8%, 200 mL) previously cooled to -20 °C, leading to the precipitation of a white powder. After centrifugation, the solid was thoroughly dried under vacuum, then reduced to a fine powder and sealed under reduced pressure to prevent moisture uptake. The purity of GRA was further improved by gel filtration performed on a XK 26/100 column packed with

Sephadex G-10 connected to an AKTA fast protein liquid chromatograph system (FPLC) (GE Healthcare, Milan, Italy). The isolated GLs powder was dissolved in ultrapure water (0.5 g mL^{-1}), filtered through a $0.45 \text{ }\mu\text{m}$ membrane filter (Gema Medical S.L., Barcelona, Spain), charged (2 mL) onto the column and eluted using a mobile phase of ultrapure water at a flow rate of 2.0 mL min^{-1} monitoring the absorbance at 254 nm (Figure 8.4). Individual fractions (6 mL) of seven runs were analyzed by HPLC and those containing pure GRA were pooled and freeze-dried. GRA (potassium salt) was characterized by NMR and the purity was assayed by HPLC analysis of its desulfo-derivative (Figure 8.5).

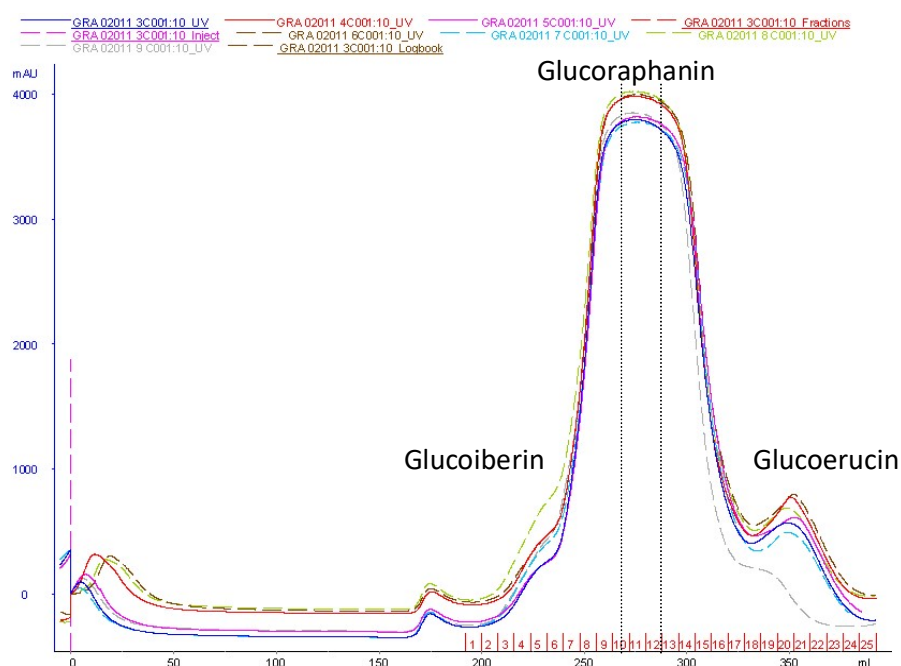


Figure 8.4 Chromatogram of a gel-filtration run performed using a XK 26/100 column packed with Sephadex G10 chromatography media, connected to an AKTA-FPLC System (GE Healthcare). Injected sample: water solution of GLs mix powder (containing main glucoraphanin and minor glucoiberin and glucoerucin) isolated with anion exchange chromatography on DEAE-A25 resin. Mobile phase: ultrapure water; monitoring absorbance: 254 nm.

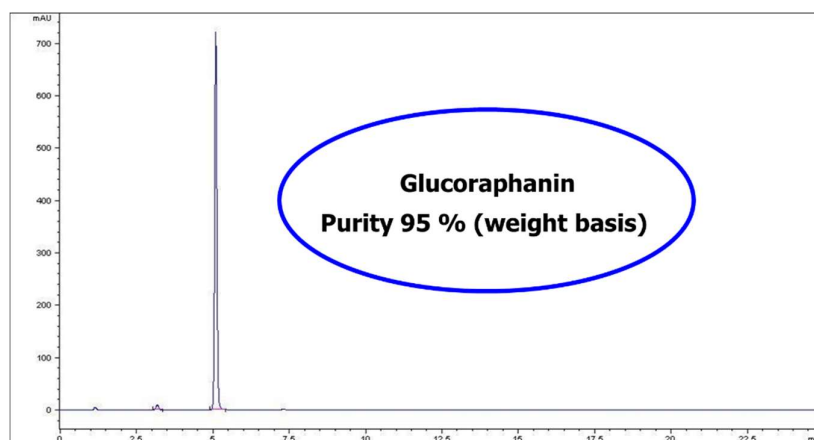


Figure 8.5 HPLC chromatogram of freeze-dried fractions of purified glucoraphanin analyzed as its desulfo counterpart.

Results and discussion of glucoraphanin purification

Individual and total GLs content in Tuscan black kale defatted seed meal are summarized (Table 8.2). Three aliphatic GLs bearing a thio-functionalized side chain accounted for 95% of the total content with predominant GRA, followed by GER and a minor amount of glucoiberin (GIB; 3-methylsulfinylpropyl GL). Two indolic GLs, namely 4-hydroxyglucobrassicin (4-OH-GBS; 4-hydroxy-3-indolylmethyl GL) and glucobrassicin (GBS; 3-indolylmethyl GL), were also present, accounting for the remaining 5% of total GLs. The starting defatted seed meal was extracted with boiling 70% ethanol with a GLs extraction yield of 78.4%. The GLs mixture isolated after anion exchange chromatography and precipitation with cold absolute ethanol consisted of GRA in a purity of 81.1% (w/w), the rest being GIB 1.4% (w/w), GER 6.7% (w/w), and most likely potassium sulfate and yellow substances which were all eliminated further on by gel filtration (Table 8.2). Enhancement of the purity level of GRA was achieved by the final gel filtration step. Seven runs of gel filtration afforded 3.10 g of purified GRA as a white amorphous solid after freeze-drying. The purity of GRA assessed by HPLC resulted to be 99% (area peak based) and 95% on weight basis.

Table 8.2 Summary of data for the purification of glucoraphanin (GRA) and the production of *R*-sulforaphane (*R*-SF) Tuscan black kale (*Brassica oleracea* (L.) ssp *acephala* (DC) var. *Sabellica* L. cv. 0D74) defatted seed meal.

Purification step	Amount	Aliphatic GLs (g)			Indole-type GLs (g)		Total GLs (g)
		GIB	GRA	GER	4-OH-GBS	GBS	
TBK-DSM	150 g	0.15 (± 0.01) ^a	7.66 (± 0.62)	1.25 (± 0.17)	0.46 (± 0.05)	0.01 (± 0.00)	9.53 (± 0.85)
Ethanolic extract	2.29 L	0.10 (± 0.00)	6.20 (± 0.02)	0.88 (± 0.00)	0.19 (± 0.07)	0.10 (± 0.00)	7.47 (± 0.09)
GLs mix powder (from DEAE A-25)	7.19 g	0.10 (± 0.00)	5.83 (± 0.14)	0.48 (± 0.06)	-	-	6.41 (± 0.20)
Purified GRA	3.10 g						
<i>R</i> -Sulforaphane	1.09 g						

^a Glucosinolate content (g) reported as the mean of eight determinations ($n = 8$). Numbers in parenthesis denote the standard deviation (\pm SD). Legend: TBK-DSM: Tuscan black kale defatted seed meal; GIB: glucoiberin; GRA: glucoraphanin; GER: glucoerucin; 4-OH-GBS: 4-hydroxy glucobrassicin; GBS: glucobrassicin

8.3.3 Glucoraphanin characterization

8.3.3.1 Glucoraphanin molar extinction coefficient determination

First, the UV spectrum of a water solution of GRA (95% pure, 2.089×10^{-4} M) was registered between 200 and 320 nm by using a computerized Varian Cary 300 Bio UV/Visible spectrophotometer (Varian, Palo Alto, CA, USA) equipped with 1 cm quartz cells. A maximum absorption at 225 nm was exhibited (Figure 8.6A). Then, the molar extinction coefficient (ϵ) of GRA was determined as follows. A stock water solution of GRA (95% pure, 10.46 mg mL^{-1}) was prepared and 10, 14, 24, 20, 30, 34 and 40 μL aliquots were diluted into the quartz cell up to 3 mL with water to achieve seven concentration levels from 0.70×10^{-4} to 2.79×10^{-4} M. The absorbance of each final solution was measured at 225 nm in triplicate against a water blank at 25 °C. Absorbance mean values were plotted against the corresponding molar concentrations and the ϵ calculated by linear regression as the slope of the plot (Figure 8.6B). This value can be of considerable importance to the analytical chemist in correcting the purity level as already pointed out (Clarke et al., 2010). The measured ϵ (225 nm, water) for GRA, potassium salt, was found to be $6634 \text{ M}^{-1} \text{ cm}^{-1}$. This value greatly differs from the previously

reported one of $6872 \text{ M}^{-1} \text{ cm}^{-1}$ measured in water at 235 nm, which is not the λ_{max} for GRA (Fahey et al., 2003).

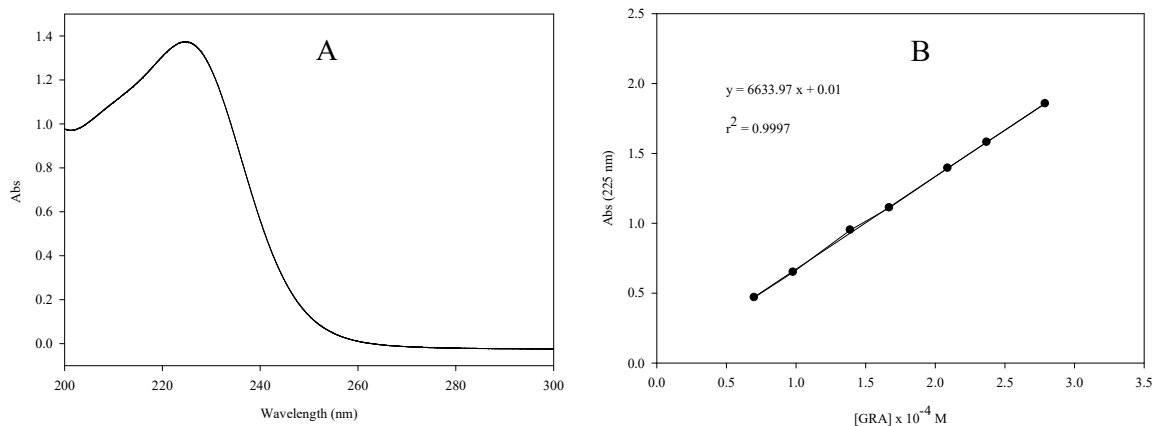
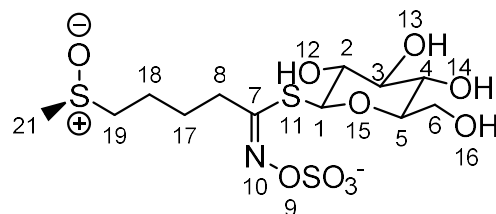


Figure 8.6 UV spectrum of purified glucoraphanin (GRA) (purity 95%) in water at a concentration value of $2.089 \times 10^{-4} \text{ M}$. λ_{max} : 225 nm (A). Absorbance vs. glucoraphanin (GRA) concentration plot used for the determination of the molar extinction coefficient (ϵ) in water at 225 nm. The ϵ calculated by linear regression as the slope of the plot resulted $6634 \text{ M}^{-1} \text{ cm}^{-1}$ (B).

8.3.3.2 NMR analysis of glucoraphanin

NMR spectra were recorded in D_2O at 298 K with TSP- d_4 as an internal reference on (i) a 500 MHz Bruker Avance III spectrometer equipped with a 5 mm BBFO+ probe and (ii) a 600 MHz Bruker Avance III spectrometer equipped with a 5 mm TCI cryoprobe, both driven by the TopSpin NMR software (v2.1), which was also used for the data processing. Spectra were recorded by means of standard Bruker pulse sequences, namely, cosygppr for COSY, hsqcedetgpsisp2.2 for HSQC, hmbcgp1pndqf for ^1H - ^{13}C HMBC and hmbcf3gpndqf for ^1H - ^{15}N HMBC as reported in Ibrahim et al. (2018).



4*R*-methylsulfinylbutyl glucosinolate (glucoraphanin, GRA)

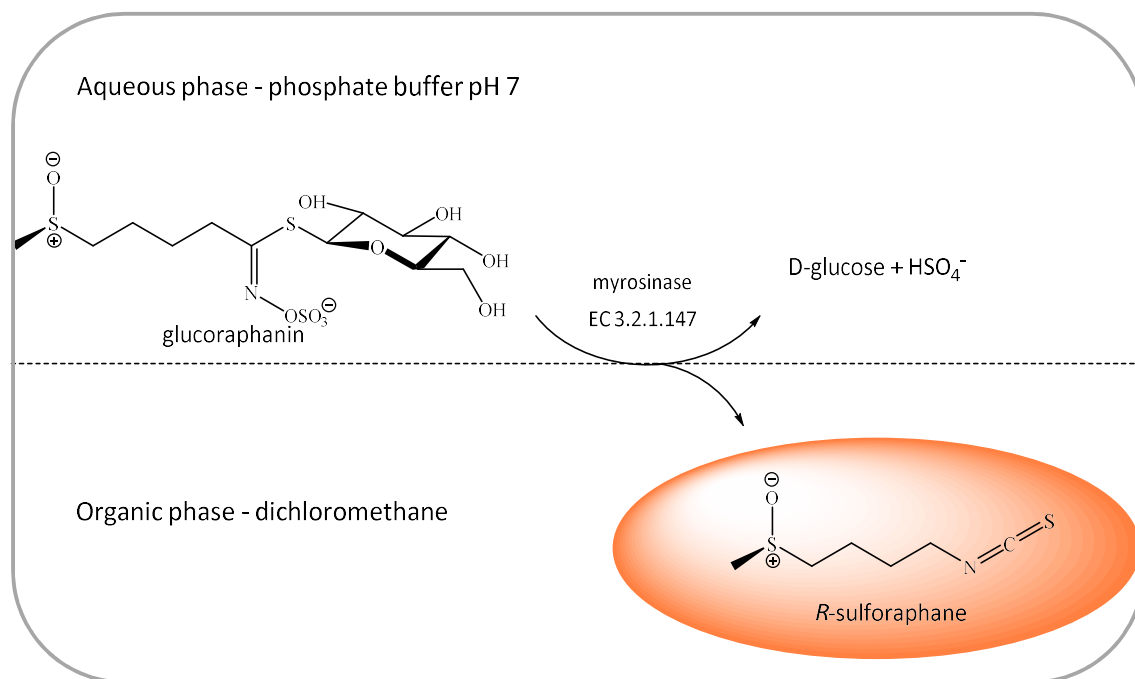
C₁₂H₂₂NO₁₀S₃ ; M = 475.59 g mol⁻¹ (potassium salt)

Table 8.3 ¹H-, ¹³C- and ¹⁵N-NMR spectral data (500 MHz, D₂O) for glucoraphanin (4-methylsulfinylbutyl glucosinolate) (Ibrahim et al., 2018).

#	δ C	#	δ H	Couplings				
C-1	84.7250	H-1	5.0276	J(H-1,H-2) = 9.8961				
C-2	74.8823	H-2	3.4483	J(H-2,H-1) = 9.8961	J(H-2,H-3) = 9.0020			
C-3	79.9776	H-3	3.5526	J(H-3,H-2) = 9.0020	J(H-3,H-4) = 9.1593			
C-4	72.1033	H-4	3.4492	J(H-4,H-3) = 9.1593	J(H-4,H-5) = 9.8367			
C-5	83.0824	H-5	3.5597	J(H-5,H-4) = 9.8367	J(H-5,H-6S) = 5.9431	J(H-5,H-6R) = 2.2233		
C-6	63.6114	H-6R	3.8883	J(H-6R,H-5) = 2.2233	J(H-6R,H-6S) = -12.6088			
		H-6S	3.6980	J(H-6S,H-5) = 5.9431	J(H-6S,H-6R) = -12.6088			
C-7	166.6598							
C-8	34.6060	H-8R	2.7953	J(H-8R,H-8S) = -14.7144	J(H-8R,H-17R) = 8.1568	J(H-8R,H-17S) = 9.2756		
		H-8S	2.7897	J(H-8S,H-8R) = -14.7144	J(H-8S,H-17R) = 5.0333	J(H-8S,H-17S) = 6.5919		
N-10	346.1800							
C-17	28.3292	H-17R	1.9061	J(H-17R,H-8S) = 5.0333	J(H-17R,H-8R) = 8.1568	J(H-17R,H-17S) = -13.3531	J(H-17R,H-18S) = 7.5533	J(H-17R,H-18R) = 7.4683
		H-17S	1.8824	J(H-17S,H-8S) = 6.5919	J(H-17S,H-8R) = 9.2756	J(H-17S,H-17R) = -13.3531	J(H-17S,H-18S) = 5.2948	J(H-17S,H-18R) = 7.4205
C-18	24.1367	H-18R	1.8196	J(H-18R,H-17R) = 7.4683	J(H-18R,H-17S) = 7.4205	J(H-18R,H-18S) = -12.0042	J(H-18R,H-19R) = 5.5044	J(H-18R,H-19S) = 9.1477
		H-18S	1.8466	J(H-18S,H-17R) = 7.5533	J(H-18S,H-17S) = 5.2948	J(H-18S,H-18R) = -12.0042	J(H-18S,H-19R) = 9.0214	J(H-18S,H-19S) = 6.6860
C-19	55.0411	H-19R	2.9185	J(H-19R,H-18S) = 9.0214	J(H-19R,H-18R) = 5.5044	J(H-19R,H-19S) = -13.3586		
		H-19S	2.9563	J(H-19S,H-18S) = 6.6860	J(H-19S,H-18R) = 9.1477	J(H-19S,H-19R) = -13.3586		
C-21	39.3269	H-21	2.6924					

8.4 Production of enantiopure *R*-sulforaphane on the gram scale

A sample of purified GRA (95% weight based, 3.10 g; 6.192 mmol) was dissolved in PPB pH 7.0 (0.3 M, 120 mL) and mixed with DCM (160 mL). After addition of MYR (1 mL, 12 U mL⁻¹), the mixture was vigorously stirred at 37 °C overnight (Scheme 8.2). After cooling at room temperature, the organic phase was decanted, and the aqueous phase extracted with DCM (3 × 10 mL). The organic layers were pooled, dried over anhydrous sodium sulfate, and the solvent was then removed by rotary evaporation at room temperature yielding enantiopure *R*-SF (1.09 g, 6.130 mmol) as a light-yellow oil with a 99% conversion of GRA. *R*-SF was sealed under reduced pressure and stored at -28 °C. Characterization of *R*-SF is reported at Chapter nine (See Section 9.4.1).



Scheme 8.2 Production of enantiopure *R*-sulforaphane. Myrosinase (β -thioglucoside glucohydrolase; E.C. 3.2.1.147; MYR) catalyzed hydrolysis reaction of glucoraphanin (GRA), purified from Tuscan black kale defatted seed meal, in a biphasic system. Upper layer: phosphate buffer 0.3 M pH 7.0, lower layer: dichloromethane.

8.5 Production of a standardized freeze-dried Tuscan black kale seed extract powder

Tuscan black kale seeds were dehulled, ground to a fine powder and defatted overnight by stirring in hexane. After filtration on filter paper (Whatman No. 1) the residue was let to dry completely in a fume hood obtaining the defatted seed meal (DSM) as a yellow fine powdered cake. A sample of DSM (25.4 g) was extracted in boiling 70% (v/v) ethanol (750 mL) for 5 min at 75°C using an Ultra-Turrax T25 homogenizer (IKA-Werk, Staufen, Germany), and then centrifuged with a J2-MC centrifuge (Beckman, Palo Alto, CA, USA) at 10000g for 45 min at 10 °C. The solid residue was extracted a second time (500 mL solvent) and centrifuged as before. The two supernatants (514 + 335 mL) were pooled and reduced in a rotary evaporator at a temperature of 40 °C. The concentrated extract (230 mL) was kept in an ice bath and left overnight at 4 °C for protein precipitation. After centrifugation ultrapure water was added (up to 450 mL) to the slightly yellow clear solution. The extract was then frozen and finally freeze-dried (DLAB 500, Italian Vacuum Technology) obtaining a light yellow fine powder (4.695 g) that was analyzed for GL profile and content. The freeze-dried seed extract resulted to be highly enriched in GRA containing 26.7% (w/w) of the GL of interest.

Table 8.3 Glucosinolate (GL) content of Tuscan black Kale (*Brassica oleracea* (L.) ssp *acephala* (DC) var. *Sabellica* L. cv. 0D74) freeze-dried seed extract powder.

	Aliphatic GLs		Total Aliphatic GLs	Indole-type GLs	Total GLs
	GRA	GER		4-OH-GBS	
μmol/g	561.8 ± 18.4	96.1 ± 2.9	657.9 ± 21.3	23.6 ± 2.6	681.5 ± 23.9
mg/g	267.2 ± 8.8	44.2 ± 1.3	311.4 ± 10.1	11.9 ± 1.3	323.3 ± 11.4
% (w/w)	26.7	4.4	31.1	1.2	32.3

8.6 Production of a standardized freeze-dried Tuscan black kale sprout powder

Tuscan black kale seeds were surface sterilised by soaking for 30 min in 1% sodium hypochlorite and rinsed with tap water. Sprouts were grown at room temperature by using an automatic sprouter VitaSeed (Suba Seeds, Longiano, FC, Italy) under an 8h/16h light/dark cycle. Four-day old sprouts were gently washed with tap water, whole frozen, freeze-dried and ground to a fine powder. The obtained powder was analyzed for GLs and results are reported in Table 8.4.

Table 8.4 Glucosinolate (GL) content of Tuscan black Kale (*Brassica oleracea* (L.) ssp *acephala* (DC) var. *Sabellica* L. cv. 0D74) freeze-dried four-day old sprout powder.

	Aliphatic GLs		Indole-type GLs				Total GLs
	GRA	GER	4-OH-GBS	GBS	4-OMe-GBS	Neo-GBS	
μmol/g	90.2 ± 2.2	19.8 ± 0.1	6.4 ± 0.2	1.1 ± 0.1	1.2 ± 0.1	3.5 ± 0.1	122.2 ± 2.8
mg/g	42.9 ± 1.1	9.1 ± 0.0	2.6 ± 0.1	0.6 ± 0.1	0.8 ± 0.0	1.8 ± 0.1	57.6 ± 1.3
% (w/w)	4.3	0.9	0.3	0.1	0.1	0.2	5.9

8.7 Production of a standardized freeze-dried Tuscan black kale sprout powder

Fine powdered freeze-dried four-day old sprouts (30 g) were extracted in boiling 70% (v/v) ethanol (800 mL) for 5 min at 80°C using an Ultra-Turrax T25 homogenizer (IKA-Werk, Staufen, Germany), and then centrifuged with a J2-MC centrifuge (Beckman, Palo Alto, CA, USA) at 17700g for 40 min at 10 °C. The solid residue was extracted a second time with the same w/v ratio and centrifuged as before. The two supernatants were collected and the volume was reduced three fold in a rotary evaporator at a temperature of 40 °C. The concentrated extract was kept in an ice bath overnight. Precipitated proteins were removed by centrifugation, and finally the extract was freeze-dried (DLAB 500, Italian Vacuum Technology) obtaining a fine green powder (TBK-SE). Individual and total content of GLs in TBK-SE are reported in Table 8.5, and Figure 8.7 shows a typical HPLC chromatogram of derived DS-GLs. The extract resulted to be highly enriched in GLs containing 20.3% (w/w) of total GLs. The most abundant were two aliphatic GL with sulfur-containing side chain, with predominant GRA, followed by glucoerucin (GER, 4-methylsulfanylbutyl GL) the precursor of erucin, representing 74% and 18% of total GLs, respectively. It is worth noting that, TBK-SE was free of the goitrogenic progoitrin ((2S)-2-hydroxy-3-butenyl GL) and contained only limited amount of indole GLs, 0.98% (w/w) 4-hydroxy-glucobrassicin (4-OH-GBS, 4-hydroxy-3-indolylmethyl GL), 0.18% (w/w) glucobrassicin (GBS, 3-indolylmethyl GL), 0.02% (w/w) 4-methoxy glucobrassicin (4-OMe-GBS, 4-methoxy-3-indolylmethyl GL) and 0.07% (w/w) neoglucobrassicin (Neo-GBS, N-methoxy-3-indolylmethyl).

Table 8.5 Glucosinolate (GL) content of Tuscan black Kale (*Brassica oleracea* (L.) ssp *acephala* (DC) var. *Sabellica* L. cv. 0D74) freeze-dried four-day old sprout extract.

	Aliphatic GLs			Indole-type GLs				Total GLs
	GIB	GRA	GER	4-OH-GBS	GBS	4-OMe-GBS	Neo-GBS	
μmol/g	6.5 ± 0.4	317.2 ± 8.2	79.5 ± 2.8	19.4 ± 1.8	3.7 ± 0.5	0.4 ± 0.5	1.4 ± 0.3	428.1 ± 14.5
mg/g	3.0 ± 0.2	150.9 ± 3.9	36.5 ± 1.3	9.8 ± 0.9	1.8 ± 0.2	0.2 ± 0.3	0.7 ± 0.2	202.9 ± 7.0
%(w/w)	0.3	15.1	3.6	1.0	0.2		0.1	20.3

The data represent the mean ± SD of two replicates experiments with 4 samples analysed per replicate ($n = 8$). Legend: GIB, glucoiberin; GRA, glucoraphanin; GER, glucoerucin; 4-OH-GBS, 4-hydroxy glucobrassicin; GBS, glucobrassicin, 4-OMe-GBS, 4-methoxy glucobrassicin; Neo-GBS, neoglucobrassicin.

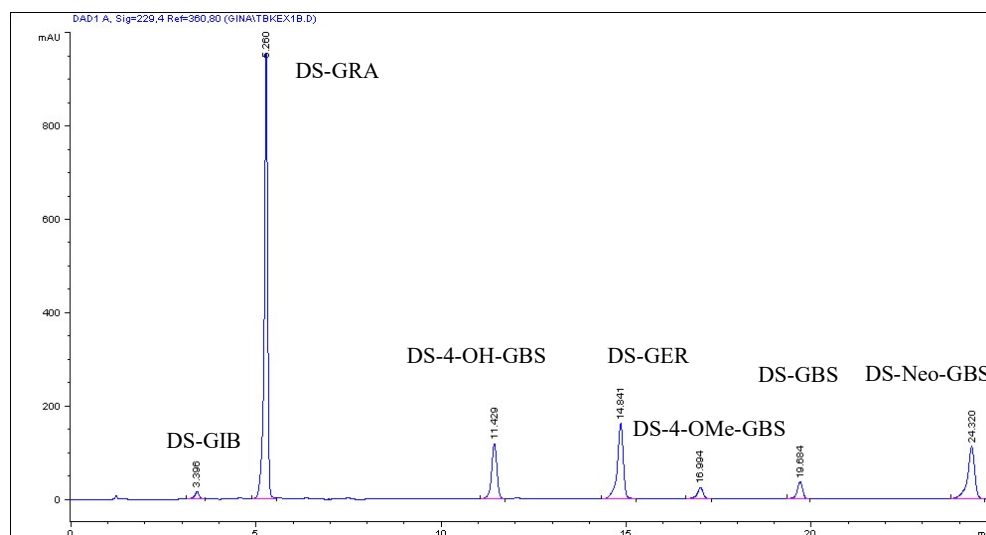


Figure 8.7. HPLC chromatogram of desulfo glucosinolates (DS-GLs) isolated from Tuscan black kale (*Brassica oleracea* (L.) ssp *acephala* (DC) var. *Sabellica* L. cv. 0D74) freeze-dried sprout extract (TBK-SE). Legend: DS-GIB, desulfo glucoiberin; DS-GRA, desulfo glucoraphanin; DS-GER, desulfo glucoerucin; DS-4-OH-GBS, desulfo 4-hydroxy glucobrassicin; DS-GBS, desulfo glucobrassicin, DS-4-OMe-GBS, desulfo 4-methoxy glucobrassicin; DS-Neo-GBS, desulfo neoglucobrassicin.

8.8 TBK-SE treatment with myrosinase

TBK-SE (17 mg) was dissolved in PBS pH 7.4 (1 mL, 0.01 M), and ITCs were produced by MYR (*S. alba* L.) (0.64 U) enzymatic hydrolysis performed at 37 °C. After 10 min, the resulting ITCs were analyzed via GC-MS for profile determination and quantified as total ITCs via HPLC analysis.

8.8.1 GC-MS analysis of isothiocyanates

The buffered solution containing ITCs (1 mL) was withdrawn and extracted with DCM (2 mL). After drying with K_2SO_4 , the organic phase was analyzed by GC-MS. GC-MS analyses of ITCs were carried out using a Bruker Scion SQ Premium (Bruker Daltonics) equipped with a 30 m x 0.25 mm capillary column (HP-5MS). The flow rate of the carrier gas He was 1 mL min⁻¹. Temperature programming was from 60 °C (hold 4 min) to 200 °C at 10 °C min⁻¹ (hold 1 min). The temperature of the injector and of the detector was 180 and 280 °C, respectively. All MS

analyses were conducted in the electron impact (EI+) mode at 70 eV, the mass range was from 40 to 650 m/z and the chromatogram acquired in total ion current (TIC). The identification of ITCs was assigned based on retention times and mass spectra of standard ITCs obtained by MYR-catalyzed conversion of pure GLs.

8.8.2 HPLC analysis of total isothiocyanates

The buffered solution containing ITCs was analyzed as reported by Matera et al. (2012) by adding 40 μL of the sample to 600 μL of a solution of 1,2-benzenedithiol (10 mM) in *i*-PrOH and 500 μL of phosphate buffer pH 8.5 (0.1 M). Solutions were incubated for 2 h at 65 °C and then left to cool to room temperature, centrifuged 20 min at 13 000 g with a 5415C centrifuge (Eppendorf) and the supernatants (20 μL) were injected in HPLC. Analyses were performed with an Agilent 1100 system equipped with a photodiode array detector on a Zorbax SB-C18 column (150 x 4.6 mm, 3.5 μm) and thermostated at 30 °C. Separation and quantification was achieved as previously described (Matera et al., 2012). The pretreatment of TBK-SE solution with MYR was performed twice and each cyclo-condensation assay was done in triplicate.

8.3 Results

GLs contained in TBK-SE were hydrolyzed by the exogenous MYR treatment, and the resulting ITCs were identified and quantified. Identification was achieved by GC–MS analysis after DCM extraction of the buffered hydrolysate. As a result, three ITCs, SF, erucin (ER) and minor iberin, were detected confirming the presence of the precursors GRA, GER and glucoiberin (GIB) in the extract. The total ITCs were determined according to the well-established cyclo-condensation assay (Zhang, 2012) and quantified by HPLC. By treating 17 mg mL⁻¹ of TBK-SE containing 3.2 \pm 0.1 mmol mL of GLs (GIB, GRA and GER) the cyclo-condensation assay gave a result of 3.3 \pm 0.1 mmol mL of total ITCs, showing a quantitative transformation of aliphatic GLS into ITCs, thus indole GLs are known to be hydrolyzed into highly unstable ITCs and are spontaneously transformed to carbinols.

8.9 Conclusions

Tuscan black kale seed has shown to be a valuable vegetable source of GRA, particularly suitable for purification purposes. In fact, the defatted seed meal contained a high percentage (5.1% w/w) of GRA which was also the most abundant among a limited number of only five GLs, representing 80% of the total GL content. Those data fulfilled the starting conditions to make it a remarkable candidate amongst brassica vegetables for an efficient purification of GRA through a simple procedure. Although broccoli seeds have also been reported to be a good source of GRA, the investigated Tuscan black kale seeds showed a higher amount of GRA compared with different commercial broccoli seeds cultivars that were obtained locally. Moreover, GRA only constitutes approximately 50% of the GLs present in broccoli, which represents a major drawback for the purification of this GL (Lai et al., 2008). In this study, a complete and detailed strategy to purify GRA via a two-step chromatographic process starting from Tuscan black kale defatted seed meal is described. The purification procedure involves the initial inactivation of MYR by use of boiling 70% ethanol. After extraction, GLs are isolated using an anion exchange column chromatography on DEAE Sephadex A-25, well adapted for optimum recovery of the loaded mixture of methionine-derived GLs, namely GIB, GRA and GER, by eluting with a 0.2 M aqueous solution of potassium sulfate. The DEAE Sephadex A-25 resin proved to be suited to our purpose, further allowing isolation of the GLs mixture as a fine powder with a good purity level of 81.1% after precipitation with cold absolute ethanol. Both indole-type GLs (4-OH-GBS and GBS) are retained by the resin and can therefore be eluted at higher salt concentration (Agerbirk et al., 1998). After the first chromatographic step, GRA is further purified by gel filtration on Sephadex G-10, which enables to discard the yellow contaminants present in the starting mixture, and to separate GIB and GER from GRA. The gram-scale availability of highly pure GRA allowed to design a strategy to easily produce amounts of the naturally occurring enantiopure *R*-SF. *R*-SF is a potential chemopreventive agent and it has proven furthermore to be a promising molecule for the prevention/treatment of neurological diseases in an animal model of multiple sclerosis and Parkinson's disease (Giacoppo et al., 2013; Galuppo et al., 2013). It is therefore important to dispose of a simple and efficient method for the preparation of enantiopure *R*-SF. It is worth mentioning that the novel method disclosed herein conveniently allows gram-scale production of the target compound without requiring any purification steps as it is further

discussed next at Chapter nine. SF is usually regarded as a labile compound and moreover, because of its poor solubility in water, several difficulties are met during *in vitro* and *in vivo* testing of SF to correctly assess its biological properties. To overcome these drawbacks, the presented strategy of producing large amounts of R-SF can be positively combined with already reported effective methods to enhance its stability such as the inclusion in cyclodextrins (Lai et al., 2008; Roselli et al., 1999) or its formulation in polyethylene glycol successfully applied for topical applications (Franklin et al., 2013). Tuscan blake kale seed represents an ideal multifunctional starting material to realize also glucoraphanin enriched powder such as a freeze-dried four-day old sprouts, a freeze-dried sprouts extract and a freeze-dried seed extract. These latter materials were all standardized for GLs content and resulted to contain GRA in the following amount 4.3% (w/w), 15.1% (w/w) and 26.7% (w/w), respectively. Enriched GRA powders can be usefully used in *in vitro* and *in vivo* studies to assess their biological properties and can be promising ingredients for applications in food/nutraceutical industry.

References

Abdull Razis AF, Iori R, Ioannides C (2011) The natural chemopreventive phytochemical *R*-sulforaphane is a far more potent inducer of the carcinogen-detoxifying enzyme systems in rat liver and lung than the *S*-isomer. *Int. J Cancer* 128:2775-2782.

Abdull Razis AF and Noor NM (2013) Cruciferous vegetables: dietary phytochemicals for cancer prevention. *Asian Pac J Cancer Prev* 14:1565-1570.

Agerbirk N, Olsen CE, Sørensen H (1998) Initial and final products, nitriles, and ascorbigens produced in myrosinase-catalyzed hydrolysis of indole glucosinolates. *J Agric Food Chem* 46:1563-1571.

Clarke DB (2010) Glucosinolates, structures and analysis in food. *Anal Methods* 2(4):310-325.

ClinicalTrials.gov. Available online: <http://clinicaltrials.gov> (accessed on 16 February 2018).

De Nicola GR, Rollin P, Mazzon E, Iori R (2014) Novel gram-scale production of enantiopure *R*-Sulforaphane from Tuscan black kale seeds. *Molecules* 19 (6):6975-6986.

Fahey JF, Wade KL, Stephenson KK, Chou FE (2003) Separation and purification of glucosinolates from crude plant homogenates by high-speed counter-current chromatography. *J Chromatogr A* 996:85-93.

Franklin SJ, Dickinson SE, Karlage KL, Bowden GT, Myrdal PB (2013) Stability of sulforaphane for topical formulation. *Drug Dev Ind Pharm* 40:494-502.

Giacoppo S, Galuppo M, Iori R, De Nicola GR, Cassata G, Bramanti P, Mazzon E (2013) Protective role of (*R*_S)-glucoraphanin bioactivated with myrosinase in an experimental model of multiple sclerosis. *CNS Neurosci Ther* 19:577-584.

Galuppo M, Iori R, De Nicola GR, Ferrantelli V, Bramanti P, Mazzon E (2013) Anti-inflammatory and anti-apoptotic effects of (*R*_S)-glucoraphanin bioactivated with myrosinase

in murine sub-acute and acute MPTP-induced Parkinson's Disease. *Bioorg Med Chem* 21:5532-5547.

Ibrahim N, Allart-Simon I, De Nicola GR, Iori R, Renault J-H, Rollin P, Nuzillard J-M (2018) Advanced NMR-based structural investigation of glucosinolates and desulfoglucosinolates. *J Nat Prod* 81:323-334.

Johnson TL. Paul Talalay: the catalyst. In Bernhard HJ Juurlink (ed), *Broccoli*. Nova Science Publishers Inc. 2016: pp. 1-8.

Kelsey NA, Wilkins HM, Linseman DA (2010) Nutraceutical antioxidants as novel neuroprotective agents. *Molecules* 15:7792-7814.

Lai RH, Keck AS, Wallig MA, West LG, Jeffery EH (2008) Evaluation of the safety and bioactivity of purified and semi-purified glucoraphanin. *Food Chem Toxicol* 46:195-202.

Li C, Liang H, Yuana Q, Houa X (2008) Optimization of sulforaphane separation from broccoli seeds by macroporous resins. *Separ Sci Technol* 43:609-623.

Liang H, Yuan Q, Xiao Q (2005) Purification of sulforaphane from *Brassica oleracea* seed meal using low-pressure column chromatography. *J Chromatogr B* 828:91-96.

Liang H, Li C, Yuan Q, Vriesekoop F (2007) Separation and purification of sulforaphane from broccoli seeds by solid phase extraction and preparative high-performance liquid chromatography. *J Agric Food Chem* 55:8047-53.

Matera R, Gabbanini S, De Nicola GR, Iori R, Petrillo G, Valgimigli L (2012) Identification and analysis of isothiocyanates and new acylated anthocyanins in the juice of *Raphanus sativus* cv. Sango sprouts. *Food Chemistry* 133:563-572.

Procházka Ž. (1959) Isolation of sulforaphane from hoary cress (*Lepidium draba* L.) *Collection of Czechoslovak Chemical Communications* 24(7):2429-2430.

Roselli C, Perly B, Rollin P. Inclusion Compounds of Natural Precursors of Isothiocyanates in Cyclodextrins, Their Preparation and Use. International application PCT/FR99/00720, 29 March 1999.

Sasaki K, Neyazaki M, Shindo K, Ogawa T, Momose M (2012) Quantitative profiling of glucosinolates by LC-MS analysis reveals several cultivars of cabbage and kale as promising candidates for sulforaphane production. *J Chromatogr B* 903:171-176.

Scopus Database. Available on line: www.scopus.com (accessed on 16 February 2018).

Vergara F, Wenzler M, Hansen BG, Kliebenstein DJ, Halkier BA, Gershenzon J, Schneider, B (2008) Determination of the absolute configuration of the glucosinolate methyl sulfoxide group reveals a stereospecific biosynthesis of the side chain. *Phytochemistry* 69:2737-2742.

Zhang Y, Talalay P, Cho CG, Posner GH (1992) A major inducer of anticarcinogenic protective enzymes from broccoli: isolation and elucidation of structure. *Proc Natl Acad Sci USA* 89(6):2399-403.

Zhang Y (2012) The 1,2-benzenedithiole-based cyclocondensation assay: a valuable tool for the measurement of chemopreventive isothiocyanates. *Crit Rev Food Sci Nutr* 52, 525-532.

PART FOUR

GLUCOSINOLATE MYROSINASE ASSISTED HYDROLYSIS

CHAPTER NINE

Isothiocyanates and dithiocarbamates production in a biphasic system

Contents

Summary

- 9.1** Availability of natural isothiocyanates
- 9.2** A new strategy – The phosphate buffer/dichloromethane biphasic system
 - 9.2.1** Glucosinolate isolation and purification
 - 9.2.2** Myrosinase purification
 - 9.2.3** General procedure for isothiocyanates production
 - 9.2.4** Isothiocyanates characterization
 - 9.2.4.1 NMR analysis*
 - 9.2.4.2 Infrared analysis*
 - 9.2.4.3 Optical rotation determination*
- 9.3** Erucin production
 - 9.3.1** Erucin characterization
- 9.4** *R*-Sulforaphane production
 - 9.4.1** *R*-Sulforaphane characterization
- 9.5** *E*-Raphasatin production
 - 9.5.1** *E*-Raphasatin characterization
- 9.6** *ER*-Sulforaphene production
 - 9.6.1** *ER*-Sulforaphene characterization
- 9.7** Discussion of the isothiocyanates production yields
- 9.8** One-pot production of dithiocarbamates
 - 9.8.1** General procedure for dithiocarbamates production
 - 9.8.2** Dithiocarbamates characterization
 - 9.8.2.1 NMR analysis*
- 9.9** Erucin-dithiocarbamate production
 - 9.9.1** Erucin-dithiocarbamate characterization

- 9.10** *R*-Sulforaphane-dithiocarbamate production
 - 9.10.1** *R*-Sulforaphane-dithiocarbamate characterization
- 9.11** *E*-Raphasatin-dithiocarbamate production
 - 9.11.1** *E*-Raphasatin-dithiocarbamate characterization
- 9.12** *ER*-Sulforaphene-dithiocarbamate production
 - 9.12.1** *ER*-Sulforaphene-dithiocarbamate characterization
- 9.13** Discussion of the dithiocarbamates production yields
- 9.14** Further exploration of glucoraphenin myrosinase assisted hydrolysis
 - 9.14.1** Solvent effect
 - 9.14.1.1 Hydrolysis in phosphate buffer*
 - 9.14.1.2 Hydrolysis in phosphate buffer/ethyl acetate biphasic system*
 - 9.14.2** Time effect
 - 9.14.3** Myrosinase/glucoraphenin ratio effect
 - 9.14.4** Ascorbic acid effect
 - 9.14.5** Effects of enzymolysis conditions on glucoraphenin conversion into *ER*-sulforaphene
 - 9.14.6** Autolysis of Japanese radish seed
 - 9.14.6.1 Daikon defatted seed meal preparation*
 - 9.14.6.2 Daikon defatted seed meal autolysis in the biphasic system*
 - 9.14.6.3 Daikon myrosinase crude extract preparation*
 - 9.14.6.4 Daikon myrosinase assisted hydrolysis of glucoraphenin*
- 9.15** Stability test and transformation of *ER*-sulforaphene in water
- 9.16** Investigation of the aqueous phase in myrosinase assisted glucoraphenin hydrolysis
 - 9.16.1** Isolation and purification of P3
 - 9.16.1.1 P3 characterization*
- 9.17** Conclusion

References

Keywords

Glucosinolates, Isothiocyanates, Dithiocarbamates, Glucoerucin, Glucoraphenin, Glucoraphasatin, Glucoraphenin, Erucin, *R*-Sulforaphane, *E*-Raphasatin, *ER*-Sulforaphene

Abbreviations

AcOEt: Ethyl Acetate;

DCM: Dichloromethane;

DS-GL: Desulfo-glucosinolate;

DTC: Dithiocarbamate;

ER: Erucin;

E-RH: *E*-Raphasatin;

ER-SFE: *ER*-Sulforaphene;

R-SF: *R*-Sulforaphane;

GER: Glucoerucin;

GL: Glucosinolate;

GRA: Glucoraphanin;

GRE: Glucoraphenin;

GRH: Glucoraphasatin;

ITC: Isothiocyanate;

MYR: Myrosinase;

PPB: Potassium phosphate buffer.

Summary

In this Chapter a new simple method to produce pure isothiocyanates and dithiocarbamates is described. Pure glucosinolates were hydrolyzed by the action of myrosinase in a phosphate buffer/dichloromethane biphasic system. The conversion of a set of four glucosinolates to isothiocyanates namely glucoerucin, glucoraphanin, glucoraphasatin and glucoraphenin, was investigated. The same glucosinolates were hydrolyzed using the biphasic system with the addition of benzyl mercaptan used as a model thiol to trap *in situ* the corresponding isothiocyanates intermediate and directly transform them into dithiocarbamates. This new strategy gave a quantitative transformation of glucoerucin and glucoraphanin into the desired isothiocyanates, and dithiocarbamates in good yield. Conversely, glucoraphasatin and glucoraphenin gave lower results. Glucoraphenin myrosinase assisted hydrolysis, as well as the stability in water of its enantiopure isothiocyanate, *ER*-sulforaphene, were further investigated showing an interesting and peculiar reactivity. A new small molecule bearing 3 sulfur atoms was isolated and characterized for the first time.

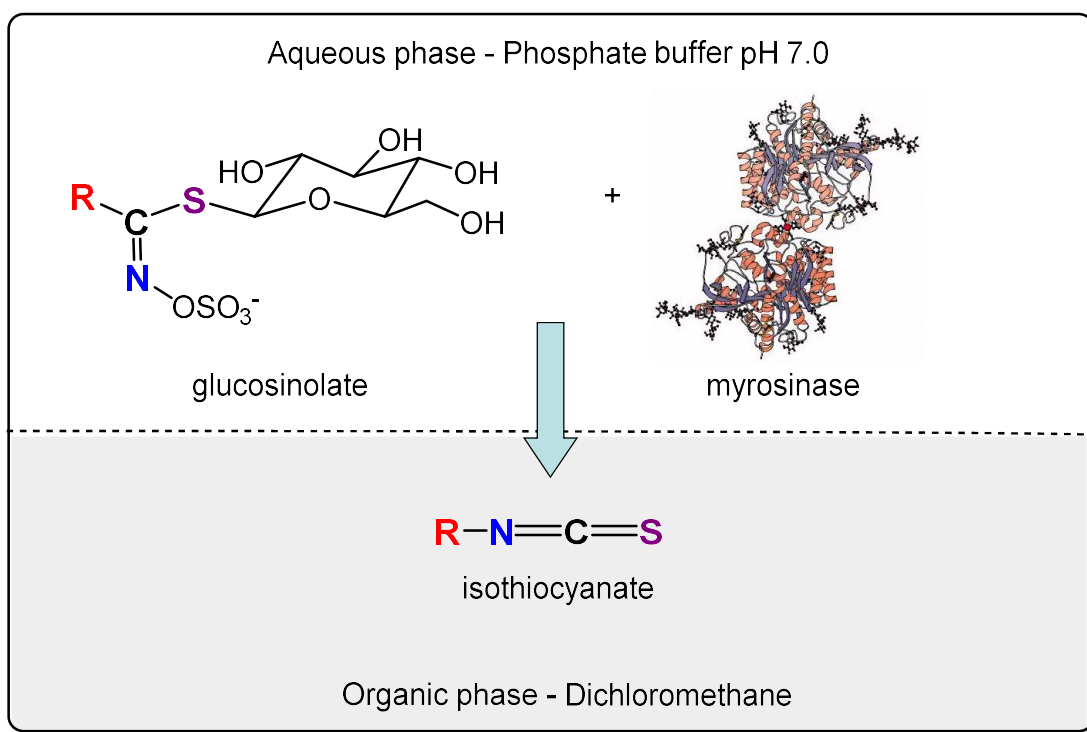
9.1 Availability of natural isothiocyanates

Isothiocyanates (ITCs) are the main breakdown products of glucosinolates (GLs) myrosinase (MYR) assisted hydrolysis at neutral pH. Many ITCs are of interest because of their biological activities. Indeed, some of them have proven biocidal activity against a wide variety of organisms, such as insects, plants, fungi and bacteria (Vig et al., 2009), whereas others can provide human health benefits (Traka, 2016). Nutritional/health studies require gram quantities of ITCs and the utilization of these compounds is often limited because either they are not commercially available, or their cost is very high. For instance, 5 mg of pure *R*-sulforaphane ($\geq 95\%$ HPLC grade) currently costs 222 € (Sigma-Aldrich Italy). Most studies are focused on sulforaphane (see Chapter five of this PhD thesis), though in nature there are at least 134 documented GLs and it would be valuable to investigate how different side chain structures could modulate the biological activity and the possible health promoting properties of the corresponding ITCs. Therefore, there is the need to make these biomolecules available on the multigram scale. Several methods to produce natural ITCs have been reported in the literature. You et al. (2008) screened 28 varieties of brassica seeds to select the most suitable source for the isolation of sulforaphane and erucin on the gram scale. In that study, seeds were autolyzed (hydrolyzed by the action of endogenous MYR) releasing a pool of ITCs, nitriles and goitrin that needed to be purified with chromatographic techniques for the isolation of the pure target compounds. In a previous study, Vaughn and Berhow (2005) described a procedure for the gram-scale preparation of several GL hydrolysis products autolyzing suitable defatted seed meals in variable reaction conditions, without necessitating chromatography of any kind. Although the focus of their study was to qualitatively produce the compounds without using chromatography, they also reported the yield of conversion for one of the selected GL into the corresponding ITC. Pure 3-methylsulfinylpropyl ITC (iberin) was obtained in a yield of 90% after several solvent extractions of autolyzed defatted *Lesquerella fendleri* seed meal (rich in the parent GL) in a mixture of HCl 0.1 M and dichloromethane (DCM). A different strategy evaluated the transformation of purified GLs using free and immobilized MYR followed by water/DCM liquid/liquid extraction. It was shown that, starting from 2-propenyl GL (sinigrin), 3-butenyl GL (gluconapin), benzyl GL (glucotropaeolin), 4-hydroxybenzyl GL (sinalbin), 4-methylsulfonylbutyl GL (glucoerucin), 4-methylsulfinylbutyl GL (glucoraphanin) and 3-methylsulfonylpropyl GL (glucocheirolin)

obtained in a pure form from suitable GL rich seeds, only ITCs were produced at pH value of 6.5. However, the yield of transformation of starting GLs into ITCs was not mentioned. The authors reported only the ratio of ITCs to nitriles determined qualitatively via GC-MS analysis (Leoni et al., 1997; 2000).

9.2 A new strategy – The phosphate buffer/dichloromethane biphasic system

The aim of the present study was to test the feasibility of hydrolyzing pure GLs with MYR using a simple potassium phosphate buffer (PPB)/DCM biphasic system to recover a single highly pure ITC in the organic phase without the need of any chromatographic separation (Scheme 9.1).



Scheme 9.1 General scheme of the production of isothiocyanates from myrosinase catalyzed hydrolysis of glucosinolates in a biphasic system. Aqueous phase is potassium phosphate buffer pH 7.0 (upper layer) and organic phase is dichloromethane (lower layer). The reported dimeric structure of myrosinase purified from white mustard seeds (*Sinapis alba* L.) is taken from Burmeister et al. (1997).

The presented new procedure has been applied to the conversion of a set of four thio-functionalized GLs into the corresponding ITCs and DTCs (Figure 9.1). Two bio-relevant redox couples have been chosen: 4-methylsulfanylbutyl GL (glucoerucin; GER)/ 4*R*-methylsulfanylbutyl GL (glucoraphanin; GRA) and (*E*)-4-methylsulfanyl-3-butenyl GL (glucoraphasatin; GRH)/(*E*)-4*R*-methylsulfanyl-3-butenyl GL (glucoraphanin; GRE). Both examined GL couples are present in vegetables widely consumed worldwide. The couple GER/GRA is present in crucifers such as broccoli (*Brassica oleracea* (L.) spp. *italica*), Tuscan black kale (*Brassica oleracea* (L.) ssp *acephala* (DC) var. *sabellica* L.) and rocket (*Eruca sativa* (Mill.)). The corresponding ITCs, 4-methylsulfanylbutyl ITC (erucin; ER) and especially 4*R*-methylsulfanylbutyl ITC (*R*-sulforaphane; *R*-SF) are the most studied amongst dietary ITCs. The couple GRH/GRE can be found in radish (*Raphanus sativus* (L.)) which consumption is increasing together with the interest of the scientific community in investigating the promising positive health effects of its derived ITCs, namely (*E*)-4-methylsulfanyl-3-butenyl ITC (*E*-raphasatin; *E*-RH) and (*E*)-4*R*-methylsulfanyl-3-butenyl ITC (*ER*-Sulforaphene, *ER*-SFE) (Hanlon and Barnes, 2011, De Nicola et al., 2013a, Abdul Razis et al., 2013). The dried ripe seed of raphanus is used as traditional Chinese medicine and is listed in Pharmacopoeia of the People's Republic of China (Sham et al., 2013). In particular, raphanus var. Sango has gained attention because it is rich of GLs and anthocyanins. A freeze-dried juice obtained by 7-day old Sango sprouts, standardized for total ITCs and anthocyanins (Matera et al., 2012; Matera et al., 2015), was prepared as a side activity of this PhD thesis project and recently studied in a rat model of obesity (Vivarelli et al., 2016; Vivarelli et al., 2017).

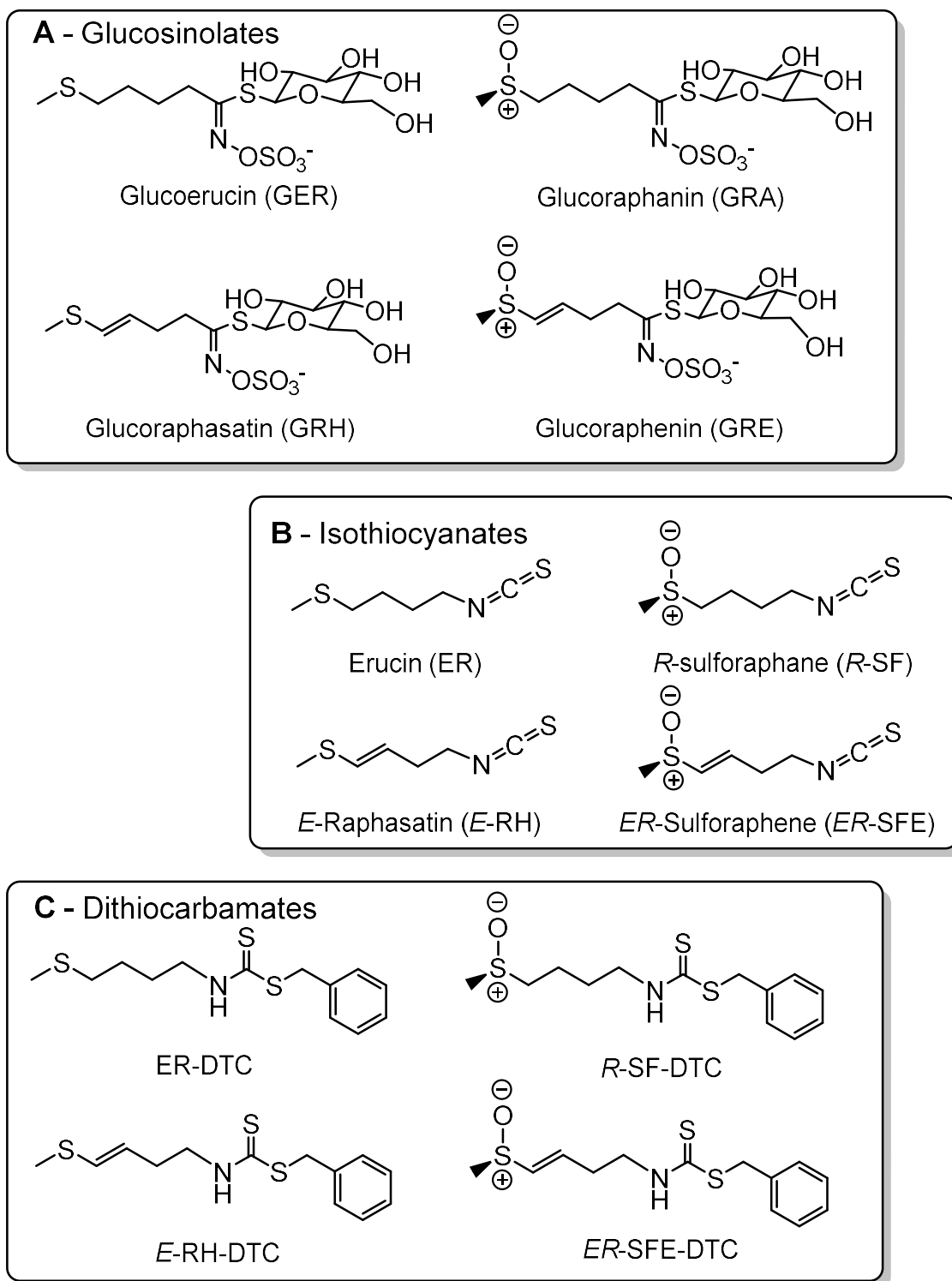


Figure 9.1 Structures of isothiocyanates (B) and dithiocarbamates (C) produced from purified glucosinolates (A) myrosinase assisted hydrolysis in a phosphate buffer/dichlorometane biphasic system.

9.2.1 Glucosinolate isolation and purification

To test the presented original method, natural purified GLs have been used. Purification of GRA isolated from Tuscan black kale seeds has been already described in detail at Chapter eight and published in De Nicola et al. (2014). The same two-step chromatography procedure, namely anion exchange followed by gel filtration, described for GRA, was applied to purify GER, GRH and GRE extracted from a suitable plant source. NMR spectra of each purified GL were recorded in D₂O as described for GRA (see section 8.3.3.2) and reported in Ibrahim et al. (2018).

Glucorucin purification and characterization

GER was extracted from rocket (*Eruca sativa* Mill.) ripe seeds as described in Barillari et al. (2005a). Briefly, rocket seeds were first ground to a fine powder and defatted in hexane. The solvent was removed, and the defatted seed meal was then treated with boiling 70% ethanol to produce a quick deactivation of endogenous MYR and to extract the intact GL. The isolation of GER from the extract was carried out by one-step anion-exchange chromatography and the purity was further improved by gel-filtration by using water as mobile phase. Fractions containing pure GER were freeze-dried obtaining a white solid. GER was characterized by NMR spectrometry (Table 9.1), and the absolute purity estimated by HPLC analysis of its desulfo counterpart was 96%.

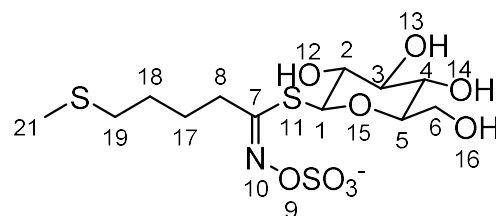
Glucoraphasatin purification and characterization

GRH was purified from 10-day old Daikon (*Raphanus sativus* L.) sprouts as described in Barillari et al., (2005b). A sample of fine freeze-dried powder (35g) was extracted twice with 500 mL of boiling ethanol 70% (v/v). The pooled extracts were filtered by using Hyflo Supercel Filter Aid (BDH Chemicals Ltd., Poole, U.K.) and subjected to chromatography procedures. The extract was loaded onto an open preparatory column (25x200 mm i.d., Pharmacia) containing DEAE-Sephadex A-25 conditioned with 25 mM acetate buffer (pH 5.6). After loading, the column was washed in sequence with starting buffer, formic acid/2-propanol/water (3:2:5) solution, and the buffer again. The column was then eluted stepwise with 5x100 mL of 25 mM

aqueous K_2SO_4 and finally with 2x150 mL of 50 mM aqueous K_2SO_4 . Each fraction collected was then checked for GL content by HPLC, and those containing GRH (about 95%) were pooled and concentrated to 1/10 of the initial volume. Inorganic salts were removed from the concentrate by adding absolute ethanol in 1:1 (v/v) ratio. After removal of precipitated salts by centrifugation, the ethanol was evaporated, and the aqueous solution containing GRH was freeze-dried. The GRH-containing freeze-dried sample of about 1.6 g was dissolved in water (400 mg mL^{-1}), and 2 mL sample was loaded onto an XK 26/100 column containing Sephadex G-10 (GE Healthcare, Milano, Italy) connected to an AKTA FPLC equipped with a Frac-900 fraction collector and UV monitor UPC-900 (GE Healthcare, Milano, Italy). Elution was performed using water as mobile phase at a flow rate of 2.0 mL min^{-1} , and the eluate was monitored at 254 nm. After the void volume was discarded, 10-mL fractions were collected. Individual fractions were then analyzed by HPLC and those containing pure GRH were pooled and freeze-dried obtaining pure GRH as a white solid. GRH was characterized by NMR spectrometry (Table 9.2), and the absolute purity estimated by HPLC analysis of its desulfo counterpart was 94%.

Glucoraphenin purification and characterization

GRE was extracted from Daikon (*Raphanus sativus* L.) ripe seeds and purified through a sequential two-step ion exchange and size exclusion chromatography, as reported in De Nicola et al. (2013b). After the two-step chromatography process, water aliquots containing pure GRE were lyophilized obtaining a white solid. GRE was characterized by NMR spectrometry (Table 9.3), and the absolute purity estimated by HPLC analysis of its desulfo counterpart was 95%.

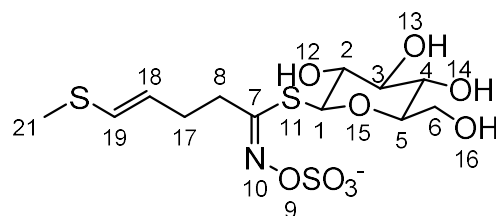


4-methylsulfanylbutyl glucosinolate (glucoerucin, GER)

$C_{12}H_{22}NO_9S_3$; $M = 459.58 \text{ g mol}^{-1}$ (potassium salt)

Table 9.1 ^1H -, ^{13}C - and ^{15}N -NMR spectral data (500 MHz, D_2O) for glucoerucin (4-methylsulfanylbutyl glucosinolate) (Ibrahim et al., 2018).

#	$\delta \text{ C}$	#	$\delta \text{ H}$	Couplings				
C-1	84.7308	H-1	5.0631	$J(\text{H-1},\text{H-2}) = 9.9024$				
C-2	74.8860	H-2	3.4649	$J(\text{H-2},\text{H-1}) = 9.9024$	$J(\text{H-2},\text{H-3}) = 8.9435$			
C-3	79.9919	H-3	3.5721	$J(\text{H-3},\text{H-2}) = 8.9435$	$J(\text{H-3},\text{H-4}) = 9.2058$			
C-4	72.0727	H-4	3.4734	$J(\text{H-4},\text{H-3}) = 9.2058$	$J(\text{H-4},\text{H-5}) = 9.9469$			
C-5	83.0913	H-5	3.5821	$J(\text{H-5},\text{H-4}) = 9.9469$	$J(\text{H-5},\text{H-6S}) = 2.2386$	$J(\text{H-5},\text{H-6R}) = 5.8203$		
C-6	63.5812	H-6R	3.7210	$J(\text{H-6R},\text{H-5}) = 5.8203$	$J(\text{H-6R},\text{H-6S}) = -12.6141$			
		H-6S	3.9077	$J(\text{H-6S},\text{H-5}) = 2.2386$	$J(\text{H-6S},\text{H-6R}) = -12.6141$			
C-7	167.3351							
C-8	34.5900	H-8R	2.7522	$J(\text{H-8R},\text{H-8S}) = -15.7577$	$J(\text{H-8R},\text{H-17R}) = 8.9934$	$J(\text{H-8R},\text{H-17S}) = 5.9266$		
		H-8S	2.7522	$J(\text{H-8S},\text{H-8R}) = -15.7577$	$J(\text{H-8S},\text{H-17R}) = 6.1395$	$J(\text{H-8S},\text{H-17S}) = 9.1683$		
N-10	345.5810							
C-17	28.6469	H-17R	1.8297	$J(\text{H-17R},\text{H-8S}) = 6.1395$	$J(\text{H-17R},\text{H-8R}) = 8.9934$	$J(\text{H-17R},\text{H-17S}) = -12.2374$	$J(\text{H-17R},\text{H-18S}) = 11.8729$	$J(\text{H-17R},\text{H-18R}) = 2.7275$
		H-17S	1.8153	$J(\text{H-17S},\text{H-8S}) = 9.1683$	$J(\text{H-17S},\text{H-8R}) = 5.9266$	$J(\text{H-17S},\text{H-17R}) = -12.2374$	$J(\text{H-17S},\text{H-18S}) = 7.4241$	$J(\text{H-17S},\text{H-18R}) = 8.7904$
C-18	30.1943	H-18R	1.7250	$J(\text{H-18R},\text{H-17R}) = 2.7275$	$J(\text{H-18R},\text{H-17S}) = 8.7904$	$J(\text{H-18R},\text{H-18S}) = -12.4219$	$J(\text{H-18R},\text{H-19R}) = 7.3033$	$J(\text{H-18R},\text{H-19S}) = 6.1088$
		H-18S	1.7250	$J(\text{H-18S},\text{H-17R}) = 11.8729$	$J(\text{H-18S},\text{H-17S}) = 7.4241$	$J(\text{H-18S},\text{H-18R}) = -12.4219$	$J(\text{H-18S},\text{H-19R}) = 7.1637$	$J(\text{H-18S},\text{H-19S}) = 8.3911$
C-19	35.5165	H-19R	2.6068	$J(\text{H-19R},\text{H-18S}) = 7.1637$	$J(\text{H-19R},\text{H-18R}) = 7.3033$	$J(\text{H-19R},\text{H-19S}) = -21.1761$		
		H-19S	2.6008	$J(\text{H-19S},\text{H-18S}) = 8.3911$	$J(\text{H-19S},\text{H-18R}) = 6.1088$	$J(\text{H-19S},\text{H-19R}) = -21.1761$		
C-21	16.9564	H-21	2.1119					

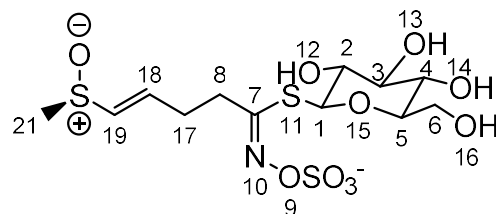


4-methylsulfanyl-3-butenyl glucosinolate (glucoraphasatin, GRH)

$C_{12}H_{20}NO_9S_3$; $M = 457.57 \text{ g mol}^{-1}$ (potassium salt)

Table 9.2 ^1H - and ^{13}C -NMR spectral data (500 MHz, D_2O) for glucoraphasatin (4-methylsulfanyl-3-butenyl glucosinolate) (Ibrahim et al., 2018).

#	$\delta \text{ C}$	#	$\delta \text{ H}$	Couplings				
C-1	84.7292	H-1	5.0284	$J(\text{H-1}, \text{H-2}) = 9.8978$				
C-2	74.8384	H-2	3.4660	$J(\text{H-2}, \text{H-1}) = 9.8978$	$J(\text{H-2}, \text{H-3}) = 8.9132$			
C-3	79.9636	H-3	3.5671	$J(\text{H-3}, \text{H-2}) = 8.9132$	$J(\text{H-3}, \text{H-4}) = 9.2147$			
C-4	72.0373	H-4	3.4716	$J(\text{H-4}, \text{H-3}) = 9.2147$	$J(\text{H-4}, \text{H-5}) = 9.9575$			
C-5	82.9952	H-5	3.5655	$J(\text{H-5}, \text{H-4}) = 9.9575$	$J(\text{H-5}, \text{H-6S}) = 2.2891$	$J(\text{H-5}, \text{H-6R}) = 5.7865$		
C-6	63.5225	H-6R	3.7181	$J(\text{H-6R}, \text{H-5}) = 5.7865$	$J(\text{H-6R}, \text{H-6S}) = -12.6229$			
		H-6S	3.9024	$J(\text{H-6S}, \text{H-5}) = 2.2891$	$J(\text{H-6S}, \text{H-6R}) = -12.6229$			
C-7	166.2401							
C-8	34.9731	H-8R	2.8000	$J(\text{H-8R}, \text{H-8S}) = -15.4956$	$J(\text{H-8R}, \text{H-17R}) = 6.2545$	$J(\text{H-8R}, \text{H-17S}) = 7.8589$		
		H-8S	2.8204	$J(\text{H-8S}, \text{H-8R}) = -15.4956$	$J(\text{H-8S}, \text{H-17R}) = 6.5029$	$J(\text{H-8S}, \text{H-17S}) = 8.2421$		
C-17	32.9793	H-17R	2.5336	$J(\text{H-17R}, \text{H-8S}) = 6.5029$	$J(\text{H-17R}, \text{H-8R}) = 6.2545$	$J(\text{H-17R}, \text{H-17S}) = -19.0478$	$J(\text{H-17R}, \text{H-18}) = 7.6040$	$J(\text{H-17R}, \text{H-19}) = -1.1685$
		H-17S	2.5382	$J(\text{H-17S}, \text{H-8S}) = 8.2421$	$J(\text{H-17S}, \text{H-8R}) = 7.8589$	$J(\text{H-17S}, \text{H-17R}) = -19.0478$	$J(\text{H-17S}, \text{H-18}) = 6.4934$	$J(\text{H-17S}, \text{H-19}) = -1.3230$
C-18	127.5983	H-18	5.5596	$J(\text{H-18}, \text{H-17R}) = 7.6040$	$J(\text{H-18}, \text{H-17S}) = 6.4934$	$J(\text{H-18}, \text{H-19}) = 15.0474$		
C-19	128.0764	H-19	6.2140	$J(\text{H-19}, \text{H-17R}) = -1.1685$	$J(\text{H-19}, \text{H-17S}) = -1.3230$	$J(\text{H-19}, \text{H-18}) = 15.0474$		
C-21	16.6233	H-21	2.2555					



4*R*-methylsulfinyl-3-butenyl glucosinolate (glucoraphenin, GRE)

$C_{12}H_{20}NO_{10}S_3$; $M = 473.57 \text{ g mol}^{-1}$ (potassium salt)

Table 9.3 ^1H -, ^{13}C - and ^{15}N -NMR spectral data (500 MHz, D_2O) for glucoraphenin (4-methylsulfinyl-3-butenyl glucosinolate) (Ibrahim et al., 2018).

#	$\delta \text{ C}$	#	$\delta \text{ H}$	Couplings					
C-1	84.5130	H-1	5.0596	$J(\text{H-1}, \text{H-2}) = 9.9004$					
C-2	74.7751	H-2	3.4716	$J(\text{H-2}, \text{H-1}) = 9.9004$	$J(\text{H-2}, \text{H-3}) = 8.9201$				
C-3	79.8731	H-3	3.5708	$J(\text{H-3}, \text{H-2}) = 8.9201$	$J(\text{H-3}, \text{H-4}) = 9.2076$				
C-4	71.9950	H-4	3.4677	$J(\text{H-4}, \text{H-3}) = 9.2076$	$J(\text{H-4}, \text{H-5}) = 9.9777$				
C-5	82.9455	H-5	3.5811	$J(\text{H-5}, \text{H-4}) = 9.9777$	$J(\text{H-5}, \text{H-6S}) = 5.9737$	$J(\text{H-5}, \text{H-6R}) = 2.2149$			
C-6	63.4793	H-6R	3.9055	$J(\text{H-6R}, \text{H-5}) = 2.2149$	$J(\text{H-6R}, \text{H-6S}) = -12.6152$				
		H-6S	3.7127	$J(\text{H-6S}, \text{H-5}) = 5.9737$	$J(\text{H-6S}, \text{H-6R}) = -12.6152$				
C-7	165.1462								
C-8	33.2952	H-8R	2.9483	$J(\text{H-8R}, \text{H-8S}) = -17.7470$	$J(\text{H-8R}, \text{H-17R}) = 6.9221$	$J(\text{H-8R}, \text{H-17S}) = 6.9861$			
		H-8S	2.9523	$J(\text{H-8S}, \text{H-8R}) = -17.7470$	$J(\text{H-8S}, \text{H-17R}) = 7.4720$	$J(\text{H-8S}, \text{H-17S}) = 7.0568$			
N-10	347.6290								
C-17	31.4656	H-17R	2.7261	$J(\text{H-17R}, \text{H-8S}) = 7.4720$	$J(\text{H-17R}, \text{H-8R}) = 6.9221$	$J(\text{H-17R}, \text{H-17S}) = -15.0413$	$J(\text{H-17R}, \text{H-18}) = 7.1162$	$J(\text{H-17R}, \text{H-19}) = -1.7910$	
		H-17S	2.7376	$J(\text{H-17S}, \text{H-8S}) = 7.0568$	$J(\text{H-17S}, \text{H-8R}) = 6.9861$	$J(\text{H-17S}, \text{H-17R}) = -15.0413$	$J(\text{H-17S}, \text{H-18}) = 6.4611$	$J(\text{H-17S}, \text{H-19}) = -1.4115$	
C-18	144.2535	H-18	6.6057	$J(\text{H-18}, \text{H-17R}) = 7.1162$	$J(\text{H-18}, \text{H-17S}) = 6.4611$	$J(\text{H-18}, \text{H-19}) = 15.2297$			
C-19	135.7740	H-19	6.5936	$J(\text{H-19}, \text{H-17R}) = -1.7910$	$J(\text{H-19}, \text{H-17S}) = -1.4115$	$J(\text{H-19}, \text{H-18}) = 15.2297$			
C-21	41.5544	H-21	2.7434						

9.2.2 Myrosinase purification

MYR was isolated from seeds of *Sinapis alba* L. according to a published method (Pessina et al., 1990) with some modifications (Bernardi et al., 2003). Briefly, the enzyme was extracted from white mustard seeds with water and purified by affinity chromatography on Con A-Sepharose. Then, the active fractions coming from affinity chromatography were pooled and dialyzed against 50 mM phosphate buffer pH 6.5 containing 0.15 M NaCl. The dialyzed MYR solution was concentrated and loaded into a prepacked Superdex 200 HiLoad 26/60 gel filtration column (GE Healthcare) equilibrated with 50 mM phosphate buffer pH 6.5 containing 0.15 M NaCl connected with a fast protein liquid chromatography system (AKTA FPLC System, GE Healthcare, Milan, Italy). The active fractions were pooled and concentrated by Millipore Amicon Stirred Cell Model 8400 using a UF membrane 30 KDa MWCO (Millipore). MYR activity was determined by spectrophotometric analysis. One MYR unit (U) was defined as the amount of enzyme able to hydrolyze 1 μmol of sinigrin (SIN; 2-propenyl GL) per minute at pH 6.5 and 37 °C (Palmieri et al., 1982). The stock solution used in the present PhD thesis study had a specific activity of 60 U mg^{-1} of soluble protein. The enzymatic activity was 32 U mL^{-1} and the solution was stored at 4 °C in sterile saline solution at neutral pH until use.

9.2.3 General procedure for isothiocyanates production

A solution of GL (0.2 mmol) in PPB pH 7.0 (1 mL, 0.5 M) and water (2 mL) was mixed with DCM (4 mL). After addition of MYR (3.2 U) the mixture was stirred vigorously at 37 °C for 4 hours. After cooling at room temperature, the organic phase was decanted, and the aqueous phase extracted with DCM (3 x 10 mL). The combined organic extracts were dried over MgSO_4 and the DCM then removed under reduced pressure at 35°C. The obtained ITC was weighed and characterized by NMR, IR, and optical rotation analysis. The efficiency of GL enzymolysis was quantified by the rate of conversion of the precursor GL to its ITC and was expressed as the percentage (%) obtained by the following equation: $\text{Yield (\%)} = [\text{ITC (mol)}/\text{GL (mol)}] \times 100$.

9.2.4 Isothiocyanate characterization

Each ITC was characterized through ^1H - and ^{13}C -NMR, and IR. The optical rotation was measured for chiral *R*-SF and *ER*-SFE. For each ITC, the Compound Identification (CI) number found in the PubChem Open Chemistry Database (National Center for Biotechnology Information, 2018), was also given.

9.2.4.1 NMR analysis

^1H - and ^{13}C -NMR spectra were recorded on a 400 MHz Avance 2 spectrometer (Bruker Biospin SA, Wissembourg, France). ITCs were dissolved in deuterated chloroform (CDCl_3) and chemical shift (δ) values were reported in ppm referenced to residual CHCl_3 at 7.26 ppm. The δ assignments were supported by 2D COSY, HSQC, and HBMC spectra. Following abbreviations are used to designate δ multiplicities: s, singlet; d, doublet; t, triplet; q, quartet; m, multiplet; and coupling constants (J) are given in Hertz (Hz).

9.2.4.2 Infrared analysis

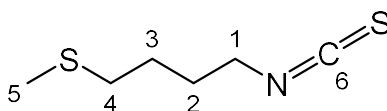
Infrared spectra were recorded on an Attenuated Total Reflectance Thermo-Nicolet AVATAR 320 AEK0200713 instrument (Perkin Elmer Instruments, Courtaboeuf, France).

9.2.4.3 Optical rotation determination

ITCs were weighed in a 1 mL volumetric flask and dissolved in CHCl_3 . The solution was transferred into a 1 mL cell (path length 1 dm) and the optical rotation was measured at 25 °C on a Perkin-Elmer 141 polarimeter (Perkin Elmer Instruments, Courtaboeuf, France) and reported as $[\alpha]_{\text{D}}^{25}$ values. Concentration (c) was expressed in g per 100 mL of solvent.

9.3 Erucin production

GER (96% pure, 0.27 mmol) was hydrolyzed as described before in the general procedure. The crude product from DCM was analyzed by $^1\text{H-NMR}$ and any purification was needed. ER (42.5 mg) was obtained as an oil with a yield of 97%.



4-methylsulfanylbutyl isothiocyanate

PubChem Compound Database; CID=78160

CAS Registry Number: 4430-36-8

$\text{C}_6\text{H}_{11}\text{NS}_2$; $M = 161.28 \text{ g mol}^{-1}$

9.3.1 Erucin characterization

IR (cm^{-1}): 2915, 2856, 2179, 2089, 1448, 1346, 1269, 1070, 958, 765, 685. Data are in accordance with Kuhnert et al. (2001).

Table 9.4 $^1\text{H-}$ and $^{13}\text{C-NMR}$ spectral data (400 MHz, CDCl_3) for erucin (4-methylsulfanylbutyl isothiocyanate; ER). Data are in accordance with those reported by Kuhnert et al. (2001).

Position	$\delta \text{ C}$	Position	$\delta \text{ H}$	δ Multiplicities and J
C-1	44.8	H-1	3.55	t, 2H, $J = 6.3$
C-2	26.0	H-2	1.76-1.85	m, 2H
C-3	29.0	H-3	1.69-1.75	m, 2H
C-4	33.4	H-4	2.53	t, 2H, $J = 6.9$
C-5	15.6	H-5	2.10	s, 3H
C-6	130.4			

9.4 R-Sulforaphane production

GRA (96% pure, two experiments: 0.51 mmol; 1.30 mmol) was hydrolyzed as described before in the general procedure. The crude product from DCM was analyzed by $^1\text{H-NMR}$ and any purification was needed. *R-SF* (90 mg; 230 mg) was obtained as a light-yellow oil with an average yield of 100%. Production of enantiopure *R-SF* was also easily scaled-up using this new methodology converting 3.10 g of GRA to 1.09 g of *R-SF* as described at Chapter eight.

9.4.1 R-Sulforaphane characterization

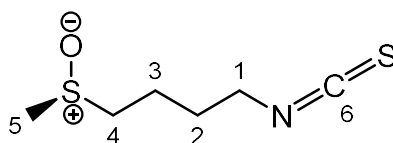
Besides NMR, optical rotation and infrared spectra analysis, *R-SF* was also analyzed by HPLC and GC-MS as follows.

HPLC-PDA Analysis of R-sulforaphane

Pure *R-* was dissolved in 10% aqueous acetonitrile and analyzed using an Agilent 1100 HPLC system (Agilent, Waldbronn, Germany) with an Inertsil ODS-3 column (250 × 3.0 mm, 5 μm particle size), thermostated at 30°C, and equipped with a PDA detector. The chromatography was performed at a flow rate of 0.8 mL min⁻¹ eluting with a gradient of H₂O (A) and acetonitrile (B) following the program: 1 min 10% B; 16 min linear gradient up to 40% B; 3 min linear gradient down to 10% B. *R-SF* was detected by absorbance monitoring at 240 nm.

GC/MS Analysis of R-sulforaphane

GC-MS analyses of pure *R-SF* was carried out using a Bruker Scion SQ Premium (Bruker Daltonics, Macerata, Italy) equipped with a 30 m × 0.25 mm capillary column HP-5ms. The flow rate of the carrier gas (He) was 1 mLmin⁻¹. Temperature programming was from 60 °C (hold 4 min) to 200 °C at 10 °Cmin⁻¹ (hold 1 min). The temperature of the injector and of the detector was 180 °C and 280 °C, respectively. All MS analyses were made in the electron impact (EI+) mode at 70 eV, the mass range was from 40 to 650 *m/z* and the chromatogram acquired in total ion current (TIC).



4*R*-methylsulfinylbutyl isothiocyanate

PubChem Compound Database; CID=9577379

CAS Registry Number: 142825-10-3

C₆H₁₁NOS₂ ; M = 177.28 g mol⁻¹

[α]_D²⁵: -76.0 (*c* 1.3, CHCl₃); literature data: -78.2 (*c* 0.6, CHCl₃) (Khiar et al., 2009).

IR (cm⁻¹): 3426 (O-H from H₂O adsorbed), 2923, 2867 (C-H), 2179, 2100 (N=C=S), 1451, 1349 (C-H), 1260 (C-N), 1021 (S=O), 739 (C-H), 688 (C-S), in accordance with literature data (Wu et al., 2010).

HPLC, *t* = 5.8 min.

GC-MS, *t*_R = 18.7 min; EIMS 70 eV *m/z* (rel. int.): 72 (100), 160 (64), 55 (43), 39 (15), 45 (13), 64 (12), 63(10), 41(10), 114 (8), 74 (6). The observed data are in agreement with literature values (Chiang et al., 1998).

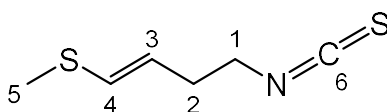
Table 9.5 ¹H- and ¹³C-NMR spectral data (400 MHz, CDCl₃) for *R*-sulforaphane (4*R*-methylsulfinylbutyl isothiocyanate; *R*-SF). Data are in accordance with those reported by Khiar et al. (2009).

Position	δ C	Position	δ H	δ Multiplicities and <i>J</i>
C-1	44.8	H-1	3.59	t, 2H, <i>J</i> = 6.0
C-2	29.1	H-2 and H-3	1.83-1.97	m, 4H
C-3	20.2			
C-4	53.6	H-4	2.66-2.80	m, 2H
C-5	38.9	H-5	2.59	s, 3H
C-6	Not Detected			

9.5 *E*-Raphasatin production

GRH (94% pure, two experiments: 0.14 mmol; 0.13 mmol) was hydrolyzed as described before in the general procedure. The crude product from DCM was analyzed by ¹H-NMR and any purification was needed. *E*-RH (12.84 mg; 11.5 mg) was obtained as an oil with an average yield of 56%.

9.5.1 *E*-Raphasatin characterization



(*E*)-4-methylsulfanyl-3-butenyl isothiocyanate

PubChem Compound Database; CID=5368086

CAS Registry Number: 13028-50-7

C₆H₉NS₂ ; M = 159.27 g mol⁻¹

IR (cm⁻¹): 2917, 2178, 2077, 1613, 1448, 1345, 1259, 1079, 1011, 935, 818, 684.

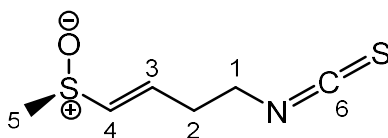
Table 9.6 ¹H- and ¹³C-NMR spectral data (400 MHz, CDCl₃) for *E*-Raphasatin ((*E*)-4-methylsulfanyl-3-butenyl isothiocyanate; *E*-RH).

Position	δ C	Position	δ H	δ Multiplicities and <i>J</i>
C-1	45.3	H-1	3.53	t, 2H, <i>J</i> = 6.5
C-2	34.0	H-2	2.47-2.52	m, 2H
C-3	120.2	H-3	5.31-5.38	m, 2H
C-4	129.3	H-4	6.20	d, 2H, <i>J</i> _{trans} = 15.0
C-5	14.9	H-5	2.27	s, 3H
C-6	Not detected			

9.6 *ER*-Sulforaphene production

GRE (95% pure, 0.2 mmol) was hydrolyzed as described before in the general procedure. The crude product from DCM was analyzed by $^1\text{H-NMR}$ and any purification was needed. *ER*-SFE was obtained as an oil (11.4 mg) with a yield of 33%.

9.6.1 *ER*-Sulforaphene characterization



(*E*)-4*R*-methylsulfinyl-3-butenyl isothiocyanate

PubChem Compound Database; CID=5368086

CAS Registry Number: 592-95-0

$\text{C}_6\text{H}_9\text{NOS}_2$; $M = 175.26 \text{ g mol}^{-1}$

$[\alpha]_{\text{D}}^{25}$: -115.8 (c 1.3, CHCl_3).

IR (cm^{-1}): 3442, 2998, 2913, 2180, 2085, 1732, 1634, 1452, 1417, 1344, 1295, 1249, 1174, 1039, 958, 912, 873, 801, 730, 680.

Table 9.7 ^1H - and ^{13}C -NMR spectral data (400 MHz, CDCl_3) for *ER*-sulforaphene ((*E*)-4*R*-methylsulfinyl-3-butenyl isothiocyanate; *ER*-SFE). Data are in accordance with those reported by Brinker and Spencer (1993).

Position	δ C	Position	δ H	δ Multiplicities and J
C-1	43.8	H-1	3.67	t, 2H, $J = 6.4$
C-2	32.8	H-2	2.71-2.61	m, 2H
C-3	133.3	H-3 and H-4	6.54-6.38	m, 2H
C-4	133.3			
C-5	40.7	H-5	2.65	s, 3H
C-6	138.2			

9.7 Discussion of the isothiocyanates production yields

Yield data of the production of the four investigated ITCs are summarized in Table 9.8. Both GER and GRA were quantitatively converted to the corresponding ITCs affording ER and *R*-SF in a 97% and 100% yield respectively, without the need of any chromatographic step. The system has also proven to be easily scaled-up to produce pure enantiomeric *R*-SF on the gram scale, as described at Chapter eight. Conversely, the transformation of GRH and GRE was not as effective as for the redox couple GER/GRA. GRH yielded *E*-RH in a 56% of the expected amount based on an equimolar conversion rate of the starting GL to final ITC. This result was somehow expected since *E*-RH is known to be unstable in aqueous environment and to spontaneously change to other compounds (Montaut et al., 2010, Kim et al., 2015). The lowest transformation rate was obtained with GRE which displayed only a 33% of formation of *ER*-SFE. *E*-RH is more hydrophobic than *ER*-SFE (Holst and Williamson, 2004) therefore, *E*-RH produced by hydrolysis in water migrates to the non-polar DCM phase faster than *ER*-SFE resulting in this way more protected from degradation. Moreover, GRE, as well as its corresponding ITC, *ER*-SFE, holds the unique structural specificity of a Michael acceptor vinyl sulfoxide site and several unexpected transformations have been already reported, such as Michael-induced ring closures (Iori et al., 2008, De Nicola et al., 2013b).

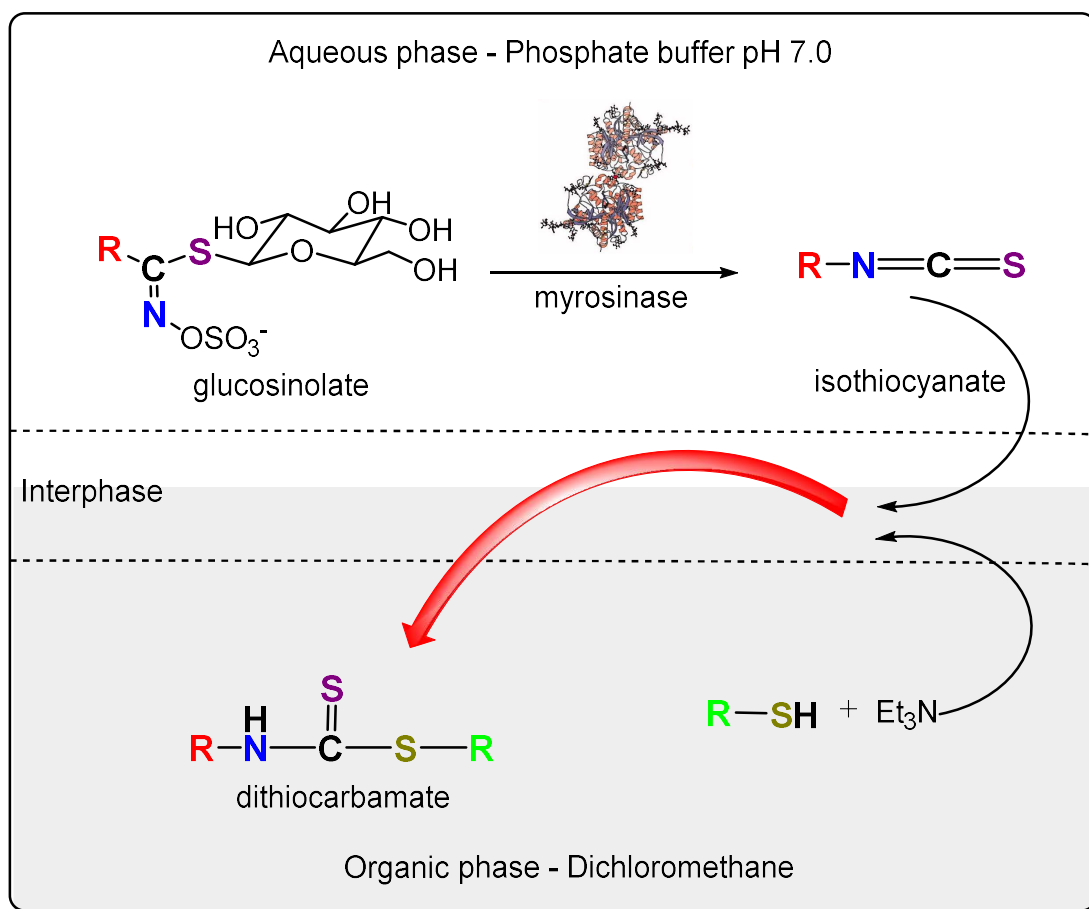
Table 9.8 Isothiocyanates (ITCs) and dithiocarbamates (DTCs) production from glucosinolates (GLs) myrosinase (MYR) catalyzed hydrolysis in a potassium phosphate buffer/dichloromethane biphasic system. MYR was isolated and purified from white mustard seeds (*Sinapis alba* L.). Yield is expressed as the % of starting glucosinolate conversion rate.

Glucosinolate	Code	Purity	Isothiocyanate	Code	Yield	DTC	Yield
Glucoerucin	GER	96%	Erucin	ER	97%	ER-DTC	68%
Glucoraphanin	GRA	96%	<i>R</i> -Sulforaphane	<i>R</i> -SF	100%	<i>R</i> -SF-DTC	90%
Glucoraphasatin	GRH	94%	<i>E</i> -Raphasatin	<i>E</i> -RH	56%	<i>E</i> -RH-DTC	90%
Glucoraphenin	GRE	95%	<i>ER</i> -Sulforaphene	<i>ER</i> -SFE	33%	<i>ER</i> -SFE-DTC	20%

The last column of Table 9.8 shows the results obtained with the one-pot DTCs production in the biphasic system that will be discussed at section 9.13.

9.8 One-pot production of dithiocarbamates

Based on the results discussed at section 9.7, the new methodology for GL hydrolysis in a biphasic system was tested to assess the ability of an added model thiol to trap *in situ* the intermediate ITC to directly produce dithiocarbamates (DTCs) (Scheme 9.2).



Scheme 9.2 General scheme of the one-pot production of dithiocarbamates from myrosinase catalyzed hydrolysis of glucosinolates in a biphasic system in the presence of triethylamine (NEt_3) and a model thiol to trap *in situ* the intermediate isothiocyanate. Aqueous phase is phosphate buffer pH 7.0 and organic phase is dichloromethane. The reported dimeric structure of myrosinase purified from white mustard seeds (*Sinapis alba* L.) is taken from Burmeister et al. (1997).

9.8.1 General procedure for the production of dithiocarbamates

To a solution of benzylmercaptan (0.24 mmol) and triethylamine (0.24 mmol) in DCM (4 mL), a solution of GL (0.2 mmol) in PPB pH 7.0 (1 mL, 0.5 M) and water (2 mL) was added. After addition of MYR (3.2 U) the mixture was vigorously stirred at 37 °C for 4 hours. After cooling at room temperature, the organic phase was decanted, and the aqueous phase extracted with DCM (3 x 10 mL). The combined extracts were dried over MgSO₄ and the DCM removed under reduced pressure at 35 °C.

9.8.2 Dithiocarbamates characterization

Each DTC was characterized through ¹H- and ¹³C-NMR analysis.

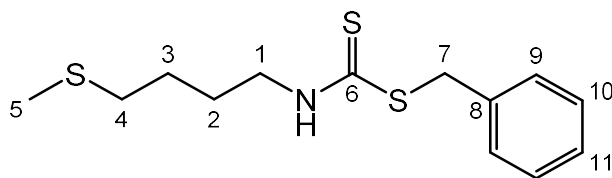
9.8.2.1 NMR analysis

¹H- and ¹³C-NMR spectra were recorded on a 400 MHz Avance 2 spectrometer (Bruker Biospin SA, Wissembourg, France). DTCs were dissolved in dimethyl sulfoxide-d₆ (DMSO-d₆) and chemical shift (δ) values were reported in ppm referenced to DMSO at 2.54 and 40.5 ppm, respectively. Following abbreviations are used to designate δ multiplicities: s, singlet; d, doublet; t, triplet; q, quartet; m, multiplet; br, broad; and coupling constants are given in Hertz (Hz).

9.9 Erucin-dithiocarbamate production

GER (96% pure, 0.2 mmol) was hydrolyzed as described before in the general procedure in the presence of benzylmercaptan (1.2 eq) and NEt₃ (1.2 eq). Crude product (55.4 mg) was purified by flash chromatography (petroleum ether/AcOEt 10:1) to give ER-DTC (38.8 mg) as a clear transparent oil in a 68% yield.

9.9.1 Erucin-dithiocarbamate characterization



Benzyl 4-methylsulfanylbutyldithiocarbamate

Original compound

C₁₃H₁₉NS₃; M = 285.48 g mol⁻¹

Table 9.9 ¹H- and ¹³C-NMR spectral data (400 MHz, DMSO-*d*₆) for erucin-dithiocarbamate (benzyl 4-methylsulfanylbutyldithiocarbamate; ER-DTC).

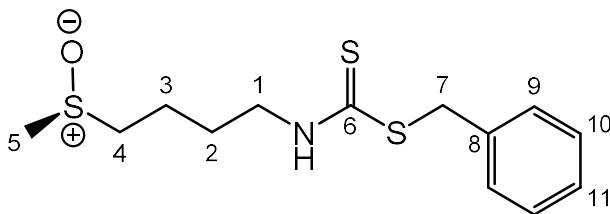
Position	δ C	Position	δ H	δ Multiplicities and <i>J</i>
C-1	46.4	H-1	3.60-3.65	m, 2H
C-2	25.9 or 26.7	H-2	1.62-1.69	m, 2H
C-3	25.9 or 26.7	H-3	1.50-1.57	m, 2H
C-4	32.8	H-4	2.47	t, 2H, <i>J</i> = 7.2
C-5	14.6	H-5	2.02	s, 3H
C-6	195.4			
C-7	38.1	H-7	4.50	s, 2H
C-8	137.4	H-Ar	7.22-7.42	s, 5H
C-9	128.4 or 128.8	N-H	9.98	br s, 1H
C-10	127.9			
C-11	128.4 or 128.8			

In the ¹H-NMR spectrum of ER-DTC peaks corresponding to a minor rotamer (7% ca.) could be detected at δ: 10.17 (br s, 1H, N-H), 4.55 (s, 2H, H-7), 3.32-3.37 (m, 2H, H-1).

9.10 R-Sulforaphane-dithiocarbamate production

GRA (96% pure, 0.2 mmol) was hydrolyzed as described before in the general procedure in the presence of benzylmercaptan (1.2 eq) and NEt₃ (1.2 eq). Crude product (69.3 mg) was purified by flash chromatography (CHCl₃/MeOH 9:1) to give (54.2 mg) of a white solid in a 90% yield.

9.10.1 R-Sulforaphane-dithiocarbamate characterization



Benzyl 4*R*-methylsulfinylbutyldithiocarbamate

PubChem Compound Database; CID = 11500431

CAS Registry Number: 884523-01-7

C₁₃H₁₉NOS₃; M = 301.49 g mol⁻¹

Table 9.10 ¹H- and ¹³C-NMR spectral data (400 MHz, CDCl₃) for *R*-sulforaphane-dithiocarbamate (Benzyl 4*R*-methylsulfinylbutyldithiocarbamate; *R*-SF-DTC). Data are in accordance with those reported by Moriarty et al. (2006).

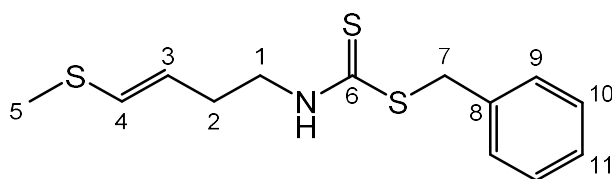
Position	δ C	Position	δ H	δ Multiplicities and <i>J</i>
C-1	46.5	H-1	3.76	d, 2H, <i>J</i> = 5.5
C-2	39.8	H-2, H-3	1.83-1.85	m, 4H
C-3	27.1			
C-4	53.5	H-4	2.73	t, 2H, <i>J</i> = 6.0
C-5	20.3	H-5	2.53	s, 3H
C-6	197.7			
C-7	38.6	H-7	4.53	s, 2H
C-8	136.8	H-Ar	7.24-7.38	s, 5H
C-9	128.7 or 129.2	N-H	8.16	br s, 1H
C-10	127.5			
C-11	128.7 or 129.2			

In the ¹H-NMR spectrum of *R*-SF-DTC peaks corresponding to a minor rotamer (20% ca.) could be detected at δ: 8.34 (br s, 1H, N-H), 3.45 (s, 2H, H-1). Minor peaks were also detected in the ¹³C-NMR spectrum at δ: 45.8 (C-1), 41.0 (C-2), 27.9 (C-3).

9.11 *E*-raphasatin-dithiocarbamate production

GRH (94% pure, 0.2 mmol) was hydrolyzed as described before in the general procedure in the presence of benzylmercaptan (1.2 eq) and NEt₃ (1.2 eq). Crude product (68 mg) was purified by flash chromatography (petroleum ether/AcOEt 95:5) to give *E*-RH-DTC (51 mg) as a yellow oil in a 90% yield.

9.11.1 *E*-raphasatin-dithiocarbamate characterization



Benzyl (*E*)-4-methylsulfanyl-3-butenyl dithiocarbamate

Original compound

C₁₃H₁₇NS₃; M = 283.48 g mol⁻¹

Table 9.11 ¹H- and ¹³C-NMR spectral data (400 MHz, DMSO-*d*₆) for *E*-raphasatin-dithiocarbamate Benzyl (*E*)-4-methylsulfanyl-3-butenyl dithiocarbamate; *E*-RH-DTC).

Position	δ C	Position	δ H	δ Multiplicities and <i>J</i>
C-1	46.6	H-1	3.62-3.65	m, 2H
C-2	31.0	H-2	2.31-2.40	m, 2H
C-3	122.2	H-3	5.34	dt, 1H, <i>J</i> = 7.0, <i>J</i> _{trans} = 15.0
C-4	125.9	H-4	6.15	d, 2H, <i>J</i> _{trans} = 15.0 Hz
C-5	13.9	H-5	2.19	s, 3H
C-6	195.6			
C-7	38.1	H-7	4.50	s, 2H
C-8	137.4	H-Ar	7.22-7.40	s, 5H
C-9	128.4 or 128.9	N-H	10.00	br s, 1H
C-10	127.1			
C-11	128.4 or 128.9			

In the ^1H -NMR spectrum of *E*-RH-DTC peaks corresponding to the *Z* stereoisomer (35% ca.) could be detected at δ : 6.11 (d, 1H, $J_{cis} = 9.0$ Hz, H-4), 5.49 (dt, 1H, $J_{cis} = 9.0$ Hz, $J = 7.0$ Hz, H-3), 2.26 (s, 3H, H-5). ^{13}C -NMR signals due to the *Z* stereoisomer were detected at δ : 129.5 (C-4), 123.6 (C-3), 16.1 (C-5).

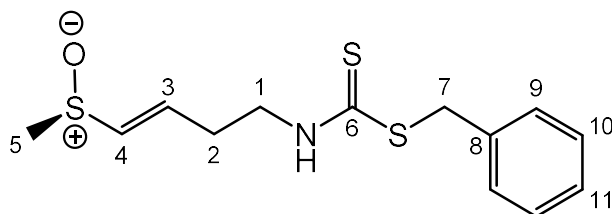
Moreover, signals due to a minor rotamer (12% ca.) were also detected in the ^1H -NMR spectrum at δ : 10.13 (br s, 1H, N-H), 4.55 (s, 2H, H-7), 3.40-3.35 (m, 2H, H-1), 2.17 (s, 3H, H-5) and in the ^{13}C -NMR spectrum at δ : 27.5 (C-2), 45.7 (C-1).

Also, a strong shielding effect (^1H and ^{13}C) was observed on the C-3 vinylic β -site of *E*-RH-DTC for which the normal positioning compared to the α -site C-4 was inverted both in $\text{DMSO}-d_6$ and CDCl_3 solutions. Such observation was already reported for RH and methyl 4-methylthio-3-butenyl dithiocarbamate in $\text{DMSO}-d_6$ (Kosemura et al., 1993; Matsuoka et al., 1997).

9.12 *ER*-sulforaphene-dithiocarbamate production

GRE (95% pure, 0.2 mmol) was hydrolyzed as described before in the general procedure in the presence of benzylmercaptan (1.2 eq) and Net_3 (1.2 eq). Crude product (32.60 mg) was purified by flash chromatography (petroleum ether/ AcOEt 9:1) to give *ER*-SFE-DTC (11.8 mg) a white solid with a 20% yield.

9.12.1 *ER*-sulforaphene-dithiocarbamate characterization



Benzyl (*E*)-4*R*-methylsulfinyl-3-butenyl dithiocarbamate

Original compound

$\text{C}_{13}\text{H}_{17}\text{NOS}_3$; $M = 299.48 \text{ g mol}^{-1}$

Table 9.12 ^1H - and ^{13}C -NMR spectral data (400 MHz, $\text{DMSO-}d_6$) for *ER*-sulforaphene-dithiocarbamate (Benzyl (*E*)-4*R*-methylsulfinyl-3-butenyl dithiocarbamate; *ER*-SFE-DTC).

Position	δ C	Position	δ H	δ Multiplicities and J
C-1	45.4	H-1	3.68-3.76	m, 2H
C-2	29.6	H-2	2.49-2.58	m, 2H
C-3	133.8	H-3	6.26	dt, 1H, $J = 6.8$, $J_{trans} = 15.2$
C-4	136.8	H-4	6.63	d, 1H, $J_{trans} = 15.2$
C-5	40.1	H-5	2.54	s, 3H
C-6	196.0			
C-7	38.1	H-7	4.50	s, 2H
C-8	137.3	H-Ar	7.24-7.37	s, 5H
C-9	128.4 or 128.9	N-H	10.08	br s, 1H
C-10	127.1			
C-11	128.4 or 128.9			

In the ^1H -NMR spectrum of *ER*-SFE-DTC peaks corresponding to a minor rotamer (9% ca.) could be detected at δ : 10.16 (br s, 1H, N-H) and 4.54 (s, 2H, H-7). The same shielding effect described before for *E*-RH-DTC was observed also for *R*-SFE-DTC and reported already for GRE and DS-GRE (Iori et al., 2008).

9.13 Discussion of the dithiocarbamate yields

Yield data of the production of the four investigated DTCs are summarized in Table 9.8 together with results obtained for ITCs production. DTCs are known to exert promising biorelevant activity such as chemoprevention (Moriarty et al., 2006; Qian et al., 2010) and they offer a better stability than ITCs. The proposed system proved to be effective, excluding the exceptional behavior of GRE, and it will be further investigated to produce a wider portfolio of DTCs. GER and GRA gave again good results, though in a lower yield compared to their transformation into the corresponding ITCs. Interestingly, the yield increased for the one pot direct transformation of GRH to DTC, if compared to the yield of production of its ITC, RH. Hence, the addition of benzylmercaptan to trap the *in situ* intermediate *E*-RH facilitated the migration of the hydrophobic *E*-RH into the DCM phase successfully stabilizing it in the DTC form. It is to be noted that the aglycone of starting GRH was mainly in the *E* conformation with minor *Z* (10%) assessed by ¹H-NMR analysis whereas, the recovered *E*-RH-DTC after chromatography showed an increase of *Z* epimer up to 35%. Recently, the same stereomutation effect of RH side chain has already been observed and reported (Montaut et al., 2010). Again, GRE showed the lowest yield (20%) and a lower result compared to the formation of *ER*-SFE in PPB/DCM. Differently from the case of *E*-RH, the idea of trapping *ER*-SFE to facilitate its migration to DCM was not effective. The MYR assisted hydrolysis of GRE, as well as the stability in water of its enantiopure ITC *ER*-SFE, was then further investigated to gain insights into its peculiar reactivity as described in the following sections.

9.14 Further exploration of glucoraphenin myrosinase assisted hydrolysis

GRE myrosinase assisted hydrolysis has been investigated under various controlled conditions to evaluate the effect of several parameters on the conversion of this GL to its corresponding ITC, *ER-SFE*.

9.14.1 Solvent effect

9.14.1.1 *Hydrolysis in phosphate buffer followed by dichloromethane extraction*

To evaluate the solvent effect, a sample of GRE (95% pure, 0.2 mmol) was hydrolyzed in PPB pH 7 (0.5 M, 3 mL) with MYR (32 U) in ten minutes to speed the reaction up and limiting the time of its possible degradation or peculiar reaction. The hydrolysis reaction was then stopped and extraction with DCM (3 x 10 mL) was performed. Pure *ER-SFE* (11.3 mg) was recovered in a yield of 32%

9.14.1.2 *Hydrolysis in phosphate buffer/ethyl acetate biphasic system*

GRE (95% pure, 0.2 mmol) was hydrolyzed with the same procedure described in section 9.6.1 using AcOEt in the biphasic system as well as in the work up phase to extract the aqueous phase after hydrolysis. Pure *ER-SFE* (12.6 mg) was recovered in a 36% yield.

9.14.2 Time effect

To learn on the effect of hydrolysis time, samples of GRE (95% pure, 0.2 mmol) were hydrolyzed with MYR (3.2U) in a PPB pH 7/DCM biphasic system for a set time of 1.5 h, 2h, 4h up to 14 hours overnight. *ER-SFE* recovery yields are reported in Table 9.13 with the indication of the reaction time.

9.14.3 Myrosinase/glucoraphenin ratio effect

Samples of GRE (95% pure, 0.2 mmol) were hydrolyzed with different amount of enzyme MYR (0.32 U, 3.2 U and 32 U) in a PPB pH 7/DCM biphasic system. *ER*-SFE recovery yields are reported in Table 9.13 with the indication of the reaction time.

9.14.4 Ascorbic acid effect

The procedure was the same as described at section 9.6.1 except ascorbic acid was added and hydrolysis was conducted in 4 hours. Two experiments were performed adding 0.012 eq and 0.15 eq of ascorbic acid (based on GRE content) to have a final concentration of 1 mM and 10 mM in the aqueous phase, respectively.

9.14.5 Effects of enzymolysis conditions on glucoraphenin conversion into *ER*-sulforaphene

Conversion rates of GRE obtained with different controlled conditions of enzymolysis are summarized in Table 9.13. A quick hydrolysis done in PPB in 10 min followed by extraction with DCM showed that DCM does not affect MYR performance. Ethyl acetate (AcOEt) was also tested as water concurrent solvent in a biphasic system to evaluate a possible better migration of *ER*-SFE into a more polar solvent than DCM. However, results indicated a minor role of the extraction solvent in the final yield. 3.2 U MYR can catalyze the hydrolysis of 0.2 mmol GL in 62 min and 0.77 mmol GL in 4 hours which was the time set in the general ITCs production procedure (section 9.2.1). Results showed that when hydrolyzing 0.2 mmol GRE conversion yield does not change with hydrolysis time from 1.5 h up to an overnight reaction for 14 h. Either decreasing or increasing the MYR/GRE ratio did not improve the conversion rate as well. It is known that MYR is activated by ascorbic acid at low millimolar concentrations typically 1-2 mM (Wittstock et al., 2016), anyway the addition of ascorbic acid did not have any effect in terms of *ER*-SFE production with both tested concentrations (1 and 10 mM).

Table 9.13 Conversion rate of pure GRE to *ER*-SFE using MYR (from *Sinapis alba* L.) in different hydrolysis conditions. All the experiments have been done using GRE (95% pure, 0.2 mmol).

	Solvent	MYR (U)	Time	Ascorbic acid	Yield
<i>Solvent effect</i>	PPB	32	10 min	-	32%
	PPB/AcOEt	3.2	2.5 h	-	36%
<i>Time effect</i>	PPB/DCM	3.2	1.5 h	-	33%
	PPB/DCM	3.2	2 h	-	29%
	PPB/DCM	3.2	4	-	33%
	PPB/DCM	3.2	14	-	33%
<i>MYR/GRE ratio</i>	PPB/DCM	3.2	1.5 h	-	33%
	PPB/DCM	32	1 h	-	39%
	PPB/DCM	0.32	14	-	37%
	PPB/DCM	3.2	14	-	33%
<i>Ascorbic acid effect</i>	PPB/DCM	3.2	1.5	1 mM	32%
	PPB/DCM	3.2	4	10 mM	35%

9.14.6 Autolysis of Japanese radish seed

In a previous study, the autolysis of radish sprouts proved a high conversion of GRE and GRH to the corresponding ITCs. In particular, Daikon *var.*, known as Japanese radish, exhibited an almost complete transformation of GRE and GRH to ITCs, analyzed as total ITCs, in autolysis experiments of freeze-dried powdered sprouts both in water and phosphate buffer pH 6.5 (De Nicola et al., 2013a). This result lead to reasonably think that Daikon endogenous MYR (Daikon MYR) is specific for its substrates GRH and GRE. It is known, indeed, that MYRs accept GLs of different structural types as substrates but differ in their affinity to individual GLs and in the efficiency of their conversion. In some cases, substrate specificity of MYRs roughly matches the GL profile of the plant organ in which the enzyme is expressed indicating some degree of specialization (Wittstock et al., 2016). Based on these considerations, the following experiments were examined: the autolysis of Daikon defatted seed meal, and the hydrolysis of pure GRE by the action of a crude extract of Daikon MYR.

9.14.6.1 *Daikon defatted seed meal preparation*

Daikon (*R. sativus* (L.) major cv. OP38) seed (50 g) was ground to a fine powder and defatted overnight by stirring in hexane (500 mL). After filtration on filter paper (Whatman No. 1) the residue was allowed to dry completely in a fume hood obtaining the defatted seed meal (DSM) (20 g). GRE content in Daikon DSM was quantified to be 130 μmolg^{-1} (6.1%) by HPLC-DAD analysis of the corresponding DS-GRE.

9.14.6.2 *Daikon defatted seed meal autolysis in the biphasic system*

A sample of Daikon DSM (1.547 g; containing 0.2 mmol GRE) was autolyzed by the action of the endogenous MYR in a PPB/DCM (3 mL/4 mL) biphasic system at 37 °C overnight (14 h). The mixture was centrifuged, and the aqueous phase extracted with DCM (3x10 mL) by vortex agitation. The crude product (90 mg) obtained after DCM evaporation contained a mix of ER-SFE and lipids. ER-SFE was purified by flash chromatography eluting first the lipidic fraction with CHCl_3 and then the target ITC with $\text{CHCl}_3/\text{MeOH}$ (20:1) to give ER-SFE (22.8 mg) in a 65% yield.

9.14.6.3 *Daikon MYR crude extract preparation*

A crude Daikon MYR extract was obtained by treating the freeze-dried powder of seven-day old Daikon sprouts (1 g) with PPB pH 6.5 (50 Mm, 10 mL) using an Ultra-Turrax T25 homogenizer in an ice bath. After centrifugation, the activity of soluble Daikon MYR was determined by spectrophotometric analysis performed with a computerized Varian Cary 300 Bio UV/vis spectrophotometer equipped with a dual cell Peltier accessory, as previously described (Palmieri et al., 1982). Two replicate experiments with three samples analyzed per replicate gave a soluble Daikon MYR activity of 1.2 U/mL.

9.14.6.4 *Daikon MYR assisted hydrolysis of glucoraphenin*

GRE (95% pure, 0.2 mmol) was hydrolyzed using the Daikon MYR crude extract (1.2 U) in a PBB/DCM biphasic system at 37 °C overnight (14 h). The crude product from DCM extraction

was analyzed by $^1\text{H-NMR}$ and any purification was needed. *ER-SFE* (24.2 mg) was obtained as an oil with a yield of 65%.

Results

Both experiments proved a better catalysis performance of Daikon MYR in comparison of *Sinapis alba* MYR at hydrolyzing GRE that is one of its natural substrate present in radish seed and sprouts, allowing to obtain enantiopure *ER-SFE* in a 65% yield. Since a better result of *ER-SFE* recovery in DCM was achieved, the focus of the study was shifted to the aqueous phase with the following objectives:

- to learn about the stability of *ER-SFE* in water with the isolation and characterization of eventual degradation products,
- the isolation and characterization of a water soluble by-product of MYR catalyzed hydrolysis of GRE.

9.15 Stability test and transformation of *ER*-sulforaphene in water

One week, room temperature

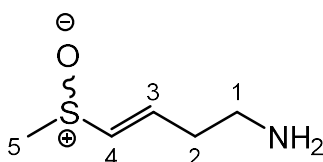
Enantiopure *ER-SFE* (22 mg, 0.12), obtained by myrosinase-catalyzed hydrolysis of GRE in PPB/DCM biphasic system, was stirred at room temperature in ultrapure water (5 mL). After one week, water was evaporated obtaining an oil that was analyzed by NMR. Only *ER-SFE* could be detected and no degradation products.

Three days, 40 °C

Enantiopure *ER-SFE* (22 mg, 0.12 mmol), obtained by MYR catalyzed hydrolysis of GRE in PPB/DCM biphasic system, was stirred at 40 °C in ultrapure water (5 mL). *ER-SFE* stability was checked by TLC. After three days a TLC analysis ($\text{CHCl}_3/\text{MeOH}$ 9/1) showed three spots corresponding to starting *ER-SFE* and two other compounds. The reaction was stopped, and flash-chromatography performed. The two isolated compounds, P1 (1 mg) and P2 (white solid, 4 mg) were identified by NMR characterization and HR-MS analysis, as follows.

P1 Characterization

P1 was dissolved in DMSO- d_6 and ^1H -NMR and bidimensional COSY spectra were recorded as described at section 9.8.2.1. The quantity of P1 recovered by flash chromatography was not enough to register the ^{13}C -NMR spectrum.



(*E*)-4-(methylsulfinyl)-3-butenamine

Original compound

$\text{C}_5\text{H}_{11}\text{NOS}$; MW = 133.21 g mol $^{-1}$

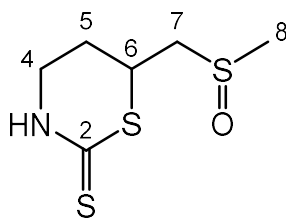
Table 9.14 ^1H -NMR spectral data (400 MHz, DMSO- d_6) of P1 isolated after *ER*-SFE degradation in water at 40 °C and characterized as (*E*)-4-(methylsulfinyl)-3-butenamine.

Position	δ H	δ Multiplicities and J
H-1	3.49	br s, 2H
H-2	2.43	q, 2H
H-3	6.24	dt, 1H, $J_{trans} = 15.2\text{Hz}$, $J_{2,3} = 6.9$
H-4	6.62	d, 1H, $J_{trans} = 15.2$
H-5	2.56	s, 3H
N-H	7.55	br s, 2H

P2 Characterization

P2 was dissolved in DMSO- d_6 and NMR spectra (^1H , ^{13}C , COSY, DEPT135 and HSQC) were recorded as described at section 9.8.2.1.

Mass spectra were recorded on a Perkin-Elmer SCIEX API-300 spectrometer (electrospray, positive mode).



6-methylsulfinylmethyl-1,3-thiazinan-2-thione

CCDC ID = 742902 (Cambridge Structural Database)

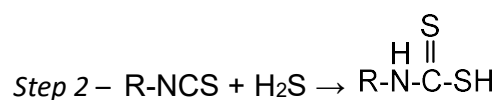
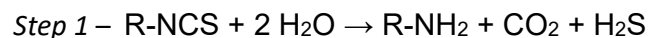
$\text{C}_6\text{H}_{11}\text{NOS}_3$; MW = 209.34 g mol $^{-1}$

MS m/z = 146 [M-CH $_3$ SO] $^+$, 210 [M+H] $^+$, 232 [M+Na] $^+$

Table 9.15 ^1H - and ^{13}C -NMR spectral data (400 MHz, DMSO- d_6) of P2 isolated from ER-SFE degradation in water at 40 °C and characterized as 6-methylsulfinylmethyl-1,3-thiazinan-2-thione. Data are in accordance with that reported in literature (Zhang et al., 2010; Song et al., 2013).

Position	δ C	Position	δ H	δ Multiplicities and J
C-2	190.9			
C-4	42.2	H-4	3.36-3.39	m, 1H
		H-4	3.40-3.51	m, 1H
C-5	25.6	H-5	1.78-1.91	m, 1H
		H-5	2.23-2.35	m, 1H
C-6	38.5	H-6	3.69-3.80	m, 1H
C-7	57.2	H-7	2.93	dd, 1H, $J_{7a,7b} = 13.1$, $J_{7,6} = 5.13$
		H-7	3.14	dd, 1H, $J_{7a,7b} = 13.1$, $J_{7,6} = 9.2$
C-8	38.4	H-8	2.61	s, 3H
		N-H	10.40	br s, 1H

Degradation product P2 characterized as 6-methylsulfinylmethyl-1,3-thiazinan-2-thione has been previously fully described by Zhang et al. (2010). In that study authors evaluated the effect of the roasting process of *Raphanus sativus* L. seeds on sulforaphene chemistry. They also established the absolute stereochemistry of the degradation compound by X-ray crystallographic analysis as S-6-methylsulfinylmethyl-1,3-thiazinan-2-thione. The same product was identified later by Song et al. (2013) as a degradation product of SFE in the autolysis of radish seeds in PPB pH 7. It's fascinating that *ER*-SFE and its possible degradation compound were studied for the first time back in the years in 1950. Indeed, enantiopure *ER*-SFE isolated from radish in 1948, has been claimed as the first natural product with optical activity due to sulfur (Schmid and Karrer, 1948). Moreover, Koczka et al. (1950) showed that *ER*-SFE treated with a water solution of Ba(OH)₂ was transformed in a compound with melting point of 192-193 °C, and formula C₆H₁₁NOS₃, same as P2. Koczka et al. (1950) also showed that the same compound was obtained by treating *ER*-SFE with H₂S. That new compound was not characterized in that first document and authors explained the addition of H₂S to *ER*-SFE by means of a two-step process as follow:



Recently, Song et al. (2013) found that SFE degraded and converted completely to product P2 when H₂S was passed through a water solution of SFE. On the basis of the aforementioned finding the authors proposed the following degradation pathway for SFE (Chart 9.1).

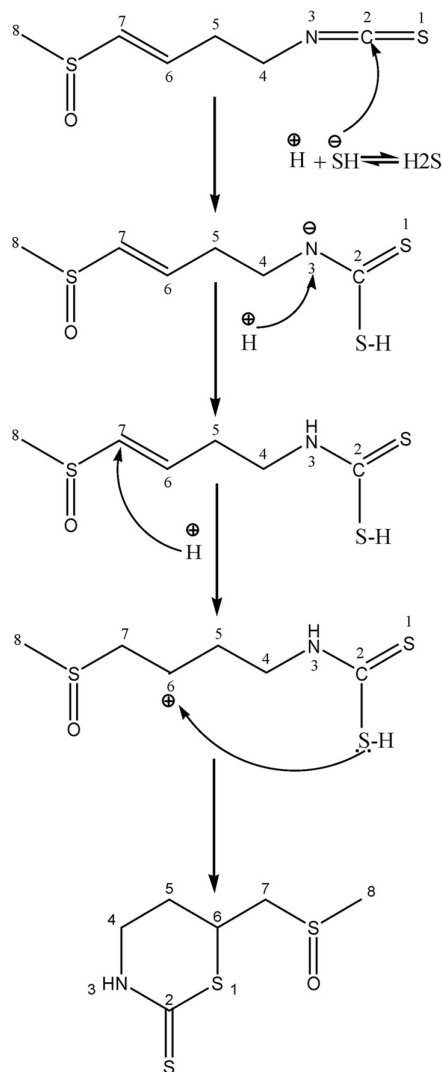


Chart 9.1 Proposed degradation pathway of sulfuraphene into 6-methylsulfinylmethyl-1,3-thiazinan-2-thione (P2). Taken from Song et al. (2013).

The isolation of P1 in the process of *ER*-SFE degradation in water solution is unprecedented in the literature and strongly support the already proposed pathway for the degradation of SFE.

Indeed, the isolation of P1 justifies the hydrolytic generation of H₂S according to Koczka et al., which in turn is necessary to explain the subsequent conversion of SFE into P2 by the mechanism proposed by Song et al (Chart 9.1).

9.16 Investigation of the aqueous phase after myrosinase assisted glucoraphenin hydrolysis

To learn on the formation of a side product during the hydrolysis of GRE to SFE, so to fully rationalize the lower yields of conversion as compared to other ITCs, four kinds of experiments have been done with GRE:

- pure GRE hydrolyzed with *Sinapis alba* MYR to produce *ER*-SFE in different controlled reaction conditions as summarized in Table 9.13;
- pure GRE hydrolyzed with *Sinapis alba* MYR in the presence of benzyl mercaptan and NEt₃ to produce *ER*-SFE-DTC (Table 9.8);
- Daikon DSM (containing GRE) autolyzed by the action of the endogenous MYR;
- pure GRE hydrolyzed with Daikon MYR to produce *ER*-SFE.

In all these experiments, the aqueous phase has always been checked by ¹H-NMR analysis in DMSO-*d*₆ after the following work-up. The aqueous phase was co-evaporated with toluene, the residue partly re-dissolved with anhydrous MeOH and evaporated to dryness after filtration on celite. Preliminary NMR investigation indicated a new compound, P3, probably derived by a different cyclization of *ER*-SFE leading to P2.

9.16.1 Isolation and purification of P3

A solution of GRE (95% pure, 0.74 mmol) in PPB pH 7.0 (3 mL, 0.5 M) and water (7 mL) was mixed with DCM (12 mL). After addition of *Sinapis alba* MYR (10.5 U) the mixture was stirred vigorously at 37 °C for 4 hours. Hydrolysis reaction was monitored via HPLC-DAD analysis. Diluted samples (1:1000 with ultrapure water) were injected on a Hewlett-Packard HP1090 model equipped with a hydrophilic C18 column ODS-AQ (Waters) thermostated at 30 °C. The chromatography was performed at a flow rate of 0.8 mLmin⁻¹, using isocratic ammonium acetate 50 mM as eluent and monitoring the absorbance at 226 nm. GRE consumption was

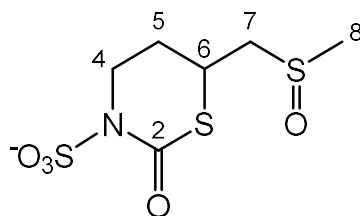
observed by the area decrease of the peak eluting at 9.5 min. Simultaneous formation of P3 was observed with the appearance and increase of a peak at 8 min. After 220 min GRE resulted completely transformed and the hydrolysis was stopped after a reaction time of 4 hours. After cooling at room temperature, the organic phase was decanted, and the aqueous phase extracted with DCM (3 x 10 mL) to eliminate any trace of *ER-SFE*. Pooled DCM extracts gave *ER-SFE* (38.7 mg) with a 30% yield in line with previous observations of several replicated experiments. The aqueous phase was quickly frozen (-80°C) and then freeze-dried obtaining a crude product (617 mg) that was extracted with anhydrous MeOH and filtered on celite giving pure P3 (64.7 mg) as a hygroscopic white solid.

9.16.1.1 *P3 characterization*

The UV spectrum of P3 was registered between 200 and 320 nm in water solution using a computerized Varian Cary 300 Bio UV/Visible spectrophotometer (Varian, Palo Alto, CA, USA) equipped with 1 cm quartz cells. A maximum absorption at 226 nm was exhibited. The structure of the degradation product P3 was identified by HR-MS and NMR analysis. P3 was dissolved in DMSO-*d*₆ and NMR spectra (¹H, ¹³C, COSY, DEPT135, HSQC and HMBC) were recorded as described at section 9.8.2.1.

HRMS was measured on a MicrOTOF-QII (ESI mode).

The ESI-HRMS spectrum showed the compound had a molecular formula of C₆H₁₀NO₅S₃ with mass 271.9720 (calculated: 271.9721). ¹H- and ¹³C-NMR data as well as DEPT135 and the correlation in bi-dimensional COSY, HSCQ and HMBC spectrum are listed in Table 9.16 for P3 that was characterized as 6-(methylsulfinylmethyl)-2-oxo-1,3-thiazinane-3-sulfonate.



6-(methylsulfinylmethyl)-2-oxo-1,3-thiazinane-3-sulfonate

$C_6H_{10}NO_5S_3$; MW = 271.97 g mol⁻¹

Table 9.16 NMR spectral data (400 MHz, DMSO-*d*₆) of P3 isolated from the aqueous phase of myrosinase-assisted hydrolysis of glucoraphenin in a phosphate buffer/dichlorometane biphasic system and characterized as 6-(methylsulfinylmethyl)-2-oxo-1,3-thiazinane-3-sulfonate.

#	δ H	Couplings (Hz)	COSY (H-H)	HSQC (H-C)	δ C	DEPT 135	HMBC (H-C)
2					162.37	C	
3							
4a	2.82 (dt, 1H)	$J_{4a,5a}=J_{4a,5b}=6.0$, $J_{4a,4b}=15.6$	H ₄ , H ₅	C ₄	31.89	CH ₂	C ₂ , C ₅ , C ₆
4b	2.69 (ddd, 1H)	$J_{4b,5a}=6.6$, $J_{4b,5b}=9.0$, $J_{4a,4b}=15.6$	H ₄ , H ₅				C ₂ , C ₅ , C ₆
5a	2.34 (dddd, 1H)	$J_{4b,5a}=J_{5a,6}=6.0$, $J_{4a,5a}=6.6$, $J_{5a,5b}=12.2$	H ₄ , H ₅ , H ₆	C ₅	32.95	CH ₂	C ₂ , C ₄ , C ₆ , C ₇
5b	1.90-1.99 (m, 1H)		H ₄ , H ₅ , H ₆				C ₂ , C ₄ , C ₆ , C ₇
6	3.96 (ddd, 1H)	$J_{6,5a}=J_{6,5b}=6.0$, $J=7.8$	H ₅ , H ₇	C ₆	43.86	CH	C ₂ , C ₅ , C ₇
7a	3.24 (dd, 1H)	$J_{7a,6}=8.3$, $J_{7a,7b}=13.1$	H ₅ , H ₇	C ₇	57.77	CH ₂	C ₅ , C ₆ , C ₈
7b	3.24 (dd, 1H)	$J_{7b,6}=6.1$, $J_{7a,7b}=13.1$	H ₅ , H ₇				C ₅ , C ₆ , C ₈
8	2.61 (s, 3H)			C ₈	38.35	CH ₃	C ₆ , C ₇

9.17 Conclusion

The new presented biphasic system proved to be effective at obtaining pure ITCs and DTCs without the need of any further chromatographic step. In this study, the MYR assisted hydrolysis in a biphasic PPB/DCM system has been applied to the conversion of four thio-functionalized GLs, namely the two redox couples GER/GRA and GRH/GRE. The system allowed to modify GER, GRA and GRH in a very good yield. Conversely GRE showed the lowest yield of transformation when hydrolyzed in the same reaction conditions used for the other three GLs. Indeed, GRE was not an ideal substrate for MYR purified from white mustard (*S. alba* L.). The transformation of GRE to its corresponding ITC, *ER*-SFE was enhanced from about 30% to 65% by using a crude extract of Daikon MYR. Hence, this finding highlighted the importance of studying each GL-MYR system modification with attention. This finding opened the way to further investigate the peculiar reactivity of GRE and *ER*-SFE. Studying the stability of *ER*-SFE in water it was possible to isolate (*E*)-4-(methylsulfinyl)-3-butenamine (P1) for the first time, strongly supporting the hydrolytic generation of H₂S which in turn is necessary to explain the subsequent conversion of *ER*-SFE into cyclic 6-methylsulfinylmethyl-1,3-thiazinan-2-thione (P2). Moreover, a new small hydrophobic cyclic molecule bearing three sulfur atom was isolated from the MYR assisted hydrolysis of GRE and characterized as 6-(methylsulfinylmethyl)-2-oxo-1,3-thiazinane-3-sulfonate (P3).

References

Abdull Razis AF, De Nicola GR, Pagnotta E, Iori R, Ioannides C (2013) A glucosinolate-rich extract of Japanese Daikon perturbs carcinogen-metabolizing enzyme systems in rat, being a potent inducer of hepatic glutathione S-transferase. *Eur J Nutr* 52:1279-1285.

Barillari J, Canistro D, Paolini M, Ferroni F, Pedulli GF, Iori R, Valgimigli L (2005a) Direct antioxidant activity of purified glucoerucin, the dietary secondary metabolite contained in rocket (*Eruca sativa* Mill.) seeds and sprouts. *J Agric Food Chem* 53:2475-2482.

Bernardi R, Finiguerra MG, Rossi A, Palmieri S (2003) Isolation and biochemical characterization of a basic myrosinase from ripe *Crambe abyssinica* seeds, highly specific for epi-progoitrin. *J Agric Food Chem* 51, 2737-2744.

Brinker and Spencer (1993) Herbicidal activity of sulforaphane from stock (*Matthiola incana*). *J of Chemical Ecology* 19: 2279-2284.

Burmeister WP, Cottaz S, Driguez H, Iori R, Palmieri S, Henrissat B (1997) The crystal structures of *Sinapis alba* myrosinase and a covalent glycosyl-enzyme intermediate provide insights into the substrate recognition and active-site machinery of an S-glycosidase. *Structure* 5:663-675.

Cambridge Structural Database. www.ccdc.cam.ac.uk/structures (accessed Jan. 24, 2018).

Chiang WCK, Pusateri DJ, Leitz REA (1998) Gas chromatography/mass spectrometry method for the determination of sulforaphane and sulforaphane nitrile in broccoli. *J Agric Food Chem* 46:1018-1021.

De Nicola GR, Bagatta M, Pagnotta E, Angelino D, Gennari L, Ninfali P, Rollin P, Iori R. (2013a) Comparison of bioactive phytochemical content and release of isothiocyanates in selected brassica sprouts. *Food Chem* 141(1):297-303.

De Nicola GR, Tatibouet A, Iori R, Rollin P (2013b) Sulfur-containing metabolites in radishes. Further exploration of glucoraphenin desulfation. *J of Sulfur Chemistry* 34:48-54.

De Nicola GR, Rollin P, Mazzon E, Iori R (2014) Novel gram-scale production of enantiopure R-Sulforaphane from tuscan black kale seeds. *Molecules* 19 (6):6975-6986.

Hanlon PR, Barnes DM (2011) Phytochemical composition and biological activity of 8 varieties of radish (*Raphanus sativus* L.) sprouts and mature taproots. *J of Food Science* 76:C185-C192.

Holst B, Williamson G (2004) A critical review of the bioavailability of glucosinolates and related compounds. *Nat Prod Rep* 21:425-447.

Khier N, Werner S, Mallouk S, Lieder F, Alcludia A, Fernández I (2009) Enantiopure sulforaphane analogues with various substituents at the sulfinyl sulfur: asymmetric synthesis and biological activities. *J Org Chem* 74: 6002-6009.

Kim JW, Kim MB, Lim SB (2015) Formation and stabilization of raphasatin and sulforaphane from radish roots by endogenous enzymolysis. *Prev Nutr Food Sci* 20(2):119-125.

Kosemura S, Yamamura S, Hasegawa K (1993) Chemical studies on 4-methylthio-3-butenyl isothiocyanate from roots of Japanese radish (*Raphanus sativus* L.) in connection with raphanusanins, phototropism-regulating substances of radish hypocotyls. *Tetrahedron Lett* 34:481-484.

Koczka I (1950) Über die Umsetzung des Raphanins mittels Barytlaug. *Acta Chem Phys* 3(1):38-42.

Kuhnert N, Holst B, Williamson G (2001) Synthesis of ¹⁴C-labelled sulforaphane. *J of Labelled Cpd Radiopharm* 44:347-354.

Ibrahim N, Allart-Simon I, De Nicola GR, Iori R, Renault J-H, Rollin P, Nuzillard J-M (2018) Advanced NMR-based structural investigation of glucosinolates and desulfoglucosinolates. *J Nat Prod* 81:323-334.

Iori R, Barillari J, Gallienne E, Bilardo C, Tatibouet A, Rollin P (2008) Thio-functionalised glucosinolates: unexpected transformation of desulfoglucoraphenin. *Tetrahedron Lett* 49:292-295.

Leoni O, Iori R, Palmieri S, Esposito E, Menegatti E, Cortesi R, Nastruzzi C (1997) Myrosinase-generated isothiocyanate from glucosinolates: isolation, characterization and in vitro antiproliferative studies. *Bioorg Med Chem* 5:1799-1806.

Leoni O, Iori R, Palmieri S (2000) Hydrolysis of glucosinolates using nylon-immobilized myrosinase to produce pure bioactive molecules. *Biotechnol Bioeng* 68:660-664.

Matera R, Gabbanini S, De Nicola GR, Iori R, Petrillo G, Valgimigli L (2012) Identification and analysis of isothiocyanates and new acylated anthocyanins in the juice of *Raphanus sativus* cv. Sango sprouts. *Food Chemistry* 133:563-572.

Matera R, Gabbanini S, Berretti S, Amorati R, De Nicola GR, Iori R, Valgimigli L (2015) Acylated anthocyanins from sprouts of *Raphanus sativus* cv. Sango: isolation, structure elucidation and antioxidant activity. *Food Chemistry* 166:397-406.

Matsuoka et al (1997) Formation of thioxopyrrolidines and DTC from GRH-ITC in aqueous media. *Biosci Biotech Biochem* 61:2109-2112.

Montaut S, Barillari J, Iori R, Rollin P (2010) Glucoraphasatin: chemistry, occurrence and biological properties. *Phytochemistry* 71:6-12.

Moriarty RM, Naithani R, Kosmeder J, Prakash O (2006) Cancer chemopreventive activity of sulforamate derivatives. *Eur J Med Chem* 41:121-124

National Center for Biotechnology Information. PubChem Compound Database
<https://pubchem.ncbi.nlm.nih.gov> (accessed Jan. 24, 2018).

Palmieri S, Leoni O, Iori R. (1982) A steady-state kinetics study of myrosinase with direct ultraviolet spectrophotometric assay. *Anal Biochem* 123:320-324.

Pessina A, Thomas RM, Palmieri S, Luisi, PL (1990) An improved method for the purification of myrosinase and its physicochemical characterization. *Arch Biochem Biophys* 280:383-389.

Qian Y, Ma G-Y, Yang Y, Cheng K, Zheng Q-Z, Mao W-J, Shi L, Zhao J, Zhu H-L (2010) Synthesis, molecular modelling and biological evaluation of dithiocarbamates as novel antitubulin agents. *Bioorg Med Chem* 18:4310-4316.

Schmid H, Karrer P (1948) Über Inhaltsstoffe des Rettichs I. Über Sulforaphen, ein Senföl aus Rettichsamen (*Raphanus sativus* L. var. *alba*). *Helv Chim Acta* 31:1017-1028

Sham T-T, Yuen A C-Y, Ng Y-F, Chan C-O, Mok D K-W, Chan S-W (2013) A review of the phytochemistry and pharmacological activities of Raphani semen. *J Evidence-Based Complementary Altern Med* ID 636194.

Song D, Liang H, Kuang P, Tang P, Hu G, Yuan Q (2013) Instability and structural change of 4-methylsulfinyl-3-butenyl isothiocyanate in the hydrolytic process. *J Agric Food Chem* 61:5097-5102.

Traka MH. Health benefits of glucosinolates. In Kopriva S (ed), *Glucosinolates, Advances in Botanical Research* Volume 80. Elsevier Ltd. 2016: pp. 247-279.

Vaughn SF, Berhow MA (2005) Glucosinolate hydrolysis products from various plant sources: pH effects, isolation, and purification. *Ind Crops Prod* 21:193:202.

Vig AP, Rampal G, Thind TS, Arora S (2009) Bio-protective effects of glucosinolates – A review. *LTW Food Sci Technol* 42:1561-1572.

Vivarelli F, Canistro D, Sapone A, De Nicola GR, Babot Marquillas C, Iori R, Antonazzo IC, Gentilini F, Paolini M (2016) *Raphanus sativus* cv. Sango sprout juice decreases diet-induced obesity in Sprague Dawley rats and ameliorates related disorders. PLoS ONE 11(3):e0150913. doi:10.1371/journal.pone.0150913.

Vivarelli F, Canistro D, Babot Marquillas C, Cirillo S, De Nicola GR, Iori R, Biagi G, Pinna C, Gentilini F, Pozzo L, Longo V, Paolini M (2017) The combined effect of Sango sprout juice and caloric restriction on metabolic disorders and gut microbiota composition in an obesity model. Int J Food Sci Nutr DOI: 10.1080/09637486.2017.1350940

Wittostock U, Kurzbach E, Herfurth AM, Stauber EJ. Glucosinolate breakdown. In Kopriva S (ed), Glucosinolates, Advances in Botanical Research Volume 80. Elsevier Ltd. 2016:125-169.

Wu H, Liang H, Yuan Q, Wang T, Yan X (2010) Preparation and stability investigation of the inclusion complex of sulforaphane with hydroxypropyl- β -cyclodextrin. Carbohydr Polym 82: 613-617.

You Y, Wu Y, Mao J, Zou L and Liu S (2008) Screening of Chinese brassica species for anti-cancer sulforaphane and erucin. Afr J of Biotechnol 7:147-152.

Zhang X, Liu H-B, Jia J-J, Lv W-H (2010) Two novel sulfur compounds from the seeds of *Raphanus sativus* L. J Asian Nat Prod Res 12:113-118.

PART FIVE

*GLUCOMORINGIN PURIFICATION AND
DERIVATIVES PRODUCTION*

CHAPTER TEN

Moringa oleifera seed cake as a source of medicinal glucomoringin, moringin and other derivatives

Contents

Summary

- 10.1** *Moringa oleifera* – Botanical classification and its use
- 10.2** Glucomoringin and its derivatives
- 10.3** Plant material
 - 10.3.1** PKM-2 *Moringa oleifera* seed cake
 - 10.3.2** PKM-2 *Moringa oleifera* seed cake freeze-dried extract
- 10.4** Analysis
 - 10.4.1** Determination of glucomoringin content
 - 10.4.2** NMR analysis of moringin derivatives
 - 10.4.3** Infrared analysis
 - 10.4.4** Optical rotation determination
- 10.5** Glucomoringin purification
 - 10.5.1** Glucomoringin characterization
- 10.6** Moringin production
 - 10.6.1** *Moringa* PKM-2 hydrolysis in a biphasic system
 - 10.6.2** *Moringa* PKM-2 hydrolysis in phosphate buffer
 - 10.6.3** Freeze-dried *Moringa* PKM-2 seed cake water extract hydrolysis
 - 10.6.4** Pure glucomoringin hydrolysis in a biphasic system
 - 10.6.5** Moringin characterization
- 10.7** One-pot production of a model glucomoringin-dithiocarbamate
 - 10.7.1** Glucomoringin-dithiocarbamate characterization
- 10.8** Moringin peracetylated production
 - 10.8.1** Moringin peracetylated characterization
- 10.9** Discussion and conclusions

References

Keywords

Moringa oleifera, Periyakulam-2, PKM-2, Glucomoringin, Moringin, Peracetylated moringin

Summary

Moringa (*Moringa oleifera* Lam.) belongs to the family Moringaceae within the order Brassicales and it is an extraordinary source of a unique dietary glycosylated glucosinolate, namely 4-(α -L-rhamnosyloxy)benzyl glucosinolate (glucomoringin). In this chapter the utilization of the commercially available Moringa PKM-2 seed cake was investigated for several purposes. First, the production of a freeze-dried glucomoringin-rich extract, as well as the isolation and purification of glucomoringin to a high level purity are described. The myrosinase catalyzed hydrolysis of glucomoringin to its isothiocyanate counterpart, moringin, has also been investigated. The feasibility of exogenous enzymolysis of glucomoringin was evaluated testing different glucomoringin sources: Moringa PKM-2 seed cake, the enriched extract and the pure glucomoringin. Moreover, the one-pot production of a model dithiocarbamate as already described at Chapter nine for four different dietary glucosinolates, has been applied hydrolyzing glucomoringin in a phosphate buffer/dichloromethane biphasic system in the presence of benzylmercaptan to trap the *in situ* produced moringin. Finally, a third derivative, the peracetylated moringin, was prepared in a semi synthetic way and characterized. Based on literature data about the mono-acylated isomer, this latter compound could be attractive for testing its possible anti-inflammatory properties.

10.1 *Moringa oleifera* – Botanical classification and its use

The Moringaceae family consists of a single genus *Moringa* with 13 different species, namely – *M. arborea*, indigenous to Kenya; *M. rivae* indigenous to Kenya and Ethiopia; *M. borziana*, indigenous to Somalia and Kenya; *M. pygmaea* indigenous to Somalia; *M. longituba* indigenous to Kenya, Ethiopia and Somalia; *M. stenopetala* indigenous to Kenya and Ethiopia; *M. ruspoliana* indigenous to Ethiopia; *M. ovalifolia* indigenous to Namibia and Angola; *M. drouhardii*, *M. hildebrandi* indigenous to Madagascar; *M. peregrine* indigenous of Red sea and Horn of Africa, *M. concanensis*, *M. oleifera* indigenous to sub-Himalayan tracts of Northern India (Leone et al., 2015). The best known and most widely distributed species is by far *M. oleifera* Lam. (*Moringa pterygosperma* Gaerthn), referred as Moringa or drumstick tree for the shape of its seed pods (Figure 10.2). Moringa is an exceptionally useful multipurpose plant that is native to northwestern India and now cultivated in all tropical countries. It has been used for millennia for human nutrition, animal feeding, and traditional medicine purposes (Fahey, 2005; Anwar et al., 2007). Pods and leaves are very popular vegetables and the plant is used extensively for low-cost nutrition. All parts of the tree are used medicinally and appear to have potent antioxidant, antimicrobial and chemoprevention activity. Seeds contain a high-oleic oil used in cooking, cosmetics and as a machinery lubricant. The seed cake remaining after oil extraction can be used to clarify turbid water or to increase protein in animal feed or crop fertilizer (Olson et al., 2016). Moringa derives from a Tamil (the official language spoken in the State of Tamil Nadu, India) word, murungai, meaning "twisted pod", alluding to young Moringa fruit. Interestingly, the Agricultural University of Periyakulam, in the State of Tamil Nadu pioneered in the development of Moringa cultivars. Periyakulam (PKM) is one of the most fertile places in the state of Tamil Nadu and agriculture is the primary occupation for the population there. Since Moringa is emerging as a future crop across the globe for health management due to its nutraceutical traits, multidisciplinary efforts are needed to answer to the concern to produce more Moringa with less water and land, along with the pressure of biotic and abiotic stress. In this scenario, scientists at the Agricultural University of Periyakulam have succeeded in developing seed-propagated Moringa types, which has revolutionized the Moringa cultivation in India releasing two commercially available high yielding annual Moringa cultivars: Periyakulam-1 (PKM-1), and Periyakulam-2 (PKM-2) (AICRP, 2017). Considering the potential of Moringa, more intensive research is needed. Despite the clear utility of the tree, crucial information gaps impede its optimal use in all its applications,

including nutrition. Many reports of its efficacy have not been published in high impact journals in the past limiting their visibility and there are still too few clinical studies to recommend Moringa parts as medication in the prevention or treatment of diseases. Noteworthy, the efforts of the scientific community are going towards that direction and the literature about Moringa has had an exponential increase (Figure 10.1) especially during the last ten years witnessing the great interest about this plant (Scopus, 2018).

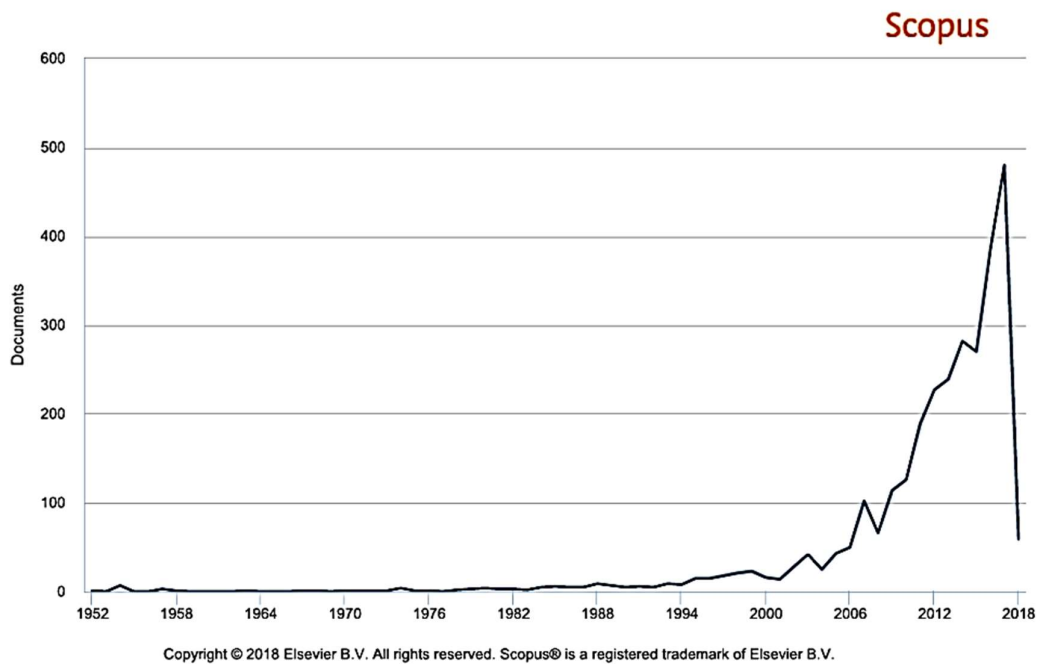


Figure 10.1 Chronology of the number of publications appearing in Scopus between 1952 and 2018 by using the keyword 'Moringa'.

10.2 Glucomoringin and its derivatives

Seeds and leaves of *M. oleifera* contain several phytochemicals (Maldini et al., 2014; Leone et al., 2015), and in particular they are rich in a structurally unusual glucosinolate (GL), 4-(α -L-rhamnosyloxy)benzyl GL (glucomoringin, GMG). Structurally speaking (Figure 10.1), GMG is a unique *O*-glycosylated form of the ubiquitous phenolic GL, 4-hydroxybenzyl GL (glucosinalbin; SNB), broadly represented among Brassicaceae, Resedaceae and other families of the order Brassicales (Fahey et al. 2001; Agerbirk and Olsen, 2012; Pagnotta et al., 2017). The therapeutic value of the seeds and other parts of the plant has long been recognized in folk medicine, and different extracts have also been tested as anticancer and anti-inflammatory agents (Padayachee, 2012; Biswas et al., 2012; Berkovich et al., 2013). Those properties are mainly attributed to the glycosylated isothiocyanate (ITC), 4-(α -L-rhamnosyloxy)benzyl ITC (moringin, MO), resulting from myrosinase (MYR) hydrolysis of GMG (Figure 10.2). Recently, it has been demonstrated that MO, produced from GMG, constitutes an innovative and effective antibiotic against strains of Gram positive bacteria with new promising application for the clinical practice in the treatment of nosocomial infections (Galuppo et al., 2013). In this context, there is the need to make GMG and its derivative MO available in large quantities to study their properties. Easy accessible procedures to obtain GMG and MO on the gram-scale are described here in this Chapter (Chart 10.1). Furthermore, it has been reported that naturally-occurring *O*-acetylated forms of MO on the L-rhamno unit led to higher anti-inflammatory activity, investigated with the lipopolysaccharide (LPS)-induced murine macrophage RAW 264.7 cell line, versus the non-acetylated MO (Cheenpracha et al., 2010). Considering this enhancement of bioactivity from partial acetylation of the carbohydrate moiety of MO, a semi-synthetic route to produce the peracetylated derivative, *i.e.* 4-(2',3',4'-tri-*O*-acetyl- α -L-rhamnosyloxy)benzyl isothiocyanate (MO-TRIAC) (Chart 10.1) from MO is also described in this Chapter.

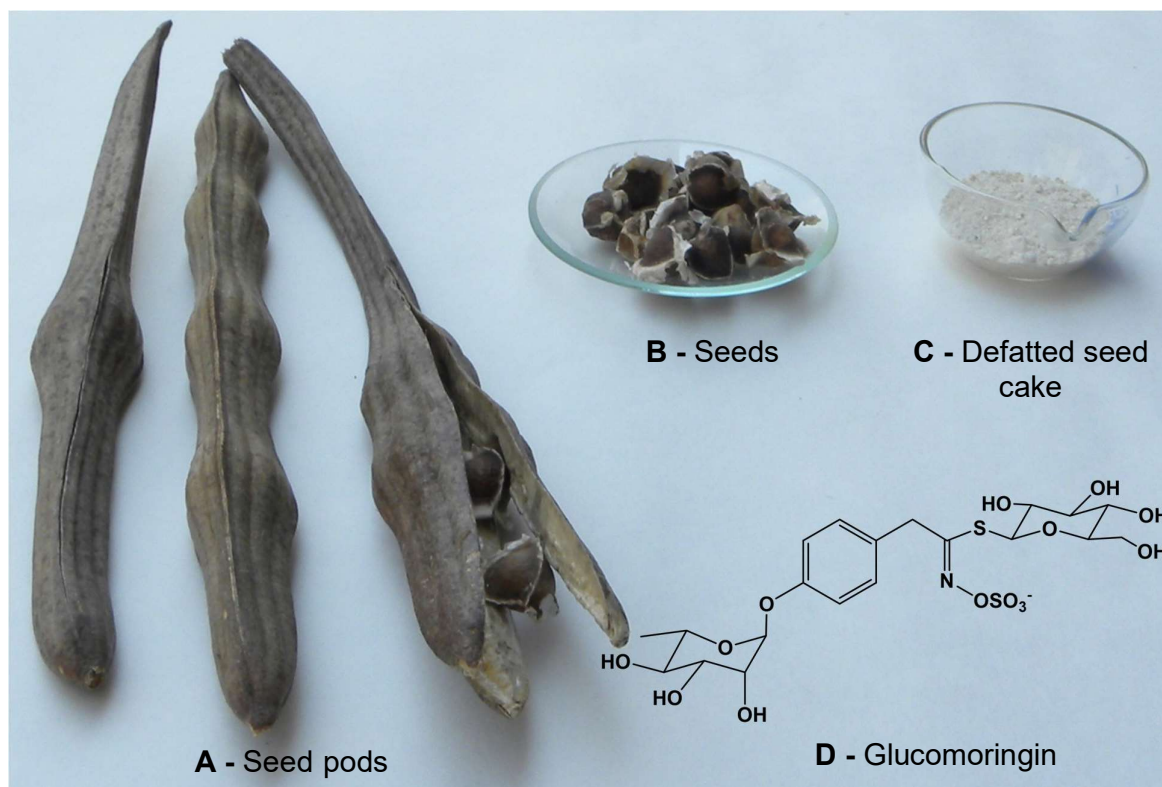


Figure 10.2 *Moringa oleifera* as a source of 4-(α -L-rhamnosyloxy)benzyl glucosinolate (glucomoringin; GMG) (D). Pictured: seed pods known as Moringa drumsticks (A), seeds (B) and defatted seed cake (C).

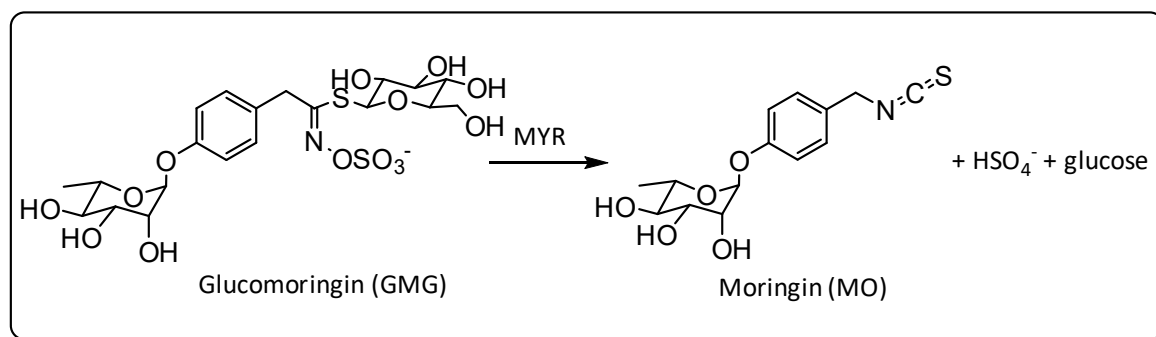


Figure 10.3 Reaction of myrosinase catalyzed hydrolysis of 4-(α -L-rhamnosyloxy)benzyl glucosinolate (glucomoringin; GMG) to produce 4-(α -L-rhamnosyloxy)benzyl isothiocyanate (moringin; MO).

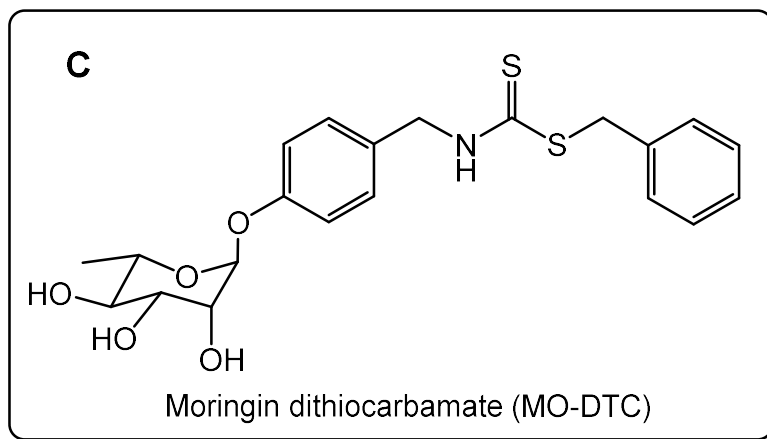
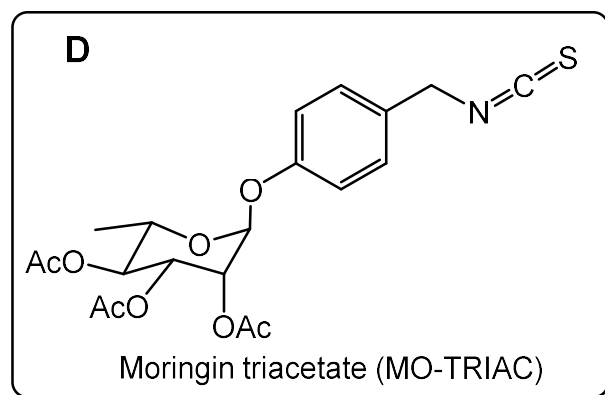
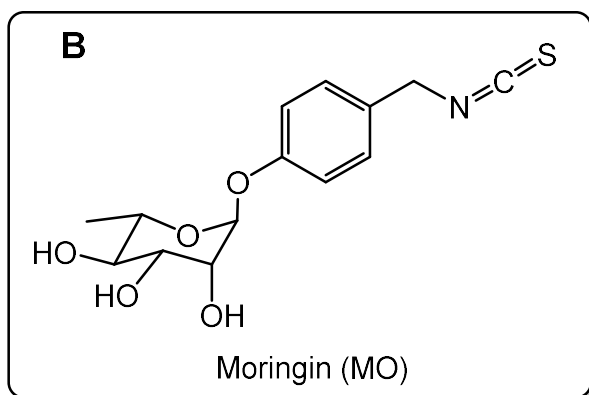
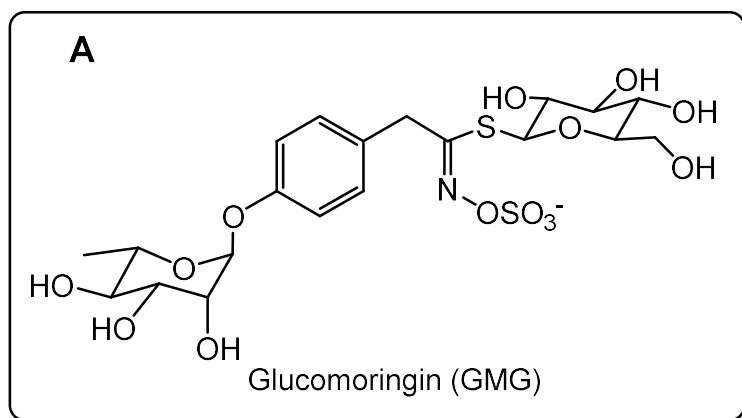


Chart 10.1 Structures of Glucomoringin (GMG) (A) and its derivatives. The isothiocyanate moringin (MO) (B), a model moringin dithiocarbamate (MO-DTC) (C) and the moringin peracetylated (MO-TRIAC) (D).

10.3 Plant material

10.3.1 *Moringa oleifera* PKM-2 seed cake

The plant material used for this research activity was *M. Oleifera* PKM-2 cake powder provided by Indena India Pvt. Ltd.; Bangalore, India. Figure 10.3 shows the chromatogram of DS-GMG isolated from *M. oleifera* PKM-2 seed cake powder ethanolic extract. *M. oleifera* PKM-2 seed cake powder contains $227.7 \pm 8.6 \mu\text{mol g}^{-1}$ of GMG as a single glucosinolate in the percentage of 13.9% (w/w).

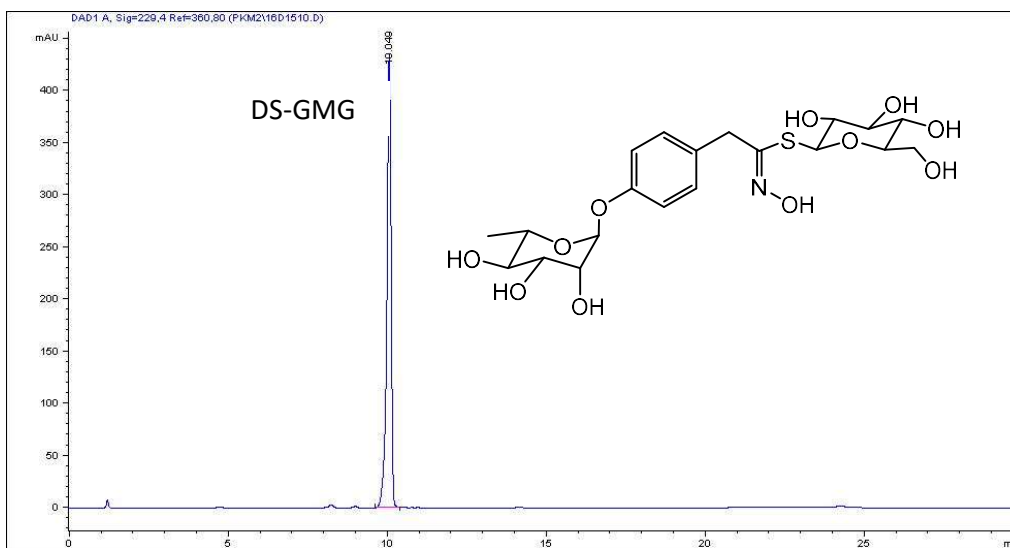


Figure 10.4 HPLC chromatogram of desulfo-glucomoringin (DS-GMG) isolated from *Moringa oleifera* PKM-2 seed cake powder ethanolic extract.

10.3.2 *Moringa oleifera* PKM-2 seed cake freeze dried extract

M. oleifera PKM-2 seed cake powder (50 g containing 6.95 g of GMG) was extracted in boiling water (500 mL) for 15 min at 80°C using an Ultra-Turrax T25 homogenizer (IKA-Werk, Staufen, Germany), and then centrifuged with a J2-MC centrifuge (Beckman, Palo Alto, CA, USA) at 10000g for 30 min at 10 °C. The solid residue was extracted a second time with the same w/v ratio and centrifuged as before. The two extracts were pooled, and zinc acetate (1M) was added in the ratio 50:1 (v/v), and left overnight at 4 °C for protein precipitation. After centrifugation (10000g, 40 min, 10 °C) a slightly yellow clear solution (940 mL) was obtained

and freeze-dried. After lyophilization a slightly yellow fine powder (PKM2EXT) was obtained (16.79 g). The content of GMG in the water extract was determined to be 5.5 (± 0.3) g (8.97 ± 0.55 mmol) with an extraction efficacy of 85% on the starting brown Moringa PKM-2 seed cake. The freeze-dried water extract (PKM2EXT) resulted to be highly enriched in GMG containing 32.8% (w/w) of the GL of interest.

10.4 Analysis

10.4.1 Determination of glucomoringin content

GMG content was analyzed in *M. oleifera* PKM-2 seed cake powder and in the freeze-dried PKM2EXT as desulfo-GMG (DS-GMG). Two fine powder samples were extracted twice with boiling EtOH/H₂O 80/20. Combined extracts were analyzed twice on two minicolumns by means of desulfation (n=4) and analyzed by HPLC-DAD. Purity level of purified GMG was assessed in the same way after water dilution.

10.4.2 NMR analysis of moringin derivatives

¹H- and ¹³C-NMR spectra were recorded on a 400 MHz Avance 2 spectrometer (Bruker Biospin SA, Wissembourg, France). Following abbreviations are used to designate δ multiplicities: s, singlet; d, doublet; t, triplet; q, quartet; m, multiplet; br, broad; and coupling constants are given in Hertz (Hz).

10.4.3 Infrared analysis

Infrared spectra were recorded on an Attenuated Total Reflectance Thermo-Nicolet AVATAR 320 AEK0200713 instrument (Perkin Elmer Instruments, Courtaboeuf, France).

10.4.4 Optical rotation determination

ITCs were weighed in a 1 mL volumetric flask and dissolved in CHCl₃. The solution was transferred into a 1 mL cell (path length 1 dm) and the optical rotation was measured at 25

°C on a Perkin-Elmer 141 polarimeter (Perkin Elmer Instruments, Courtaboeuf, France) and reported as $[\alpha]_D^{25}$ values. Concentration (c) was expressed in g per 100 mL of solvent.

10.5 Glucomoringin purification

Glucomoringin was purified by means of two chromatographic steps following the same procedure as reported for GRA purification at Chapter eight.

- *Glucomoringin isolation*

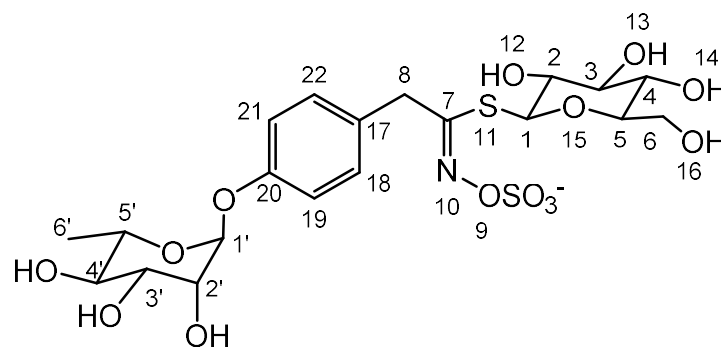
A sample of PKM2EXT (50 g) was dissolved in ultrapure water (50 mL). The isolation of GMG from the extract was carried out by one-step ion exchange chromatography. The extract was loaded on a glass column (Econo-Column 2.5 × 20 cm, Bio-Rad Laboratories, Milan, Italy) packed with DEAE Sephadex A-25 anion exchanger (GE Healthcare, Milan, Italy) (90 mL) conditioned with 25 mM acetate buffer (pH 4.2). After washing with distilled water (2 L), GMG was eluted with a water solution of potassium sulfate (0.5 M, 500 mL). The collected solution was concentrated to dryness using a rotary evaporator Laborota 4002 (Heidolph Instruments, Schwabach, Germany). The solid residue was then submitted to three subsequent extractions with boiling methanol (3 × 100 mL). The alcoholic extracts were pooled, then filtered and concentrated by rotary evaporation to about 10% of the initial volume. Afterwards, the solution was warmed, and slowly added dropwise under stirring to absolute ethanol ($\geq 99.8\%$, 2 portions of 200 mL) previously cooled to -20 °C, leading to the precipitation of a white powder. After centrifugation, the solid was thoroughly dried under vacuum, then reduced to a fine powder and sealed under reduced pressure to prevent moisture uptake.

- *Glucomoringin purification*

The purity of GMG was further improved by gel filtration performed on a XK 26/100 column packed with Sephadex G-10 connected to an AKTA fast protein liquid chromatograph system (FPLC) (GE Healthcare, Milan, Italy). The isolated GL powder was dissolved in ultrapure water (0.5 g mL^{-1}), filtered through a $0.45 \mu\text{m}$ membrane filter (Gema Medical S.L., Barcelona, Spain), charged (2 mL) onto the column and eluted using a mobile phase of ultrapure water at a flow rate of 2.0 mL min^{-1} monitoring the absorbance at 254 nm. Individual fractions (6 mL) of seven runs were analyzed by HPLC and those containing pure GMG were pooled and freeze-dried. GMG (9.1 g) was obtained as a white solid and characterized by ^1H - and ^{13}C -NMR. The purity of GMG assessed by HPLC resulted to be 99% (area peak based) and 95% on weight basis.

10.5.1 Glucomoringin characterization

NMR spectra of pure GMG were recorded in D₂O as described for GRA (see Section 8.3.3.2) and reported in Ibrahim et al. (2018).



4-(α -L-rhamnosyloxy)benzyl glucosinolate

PubChem Compound Database; CID = 102222710

C₁₉H₂₆NO₁₄S₂K; M = 595.18 g mol⁻¹ (potassium salt)

Table 10.1 ^1H -, ^{13}C - and ^{15}N -NMR spectral data (500 MHz, D_2O) for glucomoringin (4-(α -L-rhamnosyloxy)benzyl glucosinolate; GMG) (Ibrahim et al., 2018).

#	δ C	#	δ H	Couplings			
C-1	84.2256	H-1	4.7204	J(H-1,H-2) = 9.7185			
C-2	74.6341	H-2	3.3394	J(H-2,H-1) = 9.7185	J(H-2,H-3) = 8.9375		
C-3	79.8478	H-3	3.3420	J(H-3,H-2) = 8.9375	J(H-3,H-4) = 9.1790		
C-4	71.5814	H-4	3.4194	J(H-4,H-3) = 9.1790	J(H-4,H-5) = 9.9289		
C-5	82.7088	H-5	3.2429	J(H-5,H-4) = 9.9289	J(H-5,H-6S) = 3.6733	J(H-5,H-6R) = 3.6532	
C-6	63.1380	H-6R	3.6468	J(H-6R,H-5) = 3.6532	J(H-6R,H-6S) = -12.0277		
		H-6S	3.6512	J(H-6S,H-5) = 3.6733	J(H-6S,H-6R) = -12.0277		
C-7	165.5820						
C-8	40.3724	H-8R	4.1055	J(H-8R,H-8S) = -16.2722			
		H-8S	4.1210	J(H-8S,H-8R) = -16.2722	J(H-8S,H-18) = -0.8725	J(H-8S,H-22) = -0.8725	
N-10	346.8470						
C-17	132.3216						
C-18	132.2893	H-18	7.3771	J(H-18,H-8S) = -0.8725	J(H-18,H-19) = 8.5543	J(H-18,H-21) = 0.3012	J(H-18,H-22) = 2.7731
C-19	120.4358	H-19	7.1651	J(H-19,H-18) = 8.5543	J(H-19,H-21) = 2.4060	J(H-19,H-22) = 0.3012	
C-20	157.5697						
C-21	120.4358	H-21	7.1651	J(H-21,H-18) = 0.3012	J(H-21,H-19) = 2.4060	J(H-21,H-22) = 8.5543	
C-22	132.2893	H-22	7.3771	J(H-22,H-8S) = -0.8725	J(H-22,H-18) = 2.7731	J(H-22,H-19) = 0.3012	J(H-22,H-21) = 8.5543
C-1'	101.0160	H-1'	5.5668	J(H-1',H-2') = 1.8624			
C-2'	72.8453	H-2'	4.1789	J(H-2',H-1') = 1.8624	J(H-2',H-3') = 3.4801		
C-3'	72.9493	H-3'	4.0143	J(H-3',H-2') = 3.4801	J(H-3',H-4') = 9.7866		
C-4'	74.9041	H-4'	3.5282	J(H-4',H-3') = 9.7866	J(H-4',H-5') = 9.6315		
C-5'	72.2952	H-5'	3.8156	J(H-5',H-4') = 9.6315	J(H-5',H-6') = 6.2715		
C-6'	19.5356	H-6'	1.2464	J(H-6',H-5') = 6.2715			

10.6 Moringin production

Several ways to produce MO are described. Enzymolysis by using MYR purified from *Sinapis alba* L. was tested on different GMG containing material starting from Moringa PKM-2 seed cake powder as such, to a GMG enriched extract, up to purified GMG.

10.6.1 Moringa PKM2 hydrolysis in a biphasic system

A sample of Moringa PKM2 seed cake powder (10.32 g containing 1.43 g of GMG, 2.34 mmol GMG) was dispersed in freshly prepared potassium phosphate buffer (PPB) pH 7.0 (0.25 M, 50 mL) and mixed with DCM (40 mL). After addition of MYR (7.5 U), the mixture was vigorously stirred at 37 °C overnight. After cooling at room temperature recovery of the organic phase was tried in two ways. Filtration on cotton was not successful. Filtration on a glass filter was possible although not optimal. The organic phase was washed with brine, dried over anhydrous sodium sulfate, and the solvent was then removed by rotary evaporation at room temperature. The oily residue was dissolved in aqueous ACN (30%, 21 mL) and freeze-dried. MO (692 mg) was obtained as a slightly yellow oily gum and the purity level was not assessed. The system used resulted not easy to be treated and in particular, the work up phase was not handy. DCM extracted MO together with the residual oil of the seed meal. For this reason, the freeze-dried MO was not obtained as a white solid but as an oily gum. Taking these considerations into account, Moringa PKM-2 seed cake powder was hydrolyzed in PPB followed by DCM extraction after centrifugation to eliminate the solid residue.

10.6.2 Moringa PKM2 seed cake powder hydrolysis in phosphate buffer

A sample of Moringa PKM-2 seed cake powder (10.17 g containing 1.41 g of GMG, 2.31 mmol GMG) was dispersed in freshly prepared PPB pH 7.0 (0.25 M, 50 mL). After addition of MYR (7.5 U), the mixture was stirred at 37 °C overnight. After cooling at room temperature, the mixture was centrifuged at 10 °C (14000 g, 30 min). The supernatant was left overnight in an ice bath for protein precipitation and then centrifuged again at 10 °C (17000g, 30 min). Extraction with DCM was tried on the clear slightly yellow aqueous phase, but it resulted not

handy for the formation of a lot of foam. Addition of brine did not improve the extraction process.

10.6.3 Freeze-dried Moringa PKM2 seed cake water extract hydrolysis in a biphasic system

A sample of freeze-dried Moringa PKM-2 seed cake powder water extract (PKM2EXT) (7.19 g containing 2.36 g of GMG, 3.87 mmol GMG) was solubilized in freshly prepared PPB pH 7.0 (0.25 M, 100 mL) and mixed with DCM (140 mL). After addition of MYR (6 U), the solution was stirred at 37 °C overnight. After cooling at room temperature, the mixture was transferred into a separatory funnel and extracted with DCM (3 x 10 mL). The formation of three phases in the separatory funnel was observed: the bottom-heavy DCM phase, an intermediate fine solid phase and an upper slightly yellow aqueous phase. DCM extractions were pooled together, and the solvent removed by rotatory evaporator at room temperature. The solid residue was dissolved in aqueous ACN (22%, 90 mL) and freeze-dried. MO (548 mg) was obtained as a white solid with a yield of 46.8% and purity level determined by HPLC was >99%. The aqueous phase was freeze-dried obtaining a slightly yellow powder (7.0 g). The powder was analyzed for not hydrolyzed GMG and its content was assessed to be 8.0% (w/w).

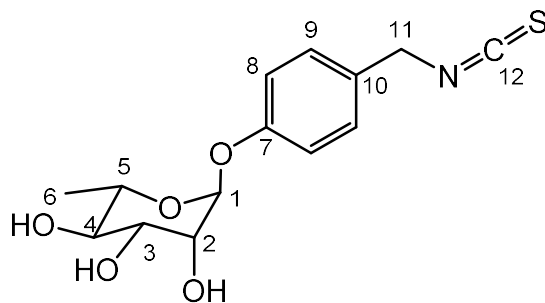
10.6.4 Moringin from pure glucomoringin hydrolysis in a biphasic system

A sample of purified GMG ($\geq 95\%$; 3.55 g; 5.82 mmol) was dissolved in freshly prepared PPB pH 7.0 (0.25 M, 120 mL) and mixed with DCM (140 mL). After addition of MYR (15 U) the mixture was vigorously stirred at 37 °C for 18 hours. After cooling at room temperature, the organic phase was decanted, and the aqueous phase extracted with DCM (3 x 10 mL). The organic layers were pooled, dried over anhydrous sodium sulfate, and the solvent was then removed by rotary evaporation at room temperature. The residue was dissolved in aqueous ACN (30%, 150 mL) and freeze-dried. Pure MO (876 mg, 2.81 mmol) was obtained as a white powder with a yield of 48.4%.

The aqueous phase was added with additional MYR (15 U) and mixed with DCM (100 mL). The mixture was vigorously stirred at 37 °C for 17 hours. After cooling at room temperature, the organic phase was decanted, and the aqueous phase extracted with DCM (3 x 10 mL). The organic layers were pooled, dried over anhydrous sodium sulfate, and the solvent was then

removed by rotary evaporation at room temperature. The residue was dissolved in aqueous ACN (30%, 140 mL) and freeze-dried. Pure MO (605 mg, 1.94 mmol) was obtained as a white powder with a yield of 33.3%. The starting GMG was hydrolyzed to the desired ITC MO by means of two subsequent hydrolysis processes with a total yield of 81.7%.

10.6.5 Moringin characterization



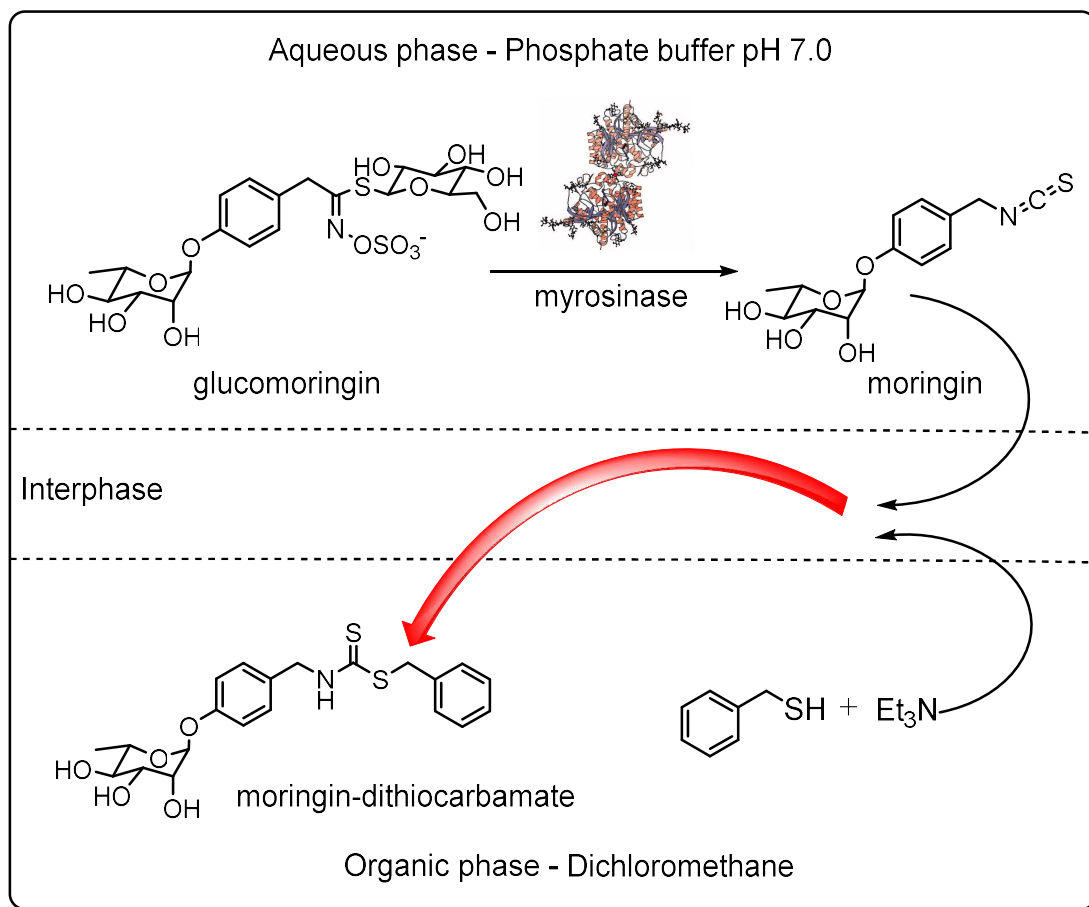
4-(α -L-rhamnosyloxy)benzyl isothiocyanate
 PubChem Compound Database; CID = 153557
 CAS Registry Number: 73255-40-0
 $C_{14}H_{17}NO_5S$; $M = 311.35 \text{ g mol}^{-1}$

Table 10.2 ^1H - and ^{13}C -NMR spectral data (400 MHz, CD_3OD) for moringin (4-(α -L-rhamnosyloxy)benzyl isothiocyanate; MO).

Position	$\delta \text{ C}$	Position	$\delta \text{ H}$	δ Multiplicities and J
C-1	99.9	H-1	5.4	d, 1H, $J = 1.9$
C-2	72.0	H-2	3.99	dd, 1H, $J = 3.6$, $J = 1.9$
C-3	72.3	H-3	3.83	dd, 1H, $J = 9.5$, $J = 3.7$
C-4	73.9	H-4	3.28	t, 1H, $J = 9.5$
C-5	70.8	H-5	3.62	m, 1H
C-6	18.1	H-6	1.22	d, 3H, $J = 6.1$
C-7	157.8			
C-8	117.9	H-8	6.99	d, 2H, $J = 8.9$
C-9	129.7	H-9	7.30	d, 2H, $J = 8.9$
C-10	130.1			
C-11	49.0	H-11	4.69	s, 2H
C-12	133			

10.7 One-pot production of a model glucomoringin-dithiocarbamate

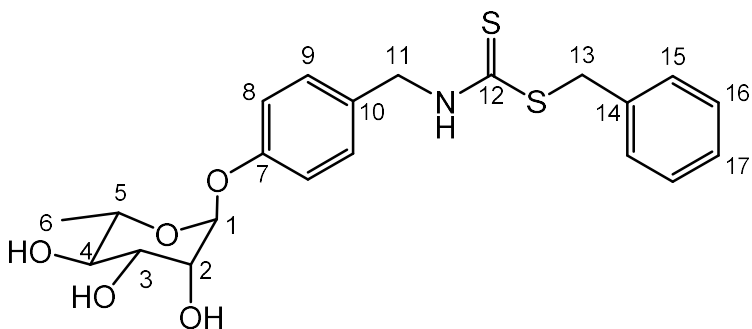
The same procedure used for four dietary GLs (see Chapter nine) for the direct transformation of GMG into a model MO-DTC was tested in a PPB/DCM biphasic system in the presence of benzyl mercaptan to trap the *in-situ* MO produced by the action of exogenous MYR purified from *Sinapis alba* L.



Scheme 10.1 One-pot production of moringin-dithiocarbamate from myrosinase catalyzed hydrolysis of glucosinolates in a biphasic system in the presence of triethylamine (NEt_3) and a model thiol to trap *in situ* the intermediate moringin. Aqueous phase is phosphate buffer pH 7.0 and organic phase is dichloromethane. The reported dimeric structure of myrosinase purified from white mustard seeds (*Sinapis alba* L.) is taken from Burmeister et al. (1997).

GMG (95% pure, 0.2 mmol) was hydrolyzed as described at chapter nine (see section 9.8.1 General procedure for dithiocarbamates production) in the presence of benzylmercaptan (1.2 eq) and NEt_3 (1.2 eq). Crude product (41.3 mg) was purified by flash chromatography ($\text{CHCl}_3/\text{MeOH}$ 9:1) to give MO-DTC (33.5 mg) as a white oil in a 38.4% yield.

10.7.1 Moringin-dithiocarbamate characterization



Benzyl 4-(α -L-rhamnosyloxy)benzylidithiocarbamate

Original compound

$C_{21}H_{25}NO_5S_2$; $M = 435.56 \text{ g mol}^{-1}$

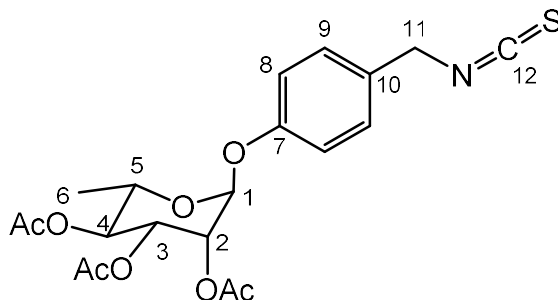
Table 10.3 ^1H - and ^{13}C -NMR spectral data (400 MHz, $\text{DMSO-}d_6$) for moringin-dithiocarbamate (benzyl 4-(α -L-rhamnosyloxy)benzylidithiocarbamate; MO-DTC).

Position	$\delta \text{ C}$	Position	$\delta \text{ H}$	δ Multiplicities and J
C-1	98.4	H-1	5.35	br s, 1H
C-2	70.22	H-2	3.82	m, 1H
		OH ₂	5.02	d, 1H, $J = 4.3$
C-3	70.44	H-3	3.64	m, 1H
		OH ₃	4.72	d, 1H, $J = 6.0$
C-4	71.81	H-4	3.28	m, 1H
		OH ₄	5.02	d, 1H, $J = 5.8$
C-5	69.48	H-5	3.45	m, 1H
C-6	17.94	H-6	1.10	d, 3H, $J = 6.3$
C-7	155.34			
C-8	116.2	H-8	6.99	d, 1H, $J = 8.8$
	128.46, 128.95, 129.15	H-Ar H-9, H-15, H-16, H-17	7.30	m, 7H
C-9 or C-15 or C-16				
C-10	130.54			
C-11	49.23	H-11	4.79	br s, 2H
C-12	196.11			
C-13	38.31	H-13	4.79	br s, 2H
C-14	137.19			
C-17	127.18			
		N-H	10.40	br s, 1H

10.8 Moringin peracetylated production

The production of MO-TRIAC was carried out as briefly described in Kjaer (1979). MO (2.150 g, 6.9 mmol) was dissolved in pyridine (20 mL) and cooled in a NaCl/ice bath. Acetic anhydride (4 mL, 42.4 mmol) was added dropwise to the solution and then stirred overnight at room temperature. After coevaporation with toluene in a rotatory evaporator at 40 °C, the yellow oily residue was dissolved in DCM (20 mL) and washed with water (20 mL). The aqueous phase was extracted with DCM and the two pooled organic layers were washed consecutively with HCl 1N (2 x 20 mL), saturated NaHCO₃ (2 x 20 mL), distilled water until neutral pH. The organic phase was then dried over anhydrous potassium sulfate and the solvent was then removed by rotary evaporation. The oily MO-TRIOAC was dissolved in aqueous ACN 40% and freeze-dried to obtain a slightly yellow crystalline compound (3.0 g) with a yield of 99%.

10.8.1 Moringin peracetylated characterization



4-(2',3',4'-O-triacetyl- α -L-rhamnosyloxy)benzyl isothiocyanate

Original compound

C₂₀H₂₃NO₈S; M = 437.46 g mol⁻¹

HPLC, t_R = 12.2 min. UV (λ_{max}): 222 nm. $[\alpha]_D^{25}$: -81.0 (c 1, CHCl₃).

IR (cm⁻¹): 2983, 2167, 2085 (N=C=S), 1744, 1612, 1510, 1438, 1368, 1213, 1180, 1129, 1031, 983, 936, 828, 761, 733, 672.

ESI⁺-MS m/z = 438 [M+H]⁺, 460 [M+Na]⁺, 476 [M+K]⁺ and a signal with m/z 273 corresponding to the fragment of a peracetylated α -L-rhamnosyloxyl ion.

Table 10.4 ^1H - and ^{13}C -NMR spectral data (400 MHz, CDCl_3) for moringin-peracetylated (4-(2',3',4'-*O*-triacetyl- α -L-rhamnosyloxy)benzyl isothiocyanate; MO-TRIAC).

Position	δ C	Position	δ H	δ Multiplicities and <i>J</i>
C-1	95.77	H-1	5.46	d, 1H, <i>J</i> = 1.6
C-2	69.74	H-2	5.42	dd, 1H, <i>J</i> = 3.5, <i>J</i> = 1.9
C-3	68.92	H-3	5.50	dd, 1H, <i>J</i> = 10.1, <i>J</i> = 3.5
C-4	71.01	H-4	5.16	t, 1H, <i>J</i> = 9.9
C-5	67.42	H-5	3.95	dq, 1H, <i>J</i> = 9.8, <i>J</i> = 6.2
C-6	17.59	H-6	1.21	d, 3H, <i>J</i> = 6.2
C-7	155.94			
C-8	116.91	H-8	7.09	d, 2H, <i>J</i> = 8.7
C-9	128.59	H-9	7.26	d, 2H, <i>J</i> = 8.7
C-10	125.45			
C-11	48.33	H-11	4.66	s, 2H
C-12	128.63			
OAc	20.89		2.03	s, 3H
OAc	20.94		2.06	s, 3H
OAc	21.05		2.17	s, 3H

10.9 Discussion and conclusions

Moringa PKM-2 seed cake represents a very good source of GMG. It is commercially available, rich in GMG 13.9% (w/w), and has the advantage to be defatted when compared to the whole seed. Starting from this advantageous material an extract was prepared using boiling water obtaining a GMG enriched freeze-dried extract containing GMG in a 32.8% (w/w). This product was the starting material for the purification of GMG by a sequential two-step process, anion exchange chromatography followed by gel filtration, that allowed to obtain GMG on a gram scale as a white solid 99% pure (HPLC peak based) and $\geq 95\%$ (weight based). Moringa PKM-2 seed cake, the rich GMG extract, as well as pure GMG were all tested to produce MO by enzymolysis using exogenous MYR purified from white mustard seeds (*Sinapis alba* L.). The best way resulted to be the hydrolysis of pure GMG. Interestingly, a second

addition of MYR was necessary to almost complete the conversion of GMG to MO. Considering the results, GMG was indeed converted to MO with the rate of 46.8% and 48.4% when hydrolyzing PKM2EXT and pure GMG, respectively, with the first MYR treatment. A similar yield was obtained when hydrolyzing GMG with the addition of benzyl mercaptan resulting in the production of MO-DTC in a 38.4% rate. This occurrence leads to consider the hydrolysis of GMG with endogenous Moringa MYR to further investigate the process, similarly to what I have done studying glucoraphenin (GRE) conversion to its ITC and described at Chapter nine. The second MYR addition made it possible to reach 81.7% MO production, when hydrolyzing pure GMG. The dietary ITC MO is different from most ITCs since it can be produced as a white solid after lyophilization. It is stable, odorless and water soluble up to a concentration of about 1 mg mL⁻¹. The procedure described here to obtain MO in a biphasic system made it possible to have it in a pure form without the need of any chromatographic step and it represents a simplification of a previously reported method (Brunelli et al., 2010). In that cited study, pure GMG was hydrolyzed in PPB followed by a C-18 reverse phase chromatography step to release pure MO. Finally, a third GMG derivative has been described here; the peracetylated MO was obtained in a semi synthetic way transforming natural MO in a quantitative yield. To sum up, GMG and its derivatives MO, MO-DTC and MO-TRIAC can easily be obtained on the gram scale making these molecules available for new research studies on their activity in many fields from nutrition to several pathologies to prove the efficacy of the use of Moringa “the Miracle tree” as an edible medicinal plant.

References

Agerbirk N and Olsen CE (2012) Glucosinolate structures in evolution. *Phytochemistry* 77:16-45.

AICRP (2017) Advances in production of Moringa. Available on line at agritech.tnau.ac.in/horticulture/pdf/Moringa%20English%20book.pdf (accessed on 28 february 2018).

Anwar F, Latif S, Ashraf M, Gilani AH (2007) *Moringa oleifera*: a food plant with multiple medicinal uses. *Phytother Res* 21:17.

Berkovich L, Earon G, Ron I, Rimmon A, Vexler A, Lev-Ari, S (2013) *Moringa oleifera* aqueous leaf extract downregulates nuclear factor-kappaB and increases cytotoxic effect of chemotherapy in pancreatic cancer cells. *BMC Complementary and Alternative Medicine* 13:212-218.

Biswas SCA, Das J, Roy A, Zahid Hosen SM (2012) Pharmacological potentials of *Moringa oleifera* Lam.: a review. *Int J Pharm Sci Res* 3:305-310.

Brunelli D, Tavecchio M, Falcioni C, Frapolli R, Erba E, Iori R, Rollin P, Barillari J, Manzotti C, Morazzoni P, D'Incalci M (2010) The isothiocyanate produced from glucomoringin inhibits NF- κ B and reduces myeloma growth in nude mice in vivo. *Biochem Pharmacol* 79:1141–1148.

Burmeister WP, Cottaz S, Driguez H, Iori R, Palmieri S, Henrissat B (1997) The crystal structures of *Sinapis alba* myrosinase and a covalent glycosyl-enzyme intermediate provide insights into the substrate recognition and active-site machinery of an S-glycosidase. *Structure* 5:663-675.

Cheenpracha S, Park EJ, Yoshida WY, Barit C, Wall M, Pezzuto GM, Chang LC (2010) Potential anti-inflammatory phenolic glycosides from the medicinal plant *Moringa oleifera* fruits. *Bioorg Med Chem* 18:6598-6602.

Fahey JW, Zalcmann AT, Talalay P (2001) The chemical diversity and distribution of glucosinolates and isothiocyanates among plants. *Phytochemistry* 56(1):5-51.

Fahey JW (2005) *Moringa oleifera*: A review of the medical evidence of its nutritional, therapeutic and prophylactic properties. *Trees for Life J* 1:5.

Galuppo M, De Nicola GR, Iori R, Dell'Utri P, Bramanti P, Mazzon E (2013) Antibacterial activity of glucomoringin bioactivated with myrosinase against two important pathogens affecting the health of long-term patients in hospitals. *Molecules* 18:14340–14348.

Ibrahim N, Allart-Simon I, De Nicola GR, Iori R, Renault J-H, Rollin P, Nuzillard J-M (2018) Advanced NMR-based structural investigation of glucosinolates and desulfoglucosinolates. *J Nat Prod* 81:323-334.

Kjaer A, Malver O, El-Menshawi B, Reisch J (1979) Isothiocyanates in myrosinase-treated seed extracts of *Moringa Peregrina*. *Phytochemistry* 18:1485-1487.

Leone A, Spada A, Battezzati A, Schiraldi A, Aristil J, Bertoli S (2015) Cultivation, genetic, ethnopharmacology, phytochemistry and pharmacology of *Moringa oleifera* leaves: an overview. *Int J Mol Sci* 16:12791-12835.

Maldini M, Maksoud SA, Natella F, Montoro P, Petretto GL, Foddai M, De Nicola GR, Chessa M, Pintore G (2014) *Moringa oleifera*: Study of phenolics and glucosinolates by mass spectrometry (2014) *J of Mass Spectrometry* 49(9):900-910.

Olson ME, Sankaran RP, Fahey JW, Grusak MA, Odee D, Nouman W (2016) Leaf protein and mineral concentrations across the “Miracle Tree” genus *Moringa*. *PLoS ONE* 11(7):e0159782.

Padayachee B (2012) An overview of the medicinal importance of Moringaceae. *J Med Plants Res* 6:5831-5839.

Pagnotta E, Agerbirk N, Olsen CE, Ugolini L, Cinti S, Lazzeri L (2017) Hydroxyl and methoxyl derivatives of benzylglucosinolate in *Lepidium densiflorum* with hydrolysis to isothiocyanates and non-isothiocyanate products: substitution governs product type and mass spectral fragmentation. *J Agric Food Chem* 63:3167-3178.

Scopus Database. Available on line: www.scopus.com (accessed on 16 February 2018).

PART SIX

*IN VIVO PHARMACOLOGICAL STUDIES –
ROLE OF R-SULFORAPHANE AND MORINGIN
IN THE PREVENTION OF PATHOLOGIES
OF THE CENTRAL NERVOUS SYSTEM*

CHAPTER ELEVEN

Glucoraphanin purified from Tuscan black kale and bioactivated with myrosinase enzyme protects against cerebral ischemia/reperfusion injury in rats

Contents

Summary

11.1 Cerebral ischemia/reperfusion

11.2 Materials and Methods

11.2.1 Animals

11.2.2 Induction of cerebral I/R

11.2.3 Myrosinase bioactivation of glucoraphanin

11.2.4 Experimental groups

11.2.5 Light microscopy

11.2.6 Immunohistochemical localization of ICAM-1, iNOS, I κ B- α and NF- κ B

11.2.7 Protein extraction from formalin-fixed paraffin-embedded tissues (FFPE)

11.2.8 Terminal deoxynucleotidyltransferase-mediated UTP end labeling (TUNEL) assay

11.2.9 Statistical evaluation

11.3 Results

11.3.1 Effect of *R*-SF on carotid artery ischemia/reperfusion injury rats

11.3.2 Effect of *R*-SF on ICAM-1 expression in ischemic cerebral tissues

11.3.3 Effect of *R*-SF on I κ B- α and NF- κ B expression in ischemic cerebral tissues

11.3.4 Effect of *R*-SF on iNOS expression in ischemic cerebral tissues

11.3.5 Effect of *R*-SF on apoptosis in brain after ischemia

11.3.6 Effect of *R*-SF on Caspase 3 expression in ischemic cerebral tissues

11.4 Discussion

11.5 Conclusion

References

Keywords

Cerebral ischemia-reperfusion; Glucoraphanin; *R*-Sulforaphane; Inflammation; Oxidative stress; Apoptosis

Abbreviations

GLs: glucosinolates;

FFPE: formalin-fixed paraffin-embedded;

H&E: hematoxylin/eosin;

iNOS: inducible nitric oxide synthase expression;

ICAM-1: intercellular adhesion molecule 1;

I/R: ischemia/reperfusion;

ITCs: isothiocyanates;

MYR: myrosinase;

NF- κ B: nuclear factor κ B;

NO: nitric oxide;

ONOO⁻: peroxynitrite;

RNS: reactive nitrogen species;

ROS: reactive oxygen species;

Bioactive *R*_S-GRA: myrosinase bioactivated GRA;

O₂⁻: superoxide anion;

TdT: terminal deoxynucleotidyltransferase;

TUNEL: terminal deoxynucleotidyltransferase-mediated UTP end labeling.

Summary

Ischemic stroke is the result of a transient or permanent reduction in cerebral blood flow caused by the occlusion of a cerebral artery via an embolus or local thrombosis. Restoration of blood supply to ischemic tissues can cause additional damage known as reperfusion injury that can be more damaging than the initial ischemia. This study was aimed to examine the possible neuroprotective role of enantiopure *R*-sulforaphane *R*-SF in an experimental rat model of brain ischemia/reperfusion injury (I/R). The mechanism underlying the inhibitory effects of *R*-SF on inflammatory and apoptotic responses, induced by carotid artery occlusion in rats, was carefully examined. Cerebral I/R was induced by the clamping of carotid artery for 1 h, followed by 40 min of reperfusion through the release of clamp. The results have clearly shown that administration of *R*-SF (GRA 10 mg Kg⁻¹, i.p. + myrosinase) 15 min after ischemia, significantly reduces proinflammatory parameters, such as inducible nitric oxide synthase expression (iNOS), intercellular adhesion molecule 1 (ICAM-1), nuclear factor (NF)-κB translocation as well as the triggering of the apoptotic pathway (TUNEL and Caspase 3 expression). Results have shown that *R*-SF possesses beneficial neuroprotective effects in counteracting the brain damage associated to I/R.

11.1 Cerebral ischemia reperfusion

Stroke is the third leading cause of death (Lo et al., 2003) and the most severe cause of acquired adult disability (Donnan et al., 2008). With high incidence, stroke survivors are permanently disabled, and they require institutional care. Deficits can include partial paralysis, difficulties in memory, thinking, language, and movements. Ischemic stroke results by a transient or permanent reduction in cerebral blood flow, that is restricted to the territory of a major brain artery. The reduction in flow is, in most cases, caused by the occlusion of a cerebral artery either by an embolus or by local thrombosis. This leads to a complex sequence of pathophysiological events, that evolve in time and space and which includes mechanisms of excitotoxicity, release of neurotransmitters, breakdown of blood–brain barrier, cytokine production, adhesion molecule upregulation, oxidative and nitrosative stress and apoptosis (Sahota and Savitz, 2011; Brouns and De Deyn, 2009). Although several mechanisms are involved in cerebral ischemic stroke pathogenesis, increasing evidences demonstrate that inflammation plays a key role in the pathogenesis of ischemic stroke and other forms of ischemic brain injury (Moskowitz et al., 2010; Jin et al., 2010). Cerebral ischemia initiates a significant inflammatory cascade, which involves the activation of brain microglia, upregulation of proinflammatory cytokines, such as tumor necrosis factor-alpha (TNF- α), interleukin (IL)-1 β and others (Jin et al., 2010; del Zoppo et al., 2000), infiltration of various types of inflammatory cells (including neutrophils, different subtypes of T cells, monocyte/macrophages and other cells) into the ischemic brain tissue (Jin et al., 2010; Yilmaz and Granger, 2010). Reperfusion is the restoration of blood flow to the ischemic tissue. Despite the unequivocal benefit of blood reperfusion to an ischemic tissue, itself can elicit a cascade of adverse reactions that paradoxically injure the tissue (Bonventre, 1993). It has been amply demonstrated that there are a series of reactions following brain reperfusion, such as inflammation and a rapid increase of reactive oxygen species (ROS) and reactive nitrogen species (RNS), which can produce significant quantities of tissue damage, thereby contributing to neuronal cell death (Kahles et al., 2007; Maneen and Cipolla, 2007). Therefore, antiinflammatory or antioxidant approach may be a potential therapeutic strategy of preserving against ischemia/reperfusion (I/R) cerebral injury. Despite advances in the understanding of the cerebral ischemia pathophysiology, therapeutic options remain limited. Numerous clinical trials failed in the past decades because either these agents showed no

protective effects in patients or their toxicity/side effects cannot be tolerated by patients. The aim of this study was to evaluate the possible positive effect of *R*-SF in the treatment of cerebral I/R rat model.

11.2 Materials and Methods

11.2.1 Animals

Male Wistar rats (Harlan, Italy) weighing 200–250 g were used. Rats were housed in a controlled environment and provided with standard rodent chow and water. Animal care followed Italian regulations on the protection of animals used for experimental and other scientific purpose (D.M. 116/92) as well as with the EEC regulations (O.J. of E.C. L358/112/18/1986). Experimental procedures did not cause any significant animal suffering.

11.2.2 Induction of cerebral I/R

After anesthesia, cerebral I/R was induced in rats. In brief, in the supine position, a midline ventral incision was made in the neck of each animal, carotid artery was exposed, separated from the vagus nerve and occluded for 1 h by clamping with small vascular clips and by inducing hypotension to generate a cerebral ischemia animal model. *R*-SF was administered 15 min after ischemia and at the end of clamping time, a phase of reperfusion of blood flowing the duration of 40 min was followed. Finally, rats were sacrificed to perform subsequent morphological evaluation and Western blot analysis.

11.2.3 Myrosinase bioactivation of pure glucoraphanin

GRA and MYR were purified as described at Chapter eight (see Section 8.3.2) and at Chapter nine (see Section 9.2.2), respectively.

Pure GRA (95%) was dissolved in PBS solution pH 7.2 at room temperature (2.5 mg mL⁻¹) and hydrolyzed by the action of MYR (12.5 µl; 32 U mL⁻¹) for 15 min at 37 °C right before animal treatment. Starting GRA was quantitatively transformed into *R*-SF and rats were then administered with the resulting solution as such.

11.2.4 Experimental design

Rats were randomly allocated into the following groups (N=20 total animals):

- I/R + saline group: rats were subjected to artery occlusion (1 h) followed by reperfusion (40 min) and were administered with saline (N=10);
- I/R + R-SF group: rats were subjected to surgical procedures described as above and R-SF (GRA 10 mg Kg⁻¹ + 50 µl/rat MYR) was administered 15 min after ischemia (N=10).

At the end of the experiment, blood from each animal was collected by cardiac puncture for hemogram analysis, following animals were sacrificed. Brain tissues were sampled and processed, to evaluate some disease parameters.

11.2.5 Light microscopy

Brain tissues were taken at 40 min following I/R (Lu et al., 2003). Tissues were fixed in 10% formalin, pH 7.4. After dehydration in graded ethanol and xylene, the tissues were paraffin embedded and cut into coronal sections (7 µm thick) to observe hippocampus area, a vital center for learning and memory, which is extremely vulnerable to various insults such as ischemia (Nakatomi et al., 2002). Tissue sections were stained with hematoxylin/eosin (H&E) and studied using light microscopy (Leica ICCS50HD).

11.2.6 Immunohistochemical localization of ICAM-1, iNOS, IκB-α and NF-κB

About 40 min following I/R tissues were fixed in 10% (w/v) PBS-buffered formaldehyde, and 6-µm sections were prepared from paraffin-embedded tissues. After deparaffinization, endogenous peroxidase was quenched with 0.3% (v/v) hydrogen peroxide in 60% (v/v) methanol for 30 min. Nonspecific adsorption was minimized by incubating the section in 2% (v/v) normal goat serum in PBS for 20 min. Endogenous biotin or avidin binding sites were blocked by sequential incubation for 15 min with biotin and avidin (DBA, Milan, Italy), respectively. Sections were incubated overnight with anti-ICAM-1 monoclonal antibody (1:100 in PBS v/v; Santa Cruz Biotechnology. INC), anti-iNOS polyclonal antibody (1:100 in PBS v/v; Santa Cruz Biotechnology. INC), anti-IκB-α polyclonal antibody (1:100 in PBS v/v; Santa Cruz Biotechnology. INC), and anti-NF-κB monoclonal antibody (1:100 in PBS v/v; Cell

Signaling). Sections were washed with PBS and incubated with secondary antibody. Specific labeling was detected with a biotin conjugated goat anti-rabbit IgG and avidin–biotin peroxidase complex (DBA). The counterstain was developed with diaminobenzidine (brown color) and ematosilin (blue background). To verify the binding specificity, some sections were also incubated with only the primary antibody (no secondary) or with only the secondary antibody (no primary). In these situations, no positive staining was found in the sections, indicating that the immunoreaction was positive in all the experiments carried out. All sections were obtained using light microscopy (LEICA ICC50 HD) and studied via an Imaging computer program (Leica Application Suite V4.1).

11.2.7 Protein extraction from formalin-fixed paraffin-embedded tissues (FFPE)

For Western blotting analysis, according to Rodriguez-Rigueiro et al. (2011), we obtained a total protein extract from formalin-fixed paraffin-embedded tissue (FFPE) blocks. Briefly, 6 × 15µm sections for each paraffin embedded sample were deparaffinated with xylene and rehydrated with decreasing scale of alcohols. After centrifugation, pellets were resuspended in 50 µl of buffer, containing 200 mM Tris HCl, pH 7.5, 200 mM NaCl, 5% SDS and 100 mM sodium citrate, and incubated in a thermomixer comfort (Eppendorf) first at the temperature of 100 °C for 20 min and then at 80 °C for 2 h, under continuous shaking at 1000 rpm. Samples were ice cooled for 1 min, purified by centrifugation at 14000 ×g for 15 min at 4 °C and the supernatants were recovered, and protein quantification was carried out by using Biorad protein assay kit (Bio-Rad Milan, Italy). According to the molecular weight of the protein to investigate, extracts were loaded in polyacrilamide gels at different percentage for SDS-PAGE and after electrophoresis and blotting, Westran S PVDF Blotting Membranes, (Labcenter EXACTA + OPTTECH) were blocked with 1×PBS, 5% (w/v) nonfat dried milk (PM) for 1 h at room temperature and subsequently probed at 4 °C overnight with specific antibodies for Caspase 3 (1:1000; Cell Signaling), in 1×PBS, 5% (w/v) nonfat dried milk, 0.1% Tween-20 (PMT). Membranes were incubated with peroxidase-conjugated bovine anti-mouse IgG secondary antibody or peroxidase-conjugated goat anti-rabbit IgG (1:2000, Santa Cruz Biotechnology. INC) for 1 h at room temperature. To verify that blots were loaded with equal amounts of protein extract, they were also incubated in the presence of the antibody against α-tubulin (1:250, Santa Cruz Biotechnology. INC). The relative expression of the protein bands of

Caspase 3 (~35 kDa), was visualized using an enhanced chemiluminescence system (Luminata Western HRP Substrates, Millipore). The protein bands were scanned and quantitated with ChemiDoc™ MP System (Bio-Rad) and a computer program (ImageJ).

11.2.8 Terminal deoxynucleotidyltransferase-mediated UTP end labeling (TUNEL) assay

To test whether I/R was associated with cell death by apoptosis, we measured TUNEL-like staining in brain tissues. TUNEL assay was conducted by using a TUNEL detection kit according to the manufacturer's instruction (Apotag, HRP kit DBA, Milan, Italy). Sections were incubated with 15 mg mL⁻¹ proteinase K for 15 min at room temperature and then washed with PBS. Endogenous peroxidase was inactivated by 3% H₂O₂ for 5 min at room temperature and then washed with PBS. Sections were immersed in terminal deoxynucleotidyltransferase (TdT) buffer containing deoxynucleotidyl transferase and biotinylated dUTP in TdT buffer, incubated in a humid atmosphere at 37 °C for 1 h, and then washed with PBS. Sections were incubated at room temperature for 30 min with anti-horseradish peroxidase conjugated antibody, and signals were visualized with diaminobenzidine and counterstained with methyl green.

11.2.9 Statistical evaluation

Data were analyzed in GraphPad Prism version 6.0 (GraphPad Software, La Jolla, CA). The results were analyzed by unpaired Student's t-test. A p value of ≤0.05 was considered to be statistically significant. Results are expressed as the mean ± S.E.M. of n experiments.

11.3 Results

11.3.1 Effect of R-SF on carotid artery ischemia/reperfusion injury in rats

Cerebral infarction was examined using slices of brain after I/R in rats through H&E staining. The infarct area was larger in brain sections obtained from rat subjects to I/R. In addition, histological examination showed severe damage to the brain tissue in different sections, as demonstrated by the presence of edema (Figure 11.1A, B, E and F), infiltration of

inflammatory cells, such as leukocytes (neutrophils and/or lymphocytes), as well as alteration of the frame 40 min after injury. These data were also supported by the results obtained through hemogram analysis, that have demonstrated an increase in inflammatory cells in rats subjected to cerebral I/R. On the contrary, an attenuation of these indices of inflammation was observed in rats treated with *R-SF* (Table 11.1). Moreover, presence of mast cells (Figure 11.2A) was observed in brain tissues collected after 40 min of reperfusion in perivascular area (arrows indicate the presence of mast cells characterized by metachromatic granules basophils rich in histamine). On the contrary, significant less mast cells density and degranulation were observed in brain tissue after I/R, collected from rats which have been treated with *R-SF* (Figure 11.2B). Also, *R-SF* administration showed reductions in infarct volume and a significant protection from I/R-associated damage was observed in tissue samples collected from *R-SF* treated rats (Figure 11.1C, D).

Table 11.1 Hemogram analysis. The results obtained through hemogram analysis, demonstrated an increase in inflammatory cells in rats subjected to cerebral I/R. On the contrary, an attenuation of these indices of inflammation was observed in rats treated with *R-SF*. Values shown are the mean of multiple observations.

Parameters	I/R (K/μL)	I/R + <i>R-SF</i> (K/μL)
WBC	1.37	0.5355
NEU	0.42967	0.236
LYM	0.837	0.2715
MONO	0.027	0.0065
EOS	0.058	0.02
BASO	0.01867	0.001

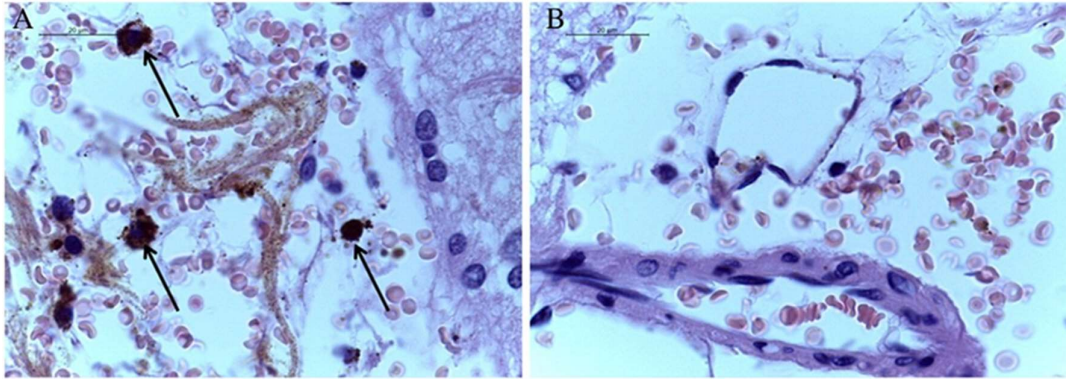


Figure 11.2 Staining of mast cells. In the vascular endothelium the presence of metachromatic granules basophils rich in histamine was shown, indicated by the arrows, which identifies the cells as mast cells. Many of the mast cells are arranged separately in concentric rings around small blood-vessels. In the brain tissue collected after 40 min of reperfusion there is presence of mast cells mainly localized in the perivascular area (A). On the contrary, administration of *R-SF* showed reduction in mast cell infiltration and activation (B).

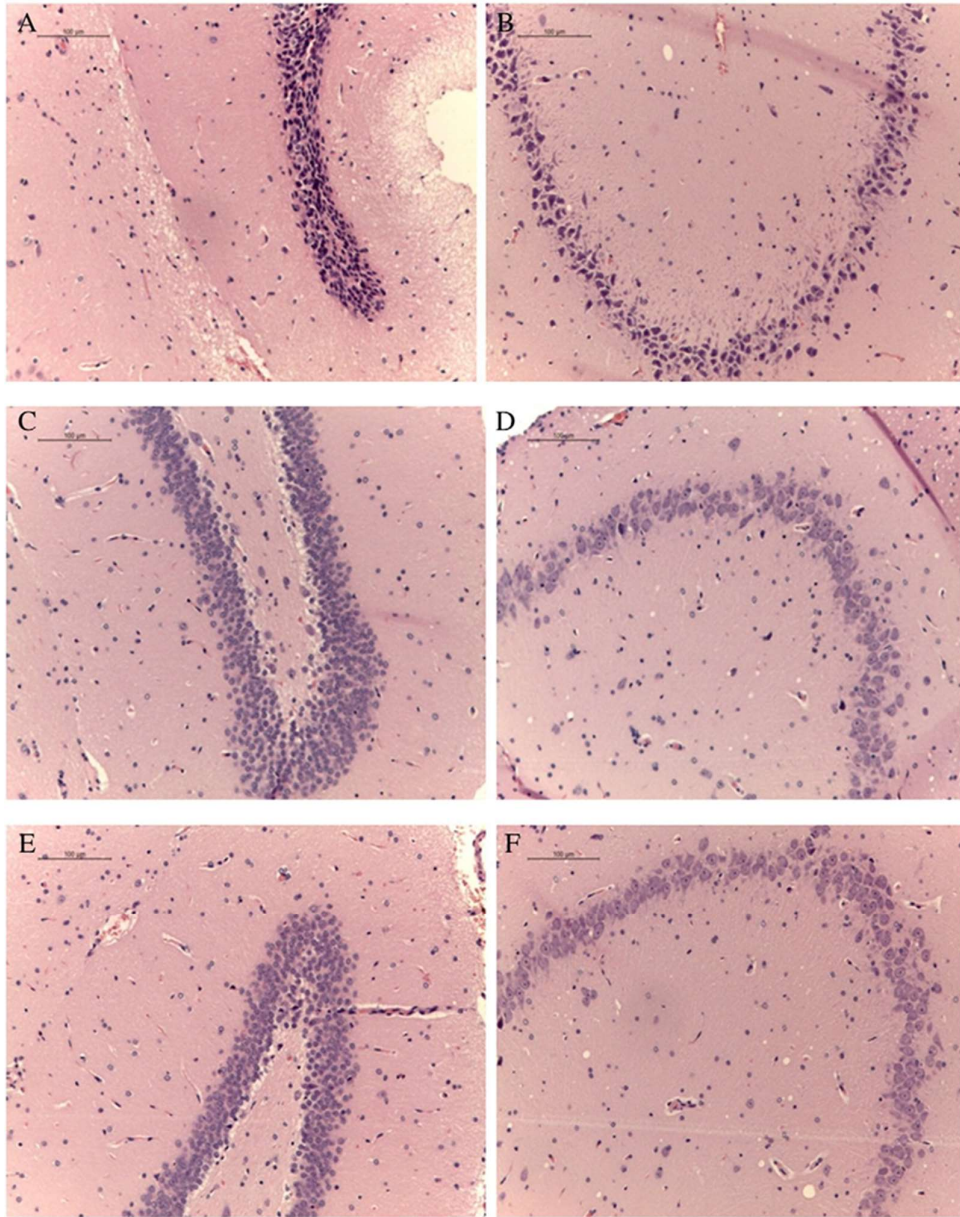


Figure 11.1 Effect of *R-SF* on histological alterations of the brain tissue. Significant damage to the brain tissue in rats subjected to I/R was apparent, as demonstrated by the presence of edema as well as frame alteration 40 min after injury (A, B, E and F). Also, a significant protection from I/R-associated damage was observed in tissue samples collected from *R-SF* treated rats (C,D).

11.3.2 Effect of *R*-SF on ICAM-1 expression in ischemic cerebral tissues

Since ICAM-1 in post-ischemic cerebral stroke has a role in the recruitment of inflammatory cells, such as leukocytes and lymphocytes from the blood into the brain parenchyma, we evaluated ICAM-1 expression in ischemic cerebral tissue collected after 40 min of reperfusion. Our results clearly showed that increased expression of adhesion molecules following carotid artery I/R in the vascular endothelium (Figure 11.3A, C) could be reverted by *R*-SF treatment that significantly reduces degree of positive staining for ICAM-1 (Figure 11.3B, D).

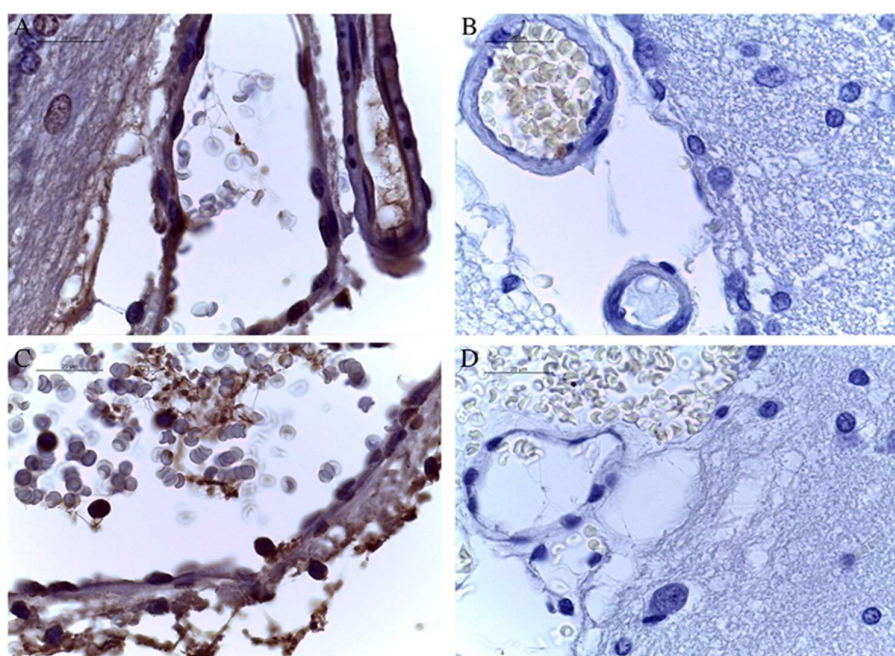


Figure 11.3 Effect of *R*-SF on ICAM-1 expression. A substantial increase in ICAM-1 expression was found in brain tissues from I/R rats 40 min after reperfusion localized in the vascular endothelium (A, C). Treatment with *R*-SF significantly reduced the degree of positive staining for ICAM-1 (B, D).

11.3.3 Effect of *R*-SF on I κ B- α and NF- κ B expression in ischemic cerebral tissues

To investigate the cellular mechanism by which *R*-SF treatment may attenuate development of I/R and damage associated with it, we evaluated in the brain sections collected after 40 min of reperfusion, I κ B- α degradation and nuclear NF- κ B activation by immunohistochemical analysis. Brain sections obtained from rats subjected to I/R did not stain for I κ B- α (Figure 11.4 A, C), whereas brain sections obtained from rats treated with *R*-SF exhibited positive staining

for I κ B- α (Figure 11.4B, D). In addition, brain sections obtained from rats subjected to I/R exhibited positive staining for NF- κ B (Figure 11.4E, G). On the contrary, *R*-SF treatment significantly reduced degree of positive staining for NF- κ B (Figure 11.4F, H).

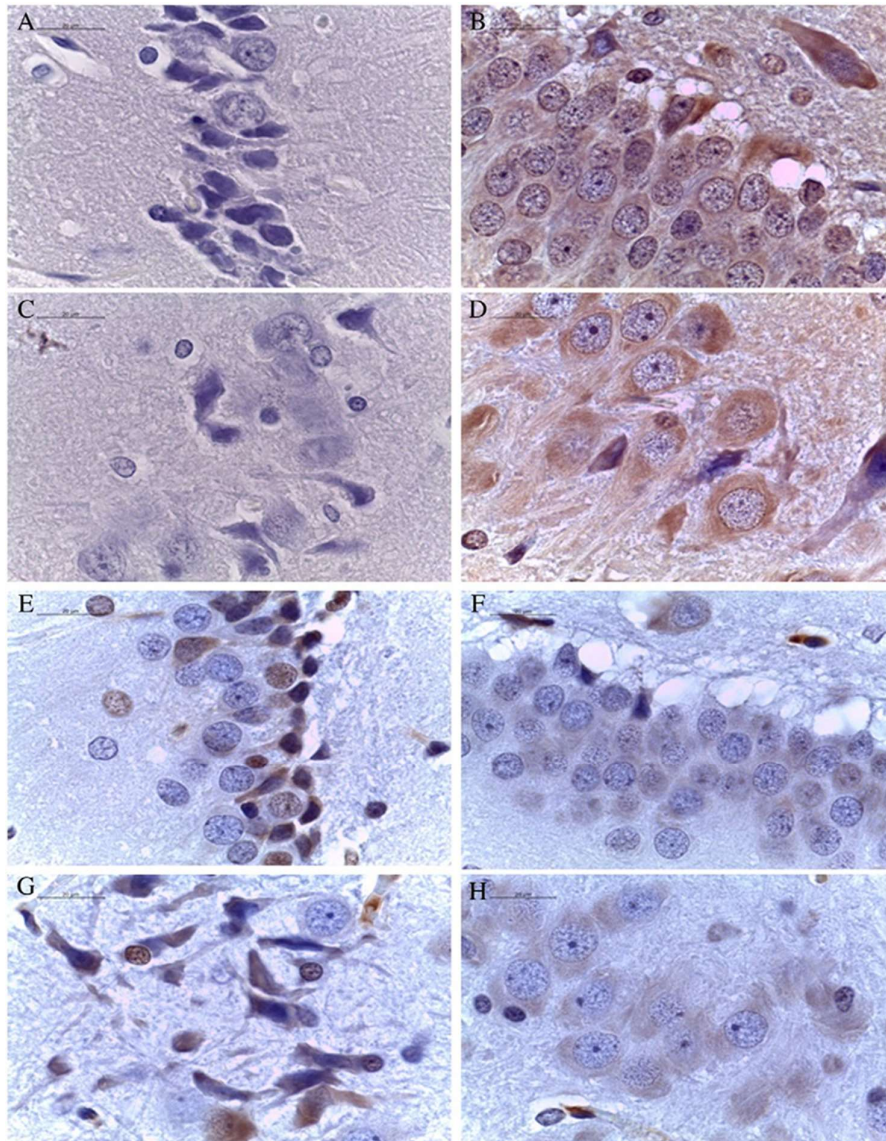


Figure 11.4 Effect of *R*-SF on I κ B- α and NF- κ B expression. I κ B- α and NF- κ B expression was evaluated by immunohistochemical analysis. Brain sections obtained from rats subjected to I/R did not stain for I κ B- α (A, C), whereas brain sections obtained from rats treated with *R*-SF exhibited positive staining for I κ B- α (B, D). In addition, brain sections obtained from rats subjected to I/R exhibited positive staining for NF- κ B (E, G). On the contrary, treatment with *R*-SF significantly reduced the degree of positive staining for NF- κ B (F, H).

11.3.4 Effect of *R*-SF on iNOS expression in ischemic cerebral tissues

To determine the role of nitric oxide (NO) produced during I/R and to verify whether treatment with *R*-SF is able to counteract oxidative and nitrosative stress resulting from ischemic damage, we evaluated iNOS expression by immunohistochemical analysis, after 40 min of reperfusion. Brain section obtained from rats subjected to I/R exhibited positive staining for iNOS (Figure 11.5A, C, see densitometry analysis E). *R*-SF treatment clearly reduced the degree of positive staining for iNOS (Figure 11.5B, D see densitometry analysis E).

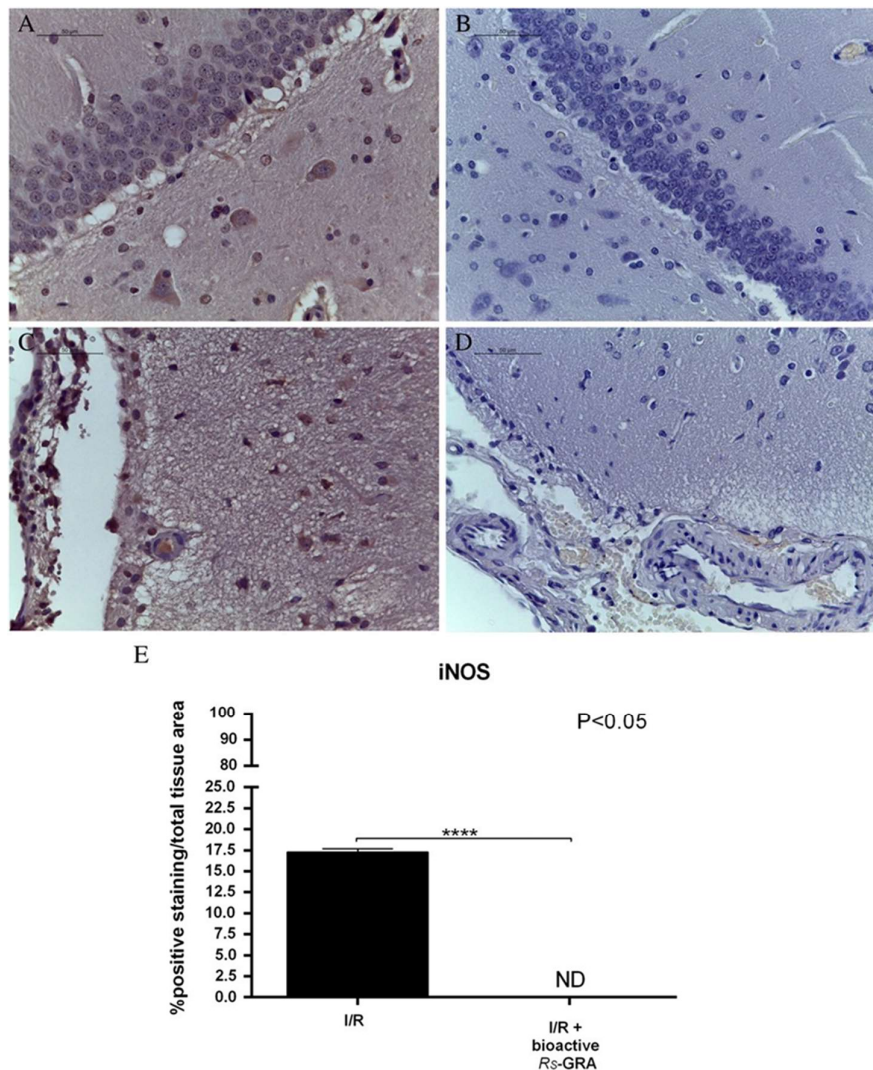


Figure 11.5 Effect of *R*-SF (bioactive *R*₅-GRA) on iNOS expression. A substantial increase in iNOS expression was found in inflammatory cells, in the white matter nuclei of hippocampus from I/R rats (A) and in blood–brain barrier (C). Brain levels of iNOS were significantly attenuated in *R*-SF treated rats (B, D). Densitometric analysis is shown in E: a *p* value ≤ 0.05 was considered statistically significant. ND: not detectable.

11.3.5 Effect of *R*-SF on apoptosis in brain after ischemia

Morphological and biochemical criteria of apoptosis are the condensation of chromatin leading to the development of apoptotic bodies or membrane-enclosed vesicles containing oligonucleosomal DNA fragments. Important diagnostic tools of death, such as TUNEL test, are based on the biochemical characteristics mentioned above. To test whether tissue damage was associated with apoptosis induction, we evaluated TUNEL-like staining in the brain tissue. After 40 min of reperfusion, brain tissue demonstrated a marked appearance of dark-brown apoptotic cells and intercellular apoptotic fragments (Figure 11.6A, see particle A1 and C). In contrast, tissues obtained from rats treated with *R*-SF demonstrated no apoptotic cells or fragments (Figure 11.6B, D).

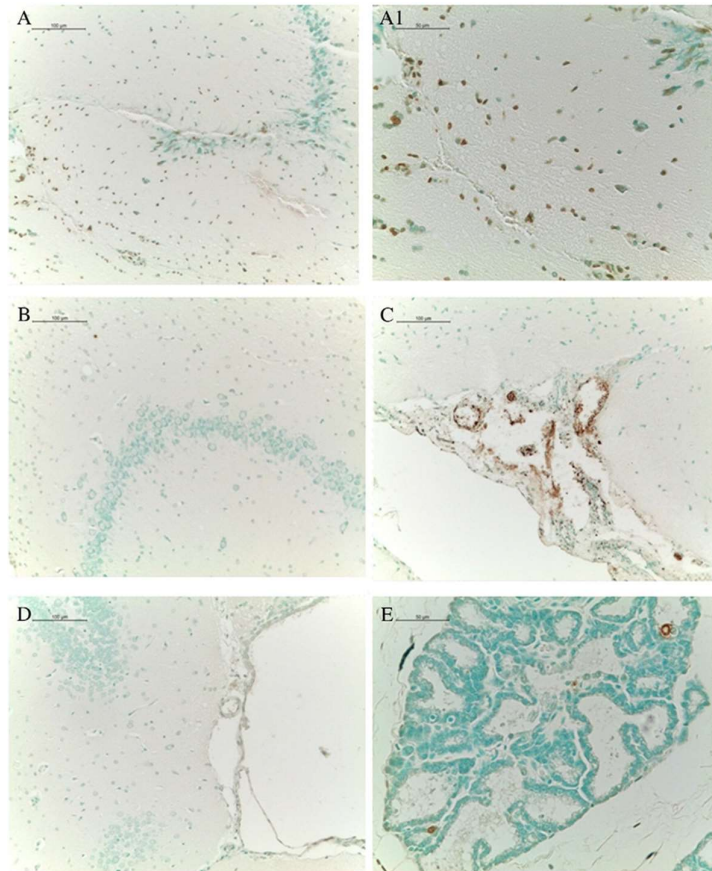


Figure 11.6 Effect of *R*-SF on TUNEL-like staining in brain tissue. At 40 min after reperfusion, tissues obtained from rats subjected to I/R demonstrated a marked appearance of dark-brown apoptotic cells and intercellular apoptotic fragments both in hippocampus (A, see particle A1,) and in the vascular endothelium (C). In contrast, tissues obtained from rats treated with *R*-SF demonstrated no apoptotic cells or fragments in hippocampus areas (B) and in vascular endothelium (D). Panel E is a positive control of kit.

11.3.6 Effect of *R*-SF on Caspase 3 expression in ischemic cerebral tissues

By Western blot, we evaluated Caspase 3 activation, since sequential activation of caspase plays a key role in the execution phase of cell apoptosis. Caspase 3 levels were appreciably increased in the brain from rats subjected to I/R. On the contrary, treatment with *R*-SF prevented I/R-induced Caspase 3 expression (Figure 11.7).

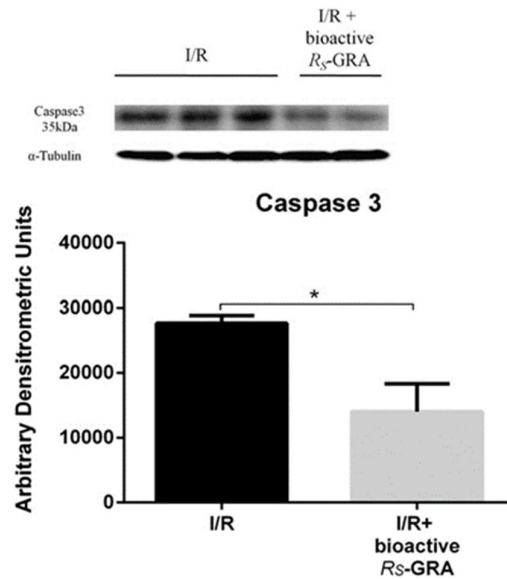


Figure 11.7 Western blot for Caspase 3. By Western blot, Caspase 3 activation was evaluated. Caspase 3 levels were appreciably increased in the brain from rats subjected to I/R. On the contrary, treatment with *R*-SF (bioactive *R*₅-GRA) prevented the I/R-induced Caspase 3 expression. α -tubulin was used as internal control. * $p \leq 0.0112$ vs. I/R.

11.4 Discussion

I/R is characterized by initial tissue damage during the ischemic period to cell structures and following the restoration of blood flow (I/R), lesions produced are exacerbated further. Moreover, it is believed that several mediators, such proinflammatory cytokines (Husted and Lentsch, 2006), chemokines, excess of NO (Masini et al., 2006) and ROS contribute significantly to the degree of injury (Serracino-Inglott et al, 2001; Ayub et al., 2001). Previous studies have demonstrated that inflammation has been implicated in the pathogenesis of ischemic stroke and inflammatory cell recruitment, appears to aggravate ischemic brain injury (Planas et al., 2006; Wang et al., 2007). Since leukocyte-endothelial cell adhesion is a rate-

determining step in the recruitment of leukocytes into post-ischemic brain tissue, much attention has been devoted to defining the contribution of different adhesion molecules, expressed either on leukocytes or endothelial cells, to the leukocyte recruitment process, like ICAM-1 (Yilmaz and Granger, 2008). ICAM-1 is a member of the immunoglobulin superfamily and among all, ICAM-1 has been the most extensively investigated in cerebral ischemia since it plays an important role in its pathophysiology (Yilmaz and Granger, 2008). Indeed, results of several studies have revealed significant ICAM-1 expression in the post-ischemic brain and a role for this adhesion molecule in the recruitment of inflammatory cells, such as leukocytes and lymphocytes from the bloodstream into the brain parenchyma (Chen et al., 2003; Okada et al., 1994; Jander et al., 1995; Zhang et al., 1995; Wang et al., 1995). In normal rat brain, ICAM-1 is constitutively expressed in low concentrations in the membranes of leukocytes and endothelial cells. In certain circumstances, concentrations greatly increase. In response to I/R, it is super expressed in the vascular endothelium cells, connective tissue, lamina propria and inflammatory cells. This super expression of ICAM-1 accentuates the leukocyte adhesion and promotes their migration to the injured brain during I/R. We have shown significant increase ICAM-1 levels in the brain tissues from I/R rats and that treatment with *R*-SF significantly reduced degree of positive staining for ICAM-1. Also, resident mast cells contribute to dysfunction of the I/R brain through the release of histamine and other mediators, mainly after the formation of large quantities of ROS (Mannaioni and Masini, 1988). These in turn contribute to the up-regulation of ICAM-1 expression on endothelial cells and play a key role in inflammatory process (Clark et al., 1995). Mast cells are implicated in leukocyte recruitment and tissue injury following acute brain I/R, in specific, through their degranulation is released histamine. It is a vasoactive amine which increases the caliber and permeability of blood vessels by promoting the extravasation of plasma and plasma proteins in the extracellular environment, with consequent formation of edema and promoting the release neutrophils (Strbian et al., 2006; Lindsberg et al., 2010). By histological examination we demonstrated that cerebral ischemia causes edema and infiltration of inflammatory cells, such as leukocytes (neutrophils and/or lymphocytes) and mast cells in brain tissues from I/R rats. *R*-SF administration significantly reduced degree of the severity of I/R through reduction of mast cell infiltration and activation. NF- κ B plays a central role in the regulation of many genes responsible for generation of mediators or proteins in secondary inflammation associated to I/R. NF- κ B is normally sequestered in the cytoplasm, bound to regulatory protein I κ Bs. In

response to a wide range of stimuli including oxidative stress, infection, hypoxia, extracellular signals, and inflammation, I κ B is phosphorylated by I κ B kinase enzyme (Bowie and O’Niell, 2000). The net result is release of the NF- κ B dimer, which is then free to translocate into the nucleus. We reported here that carotid artery occlusion caused a significant increase in the NF- κ B levels in brain tissues, whereas treatment with *R*-SF significantly reduced this expression. Moreover, we also demonstrated that *R*-SF inhibited I κ B- α degradation, as well as the consequent NF- κ B translocation and subsequent activation of many proinflammatory mediators under its control, such as iNOS (Attuwaybi et al., 2004). ROS and RNS are produced during an acute ischemic stroke and it is known that oxidative stress is a key mediator of tissue damage in it (Cuzzocrea et al., 2001). NO is also important among the free radicals produced during I/R. It is normally synthesized by L-arginine through NO synthase, which can have constitutive (cNOS) and induced (iNOS) isoforms. The excess production of NO through induced NO synthase (iNOS) contributes to the pathophysiology of I/R in the brain. NO presents beneficial vasodilatory effects in the microvascular system through the relaxation of the smooth vascular muscle cells, but, paradoxically, could be involved in the production of cytotoxic radicals (Chan et al., 1999). According to Sekhon et al. (2003), NO is beneficial as a modulator or messenger, but during oxidative stress it is potentially toxic. NO cytotoxicity emerges, in part, by reaction with superoxide anion (O₂⁻) to generate peroxynitrite (ONOO⁻), which then causes accentuated lipid peroxidation, proteic and DNA modifications resulting in cellular damage (Montalto et al., 2003). All cellular components are susceptible to the action of ROS, though the membrane is one of the most affected because of lipid peroxidation, which causes alterations in the structure and permeability of cellular membranes. We showed that cerebral I/R results in expression of iNOS in rats brain 40 min after reperfusion. We further demonstrated that *R*-SF administration protected brain morphology and reduced I/R-induced activation of iNOS after reperfusion. Therefore, it is possible that *R*-SF by counteracting oxidative and nitrosative stress prevents inflammatory and toxic events during I/R injury. Moreover, it is well known that isothiocyanates may exert their cytoprotective effects by the ability to induce the expression of several enzymes via the Keap1/Nrf2/ARE pathway (Baird et al., 2014). Nrf2, is believed one of the most important transcription factors involved in the protection of the cells by oxidative stress, regulating cytoprotective genes and triggering the activation of the antioxidant glutathione pathway (Harvey et al., 2009). Therefore, after damage, Nrf2 could play a protective action in astrocytes, decreasing GFAP expression

probably through the mechanism related to the glutathione activity, according to other studies reported in literature (Harvey et al., 2009; LaPash Daniels et al., 2012). Thus, it seems that astrocyte specific Nrf2 mediated protection due to treatment with *R*-SF could have beneficial effects in counteracting the damage after I/R and this could be associated with the production of several growth factors that may protect neurons from damage. Finally, we have demonstrated that *R*-SF treatment has proved to be able to attenuate degree of apoptosis in brain after I/R induction, measured by TUNEL. Apoptosis is a natural form of cell death, which can be induced by an “intrinsic” mitochondria mediated pathway. Activation of caspases (in particular Caspase 3) followed by cleavage of cellular substrates, leads to programmed cell death (Green and Reed, 1998). Caspase 3 is a key regulator of apoptosis, essential for some of the characteristic changes in cell morphology and in some biochemical events associated with the execution and completion of this process (Porter and Janicke, 1999). Since apoptosis is present in dying neurons after ischemia, we considered Caspase 3 overexpression as marker of apoptosis. Our data demonstrated a significant increase of cleaved Caspase-3 after I/R. A protective effect of *R*-SF suggests that this treatment could interfere with the I/R induced neuronal death, preserving cells by injury.

11.5 Conclusion

Taken together, the results of the present study have shown that the *R*-SF treatment is associated with neuroprotective effects due to an anti-inflammatory and antiapoptotic activity during cerebral I/R in rats. These results provide a new and interesting possible application of *R*-SF in the clinical treatment of cerebral ischemia.

References

Attuwaybi BO, Kozar RA, Moore-Olufemi SD, Sato N, Hassoun HT, Weisbrodt NW et al. (2004) Heme oxygenase-1 induction by hemin protects against gut ischemia/reperfusion injury. *J Surg Res* 118:53-7.

Ayub K, Serracino-Inglott F, Williamson RC, Mathie RT (2001) Expression of inducible nitric oxide synthase contributes to the development of pancreatitis following pancreatic ischemia and reperfusion. *Br J Surg* 88:1189-93.

Baird L, Swift S, Lleres D, Dinkova-Kostova AT (2014) Monitoring Keap1-Nrf2 interactions in single live cells. *Biotechnol Adv* 32:1133-44.

Bonventre JV (1993) Mechanisms of ischemic acute renal failure. *Kidney Int* 43:1160-78.

Bowie A and O'Neill LA (2000) Oxidative stress and nuclear factor-kappa B activation: a reassessment of the evidence in the light of recent discoveries. *Biochem Pharmacol* 59:13-23.

Brouns R and De Deyn PP (2009) The complexity of neurobiological processes in acute ischemic stroke. *Clin Neurol Neurosurg* 111:483-95.

Chan KL, Zhang XH, Fung PC, Guo WH, Tam PK (1999) Role of nitric oxide in intestinal ischemia–reperfusion injury studied using electron paramagnetic resonance. *Br J Surg* 86:1427-32.

Chen Y, Ruetzler C, Pandipati S, Spatz M, McCarron RM, Becker K et al. (2003) Mucosal tolerance to E-selectin provides cell-mediated protection against ischemic brain injury. *Proc Natl Acad Sci USA* 100:15107-12.

Clark WM, Lauten JD, Lessov N, Woodward W, Coull BM (1995) Time course of ICAM-1 expression and leukocyte subset infiltration in rat forebrain ischemia. *Mol Chem Neuropathol* 26:213-30.

Cuzzocrea S, Riley DP, Caputi AP, Salvemini D (2001) Antioxidant therapy: a new pharmacological approach in shock, inflammation, and ischemia/reperfusion injury. *Pharmacol Rev* 53:135-59.

del Zoppo G, Ginis I, Hallenbeck JM, Iadecola C, Wang X, Feuerstein GZ (2000) Inflammation and stroke: putative role for cytokines, adhesion molecules and iNOS in brain response to ischemia. *Brain Pathol* 10:95-112.

Donnan GA, Fisher M, Macleod M, Davis SM (2008) Stroke. *Lancet* 371:1612-23.

GreenDR and Reed JC (1998) Mitochondria and apoptosis. *Science* 281:1309-12.

Harvey CJ, Thimmulappa RK, Singh A, Blake DJ, Ling G, Wakabayashi N et al. (2009) Nrf2-regulated glutathione recycling independent of biosynthesis is critical for cell survival during oxidative stress. *Free Radic Biol Med* 46:443-53.

Husted TL, Lentsch AB (2006) The role of cytokines in pharmacological modulation of hepatic ischemia/reperfusion injury. *Curr Pharm Des* 12:2867-73.

Jander S, Kraemer M, Schroeter M, Witte OW, Stoll G (1995) Lymphocytic infiltration and expression of intercellular adhesion molecule-1 in photochemically induced ischemia of the rat cortex. *J Cereb Blood Flow Metab* 15:42-51.

Jin R, Yang G, Li G (2010) Inflammatory mechanisms in ischemic stroke: role of inflammatory cells. *J Leukoc Biol* 87:779-89.

Kahles T, Luedike P, Endres M, Galla HJ, Steinmetz H, Busse R et al. (2007) NADPH oxidase plays a central role in blood-brain barrier damage in experimental stroke. *Stroke* 38:3000-6.

LaPash Daniels CM, Austin EV, Rockney DE, Jacka EM, Hagemann TL, Johnson DA et al. (2012) Beneficial effects of Nrf2 overexpression in a mouse model of Alexander disease. *J Neurosci* 32:10507-15.

Lindsberg PJ, Strbian D, Karjalainen-Lindsberg ML (2010) Mast cells as early responders in the regulation of acute blood–brain barrier changes after cerebral ischemia and hemorrhage. *J Cereb Blood Flow Metab* 30:689-702.

Lo EH, Dalkara T, Moskowitz MA (2003) Mechanisms, challenges and opportunities in stroke. *Nat Rev Neurosci* 4:399-415.

Lu XC, Massuda E, Lin Q, LiW, Li JH, Zhang J (2003) Post-treatment with a novel PARG inhibitor reduces infarct in cerebral ischemia in the rat. *Brain Res* 978:99-103.

Maneen MJ and Cipolla MJ (2007) Peroxynitrite diminishes myogenic tone in cerebral arteries: role of nitrotyrosine and F-actin. *Am J Physiol Heart Circ Physiol* 292:H1042-50.

Mannaioni PF and Masini E (1988) The release of histamine by free radicals. *Free Radic Biol Med* 5:177-97.

Masini E, Cuzzocrea S, Mazzon E, Muia C, Vannacci A, Fabrizi F et al. (2006) Protective effects of relaxin in ischemia/reperfusion-induced intestinal injury due to splanchnic artery occlusion. *Br J Pharmacol* 148:1124-32.

Montalto MC, Hart ML, Jordan JE, Wada K, Stahl GL (2003) Role for complement in mediating intestinal nitric oxide synthase-2 and superoxide dismutase expression. *Am J Physiol Gastrointest Liver Physiol* 285:G197-206.

Moskowitz MA, Lo EH, Iadecola C (2010) The science of stroke: mechanisms in search of treatments. *Neuron* 67:181-98.

Nakatomi H, Kuriu T, Okabe S, Yamamoto S, Hatano O, Kawahara N et al. (2002) Regeneration of hippocampal pyramidal neurons after ischemic brain injury by recruitment of endogenous neural progenitors. *Cell* 110:429-41.

Okada Y, Copeland BR, Mori E, Tung MM, Thomas WS, del Zoppo GJ (1994) P-selectin and intercellular adhesion molecule-1 expression after focal brain ischemia and reperfusion. *Stroke* 25:202-11.

Planas AM, Gorina R, Chamorro A (2006) Signalling pathways mediating inflammatory responses in brain ischemia. *Biochem Soc Trans* 34:1267-70

Porter AG and Janicke RU (1999) Emerging roles of caspase-3 in apoptosis. *Cell Death Differ* 6:99-104.

Rodriguez-Rigueiro T, Valladares-Ayerbes M, Haz-Conde M, Blanco M, Aparicio G, Fernandez-Puente P et al. (2011) A novel procedure for protein extraction from formalin-fixed paraffin-embedded tissues. *Proteomics* 11:2555-9.

Sahota P and Savitz SI (2011) Investigational therapies for ischemic stroke: neuroprotection and neurorecovery. *Neurotherapeutics* 8:434-51.

Sekhon B, Sekhon C, Khan M, Patel SJ, Singh I, Singh AK (2003) N-acetyl cysteine protects against injury in a rat model of focal cerebral ischemia. *Brain Res* 971:1-8.

Serracino-Inglott F, Habib NA, Mathie RT (2001) Hepatic ischemia–reperfusion injury. *Am J Surg* 181:160-6.

Strbian D, Karjalainen-Lindsberg ML, Tatlisumak T, Lindsberg PJ (2006) Cerebral mast cells regulate early ischemic brain swelling and neutrophil accumulation. *J Cereb Blood Flow Metab* 26:605-12.

Wang Q, Tang XN, Yenari MA (2007) The inflammatory response in stroke. *J Neuroimmunol* 184:53-68.

Wang X, Yue TL, Barone FC, Feuerstein GZ (1995) Demonstration of increased endothelial-leukocyte adhesion molecule-1 mRNA expression in rat ischemic cortex. *Stroke* 26:1665-8.

Yilmaz G and Granger DN (2008) Cell adhesion molecules and ischemic stroke. *Neurol Res* 30:783-93.

Yilmaz G and Granger DN (2010) Leukocyte recruitment and ischemic brain injury. *Neuromolecular Med* 12:193-204.

Zhang RL, Chopp M, Zaloga C, Zhang ZG, Jiang N, Gautam SC et al. (1995) The temporal profiles of ICAM-1 protein and mRNA expression after transient MCA occlusion in the rat. *Brain Res* 682:182-8.

CHAPTER TWELVE

Tuscan black kale sprout extract bioactivated with myrosinase: a novel natural product for neuroprotection by inflammatory and oxidative response during cerebral ischemia/reperfusion injury in rat

Contents

Summary

- 12.1** Cerebral ischemic stroke
 - 12.2** Materials and Methods
 - 12.2.1** Animals
 - 12.2.2** Induction of CIR
 - 12.2.3** Myrosinase bioactivation of TBK-SE
 - 12.2.4** Experimental design
 - 12.2.5** Immunohistochemical evaluation
 - 12.2.6** Western blot analysis
 - 12.2.7** Blood sampling
 - 12.2.8** TNF- α assay
 - 12.2.9** Statistical evaluation
 - 12.3** Results
 - 12.3.1** Bioactive TBK-SE restores BBB vascular endothelium after CIR induction
 - 12.3.2** Bioactive TBK-SE modulates GFAP and Iba-1 expression after CIR
 - 12.3.3** Bioactive TBK-SE regulates iNOS, nitrotyrosine and Nrf2 expression
 - 12.3.4** Effect of bioactive TBK-SE on Phospho-p44/42 MAPK (ERK1/2) expression and TNF- α following CIR
 - 12.3.5** Bioactive TBK-SE treatment inhibits CIR induced apoptosis
 - 12.4** Discussion
 - 12.5** Conclusion
- References

Keywords

Glucosinolates, Glucoraphanin, *R*-Sulforaphane, Tuscan black kale extract, Blood–brain barrier, Oxidative stress, Apoptosis, Inflammation

Abbreviations

(2S)-2-hydroxy-3-butenyl GL: progoitrin;
4-OH-GBS: 4-hydroxy-3-indolylmethyl GL, 4-hydroxy-glucobrassicin;
4-OMe-GBS: 4-methoxy-3-indolylmethyl GL, 4-methoxy glucobrassicin;
BBB: blood–brain barrier;
CIR: Cerebral ischemia and reperfusion;
CNS: central nervous system;
GBS: 3-indolylmethyl GL, glucobrassicin;
GER: 4-methylsulfanylbutyl GL, glucoerucin;
GLs: glucosinolates;
GRA: 4(R)-methylsulfinylbutyl GL, glucoraphanin;
ICAM-1: adhesion molecule 1;
iNOS: inducible nitric oxide synthase;
ITCs: isothiocyanates;
MYR: myrosinase;
Neo-GBS: N-methoxy-3-indolylmethyl, neoglucobrassicin;
NO: nitric oxide;
RNS: reactive nitrogen species;
ROS: reactive oxygen species;
TBK-SE: Tuscan black kale sprout extract;
TJ: tight junction;
t-PA: tissue plasminogen activator.

Summary

Cerebral ischemia and reperfusion (CIR) is a pathological condition characterized by a first blood supply restriction to brain followed by the consequent restoration of blood flow and simultaneous reoxygenation. The aim of this study was to evaluate the neuroprotective effects of Tuscan black kale sprout extract (TBK-SE) bioactivated with myrosinase enzyme, assessing its capability to preserve blood–brain barrier (BBB), in a rat model of CIR.

CIR was induced in rats according to a classic model of carotid artery occlusion for a time of 1 h and the reperfusion time was prolonged for seven days. By immunohistochemical evaluation and western blot analysis of brain and cerebellum tissues, our data have clearly shown that administration of bioactive TBK-SE is able to restore alterations of tight junction components (claudin-5 immunolocalization). Also, bioactive TBK-SE reduces some inflammatory key-markers (p-selectin, GFAP, Iba-1, ERK1/2 and TNF- α), as well as the triggering of neuronal apoptotic death pathway (data about Bax/Bcl-2 balance, p53 and cleaved-caspase 3) and the generation of radicalic species by oxidative stress (results focused on iNOS, nitrotyrosine and Nrf2). Taken together, the results showed that bioactive TBK-SE exerts pharmacological properties in protecting BBB integrity through a mechanism of action that involves a modulation of inflammatory and oxidative pathway as well into control of neuronal death.

12.1 Cerebral ischemic stroke

Cerebral ischemic stroke regards for approximately 80% of all strokes (Feigin et al., 2003) and often it results from the occlusion of a cerebral artery caused by a thrombus or embolus that leads to an immediate loss of the normal intake of oxygen and glucose to cerebral tissues (Go et al., 2014). Ready initiation of reperfusion is the most effective treatment for reducing infarct area and behavioral deficits caused by ischemia. Paradoxically, however, blood flow restoration is causative of additional injury during the cascade of events that characterize and identify the so-called cerebral ischemia/reperfusion (CIR) injury (Dong et al., 2013). It has been widely demonstrated that excitotoxicity, ionic imbalance, adhesion molecules upregulation, reactive oxygen and nitrogen species (ROS/RNS) formation, inflammation and apoptosis are the main mechanisms involved in CIR (Doyle et al., 2008; Ritz et al., 2008). It is well known also that all these events contribute to blood–brain barrier (BBB) breakdown, considered as a critical step in cerebral ischemia pathogenesis (Sandoval and Witt, 2008). BBB integrity and maintenance of homeostasis in central nervous system (CNS) are critically dependent of tight junctions (TJs) between cerebrovascular endothelial cells. Any abnormality in the structure or function of TJs can lead to BBB dysfunction that consequently may contribute to the development of neurological damage (Sandoval and Witt, 2008). Several experimental data showed that oxidative stress may affect TJ components of BBB through the activation of several pathways (Lochhead et al., 2010). In fact, during CIR, production of ROS is dramatically increased and involves endogenous antioxidant systems leading to oxidative stress and ultimately contributing to neuronal cell death (Sugawara and Chan, 2003). For this reason, antioxidants have been the focus of studies for developing neuroprotective drugs to be used in cerebral ischemia treatment. To date there is no clinically effective therapy for stroke management except tissue-plasminogen activator (t-PA) (Alavijeh et al., 2005). The purpose of our study was to investigate whether a freeze-dried Tuscan black kale sprouts extract containing about 15% of GRA and other minor GLs and bioactivated with MYR (bioactive TBK-SE) has neuroprotective effects in a chronic experimental model of CIR. Also, we investigated the possible neuroprotective role of bioactive TBK-SE, as a novel important field of action potentially applicable in BBB dysfunctions through a repair mechanism at the level of TJs proteins and thus, the progression of neurological injury. Finally, other important aim of this study was to suggest this natural extract as a promising source of alternative

medicine for the prevention and/or treatment of cerebral ischemia. In addition, as being a natural phytochemical, we believe that bioactive TBK-SE could be introduced as an herbal medicine without adverse effects, at least in association with current conventional therapies.

12.2 Materials and Methods

12.2.1 Animals

Male Sprague–Dawley rats (about 9 weeks old) (Harlan, Italy) 200–250 g weight were used. Rats were housed in a controlled environment and provided with standard rodent chow and water. Animal care was in compliance with Italian regulations on protection of animals used for experimental and other scientific purposes (D.M. 116/92) as well as with the EEC regulations (O.J. of E.C.L 358/1 12/18/1986).

12.2.2 Induction of CIR

After anesthesia induced with an anesthetic cocktail composed of tiletamine plus xylazine (1 mL Kg⁻¹ i.p.), CIR was induced in rats according to Awooda et al. (2013). In brief, in the supine position, a midline ventral incision was made in the neck of each animal; the left carotid artery was exposed, separated from the vagus nerve and occluded for 1 h by clamping with small vascular clips and by inducing hypotension to generate a cerebral ischemia animal model. A phase of reperfusion of blood flow of the duration of seven days was followed. Blood pressure was continuously monitored through a blood pressure recorder (Ugo Basile, Varese, Italy), a noninvasive method that allows to check on a display the systolic and diastolic blood pressure of rat during the surgical procedures by the application of a tail cuff. This allowed to ascertain the reduction of blood flow following carotid artery occlusion and the increasing after blood flow restoration. In specific, before the start surgical procedures, it was recorded a baseline blood pressure value of about 108 ± 5 mmHg in rats and a blood pressure value of about 49 ± 5 mmHg immediately after the clamping, indicating that cerebral ischemia was successful induced. Following removal of vascular clip, blood pressure returned to the value of about 108 ± 5 mmHg. In addition, during the observation period of seven days, we have recorded

eyelid edema associated to hemorrhagic lachrymation in animal subjected to CIR, further indicating that there had been alteration in cerebral blood flow circulation.

12.2.3 Myrosinase bioactivation of TBK-SE

TBK-SE was prepared as described at Chapter eight (see section 8.7). TBK-SE was dissolved in PBS solution pH 7.2 (17 mg mL⁻¹, containing 2.6 mg GRA) and hydrolyzed by the action of MYR (20 µl; 32 U mL⁻¹) for 15 min at 37 °C, right before animal treatment. The resulting solution was labeled as bioactive TBK-SE and used for animal treatment in this study. MYR treatment transformed quantitatively aliphatic GLs into ITCs, *R*-sulforaphane being the major one as described at Chapter eight (see section 8.8).

12.3.4 Experimental design

Rats were randomly allocated into the following groups (N=20 total animals):

- Untreated CIR group: rats were subjected to 1 h of carotid artery occlusion followed by 7 days of reperfusion (N=10);
- Bioactive TBK-SE-treated CIR group: rats were subjected to surgical procedures described as above and bioactive TBK-SE (17 mg TBK-SE/rat plus 20 µl MYR) was administered 15 min after ischemia and daily for seven days (N=10).

At the end of the experiment, blood was collected by cardiac puncture and animals were euthanized. Brain and cerebellum tissues were sampled and processed to perform morphological evaluation and molecular biology analysis.

12.3.5 Immunohistochemical evaluation

At 7 days following CIR-induction, brains were sampled and fixed in 10 % (w/v) PBS-buffered formaldehyde and 7 µm sections were prepared from paraffin-embedded tissues. After deparaffinization with xylene, sections of brain samples were hydrated in graded ethanol. Detection of claudin-5, p-selectin, GFAP and iNOS, Nitrotyrosine, Nrf2 and Bax was carried out after boiling in citrate buffer 0.01 M pH 6 for 4 min. Endogenous peroxidase was quenched with 0.3% (v/v) hydrogen peroxide in 60% (v/v) methanol for 30 min. Nonspecific adsorption

was minimized by incubating the section in 2% (v/v) normal goat serum in PBS for 20 min.

Sections were incubated overnight with:

- anti-Claudin-5 monoclonal antibody (1:100 in PBS v/v; Novus Biologicals);
- anti-p-selectin polyclonal antibody (1:100 in PBS v/v; Santa Cruz Biotechnology, Inc.);
- anti-GFAP monoclonal antibody (1:50 in PBS v/v; Cell Signaling Technology);
- anti-iNOS polyclonal antibody (1:100 in PBS v/v; Santa Cruz Biotechnology, Inc.);
- anti-Nitrotyrosine polyclonal antibody (1:1000 in PBS v/v; Millipore);
- anti-Nrf2 polyclonal antibody (1:100 in PBS v/v; Santa Cruz Biotechnology, Inc.);
- anti-Bax polyclonal antibody (1:100 in PBS v/v; Santa Cruz Biotechnology, Inc.).

Endogenous biotin or avidin binding sites were blocked by sequential incubation for 15 min with biotin and avidin (DBA, Milan, Italy), respectively. Sections were washed with PBS and incubated with secondary antibody. Specific labelling was detected with a biotin-conjugated goat anti-rabbit IgG and avidin–biotin peroxidase complex (Vectastain ABC kit, VECTOR). The counterstain was developed with peroxidase substrate kit DAB (brown colour) or DAB nickel solution adducted (black colour) (Vector Laboratories, Inc.) and Hematoxylin (blue background) or nuclear fast red (Vector Laboratories, Inc.). To verify the binding specificity, some sections were also incubated with only the primary antibody (no secondary) or with only the secondary antibody (no primary). In these cases, no positive staining was found in the sections, indicating that the immunoreaction was positive in all the experiments carried out. All sections were obtained using light microscopy (LEICA DM 2000 combined with LEICA ICC50 HD camera). To perform densitometric analysis, quantitative data were carried out using Leica Application Suite V4.2.0 software.

12.3.6 Western blot analysis

All the extraction procedures were performed on ice using ice-cold reagents. In brief, cerebellum tissues were suspended in extraction buffer containing 0.32 M sucrose, 10 mM Tris–HCl, pH 7.4, 1 mM EGTA, 2 mM EDTA, 5 mM NaN₃, 10 mM 2-mercaptoethanol, 50 mM NaF, protease inhibitor tablets (Roche Applied Science, Monza, Italy), and they were homogenized at the highest setting for 2 min. The homogenates were chilled on ice for 15 min and then centrifuged at 1000 g for 10 min at 4°C, and the supernatant (cytosol + membrane extract from brain tissue) was collected to evaluate content of cytoplasmatic

proteins. The pellets were suspended in the supplied complete lysis buffer containing 1 % Triton X-100, 150 mM NaCl, 10 mM Tris-HCl, pH 7.4, 1 mM EGTA, 1 mM EDTA protease inhibitors (Roche), and then were centrifuged for 30 min at 15.000 g at 4 °C. Then, supernatant containing nuclear extract was collected to evaluate the content of nuclear proteins. Supernatants were stored at -80°C until use. Protein concentration in homogenate was estimated by Bio-Rad Protein Assay (Bio-Rad, Segrate, Italy) using BSA as standard, and 20 µg of cytosol and nuclear extract from each sample were analyzed. Proteins were separated on sodium dodecyl sulfate polyacrylamide minigels and transferred onto PVDF membranes (Immobilon-P Transfer membrane, Millipore), blocked with PBS containing 5 % nonfat dried milk (PM) for 45 min at room temperature, and subsequently probed at 4 °C overnight with specific antibodies for Phospho-p44/42 MAPK (ERK1/2) (1:2000; Cell Signaling Technology), Bcl-2 (1:500; Cell Signaling Technology), Bax (1:500; Cell Signaling Technology), Nrf2 (1:100; Cell Signaling Technology), Nitrotyrosine (1:2000; Millipore), Iba-1 (1:1000; Abcam), p53 (Abcam 1:2000;) and cleaved caspase 3 (1:500; Cell Signaling Technology), in 1x PBS, 5% (w/v) nonfat dried milk, 0.1 % Tween-20 (PMT). HRP-conjugated goat anti-rabbit IgG or goat anti-mouse IgG were incubated as secondary antibodies (1:2000; Santa Cruz Biotechnology, Inc.) for 1 h at room temperature. To ascertain that blots were loaded with equal amounts of protein lysates, they were also incubated with antibody for GAPDH HRP Conjugated (1:1000; Cell Signaling Technology), p42 MAP Kinase (Erk 2) (1:1000; Cell Signaling Technology) and beta-actin (1:1000; Santa Cruz Biotechnology, Inc). The relative expression of protein bands was visualized using an enhanced chemiluminescence system (Luminata Western HRP Substrates, Millipore) and proteic bands were acquired and quantified with ChemiDoc™ MP System (Bio-Rad) and a computer program (ImageJ software) respectively. Blots are representative of three separate and reproducible experiments. The statistical analysis was carried out on three repeated blots performed on separate experiments.

12.3.7 Blood sampling

At the sacrifice, blood samples were collected via cardiac puncture in Serum Separator Tubes (Vacutainer® SSTTMII Advance, BD Diagnostic, Milan, Italy) and centrifuged following at least 30 min from the collection at 2000 g speed for 10 min. The achieved serum was collected, aliquoted and stored at -80 °C to be used in next investigations.

12.3.8 TNF- α assay

ELISA kit for TNF- α parameter assay (R&D system Europe, Ltd, Abingdon, UK) was purchased to detect TNF- α levels in serum samples. The kit was used according to the manufacturer's instruction and achieved O.D. were tabulated and analyzed using a software of elaboration data.

12.3.9 Statistical evaluation

Data were analyzed in GraphPad Prism version 6.0 (GraphPad Software, La Jolla, CA). The results were analyzed by unpaired Student's t-test. A p value of <0.05 was considered to be statistically significant. Results are expressed as the mean \pm S.E.M. of n experiments.

12.3 Results

12.3.1 Bioactive TBK-SE restores BBB vascular endothelium after CIR induction

To evaluate whether BBB breakdown is accompanied by the loss or alterations of TJ-associated molecules from the BBB TJs following CIR induction, we investigated the claudin-5 expression by immunohistochemical evaluation. Sections obtained from CIR rats did not show positive staining for claudin-5 in temporal lobe of brain tissue (Figure 12.1a) as well as at the level of vascular endothelium of BBB in temporal lobe area of the brain (Figure 12.1b). In contrast, bioactive TBK-SE treatment normalized the positive staining for claudin-5 in different districts, as shown by immunohistochemical localization in brain section and in BBB vascular endothelium of CIR rats (Figure 12.1c and d, see densitometric analysis Figure 12.2). Also, immunohistochemical localization of p-selectin showed an increased expression of adhesion molecules following CIR in the vascular endothelium (Figure 12.1e), while treatment with bioactive TBK-SE clearly reduced the degree of positive staining for p-selectin in brain tissues (Figure 12.1f, see densitometric analysis Figure 12.2).

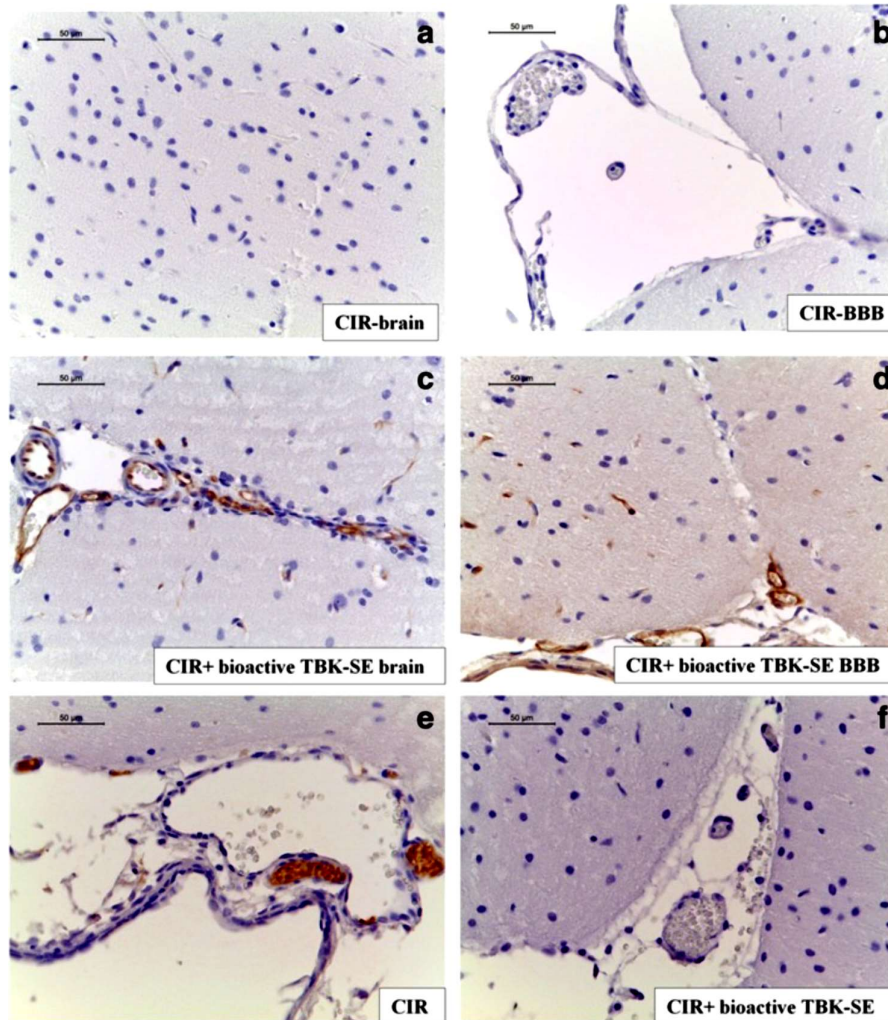


Figure 12.1 Bioactive TBK-SE restores BBB vascular endothelium. Sections from CIR rats did not show positive staining for claudin-5 in temporal lobe of brain tissue (a) as well as at the level of vascular endothelium of BBB in temporal lobe area of the brain (b). In contrast, in both two sections obtained from bioactive TBK-SE-treated rats it was observed a normal distribution of claudin-5 (c and d). Also, immunohistochemical localization of p-selectin displayed an increased expression of adhesion molecules following CIR in the vascular endothelium (e), while treatment with bioactive TBK-SE clearly reduced the degree of positive staining for p-selectin in brain tissues (f).

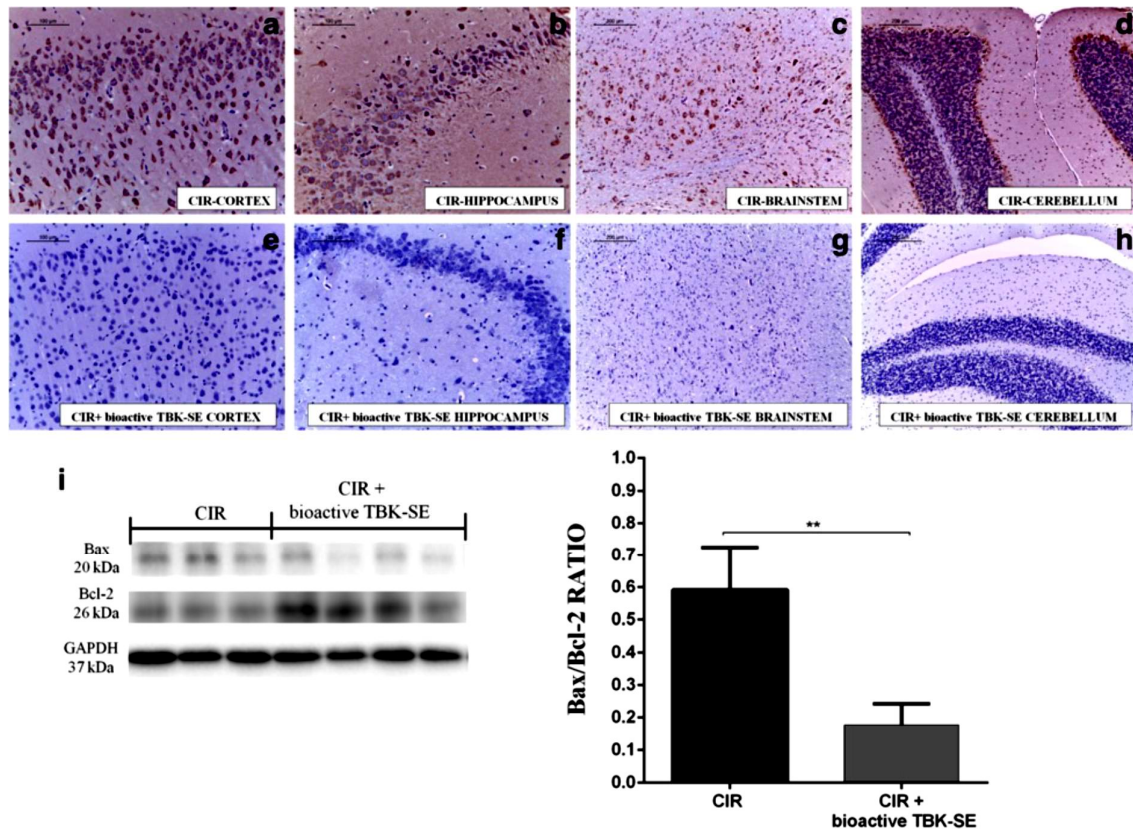


Figure 12.2 Bioactive TBK-SE treatment modulates unbalance between Bax and Bcl-2. Bax was evaluated by immunohistochemical evaluation in brain sections after CIR induction. Brain sections obtained from CIR untreated rats exhibited positive staining for Bax in cortex (a), hippocampus (b), brainstem (c) and cerebellum (d) of CIR rats, while rats treated with bioactive TBK-SE showed negative staining for Bax in cortex (e), hippocampus (f), brainstem (g) and cerebellum (h). Panel I shows ratio between Bax and Bcl-2 in cerebellum tissues, showing an higher expression of Bax/Bcl-2 in CIR untreated rats, attenuated by administration of bioactive TBK-SE (i). GAPDH was used as internal control. **p < 0.05 vs CIR.

12.3.2 Bioactive TBK-SE modulates GFAP and Iba-1 expression after CIR

Moreover, with the purpose to investigate the cellular mechanisms by which the treatment with bioactive TBKSE may modulate the astrocyte activation during CIR, we evaluated the GFAP expression by immunohistochemical analysis. GFAP is considered a marker protein for astrogliosis. It was observed a marked positive staining for GFAP in the sections from CIR rats, both in brain (Figure 12.3a) and cerebellum sections (Figure 12.3b). In contrast, a reduction of GFAP positive staining was evident in pharmacologically treated group (Figure 12.3c and d,

see densitometric analysis Figure 12.4). Also, western blot analysis showed that Iba-1 levels are substantially increased in cerebellum samples collected from CIR rats seven days after CIR induction, whereas Iba-1 levels were attenuated by approximately 50% with bioactive TBK-SE administration (Figure 12.3e).

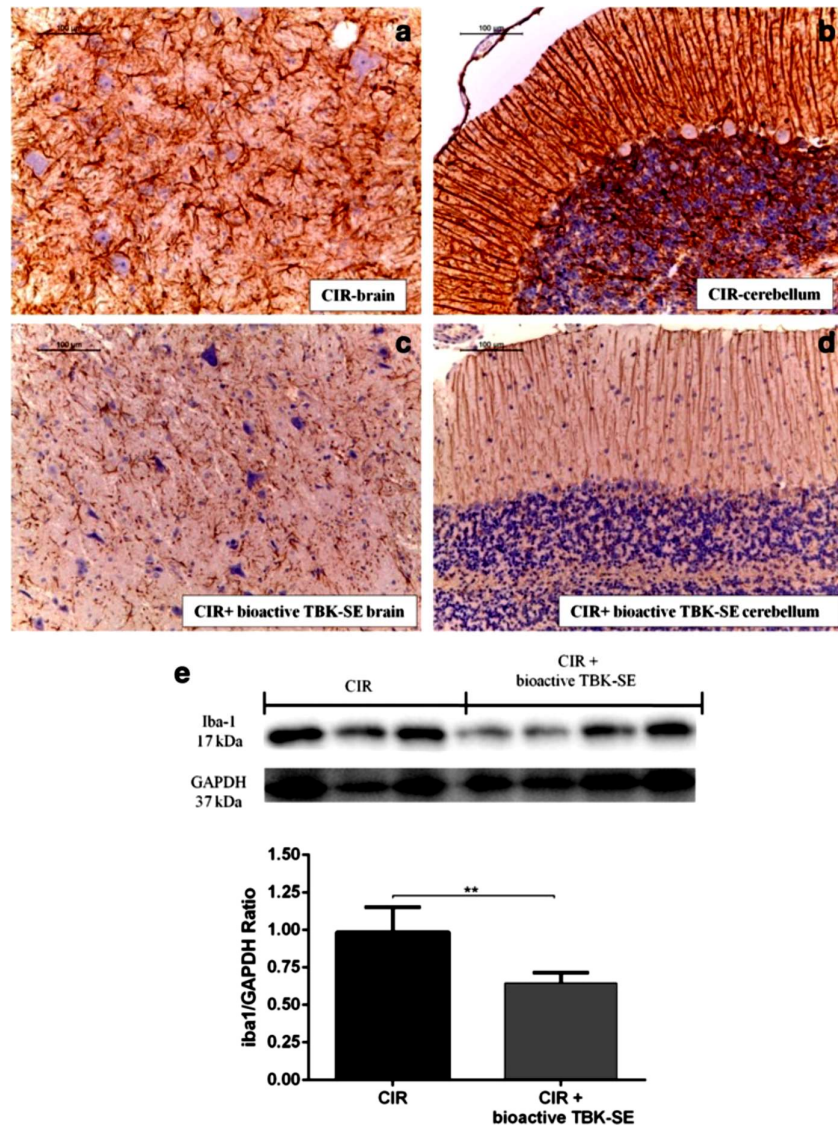


Figure 12.3 Effects of Bioactive TBK-SE on GFAP and Iba-1 expression. The immunohistochemical analysis for GFAP showed that positive staining for GFAP was observed in the tissues obtained from CIR rats both in brain (a) as well as in cerebellum sections (b). In contrast, a reduction of GFAP positive staining was evident in bioactive TBK-SE-treated group in both two different areas (c and d). By western blot analysis it has been shown a significant increase Iba-1 expression in cerebellum samples collected from CIR rats seven days after CIR induction. Conversely, levels of Iba-1 were attenuated by administration with bioactive TBK-SE attenuated Iba-1 levels by approximately 50 % (e). GAPDH was used as internal control. **p < 0.05 vs CIR

12.3.3 Bioactive TBK-SE regulates iNOS, nitrotyrosine and Nrf2 expression

To determine the role of nitric oxide (NO) produced during CIR and to verify whether treatment with bioactive TBK-SE is able to counteract oxidative and nitrosative stress resulting from ischemic damage, we evaluated iNOS and nitrotyrosine expression by immunohistochemical and western blot analysis, after seven days of reperfusion. Immunohistochemical localization of iNOS in temporal lobe area of brain tissues of untreated-CIR rats (Figure 5a) sampled showed an increased expression of this marker following CIR, while treatment with bioactive TBK-SE significantly reduces the degree of positive staining for iNOS (Figure 5b, see densitometric analysis Figure 4). Brain sections obtained from CIR untreated rats exhibited positive staining for nitrotyrosine in cortex (Figure 6a), hippocampus (Figure 6b), brainstem (Figure 6c) and cerebellum (Figure 6d) of CIR rats, while rats treated with bioactive TBK-SE showed negative staining for nitrotyrosine (Figure 6e, f, g, h, see densitometric analysis Figure 4). In addition, we analyzed cerebellum expression levels of nitrotyrosine by western blot analysis. This displayed a significant increase in nitrotyrosine expression in cerebellum samples collected 7 days after CIR-induction from untreated rats. Conversely, cerebellum levels of nitrotyrosine were reduced by administration of bioactive TBK-SE (Figure 6i). Moreover, it is known that GLs may exert their cytoprotective effects by the ability to induce expression of several enzymes via the Keap1/Nrf2/ARE pathway. Western blot analysis showed a basal level of Nrf2 expression in samples obtained from CIR rats. Treatment of rats with bioactive TBK-SE significantly increased Nrf2 expression (Figure 7i). The same result was obtained from immunohistochemical evaluation for Nrf2, showing a positive staining in cortex (Figure 7a), hippocampus (Figure 7b), brainstem (Figure 7c) and cerebellum (Figure 7d) of CIR rats treated with bioactive TBK-SE, and a negative staining in brain of CIR rats (Figure 7e, f, g, h, see densitometric analysis Figure 4).

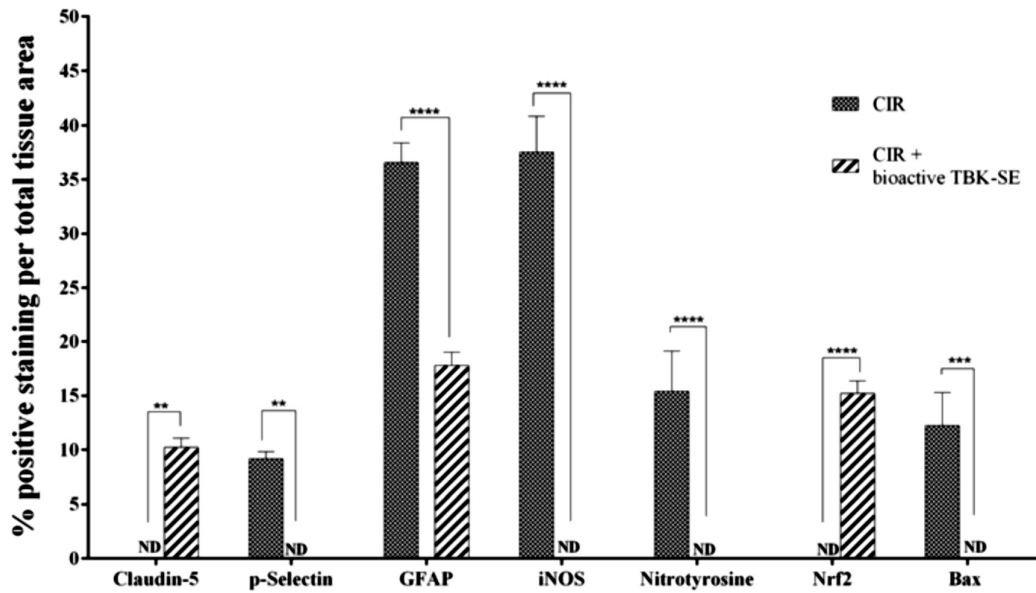


Figure 12.4 Densitometric analysis for claudin-5, p-selectin, GFAP and i-NOS, nitrotyrosine, Nrf2 and Bax. For immunohistochemical images, densitometric analysis was carried out to quantify and highlight significant differences among experimental groups. p value <0.05 was considered significant.

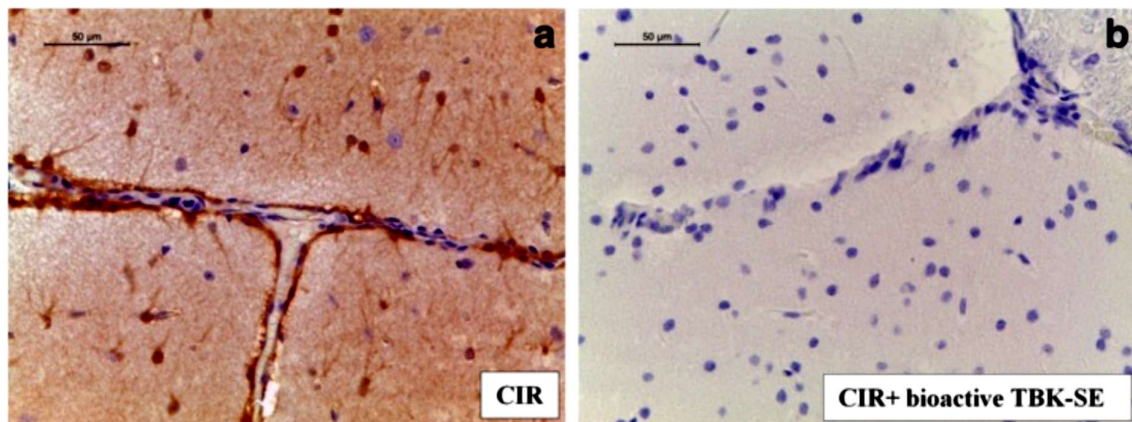


Figure 12.5 Bioactive TBK-SE modulates production of i-NOS. iNOS was evaluated by immunohistochemical analysis in brain sections 7 days after CIR. Brain sections obtained from CIR rats exhibited positive staining for iNOS (a). Bioactive TBK-SE treatment reduced the degree of positive staining for iNOS in lobe temporal area of brain (b).

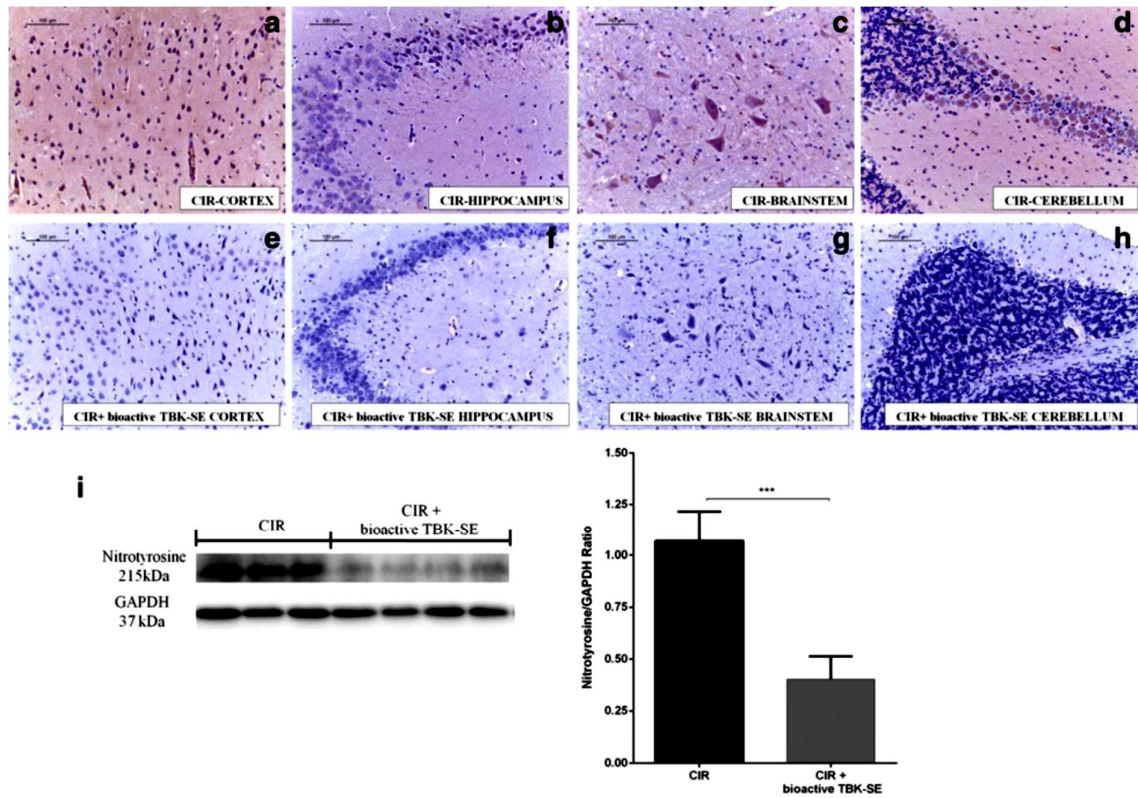


Figure 12.6 Bioactive TBK-SE modulates nitrotyrosine expression. Nitrotyrosine was evaluated by immunohistochemical evaluation in brain sections after CIR induction. Brain sections obtained from CIR untreated rats exhibited positive staining for nitrotyrosine in cortex (a), hippocampus (b), brainstem (c) and cerebellum (d) of CIR rats, while rats treated with bioactive TBK-SE showed negative staining for nitrotyrosine in cortex (e), hippocampus (f), brainstem (g) and cerebellum (h). By western blot analysis nitrotyrosine expression was evaluated. It was found a significant increase in nitrotyrosine expression in cerebellum samples collected 7 days after CIR-induction from untreated rats. Conversely, cerebellum levels of nitrotyrosine were reduced by administration of bioactive TBK-SE (i). GAPDH was used as internal control. *** $p < 0.05$ vs CIR

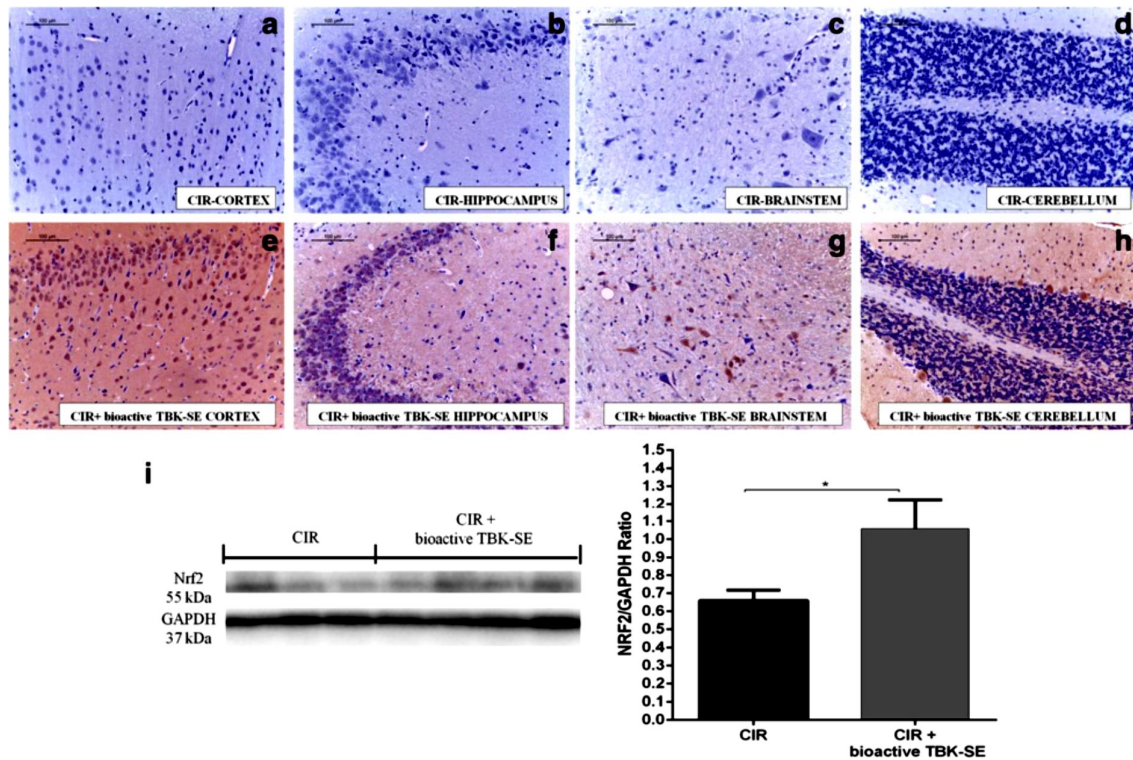


Figure 12.7 Effects of Bioactive TBK-SE on Nrf2 expression. Negative staining for Nrf2 was observed in cortex (a), hippocampus (b), brainstem (c) and cerebellum (d) of CIR rats. On the contrary, positive staining for Nrf2 was observed in cortex (e), hippocampus (f), brainstem (g) and cerebellum (h) from rats treated with bioactive TBK-SE. Also, western blot analysis showed a basal level of Nrf2 expression in cerebellum samples obtained from CIR rats. Bioactive TBK-SE treatment significantly increased Nrf2 expression (i). GAPDH was used as internal control. * $p < 0.05$ vs CIR

12.3.4 Effect of bioactive TBK-SE on Phospho-p44/42 MAPK (ERK1/2) expression and TNF- α following CIR

To investigate the cellular mechanisms whereby treatment with bioactive TBK-SE attenuates the development of CIR, we also evaluated the level of ERK1/2 which results in expression of pro-inflammatory genes mediating the inflammatory characteristic of CIR. The activation of MAPK pathways in particular the phosphorylation of ERK1/2 expression was investigated by western blot analysis in cerebellum tissue. ERK1/2 levels were appreciably increased in cerebellum samples taken from rats subjected to CIR, while the treatment of rats with bioactive TBK-SE reduced levels of ERK1/2 (Figure 12.8a). Also, in order to investigate whether treatment with bioactive TBK-SE can modulate the inflammatory processes triggered by CIR

induction through regulating secretion of pro-inflammatory cytokines, the expression levels of TNF- α , serum samples was quantified by ELISA assay. Our results showed that serum levels are significantly higher in untreated CIR rats when compared with serum levels of animals treated with bioactive TBK-SE (Figure 12.8b).

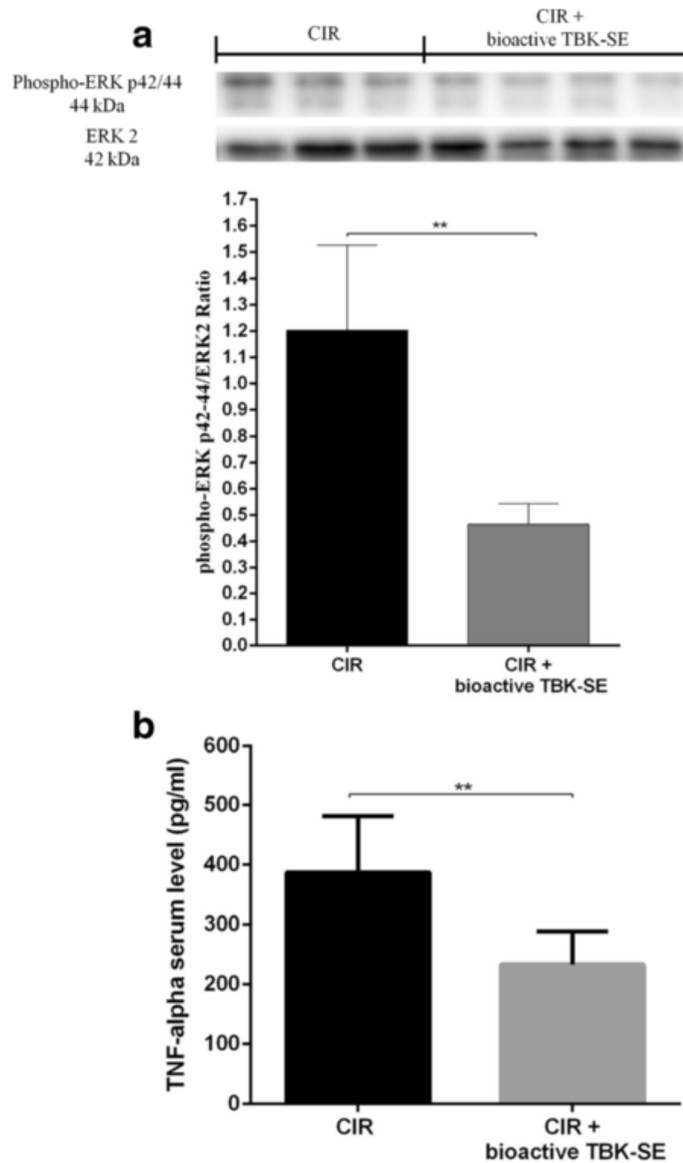


Figure 12.8 Western blot analysis of ERK1/2 expression and ELISA assay for TNF- α . ERK1/2 expression levels normalized on ERK2 display an increase in rats subjected to CIR, while administration of bioactive TBK-SE reduces levels of ERK1/2 (a). ERK2 was used as internal control. ** $p < 0.05$ vs CIR. ELISA assay showed that serum levels of TNF- α are significantly higher in untreated CIR rats when compared with TNF- α serum levels of animals treated with bioactive TBK-SE (b). ** $p < 0.05$ vs CIR.

12.3.5 Bioactive TBK-SE treatment inhibits CIR induced apoptosis

At seven days after CIR, the appearance of proteic effectors of mitochondrial apoptosis, such as pro-apoptotic Bax proteins, was evaluated by immunohistochemical evaluation and western blot. Immunohistochemical evaluation for Bax was performed in different areas of brain tissues. Specifically, a positive staining was found in cortex (Figure 12.2a), hippocampus (Figure 12.2b), brainstem (Figure 12.2c) and cerebellum (Figure 12.2d) of CIR rats. On the contrary, treatment with bioactive TBK-SE significantly reduces the degree of positive staining for Bax in all the same regions of the brain (Figure 12.2e, f, g, h, see densitometric analysis Figure 12.4). Also, by western blot was found that Bax levels were increased substantially in cerebellum tissues from CIR rats. On the contrary, bioactive TBK-SE treatment prevented the CIR-induced Bax expression (Figure 12.2i). Likewise, to detect Bcl-2 expression, extracts from cerebellum tissues of rats were also analyzed by Western blot analysis. A basal level of Bcl-2 expression was detected in samples from CIR rats. Treatment of rats with bioactive TBK-SE significantly attenuated CIR-induced inhibition of Bcl-2 expression (Figure 12.2i). In addition, proteins in the mitochondrial p53 pathway were detected by western blot analysis in cerebellum samples. Our data showed a significant expression of p53 in samples collected seven days after CIR-induction. Conversely, levels of p53 were clearly reduced by administration of bioactive TBK-SE (Figure 12.9a). Finally, sequential activation of caspases plays a central role in the execution-phase of cell apoptosis, leading to programmed cell death by cleavage of cellular substrates. By western blot analysis, we have evaluated the activation of cleaved-caspase 3. Cleaved-caspase 3 levels were appreciably increased in the cerebellum from rats subjected to CIR. On the contrary, treatment with bioactive TBK-SE prevented CIR-induced cleaved-caspase 3 expression (Figure 12.9b).

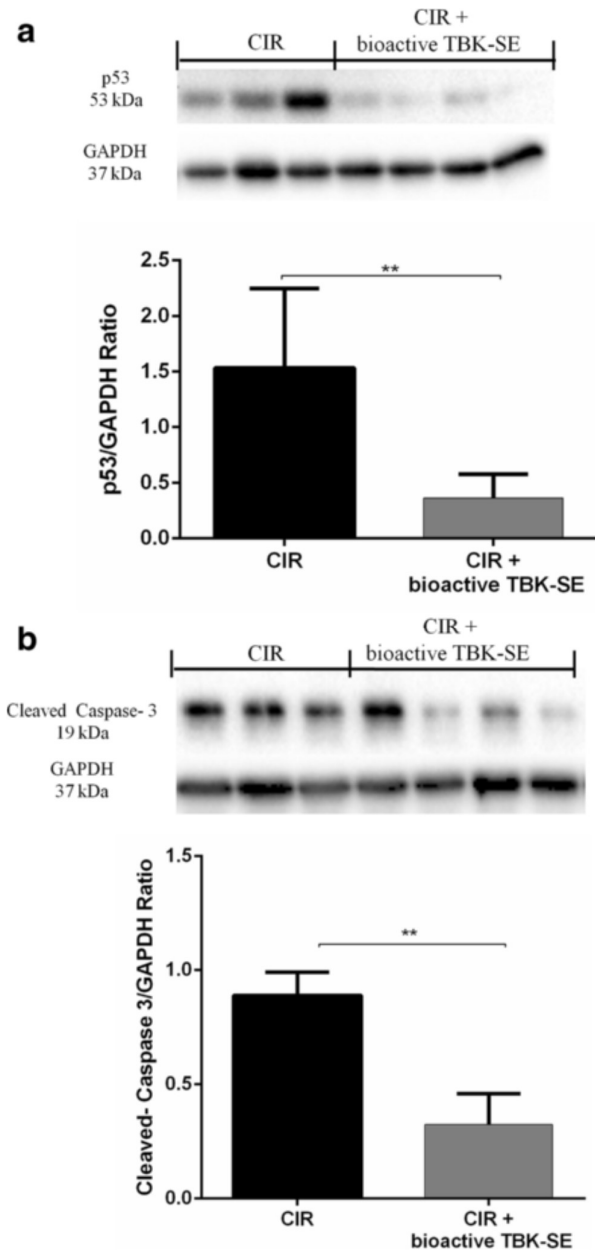


Figure 12.9 Western blot analysis for p53 and Cleaved-caspase3 expression. p53 expression was detected by western blot analysis. Our data showed a significant expression of p53 in samples collected seven days after CIR-induction. Conversely, levels of p53 were clearly reduced by administration of bioactive TBK-SE (a). GAPDH was used as internal control. **p < 0.05 vs CIR. By western blot analysis the activation of cleaved-caspase 3 was evaluated. CIR caused a significant increase in cleaved-caspase 3 expression. On the contrary, treatment with bioactive TBK-SE prevented the CIR-induced caspase 3 expression (b). GAPDH was used as internal control. **p < 0.05 vs CIR.

12.4 Discussion

Ischemic stroke is the result of a transient or permanent reduction in cerebral blood flow caused by occlusion of a cerebral artery via an embolus or local thrombosis (Pignataro et al., 2007). After the primary neuronal cell injury, secondary neuronal damage, known as reperfusion injury occurs

and exacerbates initial damage (Dong et al., 2013; Manley et al., 2000). It is well known that cerebral ischemia rapidly raises inflammatory responses in brain, by activating different resident cell populations such as endothelial cells, microglia and astrocytes, as well as inflammatory cytokines release, thereby contributing to BBB breakdown (Yilmaz and Granger, 2010; Skaper et al., 2012). In fact, BBB disruption is considered as a critical event in the pathogenesis of cerebral stroke. However, the molecular mechanisms involved are not completely understood (Sandoval and Witt, 2008). Among various components of the BBB, the tight junction (TJs) protein claudins are the most widely studied, which are critical for maintaining the BBB structural integrity and permeability. The disruption of the cerebrovascular claudin-5 has been strongly correlated with the dynamic event of BBB breakdown after cerebral ischemia (McColl et al., 2008; Nitta et al., 2003). Immunohistochemical evaluation was performed to demonstrate that CIR induced changes in claudin-5 expression and as well as bioactive TBK-SE can control TJs permeability, modulating claudin-5 expression. Following an impairment of BBB, peripheral leukocytes infiltrate into the brain and the normally immune privileged cerebral environment is exposed to systemic responses that further aggravate inflammation and brain injury (Patel et al., 2013). According to Jin et al. (2011), our data have revealed an increased expression of p-selectin, an adhesion molecule that stimulates rolling of leukocytes and other inflammatory cell infiltration following induced damage, demonstrating that it was modulated by bioactive TBK-SE administration. About the untreated rats the up-regulation of p-selectin seems to reflect both increased expression of the endothelial cells and the binding of p-selectin positive platelets to the vessel wall, leading in turn an exacerbation of the neuroinflammation status (Ishikawa et al., 2003). In addition, we evaluated expression of Iba-1, a novel calcium-binding protein that plays an important role in regulation of microglia function, in which it is

specifically expressed (Ito et al., 2001). Also, it was found that Iba-1 expression is up-regulated in microglia following cerebral ischemia (Ito et al., 2001).

Indeed, according to Ohsawa et al. (2000), seems that Iba-1 is involved in the Rho family of small GTPase, Rac, and calcium signaling pathways and may be required for cell mobility and phagocytosis of microglia/macrophages. Once activated, microglia develops macrophage-like capabilities including cytokine production, antigen presentation and the release of matrix metalloproteinases that weaken the BBB (Iadecola and Anrather, 2011). Our data confirmed an up-regulation of Iba-1 in CIR rats compared with pharmacologically treated ones. Moreover, looking at proinflammatory cytokine profile classically activated by microglia during CIR, levels of TNF- α result significantly decreased following bioactive TBK-SE treatment. It was consistently demonstrated that astrocytes the most abundant population of glial cells, are essential for brain homeostasis and maintenance and maturation of the BBB (Abbott et al., 2006; Liu et al., 2012; Barreto et al., 2011). While astrocytes show a good capability repairing in many CNS processes, they are also capable of secreting inflammatory factors such as cytokines and chemokines, which aggravate brain damage (Sun et al., 2009). In fact, astrocytes were found to play an important role also in CIR injury (Burnstock, 2008). Moreover, the induction of Nrf2-mediated transcription, particularly in astrocytes, has been shown to protect against neurotoxicity from a variety of injuries, such as cerebral ischemia (Narayanan et al., 2015; Jing et al., 2013). According to other studies reported in literature, Nrf2 could play a protective action in astrocytes, decreasing GFAP expression probably through the mechanism related to the glutathione activity (Calkins et al., 2010; Vargas and Johnson, 2009). Our results confirmed that treatment with bioactive TBK-SE in CIR rats leads to an upregulation of Nrf2 expression, while GFAP expression was significantly inhibited. This balance prevents that GFAP expressing astrocytes may regulate the integrity of BBB, damaging TJ components and interfering with the normal astrocyte interactions (LaPash Daniels et al., 2012; Mignot et al., 2004; Willis, 2012). Probably, astrocyte specific Nrf2-mediated protection due to treatment with bioactive TBK-SE could have beneficial effects in counteracting the damage after CIR and this could be associated with the production of several growth factors that may protect neurons from damage. The local accumulation of NO is also involved in the inflammatory cascade after cerebral ischemia (Mitrasinovic et al., 2005; Awooda et al., 2015). This mediator enhances cell adhesion molecules expression on endothelial cells and promotes adhesion and transendothelial migration of immune cells

(Kubes et al., 1991). The role of iNOS in ischemia is yet controversial, it was demonstrated that has a beneficial role as modulator or messenger but during oxidative stress condition it is potentially toxic (Sekhon et al., 2003). In fact, over-production of NO through iNOS causes accentuated lipid peroxidation, protein and DNA modifications that result in cellular damage (Montalto et al., 2003). Our study demonstrates that bioactive TBK-SE reduces the expression of iNOS in tissues from CIR treated rats. Likewise, our results demonstrated that bioactive TBK-SE reduced the generation of reactive species through the evaluation of nitrotyrosine expression, chosen as an indirect marker of peroxynitrite activity. MAP kinase (MAPKs) pathway, investigated through detection of ERK1/2 expression, resulted upregulated in CIR related mechanisms of pathology but attenuated by bioactive TBK-SE administration. Although it has been demonstrated that ERK1/2 is a pro-survival factor in the MAP kinase family and contributes to the regulation of cell proliferation and differentiation, under some circumstances, it can function in a pro-apoptotic manner in the neuronal system (Cheung and Slack, 2004; Lu and Xu, 2006). Protective effects of bioactive TBK-SE in counteracting apoptosis are evaluable looking to the main apoptosis regulatory genes, such Bax and Bcl-2. The changes in the Bax to Bcl-2 ratio have also been studied in several experimental ischemic models proving that excess of Bcl-2 promotes cell survival, while Bax excess induces cell death. Our data showed an upregulation of Bcl-2 and a downregulation of Bax in pharmacologically treated rats. The transcription factor and mediator of apoptosis p53 was also found to be upregulated following stroke (Leker et al., 2004). p53 is able to induce apoptosis both by controlling translation of pro-apoptotic p53-checked mediators and by non-transcriptional mechanisms (Sheikh and Fornace, 2000), including upregulation of pro-apoptotic Bax and downregulation of Bcl-2 (Cregan et al., 1999; Xiang et al., 1998). In specific, according to Leker et al. (2004), translocation of resident p53 into the nucleus is an early event in p53-induced apoptosis in ischemic brain cells and that the prevention of this early translocation could reduce brain damage. Our data showed an increased nuclear expression in brain ischemic tissues, on the contrary attenuated by treatment with bioactive TBK-SE. Also, supporting above cited results and adding further evidences about effects of bioactive TBK-SE, we found a modulated cleaved-caspase 3 activity in CIR pharmacologically treated rats. A protective effect of bioactive TBK-SE suggests that this treatment could interfere with the CIR-induced neuronal death, preserving cells by the injury.

12.5 Conclusion

Alternative medicine is an interesting research field in to discovering potential active substances found in nature for a wide range of applications. Here, results showed that bioactive TBK-SE could represent a good and effective approach in the treatment of experimental CIR. This study was designed and performed considering the results reported at Chapter eleven when investigating the neuroprotective effects *R*-SF in an acute experimental model of CIR. *R*-SF proved to be active on central and peripheral nervous system, through mechanisms which involved both the modulation of the inflammatory pathways and the reduction in the activation of cell death by apoptosis. In the present study, TBK-SE exerted pharmacological properties protecting BBB integrity through a mechanism of action that involved a modulation of the inflammatory and oxidative pathway in a chronic experimental model of CIR. Also, TBK-SE could have an action in controlling neuronal death by apoptosis. In summary, the relevance of the present study consists in the possible use of TBK-SE activated with myrosinase, as a novel natural product for the treatment of damage associated with CIR, at least in association with current conventional therapies.

References

- Abbott NJ, Ronnback L, Hansson E (2006) Astrocyte-endothelial interactions at the blood–brain barrier. *Nat Rev Neurosci* 7:41-53.
- Alavijeh MS, Chishty M, Qaiser MZ, Palmer AM (2005) Drug metabolism and pharmacokinetics, the blood–brain barrier, and central nervous system drug discovery. *Neuro Rx* 2:554-71.
- Awooda HA, Lutfi MF, Sharara GGM, Saeed AM (2015) Oxidative/nitrosative stress in rats subjected to focal cerebral ischemia/reperfusion. *Int J Health Sci (Qassim)* 9:17–24.
- Awooda HA, Lutfi MF, Sharara GM, Saeed AM (2013) Role of N-nitro-L-arginine-methylester as anti-oxidant in transient cerebral ischemia and reperfusion in rats. *Exp Transl Stroke Med* 5:1.
- Barreto G, White RE, Ouyang Y, Xu L, Giffard RG (2011) Astrocytes: targets for neuroprotection in stroke. *Cent Nerv Syst Agents Med Chem* 11:164-73.
- Burnstock G (2008) Purinergic signaling and disorders of the central nervous system. *Nat Rev Drug Discov* 7:575-90.
- Calkins MJ, Vargas MR, Johnson DA, Johnson JA (2010) Astrocyte-specific overexpression of Nrf2 protects striatal neurons from mitochondrial complex II inhibition. *Toxicol Sci* 115:557-68.
- Cheung ECC and Slack RS (2004) Emerging role for ERK as a key regulator of neuronal apoptosis. *Sci STKE* 2004:PE45.
- Cregan SP, MacLaurin JG, Craig CG, Robertson GS, Nicholson DW, Park DS et al. (1999) Bax-dependent caspase-3 activation is a key determinant in p53- induced apoptosis in neurons. *J Neurosci* 19:7860-9.

Dong S, Tong X, Li J, Huang C, Hu C, Jiao H, et al. (2013) Total flavonoid of *Litsea coreana* leaf exerts anti-oxidative effects and alleviates focal cerebral ischemia/reperfusion injury. *Neural Regen Res* 8:3193-202.

Doyle KP, Simon RP, Stenzel-Poore MP (2008) Mechanisms of ischemic brain damage. *Neuropharmacology* 55:310-8.

Feigin VL, Lawes CM, Bennett DA, Anderson CS (2003) Stroke epidemiology: a review of population-based studies of incidence, prevalence, and case fatality in the late 20th century. *Lancet Neurol* 2:43-53.

Go AS, Mozaffarian D, Roger VL, Benjamin EJ, Berry JD, Blaha MJ et al. (2014) Heart disease and stroke statistics—2014 update: a report from the American Heart Association. *Circulation* 129:e28-e292.

Iadecola C and Anrather J (2011) The immunology of stroke: from mechanisms to translation. *Nat Med* 17:796-808.

Ishikawa M, Cooper D, Russell J, Salter JW, Zhang JH, Nanda A et al. (2003) Molecular determinants of the prothrombotic and inflammatory phenotype assumed by the post ischemic cerebral microcirculation. *Stroke* 34:1777-82.

Ito D, Tanaka K, Suzuki S, Dembo T, Fukuuchi Y (2001) Enhanced expression of Iba1, ionized calcium-binding adapter molecule 1, after transient focal cerebral ischemia in rat brain. *Stroke* 32:1208-15.

Jin R, Song Z, Yu S, Piazza A, Nanda A, Penninger JM et al. (2011) Phosphatidylinositol-3-kinase gamma plays a central role in blood–brain barrier dysfunction in acute experimental stroke. *Stroke* 42:2033-44.

Jing X, Ren D, Wei X, Shi H, Zhang X, Perez RG et al. (2013) Eriodictyol-7-O-glucoside activates Nrf2 and protects against cerebral ischemic injury. *Toxicol Appl Pharmacol* 273:672-9.

Kubes P, Suzuki M, Granger DN (1991) Nitric oxide: an endogenous modulator of leukocyte adhesion. *Proc Natl Acad Sci USA* 88:4651-5.

LaPash Daniels CM, Austin EV, Rockney DE, Jacka EM, Hagemann TL, Johnson DA et al. (2012) Beneficial effects of Nrf2 overexpression in a mouse model of Alexander disease. *J Neurosci* 32:10507-15.

Leker RR, Aharonowiz M, Greig NH, Ovadia H (2004) The role of p53-induced apoptosis in cerebral ischemia: effects of the p53 inhibitor pifithrin alpha. *Exp Neurol* 187:478-86.

Liu Y, Hu J, Wu J, Zhu C, Hui Y, Han Y et al. (2012) alpha7 nicotinic acetylcholine receptor-mediated neuroprotection against dopaminergic neuron loss in an MPTP mouse model via inhibition of astrocyte activation. *J Neuroinflammation* 9:98.

Lochhead JJ, McCaffrey G, Quigley CE, Finch J, DeMarco KM, Nametz N et al. (2010) Oxidative stress increases blood–brain barrier permeability and induces alterations in occludin during hypoxia-reoxygenation. *J Cereb Blood Flow Metab* 30:1625-36.

Lu Z and Xu S (2006) ERK1/2 MAP kinases in cell survival and apoptosis. *IUBMB Life* 58:621-31.

Manley GT, Fujimura M, Ma T, Noshita N, Filiz F, Bollen AW et al. (2000) Aquaporin-4 deletion in mice reduces brain edema after acute water intoxication and ischemic stroke. *Nat Med* 6:159-63.

McCull BW, Rothwell NJ, Allan SM (2008) Systemic inflammation alters the kinetics of cerebrovascular tight junction disruption after experimental stroke in mice. *J Neurosci* 28:9451-62.

Mignot C, Boespflug-Tanguy O, Gelot A, Dautigny A, Pham-Dinh D, Rodriguez D (2004) Alexander disease: putative mechanisms of an astrocytic encephalopathy. *Cell Mol Life Sci* 61:369-85.

Mitrasinovic OM, Grattan A, Robinson CC, Lapustea NB, Poon C, Ryan H et al. (2005) Microglia overexpressing the macrophage colony-stimulating factor receptor are neuroprotective in a microglial-hippocampal organotypic coculture system. *J Neurosci* 25:4442-51.

Montalto MC, Hart ML, Jordan JE, Wada K, Stahl GL (2003) Role for complement in mediating intestinal nitric oxide synthase-2 and superoxide dismutase expression. *Am J Physiol Gastrointest Liver Physiol* 285:G197-206.

Narayanan SV, Dave KR, Saul I, Perez-Pinzon MA (2015) Resveratrol preconditioning protects against cerebral ischemic injury via nuclear erythroid 2-related factor 2. *Stroke* 46:1626-32.

Nitta T, Hata M, Gotoh S, Seo Y, Sasaki H, Hashimoto N et al. (2003) Size-selective loosening of the blood–brain barrier in claudin-5-deficient mice. *J Cell Biol* 161:653-60.

Ohsawa K, Imai Y, Kanazawa H, Sasaki Y, Kohsaka S (2000) Involvement of Iba1 in membrane ruffling and phagocytosis of macrophages/microglia. *J Cell Sci* 113:3073-84.

Patel AR, Ritzel R, McCullough LD, Liu F (2013) Microglia and ischemic stroke: a double-edged sword. *Int J Physiol Pathophysiol Pharmacol* 5:73-90.

Pignataro G, Studer FE, Wilz A, Simon RP, Boison D (2007) Neuroprotection in ischemic mouse brain induced by stem cell-derived brain implants. *J Cereb Blood Flow Metab* 27:919-27.

Ritz MF, Curin Y, Mendelowitsch A, Andriantsitohaina R (2008) Acute treatment with red wine polyphenols protects from ischemia-induced excitotoxicity, energy failure and oxidative stress in rats. *Brain Res* 1239:226-34.

Sandoval KE and Witt KA (2008) Blood–brain barrier tight junction permeability and ischemic stroke. *Neurobiol Dis* 32:200-19.

Sekhon B, Sekhon C, Khan M, Patel SJ, Singh I, Singh AK (2003) N-Acetyl cysteine protects against injury in a rat model of focal cerebral ischemia. *Brain Res* 971:1–8.

Sheikh MS and Fornace Jr AJ (2000) Role of p53 family members in apoptosis. *J Cell Physiol* 182:171-81.

Skaper SD, Giusti P, Facci L (2012) Microglia and mast cells: two tracks on the road to neuroinflammation. *Faseb J* 26:3103-17.

Sugawara T and Chan PH (2003) Reactive oxygen radicals and pathogenesis of neuronal death after cerebral ischemia. *Antioxid Redox Signal* 5:597-607.

Sun RC, Yang SD, Zhou ZY, Shen CL, Shao JF, Liang JB et al. (2009) Pathologic and immunohistochemical study on lethal primary brain stem injury. *Zhonghua Bing Li Xue Za Zhi* 38:158-62.

Vargas MR and Johnson JA (2009) The Nrf2-ARE cytoprotective pathway in astrocytes. *Expert Rev Mol Med* 11:e17.

Willis CL (2012) Imaging in vivo astrocyte/endothelial cell interactions at the blood–brain barrier. *Methods Mol Biol* 814:515-29.

Xiang H, Kinoshita Y, Knudson CM, Korsmeyer SJ, Schwartzkroin PA, Morrison RS (1998) Bax involvement in p53-mediated neuronal cell death. *J Neurosci* 18:1363-73.

Yilmaz G and Granger DN (2010) Leukocyte recruitment and ischemic brain injury. *Neuromolecular Med* 12:193-204.

CHAPTER THIRTEEN

Moringin attenuates secondary damage in an experimental model of spinal cord injury

Contents

Summary

13.1 Spinal cord injury

13.2 Materials and Methods

13.2.1 Animals

13.2.2 Induction of spinal cord injury

13.2.3 Myrosinase bioactivation of glucomoringin

13.2.4 Experimental design

13.2.5 Light microscopy

13.2.6 Silver impregnation for reticulum

13.2.7 Immunohistochemical localization for (NF)- κ Bp65, iNOS, Bcl-2-associated X protein (Bax) and B-cell lymphoma 2 (Bcl-2)

13.2.8 Western blot analysis for I κ B- α and caspase 3

13.2.9 Statistical evaluation

13.3 Results

13.3.1 Moringin reduces the severity of spinal cord trauma

13.3.2 Effect of moringin on I κ B- α degradation and (NF)- κ Bp65 activation

13.3.3 Moringin modulates expression of iNOS after SCI

13.3.4 Effect of moringin on apoptosis in spinal cord after injury

13.4 Discussion

13.5 Conclusion

References

Keywords

4(α -L-Rhamnosyloxy)-benzyl isothiocyanate; Moringin; Glucomoringin; Myrosinase; *Moringa oleifera*; Spinal cord injury; Inflammation; Oxidative stress; Apoptosis

Abbreviations

MO: moringin (4(α -L-rhamnosyloxy)-benzyl isothiocyanate);

GMG: glucomoringin (4(α -L-rhamnosyloxy)-benzyl glucosinolate);

GL: glucosinolates;

ITC: isothiocyanates;

MYR: myrosinase enzyme;

(NF)- κ B: nuclear factor (NF)- κ B;

I κ B- α : nuclear factor of kappa light polypeptide gene enhancer in B-cells inhibitor, alpha;

iNOS: inducible Nitric Oxide Synthases;

SCI: spinal cord injury;

BBB: blood-brain barrier;

RO: reactive oxygen species;

RNS: reactive nitrogen species;

H&E: haematoxylin/eosin;

Bax: Bcl-2-associated X protein;

Bcl-2: B-cell lymphoma 2;

BSB: blood-spinal cord barrier;

NO: nitric oxide.

Summary

Spinal cord trauma was induced in mice by the application of vascular clips (force of 24 g) for 1 min, via four-level T5-T8 after laminectomy. The purpose of this study was to investigate the dynamic changes occurring in the spinal cord after ip treatment with moringin produced 15 min before use from myrosinase (MYR) catalyzed hydrolysis of glucomoringin (GMG) (10 mg Kg⁻¹ body weight + 5 µl MYR mouse per day). The following parameters, such as histological damage, distribution of reticular fibers in connective tissue, nuclear factor (NF)-κB translocation and nuclear factor of kappa light polypeptide gene enhancer in B-cells inhibitor, alpha (IκB-α) degradation, expression of inducible Nitric Oxide Synthases (iNOS), as well as apoptosis, were evaluated. Results showed a protective effect of MO on the secondary damage, following spinal cord injury, through an antioxidant mechanism of neuroprotection.

13.1 Spinal cord injury

Spinal cord injury (SCI) is a major cause of disability, primarily affecting young males with an incidence of 15–40 cases per million per year (Wyndaele and Wyndaele, 2006) causing enormous social and health-care costs. To date, generally accepted treatment for this disease is not available because of its complex pathophysiology. The functional decline, following SCI, is a consequence of both direct mechanical injury, which causes the death of a number of neurons that cannot be recovered and regenerated, and secondary pathophysiological mechanisms, called ‘secondary damage’, supported by a large number of cellular, molecular, and biochemical cascades (Profyris et al., 2004). The local inflammatory response in the injured spinal cord has been proposed to contribute significantly to the evolution of secondary damage. After SCI, microglia in the parenchyma are activated and macrophages in circulation pass through the blood-brain barrier (BBB) acting as intrinsic spinal phagocytes. These cells release different pro-inflammatory mediators such as cytokines, reactive oxygen species (ROS) and reactive nitrogen species (RNS) (Park et al., 2004). Increased production of ROS, which appears to play a critical role in the induction of neurological dysfunctions in SCI, causes the activation of the transcription factors such as (NF)- κ B that plays a key role in the induction of inflammatory cytokines. ROS formation and lipid peroxidation enhances damages of neuronal injury, such as spinal cord hypoperfusion, development of edema, axonal conduction failure, and breakdown of energy metabolism. The importance of free radicals and peroxidation in SCI is supported by many studies that showed neuronal protection efficacy of antioxidant agents (Scott et al., 2005).

The relevance and innovation of the present study lies in the possible use of a new formulation to deliver MO providing a therapeutic natural agent to counteract the overall cascade of events, such as oxidative injury and neuronal cell death, related to the secondary damage after spinal cord injury.

13.2 Materials and Methods

13.2.1 Animals

Male adult CD1 mice (average weight 25 g) were purchased from Harlan (Milan, Italy). Animals were housed in individually ventilated cages with food and water *ad libitum*. The room was maintained at a constant temperature and humidity on a 12 h/12 h light/dark cycle. Animal care followed Italian regulations of animal protection used for experimental and other scientific purposes (D.M. 116/92) as well as with the EEC regulations (O.J. of E.C.L 358/1 12/18/1986).

13.2.2 Induction of spinal cord injury

After anesthesia, induced with an anesthetic cocktail composed of tiletamine plus xylazine (10 mL Kg⁻¹, ip), the mice were subject to SCI, according to the model described by Rivlin and Tator (1978). A longitudinal incision was made on the midline of the back, exposing the paravertebral muscles. These muscles were dissected exposing T5-T8 vertebrae. The spinal cord was exposed via a four-level T5-T8 laminectomy and SCI was produced by extradural compression of the spinal cord at level T6-T7 using an aneurysm clip with a closing force of 24 g. In all injured groups, the spinal cord was compressed for 1 min. Following surgery, 1 mL of saline solution was administered subcutaneously to replace the blood volume lost during the surgery. The induced damage was verified and the animals were consequently awakened, evaluating the mobility of the hind limbs on a flat surface.

13.2.3 Myrosinase bioactivation of glucomoringin

GMG and MYR were purified as described at Chapter ten (see Section 10.5) and Chapter nine (see Section 9.2.2), respectively.

Pure GMG (95%) was dissolved in PBS solution pH 7.2 at room temperature (2.5 mg mL^{-1}) and hydrolyzed by the action of MYR ($5 \mu\text{l}$; 32 U mL^{-1}) for 15 min at $37 \text{ }^\circ\text{C}$ right before animal treatment. Mice were then administered the resulting solution as such.

13.2.4 Experimental design

Mice were randomly allocated into the following groups (N=25 total animals).

- SCI group (N=10): Mice were subjected to surgical operations to induce SCI.
- SCI + MO group (N=10): Mice subjected to SCI were treated with MO (GMG 10 mg Kg^{-1} body weight + $5 \mu\text{L}$ MYR mouse per day). The experiment provided a period of pretreatment with MO via ip injection once a day for 7 days. On the eighth day, the injury was induced and then the treatment was daily protracted for seven days until the sacrifice.
- Naive group: (N=5): Mice not subjected to SCI or to any injection, euthanized as control.

At the end of the experiment, the animals were euthanized, and the spinal cord corresponding to the thoracic spine was sampled, to evaluate the various parameters.

13.2.5 Light microscopy

Spinal cord biopsies, taken at 7 days following trauma, were fixed in 10% (w/v) PBS-buffered formaldehyde. Tissue segments containing the lesion (1 cm on each side of the lesion) were paraffin-embedded and cut into $7 \mu\text{m}$ -thick sections. Tissue sections were deparaffinized with xylene, stained with haematoxylin/eosin (H&E) and studied using light microscopy (LEICA ICC50 HD microscope).

13.2.6 Silver impregnation for reticulum

Silver impregnation was performed as the recommended method to show argyrophilic reticular fibers in connective tissue and specially to differentiate collagen

fibers from connective tissue. Silver impregnation was performed according to the manufacturer's protocol (<http://www.biooptica.it/pdf3/040801.pdf>, Bio-Optica, Milano S.P.A). Reticular and nervous fibers will appear in black, connective tissue in tobacco brown and collagen in gold yellow.

13.2.7 Immunohistochemical localization for (NF)- κ Bp65, iNOS, Bcl-2-associated X protein (Bax) and B-cell lymphoma 2 (Bcl-2)

After deparaffinization 7 μ m sections were hydrated in graded ethanol. Detection of (NF)- κ Bp65, iNOS, Bax and Bcl-2 was carried out after boiling in citrate buffer 0.01 M pH 6 for 4 min. Endogenous peroxidase was quenched with 0.3% (v/v) hydrogen peroxide in 60% (v/v) methanol for 30 min. Nonspecific adsorption was minimized by incubating the section in 2% (v/v) normal goat serum in PBS for 20 min. Sections were incubated overnight with anti-(NF)- κ Bp65 monoclonal antibody (Cell Signaling Technology, 1:100 in PBS); anti-iNOS monoclonal antibody (Cell Signaling Technology, 1:100 in PBS); anti-Bax polyclonal antibody (Santa Cruz Biotechnology, 1:100 in PBS) and anti-Bcl-2 polyclonal antibody (Santa Cruz Bio- technology, 1:100 in PBS). Endogenous biotin or avidin binding sites were blocked by sequential incubation for 15 min with biotin and avidin (DBA, Milan, Italy), respectively. Sections were washed with PBS and incubated with secondary antibody. Specific labelling was detected with a biotin-conjugated goat anti-rabbit IgG and avidin–biotin peroxidase complex (Vectastain ABC kit, VECTOR). The counterstain was developed with diaminobenzidine (brown color) and hematoxylin (blue background).

All images have been acquired in light microscopy using a LEICA ICC50 HD microscope. To perform densitometric analysis, quantitative data were carried out using Leica Application Suite V4.2.0 software.

13.2.8 Western blot analysis for I κ B- α and caspase 3

All the extraction procedures were performed on ice using ice-cold reagents. In brief, spinal cord tissues were suspended in extraction buffer containing 0.32 M sucrose, 10

mM Tris-HCl, pH 7.4, 1 mM EGTA, 2 mM EDTA, 5 mM NaN₃, 10 mM 2-mercaptoethanol, 50 mM NaF, and protease inhibitor tablets (Roche Applied Science, Monza, Italy), and they were homogenized at the highest setting for 2 min. The homogenates were chilled on ice for 15 min and then centrifuged at 1000g for 10 min at 4 °C, and the supernatant (cytosol + membrane extract from spinal cord tissue) was collected to evaluate content of IκB-α. The pellets were suspended in the supplied complete lysis buffer containing 1% Triton X-100, 150 mM NaCl, 10 mM Tris-HCl, pH 7.4, 1 mM EGTA, and 1 mM EDTA protease inhibitor tablets (Roche Applied Science), and then they were centrifuged for 30 min at 15,000g at 4 °C, and the supernatant (nuclear extract) was collected to evaluate the content of caspase 3. Supernatants were stored at -80 °C until use. Protein concentration in homogenate was estimated by the Bio-Rad Protein Assay (Bio-Rad, Segrate, Milan, Italy) using BSA as standard, and 50 μg of cytosol and nuclear extract from each sample was analyzed. Proteins were separated on sodium dodecyl sulfate-poly-acrylamide minigels and transferred into nitrocellulose membranes (Protran nitrocellulose transfer membrane; Whatman Schleicher and Schuell, Dassel, Germany), blocked with PBS containing 5% nonfat dried milk for 45 min at room temperature, and subsequently probed at 4 °C overnight with specific antibodies for IκB-α (1:1000; Cell Signaling Technology) and caspase 3 (1:1000; Cell Signaling Technology), in PBS, 5% (w/v) nonfat dried milk, and 0.1% Tween-20 (PMT). Membranes were incubated with peroxidase-conjugated bovine anti-mouse IgG secondary antibody or peroxidase-conjugated goat anti-rabbit IgG (1:2000; Jackson Immuno Research, West Grove, PA, USA) for 1 h at room temperature. To ascertain that blots were loaded with equal amounts of protein lysates, they were also incubated with antibody for α-tubulin (1:250; Santa Cruz Biotechnology, Inc.), and conjugated GAPDH HRP (1:1000; Cell Signaling Technology). The relative expression of the protein bands IκB-α (~37 kDa), and caspase 3 (~35 kDa) was visualized using an enhanced chemiluminescence system (Luminata Western HRP Substrates, Millipore). The protein bands were scanned and quantitated with ChemiDoc™ MP System (Bio-Rad) and a computer program (ImageJ). It is important to note that all differences in band expressions were normalized on the housekeeping control. For this reason, even if there was some

difference in the amount of protein loading, in each quantitative graph of Western blot analysis, the value was provided as ratio.

13.2.9 Statistical evaluation

Data were analyzed in GraphPad Prism version 6.0 (GraphPad Software, La Jolla, CA). The results were statistically analyzed using one-way ANOVA followed by a Bonferroni post hoc test for multiple comparisons. A *p* value of <0.05 was statistically significant. Results are expressed as the mean \pm SEM of *n* experiments.

13.3 Results

13.3.1 Moringin reduces the severity of spinal cord trauma

At day 7 after injury, the severity of the trauma of the perilesional area was analyzed by hematoxylin/eosin (H&E) staining and the presence of edema as well as alteration of the white matter and infiltration of leukocytes was assessed. Results clearly demonstrated important damage in the spinal cord tissue collected from SCI animals (Figure 13.1A) compared with naive mice (Figure 13.1C). Significant protection against the SCI was observed in MO treated mice (Figure 13.1B). Moreover, the severity of the trauma was also evaluated, investigating the alterations of reticular fibers in connective tissue by silver impregnation. Degeneration of reticular fibers in the spinal cord of SCI mice (Figure 13.1D) was found, whereas a normal distribution of reticular fibers was observed in sections of MO treated (Figure 13.1E) and naive mice (Figure 13.1F), proven by the deposit of black silver grains in the perilesional area, easily distinguishable from the brown background produced by the staining procedure.

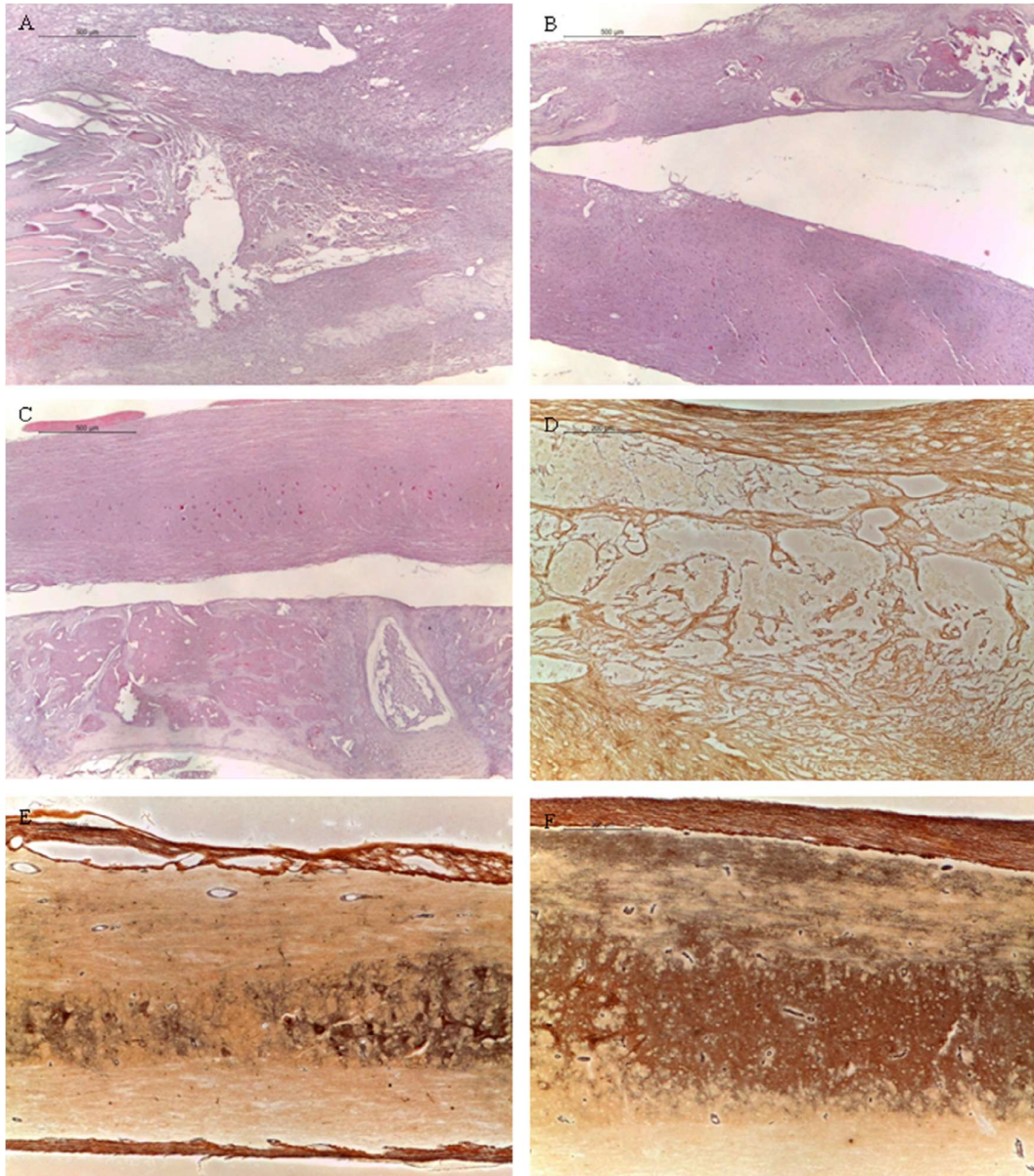


Figure 13.1 Effect of moringin (MO) on severity of spinal cord trauma (SCI). The severity of the trauma was evaluated 7 days after injury and stained with H&E. No histological alterations were observed in the spinal cord tissues from naive mice (C). 7 days after trauma, a significant damage to the spinal cord from untreated SCI operated mice at the perilesional area was assessed by the presence of edema as well as alteration of the white matter (A). It is noteworthy that a significant protection from the SCI was observed in the tissues collected from MO treated mice (B). Also, a degeneration of reticular fibers in the spinal cord from SCI mice was demonstrated (D), whereas a normal distribution of reticular fibers has been observed in sections of MO treated (E) and naive mice (F), reflected by the deposition of black silver grains in the perilesional area.

13.3.2 Effect of moringin on I κ B- α degradation and (NF)- κ Bp65 activation

Spinal cord sections were collected at 7 days after injury, to investigate cellular mechanism through which MO treatment may attenuate the damage associated with SCI. I κ B- α degradation and nuclear (NF)- κ Bp65 activation were evaluated by Western blot and immunohistochemical analysis. A basal level of I κ B- α was detected in the spinal cord from naïve mice, whereas I κ B- α levels were substantially reduced in SCI mice. MO administration attenuated the SCI induced I κ B- α degradation. Although not statistically significant, visible differences in I κ B- α expression were also found (Figure 13.2D). In addition, spinal cord sections obtained from mice subjected to SCI exhibited positive staining for (NF)- κ Bp65 in the perilesional area (Figure 13.2A). On the contrary, treatment with MO significantly reduced the degree of positive staining for (NF)- κ Bp65 (Figure 13.2B). Naive mice did not stain for (NF)- κ Bp65 (Figure 13.2C).

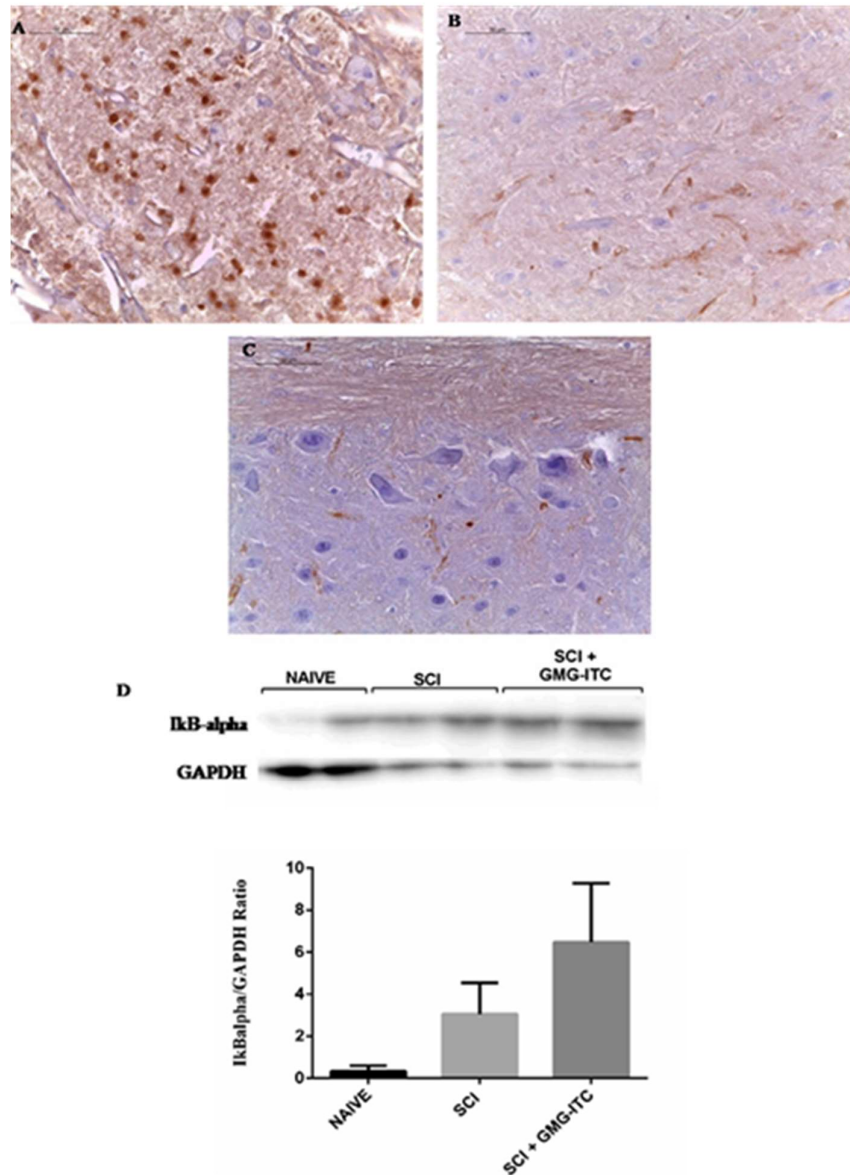


Figure 13.2 Effects of moringin (MO, labeled as GMG-ITC) on IκB-α degradation and nuclear (NF)-κBp65 expression after SCI. By Western blot analysis a basal level of IκB-α was detected in the spinal cord from naive animals and in SCI mice, whereas MO administration prevented the SCI induced IκB-α degradation. GAPDH was used as internal control. Although not statistically significant, visible differences in IκB-α expression were found. Please, note that all differences in band expression were normalized on the housekeeping control. For this reason, even if there was some difference in the amount of protein loading, in each quantitative graph of Western blot analysis, the value was provided as ratio (D). Also, (NF)-κBp65 expression was evaluated by immunohistochemical analysis. Spinal cord sections obtained from mice subjected to SCI exhibited positive staining for (NF)-κBp65 in perilesional area (A). On the contrary, treatment with MO significantly reduced the degree of positive staining for (NF)-κBp65 (B). Naive mice did not stain for (NF)-κBp65 (C).

13.3.3 Moringin modulates expression of iNOS after SCI

Evaluation of the iNOS expression by immunohistochemical analysis assessed the role of nitric oxide (NO) produced during SCI. The treatment with MO was able to counteract the oxidative and nitrosative stress resulting from the spinal cord damage. Spinal cord sections from naive mice did not stain for iNOS (Figure 15.3C), whereas spinal cord sections obtained from SCI mice exhibited positive staining for iNOS (Figure 13.3A). MO treatment reduced the degree of positive staining for iNOS in the spinal cord of mice subjected to SCI (Figure 13.3B, see densitometric analysis Figure 13.3D).

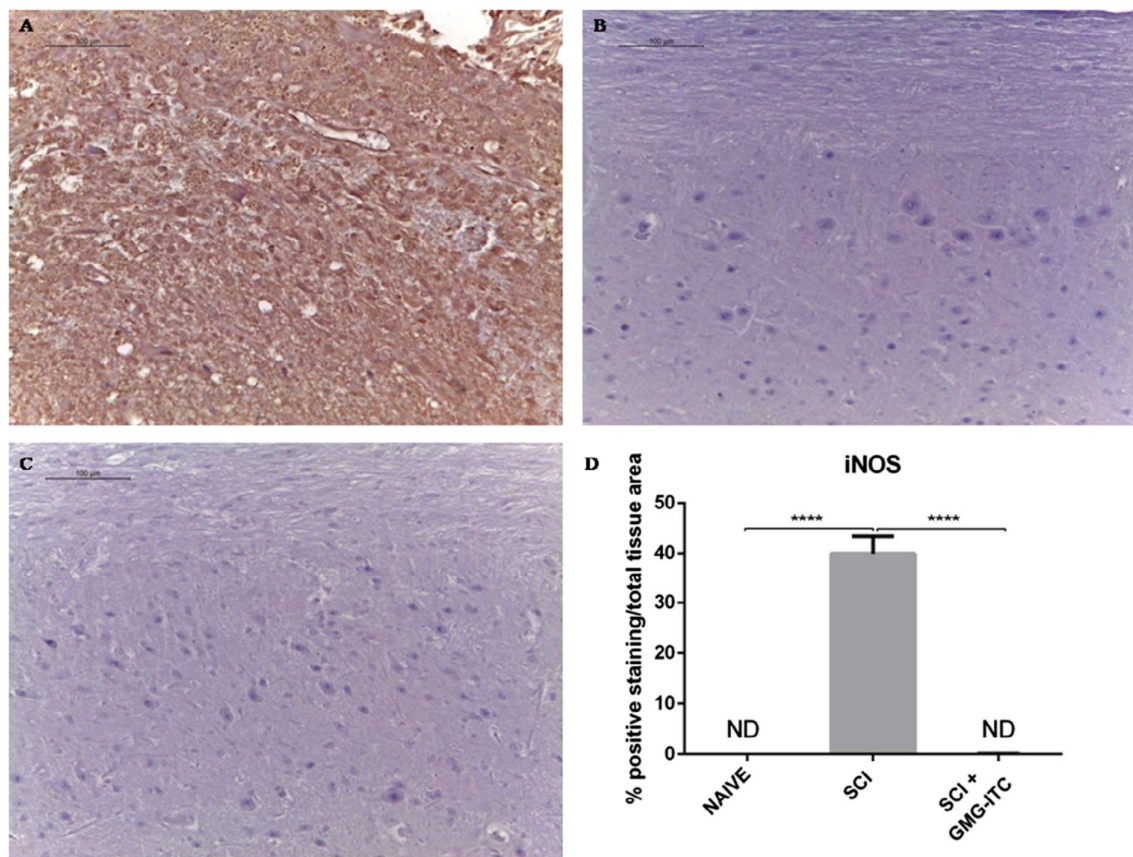


Figure 13.3 Moringin (MO, labeled as GMG-ITC) modulates expression of iNOS. iNOS was evaluated by immunohistochemical analysis in the spinal cord sections 7 days after SCI. Spinal cord sections from naive mice did not stain for iNOS (C), whereas spinal cord sections obtained from SCI mice exhibited positive staining for iNOS (A). MO treatment reduced the degree of positive staining for iNOS in the spinal cord tissues (B). Densitometric analysis of iNOS. Results were analyzed by one-way ANOVA followed by a Bonferroni post hoc test for multiple comparisons. * $p < 0.05$ versus SCI and versus naive. ND: not detectable (D).

13.3.4 Effect of moringin on apoptosis in spinal cord after injury

Samples of spinal cord tissue were taken at 7 days after SCI to determine the immunohistological staining for the apoptotic protein family. Spinal cord sections from naive mice did not stain for Bax (Figure 13.4C), whereas spinal cord sections obtained from SCI mice exhibited positive staining for Bax (Figure 13.4A). MO treatment decreased the degree of positive staining for Bax in spinal cord samples from mice subjected to SCI (Figure 13.4B, see densitometric analysis Figure 13.4D). In addition, immunohistological staining for Bcl-2 in spinal cord sections from naive mice, demonstrated positive staining (Figure 13.5C), while in SCI mice the staining was significantly reduced (Figure 13.5A). MO treatment modulates SCI induced expression of anti-apoptotic protein, increasing significantly the tissue immunolocalization of Bcl-2 protein (Figure 13.5B, see densitometric analysis Figure 13.5D). Moreover, sequential activation of caspases plays a central role in the execution-phase of cell apoptosis. Activation level of caspase 3, determined by Western blot, was appreciably increased in the spinal cord from mice subjected to SCI, while treatment with MO prevented the SCI induced expression (Figure 13.6).

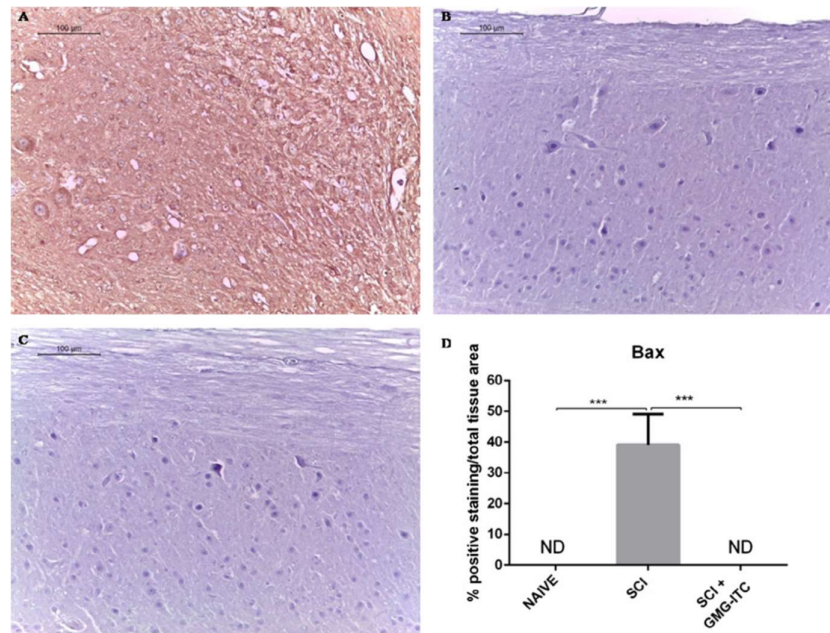


Figure 13.4 Effect of moringin (MO, labeled as GMG-ITC) on immunohistochemical expression for Bax. Spinal cord sections from naive mice did not stain for Bax (C), whereas SCI caused an increase in Bax expression at 7 days (A). MO treatment reduced the degree of positive staining for Bax in the spinal cord (B). Densitometric analysis of Bax. Results were analyzed by one-way ANOVA followed by a Bonferroni post hoc test for multiple comparisons. * $p < 0.05$ versus SCI and versus naive. ND: not detectable (D).

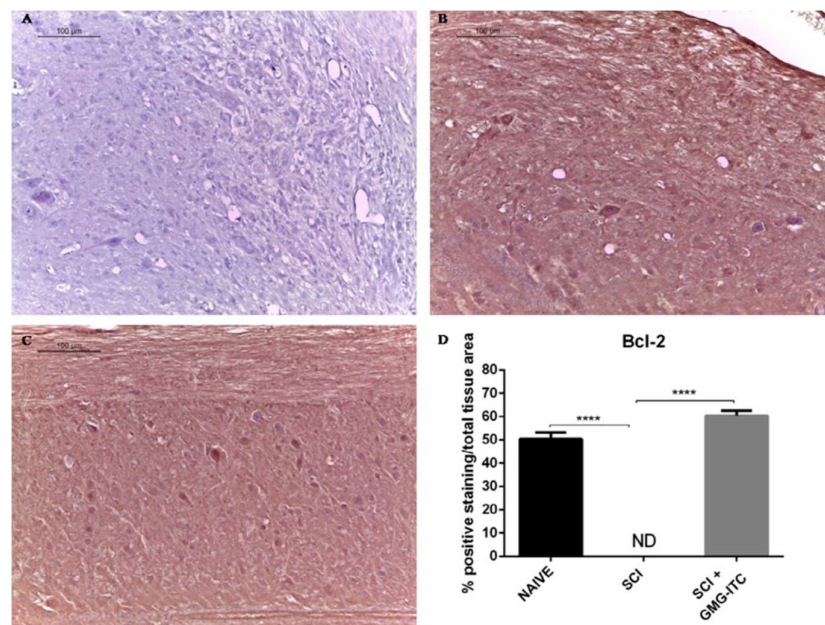


Figure 13.5 Effect of moringin (MO, labeled as GMG-ITC) on immunohistochemical expression for Bcl-2. Positive staining for Bcl-2 was observed in the spinal cord tissues from naive mice (C), while the staining was significantly reduced in SCI mice (A). MO treatment attenuated the loss of positive staining for Bcl-2 in the spinal cord from SCI subjected mice (B). Densitometric analysis of Bcl-2. Results were analyzed by one-way ANOVA followed by a Bonferroni post hoc test for multiple comparisons. * $p < 0.05$ versus SCI and versus naive. ND: not detectable (D).

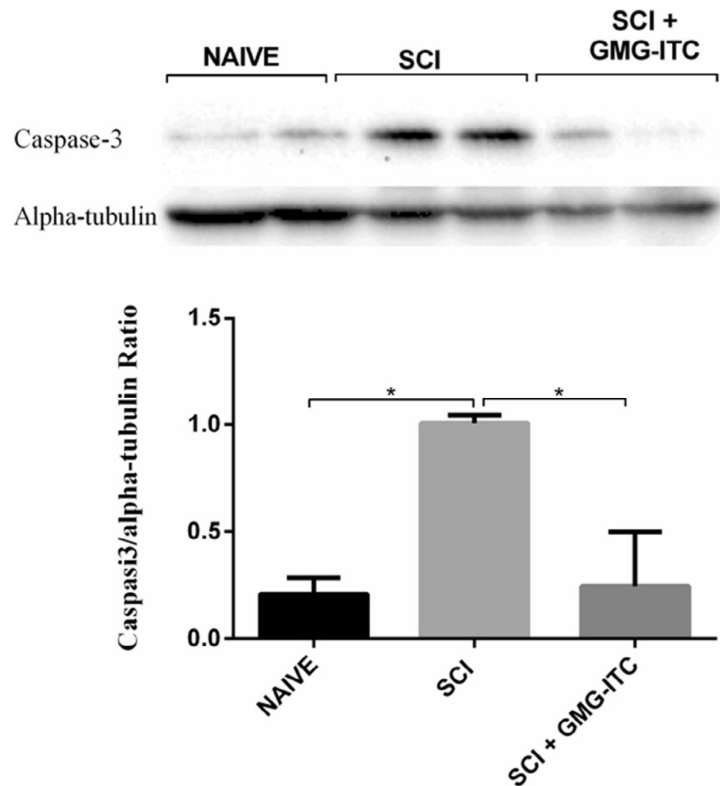


Figure 13.6 Western blot for caspase 3. By Western blot analysis the activation of caspase 3 was evaluated. SCI caused a significant increase in caspase 3 expression compare to naive mice. On the contrary, treatment with moringin (MO, labeled as GMG-ITC) prevented the SCI induced caspase 3 expression. Note that all differences in band expression were normalized on the housekeeping control. For this reason, even if there was some difference in the amount of protein loading, in each quantitative graph of Western blot analysis, the value was provided as ratio. * $p < 0.05$ versus SCI and versus naïve.

13.4 Discussion

SCI is a disease widely associated with both the inflammatory response and oxidative mechanism, as well as with the apoptotic pathway and neurodegenerative feature. In addition, in direct injury caused by primary trauma after SCI, a variety of extended neuropathophysiologic alterations occur, mediated by a series of cellular, molecular and biochemical cascades, including glutamate excitotoxicity, Ca^{2+} overload, oxygen free radical induced lipid peroxidation, inflammation, vascular events, and neuronal death (Anderson and Hall, 1993). The pharmacological window for therapeutic

intervention aimed to avoid diffused axonal injury (DAI) is between 0 and 12 h after damage. Many factors contribute to the progression of degenerative events that, in the long-term, lead to irreversible injury as well as perilesional damage. In this respect, current researches are aimed at avoiding diffused tissue degeneration at the upper level and lower the lesion with target therapies, counteracting numerous factors involved in secondary degeneration cascade (Genovese et al., 2006). By histological examination of perilesional area, untreated mice showed evident signs of inflammation and necrosis, while in spinal cord tissues of animals, treated with MO, was not observed damage. Secondary damage is related to vascular events that cause blood–spinal cord barrier (BSB) disruption, closely associated with edema formation. Moreover, BSB breakdown triggers post-traumatic inflammatory response mediated by neutrophilic infiltration and macrophage invasion. Further, trauma-activated endothelial and glial cells release vasoactive substances (reactive oxygen molecules, bradykinin, histamines and NO) that influence the spinal cord perfusion and facilitate the crossing of plasma-derived molecules into the cord (Schnell et al., 1999). Structurally, silver impregnation highlighted a degeneration of the reticular fiber in the connective tissue of the spinal cord samples collected at 7 days after the trauma, whereas a normal distribution and architecture has been observed in sections of MO treated mice. MO can hence promote a neuroprotection of microvasculature that occurs because of the trauma. Inflammatory response is the major component of secondary injury and plays a central role in regulating the pathogenesis of acute and chronic SCI. Also, it is associated with a significant production of free radicals like ROS such as superoxide anions, hydrogen peroxide and peroxynitrite (Calabrese et al., 2007). (NF)- κ B is a transcription factor, which is kept inactive by I κ B- α , that plays a central role in the regulation of many genes responsible for the generation of mediators or proteins in secondary inflammation associated with SCI. Our analysis demonstrated that MO inhibited both I κ B- α degradation, as well as (NF)- κ B translocation. A direct consequence of the inhibitory effect of MO on (NF)- κ B activation is the reduction in proinflammatory mediators production under its control, such as iNOS, involved in the development of the secondary inflammatory response and apoptosis following traumatic SCI (Genovese et al., 2006). Among

them, this factor has a beneficial role as modulator or messenger but during oxidative stress it is potentially toxic. In fact, overproduction of NO through iNOS causes accentuated lipid peroxidation, protein and DNA modifications that result in cellular damage (Ahmad et al., 2009). MO attenuates the expression of iNOS in the tissue of SCI treated mice when compared with injured mice, indicating that this compound may be able to protect the spinal cord against iNOS mediated neurodegeneration. MO influences the downstream cascade of events triggered by the inflammatory process by inhibiting (NF)- κ B pathway, that in turn regulates iNOS activation (Hsu et al., 2013). Moreover, recent studies have also demonstrated that ROS induce apoptosis in an early and likely causal event that contributes to the spinal cord motor neuron death following SCI (Siniscalco et al., 2007). Apoptosis is an important process strongly related to secondary damage after SCI which involves different cell types, especially oligodendrocytes of the white matter (Beattie et al., 2002). Chronologically, it occurs 6 h post-injury at the lesion center, where there is the highest number of apoptotic cells that increase steadily over few days. A significant intracellular signal transduction pathway that leads to apoptosis after SCI involves activation of the caspases, in particular, caspase 3 (Chittenden et al., 1995). Since SCI causes an important increase in caspase 3 and an imbalance in mitochondrial permeability with an up-regulation of proapoptotic Bax protein and a down-regulation of anti-apoptotic Bcl-2 protein, this study was aimed to understand whether MO treatment could decrease the expression level of these markers, modulating the apoptotic pathway. Interestingly, the results showed that MO can prevent transcriptional changes, playing a key role in the control of proapoptotic mechanisms following SCI-related tissue damage. Taken together, this data suggest that MO is a promising phytochemical that could be used for the management of secondary damage following SCI to counteract the overall cascade of events, such as oxidative injury and neuronal cell death, triggered by mechanical and direct damage to the spinal cord.

13.5 Conclusion

The relevance of the present study consists in the possible use of MO as a therapeutic agent in the treatment of secondary damage associated with SCI. Considering the results achieved, the neuroprotection derived by the treatment of MO could lead to an application of this drug for long term re-establishment of spinal cord functionality.

References

Ahmad R, Rasheed Z, Ahsan H (2009) Biochemical and cellular toxicology of peroxynitrite: implications in cell death and autoimmune phenomenon. *Immunopharmacol Immunotoxicol* 31(3):388-96.

Anderson DK and Hall ED (1993) Pathophysiology of spinal cord trauma. *Ann Emerg Med* 22(6):987-92

Calabrese V, Mancuso C, Calvani M, Rizzarelli E, Butterfield DA, Stella A (2007) Nitric oxide in the central nervous system: neuroprotection versus neurotoxicity. *Nat Rev Neurosci* 8(10):766-75.

Chittenden T, Harrington EA, O'Connor R, Flemington C, Lutz RJ, Evan GI, Guild BC (1995) Induction of apoptosis by the Bcl-2 homologue Bak. *Nature* 374(6524):733-6.

Genovese T, Mazzon E, Mariotto S, Menegazzi M, Cardali S, Conti A, Suzuki H, Bramanti P, Cuzzocrea S (2006) *J Neurosurg Spine* 2:145.

Hsu CC, Lien JC, Chang CW, Chang CH, Kuo SC, Huang TF (2013) *Biochem Pharmacol* 3:385.

Park E, Velumian AA, Fehlings MG (2004) The role of excitotoxicity in secondary mechanisms of spinal cord injury: a review with an emphasis on the implications for white matter degeneration. *J Neurotrauma* 21(6):754-74.

Profyris C, Cheema SS, Zang D, Azari MF, Boyle K, Petratos S (2014) Degenerative and regenerative mechanisms governing spinal cord injury. *Neurobiol Dis* 15(3):415-36.

Rivlin AS and Tator CH (1978) Effect of duration of acute spinal cord compression in a new acute cord injury model in the rat. *Surg Neurol* 10(1):38-43.

Schnell L, Fearn S, Klassen H, Schwab ME, Perry VH (1999) *Eur J Neurosci* 10:3648.

Scott GS, Cuzzocrea S, Genovese T, Koprowski H, Hooper DC (2005) Uric acid protects against secondary damage after spinal cord injury. *Proc Natl Acad Sci USA* 102(9):3483-8.

Siniscalco D, Fuccio C, Giordano C, Ferraraccio F, Palazzo E, Luongo L, Rossi F, Roth KA, Maione S, de Novellis V (2007) Role of reactive oxygen species and spinal cord apoptotic genes in the development of neuropathic pain. *Pharmacol Res* 55(2):158-66.

Wyndaele, M. and J.J. Wyndaele (2006) Incidence, prevalence and epidemiology of spinal cord injury: what learns a worldwide literature survey? *Spinal Cord* 44(9)523-9.

CHAPTER FOURTEEN

Moringin delays disease phenotype in SOD1^{G93A} rats: a transgenic model of amyotrophic lateral sclerosis

Contents

Summary

14.1 Amyotrophic lateral sclerosis

14.2 Materials and Methods

14.2.1 Animals

14.2.2 ALS model of disease

14.2.3 Myrosinase bioactivation of glucomoringin

14.2.4 Experimental design

14.2.5 Behavioral test

14.2.6 Immunohistochemistry localization

14.2.7 Western blot analysis

14.2.8 Blood sampling

14.2.9 Prostaglandin E2 (PGE2) assay

14.2.10 Chemical serum parameters

14.2.11 Golgi stain

14.2.12 Statistical evaluation

14.3 Results and discussion

14.4 Conclusion

References

Summary

The present study was designed to test the potential therapeutic effectiveness of moringin (4-(α -L-rhamnopyranosyloxy)benzyl isothiocyanate; MO) to counteract the amyotrophic lateral sclerosis (ALS) using SOD1tg rats, which physiologically develops SOD1G93A at about 16 weeks of life, and can be considered a genetic model of disease. Rats were treated once a day with glucomoringin (4-(α -L-rhamnopyranosyloxy)benzyl glucosinolate; GMG) (10mg Kg^{-1}) bioactivated with myrosinase (32 U mL^{-1} ; MYR) ($20\ \mu\text{L}/\text{rat}$) via intraperitoneal (i.p.) injection for two weeks before disease onset and the treatment was prolonged for further two weeks before the sacrifice. Immune inflammatory markers as well as apoptotic pathway were investigated to establish whether MO could represent a new promising tool in clinical practice to prevent ALS. Achieved data displayed clear differences in molecular and biological profiles between treated and untreated SOD1tg rats suggesting that MO can interfere with the pathophysiological mechanisms at the basis of ALS development. Therefore, MO could be a candidate for further studies aimed to assess its possible use in clinical practice for the prevention or to slow down this disease.

14.1 Amyotrophic lateral sclerosis

Amyotrophic lateral sclerosis (ALS) is a motor neuron disease first described by Jean-Martin Charcot in the 1800s. The disease gradually and fatally attacks both the first motor neurons in the cerebral cortex and the second motor neurons in the brainstem and spinal cord (the upper and lower motor neuron, respectively) responsible for controlling the voluntary muscles. It is a neurodegenerative pathology with a progressive and invariably fatal outcome. The disease is sometimes called Lou Gehrig's disease and, less frequently, Charcot disease (Doi et al., 2014). Sadly, as a neuromuscular disease, it is related just to the motor system so that all the neurological functions are preserved, and the patient is wholly aware of what is happening. Mostly, ALS onset occurs in late adulthood (Malaspina et al., 2015) starting in limb, axial, bulbar, or respiratory muscles and causing spasticity and severe and rapidly progressive muscle weakness and respiratory insufficiency that lead to death within few years after initial diagnosis. Sporadic (sALS) and familial (fALS) forms of the disease represent, respectively, about 90% and 10%, of all ALS cases (Rafałowska et al., 2014). To date the causes are unknown; nevertheless, it is believed that ALS could have a multifactorial etiology, where environmental factors can greatly contribute to pathology triggering (Eisen, 1995). Both a defect in glutamate transporter and calcium binding protein failure have been identified as potential causes of the corticomotoneuronal system defects (Gunther et al., 2014). Moreover, genetic mutations on chromosome 21, which codes for the cytosolic antioxidant enzyme $\text{Cu}^{2+}/\text{Zn}^{2+}$ binding superoxide dismutase gene 1 (SOD1), have been identified first as a cause associated with 20% of all familial forms (Gunther et al., 2014). Other possible genetic causes have been related to defects in transactivation response (TAR) element, DNA-binding protein 43 (TDP-43), angiogenin, and an intronic hexanucleotide expansion in the gene encoding the chromosome 9 open reading frame 72 (*C9orf72*) (Malaspina et al., 2015). Also potentiated to be involved in the genesis of the disease is the role of the innate immune system with cellular mechanisms mediated by CD8+ cytotoxic cells and CD4+ T-helper cells localized in spinal cord ventral horns, in the anterior and lateral corticospinal tracts and in the motor cortex (Malaspina et al., 2015). The most commonly used drug to treat ALS is glutamate antagonist riluzole that prolongs patient survival but has very limited benefits, since it does not show the expected efficacy that could lead to disease resolution. For this reason, new innovative and safer therapies are needed (Benatar, 2007; Stewart et al., 2001), at least aimed at delaying

the neurodegenerative processes of the ongoing disease. To discover new active compounds as alternatives to the current therapies, basic science is focused on natural products and their derivatives for the treatment of neurodegenerative diseases, such as ALS (Halliwell, 2001; Li et al., 2011). Thus, the aim of the present work was to test the potential effectiveness of MO to interfere with the mechanisms underlying ALS development and prevent or slow down the disease in transgenic SOD1^{G93A} (SOD1tg) rats, an experimental genetic model of ALS.

14.2 Materials and Methods

14.2.1 Animals

Male Sprague-Dawley rats overexpressing the mutated human gene SOD1^{G93A}, which represents a transgenic model of ALS, were purchased from Taconic Biosciences, Inc. (Hudson, NY, USA) and used for the experiment.

14.2.2 ALS model of disease

According to genetic and phenotypic description provided by Taconic industry (<http://www.taconic.com/2148>) spinal cord of SOD1^{G93A} hemizygous rats expresses about 8-fold more endogenous SOD1, which became ~16-fold by the end stages of disease. SOD1 rats have an onset of motor neuron disease after approximately 115 days.

14.2.3 Myrosinase bioactivation of glucomoringin

GMG and MYR were purified as described at Chapter ten (see Section 10.5) and Chapter nine (see Section 9.2.2), respectively.

Pure GMG (95%) was dissolved in PBS solution pH 7.2 at room temperature (2.5 mg mL⁻¹) and hydrolyzed by the action of MYR (20 µl; 32 U mL⁻¹) for 15 min at 37 °C right before animal treatment. Rats were then administered the resulting solution as such.

14.2.4 Experimental design

Rats were randomly allocated into the following groups:

- Untreated SOD1tg group (N=10): rats not pharmacologically treated.
- MO treated SOD1tg group (N=10): rats were prophylactically treated once a day with GMG (10mg Kg⁻¹) bioactivated with MYR (20 μL/rat), via i.p. injection starting from two weeks before the disease onset (about 100 days of life) and protracted for other two weeks before the sacrifice (about 130 days of life). Since the Taconic industry disease onset occurs around 115 days of life (about 16 weeks), our experiments were planned to treat SOD1tg rats starting from 14 weeks. Consequently, the sacrifice was established when in the MO SOD1tg group the first signs of disease appeared (about 18 weeks of life). At the end of the experiment, blood was collected by cardiac puncture and animals were euthanized. Brain tissue and spleen were sampled and processed to evaluate disease parameters.

14.2.5 Behavioral test

Noninvasive behavioral evaluations were made without causing excessive animal stress to provide data about muscular degeneration/locomotor activity loss. Hanging Wire Test (HWT) was performed to evaluate motor performance. The test consists in the capability of the animal at hanging from a wire for a time of 90 sec, using the paw strength. HWT was performed two times a week starting from four weeks before the disease onset and two weeks later and for a total number of fifteen tests. Also, Open Field Test (OFT) for motor function was performed to test behavior and general motor function. MO treated, as well as untreated SOD1tg rats were monitored for a time of 180 sec to assess the spontaneous activity in an open field, consisting of a white Plexiglas box (100 cm × 100 cm) with the floor divided into 16 squares. Four squares were defined as the center and 12 squares along the walls as the periphery. Each animal was placed in the center of the box and activity was scored as a line crossing when a mouse removed all four paws from one square and entered another. Immediately after each test, the apparatus was thoroughly cleaned with cotton pad wetted with 70% ethanol. The test was performed once a week starting from two weeks before the disease onset and two weeks later, with the last measure performed the day before the sacrifice and for a total number of six tests.

14.2.6 Immunohistochemistry localization

Brain tissues were fixed in 10% (w/v) PBS-buffered formaldehyde, and 6 μ m sections were prepared from paraffin-embedded tissues. After deparaffinization, endogenous peroxidase was quenched with 0.3% (v/v) hydrogen peroxide in 60% (v/v) methanol for 30 min. Nonspecific adsorption was minimized by incubating sections in 2% (v/v) normal goat serum in PBS for 20 min. Endogenous biotin or avidin binding sites were blocked by sequential incubation for 15 min with biotin and avidin, respectively. Sections were incubated overnight with the following primary antibodies:

- (i) Anti-TLR4 monoclonal antibody (1:100 in PBS v/v; Abcam).
- (ii) Anti-MMP9 polyclonal antibody (1:100 in PBS v/v; Abcam).
- (iii) Anti-NOS2 polyclonal antibody (1:100 in PBS v/v; Santa Cruz Biotechnology, Inc).
- (iv) Anti-PARP-1 polyclonal antibody (1:100 in PBS v/v; Santa Cruz Biotechnology, Inc).
- (v) Anti-CD8 α polyclonal antibody (1:100 in PBS v/v; Santa Cruz Biotechnology, Inc).
- (vi) Anti-Nrf2 polyclonal antibody (1:100 in PBS v/v; Santa Cruz Biotechnology, Inc).

Sections were washed with PBS and incubated with secondary antibody. Specific labeling was detected with a biotin conjugated goat anti-rabbit IgG and avidin-biotin peroxidase complex. The counterstain was developed with diaminobenzidine (brown color) and ematossilin (blue background). To verify the binding specificity, some sections were also incubated with only the primary antibody or with only the secondary antibody. In these situations, absence of positive staining was found in the sections, indicating that the immunoreaction was positive in all the experiments carried out. All sections were observed using light microscopy (Leica ICC50 HD). Leica Application SuiteV4.2.0 software was used as image computer program to acquire IHC (immunohistochemistry) pictures.

14.2.7 Western blot analysis

All western blot procedures aimed to assess the expression of mediators of ALS development were performed according to previously published protocols (Galuppo et al., 2014) and here modified for brain tissue and spleen. Briefly, all the extraction procedures were performed on ice using ice-cold reagents. Brain tissues or spleen were suspended in extraction buffer containing 0.32M sucrose, Tris-HCl, pH 7.4, 1 mM EGTA, 2 mM EDTA, 5 mM NaN₃, 10 mM 2-

mercaptoethanol, 50 mM NaF, and protease inhibitor tablets (Roche, Milan, Italy) and then homogenized at the highest setting for 2 min. The homogenates were chilled on ice for 15 min and then centrifuged at 1000 g for 10 min at 4 °C, and the supernatant (cytosol + membrane extract) was collected to evaluate content of cytoplasmic proteins. The pellets were suspended in the supplied complete lysis buffer containing 1% Triton X-100, 150 mM NaCl, 10 mM Tris-HCl, pH 7.4, 1 mM EGTA, and 1 mM EDTA protease inhibitors tablets (Roche), and then they were centrifuged for 30 min at 15,000 g at 4 °C, and the supernatant (nuclear extract) was collected to evaluate the content of nuclear proteins. Supernatants were stored at -80 °C until use. Protein concentration in homogenate was estimated by Bio-Rad ProteinAssay (Bio-Rad, Segrate, Italy) using BSA as standard, and 20 µg of cytosol and nuclear extract from each sample were analyzed. Proteins were separated on sodium dodecyl sulfate-polyacrylamide minigels and transferred onto nitrocellulose membranes (Protran nitrocellulose transfer membrane; Whatman Schleicher and Schuell, Dassel, Germany), blocked with PBS containing 5% nonfat dried milk (PM) for 45 min at room temperature, and subsequently probed at 4°C overnight with the following primary antibodies: TNF-alpha (1:100 in PM 0.1% Tween 20 (PMT) v/v; Cell Signaling Technologies), FoxP3 (1:500 in PMT v/v; eBioscience), and cleaved-caspase3 (1:1000 in PMT v/v; Cell Signaling Technologies). HRP-conjugated goat anti-mouse IgG or HRP-conjugated goat anti-rabbit IgG were incubated as secondary antibodies (1:2000 in PMT v/v; Santa Cruz Biotechnology, Inc.) for 1 h at room temperature. To ascertain that blots were loaded with equal amounts of proteic lysates, they were also incubated with GAPDH-HRP conjugated primary antibody (1:1000 in PMT v/v; Cell Signaling Technology). Relative protein bands expression was visualized using an enhanced chemiluminescence system (Luminata Forte, Western HRP substrate, Millipore) and proteic bands were acquired and quantified with ChemiDoc MP System (Bio-Rad, Segrate, Italy) and a computer program (ImageJ software), respectively. Blots are representative of three separate and reproducible experiments. Statistical analysis was run on three repeated blots performed on separate experiments.

14.2.8 Blood sampling

At the sacrifice, blood samples were collected via cardiac puncture in Serum Separator Tubes

(Vacutainer SSTTM II Advance, BD Diagnostic, Milan, Italy) and centrifuged following at least 30 min from the collection at 2000 g speed for 10 min. The achieved serum was collected, aliquoted, and stored at -80°C to be used in next investigations.

14.2.9 Prostaglandin E2 (PGE2) assay

ELISA kit for PGE2 parameter assay (R&D system Europe, Ltd., Abingdon, UK) was purchased to detect PGE2 levels in serum samples. The kit was used according to the manufacturer's instruction and achieved O.D. were tabulated and analyzed using a software of elaboration data.

14.2.10 Chemical Serum Parameters

VITROS MicroSlide Tests (VITROS 350 by Ortho-Clinical Diagnostics, Johnson & Johnson company, Milan, Italy) were used to assess creatine kinase (CK), sodium (Na^+), and potassium (K^+) serum levels. Data are shown as mean of achieved values for each experimental group.

14.2.11 Golgi stain

FD Neurotech kit (FD NeuroTechnologies, Ellicott City, Md, USA) was used for Golgi impregnation of tissue, according to manufacturing instruction (http://fdneurotech.com/docs/1333571253.web_pk401-401a-04042012.pdf). Briefly, brain samples were placed directly into solution (A + B) containing mercuric chloride, potassium dichromate, and potassium chromate, without rinsing, and remained there for 2weeks in the dark at room temperature. Forty-eight hours after placing in solution C (4°C), brains were frozen on dry ice and stored at -70°C until sectioning. Cryostat sections ($100\ \mu\text{m}$) were cut at -25°C and mounted onto gelatinized slides. Slides were allowed to dry in the dark, and the rest of the staining process was done as previously described (Feng et al., 2000). Cresyl violet was used as background color to counterstain.

14.2.12 Statistical evaluation

All data were elaborated using GraphPad Prism version 6.0 (GraphPad Software, La Jolla, CA). The results were statistically analyzed by performing Student's *t*-test. A *p* value of < 0.05 was considered to be statistically significant. Results are expressed as mean \pm S.E.M. of *n* experiments. For behavioral assessment, Sidak-Bonferroni method was applied using multiple *t*-tests to assess statistical differences.

14.3 Results and discussion

SOD1tg rats represent a genetic model of ALS. Our purpose was to verify whether MO could have some effects on ALS disease and, if so, to investigate the mechanism which was modulated by pharmacological treatment of animals starting two weeks before the disease onset. We aimed to assess whether MO treatment could shift the time of disease onset forward, characterized by hind limb abnormal gait associated with degeneration of muscle integrity and function. It was evident that the appearance of muscle spasticity and abdominal contortion were initially visible in untreated rats SOD1tg (16 weeks of life in untreated SOD1tg rats) and later, about two weeks of delay (18 weeks of life), in rats treated with MO. Behavioral tests were a helpful tool in monitoring disease progression and MO treatment effects. Performing OFT, we established a locomotor activity of MO treated SOD1tg rats in the arena higher than untreated SOD1tg rats (Figure 14.1).

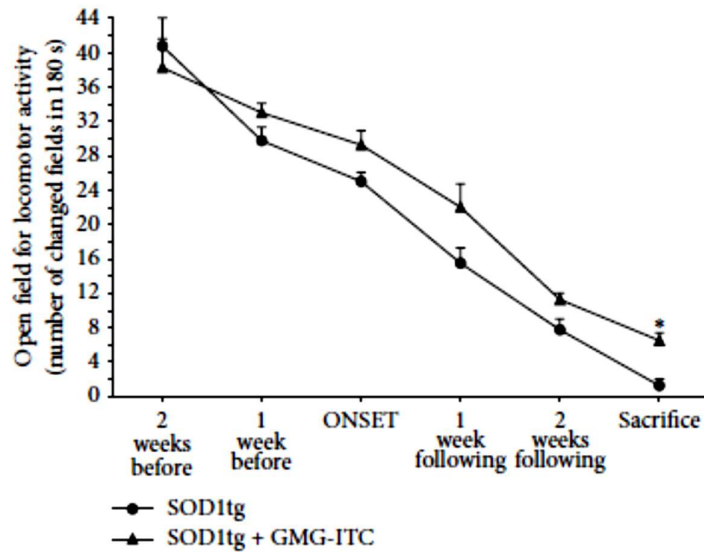


Figure 14.1 Moringin (GMG-ITC,MO) treatment delays locomotor activity loss. OFT was performed to evaluate SOD1tg rats motility in an open field, as a result of the administration or no administration of GMG-ITC treatment. Following seven measures, rats that received MO showed higher locomotor activity for the whole observational period with a significant difference at the day before the sacrifice. * $p = 0.003$.

It is noteworthy to mention that even if the motility of MO SOD1tg rats appears to decrease in the time, the last measure occurring the day before the sacrifice shows a significant difference between the two groups, leading to believe that, however, MO treatment has the capability to delay deficits by ALS. Also, WHT, often used in place of rotarod test to assess the natural course of neuromuscular disease, allowed to establish a better performance of SOD1tg rats treated with MO given by a stronger grip capability and a better muscle strength, although decreasing over time (Figure 14.2). To understand the underlying molecular and cellular mechanisms we looked at the activation of the innate and acquired immune system, since it is inextricably related to many neurodegenerative and neuromuscular diseases (Malaspina et al., 2015; Sta et al., 2011).

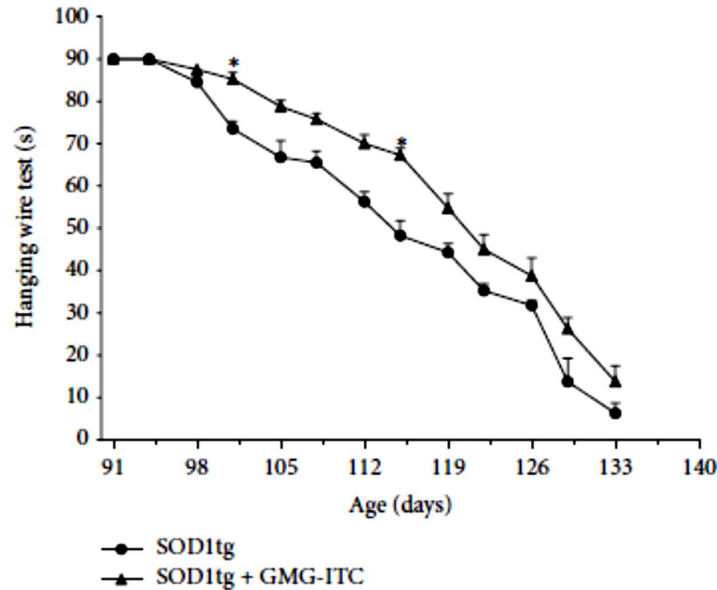


Figure 14.2 Moringin (MO; GMG-ITC) treatment delaying ALS progression maintains muscle efficiency. HWT displays an initial overlapping of performance between the two experimental groups. Nevertheless, starting from fourth test significant differences occur, showing better muscle strength and attitude in MO treated SOD1tg rats in all tests made during the experimental period. * $p = 0.002$.

As expected, we observed that both TLR4 and CD8 α detections were apparent in untreated SOD1tg rats (Figures 16.3 (a) and (c); see densitometric analysis Figure 1.9). Conversely, the effects of MO produced an immunomodulatory action reducing immune-competent cell solicitation (Figures 16.3 (b) and (d); see densitometric analysis Figure 1.9). These data have been further validated in MO treated SOD1tg rat by a high and significant FoxP3 detection, as an indirect marker of T regulatory (Treg, also known as CD4+/CD25high/FoxP3+) cell presence (Figure 14.4 (a)). Treg cell recruitment plays a key defensive role in suppression of Th1 effector cells (Dittel, 2008), which are the main T cell subtype mediating disease pathogenesis. Interestingly, it is possible that MO stimulates Th0 cell to develop into a Treg phenotype. Moreover, looking at proinflammatory cytokine profile classically activated by microglia during ALS development (Lewis et al., 2012), levels of TNF- α result significantly decreased following MO treatment (Figure 14.4 (b)). Taken together, all these parameters suggest that there is an upstream regulation of immune-inflammatory mediators as confirmed by increased PGE2 serum levels in the untreated SOD1tg rats (Shin et al., 2012) and by the modulation of this marker following MO administration (Figure 14.4 (c)). Furthermore, the influence that the prophylactic administration of MO has on ALS development is evident

assessing CK activity, an enzyme measured to monitor muscular deficit and atrophy and characteristically altered in ALS patients (Iłzecka and Stelmasiak, 2003). In fact, while no variation was detected in electrolytic balance between treated and untreated SOD1tg rats, a marked difference in serum CK was found in MO treated SOD1tg rats that show lower levels. This data demonstrated the capability of MO to interfere with motor neuron degeneration blocking radical species production, which is at the basis of many neurodegenerative diseases, including ALS (Shin et al., 2012) (Figure 14.4 (d)).

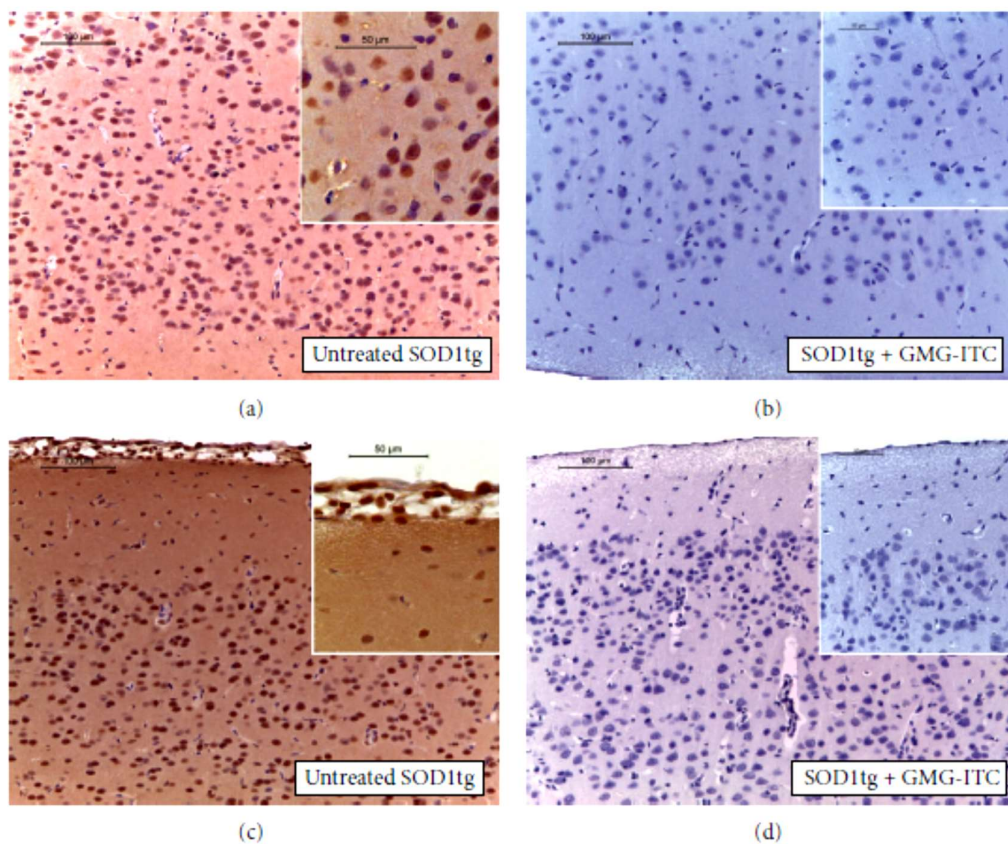


Figure 14.3 Moringin (MO; GMG-ITC) treatment modulates innate and acquired immune response. In brain sections, TLR-4 detection reveals immunopositivity in untreated SOD1tg rats (a), while SOD1tg rats treated with MO show negative staining for TLR4 (b). In untreated SOD1tg rats the immunopositivity of brain sections to CD8 antibody identified wide areas with infiltrating cells (c). MO treatment reveals the capability to counteract the release of cytotoxic T cells at level of brain sections (d).

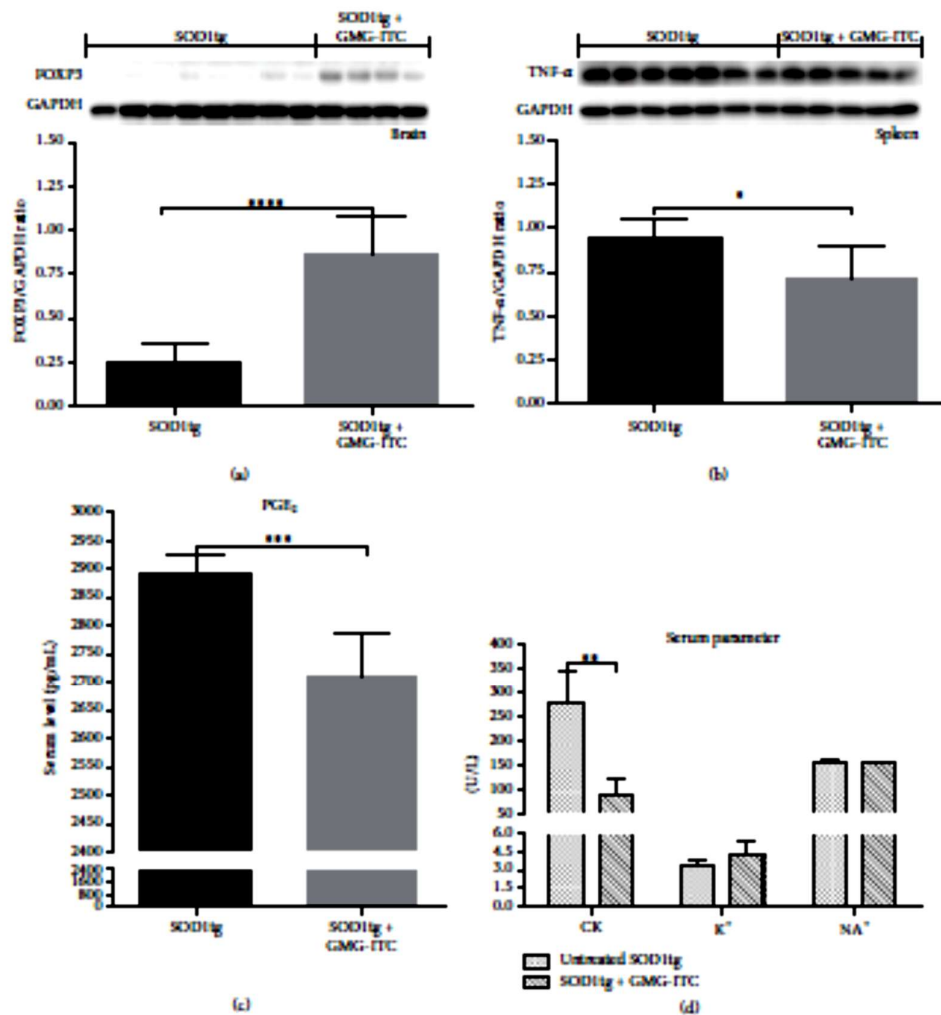


Figure 14.4 Western blot analysis of FoxP3 and TNF- α expression and serum parameters. Brain protein extracts reveal significant differences. Moringin (MO; GMG-ITC) treated SOD1tg rats present levels of FoxP3 higher than untreated animals (a) and TNF-alpha expression in spleen homogenates shows significant higher level of this marker in untreated than MO treated SOD1tg rats (b). **** $p < 0.0001$; * $p = 0.0223$. PGE₂ serum levels are significantly higher in untreated SOD1tg rats when compared with serum levels of animals treated with MO (c). *** $p = 0.0001$. About serum parameters, no electrolyte imbalance was measured in both groups looking at NA⁺/K⁺ levels, when creatine kinase (CK) enzyme was assayed, while a significant and interesting change was found comparing the CK levels of untreated SOD1tg rats higher than MO treated animals (d). ** $p = 0.008$.

Our data suggest that the high component of radicalic species is the cause of neuromuscular degeneration leading to ALS development. In this regard, it was interesting to investigate both the capability of MO to preserve brain tissue by oxidative stress and the state of the zinc dependent endopeptidase MMP9. Overall, data in literature show that this enzyme is not

specific for ALS; nevertheless, it is associated with ALS as marker of pathogenesis exerting direct neurotoxic effects or causing death by matrix proteins degradation (Łukaszewicz-Zajac, 2014). Convincing data about iNOS expression (Figure 14.5 (a) versus Figure 14.5 (b); see densitometric analysis Figure 14.9) as well as MMP-9 detection (Figure 14.5 (c) versus Figure 14.5 (d); see densitometric analysis Figure 14.9) have been produced showing tissue preservation by ALS disease in rats treated with MO. The mechanism by which MO inhibits prooxidative genes nuclear expression seems to be controlled by a nuclear factor (erythroid-derived 2)-like 2(Nrf-2)-mediated action (Figure 14.6(a) versus Figure 14.6(b); see densitometric analysis Figure 14.9). Moreover, we investigated the apoptotic pathway through different markers to evaluate how MO is able to preserve cells by dysfunction and death processes. In particular, Poly (ADP-ribose) polymerase 1 (PARP-1), which is responsible for DNA breakdown in apoptosis processes and correlated to ALS progression (Kim et al., 2004), was reduced in the MO treated rats, establishing the capability of MO to prevent tissue damage (Figure 14.6(c) versus Figure 14.6(d); see densitometric analysis Figure 14.9). Also, protective effects of MO in counteracting apoptosis are evaluable through the analysis of data regarding these markers and confirmed by the absence of apobodies in SOD1tg rats pharmacologically treated (Figures 16.7(a), 16.7(b), and 16.7(c) versus Figure 14.7(d)). A modulated cleaved-caspase 3 activity in MO treated SOD1tg rats (Figure 14.8(a)), a mediator reported to influence PARP-1 expression (Kim et al., 2004) was found. Furthermore, also a preserved neuronal cell integrity was assessed in SOD1tg rats treated with MO, resulting in normal and unaffected synaptic spine-spine communication at level of dendritic trees (Figure 14.8(b) versus Figure 14.8(c)). To compare dendritic loss, see areas in the rectangles. Finally, providing a quantification of the above displayed immunopositivity, immunohistochemical images regarding TLR-4, CD8 α , iNOS, MMP-9, Nrf-2, and PARP-1 were analyzed and the intensity was represented as % of positive staining (brown) on total tissue area (Figure 14.9).

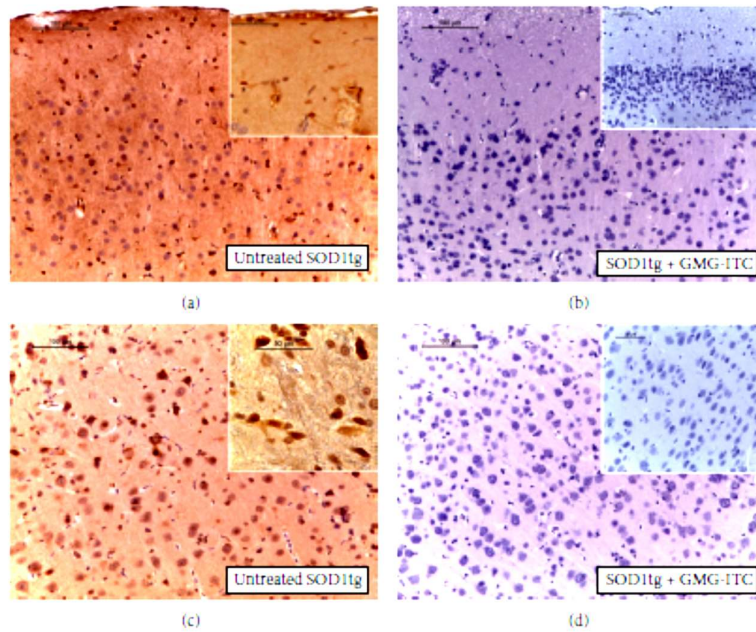


Figure 14.5 iNOS formation and MMP-9 expression. Immunohistochemical (IHC) detection of iNOS tissue expression reveals that untreated SOD1tg rats have a positive staining for this marker (a), while there is an absence of positivity in brain sections sampled from moringin (MO; GMG-ITC) treated SOD1tg rats (b). By IHC stain, brain sections sampled from untreated SOD1tg rats exhibit positive staining for MMP-9 (c), whereas brain sections obtained from MO treated SOD1tg rats do not stain for MMP-9 (d).

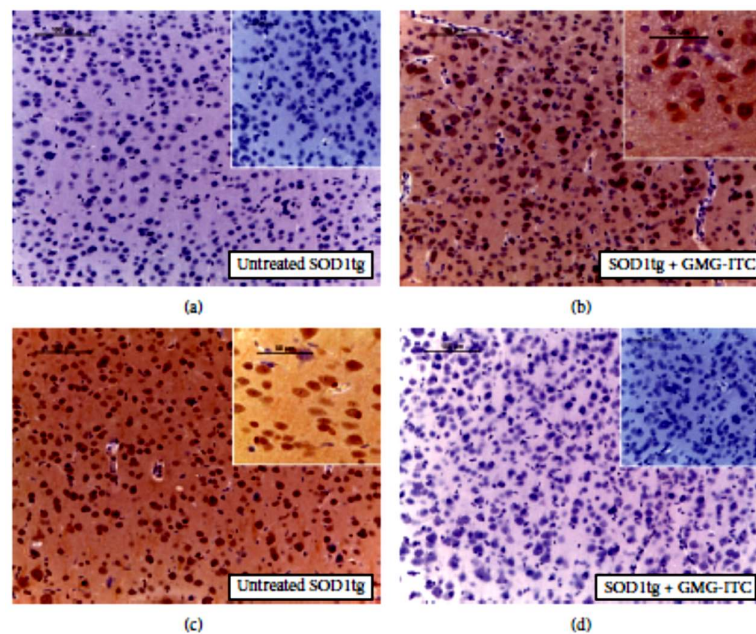


Figure 14.6 Moringin (MO; GMG-ITC) treatment promotes Nrf-2 activity and reduces PARP-1 activity. Nrf2 IHC localization shows a negative expression in brain sections sampled from untreated SOD1tg rats (a), while MO administration stimulates Nrf2 nuclear activity (b) preserving tissue damage by prooxidative gene expression. PARP-1 immunodetection shows a positive staining in untreated SOD1tg rats (c) and an IHC negative localization in MO treated SOD1tg rats (d).

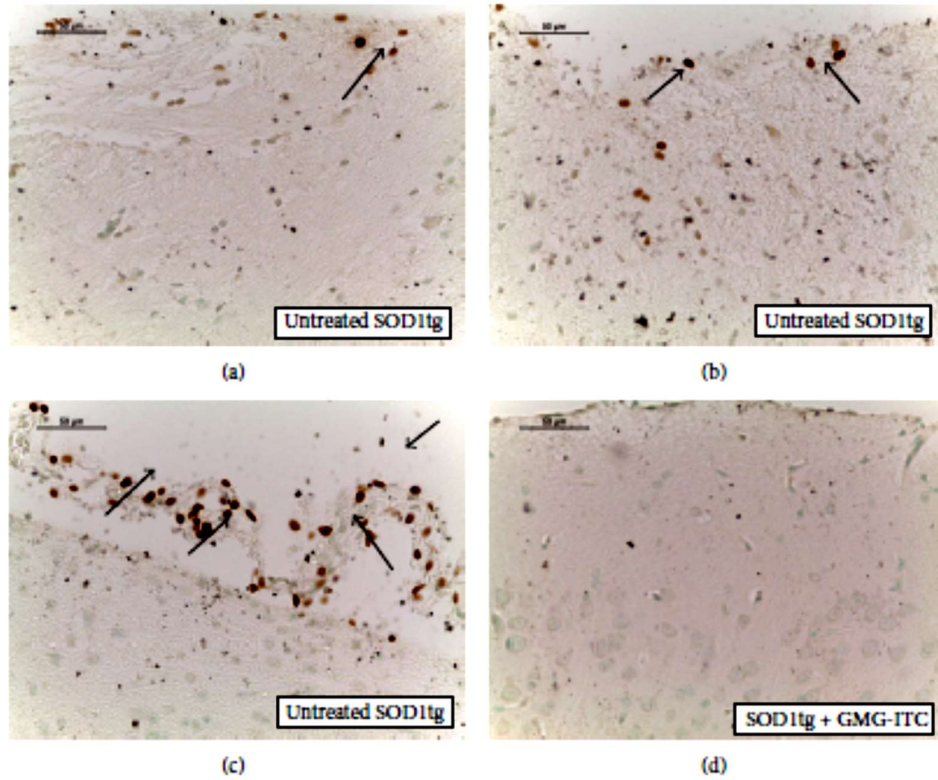
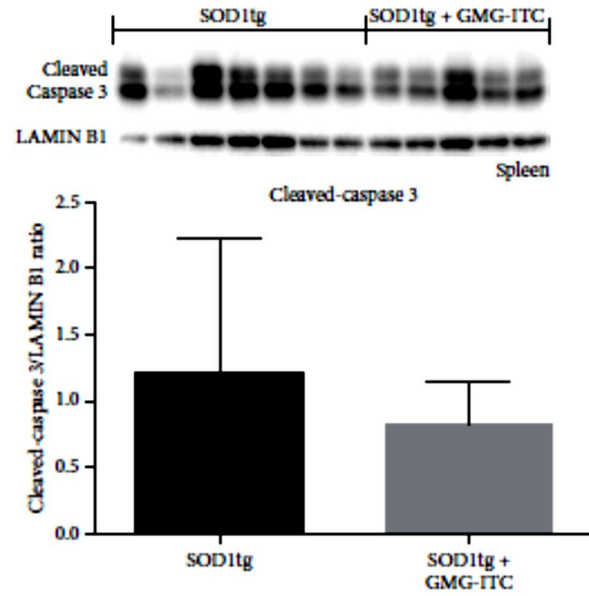
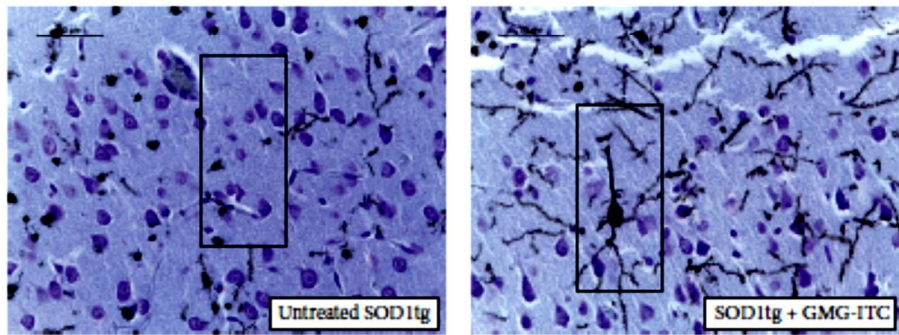


Figure 14.7 TUNEL assay for apoptosis detection. In untreated SOD1tg rats, black-brown apobodies are shown as an index of DNA breakdown (a, b, and c; see arrows). In brain sections sampled from moringin (MO; GMG-ITC) treated SOD1tg rats no apoptotic cells or fragments were present (d).



(a)



(b)

(c)

Figure 14.8 Cleaved-caspase3 activation and dendritic spine detection. Western blot analysis of spleen homogenates revealed that, although not significantly, cleaved-caspase3 levels are higher in untreated SOD1tg rats than in animals that received moringin (MO; GMG-ITC) treatment (a). Moreover, a complete loss of nerve processes was detected in untreated SOD1tg rats (b) while treatment with MO protects SOD1tg rats neurons that appear morphologically intact and with long dendrites establishing normal synapses (c).

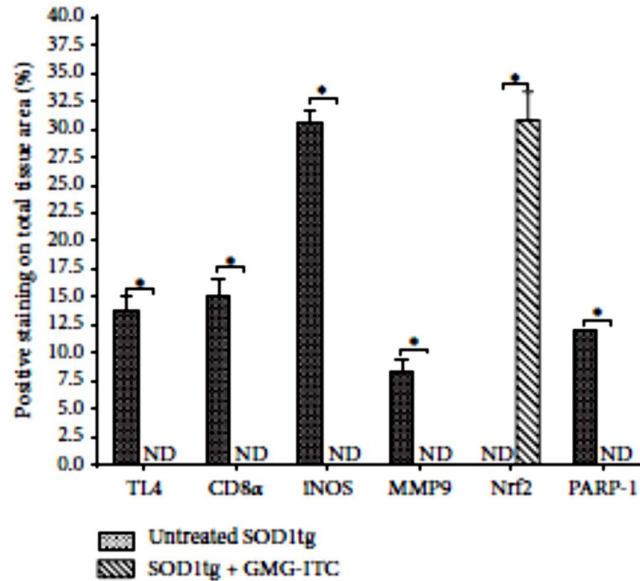


Figure 14.9 Densitometric analysis. Comparative expression between moringin (MO; GMG-ITC) treated/untreated SOD1tg rat for all evaluated immunohistochemical markers. A p value < 0.05 was considered significant. ND = not detectable.

14.4 Conclusion

The present study adds a new promising use of MO in the treatment of a so severe pathology such as ALS. SOD1tg rats, which represent a transgenic model of ALS, showed a modified phenotype following MO administration, displaying a delay in appearance of disease onset of about two weeks, and variations in serum parameters as well as in molecular and histochemical marker assessment. Overall, results support that MO treatment can interfere with the mechanisms underlying ALS development. MO, freshly produced by MYR catalyzed hydrolysis of pure GMG, could be a candidate for further studies aimed to assess its possible use in clinical practice for the prevention or attenuated progression of ALS as well as other neuromuscular pathologies.

References

Benatar M (2007) Lost in translation: treatment trials in the SOD1 mouse and in human ALS. *Neurobiology of Disease* 26(1):1-13.

Dittel BN (2008) CD4 T cells: balancing the coming and going of autoimmune-mediated inflammation in the CNS. *Brain Behavior and Immunity* 22(4):421-430.

Doi Y, Atsuta N, Sobue G, Morita M, Nakano I (2014) Prevalence and incidence of amyotrophic lateral sclerosis in Japan. *Journal of Epidemiology* 24(6):494-499.

Eisen A (1995) Amyotrophic lateral sclerosis is a multifactorial disease. *Muscle and Nerve* 18(7):741-752.

Feng J, Yan Z, Ferreira A, et al. (2000) Spinophilin regulates the formation and function of dendritic spines. *Proc Natl Acad Sci USA* 97(16):9287-9292.

Galuppo M, Giacoppo S, De Nicola GR, Iori R, Navarra M, Lombardo GE, Bramanti P, Mazzon E (2014) Antiinflammatory activity of glucomoringin isothiocyanate in a mouse model of experimental autoimmune encephalomyelitis. *Fitoterapia* 95:160-174.

Gunther R, Saal KA, Suhr M et al. (2014) The rho kinase inhibitor Y-27632 improves motor performance in male SOD1(G93A) mice. *Frontiers in Neuroscience* 8:article 304.

Halliwell B (2001) Role of free radicals in the neurodegenerative diseases: therapeutic implications for antioxidant treatment. *Drugs & Aging* 18(9):685-716.

Ihzecka J and Stelmasiak Z (2003) Creatine kinase activity in amyotrophic lateral sclerosis patients. *Neurological Sciences* 24(4):286-287.

Kim SH, Engelhardt JI, Henkel JS et al. (2004) Widespread increased expression of the DNA repair enzyme PARP in brain in ALS. *Neurology* 62(2):319-322.

Lewis C-A, Manning J, Rossi F, Krieger C (2012) The neuroinflammatory response in ALS: the roles of microglia and T cells. *Neurology Research International* ID 803701.

Li Y, Sattler R, Yang EJ, et al. (2011) Harmine, a natural beta-carboline alkaloid, upregulates astroglial glutamate transporter expression. *Neuropharmacology* 60(7-8):1168-1175.

Łukaszewicz-Zajac M, Mroczko B, Słowik A (2014) Matrix metalloproteinases (MMPs) and their tissue inhibitors (TIMPs) in amyotrophic lateral sclerosis (ALS). *Journal of Neural Transmission* 121(11):1387-1397.

Malaspina A, Puentes F, Amor S (2015) Disease origin and progression in amyotrophic lateral sclerosis: an immunology perspective. *International Immunology* 27(3):117-129.

Rafałowska J, Sulejczak D, Chrapusta SJ, Gadamski R, Dziewulska D (2014) Diverse expression of selected SMN complex proteins in humans with sporadic amyotrophic lateral sclerosis and in a transgenic rat model of familial form of the disease. *PLoS ONE* 9(8):e104614.

Shin JH, Y. A. Lee YA, Lee JK et al. (2012) Concurrent blockade of free radical and microsomal prostaglandin E synthase-1-mediated PGE production improves safety and efficacy in a mouse model of amyotrophic lateral sclerosis *Journal of Neurochemistry* 122(5):952-961.

Sta M, Sylva-Steenland RM, Casula M et al. (2011) Innate and adaptive immunity in amyotrophic lateral sclerosis: evidence of complement activation. *Neurobiology of Disease* 42(3):211-220.

Stewart A, Sandercock J, Bryan S et al. (2001) The clinical effectiveness and cost-effectiveness of riluzole for motor neuron disease: a rapid and systematic review. *Health Technology Assessment* 5(2):1-97.

CHAPTER FIFTEEN

Moringin activates Wnt canonical pathway by inhibiting GSK3 β in a mouse model of experimental autoimmune encephalomyelitis

Contents

Summary

15.1 The Wnt canonical pathway

15.2 Materials and Methods

15.2.1 Induction of experimental autoimmune encephalomyelitis

15.2.2 Experimental design

15.2.3 Myrosinase bioactivation of glucomoringin

15.2.4 Clinical disease-score evaluation

15.2.5 Immunohistochemistry

15.2.6 Western blot analysis

15.2.7 Statistical evaluation

15.3 Results

15.3.1 Moringin ameliorates clinical disease score

15.3.2 Moringin regulates the Wnt- β -catenin signaling pathway in EAE development

15.3.3 Moringin modulates apoptosis triggered by Wnt- β -catenin signaling pathway downregulation

15.3.4 Moringin regulates production of CD4 and T_{reg} cells

15.3.5 Moringin modulates neuroinflammation triggered by Wnt- β -catenin signaling pathway downregulation

15.4 Discussion

15.5 Conclusion

References

Keywords

Wnt- β -catenin pathway, GSK3 β , multiple sclerosis, moringin, glucomoringin, PPAR γ , apoptosis

Summary

Aberrant canonical Wnt- β -catenin signaling has been reported in multiple sclerosis (MS), although the results are controversial. The present study aimed to examine the role of the Wnt- β -catenin pathway in experimental MS and to test moringin (4-[α -L-rhamnopyranosyloxy]-benzyl isothiocyanate) as a modulator of neuroinflammation via the β -catenin-PPAR γ axis. Experimental autoimmune encephalomyelitis (EAE), the most common model of MS, was induced in C57BL/6 mice by immunization with MOG₃₅₋₅₅. Released moringin (10 mg Kg⁻¹ glucomoringin + 5 μ L myrosinase/mouse) was administered daily for 1 week before EAE induction and continued until mice were killed on day 28 after EAE induction. Our results clearly showed that the Wnt- β -catenin pathway was downregulated in the EAE model, whereas moringin pretreatment was able to avert this. Moringin pretreatment normalizes the aberrant Wnt- β -catenin pathway, resulting in GSK3 β inhibition and β -catenin upregulation, which regulates T-cell activation (CD4 and FoxP3), suppresses the main inflammatory mediators (IL-1 β , IL-6, and COX2), through activation of PPAR γ . In addition, moringin attenuates apoptosis by reducing the expression of the Fas ligand and cleaved caspase 9, and in parallel increases antioxidant Nrf2 expression in EAE mice. The results provided an interesting discovery in identifying moringin as a modulator of the Wnt- β -catenin signaling cascade and as a new potential therapeutic target for MS treatment.

15.1 The Wnt canonical pathway

The central logic of the Wnt- β -catenin-dependent or Wnt canonical pathway has been revealed in the past two decades. The Wnt-signaling pathway regulates many biological events occurring in the developmental and adult phases of all animals (Inestrosa and Arenas, 2010). Wnts are a family of secreted signaling proteins, which activate either β -catenin-dependent or independent intracellular pathways by binding to the seven-pass transmembrane receptors of the Frizzled family (van Amerongen et al., 2008). Generally, the Wnt1 class acts via the canonical pathway, while the Wnt5 class acts via the noncanonical pathway (Gordon and Nusse, 2006; Kikuchi et al., 2011). The key role of the canonical Wnt pathway is the stabilization of β -catenin present in the cytoplasm. When the Wnt ligand is absent, β -catenin binds with the adenomatous polyposis coli-Axin complex, which promotes β -catenin phosphorylation via the GSK3 β enzyme. Then, phosphorylated β -catenin binds with the ubiquitin complex, resulting in degradation (Gordon and Nusse, 2006; Aberle et al., 1997). Wnt signaling prevents GSK3 β activity, and thus increases the amount of β -catenin, which translocates into the nucleus and associates with TCF/LEF transcription factors, leading to the regulation of Wnt target genes (Gordon and Nusse, 2006).

Wnt- β -catenin signaling is involved in the development of sensory and motor neurons present in the brain and spinal cord via regulation of all facets of neuronal activities, including differentiation, proliferation/senescence, and survival/apoptosis (Patapoutian and Reichardt, 2000; Ciani and Salinas, 2005). Moreover, Wnt-signaling pathway aberrations are associated with the adulthood diseases of the central nervous system (CNS), which points to its critical role in the development of the mature CNS (Inestrosa and Arenas, 2010; Oliva et al., 2013). Growing evidence shows the importance of the Wnt- β -catenin pathway to stabilize neuronal cell survival and death in neurodegenerative diseases, such as Alzheimer's disease and Parkinson's disease (Inestrosa and Arenas, 2010; Toledo et al., 2008; Grand et al., 2015; Berwick and Harvey, 2012). In addition, the Wnt- β -catenin pathway seems to be involved in the pathogenesis and modulation of chronic pain in experimental autoimmune encephalomyelitis (EAE) mice (Yuan et al., 2012), the most commonly used model for multiple sclerosis (MS). However, the role of the Wnt canonical pathway in MS is still unclear. MS is a chronic inflammatory disease caused by an induction of autoreactive immune responses effected from T and B lymphocytes, which results in the demyelination of the myelin sheath

around neurons in the CNS (Trapp and Nave, 2008; Goverman, 2009). It is noteworthy to emphasize that the present-day treatments for MS provide palliative relief, but do not cure the disease. Moreover, these treatments trigger many side effects that hinder their application for a prolonged period (Weber et al., 2012). Therefore, new drugs that may act on the underlying etiology with no side effects are urgently required to treat MS. In the last few decades, PPAR γ , an important target for diabetes treatment (Willson et al., 2001) has aroused great interest for its therapeutic role in brain disorders (Haneka et al., 2007). In addition, since PPAR γ is linked with the Wnt- β -catenin pathway (Lecarpentier et al., 2014; Sabatino et al., 2014) identifying novel PPAR γ activators through Wnt- β -catenin pathway regulation has become a promising therapeutic approach for brain diseases. In the present study, we investigated moringin (4-[α -l-rhamnopyranosyloxy]-benzyl isothiocyanate, MO) as a modulator of neuroinflammation via the β -catenin-PPAR γ axis in an experimental model of MS.

15.2 Materials and Methods

15.2.1 Induction of experimental autoimmune encephalomyelitis

This study was carried out in strict accordance with the recommendations of the guide for the care and use of laboratory animals of the National Institutes of Health. The protocol was approved by the Ministry of Health “General Direction of animal health and veterinary drugs” and this study was approved by “Animal Welfare Bodies” of IRCCS Centro Neurolesi Bonino-Pulejo, Messina, Italy. Animal care followed Italian regulations on the protection of animals used for experimental and other scientific purposes (D.lgs 26/2014). All efforts were made during experimental procedures, to minimize animal suffering and to reduce the number of animal used. Male C57BL/6 mice (20–25 g) were anesthetized with an anesthetic cocktail consisting of tiletamine plus xylazine (10 mL Kg⁻¹ intraperitoneally). EAE was induced in mice using the peptide MOG_{35–55} (MEVGWYRSPFSRVVHLYRNGK, peak area by HPLC 95%; AnaSpec Inc., Fremont, CA, USA), based on Paschalidis et al. (2009). Mice were subcutaneously injected with 300 μ L/flank of the suspension consisting of an equal volume of 300 μ g MOG_{35–55} in PBS and complete Freund’s adjuvant consisting of 300 μ g heat-killed *Mycobacterium tuberculosis* H37Ra (BD, Franklin Lakes, NJ, USA). After MOG_{35–55} injection, the animals

immediately received an intraperitoneal injection of 100 μL *Bordetella pertussis* toxin (500 ng/100 μL ; Sigma-Aldrich Co., St Louis, MO, USA) and 48 hours later. EAE induction followed a sequence of progressive degeneration with visible signs, such as tail flaccidity and loss of hind-leg movement.

15.2.2 Myrosinase bioactivation of glucomoringin

GMG and MYR were purified as described at Chapter ten (see Section 10.5) and Chapter nine (see Section 9.2.2), respectively.

Pure GMG (95%) was dissolved in PBS solution pH 7.2 at room temperature (2.5 mg mL⁻¹) and hydrolyzed by the action of MYR (5 μL ; 32 U mL⁻¹) for 15 min at 37 °C right before animal treatment. Mice were then administered the resulting solution as such.

15.2.3 Experimental design

Mice were randomly separated into the following groups (n=35 total animals):

1. naïve group (n=5) – mice without any injection, serving as controls.
2. MO control group (n=5) – mice not subjected to EAE induction but injected with MO (10 mg/kg GMG + 5 μL MYR/mouse), killed as controls of drug safety and tolerance.
3. MYR control group (n=5) – mice not subjected to EAE damage, but only injected with MYR (5 μL MYR/mouse) to evaluate possible side effects, including allergenic reactions after administration.
4. EAE group (n=10) – mice receiving MOG injection.
5. EAE + MO (n=10) – MOG-injected mice administered with MO (10 mg Kg⁻¹ GMG + 5 μL MYR/mouse); MO administered intraperitoneally daily for 1 week before EAE induction and continued daily after EAE induction until death.

After 28 days of EAE induction, mice were killed and spinal cord tissues collected and processed for further analyses.

15.2.4 Clinical disease-score evaluation

Mice showed initial signs of MS, including loss of tail tonus, hind-limb paralysis, and loss of body weight, after 14 days of EAE induction. Clinical neurological score was assessed according to a standardized scoring system (Rodrigues et al., 2010): 0, no visible signs; 1, partial flaccid tail; 2, complete flaccid tail; 3, hind limb hypotonia; 4, partial hind-limb paralysis; 5, complete hind-limb paralysis; and 6, moribund or dead animal. Mice with a clinical score ≥ 5 were killed to avoid animal suffering. The following clinical disease parameters were assessed: incidence, day of onset of clinical signs, peak disease score, cumulative disease score (CDS), and mortality (Table 15.1). The first assessment of neurological disease score was measured on the day of EAE induction (day 0), and all subsequent assessments were performed every 48 hours until mice were killed. Days' difference in the disease parameter is reported compared to the day of EAE induction (day 0). Days are reported as mean \pm standard error of mean of all mice for each experimental set.

Table 15.1 Clinical parameters of EAE

Group	Incidence (%)	Day of disease onset (mean \pm SD)	Peak disease (mean \pm SD)	Cumulative disease score (mean \pm SD)	Mortality
EAE	100	12.2 \pm 0.62	3.72 \pm 0.3	28.21 \pm 10.4	0/10
EAE + moringin	100	14.3 \pm 0.5	1.26 \pm 0.2*	7.91 \pm 1.07*	0/10
Naïve	0	0	0	0	0/5

* $P < 0.005$ compared to EAE group. incidence was calculated as the percentage of mice that displayed any clinical signs of disease. One-way multiple comparisons with Tukey's test were used to determine the statistical significance of differences. All data calculated from two experiments. Day of onset: first day mice showed clinical signs; peak of disease: maximum score observed between days 0 and 28; cumulative disease score, mean of sum of daily scores observed between days 0 and 28. Abbreviations: EAE, experimental autoimmune encephalomyelitis; SD, standard deviation.

15.2.5 Immunohistochemistry

Spinal cord tissues removed from the cervical region were fixed in 10% (w/v) PBS-buffered formaldehyde and embedded in paraffin. The tissues were cut into 7 μ m sections. After deparaffinization, tissues were incubated with 0.3% (v/v) hydrogen peroxide in 60% (v/v)

methanol for 30 minutes to terminate endogenous peroxidase activity. Then, the tissue sections were blocked in 2% (v/v) normal goat serum in PBS for 20 minutes at room temperature.

Tissue sections were incubated overnight with the following primary antibodies:

- anti-IL-1 β polyclonal antibody (1:50 in PBS v/v; Santa Cruz Biotechnology Inc., Dallas, TX, USA)
- anti-IL-6 polyclonal antibody (1:100 in PBS v/v; Abcam, Cambridge, UK)
- anti-Fas-ligand polyclonal antibody (1:100 in PBS v/v; Abcam)
- anti-cleaved caspase-9 monoclonal antibody (1:200 in PBS v/v; Abcam)
- anti-CD4 polyclonal antibody (1:100 in PBS v/v; Santa Cruz Biotechnology Inc.)
- anti-FoxP3 monoclonal antibody (1:100 in PBS v/v; Santa Cruz Biotechnology Inc.).

To avoid endogenous cross-reactivity of biotin- or avidin-binding sites, tissue sections were blocked separately with biotin and avidin for 15 minutes. Tissue sections were rinsed with PBS and incubated with secondary antibody. Specific labeling was performed using a biotin-conjugated antirabbit IgG and avidin–biotin peroxidase complex (VectaStain; Vector Laboratories, Burlingame, CA, USA). Then, the tissue sections were stained using a DAB peroxidase-substrate kit (Vector Laboratories), followed by hematoxylin counterstaining. In addition, tissue sections were incubated with either primary or secondary antibody to assess antibody specificity. In these cases, no positive staining was observed in the tissue sections, indicating that the immunoreactions were positive in all the experiments carried out. Immunohistochemical staining was evaluated using light microscopy (Leica DM 2000 combined with Leica ICC50 HD camera), and images were acquired by Leica Application Suite version 4.2.0 software.

15.2.6 Western blot analysis

Spinal cord tissues were homogenized in ice-cold extraction buffer consisting of 0.32 M sucrose, 10 Mm Tris–HCl (pH 7.4), 5 Mm NaN₃, 2 Mm ethylenediaminetetraacetic acid (EDTA), 1 Mm ethyleneglycoltetraacetic acid (EGTA), 50 Mm NaF, 10 Mm 2-mercaptoethanol, and protease-inhibitor tablets (Hoffman-La Roche Ltd, Basel, Switzerland). The homogenates were kept on ice for 15 minutes, centrifuged (1,000 *g* for 10 minutes at 4°C), and the supernatant removed to estimate cytosolic proteins. The pellets were resuspended in ice-cold

lysis buffer consisting of 10 Mm Tris–HCl (Ph 7.4), 150 Mm NaCl, 1 Mm EDTA, 1 Mm EGTA, 1% Triton X-100, and protease-inhibitor tablets. The resuspended pellets were kept on ice for 10 minutes, centrifuged (15,000× *g* for 30 minutes at 4°C), and the supernatant removed to estimate nuclear proteins. Supernatants were preserved at -80°C until use. The quantity of protein was calculated with protein-assay reagent (Bio-Rad Laboratories Inc., Hercules, CA, USA). Bovine serum albumin was used as the standard. Proteins (30 µg) were resolved on sodium dodecyl sulfate polyacrylamide minigels (8% or 12%) and transferred onto polyvinylidene difluoride membranes (Immobilon-P transfer membrane; EMD Millipore). After transfer, membranes were blocked with PBS containing 5% nonfat dried milk (PBS-milk (PM)) for 1 hour at room temperature, and incubated for overnight at 4°C overnight with specific antibodies: Wnt1 (1:250; Santa Cruz Biotechnology), β-catenin (1:500; Cell Signaling Technology, Danvers, MA, USA), CK2α (1:250; Santa Cruz Biotechnology Inc.), GSK3β (1:250; Santa Cruz Biotechnology Inc.), p-β-catenin (1:500; Santa Cruz Biotechnology Inc.), PPARγ (1:250; Santa Cruz Biotechnology Inc.), COX2 (1:250; Santa Cruz Biotechnology Inc.), and Nrf2 (1:250; Santa Cruz Biotechnology Inc.). Then, membranes were washed in PBS and incubated with horseradish peroxidase-conjugated antimouse, -goat, or -rabbit IgG secondary antibody (1:2,000; Santa Cruz Biotechnology Inc.) for 1 hour at room temperature. Membranes were stripped and reprobred with β-actin (1:1,000; Santa Cruz Biotechnology Inc.) to confirm uniform protein loading. Protein bands were detected by an enhanced chemiluminescence system (Luminata Western; EMD Millipore), and images were taken by ChemiDoc™ MP (Bio-Rad Laboratories Inc.) and quantified for relative expression of proteins using ImageJ software.

15.2.7 Statistical evaluation

Statistical analysis was performed using GraphPad Prism version 6.0 (GraphPad Software, Inc., La Jolla, CA, USA). The data were statistically analyzed by one-way analysis of variance and Bonferroni post hoc tests for multiple comparisons. A *P*-value ≤0.05 was considered statistically significant. Data are reported as mean ± standard error of mean of *n* experiments.

15.3 Results

15.3.1 Moringin ameliorates clinical disease score

Clinical disease score was evaluated as a functional neurological parameter. EAE is a well-documented model of MS in the mouse and resembles the hallmarks of the disease, such as paralysis, loss of body weight, inflammation, demyelination in the CNS and blood–brain barrier leakage (Constantinescu et al., 2011). To study the role of MO in regulating susceptibility to EAE, mice were pretreated with the phytochemical and immunized with MOG_{35–55}. The mice were monitored every 48 hours to assess clinical EAE signs. Compared to the EAE group, MO pretreated mice showed a significant reduction in disease incidence and average CDS. The lower CDS in the EAE + MO group was also reflected as a significant reduction in the severity of disease (Table 15.1). Indeed, EAE mice displayed a chronic-progressive clinical course, while significant reduction in clinical score was observed in EAE mice pretreated with MO. No sign of motor deficits was noticed in naïve animals (Figure 15.1B). These results suggest that MO reduces disease progression and increases recovery of neurological function in EAE mice.

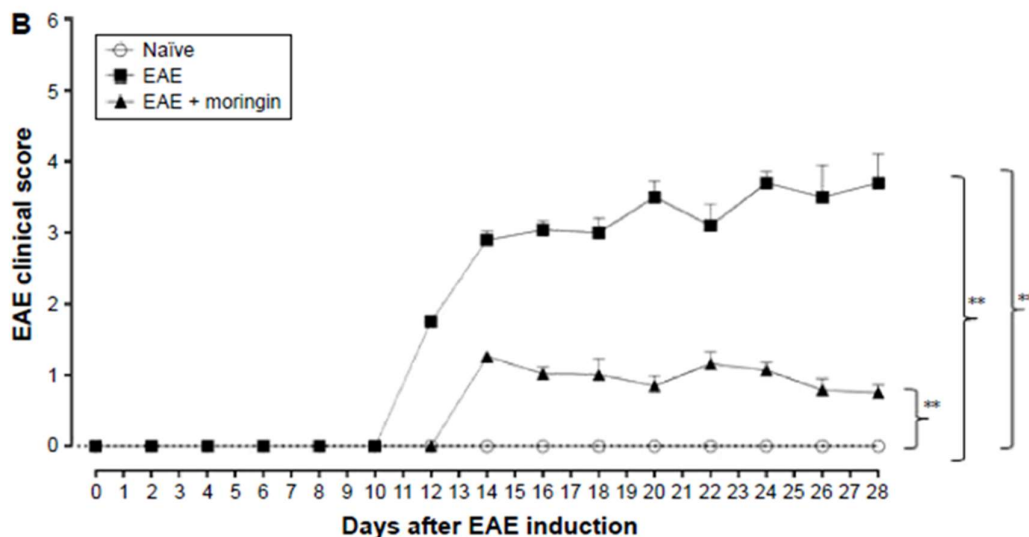


Figure 15.1 Treatment with moringin (MO) ameliorates clinical score in EAE (experimental autoimmune encephalomyelitis) mice. Scores are expressed as mean \pm SEM of all measurements of each experimental group. Naïve group (n=5), EAE group (n=10), EAE+ MO (n=10). Naïve vs EAE, ** $P=0.0018$; naïve vs EAE + MO, ** $P=0.005$; EAE vs EAE + MO, ** $P=0.0019$. One way-analysis of

variance with Bonferroni test were used to determine the statistical significance of differences. Data are expressed as mean \pm SEM (standard error of mean).

15.3.2 Moringin regulates the Wnt- β -catenin signaling pathway in EAE development

Western blot analysis was performed to observe the modulation of the Wnt- β -catenin signaling pathway after EAE induction in mouse spinal cord. Results showed that the Wnt- β -catenin canonical pathway was downregulated in EAE mice. Lower Wnt1 expression (Figure 15.2A) was found in spinal cord tissues taken from EAE mice compared to naïve and control ones, which led to enhanced expression of GSK3 β (Figure 15.2B), which acts synergistically with CK2 α (Figure 15.2C) in the multiprotein complex that phosphorylates cytoplasmic β -catenin, encouraging its ubiquitination and degradation. Indeed, β -catenin nuclear translocation was prevented in spinal cord tissues taken from EAE mice (Figure 15.2D), whereas cytoplasmic p- β -catenin expression was increased (Figure 15.2E). On the contrary, MO pretreatment positively regulated the Wnt- β -catenin signaling pathway in EAE mice. As demonstrated by Western blot analysis performed in spinal cord tissues, increased Wnt1 expression was found in pretreated EAE mice compared to untreated ones (Figure 15.2A). In addition, MO pretreatment reduced the expression levels of GSK3 β and CK2 α (Figure 15.2B and C), by inhibiting phosphorylation of cytoplasmic β -catenin (Figure 15.2D). These results were further corroborated by enhanced expression of β -catenin in the nucleus (Figure 15.2E).

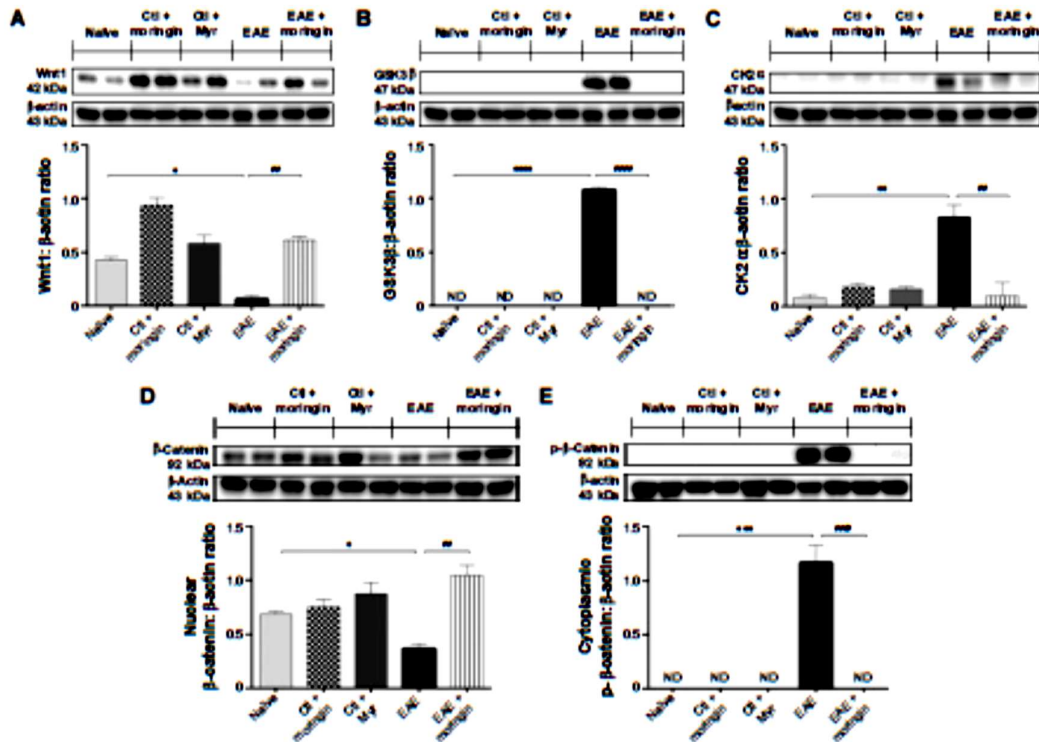


Figure 15.2 Moringin (MO) modulates the Wnt–β-catenin signaling pathway in EAE. Western blot analysis for Wnt1 (A). Naïve vs EAE, * $P=0.0108$; EAE vs EAE + MO, ### $P=0.0014$. Western blot analysis for GSK3β (B). Naïve vs EAE, **** $P,0.0001$; EAE vs EAE + MO, #### $P,0.0001$. Western blot analysis for CK2α. (C). Naïve vs EAE, ** $P=0.0022$; EAE vs EAE + MO, ### $P=0.0024$. Western blot analysis for β-catenin (D). Naïve vs EAE, * $P=0.0112$; EAE vs EAE + MO, ## $P=0.0028$. Western blot analysis for p-β-catenin (E). Naïve vs EAE, *** $P=0.0002$; EAE vs EAE + MO, #### $P=0.0002$. All Western blot analyses were performed on spinal cord tissues sampled at 28 days from EAE induction. β-Actin was used as internal control. Blots are representative of three separate and reproducible experiments. Statistical analysis was carried out on three repeated blots performed on separate experiments. One way-analysis of variance with Bonferroni test were used to determine the statistical significance of differences, Data are expressed as mean ± SEM. Abbreviations: EAE, experimental autoimmune encephalomyelitis; Ctl, control; ND, not detectable.

15.3.3 Moringin modulates apoptosis triggered by Wnt–β-catenin signaling pathway downregulation

To investigate apoptosis, we studied Fas-ligand expression by immunohistochemistry in spinal cord sections. Results showed negative staining for Fas in naïve mice (Figure 15.3A), MO controls (Figure 15.3B), and MYR control mice (Figure 15.3C). On the contrary, marked immunopositivity for Fas in untreated EAE mice (Figure 15.3D, arrows) was found. MO pretreated EAE mice showed negative staining for Fas (Figure 15.3E). It is well known that

activation of caspases is involved in apoptosis induction. Negative staining of cleaved caspase 9 was observed in naïve mice (Figure 15.4A), as well as in control groups (Figure 15.4B and C). Immunohistochemistry results also showed that cleaved caspase-9 level was considerably increased in EAE mice (Figure 15.4D). MO pretreatment totally suppressed the level of cleaved caspase 9 (Figure 15.4E).

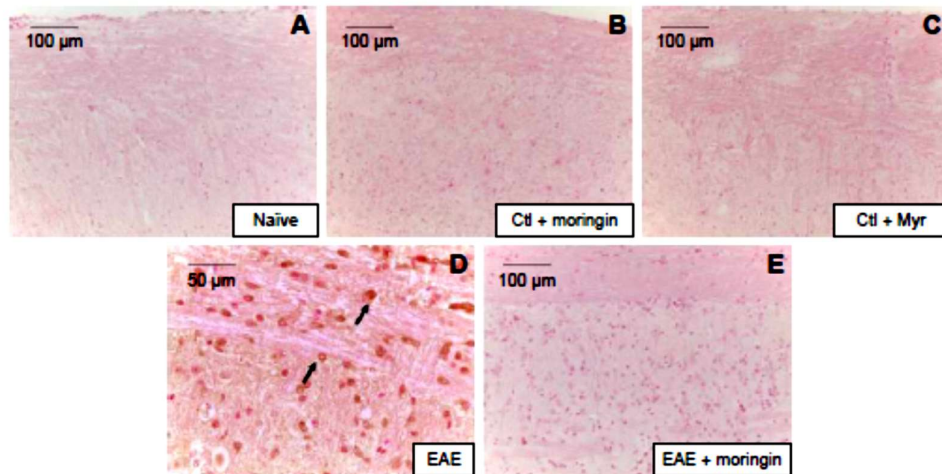


Figure 15.3 Moringin (MO) modulates Fas-ligand expression in EAE. Immunohistochemical localization for Fas ligand in spinal cord tissues from naïve mice (A), Ctl + MO (B), Ctl + MYR (C), EAE mice (D), and EAE mice pretreated with MO (E). All images are representative of three independent experiments. The arrows indicate positive staining for Fas-ligand in cytoplasmic membranes of spinal cord tissues. Abbreviations: EAE, experimental autoimmune encephalomyelitis; Ctl, control.

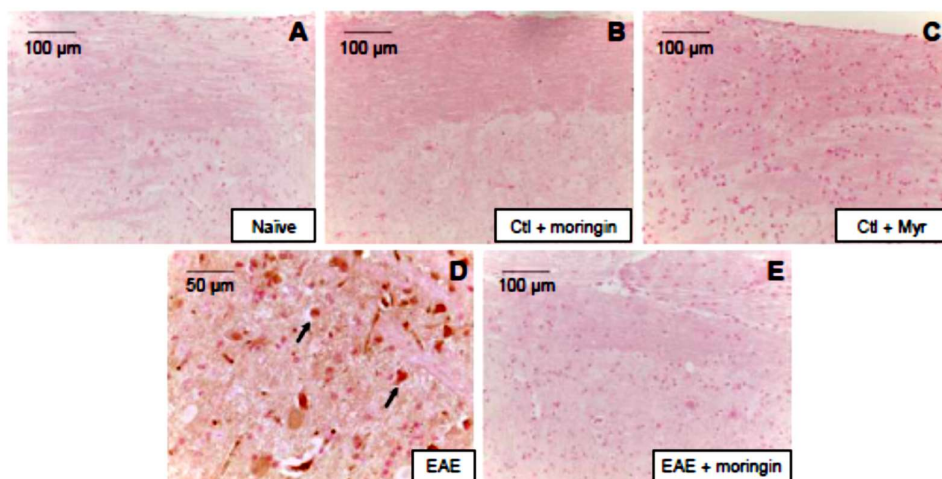


Figure 15.4 Moringin (MO) modulates cleaved caspase-9 expression in EAE. Immunohistochemical localization for cleaved caspase 9 in naïve mice (A), Ctl + MO (B), Ctl + MYR (C), EAE mice (D), and EAE mice pretreated with MO (E). All images are representative of three independent experiments. The arrows indicate positive staining for cleaved caspase-9 in nuclei of spinal cord tissues. Abbreviations: EAE, experimental autoimmune encephalomyelitis; Ctl, control.

15.3.4 Moringin regulates production of CD4 and T_{reg} cells

CD4 T-cell expression is involved in cell-mediated immunity and the pathogenesis of MS, with destruction of the axonal myelin sheath in several areas of the spinal cord mediated mainly by self-reactive CD4 T cells. Immunohistochemical analysis performed in spinal cord sections showed negative staining for CD4 in naïve (Figure 15.5A), MO controls (Figure 15.5B), and MYR control mice (Figure 15.5C). Positive staining for CD4 was observed in EAE mice (Figure 15.5D); conversely, no positive staining for CD4 expression was obtained in mice pretreated with MO (Figure 15.5E). In addition, to verify whether treatment with MO could modulate the production of regulatory T (T_{reg}) cells, we evaluated expression of the transcription factor FoxP3 by immunohistochemical analysis. Our results showed negative staining for FoxP3 in naïve mice (Figure 15.6A) and in MO, as well as the MYR control group (Figure 15.6B and C). Spinal cord sections from EAE mice showed positive staining for FoxP3 (Figure 15.6D), which was not observed in the tissues of EAE mice pretreated with MO (Figure 15.6E).

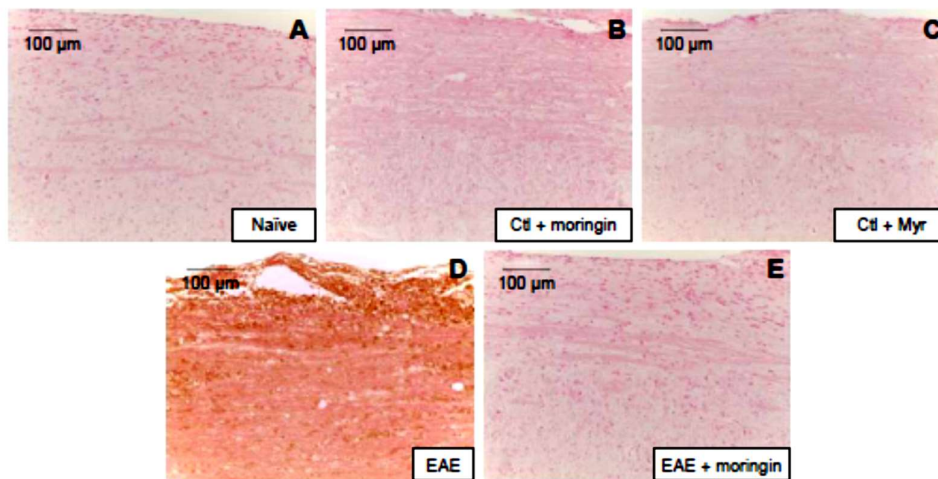


Figure 15.5 Moringin (MO) modulates CD4 expression in EAE. Immunohistochemical evaluation for CD4 in naïve mice (A), Ctl + MO (B), Ctl + MYR (C), EAE mice (D), and EAE mice pretreated with (MO) (E). All images are representative of three independent experiments.

Abbreviations: EAE, experimental autoimmune encephalomyelitis; Ctl, control.

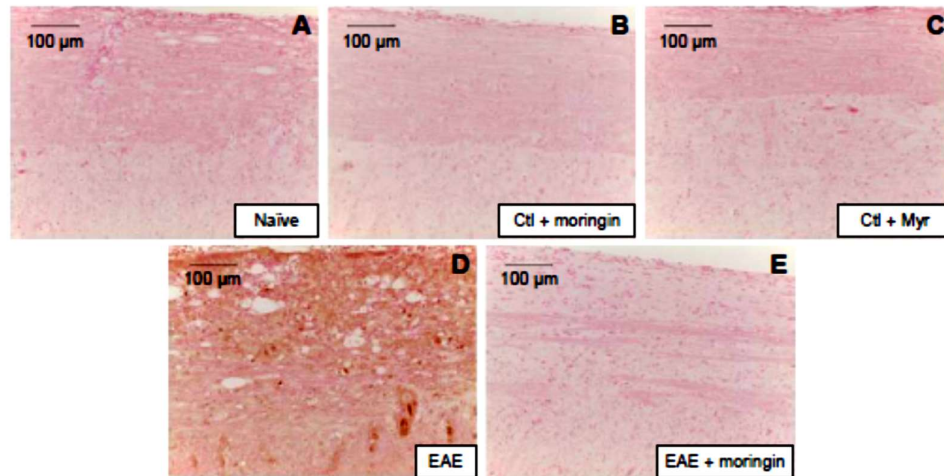


Figure 15.6 Moringin (MO) modulates FoxP3 expression in EAE. Immunohistochemical evaluation for FoxP3-naïve mice (A), Ctl + MO (B), Ctl + MYR (C), EAE mice (D), and EAE mice pretreated with MO (E). All images are representative of three independent experiments. Abbreviations: EAE, experimental autoimmune encephalomyelitis; Ctl, control.

15.3.5 Moringin modulates neuroinflammation triggered by Wnt- β -catenin signaling pathway downregulation

Enhanced expression of proinflammatory cytokines has been associated with many neurodegenerative diseases, including MS. Furthermore, as it is known that Wnt- β -catenin signaling can regulate cytokine production, we analyzed the expression of IL-1 β and IL-6 in spinal cord tissues collected from EAE untreated and MO pretreated EAE mice by immunohistochemical staining. No positive staining for IL-1 β (Figure 15.7A) or IL-6 (Figure 15.8A) was obtained in naïve mice, in the MO control group (Figures 7B and 8B), or in MYR ones (Figures 7C and 8C), while high levels of these proinflammatory mediators were noticed in spinal cord tissues of EAE mice. Specifically, positive inflammatory cells are indicated by arrows in spinal cord sections stained with IL-1 β and IL-6 (Figures 7D and 8D, respectively) and arrowheads show vascular endothelium positive for IL-6 (Figure 15.8D). Negative staining for IL-1 β and IL-6 was observed in spinal cord tissues from EAE mice pretreated with MO (Figures 7E and 8E, respectively). In addition, we investigated COX2 expression by Western blot analysis (Figure 15.9A). A basal level of COX2 was detected in naïve animals and control groups, while its level was significantly increased in EAE mice. MO pretreated EAE mice showed reduced COX2 expression. In addition, we investigated whether

MO could be a potential activator of PPAR γ via Wnt- β -catenin signaling. By Western blot analysis, a mild increase in PPAR γ expression was found in EAE mice, while administration of MO markedly increased PPAR γ levels. Neither naïve mice nor the MYR control group showed any expression for PPAR γ , whereas the MO control group showed PPAR γ expression (Figure 15.9B). Moreover, since it is widely recognized that isothiocyanates (ITCs) exert their protective effects by the capacity to induce expression of several enzymes via the Keap1-Nrf2-ARE pathway (Hu et al., 2004; Dinkova-Kostova et al., 2002) we investigated expression of Nrf2. By Western blot analysis, we found that MO pretreatment enhanced Nrf2 expression in EAE mouse spinal cord, while in untreated EAE mice, Nrf2 was absent (Figure 15.9C).

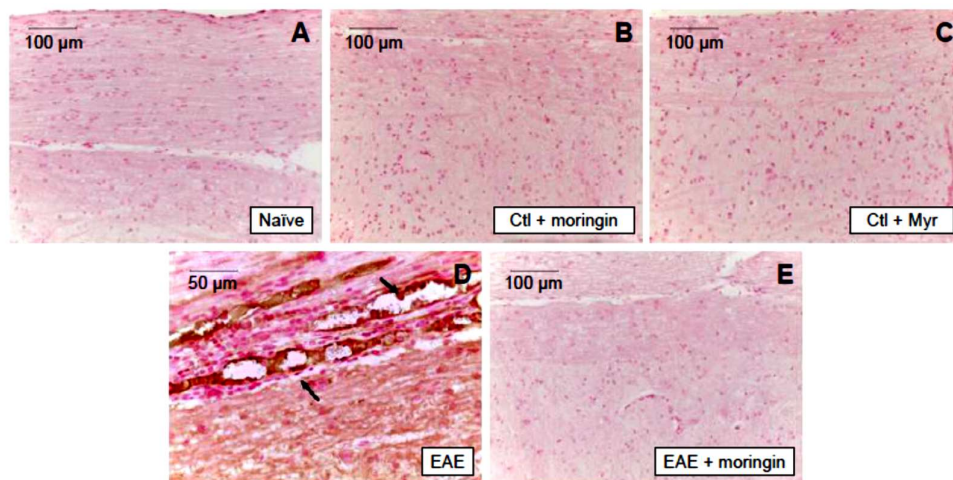


Figure 15.7 Moringin (MO) modulates IL-1 β expression in EAE. Immunohistochemical localization for IL-1 β in spinal cord tissues from naïve mice (A), Ctl + MO (B), Ctl + MYR (C), EAE mice (D), and EAE mice pretreated with MO (E). All images are representative of three independent experiments. The arrows indicate positive staining for inflammatory cells in vascular endothelium of spinal cord tissues.

Abbreviations: EAE, experimental autoimmune encephalomyelitis; Ctl, control.

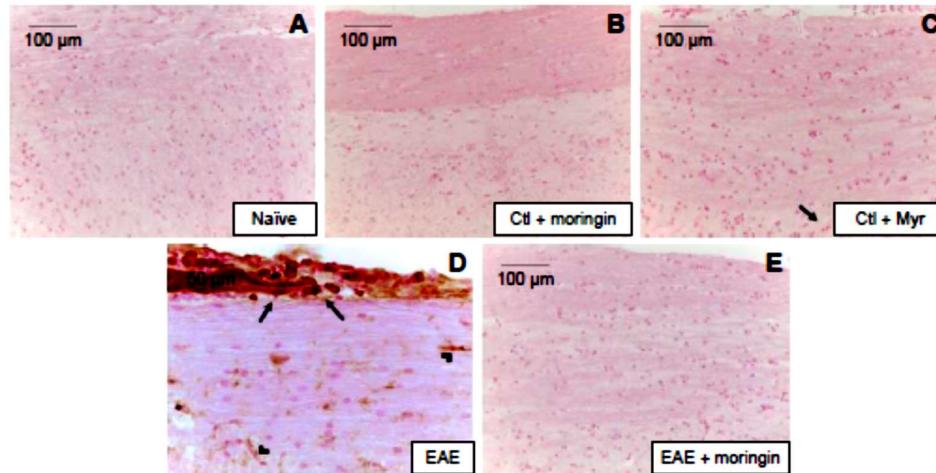


Figure 15.8 Moringin (MO) modulates IL-6 expression in EAE. Immunohistochemical evaluation for IL-6 in naïve mice (A), Ctl + MO (B), Ctl + MYR (C), EAE mice (D), and EAE mice pretreated with MO (E). All images are representative of three independent experiments. The arrows indicate positive staining for inflammatory cells in vascular endothelium of spinal cord tissues. Abbreviations: EAE, experimental autoimmune encephalomyelitis; Ctl, control.

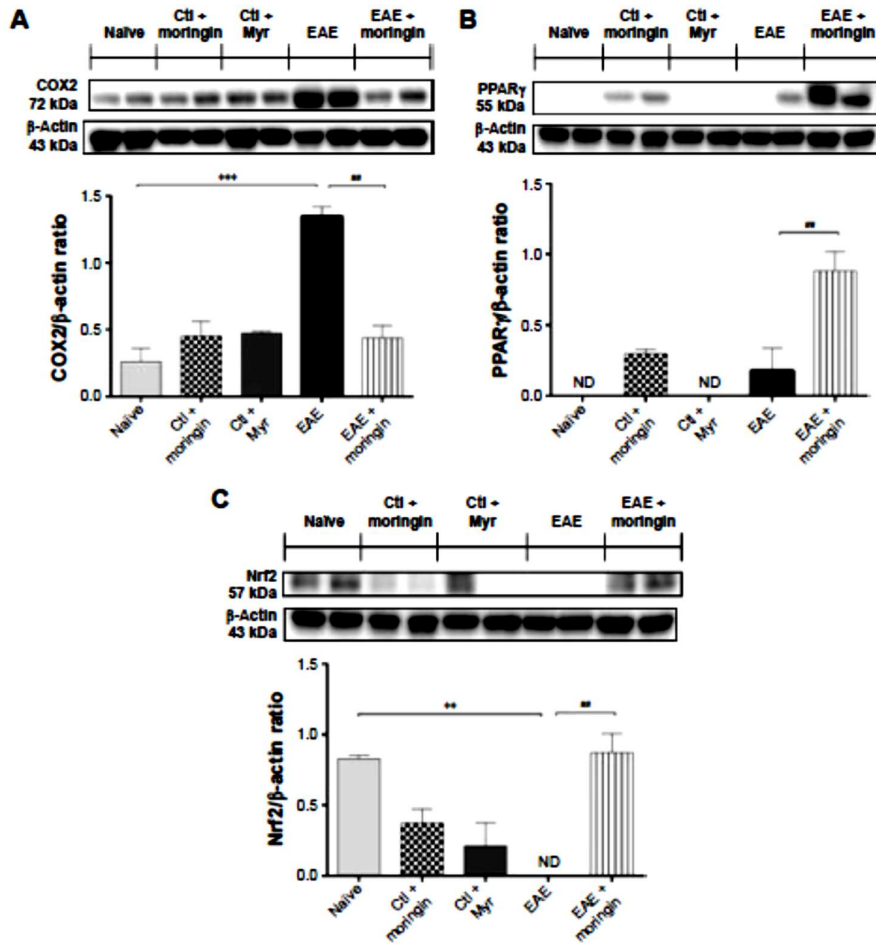


Figure 15.9 Moringin (MO) modulated inflammatory mediators and Nrf2 activity in EAE. Western blot analysis for COX2 (A). Naive vs EAE, *** $P=0.0005$; EAE vs EAE + MO, # $P=0.0012$. Western blot analysis for PPAR γ (B). EAE vs EAE + MO, # $P=0.0038$. Western blot analysis for Nrf2 (C). Naive vs EAE, ** $P=0.0039$; EAE vs EAE + MO, # $P=0.003$. All Western blot analyses were performed on spinal cord tissues sampled at 28 days from EAE induction. β -Actin was used as internal control. Blots are representative of three separate and reproducible experiments. Statistical analysis was carried out on three repeated blots performed on separate experiments. Data are expressed as mean \pm SEM. Abbreviations: EAE, experimental autoimmune encephalomyelitis; Ctl, control; ND, not detectable.

15.4 Discussion

MS is documented as the most common root of neurological disability (Nosworthy et al., 2000). Recent research has described the importance of the Wnt- β -catenin signaling pathway for normal functioning of the adult CNS, and its aberration has been reported in degenerative and inflammatory CNS diseases, like MS (Inestrosa and Arenas, 2010; Toledo et al., 2008; Yuan et al., 2012; Marchetti and Pluchino, 2013). Moreover, Wnt signaling has been reported in

immune cells present in the CNS, such as macrophages, microglia, and astrocytes, suggesting the critical role of the Wnt pathway in inflammation mediated CNS injury and recovery (Halleskog et al., 2011; L'Episcopo et al., 2011). Although it is well known that the Wnt canonical pathway can modulate the immune system by repressing the inflammatory process during MS, the role of the Wnt canonical pathway in regulating remyelination remains controversial (Xie et al., 2014). Some studies have supported the notion that the Wnt- β -catenin pathway may act as a negative modulator of the remyelination process, via inhibiting oligodendrocyte differentiation and myelin formation (Fancy et al., 2009; Shimizu et al., 2005; Gaesser and Fyffe-Maricich; 2016). Conversely, results from recent studies suggested that the Wnt canonical pathway may promote remyelination (Marchetti and Pluchino, 2013; Hanafy and Sloane, 2011; Ye et al., 2009). In the present study, we evaluated the involvement of the Wnt- β -catenin pathway in the etiopathology of an experimental EAE model and also tested MO as a modulator of neuroinflammation via the β -catenin-PPAR γ axis. In accordance with previous studies (Yuan et al., 2012; Swafford and Manicassamy, 2015) our results showed that the canonical Wnt- β -catenin pathway is inactivated in EAE development. We found that in mice subjected to EAE, cytoplasmic β -catenin was constantly phosphorylated by increased expression of CK2 α and GSK3 β , which inhibited nuclear translocation of β -catenin and consequent activation of Wnt target genes involved in cell survival. The enhanced activity of CK2 α and GSK3 β was paralleled by Wnt1 suppression. Moreover, upregulation of GSK3 β induced the degradation of β -catenin, which resulted in apoptosis of neurons. Apoptosis was confirmed by significant positive staining for proapoptotic Fas and cleaved caspase 9 in the spinal cord sections of EAE mice. Pretreatment with MO markedly ameliorated the clinical score induced by EAE. Interestingly, MO pretreatment reverted the abnormal Wnt- β -catenin signaling of EAE mice. We found that MO reduced levels of CK2 α and GSK3 β , which in turn increased Wnt1 and nuclear β -catenin levels. Reduction in GSK3 β expression was further supported by the absence of cytoplasmic phosphorylated β -catenin, which resulted in the attenuation of apoptosis, evidenced by reduction in Fas and cleaved caspase 9. Moreover, we noticed that in the spinal cord of EAE mice, CD4 and FoxP3 levels were elevated, which indicated engagement and infiltration of T_{reg} cells in the CNS. MOG-induced activation of CD4+/Foxp3+ T_{reg} cells have been already demonstrated in EAE mice (Zorzella-Pezavento et al., 2013). The proinflammatory mediators IL-1 β , IL-6, and COX2 were also increased. MO repressed EAE-associated T_{reg}-cell activation by diminishing CD4 and FoxP3 levels.

Additionally, MO decreased IL-1 β , IL-6, and COX2 levels in EAE mice. Indeed, similar suppression of T-cell response in EAE has been previously demonstrated by sulforaphane, (Geisel et al., 2014; Li et al., 2013). From our findings, we propose that MO may control EAE associated T_{reg}-cell molecules via Wnt-signaling activation. It is well known that the Wnt-signaling pathway regulates T-cell activation (van Loosdregt et al., 2013; Staal et al., 2008). Increased Wnt1/ β -catenin levels and decreased GSK3 β level in MO administered EAE mice corroborated our notion, suggesting the active inhibition of MOG induced T-cell activation via the MO mediated Wnt-signaling pathway. Studies in recent years have demonstrated the beneficial efficacy of PPAR γ agonists in the treatment of MS and other neurodegenerative diseases to suppress inflammatory and oxidative stress (Drew et al., 2008; Kaundal and Sharma, 2010; Mrak and Landreth, 2004). Since PPAR γ is associated with the Wnt- β -catenin pathway (Lecarpentier et al., 2014; Sabatino et al., 2014) we investigated whether MO could be a potential activator of PPAR γ via Wnt- β -catenin signaling. We observed a mild increase in PPAR γ levels in EAE mice, which might have resulted from an innate anti-inflammatory response. Interestingly, EAE mice administered with MO exhibited marked upregulation in PPAR γ expression. We assume that the observed reduction of the proinflammatory mediators IL-1 β , IL-6, and COX2 in MO treated EAE mice might be attributed to elevated levels of PPAR γ . Moreover, MO pretreatment augmented antioxidant Nrf2 expression in EAE mice. It has been well documented that ITCs may exert their antioxidative effects by Nrf2 activation (Dinkova-Kostova et al., 2002; Ernst et al., 2013). Of note, it is important to emphasize that GSK3 β downregulation increases Nrf2 expression (Dinkova-Kostova et al., 2002). We assume that the enhanced expression of Nrf2 might have resulted from the MO regulated reduction of GSK3 β . Our results are in line with previous studies, where it has been reported that R/S-sulforaphane, increased the level of Nrf2 by reducing GSK3 β expression (Rada et al., 2012; Shang et al., 2015; Rojo et al., 2008). Figure 15.10 shows a graphic representation of β -catenin signaling-mediated PPAR γ and Nrf2 regulation in the presence or absence of Wnt.

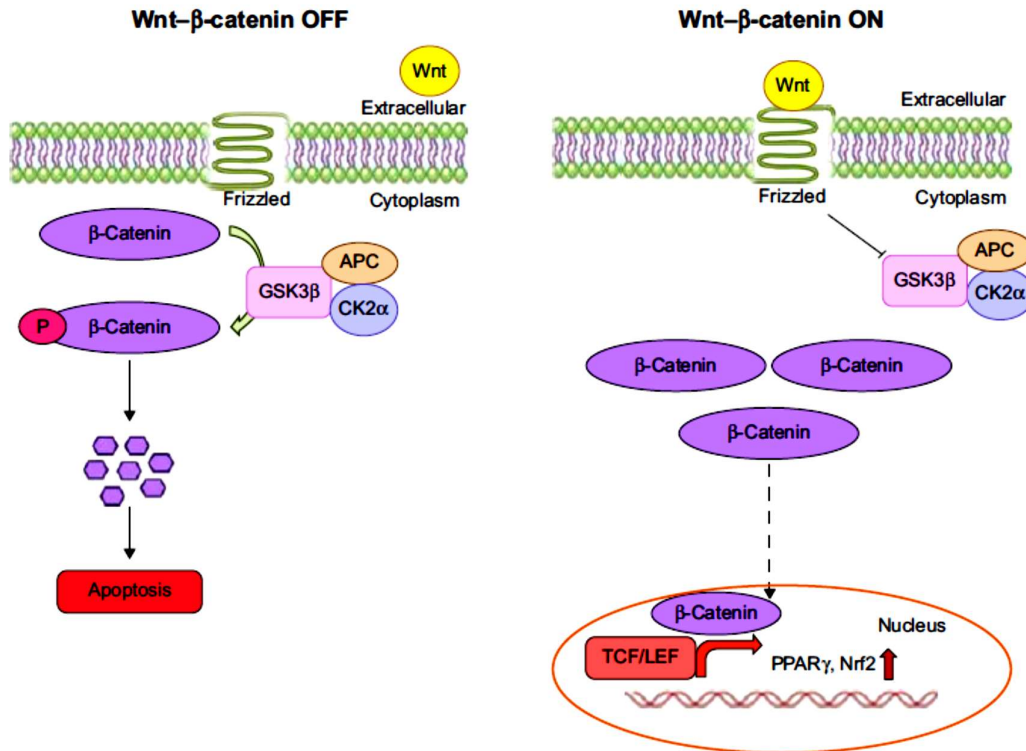


Figure 15.10 Wnt-β-catenin canonical pathway. In the absence of the Wnt ligand (off), β-catenin is phosphorylated by the destruction complex formed by Axin, APC, CK2α, and GSK3β, leading to β-catenin degradation and subsequent induction of neuronal cell death. In the presence of the Wnt ligand, the Wnt canonical pathway is activated (on), and β-catenin is not phosphorylated by the destruction complex formed by Axin, APC, CK2α, and GSK3β. Therefore, β-catenin is free to translocate into the nucleus, where it binds with the TCF/LEF transcription factors and promotes the transcription of Wnt target genes.

15.5 Conclusion

The results of the presented study demonstrated that in a mice model of EAE, MO normalizes the aberrant Wnt-β-catenin pathway and inhibits GSK3β. Furthermore, MO suppresses proinflammatory mediators via PPARγ activation and attenuates apoptosis. Therefore, MO could be considered as a potential PPARγ agonist in the treatment of MS.

References

Aberle H, Bauer A, Stappert J, Kispert A, Kemler R (1997) β -Catenin is a target for the ubiquitin-proteasome pathway. *EMBO J* 16(13):3797-3804.

Berwick DC and Harvey K (2012) The importance of Wnt signalling for neurodegeneration in Parkinson's disease. *Biochem Soc Trans* 40(5):1123-1128.

Ciani L and Salinas PC (2005) Wnts in the vertebrate nervous system: from patterning to neuronal connectivity. *Nat Rev Neurosci* 6(5):351-362.

Constantinescu CS, Farooqi N, O'Brien K, Gran B (2011) Experimental autoimmune encephalomyelitis (EAE) as a model for multiple sclerosis (MS). *Br J Pharmacol* 164(4):1079-1106.

Dinkova-Kostova AT, Holtzclaw WD, Cole RN, et al. (2002) Direct evidence that sulfhydryl groups of Keap1 are the sensors regulating induction of phase 2 enzymes that protect against carcinogens and oxidants. *Proc Natl Acad Sci USA* 99(18):11908-11913.

Drew PD, Xu J, Racke MK (2008) PPAR- γ : therapeutic potential for multiple sclerosis. *PPAR Res* 2008:627463.

Ernst IM, Palani K, Esatbeyoglu T, Schwarz K, Rimbach G (2013) Synthesis and Nrf2-inducing activity of the isothiocyanates iberberin, iberin and cheirolin. *Pharmacol Res* 70(1):155-162.

Fancy SP, Baranzini SE, Zhao C, et al. (2009) Dysregulation of the Wnt pathway inhibits timely myelination and remyelination in the mammalian CNS. *Genes Dev* 23(13):1571-1585.

Gaesser JM and Fyffe-Maricich SL (2016) Intracellular signaling pathway regulation of myelination and remyelination in the CNS. *Exp Neurol Epub* 2016 Mar 5.

Geisel J, Brück J, Glocova I, et al. (2014) Sulforaphane protects from T cell-mediated autoimmune disease by inhibition of IL-23 and IL-12 in dendritic cells. *J Immunol* 192(8):3530-3539.

Gordon MD and Nusse R (2006) Wnt signaling: multiple pathways, multiple receptors, and multiple transcription factors. *J Biol Chem* 281(32):22429-22433.

Goverman J (2009) Autoimmune T cell responses in the central nervous system. *Nat Rev Immunol* 9(6):393-407.

Halleskog C, Mulder J, Dahlström J, et al. (2011) Wnt signaling in activated microglia is proinflammatory. *Glia* 59(1):119–131.

Hanafy KA and Sloane JA (2011) Regulation of remyelination in multiple sclerosis. *FEBS Lett* 585(23):3821-3828.

Heneka MT, Landreth GE, Hull M (2007) Drug insight: effects mediated by peroxisome proliferator-activated receptor- γ in CNS disorders. *Nat Clin Pract Neurol* 3(9):496-504.

Hu R, Hebbar V, Kim BR, et al. (2004) In vivo pharmacokinetics and regulation of gene expression profiles by isothiocyanate sulforaphane in the rat. *J Pharmacol Exp Ther* 310(1):263-271.

Inestrosa NC and Arenas E (2010) Emerging roles of Wnts in the adult nervous system. *Nat Rev Neurosci* 11(2):77-86.

Kaundal RK and Sharma SS (2010) Peroxisome proliferator-activated receptor γ agonists as neuroprotective agents. *Drug News Perspect* 23(4):241–256.

Kikuchi A, Yamamoto H, Sato A, Matsumoto S (2011) New insights into the mechanism of Wnt signaling pathway activation. *Int Rev Cell Mol Biol* 291:21-71.

Kim H, Won S, Hwang DY, et al. (2011) Downregulation of Wnt/ β -catenin signaling causes degeneration of hippocampal neurons in vivo. *Neurobiol Aging* 32(12):2316.e1–e15.

Lecarpentier Y, Claes V, Duthoit G, Hebert JL (2014) Circadian rhythms, Wnt/ β -catenin pathway and PPAR α/γ profiles in diseases with primary or secondary cardiac dysfunction. *Front Physiol* 5:429.

Le Grand JN, Gonzalez-Cano L, Pavlou MA, Schwamborn JC (2015) Neural stem cells in Parkinson's disease: a role for neurogenesis defects in onset and progression. *Cell Mol Life Sci* 72(4):773-797.

L'Episcopo F, Tirolo C, Testa N, et al. (2011) Reactive astrocytes and Wnt/ β -catenin signaling link nigrostriatal injury to repair in 1-methyl-4-phenyl-1,2,3,6-tetrahydropyridine model of Parkinson's disease. *Neurobiol Dis* 41(2):508–527.

Li B, Cui W, Liu J, et al. (2013) Sulforaphane ameliorates the development of experimental autoimmune encephalomyelitis by antagonizing oxidative stress and Th17-related inflammation in mice. *Exp Neurol* 250:239-249.

Marchetti B and Pluchino S (2013) Wnt your brain be inflamed? Yes, it Wnt! *Trends Mol Med* 19(3):144–156.

Mrak RE and Landreth GE (2004) PPAR γ , neuroinflammation, and disease. *J Neuroinflammation* 1(1):5.

Noseworthy JH, Lucchinetti C, Rodriguez M, Weinshenker BG (2000) Multiple sclerosis. *N Engl J Med* 343(13):938-952.

Oliva CA, Vargas JY, Inestrosa NC (2013) Wnts in adult brain: from synaptic plasticity to cognitive deficiencies. *Front Cell Neurosci* 7:224.

Paschalidis N, Iqbal AJ, Maione F, et al. (2009) Modulation of experimental autoimmune encephalomyelitis by endogenous annexin A1. *J Neuroinflammation* 6:33.

Patapoutian A and Reichardt LF (2000) Roles of Wnt proteins in neural development and maintenance. *Curr Opin Neurobiol* 10(3):392-399.

Rada P, Rojo AI, Evrard-Todeschi N, et al. (2012) Structural and functional characterization of Nrf2 degradation by the glycogen synthase kinase 3/ β -TrCP axis. *Mol Cell Biol* 32(17):3486-3499.

Rojo AI, Rada P, Egea J, Rosa AO, Lopez MG, Cuadrado A (2008) Functional interference between glycogen synthase kinase-3 β and the transcription factor Nrf2 in protection against kainate-induced hippocampal cell death. *Mol Cell Neurosci* 39(1):125-132.

Rodrigues DH, Vilela MC, Barcelos LS, Pinho V, Teixeira MM, Teixeira AL (2010) Absence of PI3K γ leads to increased leukocyte apoptosis and diminished severity of experimental autoimmune encephalomyelitis. *J Neuroimmunol* 222(1–2):90-94.

Sabatino L, Pancione M, Votino C et al. (2014) Emerging role of the β -catenin-PPAR γ axis in the pathogenesis of colorectal cancer. *World J Gastroenterol* 20(23):7137-7151.

Shang G, Tang X, Gao P, et al. (2015) Sulforaphane attenuation of experimental diabetic nephropathy involves GSK-3 β /Fyn/Nrf2 signaling pathway. *J Nutr Biochem* 26(6):596-606.

Shimizu T, Kagawa T, Wada T, Muroyama Y, Takada S, Ikenaka K (2005) Wnt signaling controls the timing of oligodendrocyte development in the spinal cord. *Dev Biol* 282(2):397-410.

Staal FJ, Luis TC, Tiemessen MM (2008) Wnt signalling in the immune system: Wnt is spreading its wings. *Nat Rev Immunol* 8(8):581-593.

Swafford D and Manicassamy S (2015) Wnt signaling in dendritic cells: its role in regulation of immunity and tolerance. *Discov Med* 19(105):303-310.

Toledo EM, Colombres M, Inestrosa NC (2008) Wnt signaling in neuroprotection and stem cell differentiation. *Prog Neurobiol* 86(3):281-296.

Trapp BD and Nave KA (2008) Multiple sclerosis: an immune or neurodegenerative disorder? *Annu Rev Neurosci* 31:247-269.

van Amerongen R, Mikels A, Nusse R (2008) Alternative Wnt signaling is initiated by distinct receptors. *Sci Signal* 1(35):re9.

van Loosdregt J, Fleskens V, Tiemessen MM, et al. (2013) Canonical Wnt signaling negatively modulates regulatory T cell function. *Immunity* 39(2):298-310.

Weber MS, Menge T, Lehmann-Horn K et al. (2012) Current treatment strategies for multiple sclerosis: efficacy versus neurological adverse effects. *Curr Pharm Des* 18(2):209-219.

Willson TM, Lambert MH, Kliewer SA (2001) Peroxisome proliferator-activated receptor gamma and metabolic disease. *Annu Rev Biochem* 70:341-367.

Xie C, Li Z, Zhang GX, Guan Y (2014) Wnt signaling in remyelination in multiple sclerosis: friend or foe? *Mol Neurobiol* 49(3):1117-1125.

Ye F, Chen Y, Hoang T, et al. (2009) HDAC1 and HDAC2 regulate oligodendrocyte differentiation by disrupting the β -catenin-TCF interaction. *Nat Neurosci* 12(7):829-838.

Yuan S, Shi Y, Tang SJ (2012) Wnt signaling in the pathogenesis of multiple sclerosis-associated chronic pain. *J Neuroimmune Pharmacol* 7(4):904-913.

Zorzella-Pezavento SF, Chiuso-Minicucci F, Franca TG, et al. (2013) Persistent inflammation in the CNS during chronic EAE despite local absence of IL-17 production. *Mediators Inflamm* 2013:519627.

CHAPTER SIXTEEN

Moringin shows anti-inflammatory activity in the treatment of murine subacute Parkinson's disease

Contents

Summary

- 16.1** Parkinson's disease
- 16.2** Materials and Methods
 - 16.2.1** MPTP-induced subacute Parkinson's Disease
 - 16.2.2** Experimental design
 - 16.2.3** Myrosinase bioactivation of glucomoringin
 - 16.2.4** Body weight loss and behavioral test
 - 16.2.5** Immunohistochemistry on mouse brain tissues
 - 16.2.6** Golgi stain
 - 16.2.7** Cell culture conditions, drug treatment, and immunohistochemistry analysis
 - 16.2.8** Western blot analysis
 - 16.2.9** Statistical evaluation
- 16.3** Results
 - 16.3.1** Moringin avoids body weight changes and ameliorates motor deficits in MPTP mice
 - 16.3.2** Moringin prevents the decreasing of tyrosine hydroxylase expression and improves the neuronal dendrite in MPTP mice
 - 16.3.3** Moringin modulates the inflammatory pathways in MPTP mice
 - 16.3.4** Moringin modulates oxidative stress markers in MPTP mice
 - 16.3.5** Moringin pretreatment inhibits apoptosis in MPTP mice
 - 16.3.6** Moringin modulates the inflammatory pathways in LPS-activated mouse macrophage RAW 264.7
 - 16.3.7** Moringin modulates oxidative stress markers in LPS-activated mouse macrophage RAW 264.7
- 16.4** Discussion
- 16.5** Conclusion

References

Keywords

Glucomoringin; moringin, MPTP experimental model; RAW 264.7 macrophages; proinflammatory cytokines.

Summary

The present study was aimed at estimating a possible neuroprotective effect of glucomoringin (GMG) [4-(α -L-rhamnopyranosyloxy)benzyl glucosinolate] bioactivated with the enzyme myrosinase to form the corresponding isothiocyanate (4-(α -L-rhamnopyranosyloxy)benzyl C; moringin) in the treatment or prevention of Parkinson's disease (PD). The beneficial effects of moringin were compared with those of pure GMG in an *in vivo* experimental mouse model of subacute PD. Subacute PD was induced in C57BL/6 mice by administration of 1-methyl-4-phenyl-1,2,3,6-tetrahydropyridine (MPTP). Mice were pretreated daily for 1 week with moringin (GMG 10 mg Kg⁻¹ + 5 μ L MYR/mouse) and with GMG (10 mg Kg⁻¹). Behavioral evaluations were also performed to assess motor deficits and bradykinesia in MPTP mice. Besides, if pretreatment with moringin could modulate the triggering of inflammatory cascade with a correlated response, we tested its *in vitro* anti-inflammatory activity by using a model of RAW 264.7 macrophages stimulated with lipopolysaccharide. Achieved results *in vivo* showed a higher efficacy of moringin compared with GMG to modulate the inflammatory pathway as well as the oxidative stress and the apoptotic pathways. In addition, the better effectiveness of moringin in countering mainly the inflammatory pathway has been corroborated by the results obtained *in vitro*.

16.1 Parkinson's disease

Parkinson's disease (PD) is the second most common progressive neurodegenerative disorder after Alzheimer's disease that occurs mostly in older persons, but can also appear, although with a lower frequency, in young patients. Worldwide, estimated 7 to 10 million people are thought to be affected and men are 1.5 times more likely to develop PD than women (Beitz, 2014). PD is primarily characterized by extensive and progressive degeneration of dopaminergic (DA) neurons in the substantia nigra pars compacta (SNpc) with subsequent loss of dopamine in the striatum and the presence of Lewy bodies, consisting of alpha-synuclein aggregates (Braak et al., 2004; Dawson and Dawson, 2003). The neuronal connection between substantia nigra and the striatum is essential for normal motor functions of the brain; deterioration of these neurons results in dopamine depletion, which leads to major pathological hallmarks of PD (Rai et al., 2015). Although the etiology and pathogenesis of PD remain not completely understood, increasing evidences indicate oxidative stress as one of the major pathophysiological mechanisms associated with PD (Blesa et al., 2015; Jenner, 1991). However, it is still unclear whether an increase in oxidative damage, observed during progression of disease, may be the primary cause or, instead, a consequence of upstream inflammatory and excitotoxicity events. To date, DA replacement with levodopa or DA agonists is the most effective treatment against PD. Although such drugs are effective in the early stages of the disease, long-term therapy has been associated with serious adverse effects (Ceravolo et al., 2016). Over the last decade, to discover new alternative therapies for PD, basic science has focused on the discovery of natural products as a source of potent and effective antioxidant agents in the treatment of this devastating pathology.

In the present study, we investigated the neuroprotective effects of MO and we compared its efficacy with GMG in an *in vivo* 1-methyl-4-phenyl-1,2,3,6-tetrahydropyridine (MPTP)-induced subacute PD model. To provide further evidence for the potential molecular mechanisms underlying MO bioactivity, we studied its anti-inflammatory and antioxidative effects in the mouse macrophage cell line, RAW 264.7, stimulated with lipopolysaccharide (LPS).

16.2 Materials and Methods

16.2.1 MPTP-induced subacute Parkinson's Disease

Subacute PD was induced in male C57BL/6 mice by injection of MPTP hydrochloride (Sigma-Aldrich), as recognized by Langston et al. (1983). In our experimental design, five injections of MPTP (20 mg Kg⁻¹) were performed 24 hours apart to produce subacute symptoms.

16.2.2 Myrosinase bioactivation of glucomoringin

GMG and MYR were purified as described at Chapter ten (see Section 10.5) and Chapter nine (see Section 9.2.2), respectively.

Pure GMG (95%) was dissolved in PBS solution pH 7.2 at room temperature (2.5 mg mL⁻¹) and hydrolyzed by the action of MYR (5 µl; 32 U mL⁻¹) for 15 min at 37 °C right before animal treatment. Mice were then administered the resulting solution as such.

16.2.3 Experimental design

Mice were randomly allocated into the following groups (N=55 total animals):

1. NAIVE group (N=5): mice not subjected to MPTP damage or to any injection, sacrificed as control;
2. MPTP group (N=10): mice received five injections of MPTP (20 mg Kg⁻¹, intraperitoneal [i.p.]) 24 hours apart;
3. MPTP + MO group (N=10): mice were pretreated daily for 1 week with moringin (10 mg Kg⁻¹ GMG + 5 µL MYR/mouse, i.p.) before MPTP administration (20 mg Kg⁻¹, i.p.) 24 hours apart, then treatment was protracted until the sacrifice;
4. MO control group (N=5): mice not subjected to MPTP damage, but injected with MO (10 mg Kg⁻¹ GMG + 5 µL MYR/mouse, i.p.), sacrificed as control of drug safety and tolerance;

5. MPTP + GMG group (N = 10): mice were pretreated daily for 1 week with pure GMG (10 mg Kg⁻¹, i.p.) before the five injections of MPTP (20 mg Kg⁻¹, i.p.) 24 hours apart, then treatment was protracted until the sacrifice;
 6. GMG control group (N=5): mice not subjected to MPTP damage, but injected with GMG (10 mg Kg⁻¹, i.p.), sacrificed as control of drug safety and tolerance;
 7. MYR control group (N=5): mice not subjected to MPTP damage, but only injected with MYR (5 µL MYR/mouse, i.p.) to evaluate possible side effects, including allergic reactions after administration;
 8. Vehicle group (N=5): mice not subjected to MPTP damage, but only injected with MO or GMG vehicle (phosphate-buffered saline) as control of the treatment.
- At the 14th day from subacute PD induction, all animals were euthanized, and brain tissues were sampled and processed to evaluate parameters of the disease.

16.2.4 Body weight loss and behavioral test

The measure of the body weight was assessed every 48 hours, and any loss was registered as marker of pathology (Figure 16.1B). The behavior was evaluated with the pole test method (Figure 16.1C). This test is used in mice to assess basal ganglia-related movement disorders and in particular bradykinesia. The method was adapted from the protocol originally described by Ogawa et al. (1985) with minor modifications.

16.2.5 Immunohistochemistry on mouse brain tissues

All immunohistochemical evaluations were performed according to previously published protocols (Galuppo et al., 2014).

16.2.6 Golgi stain

The FD Rapid Golgi Stain™ Kit (FD NeuroTechnologies, Inc.) was used for Golgi impregnation of tissue, according to the manufacturer's instructions (http://fdneurotech.com/docs/1333571253.web_pk401-401a-04042012.pdf).

16.2.7 Cell culture conditions, drug treatment, and immunocytochemistry analysis

All experiments regarding cell culture as well as immunocytochemistry analysis were performed according to previously published protocols (Rajan et al. 2016). Untreated cells (CTR), GMG alone, and MYR alone treated cells, with or without LPS activation, were also included as controls.

16.2.8 Western blot analysis

All western blot procedures were performed according to previously published protocols (Galuppo et al., 2014).

16.2.9 Statistical evaluation

GraphPad Prism version 6.0 program (GraphPad Software) was used for statistical analysis of data. The results were statistically analyzed using one-way analysis of variance, followed by a Bonferroni post hoc test for multiple comparisons. A p-value ≤ 0.05 was considered significant. Results are expressed as $n \pm$ standard error of the mean of n experiments.

16.3 Results

16.3.1 Moringin avoids body weight changes and ameliorates motor deficits in MPTP mice

The measure of body weight was assessed every 48 hours. (Figure 16.1B). As expected, after PD induction, a significant body weight loss was observed in MPTP mice compared with naive ones. A body weight gain was also observed in MPTP mice pre-administered with moringin as well as in mice pre-administered with GMG. Likewise, no sign of any decrease in body weight was found in control groups. Pretreatment with MO as well as with pure GMG did not show any sign of toxicity in mice.

Animals were also evaluated for degree of PD-related bradykinesia during the pole test (Figure 16.1C). The results showed that MPTP mice administered with MO, more than GMG-

treated ones, did not show reluctance when placed head-up on top of the pole compared with untreated MPTP mice. MO pretreatment also resulted in faster drop time when compared with MPTP mice that did not receive pharmacological injection. As expected, control groups showed normal behavior.

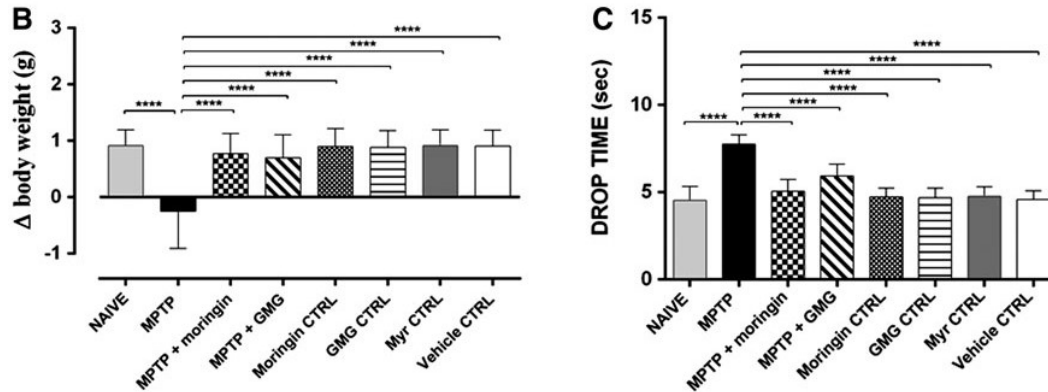


Figure 16.1 Pretreatment with MO or GMG avoids body weight changes and ameliorates motor deficits in MPTP mice. **(B)** MPTP-injected mice show a significant body weight loss. MO or GMG pretreatment significantly prevents MPTP-induced weight loss. **(C)** The same experimental group examined in a pole test gives significant results. MPTP-administrated mice pretreated with MO or GMG show a faster drop time compared with the untreated groups. The graph (B) represents Δ value for each group obtained by calculating the difference in body weight between the measures taken the day of sacrifice and those taken the day of disease induction.

(B) **** $p < 0.0001$ versus MPTP, **** $p < 0.0001$ versus MPTP+MO, **** $p < 0.0001$ versus MPTP+GMG, **** $p < 0.0001$ versus MO CTRL, **** $p < 0.0001$ versus GMG CTRL, **** $p < 0.0001$ versus MYR CTRL, **** $p < 0.0001$ versus Vehicle CTRL.

(C) **** $p < 0.0001$ versus MPTP, **** $p < 0.0001$ versus MPTP+MO, **** $p < 0.0001$ versus MPTP+GMG, **** $p < 0.0001$ versus MO CTRL, **** $p < 0.0001$ versus GMG CTRL, **** $p < 0.0001$ versus MYR CTRL, **** $p < 0.0001$ versus Vehicle CTRL. GMG, glucomoringin; MPTP, 1-methyl-4-phenyl-1,2,3,6-tetrahydropyridine; PBS, phosphate-buffered saline.

16.3.2 Moringin prevents the decreasing of tyrosine hydroxylase expression and improves the neuronal dendrite in MPTP mice

To evaluate neuronal synaptic integration following MPTP damage, we performed a qualitative analysis by Golgi impregnation in the substantia nigra area. We found that neuronal dendrites were clearly reduced in substantia nigra of MPTP mice (Figure 16.2A). In contrast with GMG pretreatment (Figure 16.2C), MO pretreatment (Figure 16.2B) exerts protection against neuronal damage with a recovery of neuronal dendrites resembling the results obtained for naive and control groups (data not shown).

As DA loss in the SNpc region is the primary feature of MPTP mice, we examined protein expression levels of tyrosine hydroxylase (TH) in brain samples to assess the neuroprotective role of MO (Figure 16.2D). In this study, we found that MPTP mice exhibited a significant reduction in the protein expression levels of TH, whereas the decreased expression of TH was significantly restored following pretreatment with MO, suggesting a neuroprotective effect protecting presumably DA neurons from MPTP-induced degeneration. Pretreatment with GMG acts only partially on restoration of TH expression. As expected, naive and control groups showed a normal expression of TH (Galuppo et al., 2013) (data not shown).

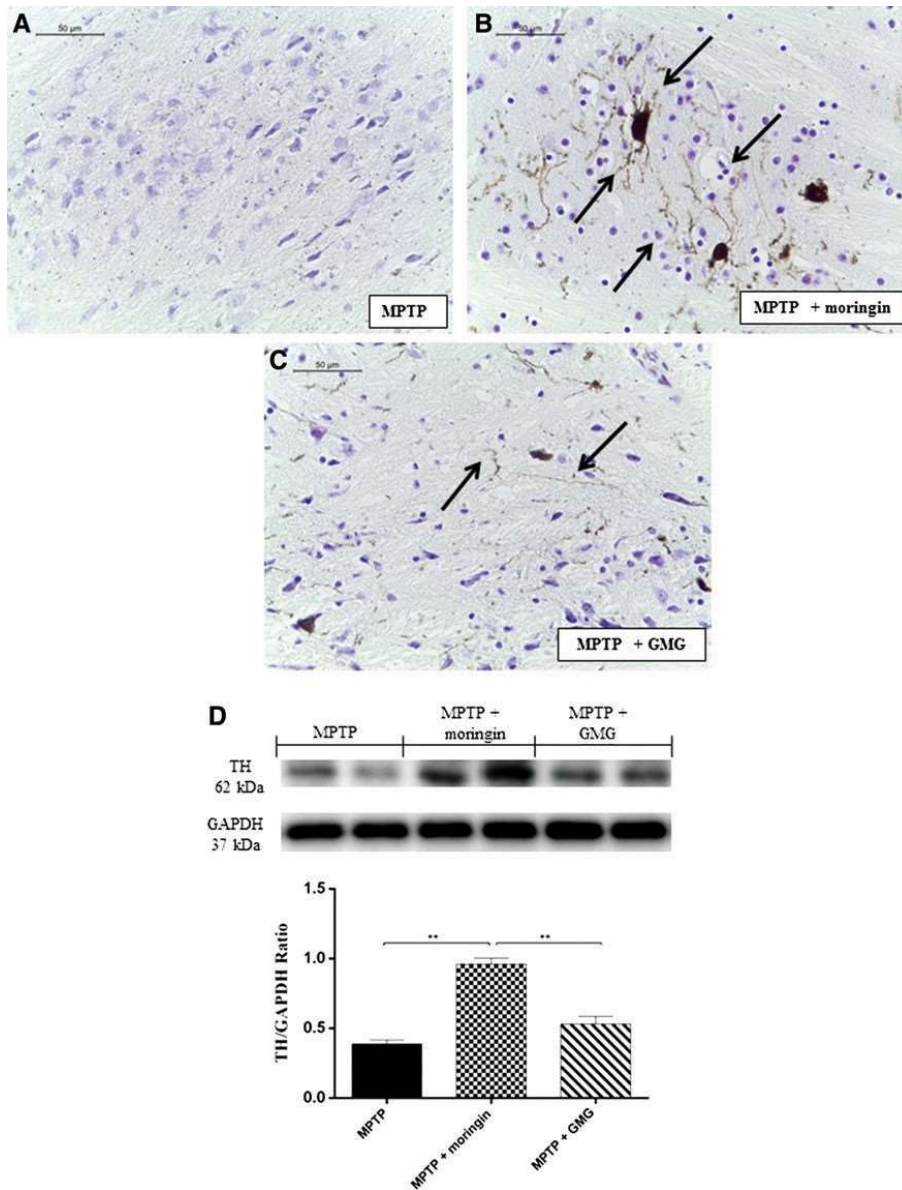


Figure 16.2 Compared with GMG, MO significantly improves the neuronal dendrites and prevents the decreasing of TH expression in MPTP mice. A severe loss of termination at the level of the dendrite tree is marked in brain samples taken from untreated MPTP mice **(A)**. Nigral DA neurons are preserved significantly by MO-pretreated MPTP mice. **(B)**, than GMG-treated MPTP mice (showed in black arrows) **(C)**. All sections were obtained using light microscopy (LEICA DM 2000 combined with LEICA ICC50 HD camera). Leica Application Suite V4.2.0 software was used as the image computer program to acquire immunohistochemical pictures. Western blot results show that expression of TH is preserved significantly by MO-treated MPTP mice than GMG-pretreated MPTP mice. A severe loss of TH level is noticed in untreated MPTP mice **(D)**. GAPDH was used as internal control. ** $p = 0.0029$ versus MPTP+MO; ** $p = 0.0067$ versus MPTP+GMG. Blots are representative of three separate and reproducible experiments. The statistical analysis was carried out on three repeated blots performed on separate experiments. DA, dopamine; TH, tyrosine hydroxylase.

16.3.3 Moringin modulates the inflammatory pathways in MPTP mice

Modulation of inflammatory mediators in mouse brain, particularly about the main cytokines involved in PD progression, was investigated to understand and assess the effects of MO pretreatment compared with GMG pretreatment on molecular mechanisms of inflammation. Specifically, the expression levels of tumor necrosis factor alpha (TNF- α) and interleukin-1 beta (IL-1 β) in brain samples were quantified by western blot and immunohistochemical analysis. By western blot analysis, an increase in TNF- α release over the course of subacute PD was found, as evidenced in samples collected from MPTP mice (Figure 16.3A). On the contrary, reduced expression of TNF- α was observed in mice having received MO administration as well as in mice pretreated with GMG. A level basal of TNF- α expression was observed in naive animals as well as in control groups (data not shown).

In addition, by western blot performed on brain extracts, we found that in MPTP mice, high expression of Toll-like receptor 4 (TLR4), which plays a fundamental role in activation of innate immunity as well as in triggering inflammatory response, was attenuated by administration of MO and less by pretreatment with GMG (Figure 16.3B). A basal level of TLR4 expression was also observed in naive animals as well as in control groups (data not shown).

Our results clearly show that brain sections from MPTP mice that did not receive pharmacological treatment displayed a marked positive staining for IL-1 β (Figure 16.3C). MPTP mice pretreated with MO (Figure 16.3D) and to a lesser extent with GMG (Figure 16.3E, densitometric analysis Figure 16.8A) displayed a reduced IL-1 β immunohistochemical localization, which supports the hypothesis of a possible mechanism of anti-inflammatory action of MO. Negative staining for IL-1 β was also found in brain sections from naive mice as well as in control groups (data not shown).

Finally, no positive staining for P-selectin was observed in sections of brain from naive mice as well as in control groups (data not shown), whereas intense positive staining in the vascular endothelium of MPTP mice was observed (Figure 16.3F, densitometric analysis Figure 16.8B). Conversely, negative staining for P-selectin was observed in brain tissues from mice pretreated with MO (Figure 16.3G) and less in GMG-pretreated mice (Figure 16.3H).

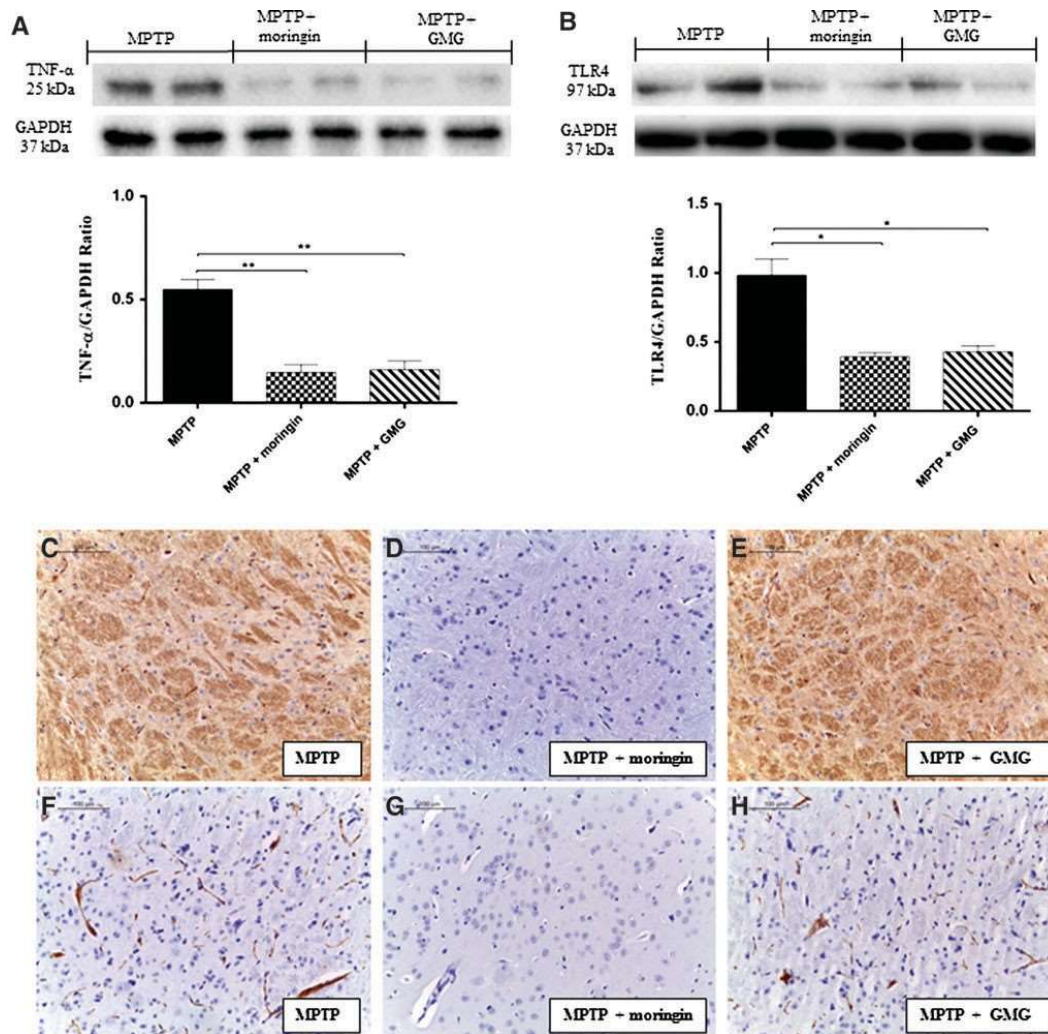


Figure 16.3 Compared with GMG, MO significantly modulates the inflammatory pathways in MPTP mice. Western blot results show enhanced expression of proinflammatory TNF- α (**A**) and TLR4 (**B**) in MPTP mice, while significant reduction is noticed in MO-pretreated MPTP mice. Similar reduction is observed in GMG-pretreated MPTP mice. GAPDH was used as internal control (**A**). ** $p = 0.0076$ versus MPTP+MO; ** $p = 0.0084$ versus MPTP+GMG; (**B**) * $p = 0.00126$ versus MPTP+MO; * $p = 0.0151$ versus MPTP+GMG. Blots are representative of three separate and reproducible experiments. The statistical analysis was carried out on three repeated blots performed on separate experiments. Proinflammatory marker IL-1 β and microglial activation marker P-selectin expression by immunohistochemical localization shows that MPTP injection causes elevated level of IL-1 β (**C**) and P-selectin (**F**), while following MO pretreatment, IL-1 β and P-selectin staining results are negative (**D** and **G**, respectively). MPTP mice pretreated with GMG show reduced expression of IL-1 β and P-selectin (**E** and **H**, respectively), although less effective than MO pretreatment. All sections were obtained using light microscopy (LEICA DM 2000 combined with LEICA ICC50 HD camera). Leica Application Suite V4.2.0 software was used as the image computer program to acquire immunohistochemical pictures. IL-1 β , interleukin-1 beta; TLR4, Toll-like receptor 4; TNF- α , tumor necrosis factor alpha.

16.3.4 Moringin modulates oxidative stress markers in MPTP mice

One possible consequence of upstream inhibition of the inflammatory pathway is the possible blockage of the oxidative stress triggering. It is known that production of radical species plays a key role in the development of severe brain damage, especially following PD. During investigation of oxidative pathways by western blot analysis, we found that samples of MPTP mice demonstrated significant increase of inducible nitric oxide synthase (iNOS), whereas in MO pretreatment, iNOS expression was clearly reduced. By comparing both pretreatments, GMG has proven to be not as effective as MO (Figure 16.4A). A basal level of iNOS was also found in naive and in control mice (data not shown). Those results were correlated with the expression of Nrf2, a transcription factor that binds to a short antioxidant response element (ARE), found in the promoters of several detoxification genes, including those involved in redox homeostasis. Immunohistochemical evaluation showed a positive staining for Nrf2 in brain samples obtained from naive mice and control ones (data not shown). The MPTP mouse group (Figure 16.4B) presents a reduced tissue expression for this protein, whereas pretreatment with MO (Figure 16.4C) and partially with GMG (Figure 16.4D, densitometric analysis Figure 16.8C) keeps Nrf2 nuclear expression at high levels, preserving tissues from MPTP damage.

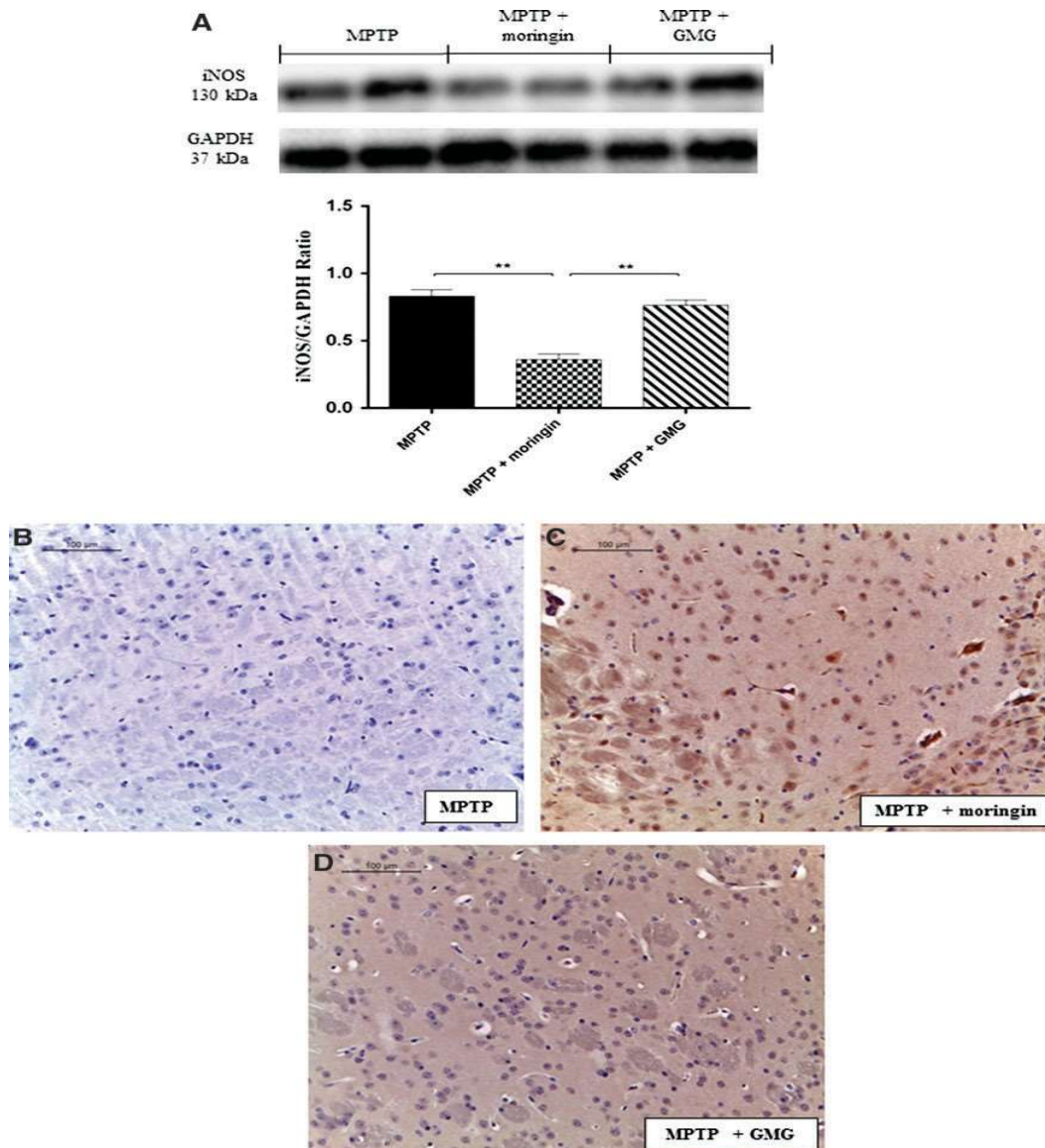


Figure 16.4 MO significantly modulates the oxidative stress markers in MPTP mice. Western blot results show enhanced expression of iNOS in MPTP mice, while significant reduction is noticed in MO-pretreated MPTP mice. MPTP mice pretreated with GMG did not show any protection (**A**). GAPDH was used as internal control. ** $p = 0.0049$ versus MPTP+MO; ** $p = 0.0076$ versus MPTP+GMG. Blots are representative of three separate and reproducible experiments. The statistical analysis was carried out on three repeated blots performed on separate experiments. Nrf2 expression by immunohistochemical localization shows that MPTP injection causes a marked reduction (**B**), while following MO pretreatment, Nrf2 staining results are significantly positive (**C**). MPTP mice pretreated with GMG show reduced expression of Nrf2 (**D**), although less effective than MO pretreatment. All sections were obtained using light microscopy (LEICA DM 2000 combined with LEICA ICC50 HD camera). Leica Application Suite V4.2.0 software was used as the image computer program to acquire immunohistochemical pictures. iNOS, inducible nitric oxide synthase.

16.3.5 MO pretreatment inhibits apoptosis in MPTP mice

Radical species production is implicated in the progression of oxidative stress-related apoptosis and cell death of the midbrain dopaminergic neurons. Therefore, we ultimately evaluated the degree of apoptosis associated with MPTP, testing the role of MO in attenuating cell death. By western blot analysis, we evaluated the activation of cleaved caspase-9 in brain tissues (Figure 16.5A). Cleaved caspase-9 levels were appreciably increased in the samples from MPTP mice, whereas pretreatment with MO prevented MPTP-induced cleaved caspase-9 expression. MPTP mice pretreated with GMG showed yet high expression of cleaved caspase-9. Naive mice as well as control ones (data not shown) showed a basal expression of cleaved caspase-9. In addition, 14 days after subacute PD induction, the appearance of protein effectors of mitochondrial apoptosis, such as proapoptotic Bax proteins, could be detected by immunohistochemical evaluation. In the study of the apoptotic pathway through immunohistochemical analysis, as expected, we assessed a completely negative staining for Bax and a marked positivity for Bcl-2 in naive animals (data not shown). Conversely, MPTP mice showed a positive expression for Bax (Figure 16.5B) and negative staining for Bcl-2 (Figure 16.5E). By comparing the two pretreatments, MO demonstrated a significant capacity in protecting the unbalance between Bax/Bcl2 (Figure 16.5C, F), while GMG possessed a lower power in downregulation of Bax (Figure 16.5D densitometric analysis Figure 16.8D) and in upregulation of Bcl-2 degradation (Figure 16.5G, densitometric analysis Figure 16.8D). The above proteins seem to be modulated by STAT-1 protein, which has been implicated in modulating pro- and antiapoptotic genes following several stress-induced responses (Cao et al., 2015). In this study, we found an increased expression of STAT-1 in MPTP mice, attenuated by administration of MO as well as by GMG pretreatment. (Figure 5H). Likewise, proteins in the mitochondrial p53 pathway (Figure 16.5I) and one of its target genes, p21 (Figure 16.5J), were detected by western blot analysis. Gene p53 is able to induce apoptosis both by controlling the translation of proapoptotic p53-checked mediators and by non-transcriptional mechanisms, including upregulation of proapoptotic proteins and downregulation of antiapoptotic mediators. MPTP mice showed a significant expression of these markers when compared with the naive group (data not shown). Conversely, expression

of p53 was reduced by administration of MO as well as by administration of GMG, while p21 was downregulated only by MO pretreatment.

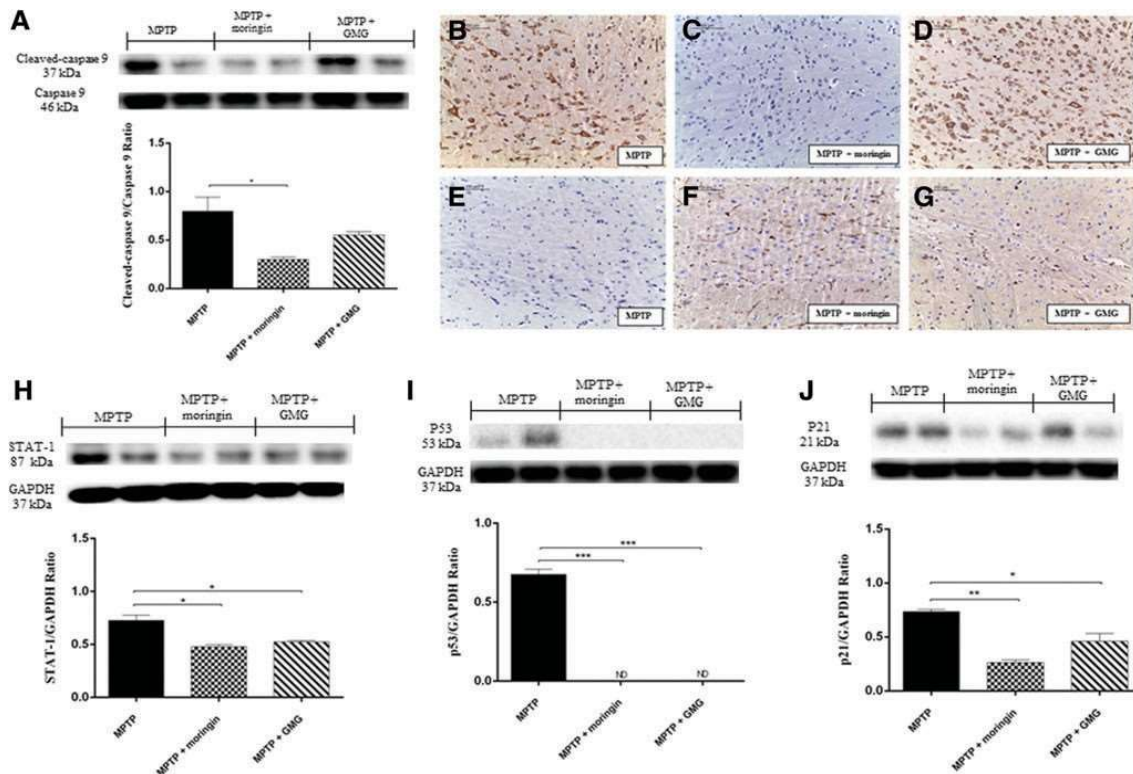


Figure 16.5 MO significantly attenuates apoptosis in MPTP mice. Western blot results show enhanced expression of cleaved caspase-9 in MPTP mice, while significant reduction is noticed in MO-pretreated MPTP mice. MPTP mice pretreated with GMG show reduced expression of cleaved caspase-9, although less effective than MO pretreatment (**A**). * $p = 0.0327$ versus MPTP+MO. Proapoptotic Bax expression by immunohistochemical localization shows that MPTP injection causes elevated level of Bax (**B**) in MPTP mice, while following MO pretreatment, Bax staining results are significantly negative (**C**). MPTP mice pretreated with GMG did not show significant reduction of Bax (**D**). Antiapoptotic Bcl-2 expression by immunohistochemical localization shows that MPTP injection causes marked reduction (**E**) in MPTP mice, while following MO pretreatment, Bcl-2 staining results are significantly positive (**F**). MPTP mice pretreated with GMG show a mild positive staining for Bcl-2 (**G**), although less effective than MO pretreatment. All sections were obtained using light microscopy (LEICA DM 2000 combined with LEICA ICC50 HD camera). Leica Application Suite V4.2.0 software was used as the image computer program to acquire immunohistochemical pictures. Western blot results show enhanced expression of STAT1 (**H**), p53 (**I**), and p21 (**J**) in MPTP mice, while significant reduction is noticed in MO-pretreated MPTP mice. MPTP mice pretreated with GMG show reduced expression of STAT1 and p53, similar to MO-pretreated MPTP mice; however, p21 reduction is less than MO pretreatment. GAPDH was used as internal control. (**H**) * $p = 0.0129$ versus MPTP+MO; * $p = 0.0229$ versus MPTP+GMG. (**I**) *** $p = 0.0002$ versus MPTP+MO; *** $p = 0.0002$ versus MPTP+GMG. (**J**) ** $p = 0.0054$ versus MPTP+MO; * $p = 0.0256$ versus MPTP+GMG. Blots are representative of three separate and reproducible experiments. The statistical analysis was carried out on three repeated blots performed on separate experiments. ND, not detectable.

16.3.6 Moringin modulates the inflammatory pathways in LPS-activated mouse macrophage RAW 264.7

To provide further evidence for the molecular mechanisms underlying the anti-inflammatory effects of MO, we performed *in vitro* studies in the mouse macrophage cell line, RAW 264.7. The cells were pretreated with MO before LPS stimulation. Eosin and hematoxylin staining showed morphological changes in LPS-stimulated macrophages (Figure 16.6B), including an increase in cell size and production of lamellipodia and filopodia compared with control cell (Figure 16.6A). MO pretreatment (Figure 16.6C) attenuated clearly these LPS-triggered morphological changes. Macrophages pretreated with GMG showed only partially reduced (Figure 16.6D) morphological changes.

Immunocytochemistry results showed dense positive staining for inflammatory markers, TLR4 (Figure 16.6F) and TNF- α (Figure 16.6J), in LPS-activated cells. On the contrary, MO pretreatment showed basal level staining for TLR4 (Figure 16.6G) similar to that of control cells (Figure 16.6E). MO pretreatment also displayed negative staining for TNF- α in LPS-activated cells (Figure 6K) as well as in control cells (Figure 16.6I). In addition, GMG pretreatment displayed partial but significant reduction of positive staining for TLR4 (Figure 16.6H, densitometric analysis Figure 16.8E) as well as for TNF- α (Figure 6L, densitometric analysis Figure 16.8F) when compared with the LPS-moringin group. Western blot data showed a reduction in I β B- α level in LPS-activated cells, while MO significantly elevated its level (Figure 16.6M). Increased expression of NF- κ B (Figure 6N) and IL-6 (Figure 16.7A) was observed in LPS-activated cells, while MO significantly reduced their levels.

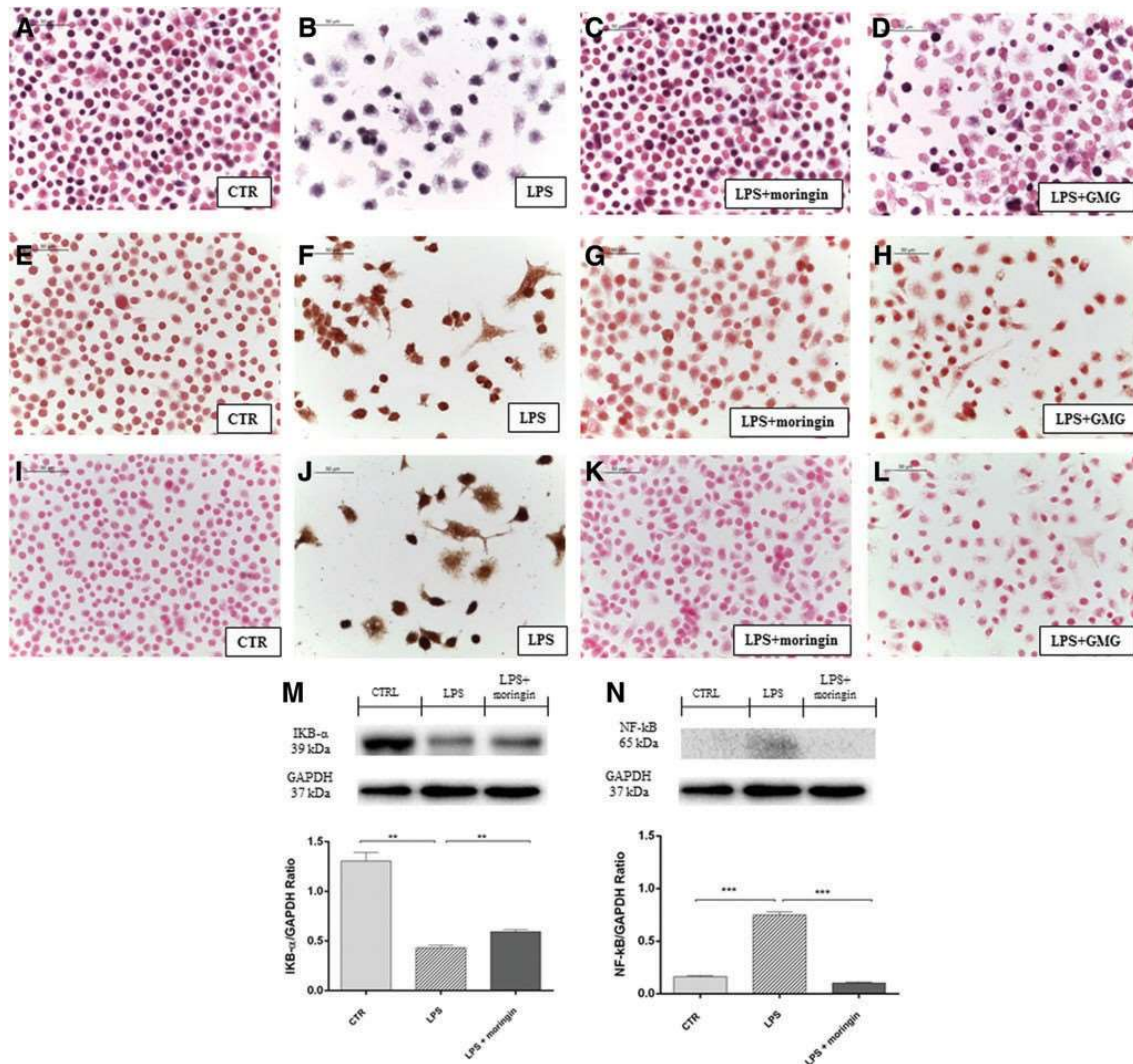


Figure 16.6 MO modulates the inflammatory pathways in LPS-activated mouse macrophage RAW 264.7. Morphological assessment in LPS-activated RAW macrophages shows increased cell size and production of lamellipodia and filopodia (**B**). MO pretreatment significantly reduced these LPS-triggered morphological features (**C**). Control cells show normal morphological appearance (**A**). GMG pretreatment reduced partially LPS-triggered morphological features (**D**). Immunocytochemistry results show that in LPS-activated macrophages, proinflammatory markers, TLR4 (**F**) and TNF- α (**J**), show enhanced expression, while MO pretreatment shows basal level staining for TLR4 (**G**) similar to that of control cells (**E**) and negative staining for TNF- α (**K**) expression. Control cells show negative staining for TNF- α (**I**). GMG pretreatment displayed partial but significant reduction of positive staining for TLR4 (**H**) as well as for TNF- α (**L**) when compared with the LPS-MO group. All sections were obtained using light microscopy (LEICA DM 2000 combined with LEICA ICC50 HD camera). Leica Application Suite V4.2.0 software was used as the image computer program to acquire immunohistochemical pictures. Western blot results show reduced expression of I κ B- α (**M**) and enhanced expression of NF- κ B (**N**) in LPS-stimulated macrophages, MO pretreatment significantly increased the I κ B- α level and decreased the NF- κ B level in LPS-activated macrophages. GAPDH was used as internal control. (**J**) $**p = 0.0014$ versus LPS; $**p = 0.0026$ versus LPS+MO. (**K**) $***p = 0.0002$ versus LPS; $***p = 0.0001$ versus LPS+MO. Blots are representative of three separate and reproducible experiments. The statistical analysis was carried out on three repeated blots performed on separate experiments. LPS, lipopolysaccharide.

16.3.7 Moringin modulates oxidative stress markers in LPS-activated mouse macrophage RAW 264.7

We assessed the antioxidative effects of MO in LPS-activated mouse macrophage RAW 264.7 cells. Immunocytochemistry results showed dense positive staining for oxidative stress marker nitrotyrosine in LPS-activated cells (Figure 7C). Only MO pretreatment (Figure 7D) significantly reduced the expression of nitrotyrosine when compared with LPS-activated cells (Figure 7C) and LPS-GMG cells (Figure 7E, densitometric analysis Figure 8G). Western blot data showed increased expression of another oxidative stress marker—iNOS—in LPS-activated cells, while MO completely inactivated iNOS expression (Figure 7F).

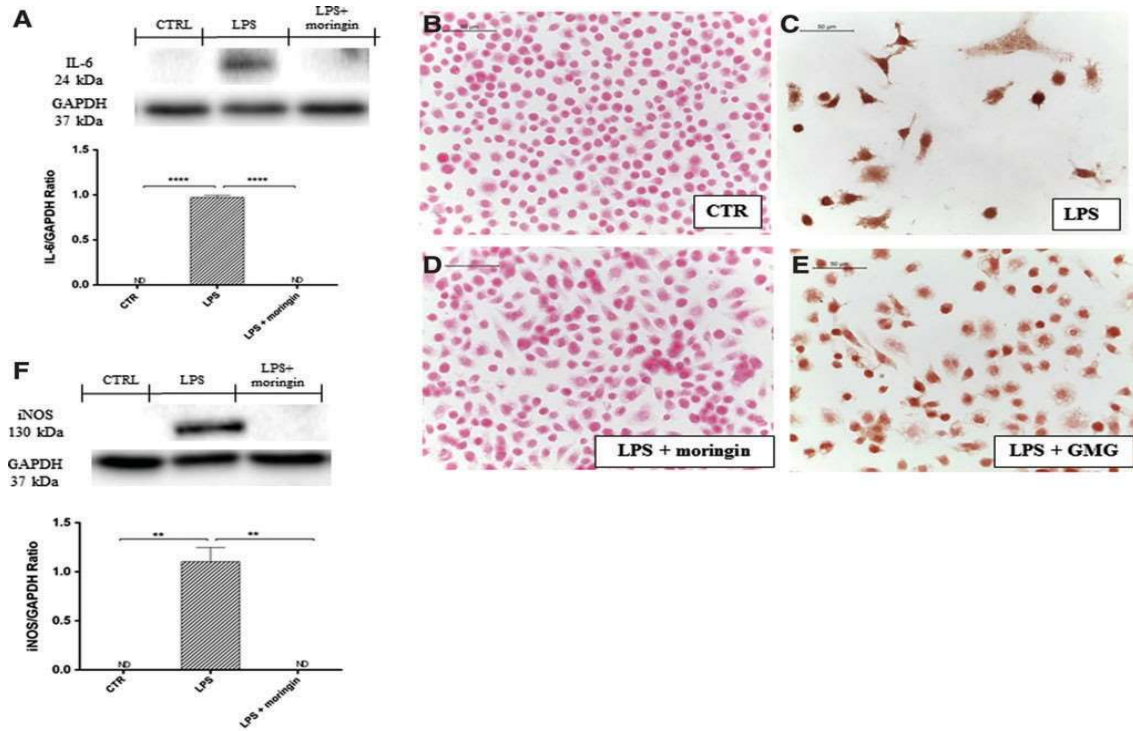


Figure 16.7 MO modulates the oxidative stress markers in LPS-activated mouse macrophage RAW 264.7. Western blot results show enhanced expression of IL-6 (**A**) and iNOS (**F**) in macrophages activated with LPS, while MO pretreatment significantly reduced the expression of IL-6 and iNOS. Immunocytochemistry results show negative staining for nitrotyrosine in normal cells (**B**). In LPS-activated macrophages, the nitrotyrosine level is markedly increased (**C**), while MO pretreatment shows negative staining for nitrotyrosine (**D**). GMG pretreatment (**E**) partially reduced the expression of nitrotyrosine when compared with LPS-activated cells. GAPDH was used as internal control. (**A**) **** $p < 0.0001$ versus LPS; **** $p < 0.0001$ versus LPS+MO. (**E**) ** $p = 0.0029$ versus LPS; ** $p = 0.0029$ versus LPS+MO. Blots are representative of three separate and reproducible experiments. The statistical analysis was carried out on three repeated blots performed on separate experiments. All sections were obtained using light microscopy (LEICA DM 2000 combined with LEICA ICC50 HD camera). Leica Application Suite V4.2.0 software was used as the image computer program to acquire immunohistochemical pictures.

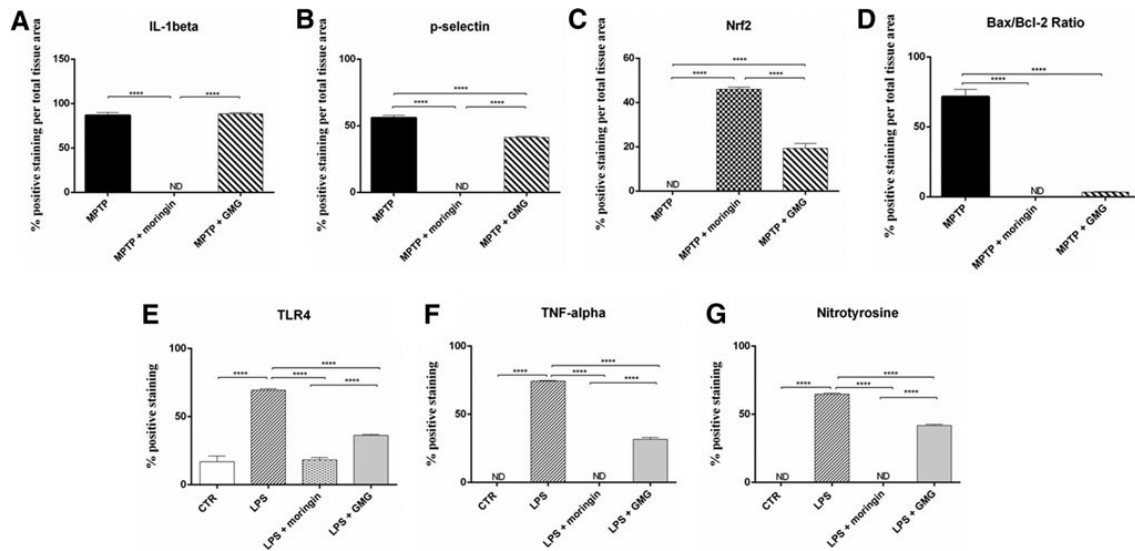


Figure 16.8 Densitometric analysis for IL-1b, P-selectin, Nrf2, Bax/Bcl-2, TLR4, TNF-a, and nitrotyrosine. For immunohistochemical images, densitometric analysis was carried out to quantify and highlight significant differences among experimental groups. p Value <0.05 was considered significant. ****p < 0.0001

16.4 Discussion

In recent years, interesting findings about the neuroprotective effects of ITCs generated from GL precursors by MYR-induced hydrolysis have been obtained in *in vitro* and *in vivo* models of neurodegeneration (Dinkova-Kostova and Kostov, 2012; Giacoppo et al. 2015a; Galuppo et al., 2014; Galuppo et al., 2015a; Galuppo et al., 2013; Galuppo et al., 2015b). The present study introduces a new promising application of MO, which is readily produced from GMG, the sole GL present in *M. oleifera* seeds. Indeed, MO might be used in the treatment of severe pathological diseases, as in PD, widely associated with both inflammatory response and oxidative mechanism, as well as apoptotic pathway and neurodegenerative feature.

As it is known, the primary pathophysiology of PD is correlated with a decrease in TH activity in the striatum. Since TH mediates the conversion of tyrosine into L-DOPA during dopamine synthesis, we investigated the changes in the expression levels of TH. In this study, the reduction in TH expression in MPTP mice was positively amended with MO pretreatment and partially by GMG pretreatment, which demonstrated the neuroprotective effect of MO against MPTP-induced dopaminergic neurotoxicity. As evidenced by our results, the behavioral deficits induced by MPTP, including motor incoordination, bradykinesia, and

weight loss, as well as damage by dendritic spine loss, were significantly improved by administration of MO and only to a small extent by GMG pretreatment. Notably, only in MO-pretreated MPTP mice and not in GMG pretreated MPTP mice, preserved neuronal cell integrity, resulting in unaffected synaptic spine-spine communication at the level of dendritic trees, was observed. Since microglial activation in the SNpc is another hallmark of PD (Galuppo et al., 2013; Mogi et al., 1994) we evaluated the immunomodulatory effects of MO and GMG in MPTP-induced neuroinflammation. TLR4 signaling promotes inflammation and oxidative stress by increasing the expression of proinflammatory cytokines, such as TNF- α , IL-1 β , and IL-6 (Sabroe et al., 2008; Tadeka and Akira; 2005). Indeed, analyses performed on postmortem brain and cerebral spinal fluid from PD patients show enhanced proinflammatory cytokine production, including TNF- α , IL-1 β , IL-6, and interferon gamma (IFN- γ) (Mogi et al., 1994; Nagatsu et al., 2000). In addition, extensive reactive microgliosis and T-cell infiltration indicate a strong proinflammatory immune response (Brochard et al., 2009; McGeer et al., 1988). All of the inflammatory features found in human PD are also observed in the MPTP model (Ramsey and Tansey, 2012), which mimics the primary pathological and biochemical features of human PD, including oxidative stress, mitochondrial dysfunction, and apoptosis (Camicioli et al., 2001). Besides, recent data indicate that TLR4 is elevated by MPTP administration in a mouse model of PD (Ros-Bernal et al., 2011). Our results showed marked upregulation of TLR4, TNF- α , and IL-1 β in the brain of MPTP mice. MO administration significantly reduced their expression. Moreover, proinflammatory cytokine triggered expression of microglial activation marker P-selectin cell adhesion molecule was reduced after MO pretreatment, which suggested a reduction in microglial activation. In addition, we noticed that GMG administration also could elicit anti-inflammatory effects, although the effects were much lower than those of MO. In a recent article (Budnowski et al., 2015) mice orally administered with other GLs, belonging to the Brassicaceae family, excreted approximately one-quarter to one-third of orally administered compounds intact in their urine. In addition, the same authors reported that intact GLs were detected not only in the urine of mice following oral administration but also in plasma. They confirmed the absorption of intact GLs in circulation and hypothesized a thioglucosidase activity as a possible account for GL hydrolysis in germ-free mice. In addition, Abdull Razis et al. (2010) reported that it has always been assumed that intact GLs, because of their hydrophilicity, would be unable to reach the bloodstream following oral intake, but these authors found that studies performed

in precision-cut rat liver slices (living tissue) demonstrate for the first time that intact GLs can modulate the hepatic activity of carcinogen-metabolizing enzyme systems. It is not possible to discern from our study whether anti-inflammatory effects of GMG, although much lower than that shown by MO, are likely derived from the GL per se or due to its derived compounds generated in small quantities by the action of a hydrolytic enzyme. Interestingly, anti-inflammatory effects of MO compared with GMG, were found in the LPS-stimulated mouse macrophage cell line, RAW 264.7. As widely known, LPS has been shown to initiate multiple intracellular signaling events by upstream TLR4, which in turn activates the NF- κ B pathway, leading to the synthesis and release of several proinflammatory mediators (Sweet and Hume, 1996; Schletter et al., 1995). In most types of cells, NF- κ B dimers are transcriptionally inactive in cytoplasm due to the inhibition of I κ B- α . In response to a wide range of stimuli, including oxidative stress, infection, extracellular signal, and inflammation, I κ B- α is phosphorylated by the enzyme, I κ B- α kinase, so that NF- κ B is free to translocate into the nucleus and to promote the expression of inflammatory cytokines (Tak and Firestein, 2001; Oeckinghaus et al., 2011). Our results showed that pretreatment with MO led to upregulation of I κ B- α and consequently downregulation of NF- κ B. These *in vivo* and *in vitro* results established a major efficacy of MO as a better anti-inflammatory agent than GMG, demonstrating the greater effectiveness of the ITC and suggesting its possible use as therapeutic agent. These results can be attributed to the electrophilicity of the ITC function, whose interaction with biological nucleophiles underlies the biological activity of ITCs (Fimognari et al., 2012), notably MO, whereas intact GLs, for example, GMG, lack such chemical behavior.

Then, we assessed the antioxidative effects of MO and GMG. It is believed that the main mechanism of DA loss in MPTP-administered animals is ascribed to an enhanced production of reactive oxygen species generated in response to MPTP exposure (Przedborski et al., 2000), which in turn can induce cell degradation and death in many forms. The antioxidative effect of ITCs has been demonstrated in previous studies and can be attributed to Nrf2-mediated action (Giacoppo et al., 2015a; Galuppo et al., 2015a; Galuppo et al., 2015b; Boddupalli et al., 2012). Nrf2 is a transcription factor that (by interacting with a short ARE) regulates phase II antioxidant response, which includes expression of free radical scavengers and cytoprotective enzymes (Scapagnini et al., 2011). Hence, these genes are upregulated in response to oxidative stress. The induction of Nrf2-mediated transcription has been shown

to protect neurons from toxic insults such as increases in intracellular calcium, oxidative stress, and mitochondrial dysfunction (Tufekci et al., 2011). With regard to ITCs, it was widely demonstrated that they can interact directly with sulfhydryl residues on the Kelch-like ECH-associated protein 1 (Keap1), the repressor of Nrf2, which is normally present in cytoplasm, leading to its release into the nucleus. Once translocated into the nucleus, Nrf2 activates ARE-responsive genes and induces the phase 2 response. In neurodegenerative diseases, Nrf2 expression has been shown to decrease, while Nrf2 overexpression was demonstrated to protect against neurodegeneration and cell death (Scapagnini et al., 2011; de Vries et al., 2008). Confirming this, in the present study, Nrf2 immunohistochemical localization shows a negative expression in brain sections sampled from MPTP mice, whereas administration of MO and, to a smaller extent, of GMG stimulates Nrf2 nuclear activity, preventing tissue damage by pro-oxidative gene expression.

Moreover, reactive nitrogen species (RNS) have been shown to play a significant role in inflammatory responses. Especially, the overproduction of nitric oxide through iNOS causes accentuated lipid peroxidation and protein and DNA modifications that result in cellular damage by exacerbating inflammatory events (Montalto et al., 2003). Our results showed that only MO pretreatment was able to inhibit iNOS production, whose expression remains, on the contrary, higher in mice pretreated with GMG. Moreover, similar inhibition of RNS was noticed in LPS-stimulated macrophages pretreated with MO. The absence of iNOS and nitrotyrosine expression found in LPS-MO cells and not in LPS-GMG ones led to suggest MO as a potent antioxidant. Finally, we investigated whether MO could potentially exert apoptosis regulatory functions in MPTP mouse brain. The mechanism of apoptosis is complex and involves a cascade of reactions; one of the key steps leading to apoptosis is the leakage of cytochrome C from the mitochondria and activation of caspases (Joshi and Bakowska, 2011). In this study, we found that MO pretreatment (and only partially GMG treatment) was able to reduce the cell death induced by MPTP in mice and this protective effect was associated with a decreased activity of cleaved caspase-9 and of Bax, a proapoptotic factor, which influences the mitochondrial outer membrane permeability and apoptotic susceptibility. In addition, MO pretreatment significantly enhanced the expression of Bcl-2 compared with both GMG-treated MPTP mice and untreated ones. In this study, we investigated also STAT1-p53-p21 pathway-mediated apoptosis in MPTP mice. As expected, upstream activation of proinflammatory cytokines and consequent oxidative stress mediators

positively recruited STAT1, p53, and p21 proteins in MPTP mouse brain. On the contrary, mice treated with MO showed significant reduction in STAT1, p53, and p21 expression when compared with mice treated with GMG, thus confirming a lower efficacy of the GL treatment in comparison with the corresponding ITC (Abdull Razis and Noor, 2013). Therefore, a protective effect of MO suggests that this pretreatment could interfere with MPTP-induced neuronal death.

16.5 Conclusion

The present study was designed to promote a new alternative therapy in the treatment or the prevention of PD, either alone or in association with the currently used therapies. For this purpose, we have compared the efficacy of the phytochemical MO obtained by MYR-catalyzed hydrolysis of the GL precursor GMG with that of GMG itself, demonstrating the greater effectiveness of a breakdown product of GL, in an experimental model of neurodegenerative disease. Therefore, we suggest MO as a good and effective candidate in the treatment of experimental PD as it is able to modulate different molecular pathways underlying the progression of this disease.

References

Abdull Razis AF, Bagatta M, De Nicola GR, Iori R, Ioannides C (2010) Intact glucosinolates modulate hepatic cytochrome P450 and phase II conjugation activities and may contribute directly to the chemopreventive activity of cruciferous vegetables. *Toxicology* 277:74-85.

Abdull Razis AF and Noor NM (2013) Sulforaphane is superior to glucoraphanin in modulating carcinogen-metabolising enzymes in Hep G2 cells. *Asian Pac J Cancer Prev* 14:4235-4238.

Beitz JM (2014) Parkinson's disease: A review. *Front Biosci* 6:65-74.

Blesa J, Trigo-Damas I, Quiroga-Varela A, Jackson-Lewis VR (2015) Oxidative stress and Parkinson's disease. *Front Neuroanat* 9:91.

Boddupalli S, Mein JR, Lakkanna S, James DR (2012) Induction of phase 2 antioxidant enzymes by broccoli sulforaphane: Perspectives in maintaining the antioxidant activity of vitamins a, C, and e. *Front Genet* 3:7.

Braak H, Ghebremedhin E, Rub U, Bratzke H, Del Tredici K (2004) Stages in the development of Parkinson's disease-related pathology. *Cell Tissue Res* 318:121-134.

Brochard V, Combadiere B, Prigent A, Laouar Y, Perrin A, Beray-Berthet V, Bonduelle O, Alvarez-Fischer D, Callebert J, Launay JM, Duyckaerts C, Flavell RA, Hirsch EC, Hunot S (2009) Infiltration of CD4⁺ lymphocytes into the brain contributes to neurodegeneration in a mouse model of Parkinson disease. *J Clin Invest* 119:182-192.

Budnowski J, Hanske L, Schumacher F, Glatt H, Platz S, Rohn S, Blaut M (2015) Glucosinolates are mainly absorbed intact in germfree and human microbiota-associated mice. *J Agric Food Chem* 63:8418-8428.

Camicioli R, Grossmann SJ, Spencer PS, Hudnell K, Anger WK (2001) Discriminating mild parkinsonism: Methods for epidemiological research. *Mov Disord* 16:33-40.

Cao ZH, Zheng QY, Li GQ, Hu XB, Feng SL, Xu GL, Zhang KQ (2015) STAT1-mediated down-regulation of Bcl-2 expression is involved in IFN-gamma/TNF-alpha-induced apoptosis in NIT-1 cells. *PLoS One* 10:e0120921.

Ceravolo R, Rossi C, Del Prete E, Bonuccelli U (2016) A review of adverse events linked to dopamine agonists in the treatment of Parkinson's disease. *Expert Opin Drug Saf* 15:181-198.

Dawson TM and Dawson VL. Molecular pathways of neurodegeneration in Parkinson's disease. *Science* 302:819-822.

de Vries HE, Witte M, Hondius D, et al. (2008) Nrf2-induced antioxidant protection: A promising target to counteract ROS-mediated damage in neurodegenerative disease? *Free Radic Biol Med* 45:1375-1383.

Dinkova-Kostova AT and Kostov RV (2012) Glucosinolates and isothiocyanates in health and disease. *Trends Mol Med* 18:337-347.

Fimognari C, Turrini E, Ferruzzi L, Lenzi M, Hrelia P (2012) Natural isothiocyanates: Genotoxic potential versus chemoprevention. *Mutat Res* 750:107-131.

Galuppo M, Iori R, De Nicola GR, Bramanti P, Mazzon E (2013) Anti-inflammatory and anti-apoptotic effects of (RS)-glucoraphanin bioactivated with myrosinase in murine subacute and acute MPTP-induced Parkinson's disease. *Bioorg Med Chem* 21:5532-5547.

Galuppo M, Giacoppo S, De Nicola GR, Iori R, Navarra M, Lombardo GE, Bramanti P, Mazzon E (2014) Antiinflammatory activity of glucomoringin isothiocyanate in a

mouse model of experimental autoimmune encephalomyelitis. *Fitoterapia* 95:160-174.

Galuppo M, Giacoppo S, Iori R, De Nicola GR, Bramanti P, Mazzon E (2015a) Administration of 4-(alpha-L-rhamnosyloxy)-benzyl isothiocyanate delays disease phenotype in SOD1 (G93A) rats: A transgenic model of amyotrophic lateral sclerosis. *Biomed Res Int* 2015:259417.

Galuppo M, Giacoppo S, Iori R, De Nicola GR, Milardi D, Bramanti P, Mazzon E (2015b) 4(alpha-L-Rhamnosyloxy)-benzyl isothiocyanate, a bioactive phytochemical that defends cerebral tissue and prevents severe damage induced by focal ischemia/reperfusion. *J Biol Regul Homeost Agents* 29:343-356.

Giacoppo S, Galuppo M, Montaut S, et al. (2015a) An overview on neuroprotective effects of isothiocyanates for the treatment of neurodegenerative diseases. *Fitoterapia* 106:12-21.

Giacoppo S, Galuppo M, De Nicola GR, Bramanti P, Mazzon E (2015) 4(Alpha-l-rhamnosyloxy)-benzyl isothiocyanate, a bioactive phytochemical that attenuates secondary damage in an experimental model of spinal cord injury. *Bioorg Med Chem* 23:80-88.

Jenner P (1991) Oxidative stress as a cause of Parkinson's disease. *Acta Neurol Scand Suppl* 136:6-15.

Joshi DC and Bakowska JC (2011) Determination of mitochondrial membrane potential and reactive oxygen species in live rat cortical neurons. *J Vis Exp* 51:pii:2704.

Langston JW, Ballard P, Tetrud JW, Irwin I (1983) Chronic Parkinsonism in humans due to a product of meperidine-analog synthesis. *Science* 219:979-980.

McGeer PL, Itagaki S, Boyes BE, McGeer EG (1988) Reactive microglia are positive for HLA-DR in the substantia nigra of Parkinson's and Alzheimer's disease brains. *Neurology* 38:1285-1291.

Mogi M, Harada M, Kondo T, Riederer P, Inagaki H, Minami M, Nagatsu T (1994) Interleukin-1 beta, interleukin-6, epidermal growth factor and transforming growth factor-alpha are elevated in the brain from parkinsonian patients. *Neurosci Lett* 180:147-150.

Montalto MC, Hart ML, Jordan JE, Wada K, Stahl GL (2003) Role for complement in mediating intestinal nitric oxide synthase-2 and superoxide dismutase expression. *Am J Physiol Gastrointest Liver Physiol* 285:G197-G206.

Nagatsu T, Mogi M, Ichinose H, Togari A (2000) Changes in cytokines and neurotrophins in Parkinson's disease. *J Neural Transm Suppl* 60:277-290.

Oeckinghaus A, Hayden MS, Ghosh S (2011) Crosstalk in NF-kappaB signaling pathways. *Nat Immunol* 12:695-708.

Ogawa N, Hirose Y, Ohara S, Ono T, Watanabe Y (1985) A simple quantitative bradykinesia test in MPTP-treated mice. *Res Commun Chem Pathol Pharmacol* 50:435-441.

Przedborski S, Jackson-Lewis V, Djaldetti R, Liberatore G, Vila M, Vukosavic S, Almer G (2000) The parkinsonian toxin MPTP: Action and mechanism. *Restor Neurol Neurosci* 16:135-142.

Rai SN, Yadav SK, Singh D, Singh SP (2015) Ursolic acid attenuates oxidative stress in nigrostriatal tissue and improves neurobehavioral activity in MPTP-induced Parkinsonian mouse model. *J Chem Neuroanat* 71:41-49.

Rajan TS, De Nicola GR, Iori R, Rollin P, Bramanti P, Mazzon (2016) Anticancer activity of glucomoringin isothiocyanate in human malignant astrocytoma cells. *Fitoterapia* 110:1-7.

Ramsey CP and Tansey MG (2014) A survey from 2012 of evidence for the role of neuroinflammation in neurotoxin animal models of Parkinson's disease and potential molecular targets. *Exp Neurol* 256:126-132.

Ros-Bernal F, Hunot S, Herrero MT, Parnadeau S, Corvol JC, Lu L, Alvarez-Fischer D, Carrillo-de Sauvage MA, Saurini F, Coussieu C, Kinugawa K, Prigent A, Hoglinger G, Hamon M, Tronche F, Hirsch EC, Vyas S (2011) Microglial glucocorticoid receptors play a pivotal role in regulating dopaminergic neurodegeneration in parkinsonism. *Proc Natl Acad Sci U S A* 108:6632-6637.

Sabroe I, Parker LC, Dower SK, Whyte MK (2008) The role of TLR activation in inflammation. *J Pathol* 214:126-135.

Scapagnini G, Vasto S, Abraham NG, Caruso C, Zella D, Fabio G (2011) Modulation of Nrf2/ARE pathway by food polyphenols: A nutritional neuroprotective strategy for cognitive and neurodegenerative disorders. *Mol Neurobiol* 44:192-201.

Schletter J, Heine H, Ulmer AJ, Rietschel ET (1995) Molecular mechanisms of endotoxin activity. *Arch Microbiol* 164:383-389.

Sweet MJ and Hume DA (1996) Endotoxin signal transduction in macrophages. *J Leukoc Biol* 60:8-26.

Tak PP and Firestein GS (2001) NF-kappaB: A key role in inflammatory diseases. *J Clin Invest* 107:7-11.

Takeda K and Akira S (2005) Toll-like receptors in innate immunity. *Int Immunol* 17:1-14.

Tufekci KU, Civi Bayin E, Genc S, Genc K (2011) The Nrf2/ARE pathway: A promising target to counteract mitochondrial dysfunction in Parkinson's disease. Parkinsons Dis 2011:314082.

SCIENTIFIC PRODUCTION

Publication list

Ibrahim N, Allart-Simon I, De Nicola GR, Iori R, Renault J-H, Rollin P, Nuzillard J-M (2018) Advanced NMR-based structural investigation of glucosinolates and desulfoglucosinolates. *J Nat Prod* 81:323-334.

Giacoppo S, Rajan TS, De Nicola GR, Iori R, Rollin P, Bramanti P, Mazzon (2017) The isothiocyanate isolated from *moringa oleifera* shows potent anti-inflammatory activity in the treatment of murine subacute Parkinson's disease. *Rejuvenation Research*, 20 (1), pp. 50-63. DOI: 10.1089/rej.2016.1828

Montaut S, De Nicola GR, Agnani H, Issembe Y, Rollin P, Menut C (2017) Probing for the presence of glucosinolates in three *Drypetes* spp. (*Drypetes euryodes* (Hiern) Hutch., *Drypetes gossweileri* S. Moore, *Drypetes laciniata* Hutch.) and two *Rinorea* spp. (*Rinorea subintegriifolia* O. Ktze and *Rinorea woermanniana* (Büttner) Engl.) from Gabon. *Natural Product Research*, 31 (3):308-313. DOI: 10.1080/14786419.2016.1236099

Vivarelli F, Canistro D, Babot Marquillas C, Cirillo S, De Nicola GR, Iori R, Biagi G, Pinna C, Gentilini F, Pozzo L, Longo V, Paolini M (2017) The combined effect of Sango sprout juice and caloric restriction on metabolic disorders and gut microbiota composition in an obesity model. *International Journal of Food Sciences and Nutrition* 1-13. DOI: 10.1080/09637486.2017.1350940

Giacoppo S, Soundara Rajan T, De Nicola GR, Iori R, Bramanti P, Mazzon E (2016) Moringin activates Wnt canonical pathway by inhibiting GSK3 β in a mouse model of experimental autoimmune encephalomyelitis. *Drug Design, Development and Therapy*, 10, pp. 3291-3304. DOI: 10.2147/DDDT.S110514

Michl C, Vivarelli F, Weigl J, De Nicola GR, Canistro D, Paolini M, Iori R, Rasclé A (2016) The chemopreventive phytochemical moringin isolated from *Moringa oleifera* seeds inhibits JAK/STAT signaling. PLoS ONE, 11 (6), art. no. e0157430. DOI: 10.1371/journal.pone.0157430

Rajan TS, De Nicola GR, Iori R, Rollin P, Bramanti P, Mazzon E (2016) Anticancer activity of glucomoringin isothiocyanate in human malignant astrocytoma cells. Fitoterapia, 110, pp. 1-7. DOI: 10.1016/j.fitote.2016.02.007

Rajan TS, Giacompo S, Iori R, De Nicola GR, Grassi G, Pollastro F, Bramanti P, Mazzon E (2016) Anti-inflammatory and antioxidant effects of a combination of cannabidiol and moringin in LPS-stimulated macrophages. Fitoterapia, 112, pp. 104-115. DOI: 10.1016/j.fitote.2016.05.008

Vivarelli F, Canistro D, Sapone A, De Nicola GR, Babot Marquillas C, Iori R, Antonazzo IC, Gentilini F, Paolini M (2016) *Raphanus sativus* cv. Sango sprout juice decreases diet-induced obesity in sprague dawley rats and ameliorates related disorders. PLoS ONE, 11 (3), art. no. e0150913. DOI: 10.1371/journal.pone.0150913

Agerbirk N, De Nicola GR, Olsen CE, Müller C, Iori R (2015) Derivatization of isothiocyanates and their reactive adducts for chromatographic analysis. Phytochemistry, 118:109-115. DOI: 10.1016/j.phytochem.2015.06.004

Blažević I, De Nicola GR, Montaut S, Rollin P, Ruščić M (2015) Glucosinolate profile of Croatian stenoendemic plant *Fibigia triquetra* (DC.) Boiss. ex Prantl. Croatica Chemica Acta, 88 (3):307-314. DOI: 10.5562/cca2687

Blažević I, Montaut S, De Nicola GR, Rollin P (2015) Long-chain glucosinolates from *Arabis turrita*: Enzymatic and nonenzymatic degradations. Natural Product Communications, 10 (6):1043-1046.

Galletti S, Bagatta M, Branca F, Argento S, De Nicola GR, Cianchetta S, Iori R, Ninfali (2015) *Isatis canescens* is a rich source of glucobrassicin and other health-promoting compounds. *Journal of the Science of Food and Agriculture*, 95 (1):158-164. DOI: 10.1002/jsfa.6697

Galuppo M, Giacoppo S, Iori R, De Nicola GR, Milardi D, Bramanti P, Mazzon E (2015) 4(α -L-rhamnosyloxy)-benzyl isothiocyanate, a bioactive phytochemical that defends cerebral tissue and prevents severe damage induced by focal ischemia/reperfusion. *Journal of Biological Regulators and Homeostatic Agents*, 29 (2), pp. 343-356.

Galuppo M, Giacoppo S, Iori R, De Nicola GR, Bramanti P, Mazzon E (2015) Administration of 4-(α -L-Rhamnosyloxy)-benzyl isothiocyanate delays disease phenotype in SOD1^{G93A} rats: A transgenic model of amyotrophic lateral sclerosis. *BioMed Research International*, 2015, art. no. 259417. DOI: 10.1155/2015/259417

Giacoppo S, Galuppo M, De Nicola GR, Iori R, Bramanti P, Mazzon E (2015) Tuscan black kale sprout extract bioactivated with myrosinase: a novel natural product for neuroprotection by inflammatory and oxidative response during cerebral ischemia/reperfusion injury in rat. *BMC Complementary and Alternative Medicine*, 15 (1), art. no. 397. DOI: 10.1186/s12906-015-0929-4

Giacoppo S, Galuppo M, De Nicola GR, Iori R, Bramanti P, Mazzon E (2015) 4(α -L-Rhamnosyloxy)-benzyl isothiocyanate, a bioactive phytochemical that attenuates secondary damage in an experimental model of spinal cord injury. *Bioorganic and Medicinal Chemistry*, 23 (1):80-88. DOI: 10.1016/j.bmc.2014.11.022

Kitamura S, Morisseau C, Inceoglu B, Kamita SG, De Nicola GR, Nyegue M, Hammock BD (2015) Potent natural soluble epoxide hydrolase inhibitors from *Pentadiplandra brazzeana* Baillon: synthesis, quantification, and measurement of biological activities in vitro and in vivo. *PLoS ONE*, 10 (2), art. no. e0117438. DOI: 10.1371/journal.pone.0117438

Matera R, Gabbanini S, Berretti S, Amorati R, De Nicola GR, Iori R, Valgimigli L (2015) Acylated anthocyanins from sprouts of *Raphanus sativus* cv. Sango: Isolation, structure elucidation and antioxidant activity. *Food Chemistry*, 166:397-406. DOI: 10.1016/j.foodchem.2014.06.056

Montaut S, Zhang W-D, Nuzillard J-M, De Nicola GR, Rollin P (2015) Glucosinolate Diversity in *Bretschneidera sinensis* of Chinese Origin. *Journal of Natural Products*, 78 (8):2001-2006. DOI: 10.1021/acs.jnatprod.5b00338

Müller C, Van Loon J, Ruschioni S, De Nicola GR, Olsen CE, Iori R, Agerbirk N (2015) Taste detection of the non-volatile isothiocyanate moringin results in deterrence to glucosinolate-adapted insect larvae. *Phytochemistry*, 118:139-148. DOI: 10.1016/j.phytochem.2015.08.007

Wagner AE, Sturm C, Piegholdt S., Wolf IMA, Esatbeyoglu T, De Nicola GR, Iori R, Rimbach G (2015) Myrosinase-treated glucoerucin is a potent inducer of the Nrf2 target gene heme oxygenase 1 studies in cultured HT-29 cells and mice. *Journal of Nutritional Biochemistry*, 26 (6):661-666. DOI: 10.1016/j.jnutbio.2015.01.004

Aissani N, Caboni P, Saba M, De Nicola GR, Iori R, Coroneo V (2014) Dicarboxylic acids from Caper leaves enhance antibiotic susceptibility of *Pseudomonas aeruginosa* to vancomycin. *International Journal of Current Microbiology and Applied Sciences* 3(11):54-64

De Nicola GR, Rollin P, Mazzon E, Iori R (2014) Novel gram-scale production of enantiopure *R*-Sulforaphane from tuscan black kale seeds. *Molecules*, 19 (6):6975-6986. DOI: 10.3390/molecules19066975

Giacoppo S, Galuppo M, Iori R, De Nicola GR, Bramanti P, Mazzon E (2014) (*R*₃)-glucoraphanin purified from Tuscan black kale and bioactivated with myrosinase enzyme protects against cerebral ischemia/reperfusion injury in rats *Fitoterapia*, 99:166-177. DOI: 10.1016/j.fitote.2014.09.016

Galuppo M, Giacoppo G, De Nicola GR, Iori R, Navarra M, Lombardo GE, Bramanti P, Mazzon E (2014) Antiinflammatory activity of glucoraphanin isothiocyanate in a mouse model of experimental autoimmune encephalomyelitis. *Fitoterapia*, 95, pp. 160-174. DOI: 10.1016/j.fitote.2014.03.018

Giacoppo S, Galuppo M, Iori R, De Nicola GR, Bramanti P, Mazzon E (2014) The protective effects of bioactive (*R_s*)-glucoraphanin on the permeability of the mice blood-brain barrier following experimental autoimmune encephalomyelitis. *European Review for Medical and Pharmacological Sciences*, 18 (2):194-204.

Maldini M, Maksoud SA, Natella F, Montoro P, Petretto GL, Foddai M, De Nicola GR, Chessa M, Pintore G (2014) *Moringa oleifera*: Study of phenolics and glucosinolates by mass spectrometry. *Journal of Mass Spectrometry*, 49 (9):900-910. DOI: 10.1002/jms.3437

ORAL PRESENTATION

G.R. De Nicola, E. Mazzon, M. Galuppo, S. Giacoppo, P. Rollin and R. Iori.
Tuscan black kale: from seeds to grams of highly pure glucoraphanin.
Proceedings 3rd International Glucosinolate Conference 2014, p. 47.

POSTER PRESENTATION

F. Burčul, I. Generalić Mekinić, A. Dulović, I. Kardum, J. Brekalo, D. Stojanov, M. Ruščić, G. R. De Nicola, S. Montaut, P. Rollin, I. Blažević.
Isothiocyanates as acetylcholinesterase inhibitors and their source from Croatian wild-growing plants. Book of abstracts Zagreb 2015, P50:p. 142.

